Multisegmented hybrid-polymers based on oligo-amino acids: synthesis and secondary structure in solution and the solid state

Dissertation

zur Erlangung des
Doktorgrades der Naturwissenschaften (Dr. rer. nat.)

der

Naturwissenschaftlichen Fakultät II
Chemie, Physik und Mathematik

der Martin-Luther-Universität
Halle-Wittenberg

vorgelegt

von Herrn Jan Freudenberg
geb. am 10.11.1992 in Weißenfels

Gutachter:

1. Prof. Dr. Wolfgang H. Binder

2. Prof. Dr. Helmut Schlaad

Verteidigung: 15.12.2020

Danksagung

„Man muss mit den richtigen Leuten zusammenarbeiten, sie achten und motivieren. Dauerhafter Erfolg ist nur im Team möglich“. Klaus Teilmann

An dieser Stelle möchte ich mich bei den Menschen bedanken, die die Erarbeitung meiner Promotionsarbeit möglich gemacht haben.

Ein großer Dank gebührt Prof. Dr. Wolfgang H. Binder, der mir das Vertrauen für die Bearbeitung dieses Themas geschenkt hat. Ich danke Ihm für seine Hilfsbereitschaft und seinem Interesse an meiner Arbeit, in der er mir bei Fragen stets zur Seite stand.

Weiterhin möchte ich mich bei der gesamten Arbeitsgruppe AG-Binder für das hervorragende Arbeitsklima und deren Unterstützung bedanken. Hervorzuheben sind Michel Biewend und Sebastian Funtan für die tolle Zeit im Büro und Ihre lustige Art, Susanne Tanner für Ihre Hilfsbereitschaft bei Fragen zu Gerätschaften, Julia Großert für die Bereitstellung der Chemikalien und Lösungsmittel und Anke Hassi für Ihr Organisationstalent. Ich habe mich in der Arbeitsgruppe stets wohl und respektiert gefühlt.

Außerdem gilt ein besonderer Dank Diana Döhler für die kritische und sachkundige Begutachtung meiner Arbeit und Ihrer Hilfsbereitschaft bei sämtlichen Fragen. Weiterhin einen großen Dank an Philipp Michael, der mit seinem fachspezifischen Wissen immer einen Ratschlag auf Lager hatte, um neue Wege zu gehen. Euch beide wünsche ich weiterhin viel Erfolg und Glück in der Zukunft.

Herrn Dr. D. Ströhl und Mitarbeiter für die Messung meiner NMR-Spektren.

Mein größter Dank gebührt meiner Freundin, meinen Eltern, meinem Bruder und allen Freunden die mich stets unterstützt und verstanden haben. Außerdem danke ich allen anderen Familienmitgliedern für das Verständnis und deren Hilfsbereitschaft und viele tolle Momente.

Bedanken möchte ich mich auch bei meinen Kommilitonen.

Diese Arbeit ist A. Kewitsch gewidmet.

Abstract

Multisegmented hybrid-polymers were synthesized on basis of single- or oligo-amino acids and investigated in view of their crystallization and secondary structure formation. Main focus was the investigation of oligo-benzyl protected glutamic acid ($O^{Bn}Glu_n$)- and oligo-benzyl protected aspartic acid ($O^{Bn}Asp_n$-) secondary structure formation, as they are usually stabilizing the α-helix, but their final conformation strongly depends on additional chemical and physical conditions introduced to the system.

First, single-amino acids were embedded in polyethylene-type middle segments as "defects" and the crystallization behavior of the alkyl chains was investigated. Therefore, polar benzyl protected glutamic acid (Glu), benzyl protected aspartic acid (Asp), as well as non-polar L-leucine (Leu), 2-aminoisobutyric acid (Aib) and 1-aminocyclohexanecarboxylic acid (ACHC) were functionalized on *N*- (**1a** – **1e**) and *C*-terminus (**2a** – **2e**) and embedded in polyethylene-type middle segments *via* ADMET-polymerization (**3a** – **3e**). Afterwards, polymers were hydrogenated (**4a** – **4e**) and the correct structures were determined by GPC, ^{1}H-NMR- and FTIR-measurements. XRD- and DSC-investigation revealed polyethylene like crystallization behavior with orthorhombic unit cells for polymers **4a** and **4b** with polar side chains, in which polymer **4a** has a lower melting point then **4b**. For the middle segments with non-polar polymers **4c** – **4e** no crystallization could be observed.

Subsequently, $O^{Bn}Glu_n$- and $O^{Bn}Asp_n$-elements with repetitive units of n=3 and n=10 were embedded in the polyethylene-type middle segments. The repetitive units were chosen as the final conformation of the oligomers depend on the molecular weight and additionally on the used solvent and the temperature, which allowed the investigation of varying secondary structure formation within the oligo-amino acids. Oligomers **$O^{Bn}Glu_{3,10}$** (**7a**, **8a**) and **$O^{Bn}Asp_{3,10}$** (**9a**, **10a**) were synthesized by ROP of **Glu-NCA** (**5**) and **Asp-NCA** (**6**) and characterized by GPC, MALDI-TOF-MS and ^{1}H-NMR-spectroscopy. ADMET-polymerization with Grubbs 1st catalyst followed by fractionation *via* preparative GPC lead to polymers **$AP_{21}(^{Bn}Glu_3)$** (**7b**), **$AP_3(^{Bn}Glu_{10})$** (**8b**), **$AP_{21}(^{Bn}Asp_3)$** (**9b**) and **$AP_4(^{Bn}Asp_{10})$** (**10b**) with define molecular weights and low *Đ*. Oligomers (**7a** – **10a**) and fractionated polymers (**7b** – **10b**) were investigated by CD- and FTIR-spectroscopy in solid state as well as in HFIP-solution to probe the secondary structure of the oligo-amino acid building blocks. Fractions of **$AP_{21}(^{Bn}Glu_3)$** (**7b**) and **$AP_3(^{Bn}Glu_{10})$** (**8b**) revealed stabilization of the β-sheet conformation in the solid state with increasing molecular weight. For polymers **$AP_{21}(^{Bn}Asp_3)$** (**9b**) and **$AP_4(^{Bn}Asp_{10})$** (**10b**) stabilization of the β-sheet conformation with increasing molecular weight in HFIP-solution was observed by CD-spectroscopy. Temperature dependent solid state FTIR-measurements show stabilization of the β-sheet conformation for all fractions of **$AP_{21}(^{Bn}Glu_3)$** (**7b**) and **$AP_3(^{Bn}Glu_{10})$** (**8b**) with increasing temperature.

Moreover, ROP of **Aib-NCA** (**11**) was studied with different initiators. First, amine initiators were used under variation of solvent, concentration and temperature. The highest molecular weights were obtained in concentrated frozen DMA-solutions. Kinetics for ROP of **Aib-NCA** (**11**) in DMF was followed *via* FTIR-spectroscopy, revealing a living character for the first 120 minutes. Furthermore, oligomers of conformational constrained amino acid Aib stabilizing a racemic mixture of left- and right-handed 3_{10}-helical conformation, which can be influenced by connection of chiral residues on the achiral Aib-domains. Subsequently, synthesized chiral amino acid-methyl esters (**16c** – **16j**) were used as initiators for ROP of **Aib-NCA** (**11**) and the obtained polymers (**17c** – **17j**) showed a preference for a left-handed helix in the case of L-amino acid-methyl esters and a preference for a right-handed helix when initiated by D-amino acid-methyl esters in HFIP-solution. Finally, bivalent azo-initiator (**19**, **20**, **21**) were used for ROP of **Aib-NCA** (**11**) as well as **ACHC-NCA** (**12**). Polymers **21a** and **21b** were investigated by UV-VIS-spectroscopy, in which both polymers revealed a thermal stabilized *cis*-conformation, which could be transferred in *trans*-conformation by irradiation of UV-light (254 nm).

Kurzdarstellung

Mutisegmente Hybrid-Polymere wurden auf Basis von Einzel- oder Oligo-Aminosäuren synthetisiert und hinsichtlich ihrer Kristallisations- und Sekundärstruktureigenschaften untersucht. Der Fokus lag auf der Untersuchung der Sekundärstrukturbildung von Oligomeren der benzylgeschützten Glutaminsäure ($O^{Bn}Glu_n$) und der benzylgeschützten Asparaginsäure ($O^{Bn}Asp_n$), welche die α-Helix stabilisieren, aber ihre endgültige Konformation stark von den Bedingungen des zu untersuchenden Systems abhängt.

Zunächst wurden einzelne Aminosäuren als "Defekte" in Polyethylen-ähnliche Mittelsegmente eingebettet und das Kristallisationsverhalten der Alkylketten untersucht. Daher wurden die polare, benzylgeschütze Glutaminsäure (Glu) und benzylgeschütze Asparaginsäure (Asp), sowie die unpolaren Aminosäuren Leucin (Leu), α-Aminobuttersäure (Aib) und 1-Aminocyclohexancarboxylsäure (ACHC) am *N*- (**1a** – **1e**) und *C*-Terminus (**2a** – **2e**) funktionalisiert und mittels ADMET-Polymerisation in Polyethylen-ähnliche Mittelsegmente eingebracht (**3a** – **3e**). Die Polymere wurden anschließend hydrogeniert und die Struktur der entstanden Polymere **4a** – **4e** konnte mittels GPC, ^{1}H-NMR- und IR-Spektroskopie nachgewiesen werden. Durch DSC- und XRD-Untersuchungen wurde für die Mittelsegmente in den Polymeren **4a** und **4b** mit polarer Seitenkette eine Kristallisation mit orthorhombischer Einheitszelle nachgewiesen, die der kommerziellen Polyethylen Kristallisation ähnelt. Für die Mittelsegmente der unpolaren Polymere **4c** – **4e** wurde keine Kristallisation beobachtet.

Anschließend wurden $O^{Bn}Glu_n$ und $O^{Bn}Asp_n$-Elemente mit den Wiederholungseinheiten von n=3 und n=10 in die polyethylen-ähnlichen Mittelsegmenten eingebracht. Die Wiederholungseinheiten wurden ausgewählt, da die endgültige Konformation der Oligomere vom Molekulargewicht abhängt, was die Untersuchung der unterschiedlichen Sekundärstrukturbildung innerhalb der Oligoaminosäuren ermöglichte. Dabei konnten die durch ROP der NCAs **Glu-NCA** (**5**) und **Asp-NCA** (**6**) entstandenen Polymere (**$O^{Bn}Glu_{3,10}$** (**7a**, **8a**) und **$O^{Bn}Asp_{3,10}$** (**9a**, **10a**)) mittels GPC, MALDI-TOF-MS und ^{1}H-NMR-Spektroskopie charakterisiert werden. Durch ADMET-Polymerisation und anschließender Auftrennung mittels präparativer GPC wurden die Polymere **$AP_{21}(^{Bn}Glu_3)$** (**7b**), **$AP_3(^{Bn}Glu_{10})$** (**8b**), **$AP_{21}(^{Bn}Asp_3)$** (**9b**) und **$AP_4(^{Bn}Asp_{10})$** (**10b**) in definierte Fraktionen mit geringen *Đ* aufgetrennt. Die Oligomere und Fraktionen der ADMET-Polymere wurden durch CD- und FTIR-Spektroskopie hinsichtlich der Sekundärstrukturbildung der Oligo-Aminosäure-Einheiten im festen Zustand und in HFIP-Lösung untersucht. Die Fraktionen von **$AP_{21}(^{Bn}Glu_3)$** (**7b**) und **$AP_3(^{Bn}Glu_{10})$** (**8b**) zeigten im festen Zustand eine Stabilisierung des β-Faltblatts mit zunehmender Kettenlänge. Für die Polymere **$AP_{21}(^{Bn}Asp_3)$** (**9b**) und **$AP_4(^{Bn}Asp_{10})$** (**10b**) konnte die Ausbildung des β-Faltblatts in HFIP-Lösung nachgewiesen werden. Temperaturabhängige FTIR-Messungen zeigten für alle Fraktionen von **$AP_{21}(^{Bn}Glu_3)$** (**7b**) und **$AP_3(^{Bn}Glu_{10})$** (**8b**) ebenfalls die Stabilisierung des β-Faltblatts mit zunehmender Temperatur.

Die ROP von **Aib-NCA** (**11**) wurde unter Verwendung verschiedener Initiator-Systeme untersucht. Zunächst wurden Amin-Initiatoren unter Variation des Lösungsmittels, der Konzentration und der Temperatur verwendet. Die höchsten Molekulargewichte wurden in konzentrierten, gefrorenen DMA-Lösungen erhalten. Die Kinetik der ROP von **Aib-NCA** (**11**) in DMF wurde mit FTIR-Messungen verfolgt und ein lebender Polymerisationscharakter für die ersten 120 Minuten nachgewiesen. Weiterhin wurden eigens synthetisierte chirale L-/D-Aminosäure Methylester (**16c** – **16j**) als Initiatoren verwendet und für die entstandenen Polymere (**17c** – **17j**) eine Bevorzugung der linksdrehenden Helix für L- und der rechtsdrehenden Helix für D-Aminosäure-Methylester Initiatoren in HFIP-Lösung nachgewiesen werden. Abschließend wurden bivalente Azo-Initiatoren (**19**, **20**, **21**) für die ROP von **Aib-NCA** (**11**) und **ACHC-NCA** (**12**) verwendet. Die Polymere **21a** und **21b** wurden mittels UV-VIS-Spektroskopie untersucht, wobei beide eine thermische Stabilisierung des *cis*-Isomers aufzeigten, das bei der Anregung mit UV-Licht (254nm) in das *trans*-Isomer überführt werden konnte.

Table of Contents

Danksagung I

Abstract II

Kurzdarstellung III

List of abbreviations VII

1. Introduction 1

1.1 Secondary structures in natural biopolymers 1

1.1.1 Determination of the secondary structure 3

1.2 Secondary structure formation of synthetic poly-amino acids 5

1.2.1 Secondary structure formation of $P^{Bn}Glu_n$ 6

1.2.2 Secondary structure formation of $P^{Bn}Asp_n$ 9

1.3 Secondary structure formation of artificial amino acids 13

1.3.1 2-Aminoisobutyric acid (Aib) as prototype for artificial amino acids 13

1.3.2 Chirality control and preference for helix direction in achiral Aib-domains 15

1.4 Ring-opening polymerization of *N*-carboxyanhydrides (ROP of NCAs) 19

1.4.1 Synthesis of common/functional NCAs 19

1.4.2 Mechanisms for ROP of NCAs 20

1.4.3 Improvements for ROP of NCAs 22

1.4.3.1 Metal-based initiators 22

1.4.3.1 Primary amino acid hydrochlorides as initiators 22

1.4.3.3 Silazane-mediated controlled polymerizations 23

1.4.3.4 Optimization of pressure, temperature and solvent systems 23

1.5 Hybrid-block copolymers based on glutamic- and aspartic acid 24

1.5.1 Non-polypeptide chain attached on the polypeptide side chain 25

1.5.2 Non-polypeptide chain attached on the *C*-terminus of the polypeptide chain 26

1.5.3 Non-polypeptide chain attached on the *N*-terminus of the polypeptide chain 28

2 Aim of the thesis 31

2.1 Objective and motivation 31

2.2 Concept 33

3 Results and discussion 36

3.1 PE-type-single amino acids hybrid polymers 36

3.1.1 Monomer synthesis 36

3.1.2 ADMET-polymerization and hydrogenation of the polymers 37

3.1.3 MALDI-TOF-MS-analysis 41

3.1.4 DSC-analysis 42
3.1.5 XRD-analysis 43
3.2 PE-type oligo-amino acid hybrid polymers 45
3.2.1 Synthesis of multisegmented polymers $AP_m(^{Bn}Glu_n)$ (**7b**, **8b**) and $AP_m(^{Bn}Asp_n)$ (**9b**, **10b**) 45
3.2.2 Solid state assembly 49
3.2.2.1 Oligomers of $O^{Bn}Glu_n$ 50
3.2.2.2 Multisegmented polymers of $AP_m(^{Bn}Glu_n)$ 51
3.2.2.3 Thermal behaviour of multisegmented polymers of $AP_m(^{Bn}Glu_n)$ 52
3.2.2.4 Multisegmented polymers of $AP_m(^{Bn}Asp_n)$ 53
3.2.3 Conformational analysis in solution 53
3.2.3.1 Oligomers of $O^{Bn}Asp_n$ and multisegmented polymers of $AP_m(^{Bn}Asp_n)$ 54
3.2.3.2 Oligomers of $O^{Bn}Glu_n$ and multisegmented polymers of $AP_m(^{Bn}Glu_n)$ 55
3.2.3.3 Fractionated multisegmented polymers of $AP_m(^{Bn}Asp_n)$ 56
3.3 Investigation of ROP of **Aib-NCA** (**11**) and **ACHC-NCA** (**12**) 57
3.3.1 ROP of **Aib-NCA** (**11**) initiated by amine initiator 58
3.3.1.1 ROP of **Aib-NCA** (**11**) with **HMDS** as initiator 59
3.3.1.2 ROP of **Aib-NCA** (**11**) with 1-dec-9-enyl-undec-10-enylamine (**A4**) as initiator 60
3.3.1.3 ROP of **Aib-NCA** (**11**) with 10-undecenamine (**A2**) as initiator 62
3.3.2 ROP of **Aib-NCA** (**11**) initiated by amino acid-methyl esters (**16a** – **16j**) 65
3.3.2.1 ^{1}H-NMR- and MALDI-TOF-MS-analysis 67
3.3.2.2 FTIR- and CD-analysis 69
3.3.3 ROP of Aib-NCA (11) and ACHC-NCA (12) initiated by bivalent azo-initiators 71
3.3.3.1 ^{1}H-NMR- and UV-VIS-analysis 72
4 Experimental part 76
4.1 Materials and methods 76
4.2 Synthesis of monomers of single-amino acid-PE(-type)-polymers (**2a** – **2e**) 78
4.2.1 *N*-terminus functionalization 78
4.2.2 Synthesis of the coupling reagent 10-undecene-1-amine (**A2**) 80
4.2.3 *C*-terminus functionalization 80
4.3 Synthesis of hydrogenated single-amino acid-PE(-type)-polymers (**4a** – **4e**) 82
4.3.1 ADMET-polymerization 82
4.3.2 Hydrogenation / deprotection of the oligomers 83
4.4 Synthesis of oligo-amino acid-PE(-type)-polymers 84
4.4.1 Synthesis of *N*-carboxyanhydrides **Glu-NCA** (**5**) and **Asp-NCA** (**6**) 84
4.4.2 Synthesis of oligomers ($O^{Bn}Glu_{3,\ 10}$ (**7a**, **8a**) and $O^{Bn}Asp_{3,\ 10}$ (**9a**, **10a**)) by ROP of NCAs 85

4.4.2.1 Oligo-β-benzyl-L-glutamate, n=3 (**$O^{Bn}Glu_3$**) (**7a**) ... 85
4.4.2.2 Oligo-β-benzyl-L-glutamate, n=10 (**$O^{Bn}Glu_{10}$**) (**8a**) ... 85
4.4.2.3 Oligo-β-benzyl-L-aspartate, n=3 (**$O^{Bn}Asp_3$**) (**9a**) ... 86
4.4.2.4 Oligo-β-benzyl-L-aspartate, n=10 (**$O^{Bn}Asp_{10}$**) (**10a**) ... 86
4.4.3 Synthesis of ADMET-polymers $AP_m(^{Bn}Glu_n)$ (**7b**, **8b**) and $AP_m(^{Bn}Asp_n)$ (**9b**, **10b**) ... 87
4.5 Synthesis of artificial oligo-amino acids ... 87
4.5.1 Synthesis of N-carboxyanhydrides (NCAs) of achiral amino acids (**11**, **12**) ... 87
4.5.1.1 Synthesis of **Aib-NCA** (**11**) ... 88
4.5.1.2 Synthesis of **ACHC-NCA** (**12**) ... 88
4.5.2 Synthesis of artificial oligo-amino acids initiated by amine initiators ... 88
4.5.2.1 Synthesis of 1-dec-9-enyl-undec-10-enylamine (initiator **A4**) ... 88
4.5.2.2 Synthesis of polymers initiated by amine initiator ... 89
4.5.3 Synthesis of artificial oligo-amino acids initiated by amino acid-methyl ester (**17a** – **17j**) 92
4.5.3.1 Synthesis of amino acid-methyl ester hydrochlorides (**16a** – **16j**) ... 92
4.5.3.2 Synthesis of polymers (**17a** – **17j**) initiated by amino acid-methyl esters ... 94
4.5.4 Synthesis of artificial oligo-amino acids initiated by azo-initiators ... 96
4.5.4.1 Synthesis of azo-initiator **Azo-OH-DFA** (**19**) and **Azo-NH_2-DFA** (**20**) ... 96
4.5.4.2 Synthesis of azo-initiator **Azo-Dop-OH** (**21**) ... 98
4.5.4.3 Synthesis of polymers (**19a, 19b, 20a, 20b, 21a, 21b**) initiated by azo-initiators . 99
5 Summary ... 101
6 References ... 106
7 Appendix ... 122
8 Curriculum vitate ... 167
9 Eigenständigkeitserklärung ... 170

List of abbreviations

Characterization methods:

CD	circular dichroism
DSC	differential scanning calorimetry
ESI-TOF-MS	electrospray ionization mass spectrometry
FTIR	Fourier-transform infrared spectroscopy
IR	infrared
MALDI-TOF-MS	matrix-assisted laser desorption/ionization time-of-flight mass spectrometry
NMR	nuclear magnetic resonance
NSR	nuclear spin relaxation
UV	ultraviolet
VCD	vibrations-circular dichroism
WAXS	wide-angle X-ray scattering
XRD	X-ray diffraction

Chemical nomenclature:

Δ^{z}Ph	α,β-dehydrophenylalanine
1,3-Bis-HFAB	1,3-bis(2-hydroxyhexafluoroisopropyl)benzene
3-phenyllacetate	benzoate ester of 2-hydroxy-3-phenylpropionic acid
AA-NPC	*N*-phenoxycarbonyl α-amino acid
Ac-$^{Bn}Glu_n$	*N*-acetyl-β-benzyl-L-glutamate
ACHC	1-aminocyclohexánecarboxylic acid
ACHC-NCA	1-aminocyclohexánecarboxylic acid *N*-carboxyanhydride
ACN	acetonitrile
ADMET	acyclic diene metathesis
AET	2-aminoethanethiol
Aib	2-aminoisobutyric acid
Aib-NCA	2-aminoisobutyric acid *N*-carboxyanhydride
Ala	alanine

allGlu-NCA	γ-allyl-L-glutamic acid *N*-carboxyanhydride
AMM	activated monomer mechanism
AOBGlu-NCA	γ-(4-Allyloxylbenzyl)-L-glutamate *N*-carboxyanhydride
Ar	aryl
Asp-NCA	β-benzyl L-aspartic *N*-carboxyanhydride
ATRP	atom transfer radical polymerization
Boc	tert-butoxycarbonyl
Boc-$^{Bn}Glu_n$	*N*-butoxycarbonyl-β-benzyl-L-glutamate
Bipy	2,2´-bipyridyl
αMe-Val	Cα-methyl-L-valine
(αMe)Phe	Cα-methyl-phenylalanine
cac	critical aggregation concentration
Cbz	benzyloxy carbonyl-group
$CDCl_3$	deuterated chloroform
CH_2Cl_2	dichloromethane
CH_3NaO	sodium methoxide
$CHCl_3$	chloroform
ClEtGlu-NCA	γ-2-chloroethyl-L-glutamate *N*-carboxyanhydride
ClPrGlu-NCA	γ-chloropropyl-L-glutamic acid *N*-carboxyanhydride
COD	1,5-cyclooctadiene
D_2O	deuterated water
D_2SO_4	deuterated sulfuric acid
Dap(pBrBz)	N^{β}-*p*-bromobenzoyl-L-α,β-diaminopropionic acid
Dab(pBrBz)	N^{γ}-*p*-bromobenzoyl-L-α,γ-diaminobutyric acid
DBU	1,8-Diazabicyclo[5.4.0]undec-7-ene
DCA	dichloroacetic acid
DCM	dichloromethane
DIPEA	*N*,*N*-diisopropylethylamine

DMA	dimethylacetamide
DMAP	4-dimethylaminopyridine
DMF	dimethylformamide
DMSO-d_6	deuterated dimethyl sulfoxide
DP	degree of polymerization
DOPC	1,2-dioleoyl-snglycero-3-phosphocholine
EA	ethyl acetate
EDC	ethylene dichloride
EDC·HCl	1-(3-dimethylaminopropyl)-3-ethylcarbodiimide hydrochloride
Et_2O	diethyl ether
EtOH	ethanol
Fib	difluoro 2-aminoisobutyric acid
Fmoc	fluorenylmethoxycarbonyl protecting group
Glu-NCA	γ-benzyl L-glutamic *N*-carboxyanhydride
Gly	glycine
Grubbs 1st	Grubbs catalyst first generation
Grubbs 2nd	Grubbs catalyst second generation
GH 1st	Grubbs-Hoveyda catalyst first Generation
HFIP-d_2	deuterated 1,1,1,3,3,3-hexafluoroisopropanol
HFIP	1,1,1,3,3,3-hexafluoroisopropanol
His	histidine
HMDS	hexamethyldisilazane
HOBt	1-hydroxybenzotriazole
HVT	high-vacuum technique
KTFA	potassium trifluoroacetate
L,L-PIAA	poly(L-isocyanoalanyl-l-alanine methyl ester)
Leu	leucine
IVA	isovaline

MCPA	mercaptopropionic acid
Me	methyl
MeO	methyl ester
MeOH	methanol
MMA	methyl methacrylate
M_n	molecular weight
MSA	methansulfonic acid
NAM	normal amine-mechanism
NCA	*N*-carboxyanhydride
NCL	native chemical ligation
NBS	*N*-bromosuccinimide
NCS	*N*-chlorosuccinimide
NEt_3	triethylamine
NIPAM	*N*-isopropylacrylamide
NMP	nitroxide-mediated polymerization
Nvoc	nitroveratryloxycarbonyl protecting group
Đ	polydispersity index (PDI)
$O^{Bn}Asp_n$/ $P^{Bn}Asp_n$	oligo/poly(β-benzyl-L-aspartate)
$O^{Bn}Glu_n$/$P^{Bn}Glu_n$	oligo/poly(γ-benzyl-L-glutamate)
OBu	butylester
OMe	methyl ester
$PAsp_n$	poly-aspartic acid
pBrBz	*p*-bromobenzoyl
PCL	poly(ε-caprolactone)
PCl_5	phosphorous pentachloride
PCl_3	phosphorous trichloride
$Pd_2(dba)_3$	tris(dibenzylideneacetone)dipalladium
PDMAEMA	poly(2-(dimethylamino)ethyl methacrylate

PE	poly(ethylene)
PEG	polyethylene glycol
PEGGlu-NCA	oligo-PEG side chain functionalized glutamic *N*-carboxyanhydride
PFS	polyferrocenylsilane
$PGlu_n$	poly-glutamic acid
Ph	phenyl
PhS-TMS	phenyl trimethylsilyl sulfide
Phe	phenylalanine
PI	poly-isobutene
PLLA	poly-L-lactide
PMBI	poly((S)-(—)-α-methylbenzyl isocyanide)
PPII	polyproline II-like conformation
Pro	proline
PS	polystyrene
RAFT	reversible addition-fragmentation chain-transfer
ROMP	ring-opening metathesis polymerization
ROP	ring-opening polymerization
Ser	serine
TEG	triethylene glycol
tert	tertiary
TFA	trifluoroacetic acid
THF	tetrahydrofuran
TFE	2,2,2-trifluoroethanol
S-TMS	trimethyl sulfide
Trp	tryptophan
$TsNHNH_2$	p-toluenesulfonyl hydrazide
TU-S	*N*,*N*′-bis[3,5-bis(trifluoromethyl)phenyl]thiourea
Val	valine

VCD	vibrational circular dichromisn
xantphos	4,5-Bis(diphenylphosphino)-9,9-dimethylxanthene
Z	carboxybenzyl
Zlys	N_{α}-(carbobenzyloxy)-L-lysine

NMR-spectroscopy:

br	broad
d	doublet
dd	doublet of doublet
m	multiplet
s	singlet
t	triplet

IR-spectroscopy:

m	middle
s	strong
ss	very strong
w	weak

Parts of the concept, results and discussion as well of the experimental part were already published in

“Precision polymers containing main-chain-amino acids: ADMET polymerization and crystallization” (Freudenberg, J., Poppe, S., Binder, W.H*. *RSC. Adv.* **2017**, *7*, 47507-47519. DOI: 10.1039/C7RA10485E) - Published by The Royal Society of Chemistry and were in parts adapted with permission from The Royal Society of Chemistry (Copyright 2016).

and

"Reprinted (adapted) with permission from (Freudenberg, J.; Binder, W. H.*, Multisegmented Hybrid Polymer Based on Oligo-Amino Acids: Synthesis and Secondary Structure in Solution and in the Solid State. *Macromolecules* **2019,** *52* (12), 4534-4544. DOI: 10.1021/acs.macromol.9b00684). Copyright (2019) American Chemical Society."

and

"Reprinted (adapted) with permission from (Freudenberg, J.; Binder, W. H.*, Chirality Control of Screw-Sense in Aib-Polymers: Synthesis and Helicity of Amino Acid Functionalized Polymers. *ACS Macro Let.* **2020**, 9 (5), 686-692. DOI: 10.1021/acsmacrolett.0c00218). Copyright (2020) American Chemical Society."

1. Introduction

1.1 Secondary structures in natural biopolymers

Folding and assembly of macromolecules is an important principle in protein fiber- and disease-formation.[1] The correct folding behavior of proteins is the prerequisite for their unique properties and proper biological function[2, 3], mainly structural support and protection, energy transduction, catalysis of reactions, transport and information transfer.[4] A variety of proteins and peptides are known[5], all built by the 22 proteogenic amino acids. In addition, over 500 amino acids with various side chain configurations could be determined up to now.[6] Although all amino acids show zwitterionic character resulting in charged COO^- and NH_3^+-group in aqueous solution[7], they can be divided in different groups due to their different side chain properties, being acid/basic (charged), polar/neutral or non-polar/hydrophobic.[8] The amino acid residues in proteins and peptides are connected by the peptide bond[9], which has a partial double bond character, thus restricting its free rotation and is therefore promoting the formation of regular 3D-structures.[10] The partial double bond character between the N-atom and the C_α-atom can be proven by the bond length of the peptide bond (133 pm) in comparison to free C-N-bonds (146 pm) and C=N-double bonds (124 pm).[11]

The structure of proteins and peptides is differentiated in four hierarchical structural levels (Figure 1): The primary structure of proteins and peptides is defined as the linear sequence of its basic building blocks, called the amino acid sequence.[12] Regular spatial structures build up by the amino acid sequence is called the secondary structure, which represents a local organization of the amino acid along the biomacromolecule-backbone (e.g. α-helix and β-sheet) in which the formation and stabilizing of the final conformation strongly depends on the intra- or intermolecular hydrogen bond interactions of the peptide bonds.[13] Secondary structure space arrangement is defined by the tertiary structure[12], which strongly depends on folded/packed side chain interactions and cross-linked disulfide bonds. The quaternary structure describes the organization from more than one peptide chain, influenced by non-covalent interactions of the macromolecular subunits.[12]

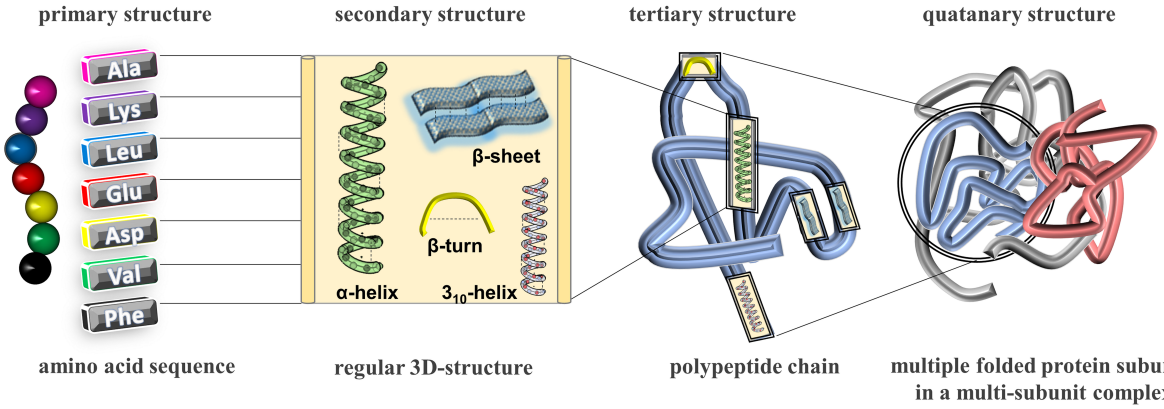

Figure 1. Demonstration of primary-, secondary-, tertiary- and quaternary structure level in proteins and peptides.[14]

As the secondary structure formation is an important feature for formation of diseases[15], its investigation in natural and synthetic polypeptides is of great interest. Additionally to the intra- or intermolecular hydrogen bond interactions, electrostatic and hydrophobic interactions have a big influence on the preorganization of the secondary structure.[16] The general formation of the various secondary structures can be attributed to the possible rotation of the N-C_α- and the C_α-C-rotation of the formed peptide bonds

around the connecting C_α-carbon atom, in which two specific rotation parameters (ϕ, ψ) describe the relative rotation angles starting from a standard configuration (ϕ=0°, ψ=0°) (Figure 2).[17] By considering and taking short contact distances of the carbon-atoms into account, the majority of ϕ,ψ-combinations are forbidden, but the limitation of these combinations depends on the choice of the permitted van der Waals contact distances. However, on the base of these model the Ramachandran-plot revealed regions with low-energy levels, depending on of the chirality of the C_α-carbon atom and the amino acid side chains.[18] Nevertheless, general observations and conclusion for ϕ,ψ-combinations could be determined: Whether the amino acid has no side chain on the C_α-carbon atom (no C_β-carbon atom), the torsion angles are close to ϕ=0°, ψ=180° or the amino acid bearing a side chain (C_β-carbon atom) the torsion angles are close to ϕ=120° and ψ=150°.[17] The most common secondary structures are the α-helix and β-sheet conformation, determined by the low-energy regions in the Ramachandran plot (Figure 2).

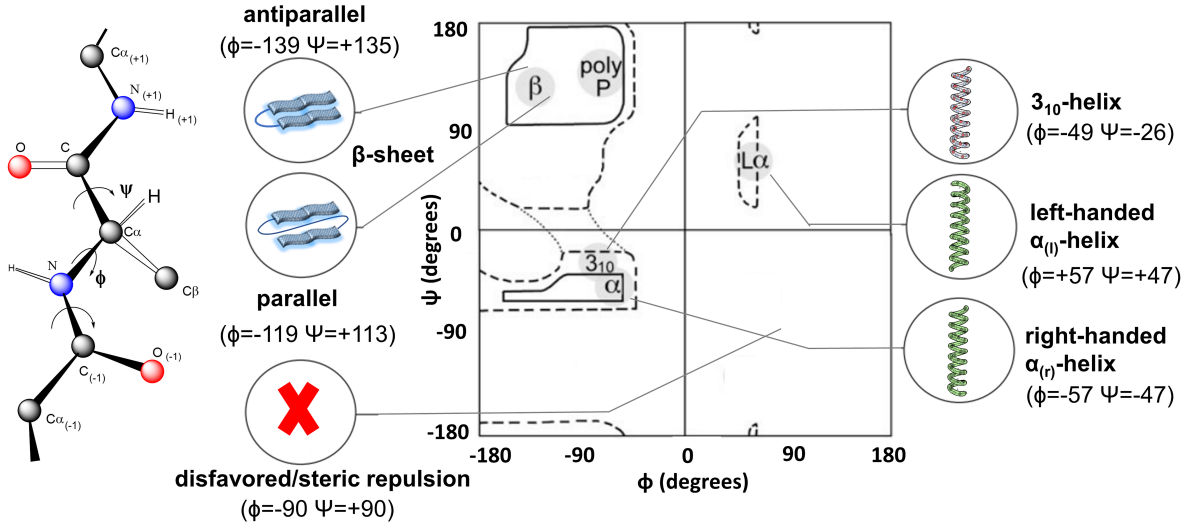

Figure 2. General demonstration of formed peptide bonds in poly-amino acids with relative rotation angles (ϕ, ψ) around the N-C_α- and the C_α-C-bond (left) and corresponding Ramachandran plot and values for ϕ and ψ for various allowed secondary structures (within the solid and dashed lines) especially right-handed α-helix (α), left-handed α-helix (Lα), 3_{10}-helix (3_{10}) and (anti-)parallel β-sheets (β) as well as other structures e.g. the poly-proline helix (polyP) or disfavored regions (white, e.g. ϕ=-90, ψ=+90 (X)) (adapted and modified from Williams et al. with permission[19]).

Discovered by Pauling, Corey and Branson in 1951[20] the α-helix is characterized by a rod like structure stabilized by intramolecular hydrogen bonds between the C=O group of each peptide bond in the strand (i) and the fourth next NH-group (i+4) (Figure 3, left), which results in 3.6 amino acid units and a length of 0.54 nm per turn.[21] The side chains of the incooperated amino acids are stretched to the outside of the tight coiled main chain, resulting in an energetically favorable formation of the right-handed helical conformation as the steric hindrance of main- and side chain is less pronounced than in the left-handed helical conformation. The critical bulding block length for the formation of the α-helix conformation was account to seven amino acids.[22]

The β-sheet or β-strand conformation is stabilized by intermolecular hydrogen bonds, resulting in a fully extended pleated arrangement of the amino acids.[13] The hydrogen bonds can be connected parallel and/or antiparallel by the C=O-group of one strand with the NH-group of the opposite strand (Figure 3, middle). If the direction of the strands are the same (*C*-terminus to *N*-terminus for both) a parallel β-sheet is formed, whereas an opposite hydrogen bonding network (*C*-terminus to *N*-terminus for the first strand and *N*-terminus to *C*-terminus for the second strand) lead to the formation of an

antiparallel β-sheet. The antiparallel conformation was found to be more stable due to the formation of a more aligned hydrogen bonding network.[23] As the side groups in a β-sheet conformation are close together, sterically demanding or equal charged side chain groups can disturb the regular arrangement of the hydrogen bonds. The hydrogen bonds interacting in a β-sheet (0.70 nm) and the distance of the vicinal amino acids (0.35 nm) is significantly longer in comparison to the α-helix (0.15 nm).[23]

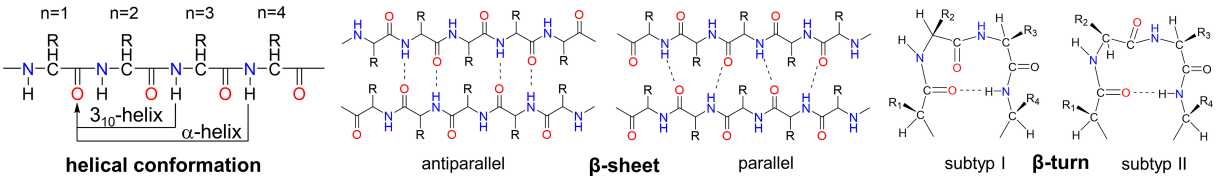

Figure 3. Hydrogen-bonding patterns in the different secondary structure elements.

Besides the two main secondary structures, other elements e.g. turn-structures or 3_{10}-helices were found in proteins and peptides. The expression of a turn is caused by intramolecular hydrogen bonds of main chain C_α-carbon atoms close to each other (0.70 nm) and can be divided in regard to the formed hydrogen bond between the C=O group (i) and the N-H group into an α-turn (i+4), a β-turn (i+3) (Figure 3, right), a γ-turn (i+2), a δ-turn (i+1) and a π-turn (i+5).[24] The most common structure in nature is the β-turn[25], consisting of four consecutive amino acids and ensures a low-energy polypeptide chain-reversal by nearly 180°.[26, 27] They are often located at surfaces of proteins comprising nearly 25% of the residues[28, 29] and have been implicated in molecular recognition and in protein folding.[30, 31]

3_{10}-helices are rarely observed in proteins[32] and were formed as extended α-helices at the end of the *N*- or *C*-terminus.[33] The 3_{10}-helix is more tightly bound than the α-helix[33] and is stabilized by intramolecular hydrogen bonds of the C=O-group (i) and the N-H group (i+3) of the third amino acid residue[34] (Figure 3, left), resulting in a ten-membered ring structure closely to β-turn subtype III, but helices of this type found in proteins and peptides generally deviate from this model due to side chain stacking.[24, 35] It is less stable than the α-helix due to less favorable van der Waals energy and not optimal hydrogen bond geometry.[32] Nevertheless, they were found in proteins such as aconitase[36] and especially in polypeptides containing C^α-disubstituted α-amino acids such as 2-aminoisobutyric acid (Aib) due to steric hindrance of the α-carbon.[37, 38]

Besides the mentioned conformations, several other torsion angles are allowed, leading to the formation of other secondary structures such as π-helix. The overall conformation depends on the propensity of the individual amino acids in the primary structure to form a defined type of secondary structures and is a combination of environmental and steric factors. Therefore, predictions which final conformation will be formed are difficult[39], nevertheless the relative frequencies of secondary structures found for individual amino acids taking part in peptides and proteins shows that the helical conformation is the most common structure.[13] If the C_β-carbon atom is branched (valine, threonine, isoleucine) the helical conformation is destabilized by steric hindrance. Furthermore, side chain-containing hydrogen bond donors or acceptors like asparagine, aspartate and serine can interact with the main chain C=O- or N-H-group and disturb the regular formation of the α-helix.[13]

1.1.1 Determination of the secondary structure

For the determination of the formed secondary structure in peptides and proteins a variety of analytical methods can be used e.g. optical rotation[40-42], X-ray diffraction (XRD)[24, 28, 30, 43, 44], Raman-spectroscopy[45-47] and nuclear magnetic resonance (NMR)[48-52]. Due to the simplicity and effectivity Fourier-transform infrared spectroscopy (FTIR) and circular dichroism (CD) have developed to the most important techniques over the years.[53-61] These analytical methods give the opportunity to determine secondary structures and their quantitative amount in complex protein and peptide systems (Figure 4).

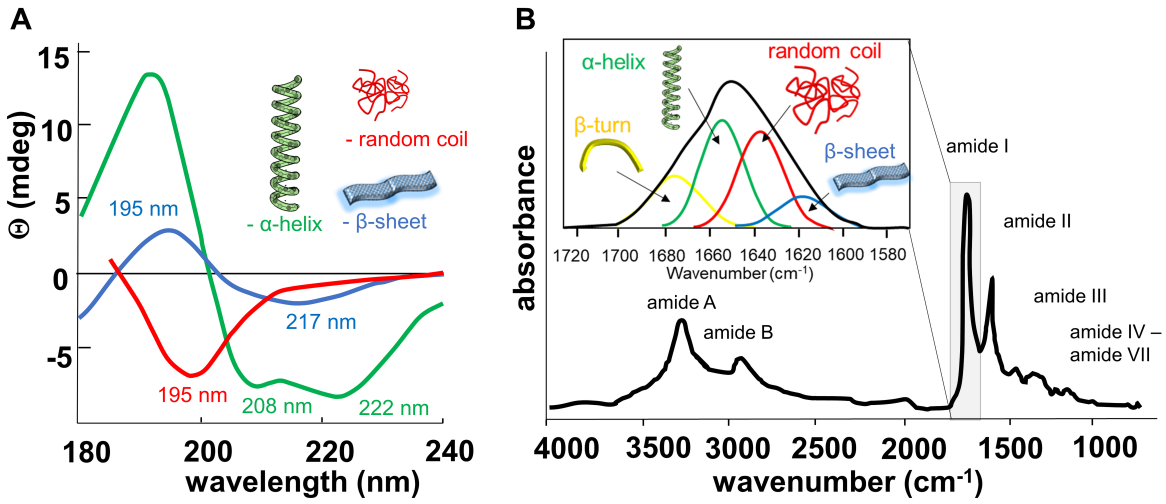

Figure 4. Determination of the individual secondary structures in a general peptide *via* **A**) CD-spectroscopy (schematic)[62] with characteristic local minima at 208 nm and 222 nm for the α-helix (green curve), local minima at 217 nm and local maxima at 195 nm for β-sheets (blue curve) and local minima at 195 nm for random coils and **B**) FTIR-spectroscopy (schematic)[63] with the amide-regions (amide A, B and amide I — amide VII) and determination of secondary structures in the amide I region (inlet) with characteristic signals at 1630 cm^{-1} for β-sheets (blue curve), 1645 cm^{-1} for random coils (red curve), 1655 cm^{-1} for the α-helix (green curve) and 1665 cm^{-1} for β-turns (yellow curve).

CD is based on the absorption of right- and left-handed polarized UV-light, which is absorbed differently by chiral molecules.[59] The basis for the investigation of poly-amino acids, peptides and proteins *via* CD-spectroscopy is the formation of the peptide bonds, in which signals in the far UV-region are based on the π-π* and n-π* transitions of the C=O-group. The π-π* and n-π* transitions of the C=O-group strongly depends on the conformation and the environment of the investigated systems, resulting in characteristic signals for the individual secondary structure in the far UV-region. Thus, helical conformation of natural peptides and proteins typically reveal two local minima at 208 nm and 222 nm, as the build secondary structures are exclusively formed from L-amino acids (Figure 4A, green curve).[60, 61] Furthermore, β-sheet conformations can be identified by a positive maximum at 195 to 197 nm (π-π*-transition) and a negative minimum at 217 nm (n-π*-transition) (Figure 4A, blue curve). The absence of a regular secondary structure is called random coil and reveals a negative signal at 195 nm (π-π*-transition) and a weak positive band at 212 nm (n-π*-transition) (Figure 4A, red curve). The individual CD-spectra of the investigated proteins and peptides always differentiating from each other, as the CD-spectroscopy reveals an average of all secondary structures in the biomacromolecule.[61] Therefore, intensities, location of the minima/maxima and the course of the curves can vary, especially in different solvents and environments.

FTIR spectroscopic investigations are based on the different stretching behavior of the main chain and side chain bonds.[64] The main advance of this technique is that the spectra can be obtained in a wide range of different environments, which leads to an advanced investigation of the secondary structure formation of proteins and peptides in different systems. The samples can be analyzed either in aqueous or organic solutions in cells as well as in solid state by attenuated total reflection (ATR-) measurements.[57] The absorption of infrared-light by the investigated peptides/proteins offers nine different characteristic regions, called amide A, B and amide I – VII (Figure 4B).
The most important information can be obtained from the amide I (Figure 4B inlet) and the amide II region, in which the C=O-stretch and N-H-stretch vibrations of the peptide bonds strongly depends on

the final conformation of the samples. The amide I region can be assigned to the vibrational bands at 1700 cm^{-1} to 1600 cm^{-1}, consisting of 80% C=O vibrational stretch, 10% N-H stretch and 10% C-N stretch absorptions directly connected to the formed peptide backbone. Characteristic signals for the individual secondary structures in this area were found to be 1662 – 1645 cm^{-1} for the α-helical conformation (Figure 4B inlet, green curve), 1630 – 1615 cm^{-1} for β-sheets (Figure 4B inlet, blue curve), 1667 – 1661 cm^{-1} for β-turns (Figure 4B inlet, yellow curve) and 1657 – 1642 cm^{-1} for random coils (Figure 4B inlet, red curve). Furthermore, amide II signals arise from 60% n-plane NH bending and 40% C-N vibration in the region of 1600 cm^{-1} to 1480 cm^{-1}.

All other amide bands (III – VII and A, B) show complex behavior and depending on the formed hydrogen bonds and the environment of the investigated systems. Thus, interpretation about the conformational analysis are less pronounced. As the signals for the individual secondary structures can overlap with each other, mathematic techniques such as second derivatization or deconvolution can enhance the resolution of the bands and increase the structural information in the FTIR-spectra.[55] The individual amide band regions in FTIR and characteristic signals for the individual secondary structures are given in Table 1.

Table 1. Characteristic regions of amide-bands and typical signals for α-helix, β-sheet, β-turn and random coil in FTIR-spectra according to literature.[53, 54, 64, 65]

	stretch	region (cm^{-1})	α-helix	β-sheet	β-turn	random coil
amide A	N-H (ν)	3300	complex amide-areas, depending on the formed hydrogen bonds and the environment of the individual investigated systems			
amide B	N-H (ν)	3100				
amide I	C=O (ν) 80% N-H (δ_i) 10% C-N (ν) 10%	1700 – 1600	1662 – 1645	1695 + 1630 – 1615	1667 – 1661	1657 – 1642
amide II	N-H (δ_i) 60% C-N (υ) 40%	1575 – 1480	1545	1530	1577 – 1528	
amide III	C-N (υ) 30% N-H (δ_i) 30% C=O (δ_i) 10% O=C-N (δ_i) 10%	1301 – 1229	1331 – 1293	1251 – 1223	1290 – 1244	1290 – 1244
amide IV	O=C-N (δ_a) 40%	767 – 625	complex amide-areas, depending on the formed hydrogen bonds and the environment of the individual investigated systems			
amide V	Out-of-plane NH bending	800 – 640				
amide VI	Skeletal torsion	606 – 537				
amide VII	Out-of-plane C=O bending	200				

[a]abbreviations: (υ) stretch vibration, (δ_i) deformation vibration in the amide-bond plane, (δa) out of plane amide-bond deformation vibration.

1.2 Secondary structure formation of synthetic poly-amino acids

The structural investigation of synthetic poly-amino acids is of fundamental importance, as they show a close relationship in structural formation to natural proteins and can therefore be used as model systems for the investigation of the fundamental properties which determine protein structure and function.[66] The final conformation of polypeptides strongly depends on the nature of the building up amino acid. Thus, poly- and oligo-amino acid can be divided into three general groups for adopting a certain secondary structure: First, amino acids exclusively adopting the β-sheet conformation such as poly-glycine, poly-valine or poly-cysteine. A special class is formed by *n*-substituted amino acids, adopting random coils e.g. poly-sarcosine, special sheet conformation or helices such as poly-proline. The main group includes poly-amino acids stabilizing the α-helical conformation as soon as the chain length is sufficiently long

and as a result the molecular weight is high enough.
Two of the most investigated homo poly-amino acid belonging to the latter group are poly-glutamic acid ($PGlu_n$) and poly-aspartic acid ($PAsp_n$) as well as their side-chain protected analogous poly-γ-benzyl-L-glutamate ($P^{Bn}Glu_n$) and poly-β-benzyl-L-aspartate ($P^{Bn}Asp_n$). In recent years, the side-chain protected forms of poly-glutamic acid and poly-aspartic acid, $P^{Bn}Glu_n$ and $P^{Bn}Asp_n$, became one of the most important class of synthetic poly-amino acids, as these two types of peptides show good solubility in organic solvents, the possibility to convert them into water-soluble polypeptides by removal of the side chain protection groups[67] and a dynamic behavior in secondary structure formation. Although these two types of poly-amino acids usually stabilizing the α-helix, the final conformation strongly depends on chemical and physical conditions introduced to the system such as molecular weight, the used solvent, end group, temperature or substitution of the side-chain benzyl-group.

1.2.1 Secondary structure formation of $P^{Bn}Glu_n$

$P^{Bn}Glu_n$ usually stabilizing the α_r-helix, but the final conformation can variy (β-sheets, β-turns, random coil) and strongly depends on chemical and physical conditions introduced to the system such as molecular weight, the used solvent, end group and temperature (Figure 5).

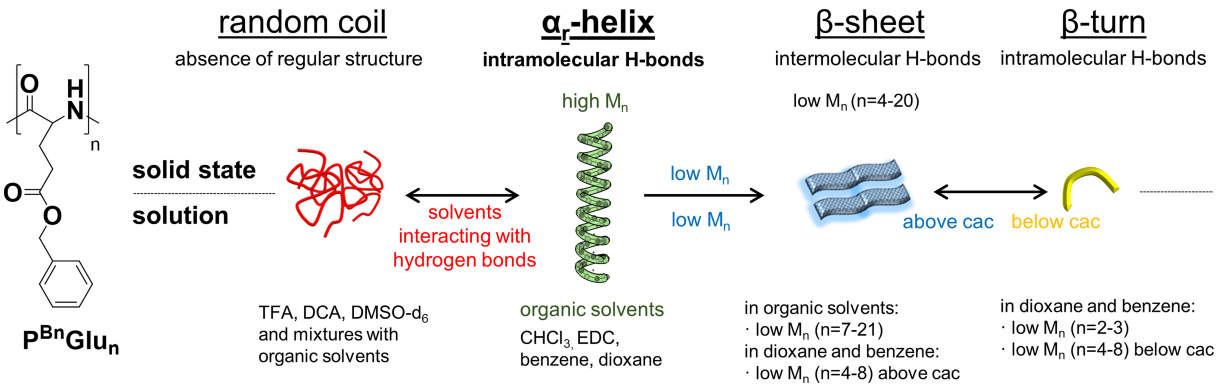

Figure 5. Secondary structure formation and transitions of $P^{Bn}Glu_n$ commonly adopting α_r-helix in solid state and solution under different physical and chemical conditions.

The molecular-weight-dependency of secondary structure formation of $P^{Bn}Glu_n$ in the solid state was first systematically investigated by Blout *et al.* [68, 69], yielding high molecular weight polymers ($P^{Bn}Glu_{91-1600}$, M_n > 100 kDa) revealing a stable α_r-helical conformation. Contrary, low molecular weight oligomers ($O^{Bn}Glu_5$, DP = 5.2) adopted the β-sheet conformation in the solid state. Furthermore, the systematic investigation of $O^{Bn}Glu_4$, $_8$, $_{20}$, and $P^{Bn}Glu_{200}$ films cast from chloroform-solutions revealed characteristic IR-bands for β-sheets at 1704 cm^{-1} and 1629 cm^{-1} as well as amide II band at 1524 cm^{-1} for $O^{Bn}Glu_4$, which was found to be coexistence to the α_r-helical conformation in $O^{Bn}Glu_{8,\ 20}$ determined by additional amide I vibration at 1650 cm^{-1}.[70] The full conversion to α_r-helix was found for high molecular weight polymer $P^{Bn}Glu_{200}$.[70] Further experiments with *N*-acetyl (Ac)-$^{Bn}Glu_n$ (of n=6, 8, 12, 14) proofed the stabilization of β-sheet conformation for low molecular weight oligomers adopted in the solid state.[71] As a result, high molecular weight polymers of $P^{Bn}Glu_n$ stabilizing the α-helix in the solid state whereas low molecular weight oligomers of $O^{Bn}Glu_n$ prefer the β-sheet conformation.

A more complex secondary structure formation was found in solution, as the final conformation not exclusively depend on the molecular weight but also on the used solvent. A stable α_r-helical conformation was found for high molecular weight polymers in $CHCl_3$- and dioxane-solution ($P^{Bn}Glu_{91-1600}$, M_n > 100 kDa), whereas oligomers ($O^{Bn}Glu_5$, DP = 5.2) stabilizing both, β-sheet and α-helix.[68, 69]

Furthermore, α-helical conformation is stabilized in DMF[72] and for high molecular weight polymers ($P^{Bn}Glu_{91-1600}$) in ethylene dichloride (EDC)[73] as well as for $P^{Bn}Glu_{132-493}$ in trichloroethylene as determined by nuclear spin relaxation- (NSR) measurements.[74] Independent of the high molecular weight, random coil conformation was found for $P^{Bn}Glu_n$ in trifluoroacetic acid (TFA)[74] and dichloroacetic acid (DCA)[73]. As the pure solvents revealed the formation of either the α -helix (EDC) or random coil (DCA), Doty *et al.*[73] demonstrated a temperature-dependent helix-coil transition for $P^{Bn}Glu_{91-1600}$ (M_n = 130 kDa) in EDC 24:76 DCA mixtures, as the final conformation at T=21 °C was determined to the random coil form which was converted into the α-helical conformation at T=40 °C. Investigation of $C_\alpha H$- and N*H*-proton shifts in ^{1}H-NMR measurements of $P^{Bn}Glu_n$ systems in DMSO-d_6 or DMSO-d_6/$CDCl_3$ revealed $C_\alpha H$-protons at 3.95 ppm for high molecular weight $P^{Bn}Glu_{100}$ characteristic for α-helical conformation, whereas $O^{Bn}Glu_7$ shows a random coil conformation under the same conditions determined by a strong shift of $C_\alpha H$-protons to 4.26 ppm.[75]

Other secondary structures, especially the formation of a β-turn, was found for oligomeric Ac-$^{Bn}Glu_{2,3}$ in dioxane and benzene solution as determined *via* FTIR. The formation of β-turns could also be found for Ac-$^{Bn}Glu_{4,5}$ and Boc-$^{Bn}Glu_{4,5,6,8}$ below the critical aggregation concentration (cac) in dioxane and benzene, whereas predominating β-sheets are formed above the cac. Furthermore, an α-helix to an unusual polyproline II (PPII)-like conformation was found in $CHCl_3$ 85:15 TFA and benzene-d_6 65:35 TFA systems as proven by FTIR and vibrational circular dichromisn (VCD). [76]

Thus, $P^{Bn}Glu_n$ build a class of polymers, which: A) adopt a stable α_r-helical conformation for high molecular weight polymers in the solid state and in weakly interacting solvents, B) form β-sheets for low molecular weight polymers in solid state and in weakly interacting solvents, C) the absence of a regular structure (random coil) in strongly interacting solvents such as DCA, presumably due to the strong solvatisation and D) form β-turns for oligomeric Ac-$^{Bn}Glu_{2,3}$ in dioxane and benzene and Ac-$^{Bn}Glu_{4,5}$ as well as Boc-$^{Bn}Glu_{4,5,6,8}$ below the critical aggregation concentration (cac) in dioxane and benzene. Detailed information about secondary structure formation of $P^{Bn}Glu_n$ and derivates under various conditions described in literature are given in Table 2.

Table 2. Summary of the secondary structures of $P^{Bn}Glu_n$ (and several substituted derivates) described in literature in dependence of the molecular weights in solid state and solution determined with various analytical methods (description: random coil; α_r: right-handed α-helix, β-sheet, β-turn, O: oligomer, P: polymer).

poly-γ-benzyl-L-glutamate ($P^{Bn}Glu_n$)							
structure	n (M_n (kDa))	conditions		α_r			Ref./ additional information
$P^{Bn}Glu_n$	n= 91 – 1600 (M_n= 20 kDa – 350 kDa)	solid state solution: $CHCl_3$ dioxane DCA	 x	x x x 	 	 	[68, 69]; ROP of Glu-NCA with NaOH or hexylammonium hydroxide as initiator; molecular weight-intrinsic viscosity; FTIR; for $O^{Bn}Glu_n$ in solution: coexistence of α-helix and β-sheet, decreasing cconcentration lead to increasing α-helix proportion
$O^{Bn}Glu_n$	n= 5	solid state solution: $CHCl_3$ dioxane	 	 x x	x x x	 	

structure	n (M_n (kDa))	conditions		α_r			Ref./ additional information
$P^{Bn}Glu_n$	n= 91 – 1600 (M_n =20 kDa – 350 kDa)	EDC DCA	x	x			[73]; ROP of Glu-NCA with NaOH as initiator; Intrinsic viscosity; optical rotation; double refraction of flow; T-dependency for helix-coil transition in EDC 24:76 DCA solutions
$P^{Bn}Glu_n$	n=594 (M_n=130 kDa)	EDC 24:76 DCA T=21 °C T=40 °C	x	x			
$O^{Bn}Glu_n$	n=4	solid state		x	X		[70]; ROP of Glu-NCA with CH_3NaO or hexylamine as initiator; orientated, solid films; increasing α-helix proportion with increasing M_n
	n=8		x	x	x		
	n=20		x	X	x		
$P^{Bn}Glu_n$	n=200			x			
$P^{Bn}Glu_n$ $O^{Bn}Glu_n$ $O^{Bn}Glu_n$	n=100 n=21 n=7	DMSO-d_6	 x X	x x x			[75]; NMR-studies of $C_\alpha H$- and N*H*-protons; increasing α-helix proportion with increasing M_n
$P^{Bn}Glu_n$	n=132 - 493	TFA trichloroethylene	x	x			[74]; ROP of Glu-NCA with CH_3NaO as initiator; NSR-measurements
Ac-$O^{Bn}Glu$	n=6 n=8 n=12 n=14	solid state and dioxane-solution			x x x x		[71]; stepwise synthesis; IR-studies in solid state and in dioxane-solution; acetyl-residue on *N*-terminus
Ac-$O^{Bn}Glu_n$	n=4-5 n≥4 n=2-3	solid state benzene and dioxane-solution: above cac* below cac* dioxane; benzene			x x 	 x x	[77]; stepwise synthesis of residues; for *N*-acetyl-$O^{Bn}Glu_n$ (n≥4) in dioxane or benzene solutions formation of antiparallel β-sheet above the cac; similar results for *N*-Boc-$O^{Bn}Glu_n$ in benzene; for *N*-acetyl-$O^{Bn}Glu_n$ (n=2-3) β-turn formation independent of concentration
Boc-$O^{Bn}Glu_n$	n=5-8 n=4-8	solid state benzene-solution: above cac* below cac*			x x 	 x	
p-substituted $P^{Bn}Glu_n$ R = H R = NO_2		DMF-solution		x x			[72]; ROP of nitrated NCA with diethylamine as initiator 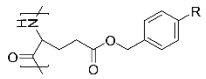
substituted $P^{Bn}Glu_n$ $R_1 = NO_2$, R_2, R_3 = H $R_2 = NO_2$, R_1, R_3 = H $R_3 = NO_2$, R_1, R_2 = H R_1 = I; R_2, R_3 = H R_1, R_2, R_3 = CH_3 benzyl	 n=80 n=250 n=330 n=190 n=270 n=60	solid state		x x x x x x			[78]; orientated films of *o*-, *m*-, *p*-substituted $P^{Bn}Glu_n$: 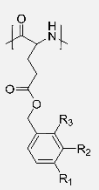 and 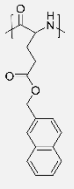 ; FTIR-measurements in solid state; optical rotatory dispersion in EDC-DCA solutions with increasing amount of EDC; random coil to α-helix-transition after adding EDC (vol%) to DCA-solutions
		EDC-DCA:					
$R_1 = NO_2$, R_2, R_3 = H $R_2 = NO_2$; R_1, R_3 = H $R_3 = NO_2$; R_1, R_2 = H R_1 = I; R_2, R_3 = H R_1, R_2, R_3 = CH_3 benzyl	n=80 n=250 n=330 n=190 n=270 n=60	≥~35% EDC ≥~25% EDC ≥~10% EDC ≥~30% EDC 0-100% EDC ≥~40% EDC	x→x x→x x→x x→x x→x	 x 			

1.2.2 Secondary structure formation of $P^{Bn}Asp_n$

Although the difference in side chain length is only one CH_2-group less than for $P^{Bn}Glu_n$, the secondary structure formation of $P^{Bn}Asp_n$ shows a more complex behavior (Figure 6). Due to the steric hindrance of the side chain, $P^{Bn}Asp_n$ usually stabilizes the rare α_l-helix, which can be converted into several secondary structures (α_r-helix, ω-helix, β-sheet, random coil) by varying the molecular weight, the used solvent, temperature, the evaporation rate and by introducing functionalities in the side-chain benzyl-group (Figure 6).

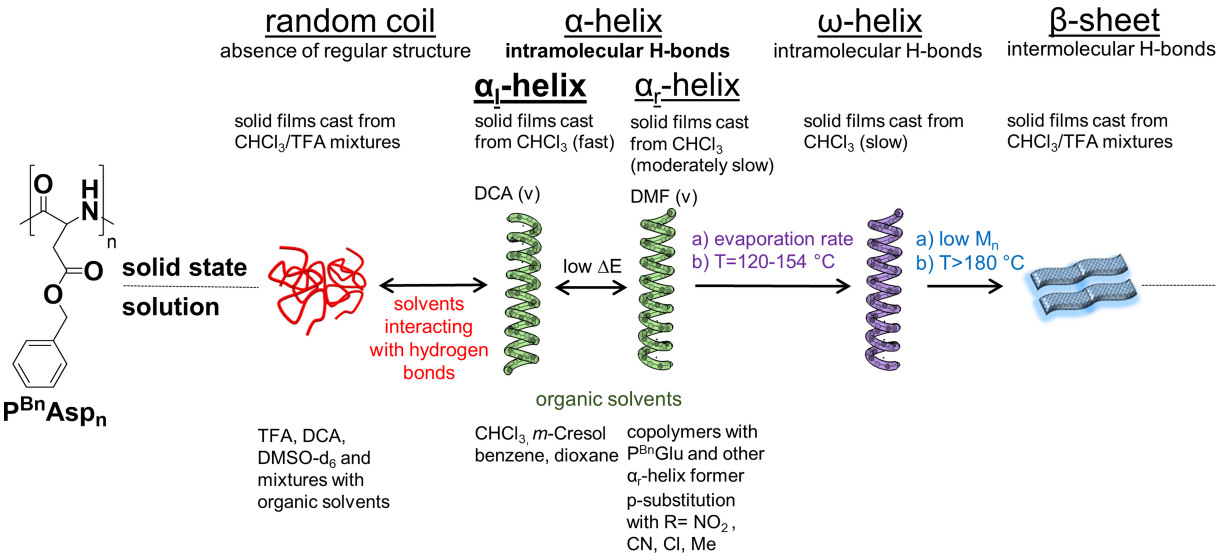

Figure 6. Secondary structure formation and transitions of $P^{Bn}Asp_n$ commonly adopting α_l-helix in solid state and solution under different physical and chemical conditions.

Similar to $P^{Bn}Glu_n$ secondary structure formation of $P^{Bn}Asp_n$ in solution strongly depends on the used solvent system. First optical rotary dispersion experiments with high molecular weight L-and D-$P^{Bn}Asp_n$ (M_n=4 kDa – 35 kDa) revealed the formation of random coils in DCA solutions equal to $P^{Bn}Glu_n$.[79] Further experiments in chloroform gave anomalous results, as L-$P^{Bn}Asp_n$ and D-$P^{Bn}Asp_n$ revealed contrary optical rotation values to the corresponding L-and D-$P^{Bn}Glu_n$ in chloroform solutions. Thus, data lead to the assumption, that the helix-sense of L-$P^{Bn}Asp_n$ is contrary to L-$P^{Bn}Glu_n$ in $CHCl_3$-solution. A possible explanation was postulated related to steric effects of the side chain benzyl groups laying closer to the main chain in the case of $P^{Bn}Asp_n$.[79] Later, Bradbury *et al.*[80, 81] demonstrated a strong molecular weight dependency for secondary structure formation of $P^{Bn}Asp_n$ as polymers with different molecular weights showed strong, small or no changes in optical rotary dispersion in a variety of solvents. Thus, they differentiate three types of behavior: With increasing molecular weights $P^{Bn}Asp_n$ showed slight increasing optical rotations values in $CHCl_3$-, $CHCl_2$-, and methyl salicylate solutions, whereas a significant change could be observed in *m*-cresol- and pyridine-solutions. Contrary, experiments in DCA and TFA revealed no molecular weight effect and constant values for the optical rotation.

As a result, the α_l-helical conformation for $P^{Bn}Asp_n$ is more stable than the α_r-helical conformation and the α_l-helix is stabilized in non-polar solvents such as $CHCl_3$ without molecular weight effects, to a lesser extent and in polar solvents such as *m*-cresol if the molecular weight is high, whereas a random coil is formed in strong interacting solvents like DCA.

As the α_l-helix formation in $P^{Bn}Asp_n$ show a strong dependency on the molecular weight and solvent system, the α_l-helix for $P^{Bn}Asp_n$ was postulated to be less stable than the α_r-helix for $P^{Bn}Glu_n$ in solution.

The random copolymerization of $P^{Bn}Asp_n$ with $P^{Bn}Glu_n$ demonstrated that only 15 mol% of $P^{Bn}Glu_n$ change the sign to opposite optical rotation values obtained for homo-$P^{Bn}Asp_n$ synonymous to change from α_l- to α_r-helix.[82] Moreover, Karlson *et al*.[83] showed, that the helix-coil transition in $CHCl_3$-DCA mixtures in $P^{Bn}Asp_n$ occurred at 8% DCA, whereas the transition could be observed at 70% DCA for $P^{Bn}Glu_n$. Similar results were obtained for high molecular weight $P^{Bn}Asp_n$ in $CHCl_3$:TFA-mixtures, as only 5 vol% TFA interrupt the α_l-helix, while it was 15 vol% for $P^{Bn}Glu_n$.[76] Furthermore, exchange of N*H* by N*D* in $CHCl_2$-solutions was found to be many times greater than for $P^{Bn}Glu_n$.[84]
As a conclusion, the α_l-helical conformation in $P^{Bn}Asp_n$ is thermodynamically less stable in relation to the solvated random coil form as for $P^{Bn}Glu_n$ and the difference in stability between α_l- and α_r-helix is much less than for $P^{Bn}Glu_n$.[81]

The reduced stability of the α_l-helical conformation for $P^{Bn}Asp_n$ was also proven by the introduction of functionalities in the side-chain benzyl-group. Goodman *et al*. introduces a nitro group in the *para*-position of the $P^{Bn}Asp_n$ side chain benzene-ring, causing a transition from α_l- to α_r-helical helical conformation in $CHCl_3$- and DMF solutions.[72, 85] They suggested that the right-handed helix sense allowed maximum interaction to occur between the aromatic groups and that the nitro-substituted aromatic rings form an electronically coupled side-chain helix rigidly arranged around the main chain helix. Ooi et a1.[86] gave another explanation, based on additional amide group interactions and the dipole of the nitro group resulting in the right-handed helix sense being the more stable. Indeed, similar reversal from the α_l- to α_r-helix of the polypeptide in a $CHCl_3$-solutions were obtained for a series of homo- and respective copolymers with $P^{Bn}Asp_n$ of *p*-methyl-, *p*-chloro-, and *p*-cyano-$P^{Bn}Asp_n$, which could not be explained by the former suggestion.[87-89] The explanation for the transition was given after copolymerization of $P^{Bn}Asp_n$ with poly-(α-ethyl L-aspartate), poly-(*p*-isopropyl L-aspartate), poly-(α-*n*-propyl L-aspartate) and poly-(*p*-phenethyl L-aspartate) (α_r-helix for homopolymers), observing a transition from right α_r-helical conformation to α_l-helix with increasing temperature.[90]
Therefore, the overall gain in entropy of the system must cause the change in conformation from the right-handed to the left-handed helix form of aspartates with increasing temperature and results from changes mainly by solvation and in change in ordering of the side chains.

The instability of the α-helical form in $P^{Bn}Asp_n$ could also be proven in the solid state by increasing the temperature during analysis of solid films. Heating of solid films of $P^{Bn}Asp_n$ to 170 °C causes a replacement of the X-ray diffraction pattern for the α-helical conformation by the ω-helix (4_{13}-helix).[80] The fourfold screw symmetric helix was found to be a form of a distorted α-helix, which has a translation of 0.133 nm with four residues per turn. Moreover, a higher ordering of the side chain than in the α-helix could be determined, in which the benzyl groups are stacked tetragonally around the helical core.

Moreover, the evaporation rate and the used solvent (-mixtures) during the preparation of solid films as well as the obtained molecular weight strongly effects secondary structure formation of $P^{Bn}Asp_n$. High molecular weight $P^{Bn}Asp_n$ films cast with different rates (fast, moderately, slow) from $CHCl_3$-solutions revealed poorly crystalline α-helical conformation for quick dried films, a mixture of α-helix and ω-helix for moderately slow dried films and the formation of high crystalline ω-helix for slowly dried films cast from chloroform solutions, as determined by FTIR- and XRD-measurements.[91] On the other hand, investigation of low molecular weight films shows the formation of the α_r-helical conformation when dried slowly from $CHCl_3$-solutions, which reverse and crystallize into the ω-form upon heating.[92] Results are mainly correlated to the extent of main chain distortion and orientation of the benzene rings. Moreover, films dried from solvent mixtures revealed the formation of various secondary structures e.g. $CHCl_3$-TFA mixtures containing 2% TFA show the formation of α-helix, β-sheet and random coil whereas DCA:ETOH mixtures revealed the formation of α-helix together with β-sheet. Heating of the

samples lead to the formation of the ω-helix at different temperatures (90 °C – 140 °C) depending on the evaporation rate, whereas the transition to β-sheet could be observed in all cases at 180 °C. A similar dynamic secondary structure formation was demonstrated by Yang *et al.*[93] by synthesizing $P^{Bn}Asp_n$ brushes by the sequential, surface-initiated vapor deposition polymerization of the corresponding NCA, revealing switchable left-handed and right-handed α-helical structures responding to DMF (α_r) or DCA (α_l) vapor exposure, which show a transition to the ω-helix when heated to 120 °C and are permanently converted to a β-sheet structure when heated to 160 °C on air.

Thus, the dynamic secondary structure behavior of $P^{Bn}Asp_n$ can be summed up to A) stabilization of the α_l-helical conformation in non-polar solvents and in polar solvents if the molecular weight is high, B) transition of the α_l-helical conformation to random coils in DCA and TFA, C) transition of the α_l-helical conformation to α_r-, ω- and β-sheet conformations in solid films in dependence of the evaporation rate, D) transition of the α_l-helical conformation to ω- and β-sheet conformation upon heating and E) transition of the α_l-helical conformation to the α_r-helical conformation by substitution of the side-chain benzene-group. Detailed information about secondary structure formation of $P^{Bn}Asp_n$ and derivates under various conditions described in literature are given in Table 3.

Table 3. Summary of the secondary structures of $P^{Bn}Asp_n$ (and several substituted derivates) described in literature in dependence of the molecular weights in solid state and solution determined with various analytical methods (description: random coil; α-helix (α_r: right-handed, α_l: left-handed), ω-helix, β-sheet, β-turn, O: oligomer, P: polymer).

poly-β-benzyl-L-aspartate ($P^{Bn}Asp_n$)							
structure	n (M_n (kDa))	conditions		α_l α_r	ω		Ref./ additional information
$P^{Bn}Asp_n$ (L- and D-conformation)	n=20-171 (M_n=4 kDa – 35 kDa)	DCA $CHCl_3$-solution: L-$P^{Bn}Asp_n$ D-$P^{Bn}Asp_n$	x	 x x			[79]; optical rotation from L- and D-$P^{Bn}Asp_n$ in solution; in $CHCl_3$ contrary helical confomormation
$P^{Bn}Asp_n$	Not exactly determined	$CHCl_3$ CH_2Cl_2 Methyl salicylate		x x x			[84]; ROP of Asp-NCA with different initiators; optical rotation dispersion; IR; deuteration of N*H*-group; T-dependency: a) in CH_2Cl_2 and $CHCl_3$: hardly any changes of b_0-values b) in *m*-cresol: with increasing T the α-helix becomes less stable in relative to the random coil, α-helix more stable in $CHCl_3$ than in *m*-cresol
	low M_n high M_n	*m*-cresol	x	x			
		DCA TFA	x x				
	high M_n	$CHCl_3$/DCA ≤ 8 % DCA ≥ 8 % DCA	 x	x			
	high M_n	*m*-cresol/DCA ≤ 2,5 % DCA ≥ 2,5 % DCA	 x	x			
$P^{Bn}Asp_n$	n=243	$CHCl_3$/DCA ≤ 8 % DCA ≥ 8 % DCA	 x	x			[83]; optical rotation; α_l-helix of $P^{Bn}Asp_n$ less stable than α_r-helix for $P^{Bn}Glu_n$
$P^{Bn}Asp_n$	Not exactly determined	solid state T = r.t. T =160 °C		x	x		[94]; IR-analysis of orientated films; α_l- to ω-helix conversion upon heating
$P^{Bn}Asp_n$	n = 1024 (M_n = 210 kDa)	solid films a) r.t. b) T =120 °C c) T=160 °C		x	x	x	[95]; solid films cast from $CHCl_3$ (fast), CD-analysis; α- to ω-helix to β-sheet transition with increasing T

structure	n (M_n (kDa))	conditions		α_l α_r	ω		Ref./ additional information
$P^{Bn}Asp_n$	n = 878 - 1220 (M_n = 180 kDa – 250 kDa)	solid state films cast from: $CHCl_3$ a) fast b)moderately slow c) slow TFA/$CHCl_3$ a) ≤ 1 vol%-TFA b) 2 vol%-TFA fast evaporation slow evaporation DCA/EtOH	 x x	 x x x x X X	 x x 	 x x x	[91]; IR-measurements of solid films cast from different solvents and evaporation time; in $CHCl_3$: α_l-helix when cast fast, ω-helix when cast slow; in TFA/$CHCl_3$ (2 vol%-TFA) and DCA/EtOH: various mixtures of secondary structures with high portion of α_l-helix
$P^{Bn}Asp_n$	n = 16 - 1220 → increasing T n = 16 → increasing T n = 112 - 1220 → increasing T	solid state, films cast from: $CHCl_3$ a) fast b) slow b) slow → increasing T	 	 x x x 	 x X x 	 X x	[92]; films with different M_n cast from $CHCl_3$ with various evaporation rate; IR- and DSC-measurements; α_l- to α_r-helix conversion for low M_n when slow casting; α- to ω-helix to β-sheet transition with increasing T
$P^{Bn}Asp_n$ on surface 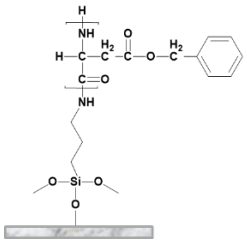	Not exactly determined	solid state: DMF (vapor) DCA (vapor) T=120 °C T=180 °C	 	 x 	 x 	 x	[93]; brushes fabricated by the sequential, surface-initiated vapor deposition polymerization of the NCA; conformational, reversable transition upon exposure to DCA (ν) or DMF (ν) between two opposite α-helix, upon heating the film permanently adopted a ω-helical or a β-sheet conformation
		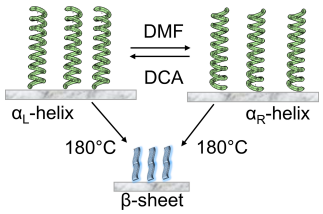					
$P^{Bn}Asp_n$	n = 20 (M_n =4 kDa)	$P^{Bn}Asp$ in $CHCl_3$: a) c = 0.08 – 0.30 T = 154 °C T > 200 °C b) c = 0.40 T=140 °C T > 200 °C c) c = 0.50 – 0.80 T=140 °C T > 200 °C d) c = 1.0 T = 120 °C T > 200 °C		 x x x x 	 x x x x	 x x x x	[96]; coacervation of $P^{Bn}Asp$ in $CHCl_3$ with different concentrations (c (mol L^{-1})) with MeOH; DSC-, TGA-, XRD-measurements; α- to ω-helix to β-sheet conversions with increasing T; α-ω-helix transition depends on concentration (lower concentration → higher transition T)
p-substituted $P^{Bn}Asp_n$ R = H R = NO_2 copolymers of $P^{Bn}Asp_n$ and R=NO_2: R=NO_2 15.0 mol% R=NO_2 26.0 mol% R=NO_2 32.0 mol% R=NO_2 0.0 mol % - 100.0 mol %	Not exactly determined	 $CHCl_3$ DCA DMF DCA $CHCl_3$ TFA	 x x x	 x x x x 	 	 	[72]; 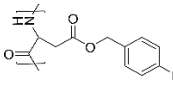 ; optical rotation dispersion; homopolymers show α_l-helical conformation for $P^{Bn}Asp_n$ and α_r-helix for NO_2 *p*-substituted $P^{Bn}Asp_n$; α_l- to α_r-helix conversion for copolymers after 26.0 mol% of *p*-NO_2-$P^{Bn}Asp_n$; in TFA random coil conformation

structure	n (M_n (kDa))	conditions		α_l α_r	ω		Ref./ additional information
p-substituted $P^{Bn}Asp_n$	Not exactly determined	solution:					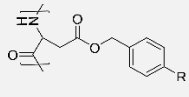 [87-89]; optical rotation dispersion and CD-measurements; *p*-substitution lead in all cases to α_l- to α_r-helix conversion for homopolymers in DMF and $CHCl_3$; α_l- to α_r-helix conversion for copolymers after the given *p*-substitution content in $CHCl_3$; random coil to α_r-helix conversion after the given *p*-substitution content; for R=Me 50 mol% α_l-helix in $CHCl_3$ and α_r-helix in DMF and conversion from α_l- to α_r-helix in $CHCl_3$:DMF (9:1)-solution
R = H		$CHCl_3$		x			
		DMF	x				
R = Me		$CHCl_3$ or DMF		x			
R = Cl				x			
R= CN				x			
Copolymers of $P^{Bn}Asp_n$ with							
R = NO_2 (20 mol%)		$CHCl_3$		x→x			
R = CN (40 mol%)		$CHCl_3$		x→x			
R = CN (30 mol%)		DMF	x	→x			
R = Me (70 mol%)		$CHCl_3$		x→x			
R = Me (30-40 mol%)		DMF	x	→x			
R = Me (50 mol%)		$CHCl_3$		x			
		DMF		x			
		$CHCl_3$:DMF (9:1)		x→x			
R= Cl (50 mol%)		$CHCl_3$		x→x			
R= Cl (15-30 mol%)		DMF	x	→x			

abbreviation: cac*: critical aggregation concentration.

1.3 Secondary structure formation of artificial amino acids

Secondary structures are not exclusively formed by biological polymers, as synthetic polymers also can form higher order structures like helices.[97] The helical conformation is a chiral structure with a preference for a left- or right-handed screw sense, usually are built from monomers with a chiral center which is essential for screw sense direction. Achiral polymers, built up from monomers without a chiral center, form enantiomeric mixtures of left- and right-handed helices, as their energy levels are equal. Although they are much rarer than polymers built from enantiomeric pure chiral monomers, achiral synthetic polymers e.g. polyisocyanates[98] and polymers on the base of achiral biological building blocks like polyamides of aromatic amino acids[99] and C_α-tetrasubstituted amino acids[100-102] such as alternating polyamides of Aib and Z-dedehydrophenylalanine polyamides[103] and 2-aminoisobutyric acid (Aib)[97, 100, 101, 104, 105] are building a class of foldamers with unique properties (Figure 7).

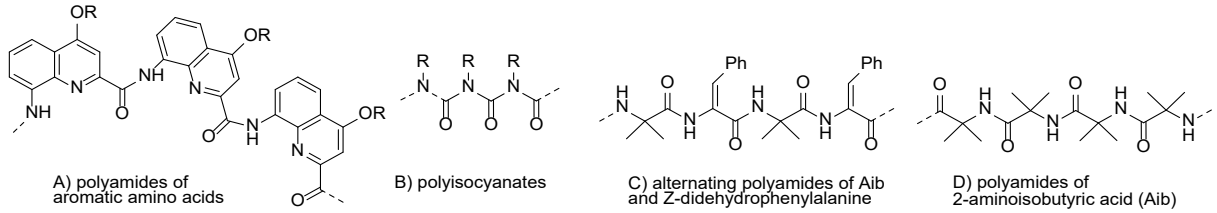

Figure 7. Structure of achiral polymers A) polyamides of aromatic amino acids, B) polyisocyanates, C) alternating polyamides of Aib- Z-dedehydrophenylalanine and D) polyamides of 2-aminoisobutyric acid (Aib).[97]

1.3.1 2-Aminoisobutyric acid (Aib) as prototype for artificial amino acids

Aib is the prototype of a non-proteogenic artificial amino acid, which is rare in nature and typically stabilizes a 3_{10}-helical conformation. The helix is formed by a series of type III/III´ β-bends[24, 30, 106-108] as the allowed angles in Ramachandran-plot are limited to helical regions (3_{10}-helix (ϕ=57°, ψ=30°) and α-helix ϕ=63°, ψ=±63°, ψ= 42°))[33, 109, 110] as well as type III/III´ β-bends caused by the two methyl groups on the C_α-carbon atom.[111] Aib-peptides strongly form single crystals, which could be isolated

for pure monomers[112, 113], dimers[114], tri- to pentamers[115], hexamers[116], octamers[117], decamers[118, 119], up to undecamers[120] (Figure 8A). Thus, it could be demonstrated that the helical conformation is built up without critical chain length, as single crystals of tripeptides revealed the formation of 3_{10}-helical conformation.

The energy difference between 3_{10}-helical and α-helical conformation is small and mainly depends on the main chain length proven by a series of $(Aib\text{-}L\text{-}Ala)_n$ oligopeptides in which the octapeptide (n=4) was found to be the shortest one for exhibiting the α-helix.[22] The strong affinity to form a helical conformation makes Aib a strong β-sheet breaker (Figure 8B). As a result, Aib was incooperated in short β-sheet forming peptides and later in complex proteins known for induce human disorders and diseases by protein misfolding and aggregation (e.g. Alzheimer's disease).[121, 122] According to literature, replacement of hydrophobic sequences (e.g. 17-21, -L-Leu-L-Val-$(L\text{-}Phe)_2$-L-Ala-), mainly responsible for β-sheet and fibril formation in amyloid beta (Aβ), with the helix supporting Aib leads to the disruption of β-sheet formation[123] even stronger than substitution with Pro.[124]

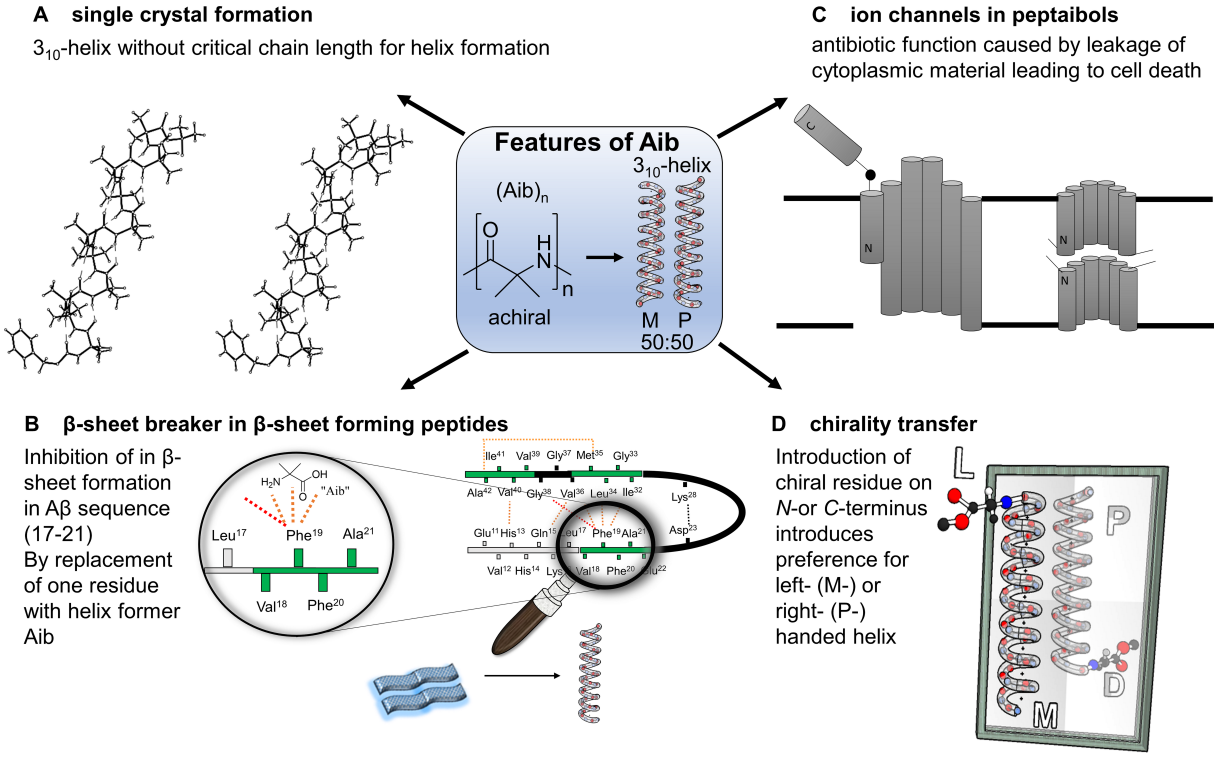

Figure 8. Features of Aib namely **A**) single crystal formation of Aib-peptides up to undecamers (Figure adapted and redrawn from reference[120] with permission of European Peptide Society and John Wiley & Sons, Ltd.) (Copyright © 2003) **B**) β-sheet breaker in β-sheet forming peptides **C**) formation of ion channels in peptaibols (Republished with permission of Biochemical Society, from literature[125]: Peptaibols: models for ion channels, J. K. Chugh; B. A. Wallace**,** 29 (4), © 2001; permission conveyed through Copyright Clearance Center, Inc. and **D**) chirality transfer in achiral helical Aib-domains by chiral residues.

In nature Aib is found in peptaibols, a class of antibiotic peptides built up from 5 to 20 amino acid units formed by the fungus species Trichoderma.[126] The over 300 peptaibols (**pep**tide, **Aib**, amino alco**hol**) found in nature[127] or synthesized analogous[128] consisting of *N*-terminal acetylated peptide group, *C*-terminal alcohols (e.g. phenylalaniol, valinol, leucinol, isoleucinol or trypthophanol) and C_α-tetrasubstituted amino acid (mainly Aib) are primilary responsible for the helical structure of peptaibols.[129-131] Due to their amphipathic character, peptaibols form voltage-depending ion channels in

liquid membranes and were also found to exhibit antibiotic activity against bacteria and fungi (Figure 8C).

1.3.2 Chirality control and preference for helix direction in achiral Aib-domains

For Aib and other artificial amino acids with C_α-tetrasubstituted carbon atom no chiral center is present in the monomer and as a result, the polymers of these type of amino acids do not have a chiral center as well.[97, 100, 101, 104, 105] Usually, the screw sense of the helical polymer depends on the nature of its chiral monomers from which they were built up. Thus, artificial amino acids without chiral center adopt a 50:50 ratio for left and right-handed- screw sense in solid state and solution, as the energy level for the different screw sense direction is equal. The left- and right-handed screw sense of the 3_{10}-helical conformation of Aib can easily inverse, undergoing the conformational change in milliseconds or less, depending on the chain length of the helical domain.[132, 133]

The preference for a certain screw sense direction can be influenced by covalently binding different type of molecules bearing a chiral center on the Aib-repeating unit as well as non-covalently interactions with chiral ligands were also found to be an effective promoter for preference of a certain screw sense in the achiral Aib-residues (Figure 8D).[97, 100, 101, 104, 105, 134] The overall preference of the screw sense depends on the nature, the position and the absolute configuration of the "guest" molecule connected to the polymer chain. In general, the chiral residue can be attached either on the *N*-terminus[99, 135-158], the *C*-terminus[135, 138, 140, 147, 149, 158-163] or in between[135, 138, 140, 143-145, 158, 160] the achiral domains (Figure 9A-E).

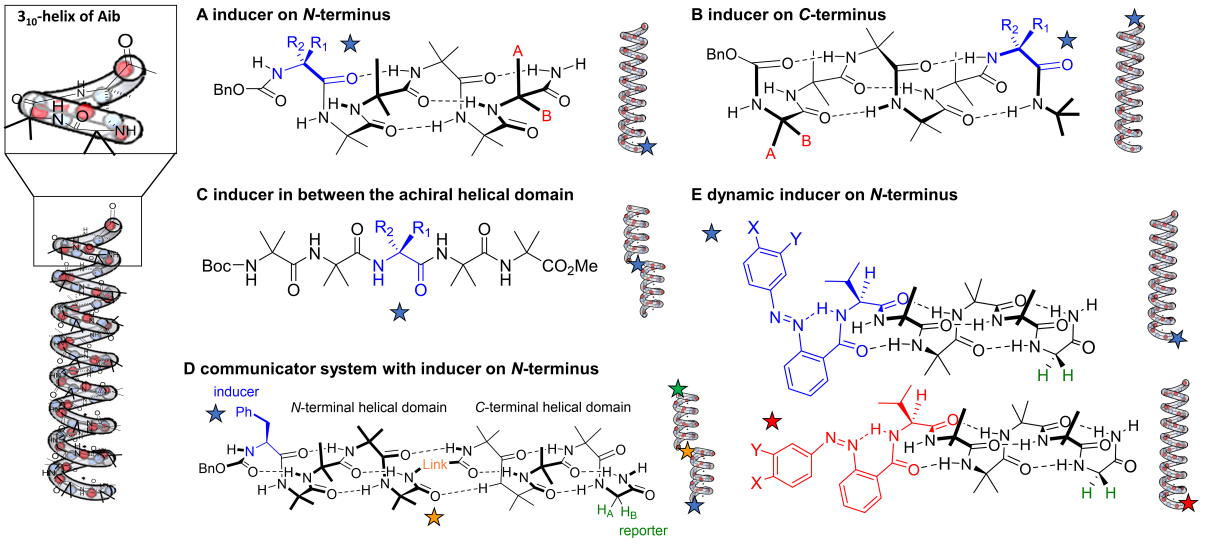

Figure 9. Chirality transfer into achiral helical Aib-domains by attachment of chiral residues on **A**) *N*-terminus[97], **B**) *C*-terminus[97], **C**) in between the achiral domain[158] and development of **D**) communication systems *via* linker molecule between two helical domains of Aib[150] and **E**) dynamic inducer introducing chirality changes in the helical domain of Aib.[164]

Already in pioneering works the location of the chiral residue was found to be an important factor for the formation of a certain screw-sense preference, as peptaibol- and related short sequences were synthesized and analyzed by XRD- and CD-measurements, in which L-Leu and L-Val segments attached on the *N*-terminus or in between the Aib-domains revealed the formation of right-handed helices, whereas a tetrapeptide with L-Val-OMe located on the *C*-terminus revealed the formation of a left-handed helix.[135, 160] The investigation on the position-influence of the guest molecule was then systematically investigated by Pengo *et al.*[140] by synthesizing L-valine-(Val) or C^α-methyl-L-valine (αMe-Val)-Aib isomers, in which the Val or αMe-Val units are connected either on the *N*- or *C*-terminus

or incorporated in the tetramer of Aib. The helix-forming, achiral Aib-tetramers clearly preferred the formation of a right-handed 3_{10}-helix when Val or αMe-Val are connected to the *N*-terminus or incorporated into the Aib repeating units, as found in proteins where L-amino acids forms right-handed helical conformations.
When the chiral center is located on the *C*-terminus, the formation of a left-handed helical screw sense is preferred, although the effect is not well pronounced as by connecting the single chiral residue on the other positions. Contrary, *C*-terminus modification with L-Val into achiral tri-, tetra-, penta- and hexapeptide segments of Aib and α,β-dehydrophenylalanine (Δ^zPh) revealed a right-handed helical conformation for the penta- and hexapeptide in TFE-solution and in solid state.[161]

The different observations clearly cut out the importance of the protection group attached on the chiral residue, as Pengo and Co-workers[140] used butyl-ester protected valine and Demizu *et al*.[161] amide protected valine for modification. The inverse behavior can be ascribed to the unfavorable O-O interaction between the main chain carbonyl group and the ester group of the connected residue, resulting in the same sign of the torsion angle of the chiral residue and the 3_{10}-helix. As a result, a "Schellmann" motif is formed by these oligomers.

Unexpected results were found by connecting a L-Val residue to the *N*-terminus of Aib-tetramers introducing a preference for the left- handed helical conformation of the overall oligomer,[151] as the L-amino acids usually form right-handed helical conformations. In contrast, a right-handed screw sense preference was found for the corresponding C^{α}-methylated amino acids such as L-αMe-Val or L-isovaline (l-Iva). Left-handed helices were also found for *N*-terminal attached tertiary L-amino acids such as Phe[99, 151, 154, 155], Pro[99, 154], Ala[141, 154, 155], Leu[154], and *tert*-Leu[154], whereas contrary quaternary L-amino acids Iva[138] and (αMe)Phe[154] induce the formation of right-handed helical screw sense. From these results, a general feature for the helix screw sense was found for *N*-terminal tertiary and quaternary L-amino acid residues, as the former adopt the left-handed helical conformation whereas the latter ones prefer the formation of right-handed helices.
The inverse behavior was attributed to the conformational change of *N*-terminal β-turn type II to type III.[151] When attached on the second position, both induce the formation of the right-handed helical conformation, in which quaternary L-amino acids revealed a more powerful effect.[154] Contrary, attachment of the tertiary and quaternary L-amino acids on the *C*-terminus revealed a conformational switch to the right-handed helical conformation[163], although the transmission of information given by the chiral residue to the achiral Aib-domain was found to more effective when the input is located on the *N*-terminus.[149]

As the chirality transfer to the achiral Aib-domain was exclusively introduced by L-amino acids, systematic investigation to corresponding D-amino acids of Pro revealed the formation of contrary helix turns, as L-Pro induces the right-helical conformation (as mentioned above), whereas D-Pro revealed the formation of left-handed helices.[139] Moreover, the direct comparison of the inducer power with location dependence of the chiral residue was investigated by simultaneously attachment of L- and D-Leu residues on Aib-tetramers *N*-and *C*-terminus or in cooperation of both species in the achiral helical domain.[158] Equal formation of right-handed helical conformation were found for tetramers in which the L-Leu residue was attached to the *C*-terminus and L- or D-Leu where attached to the *N*-terminus, whereas the attachment of L-and D-Leu in between the Aib sequence revealed the formation of a racemic mixture of left-and right-handed helical screw sense.
A summary of literature work to the chirality transfer of chiral residues to the achiral helical Aib-domain is given in Table 4.

Table 4. Summary of chosen examples in literature for chirality control in $(Aib)_n$ sequences introduced by chiral residues (**highlighted**) either on the *N*- or *C*-terminus or in between the achiral helical domain.

Ref.	*N*-terminal residue	Aib-domain $(Aib)_x$	*C*-terminal residue	P-/M-helix solution	P-/M-helix solid
Peptaibols antibiotics and related short sequences					
135	Z	-$(Aib)_3$-	**L-Val**-OMe	[a]M	M
	Z	-$(Aib)_3$-**L-Val**-	Gly-OMe	P	P
	t-Boc-**L-Leu**	-$(Aib)_2$-	OMe	P	-
	t-Boc-Gly	-**L-Leu**-$(Aib)_2$-	OMe	P	-
	t-Boc-**L-Val**	-Gly-**L-Leu**-$(Aib)_2$-	OMe	P	-
	Z	-$(Aib)_3$-**L-Val**-Gly-**L-Leu**-$(Aib)_2$-	OMe	P	-
160	Z	-$(Aib)_3$-**L-Val**-Gly-**L-Leu**-$(Aib)_2$-	OMe	[a]P	-
	Z	-$(Aib)_3$-**L-Val**-	Gly-OMe	P	P
	Z	-$(Aib)_3$-	**L-Val**-OMe	M	M
Chirality transfer of L-Val vs L-(αMe)Val with different protecting groups					
140	pBrBz-**L-Val**	-$(Aib)_4$-	OBu	[a,b]P	P
	pBrBz	-$(Aib)_2$-**L-Val**-$(Aib)_2$-	OBu	P	P
	pBrBz	-$(Aib)_4$-	**L-Val**-OBu	M	M
	pBrBz-**L-(αMe)Val**	-$(Aib)_4$-	OBu	P	P
	pBrBz	-$(Aib)_2$-**L-(αMe)Val**-$(Aib)_2$-	OBu	P	P
	pBrBz	-$(Aib)_4$-	**L-(αMe)Val**-OBu	M	M
161	Boc	-Aib-ΔPhe-$(Aib)_2$	**L-Val**-NH-Bn	P	P
	Boc	-Aib-ΔPhe-$(Aib)_3$	**L-Val**-NH-Bn	P	P
159	*p*BrBz	-$(Aib)_4$-	**L-Val**-O*t*Bu	-	P
	*p*BrBz	-$(Aib)_4$-	**L-(αMe)Val**-O*t*Bu	-	50:50
Chirality transfer of tertiary vs. quaternary amino acids on *N*-terminus					
99	Cbz-**L-Phe**	-$(Aib)_9$-	O*t*Bu	[c]M	-
	Cbz-**L-Val**	-$(Aib)_9$-	O*t*Bu	M	-
	Cbz-**L-Pro**	-$(Aib)_9$-	O*t*Bu	M	-
	Cbz-**L-(αMe)Val**	-$(Aib)_9$-	O*t*Bu	P	-
151	Ac-**L-Val**	-$(Aib)_4$-	Gly-NH_2	[a,c]M	-
	Ac-**L-Phe**	-$(Aib)_4$-	Gly-NH_2	M	-
	Ac-**L-(αMe)Val**	-$(Aib)_4$-	Gly-NH_2	P	-
152	Ac-**L-Val**	-$(Aib)_4$-	Gly-NH_2	[c]M	-
	Ac-**L-(αMe)Val**	-$(Aib)_4$-	Gly-NH_2	P	-
155	Ac-**L-Val**	-$(Aib)_4$-	$NHCH_2(C=S)$Gly-OMe	[c]M	
	Ac-**L-(αMe)Val**	-$(Aib)_4$-	$NHCH_2(C=S)$Gly-OMe	P	
	Cbz-**L-Val**	-$(Aib)_4$-	$NHCH_2(C=S)$Gly-OMe	M	50:50
	Cbz-**L-Phe**	-$(Aib)_4$-	$NHCH_2(C=S)$Gly-OMe	M	
	Cbz-**L-Ala**	-$(Aib)_4$-	$NHCH_2(C=S)$Gly-OMe	M	50:50
	Cbz-**L-(αMe)Val**	-$(Aib)_4$-	$NHCH_2(C=S)$Gly-OMe	P	
141	pBrBz-**L-Ala**	-$(Aib)_4$-	O*t*Bu	-	M
	pBrBz-**L-Val**	-$(Aib)_4$-	O*t*Bu	-	M
	pBrBz-**L-Ala**	-$(Aib)_3$-	**L-Ala**-OMe	-	M
138	Ac-**L-Iva**	-$(Aib)_4$-	OMe	-	M
	Z-**L-Iva**	-$(Aib)_4$-	OMe	-	P
145	Ac-**L-αIle**	-$(Aib)_5$-	O*t*Bu	-	50:50
154	Cbz-**L-Ser**	-$(Aib)_4$-	CH_2OH	P	-
	Cbz-**L-Ala**	-$(Aib)_4$-	CH_2OH	M	-
	Cbz-**L-Leu**	-$(Aib)_4$-	CH_2OH	M	-
	Cbz-**L-Val**	-$(Aib)_4$-	CH_2OH	M	-
	Cbz-**L-*tert*-Leu**	-$(Aib)_4$-	CH_2OH	M	-
	Cbz-**L-Pro**	-$(Aib)_4$-	CH_2OH	M	-
	Cbz-**L-Phe**	-$(Aib)_4$-	CH_2OH	M	-
	Cbz-**L-Iva**	-$(Aib)_4$-	CH_2OH	P	-
	Cbz-**L-(αMe)Val**	-$(Aib)_4$-	CH_2OH	P	-
	Cbz-**L-(αMe)Phe**	-$(Aib)_4$-	CH_2OH	P	-

Ref.	*N*-terminal residue	Aib-domain $(Aib)_x$	*C*-terminal residue	P-/M-helix solution	solid
Chirality transfer of tertiary vs. quaternary amino acids on *C*-terminus					
[162]	Z	-$(Aib)_3$-	**L-Ala**-O*t*Bu	-	M
[163]	Cbz	-$(Aib)_5$-	[c,d]**L-Ala**-NH*t*-Bu	P	-
	Cbz	-$(Aib)_5$-	**L-Val**-NH*t*-Bu	P	-
	Cbz	-$(Aib)_5$-	**L-Phe**-NH*t*-Bu	P	-
	Cbz	-$(Aib)_5$-	**L-*tert*-Leu**-NH*t*-Bu	P	-
	Cbz	-$(Aib)_5$-	**L-(αMe)Val**-NH*t*-Bu	P	-
	Cbz	-$(Aib)_5$-	**L-Ala**-O*t*-Bu	M	-
	Cbz	-$(Aib)_5$-	**L-Phe**-O*t*-Bu	M	-
	Cbz	-$(Aib)_5$-	**L-Val**-O*t*-Bu	M	-
	Cbz	-$(Aib)_5$-	**L-*tert*-Leu**-O*t*-Bu	M	-
	Cbz	-$(Aib)_5$-	**L-(αMe)Val**-O*t*-Bu	M	-
Chirality transfer of tertiary vs. quaternary amino acids in between the achiral helical domain					
[158]	Boc	-$(Aib)_2$-(**L-Leu**)$_2$-$(Aib)_2$-	OMe	P	-
[165]	Ac	-$(Aib)_2$-**L-Iva**-$(Aib)_2$-	OMe	-	50:50
[138]	Ac	-Aib-**L-Iva**-$(Aib)_3$-	OMe	-	P
	Ac	-$(Aib)_3$-**L-Iva**-Aib	OMe	-	50:50
	Z	-Aib-**L-Iva**-$(Aib)_3$-	OMe	-	P
	Z	-$(Aib)_3$-**L-Iva**-Aib	OMe	-	P
Chirality control by D- vs L- amino acids					
[139]	pBrBz-**L-Pro**	-**D-Ala**-$(Aib)_4$-	O*t*Bu	-	M
	pBrBz-**D-Pro**	-**D-Ala**-$(Aib)_4$-	O*t*Bu	-	P
[158]	Boc-**L-Leu**	-$(Aib)_4$-	**L-Leu**-OMe	50:50	P
	Boc-**D-Leu**	-$(Aib)_4$-	**L-Leu**-OMe	50:50	P
	Boc	-$(Aib)_2$-**D-Leu-L-Leu**-$(Aib)_2$-	OMe	50:50	50:50
[166]	Boc-**L-Leu**	-(**L-Leu**$_{n-1}$-**D-Leu**$_n$-$Aib_n)_3$	OMe	[a]P	-
	Boc-**D-Leu**	-(**D-Leu**$_{n-1}$-**L-Leu**$_n$-$Aib_n)_3$	OMe	M	-
Dynamic screw sense switching					
[148]	**L-3-phenyllactate**	-$(Aib)_4$-	Aib-OMe	[e]P	-
	D-3-phenyllactate	-$(Aib)_4$-	Aib-OMe	M	-
	L-3-phenyllactate	-$(Aib)_{12}$-	Aib-OMe	P	-
	D-3-phenyllactate	-$(Aib)_{12}$-	Aib-OMe	M	-
[164]	Azo(*trans*)*-**L-Val**	-$(Aib)_3$-	-Fib*-TEG*	-	M
	Azo(*cis*)*-**L-Val**	-$(Aib)_3$-	-Fib*-TEG*	-	50:50
Bivalent and further inducer					
[137]	Z-**L-Dap**(pBrBz)*	-$(Aib)_2$-	NHMe	-	M
	Z-**L-Dab**(pBrBz)*	-$(Aib)_2$-	NHMe	-	50:50
[147]	Cbz-[**(S,S)-Ac$_5$c^{dOM}**]	-$(Aib)_4$-	OEt	-	M
	Cbz	-$(Aib)_4$-	[**(S,S)-Ac$_5$c^{dOM}**]*-OMe	-	P
[142]	Bis-Boc-**L-Cis**	-$(Aib)_{3,\ 4}$-	OMe	-	50:50
[143]	CF_3CO-**L-Beg**	-$(Aib)_4$-	OEt	-	50:50
	CF_3CO	-$(Aib)_2$-**L-Beg**-$(Aib)_2$	OEt	-	P

abbreviation: solvents used for measurements: [a]TFE, [b]$CHCl_3$, [c]MeOH, [d]DMSO-d_6, [e]CD_3OD; chemical compounds*: Cbz = Z: carboxybenzyl; pBrBz: *p*-bromobenzoyl L-Dap(pBrBz): N^{β}-*p*-bromobenzoyl-L-α,β-diaminopropionic acid; L-Dab(pBrBz): N^{γ}-*p*-bromobenzoyl-L-α,γ-diaminobutyric acid; Azo: 5-fluoro-3-methoxyazobenzene; Fib: difluoroAib; TEG: triethylene glycol; [(S,S)-Ac_5c^{dOM}]: (3S,4S)-1-amino-(3,4-dimethoxy)cyclopentanecarboxylic acid; L-Beg: L-butylethylglycine.

The design of communication systems by Clayden *et al.*[150] leads to a powerful understanding of signal transmission in dependence to the nature of the different linker-molecules incooperated into the achiral domains of Aib. The system is based on an *N*-terminal inducer L-Phe, known for inducing left helical conformations, attached to achiral tetramers of Aib, connected to a linker bearing another Aib-tetramer domain. The tendency of the linker to communicate the preference for left helical screw sense to the second Aib-sequence was probed with the help of a reporting system on the *C*-terminal Aib-domain,

consisting of diastereotopic protons of glycinamide. Quaternary amino acids such as ACHC were found as effective as Aib for the communication, whereas triazolyl-based linker are isolators unable to transmit the chemical information.[150] A further extent of introducing chirality to achiral Aib-domains was the attachment of dynamic inducers, able to switch their stereoisomers. For this purpose, a benzoate ester of 2-hydroxy-3-phenylpropionic acid (L/D-3-phenyllactate) was attached on the *N*-terminus of Aib-tetramers and Aib-dodecamers, easily convertible from L-3-phenyllactate, revealing right-handed helical Aib-domains to D-3-phenyllactate by Mitsunobu reaction, tantamount with helical screw sense switching to left-handed helices. A more effective approach was the attachment of 5-fluoro-3-methoxyazobenzene to the L-Val residue on the *N*-terminus of Aib-tetramers, able to incooperate into a phospholipid 1,2-dioleoyl-snglycero-3-phosphocholine (DOPC) layer by attachment of *C*-terminal TEG (triethylene glycol) and photo switchable between *trans* and *cis* isomers by UV-irradiation directly within the phospholipid layer.[164] Storage in darkness lead to formation of fully *trans*-isomer in the *N*-terminal azobenzene revealing a left-handed helical conformation of the Aib-domains, whereas after irradiation with UV-light (365 nm) *cis*-isomerization could be observed, switching the helix ratio to equal distribution between left- and right helical screw sense, presumably by altering the geometry of the hydrogen bonding between azo-nitrogen and N*H*-proton of the *N*-terminal Val-residue.

1.4 Ring-opening polymerization of *N*-carboxyanhydrides (ROP of NCAs)

For the systematic investigation of peptide and protein folding behavior, the synthesis of polypeptides is a fundamental challenge. The synthetic access of poly-amino acids is therefore necessary and has been developed over years. Besides the stepwise solid-phase peptide synthesis[167] and the microbiological synthesis[168] whose advantages in selectivity and exact sequencing is undisputed, ring opening polymerization (ROP) of *N*-carboxyanhydrides (NCAs) offers the synthesis of high molecular weight poly-amino acids, able to introduce several functionalities and architectures into proteogenic- and artificial amino acids. Moreover, the ROP of NCAs enables new field for the systematic investigation of self-assembly behavior and the nature of secondary structure formations of polypeptides, through to research of new biological and medical applications of synthetic poly-amino acids.[169-174]

1.4.1 Synthesis of common/functional NCAs

The development of the NCA monomers found their origin in the synthesis of glycine-NCA by Leuch[175], followed by the *C*- and *N*-phenylglycine, phenylalanine and leucine.[176, 177] The synthetic approach of the "Leuchs method" was based on the one-step cyclization of halogenated *N*-alkoxycarbonyl-amino acids at high temperatures, followed by the formation of the carbonyl group after release of the halogenated alkyl-chain (Figure 10). In the pioneering works, *N*-alkoxycarbonyl-amino acids chlorides were directly generated by the reaction of the corresponding *N*-alkoxycarbonyl-amino acids with thionyl chloride[175, 178], leading to an effective removement of the gaseous by-products, but decomposition reactions of the formed NCAs as a result of the required high temperature's reduces the effectiveness of this method. Therefore, thionyl chloride was replaced by phosphorous trichloride (PCl_3) or phosphorous pentachloride (PCl_5) in further works, as the reactivity of the used phosphor-chlorides lead to the reaction under mild conditions. Due to the better nucleophile, the replacement of the phosphor-chlorides with phosphorous tribromide and the resulting synthesis of *N*-alkoxycarbonyl-amino acids bromides were found to be an effective alternative for the synthesis of the corresponding anhydrides under mild conditions (T = 4 °C).[179]

Nowadays the access of NCAs is mainly accessible directly from the corresponding amino acid *via* "Fuchs-Farthing" method[180], traditionally converted in alkalic-aqueous solutions with phosgene (Figure 10). Further investigations increases the effectivity by suspending the amino acid in an organic solvent

and treatment with phosgene(-derivates).[180, 181] The main advantages of "Fuchs-Farthing" method involve the use of low-boiling organic solvents reducing the solubility of the formed HCl, the prevention of side reactions and the simple purification by developing HCl-scavenger systems[182] and flash chromatography[183]. An improved "Fuchs-Farting" synthesis of NCAs was developed by Fuse[184], in which the fast (0.1s) and scalable synthesis (up to gram scale) of NCAs was realized in a microwave reactor, based on a fast basic-to-acid flash switching system. For the synthesis of more complex NCAs bearing side chain functional groups cursing side reactions during synthesis, protecting group strategies were used for NCA monomers. Especially for glutamic acid- (benzyl, piperonyl), aspartic acid- (benzyl) and lysine-NCA (Boc, Fmoc, Nvoc) side chain protection groups were used to detach them easily by hydrogenation, basic conditions or strong acids and to obtain the corresponding origin poly-amino acid (Figure 10).

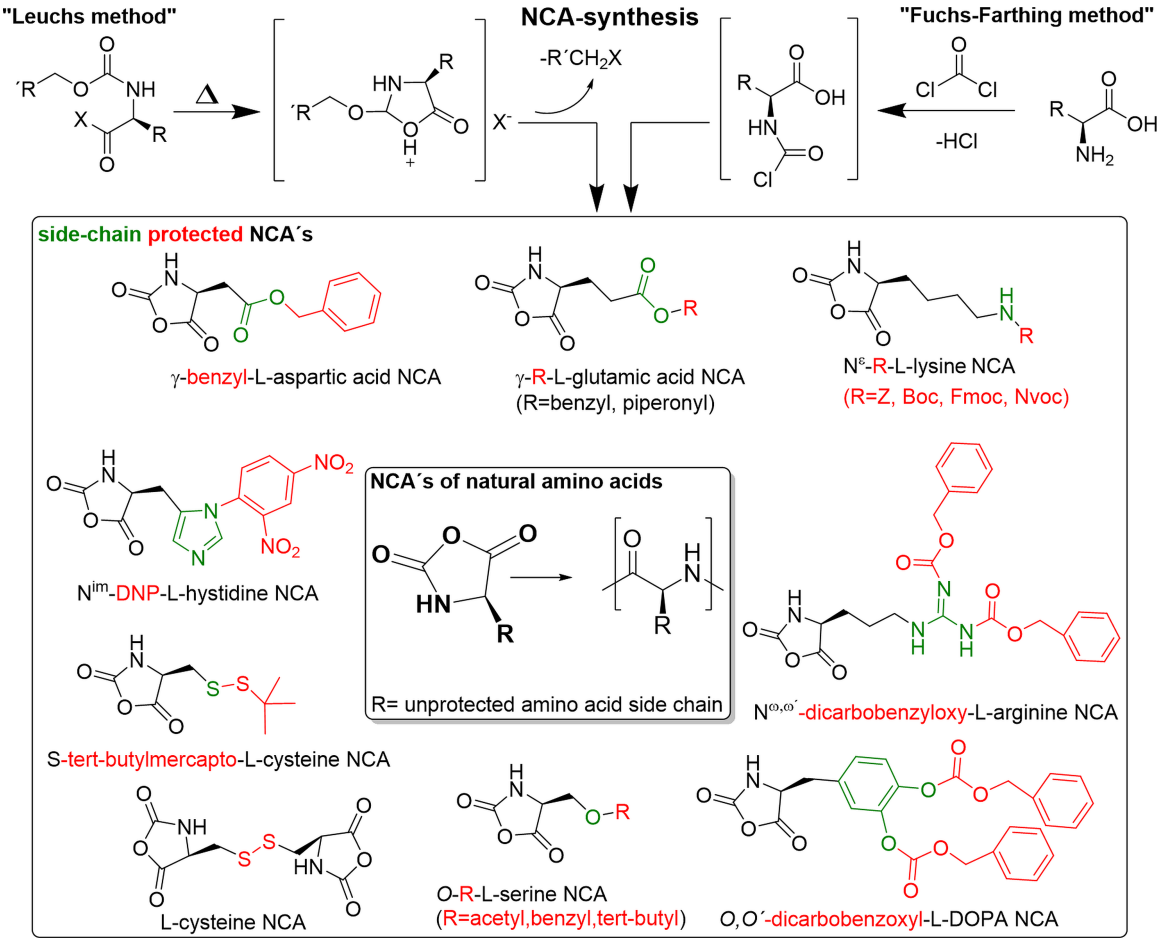

Figure 10. Synthesis of NCAs without (natural) and with side chain-protecting group *via* Leuch's method and Fuchs-Farthing method.[173]

1.4.2 Mechanisms for ROP of NCAs

Systematic investigations to the ROP of NCAs revealed two main mechanisms, depending on the used initiator: The normal amine mechanism (NAM) and the activated monomer mechanism (AMM) (Scheme 1).[170, 173, 185, 186]

NAM expire when using nucleophilic initiator, such as primary and secondary amines, alcohols and water. The nucleophilic attack takes place on the C_5-carbon atom, resulting in an unstable carbamic acid and the release of carbon dioxide. The newly formed amine group propagates the polymerization, leading to living polymerization as the initiating nucleophilic attack proceeds much faster than the

propagation step (Scheme 1, top). The AMM is based on the activation of the NCA-monomer by bases, resulting in the abstraction of the NH-proton, which leads to an initiation by activated NCA-anion´s and the formation of tadpole dimers. The propagation steps are based on the attack of NCA-monomers of the formed dimer, resulting in the creation of NCA anions at each chain end and reaction step (Scheme 1, bottom). Both mechanisms were found switch back and forth several times during the polymerization, but a propagation step for one mechanism is a side reaction for the other.[186]

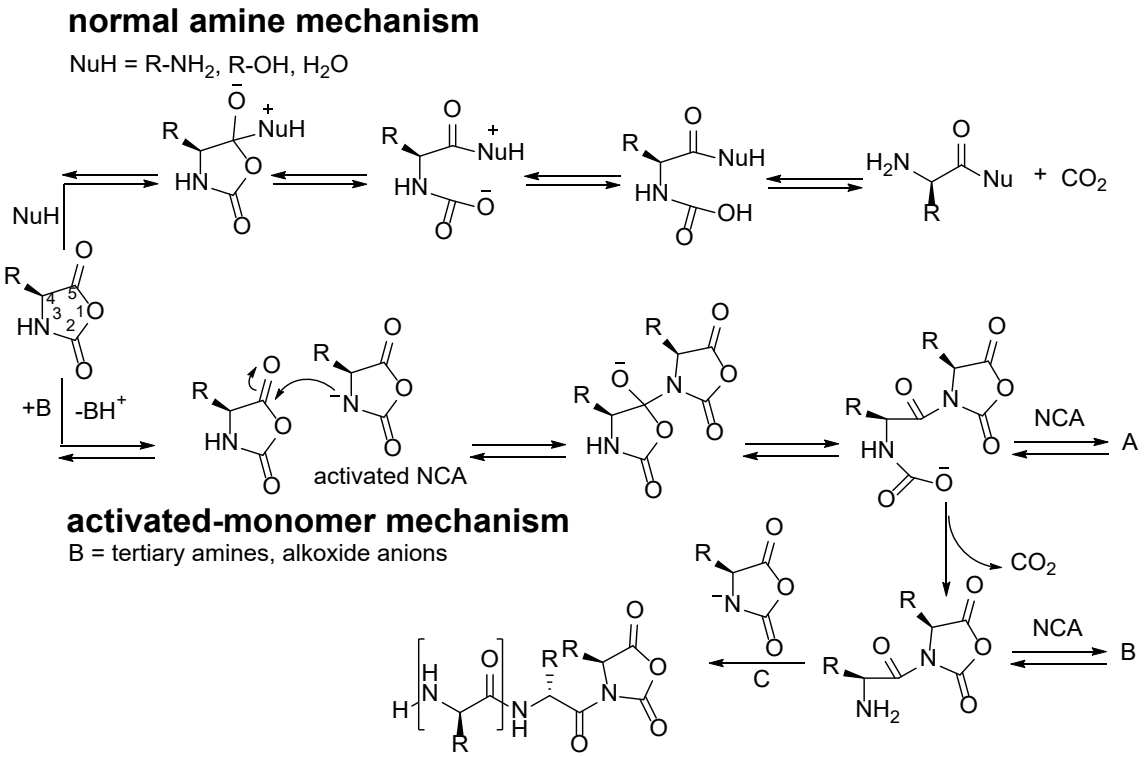

Scheme 1. General mechanism for ROP of NCAs initiated by nucleophiles (normal amine mechanism) and by bases (activated-monomer mechanism).[173]

However, the synthesis of well-defined polypeptides was often inhibited by side reactions occurring during the ROP of the NCAs, mainly deactivating the *N*-terminus and preventing the synthesis of high molecular weight polymers and further modification of the obtained polypeptides (Figure 11).[187, 188]

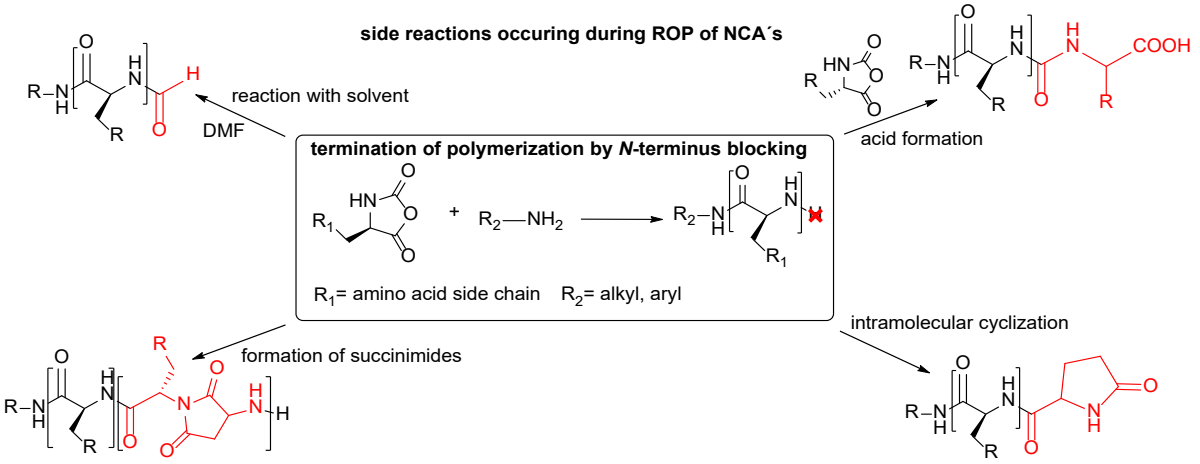

Figure 11. Side reactions occurring during the ROP of NCAs especially for ROP pf Glu-NCA and Asp-NCA.[173]

1.4.3 Improvements for ROP of NCAs

As the applications of the synthesized polymers is limited due termination reactions, the development of new *N*-terminus protecting strategies during polymerization were sophisticated. Thus, new initiator systems were developed to improve the ROP of NCAs to prevent side reactions and accelerate the polymerization (Figure 12).

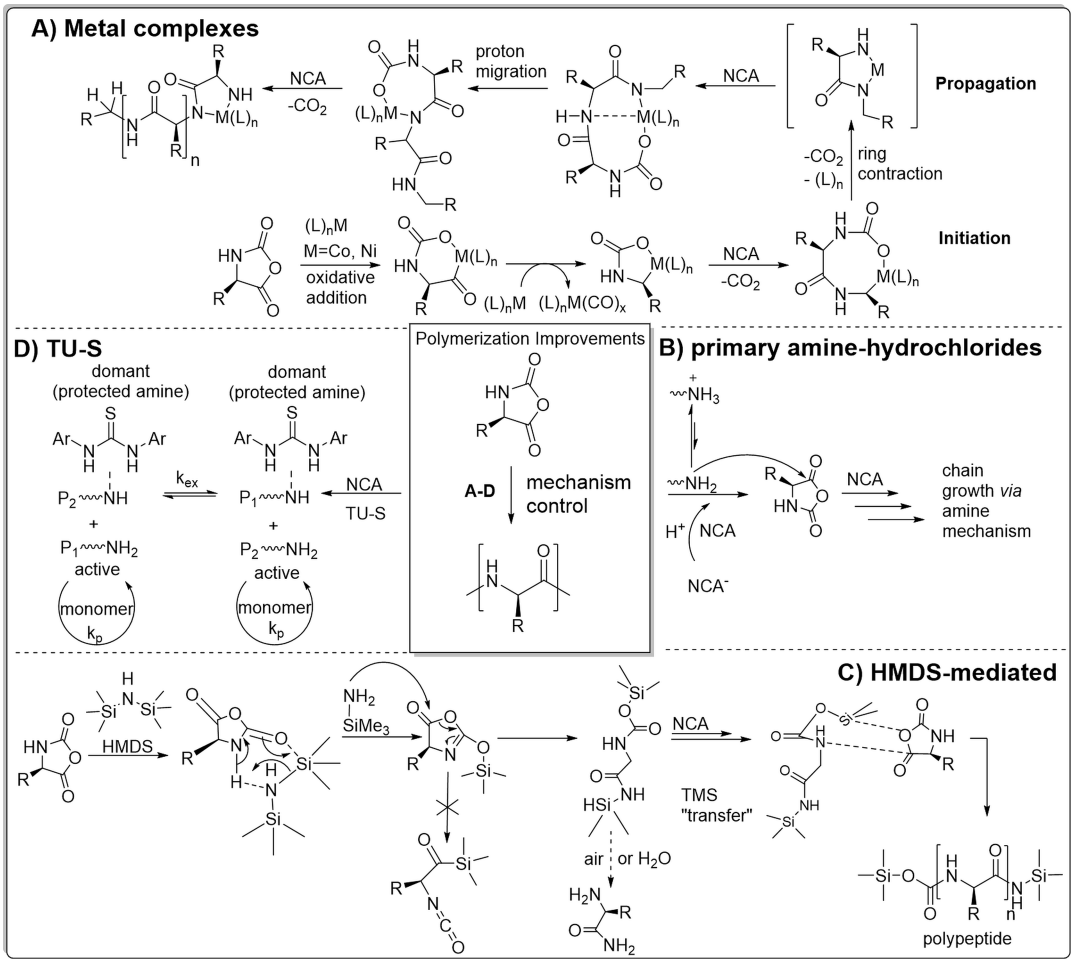

Figure 12. Improvements and mechanism in the polymerization of α-amino acid N-carboxyanhydrides by initiation *via* **A**) metal complexes[189], **B**) primary amine hydrochlorides[190], **C**) HMDS-mediated[191] and **D**) *N*,*N*′-bis[3,5-bis(trifluoromethyl)phenyl]thiourea (TU-S).[192]

1.4.3.1 Metal-based initiators

The design of amine initiators with transition metals based on organo-cobalt and nickel compounds[193] were effective to overcome side- and termination reactions during the polymerization (Figure 12A). The bipyNi(COD) (bipy = 2,2′-bipyridyl, COD = 1,5-cyclooctadiene) and the $(PMe_3)_4Co$ complexes gave living kinetics during the polymerization resulting in low PDI′s.[189] Furthermore, experiments with Pt-, Ir-, Ru- and Fe-based initiators revealed a successful initiation but the control of the molecular weight and the prevention of side reactions is limited.[194-196] The major drawback of this method is the presence of metal-ions in the final polypeptide due to the difficult purification.

1.4.3.1 Primary amino acid hydrochlorides as initiators

Another method for an enhanced control during the polymerization was reported by Schlaad[190], using primary amino acid hydrochlorides as initiators. This initiation method is based on the equilibrium of a

dormant amine hydrochloride and active amine species during the polymerization. The hydrochloride species is protecting the *N*-terminus of the propagating chain and therefore preventing side reactions due to less reactivity. The active amine group is only present for a short time period, propagating the chain by attacking new NCA monomers (Figure 12B). This method leads to polymers with low PDI´s (PDI = 1.03), but complete conversion of the NCAs was not reached after lasted 3 days and strongly depends on the used temperature. The removal of the unreacted monomers is therefore required for further addition of new NCA-monomers or additional post-functionalization of the obtained homo-poly-amino acids. This strategy was found to be effective for the initiation by hydroxyl groups, usually characterized by slow initiations, resulting in broad PDI´s of the obtained polymers due to non-living character of the polymers.[197] Methanesulfonic acid (MSA) can be used as a catalyst in the initiation step to overcome and separate the slow initiation from the propagation step[197], as the acid protonates efficiently catalyze the opening of the NCA-monomer by the hydroxyl group and to protonate the formed amine group after decarboxylation, suppressing further propagation of the chain. After a complete initiation, the protected amine end-group could be activated by addition of a base and a controlled polymerization can proceed. Moreover, the use of ammonium tetrafluoroborate initiator based on neopentyl amine, butylamine, propargyl amine, azide amine as well as polyethylene glycol monomethyl ether amine were found to be effective for the synthesis of well-defined, narrowly distributed (PDI = 1.10 – 1.19) block copolymers by adjusting a precisely degree of polymerization.

1.4.3.3 Silazane-mediated controlled polymerizations

The preventing of side reactions by protecting of the *N*-terminus was also accomplished by using silazane-mediated controlled polymerizations[191]. HMDS (hexamethyldisilazane) was found to be effective for the initiation ROP of Glu-NCA, revealing living polymerization kinetics and remarkable control over the molecular weight without detectable side reactions. The initiation is analogous to group transfer polymerizations of acrylic monomers with organosilicon compounds, but the additional use of Lewis acid activators or nucleophilic catalysts is not required, leading to a metal free, highly controlled route for the ROP of NCAs and following synthesis of block polypeptides (Figure 12C).

Further investigations showed that trimethyl sulfide (S-TMS), especially phenyl trimethylsilyl sulfide (PhS-TMS), mediated controlled ROP´s[198] accelerated the chain initiation. Thus, a better control of the living polymerization was observed. The usage of PhS-TMS leads to narrow PDI´s and controlled molecular weights, revealing a high tolerance for functional groups and the possibility for further functionalization on the *N*- and *C*-terminus, as the *in situ* formed thioester give the potential for native chemical ligation (NCL). The presence of *N*,*N´*-bis[3,5-bis (trifluoromethyl)phenyl]thiourea (TU-S) in aminoaclochol-initiaton systems stimuli activate the NCA-monomer and deactivate the propagating chain ends, resulting in high controlled polymerizations (Figure 12D).[192]

Catalyzed ROP of Glu-NCA could also be realized with the use of fluorinated alcohols without further cocatalysts or metals.[199] Therefore, 1,3-bis(2-hydroxyhexafluoroisopropyl)benzene (1,3-Bis-HFAB) or 1,3-Bis-HFAB in combination with (–)-sparteine tuned the polymerization in respective to the activity and selectivity by forming multiple dynamic hydrogen bonds with the initiator, monomer and the propagating chains, whose activating the monomer and protecting the initiator and polymer chains.[199]

1.4.3.4 Optimization of pressure, temperature and solvent systems

The traditional ROP of NCAs could be also optimized by varying experimental conditions like temperature and pressure. As mentioned above, the livingness of the ROP of NCAs strongly depends on the purity of the used monomers as well as the exclusion from water-traces and other impurities.

Hadjichristidis[200] reported about the synthesis of $P^{Bn}Glu_n$ living polypeptides *via* NAM in completely impurity-free polymerization system by using high vacuum techniques (HVT), fulfilling all

criteria of a living polymerization namely, the complete consumption of the monomer, the linearity of M_n with conversion, the stoichiometric control of the molecular weight, narrow molecular weight distributions, and the synthesis of block copolypeptides by sequential monomer addition. The polymerization of Glu-NCA initiated by *n*-hexylamine was accelerated through the use of HVT and N_2-flow, as the decarboxylation of carbamic acid intermediates and the release of nucleophilic amino groups is accelerated. The living character of the polymerization is therefore more pronounced, side reactions are prevented and the speed of the nitrogen flow clearly influences the NCA-consumption.

Furthermore, the reaction-temperature was found to be a critical parameter for the livingness of the ROP of several NCAs[187, 201], as side reactions, detectable during polymerization at room temperature, are suppressed when polymerizations are carried out at 0 °C. Especially $P^{Bn}Glu_n$ and $P^{Bn}Asp_n$ obtained by ROP of Glu-NCA reveale a strong dependency on the reaction temperature, as systematic investigations clearly show an increasing rate of intramolecular cyclization and side reactions with DMF with increasing temperature in a range of 0 °C – 60 °C, resulting in "dead" chain ends and high PDI´s.[188] The decrease in the reaction temperature to 0 °C and additional N_2-purging during the polymerization prevented the observed side reactions, resulting in the control over the molecular weights and polymers with narrowed PDI´s.

New solvent systems were found to be effective for the design of block copolypeptides, enabling a fast polymerization without side reactions in water-chloroform emulsion systems.[202] First aqueous ROP was realized by using α-amino-poly(ethylene oxide) as macroinitiator, protecting the monomers by spontaneous self-assembly and yielding the obtained deblock copolymers as nanoparticles.[203] As the polymerization also depends on the stability of the NCA`s monomers, *N*-phenoxycarbonyl α-amino acids (AA-NPC´s) were found to be stable on air and tolerant against nucleophilic impurities such as water and alcohols, enabling a controlled polymerization on air.[204]

1.5 Hybrid-block copolymers based on glutamic- and aspartic acid

Moreover, the ROP was found to be an effective tool for the synthesis of hybrid block-copolymers, combining several polymerization techniques for the attachment of non-poly-amino acid blocks to poly-amino acid chains. In general, hybrid polymers in combination with ROP of NCAs can be synthesized by three different techniques (Figure 13): A) Side chain functionalities can be introduced in the NCAs monomers and as a result in the corresponding polypeptide chain, B) the functionality is introduced by the used initiators for the ROP of NCAs on the *C*-terminus of the peptide chain and C) chemical modification of the *N*-terminus polypeptide NH_2 end-groups obtained after ROP of NCAs.

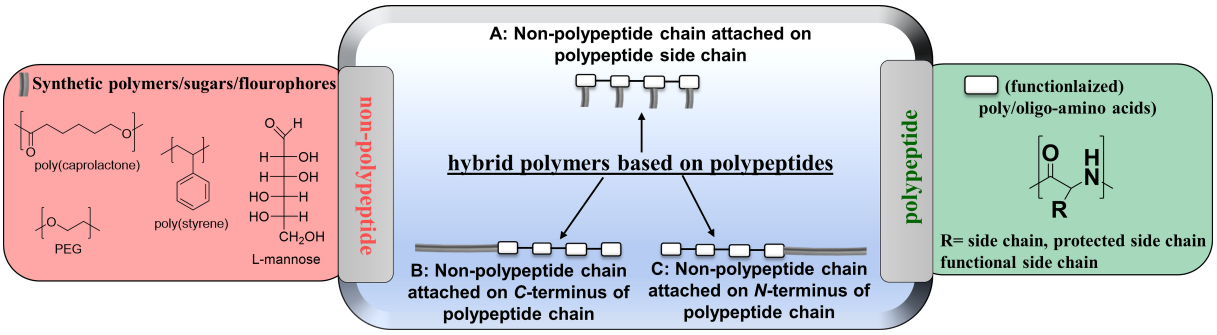

Figure 13. Routes for the synthesis of hybrid polymers based on poly/oligo amino acids with non-polypeptide blocks by **A**) introduction of the non-polypeptide block in the polypeptide side-chain or attachment on **B**) *C*- or **C**) *N*-terminus.

1.5.1 Non-polypeptide chain attached on the polypeptide side chain

The chemical modification of the side chains in NCAs allows the combination of different post-modification and polymerization techniques grafting from the side chain of the polypeptide with ROP of NCAs, especially alkene[205-213] for photo induced crosslinking[209], Michael addition[174], ozonolysis[206] and most important thiol-ene click reaction.[205, 211, 212] As also the other types of click reactions play an important role for post-modification of poly-amino acids, the incorporation of alkyne-[214-218], azide-[219] and thiol-groups[220] offer a variety of possibilities. Thioether[221-223] and selenoether[224] can be attached for oxidation reactions, halogens[225-230] for atomic transfer radical polymerization (ATRP) and nucleophilic reactions (Figure 14).

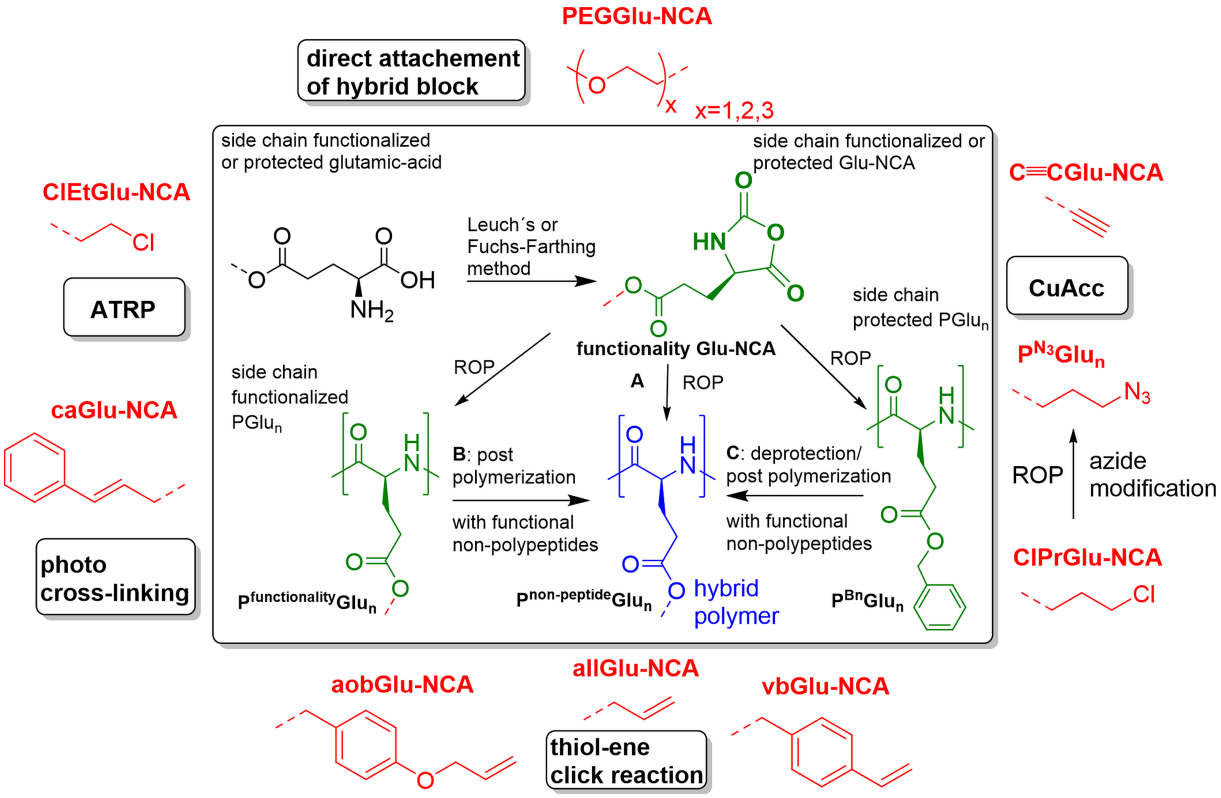

Figure 14. Methods for the synthesis of hybrid polymers on the base of side-chain functionalization of glutamic acid by **A**) ROP of non-polypeptide side-chain functionalized Glu-NCA, **B**) Introduction of various functional groups in NCAs and post polymerization with a functional non-polypeptide grafting from the side chain and **C**) the ROP of Glu-NCA, followed by deprotection and attachment of functional non-polypeptides.[171, 173]

Thus, ROP of γ-2-chloroethyl-L-glutamate NCA (ClEtGlu-NCA) and subsequent ATRP with 2-aminoethyl methacrylate hydrochloride grafting from the polypeptide side chains lead to vesicles, directly self-assemble in PBS.[231] Not even reactive groups, also long residues could include special properties into the polymeric chains, as thermo-responsive poly amino acids are available by attaching PEG[213] side chain groups on NCAs. Thus, PEG side chain functionalized P^{Bn}Glu$_n$ were synthesized directly from polymerization of oligo-PEG side chain functionalized Glu-NCA (PEGGlu-NCA), displaying lower critical solution temperature in water tunable *via* copolymerization with other NCA-monomers[232] as well as β-sheet to α-helix transition with increasing molecular weight in solid state and α-helical conformation in aqueous solution, self-assembled into nanostructures.[233] Introduction of PEG side chain functionality could also be realized by ROP of γ-propargyl-l-glutamate (C≡CGlu-NCA) and subsequent click reaction of azido functionalized PEG.[214, 234] Introduction of side chain azido

functionality by ROP of γ-chloropropyl-L-glutamic acid NCA (ClPrGlu-NCA) followed by converting to azido group and offers the opportunity for subsequent click reaction with alkyne substituted poly-L-lactide-PEG to core-shell molecular bottle-brushes with helical polypeptide backbone[235] or mannose revealing α-helical conformation in aqueous solution.[226] The latter one could also be attached on azido and allyl dual-functionalized poly(γ-allyl-L-glutamate)-*b*-poly(γ-azidopropyl-L-glutamate) block copolypeptides synthesized by ROP of γ-allyl-L-glutamic acid NCA (allGlu-NCA) and γ-chloropropyl-L-glutamic acid NCA followed by nucleophilic substitution with NaN_3, allowing the modification *via* click-chemistry and thio-ene addition.[207] UV-triggered thio-ene reaction was also used for the synthesis of charged polypeptides based on ROP of γ-(4-Allyloxylbenzyl)-L-glutamate *N*-carboxyanhydride (AOBGlu-NCA) and subsequent modification with 2-aminoethanethiol, building water-soluble materials with stable α-helical conformation unaffected by low molecular weights of the peptides, changes in pH, temperature, as well as salt and urea concentrations.[208]

1.5.2 Non-polypeptide chain attached on the C-terminus of the polypeptide chain

Hybrid polymer synthesis, based on the polypeptide chain *C*-terminus modification *via* the used initiators for the ROP of NCAs, can be differentiated between two types: A) initiation by amine-terminated macroinitiators and B) introduction of end-functionality by the used initiator (Figure 15).

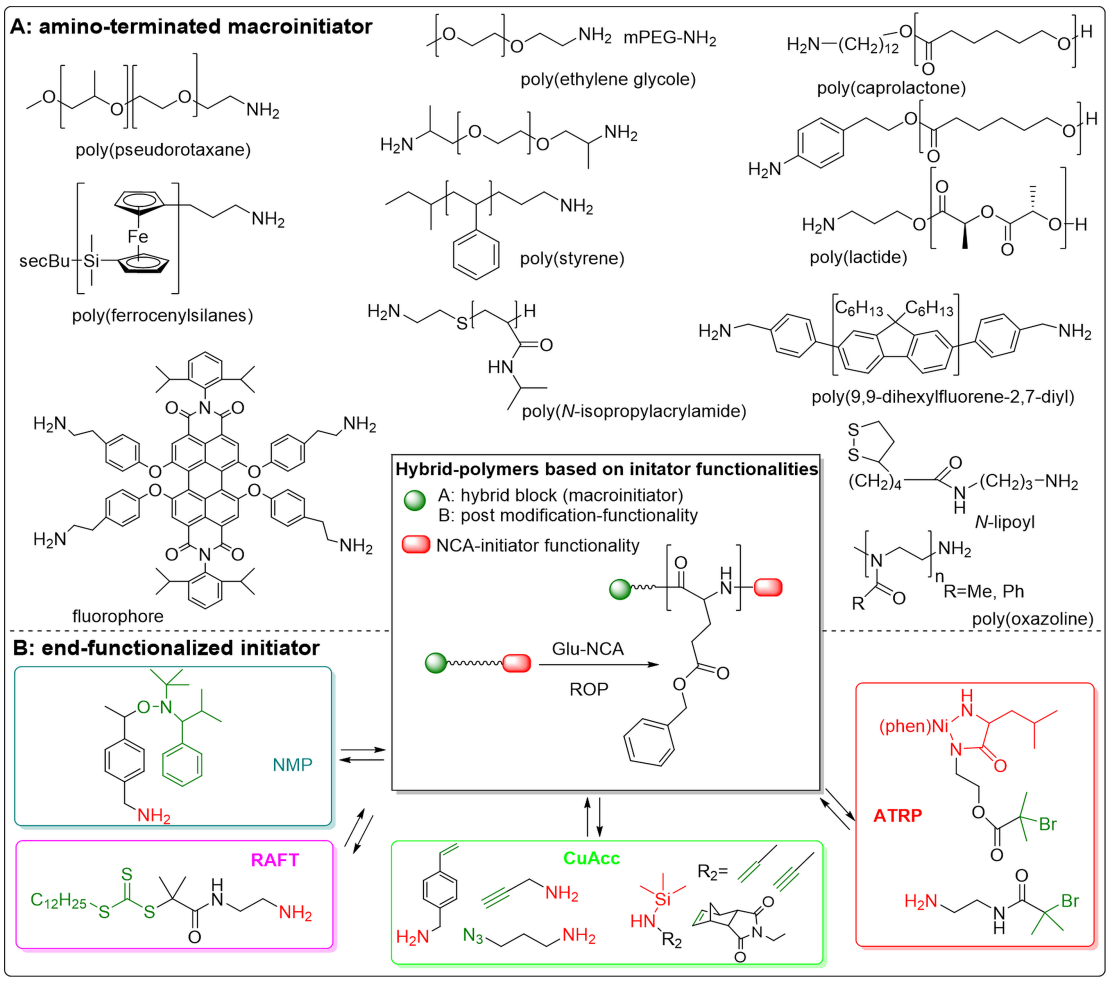

Figure 15. Synthesis of hybrid polymers with non-polypeptide attached on *C*-terminus of polypeptide by initiation of ROP of Glu-NCA with **A**) amino-terminated, non-polypeptide macroinitiators or **B**) introduction of various functional groups in polypeptides by initiation with end-functionalized initiators and further post modification with various polymerization methods.[171, 173]

As hybrid polymers are easy accessible *via* the initiation with macroinitiators (Figure 15A), the ROP of amine end group functionalized PEG[236-238] was used for the ROP of Glu-NCA, e.g. forming nanoparticles with PEO as hydrophilic and $P^{Bn}Glu_n$ as hydrophobic component, in which the PEG blocks extend out as shell in aqueous medium.[236] Moreover, the helical screw sense of the $P^{Bn}Glu_n$ block depends on the PEG content, as increasing mol% of PEG in the block copolymer lead to a change from right to left-handed helical conformation in various solvents. Furthermore, amine terminated poly(2-methyl-2-oxazoline)[239], polypseudorotaxane[240], Poly-L-Lactide[241], aminophenyl- or 4-aminobenzoyl-terminated poly(ε -caprolactone) [242-244], amine-terminated PNIPAA[245] and primary amine-terminated poly(styrene)[246] could all be successfully used for the initiation of Glu-NCA, resulting in linear hybrid block co- or triblock polymers. Moreover, ROP of Glu-NCA with *N*-lipoyl-1,3diaminopropane lead to self-assembled monolayers on gold substrates.[247, 248] and fluorescence active perlylene-initiator attached on deprotected ^{Bn}Glu-domains introduces a pH-dependent helix-coil transition of the poly-amino acid blocks in water.[249]

Introduction of functional groups on the end of the initiator offers a variety of post-modification polymerization techniques depending on the introduced functional group and the position of the functional moiety, which can be differentiated to α-position or the ω-position (Figure 15B). The combination of ROP of NCAs with controlled radical polymerization techniques, namely atom transfer radical polymerization (ATRP), reversible addition-fragmentation chain-transfer (RAFT) and nitroxide-mediated polymerization (NMP), could be realized by the ROP of the corresponding NCAs with halogen functionalized initiators and offers an opportunity for well-defined hybrid polymers with different architectures.[171] Due to the advantageous combination of controlled polymerization techniques, this route can easily carry out in one pot without intermediate purification steps.
Thus, the development of a bifunctional initiators containing either a Ni-amido amidate complex[250] or an amine group[251], useful for the controlled ROP of Glu-NCA in combination with a bromide-end group, which was used for further post-functionalization by ATRP with methyl methacrylate (MMA), lead to the controlled synthesis of well-defined rod–coil hybrid block copolymers. The combination of ROP of Glu-NCA with RAFT-polymerization was realized using an amino-functionalized RAFT-agent as dual initiator, leading to thermo- and pH-responsive hybrid-polymers consisting of $P^{Bn}Glu_n$ and poly-*N*-isopropylacrylamide (NIPAM) blocks.[252] Initiation with 4-vinyl benzylamine lead to polymers with styrene end-groups, allowing the further development of star-polymers *via* RAFT or free radical polymerization by using Divinylbenzene as cross-linking agent.[253] After deprotection of the $P^{Bn}Glu_n$ side chains and formation of $PGlu_n$, a pH-dependent solubility in water was observed, as at high pH-values (pH=8-11) the material becomes water-soluble, whereas at acidic conditions the polymers are precipitating, suggesting a core-shell structure of the hybrid-polymers and allow these materials to apply pH responsive nanocontainers. Polystyrene (PS)-$P^{Bn}Glu_n$-hybrid polymers are accessible by the combination of ROP with NMP by usage of a dual initiator containing a primary amine and a nitroxide group[254], conducted in one pot without further intermediate purification steps and allows the investigation of pH-responsive nanoparticles after deprotection of the $P^{Bn}Glu_n$-side chain.

In recent years, development of click reaction lead to a variety of opportunities for the synthesis of hybrid polymers. The modification of initiator systems bearing an amine and an azido- or alkyne-group, allows the combination of ROP of NCAs followed by post-modification with non-polypeptide blocks *via* click chemistry. Thus, α-azido-3-aminopropane and α-alkyne-propargylamine bifunctional initiators could be used for the synthesis of well-defined $P^{Bn}Glu_n$-poly(2-(dimethylamino)ethyl methacrylate (PDMAEMA) by ROP of Glu-NCA initiated by the amine group and following click-reaction of the corresponding α-azido or α-alkyne modified PDMAEMA.[255] The $P^{Bn}Glu_n$ blocks could further be deprotected in the side chain, allowing the formation of pH- and temperature responsive hydrophilic

block copolymers.[256] As mentioned above, HMDS-mediated polymerization lead to a high control of polymer mechanism, resulting in molecular weight controlled, low PDI polymers. Cheng *et al.*[257] developed *N*-TMS allylamine, propargylamine- and *N*-(aminoethylene)-5-norbornene-endo-2,3-dicarboximide-amine-functionalized initiators with allowing a facile functionalization on the *C*-terminus of poly-^{Bn}Glu peptides *via* click-chemistry or ROMP.

1.5.3 Non-polypeptide chain attached on the N-terminus of the polypeptide chain

Chemical modification of the *N*-terminus NH_2-end functional groups was realized in the synthesis of PEG-*b*-$P^{Bn}Glu_n$-*b*-(polymer)-*b*-$P^{Bn}Glu_n$-*b*-PEG (polymer = polyoctenamer, poly(ethylene glycol), or poly(dimethylsiloxane)) pentablock copolymers, in which the functionalized middle segment were used as macroinitiator for the ROP of Glu-NCA, followed by capping the *N*-terminus with isocyanate terminated PEG.[258] With this strategy, the formation of end-capped *C*-terminal functionalized polypeptides and the facile functionalization of the *N*-terminus of polypeptides from NCA polymerizations was demonstrated. Moreover, a combination of α-helical and β-sheet forming blocks could be realized by controlled ROP of Glu-NCA wit [Ni(cod)(bpy)]-complex, followed by addition of and two different polyisocyanide blocks, namely, poly((S)-(—)-α-methylbenzyl isocyanide) (PMBI) and poly(L-isocyanoalanyl-l-alanine methyl ester) (L,L-PIAA).[259] A summary for the synthesis of hybrid polymers given in literature is shown in Table 5.

Table 5. Summary for design of hybrid-polymers based on $P^{Bn}Glu_n$ and $P^{Bn}Asp_n$ as peptide blocks presented in the literature.

Ref.	polypeptide block	non-polypeptide block	functionality	hybrid polymer
A) non-polypeptide block attached on poly-amino acid side chain				
232, 233	$PGlu_n$	PEG	side chain modification of VB-Glu-NCA (PEGGlu-NCA)	$P^{PEG}Glu_n$
141, 234	$PGlu_n$	PEG	γ-propargyl-L-glutamate NCA (C≡CGlu-NCA) click-reaction with azido functionalized PEG	$P^{PEG}Glu_n$
231	$PGlu_n$	oligo(2-aminoethyl methacrylate hydrochloride) (PLG)	γ-2-chloroethyl-L-glutamate NCA (ClEtGlu-NCA) ATRP with 2-aminoethyl methacrylate hydrochloride	$P^{PLG}Glu_n$
235	$PGlu_n$	PLA-PEG	γ-chloropropyl-L-glutamic acid NCA (ClPrGlu-NCA) with subsequent azide modification and click reaction with poly-L-lactide (PLA)-PEG	$P^{PLA\text{-}PEG}Glu_n$
226	$PGlu_n$	mannose	γ-chloropropyl-L-glutamic acid NCA (ClPrGlu-NCA) with subsequent azide modification and click reaction with mannose	$P^{mannose}Glu_n$
207	$PGlu_n$	mannose and 3-mercaptopropionic acid (MCPA)	γ-allyl-L-glutamic acid NCA (allGlu-NCA) and ClPrGlu-NCA modification *via* click- and thiol-ene reaction	$P^{mannose}Glu_n$-*b*-$P^{MCPA}Glu_n$
208	$PGlu_n$	2-aminoethanethiol (AET)	γ-(4-Allyloxylbenzyl)-L-glutamate *N*-carboxyanhydride (AOBGlu-NCA) and subsequent modification with 2-aminoethanethiol (AET)	$P^{AET}Glu_n$

Ref.	polypeptide block	non-polypeptide block	functionality	hybrid polymer
B) non-polypeptide chain attached on *C*-Terminus of poly-amino acid				
(functionalized) macroinitiator				
236	$P^{Bn}Glu_n$	PEG	amine-functionalized macroinitiator	PEG-*b*-$P^{Bn}Glu_n$
237	$P^{Bn}Glu_n$ $P^{Bn}Asp_n$	PEG	ammonium-chloride functionalized macroinitiator	PEG-*b*-$P^{Bn}Glu_n$ PEG-*b*-$P^{Bn}Asp_n$
238	$P^{Bn}Glu_n$	PEG	amine-bifunctionalized macroinitiator	$P^{Bn}Glu_n$-*b*-PEO-*b*-$P^{Bn}Glu_n$
239	$P^{Bn}Glu_n$	poly(2-methyl-2-oxazoline)	ω-amine-terminated poly(2-methyl-2oxazoline)	poly(2-methyl-2-oxazoline)-*b*-$P^{Bn}Glu_n$
240	$P^{Bn}Glu_n$	$P(EO_{19}\text{-r-}PO_3)\text{-}NH_2$	macroinitiator polypseudorotaxane	$P(EO_{19}\text{-r-}PO_3)$-*b*- $P^{Bn}Glu_n$
241	$P^{Bn}Glu_n$	L-lactide	macroinitiator L-lactide, amine functionalized L-Lactide	PLLA-*b*-$P^{Bn}Glu_n$
260	$P^{Bn}Glu_n$	PEG and PLLA	Macroinitiator PEG for ROP of L-Lactide and amine-functionalized macroinitiator PLLA	PEG-*b*-PLLA-*b*- $P^{Bn}Glu_n$
261	$P^{Bn}Asp_n$	PLLA	ROP of L-Lactide and amine-functionalized macroinitiator PLLA	PLLA-*b*-$P^{Bn}Asp_n$
242	$P^{Bn}Glu_n$	PCL	amine-functionalized macroinitiator	P(ε-CL)-*b*-$P^{Bn}Glu_n$
243	$P^{Bn}Glu_n$	PCL	aminophenyl-terminated PCL	P(ε-CL)-*b*-$P^{Bn}Glu_n$
244	$P^{Bn}Glu_n$	PCL	4-aminobenzoyl-terminated poly(ε -caprolactone)	$P^{Bn}Glu_n$-P(ε-CL)-*b*-$P^{Bn}Glu_n$
245	$P^{Bn}Glu_n$	PNIPAA	amine-terminated PNIPAA	PNIPAA-*b*-$P^{Bn}Glu_n$
246	$P^{Bn}Glu_n$	PS	primary amine-terminated poly(styrene)	PS-$P^{Bn}Glu_n$
247, 248	$P^{Bn}Glu_n$ $P^{Bn}Asp_n$	SS	N-Lipoyl-1,3-diaminopropane	SS-$P^{Bn}Glu_n$
262	$P^{Bn}Glu_n$	PHF	benzylamine end-functionalized polyfluorene macroinitiators	$P^{Bn}Glu_n$-*b*-PHF-*b*-$P^{Bn}Glu_n$
263	$P^{Bn}Glu_n$	PS and PI	amine functionalized PS and PI	$P^{Bn}Glu_n$-*b*-PS-*b*-$P^{Bn}Glu_n$ $P^{Bn}Glu_n$-*b*-PI-*b*-$P^{Bn}Glu_n$ PBLL-*b*-$P^{Bn}Glu_n$-*b*-PS-*b*-$P^{Bn}Glu_n$-*b*-PBLL
264	$P^{Bn}Glu_n$	PFS (Polyferrocenylsilane)	Anionic polymerization of Dimethyl[1]silaferrocenophane and modification to amino-terminated PFS	PFS-*b*-$P^{Bn}Glu_n$
end-group functionalized initiator				
Combination of ROP of NCAs with (controlled) radical polymerization				
252	$P^{Bn}Glu_n$	P(*N*iPAM)	amine-functionalized RAFT-agent	$P^{Bn}Glu_n$-*b*-P(*N*iPAM)
250	$P^{Bn}Glu_n$	MMA	bromide- and Ni-bifunctional initiator used for a sequence of a nickel-catalyzed initiated ROP of Glu-NCA and atom transfer radical polymerization (ATRP)	$P^{Bn}Glu_n$-*b*-PMMA

Ref.	polypeptide block	non-polypeptide block	functionality	hybrid polymer
[251]	$P^{Bn}Glu_n$	MMA	bromide- and amine-bifunctional initiator used for amine initiated ROP of Glu-NCA and atom transfer radical polymerization (ATRP)	$P^{Bn}Glu_n$-*b*-PMMA
[254]	$P^{Bn}Glu_n$	PS	nitroxide- and amine-bifunctional initiator used for a sequence of an amine initiated ROP of Glu-NCA and nitroxide-mediated polymerization (NMP)	$P^{Bn}Glu_n$-*b*-PS
Combination of ROP of NCAs with CuAcc				
[255, 256]	$P^{Bn}Glu_n$	poly[2-(dimethylamino)ethyl methacrylate] (PDMAEMA)	α-alkyne or α-azide difunctional amine-initiators for ROP of Glu-NCA and subsequent Huisgen's 1,3-dipolar cycloaddition with α -alkyne-PDMAEMA or α -azido-PDMAEMA	$P^{Bn}Glu_n$-*b*- PDMAEMA and $PGlu_n$-*b*- PDMAEMA
C) non-polypeptide chain attached on *N*-Terminus of poly-amino acid				
[258]	$P^{Bn}Glu_n$	PEG POCT (polyoctenamer) PDMS poly(dimethylsiloxane)	α,ω-diamino-terminated polymers as difunctional macroinitiators for the ROP of Glu NCA to form triblock copolymers, functionalization of the *N*-terminal ends of polypeptides with end-capped isocyanate terminated poly(ethylene glycol) to give the pentablock copolymers	PEG-*b*-$P^{Bn}Glu_n$-*b*-POCT-*b*-$P^{Bn}Glu_n$-*b*-PEG, PEG-*b*-$P^{Bn}Glu_n$-*b*-PEG-*b*-$P^{Bn}Glu_n$-*b*-PEG and PEG-*b*-$P^{Bn}Glu_n$-*b*-PDMS-*b*- $P^{Bn}Glu_n$-*b*-PEG
[259]	$P^{Bn}Glu_n$	PMBI or L,L-PIAA	nickel-catalyzed ROP of Glu-NCA followed by addition of isocyanide	$P^{Bn}Glu_n$-*b*-PMBI and $P^{Bn}Glu_n$-*b*- L,L-PIAA

2 Aim of the thesis

2.1 Objective and motivation

The aim of the thesis was the development of a new class of multisegmented hybrid polymers based on (a-)chiral single-/oligo-amino acids as biochemical component in combination with synthetic segments and their systematic investigation on their properties on a molecular level (Figure 16). For this purpose, single- and oligo-amino acids embed into PE-type polymers had to be designed and investigated in the secondary structure formation of the amino acid building blocks as well as in the crystallization behavior of the middle-segments.

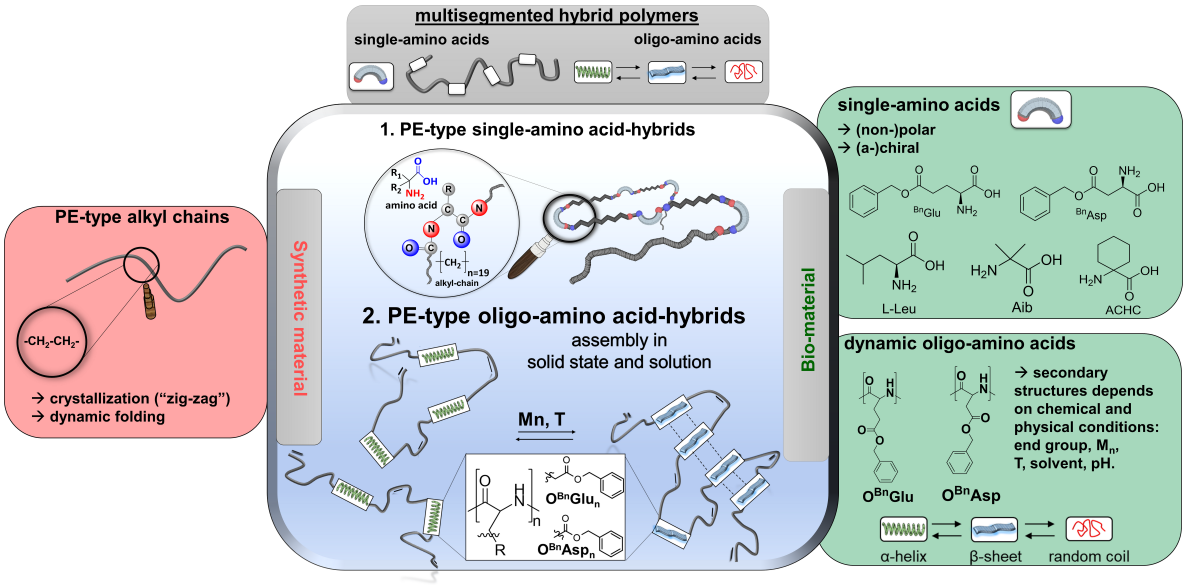

Figure 16. Design of new hybrid polymers based on the combination of dynamic-/constrained single-/oligo-amino acids as bio-component and PE-type alkyl chains or azo-compounds as synthetic material with main focus on the synthesis and investigation of PE-type oligo-amino acid hybrids.

In the first part, the crystallization of the middle-segmented PE-type chains should be prepared and investigated. Single-amino acids (chiral/achiral, polar/non-polar) had to be embeded into PE-type alkyl chains, which should act as "defects" incooperated in the PE-type middle segments (Figure 16). The individual mechanical and thermal properties as well as the crystallization behavior of these polymers should be engineered by repetitively placing the different types of amino acids at specific positions within the polymer chain of defined origin. Size, polarity and the steric structure of the amino acid-"defects" should determine the final crystallization behavior in the solid state.

In the second part, oligo-amino acids of $^{Bn}Glu_n$ and $^{Bn}Asp_n$ had to be incooperated in PE-type alkyl chain middle-segments (Figure 16). The oligo-amino acids should act as dynamic folding elements, introducing conformational changes within these multisegmented polymers. Therefore, the secondary structure formation of the oligo-amino acid building blocks had to be investigated in either HFIP-solution or the solid state. The secondary structure of $^{Bn}Glu_n$- or $^{Bn}Asp_n$-oligomers exist as a mixture of random coils, α-helices, β-sheets and other conformations and should be tuned *via* their nature, chain length or the (bio-)chemical and physical environments.

In the third part, conformational constrained-amino acids should be designed and systematically investigated in regard to their final conformation (Figure 17). The main focus should be the investigation

of the ROP of the corresponding NCAs with different classes of initiator systems and the characterization of their final chain length and end-groups. As the mechanism is not well studied yet, choice of parameters like temperature, concentration as well as solvent systems should varied. Furthermore, the different initiator systems should introduce individual properties into the oligomeric systems, which had to be investigated on a molecular level. Therefore, chiral amino acid-methyl esters should be used as initiators, leading to an attachment of a chiral residue on the *C*-terminus of the achiral helical domain. The possibility to ensure a chirality transfer of the initiator to the polymer chain and the resulting introduction of a certain screw-sense preference (P= right-handed, M=left-handed) of the helix by the ROP of the NCA should be the basic goal. Furthermore, the polymerization of the conformational constrained amino acid NCAs should initiated by bivalent azo-compounds and the final material had to be investigated in their *trans*/*cis*-isomerization behavior of the attached azo-initiator.

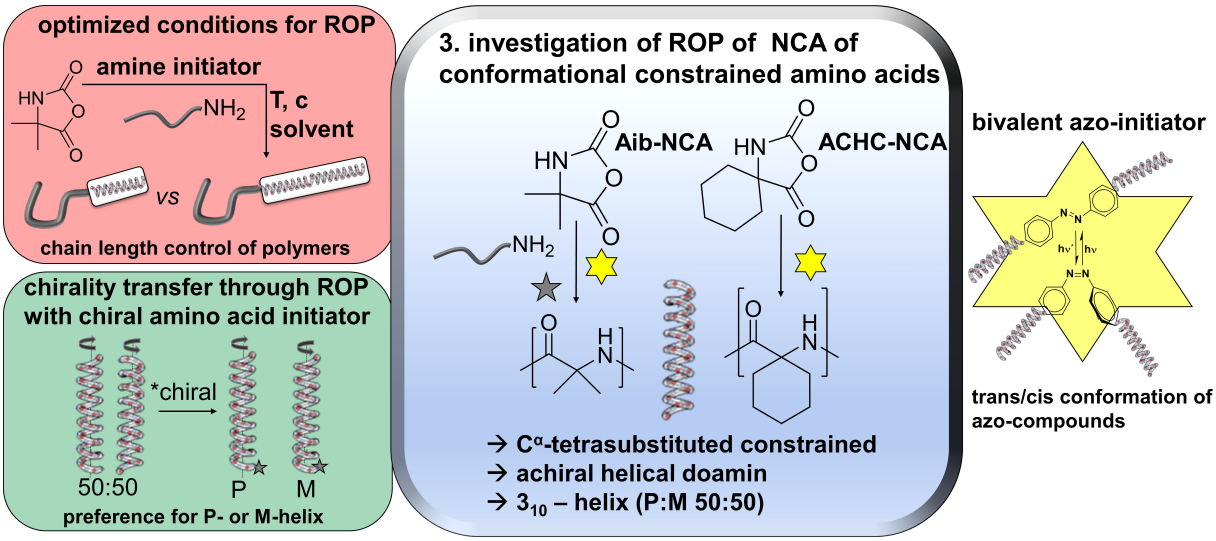

Figure 17. Investigation of the ROP of conformational constrained amino acids with different initiators and the investigation of the obtained materials with main focus on the optimized conditions for the ROP and the chirality transfer by amino acid-methyl esters.

2.2 Concept

To ensure the crystallization of the PE-type middle segments, single-amino acids were embedded in PE-type alkyl chains resulting in highly defined hybrid polymers. Therefore, *N*- and *C*-terminus ω-alkene-chain functionalized benzyl protected glutamic acid (Glu), benzyl protected aspartic acid (Asp), L-leucine (Leu), 2-aminoisobutyric acid (Aib) and 1-aminocyclohexanecarboxylic acid (ACHC) were synthesized. For *N*-terminus functionalization with 10-undecenoyl chloride Einhorn-Method were used for polar benzyl protected glutamic acid and benzyl protected aspartic acid, whereas non-polar L-leucine, 2-aminoisobutyric acid and 1-aminocyclohexanecarboxylic acid were functionalized *via* Schotten-Baumann method. *C*-terminus functionalization were realized by amidation of the *N*-terminus functionalized amino acids with 10-undecen-1-amine. The synthesis of the polymers was accomplished by ADMET polymerization of the chosen *N*- and *C*-terminus ω-alkene-chain functionalized amino acids. Acyclic diene metathesis polymerization (ADMET)[265] has proven to be an excellent tool to achieve a poly(ethylene) (PE)-like chain with functional monomers at precise locations.[266, 267] For the investigation of the influence on the chiral/achiral and polar/nonpolar nature of the amino acids on the crystallization behavior, chiral/polar amino acids glutamic (Glu) and aspartic acid (Asp), chiral/non-polar L-leucine (Leu) and achiral/non-polar 2-amino-2-methylpropanoic (Aib) acid and 1-aminocyclohexane-carboxylic acid (ACHC) ADMET-polymers were hydrogenated with *p*-toluenesulfonyl hydrazide ($TsNHNH_2$) (Figure 18).

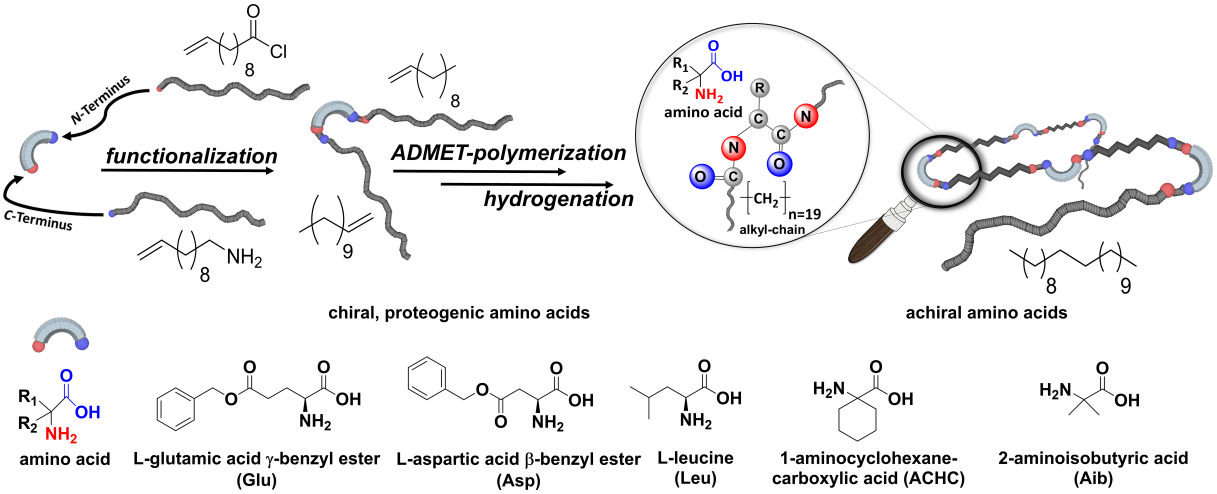

Figure 18. Schematic representation of the synthesis of PE-type precision polymers with amino acid defects.

The synthetic approach towards the multisegmented polymers containing $O^{Bn}Glu_n$ and $O^{Bn}Asp_n$ units (O^{Bn}amino $acid_{n=\text{number amino acids units}}$) is based on a combination of ring-opening polymerization (ROP) of *N*-carboxyanhydrides (NCA) followed by *N*-terminus functionalization to achieve control over the oligo-amino acids ($O^{Bn}Asp_n$, $O^{Bn}Glu_n$)-segments, followed by ADMET polymerization of appropriately *C*- and *N*-terminal bis-vinyl-functionalized oligo-amino acids to separate them by methylene-segments along a polymer chain (Figure 19). From a molecular design-point, the interrupting alkyl-units act as flexible spacer unit spatially separating the oligo-amino acids along the polymer chain, but also constraining them within the same chain. In order to check for a potential crystallization of the alkyl-units, a chain length (19-CH_2- units), able to crystallize into well-known crystal lattices as known from more simple systems with small defects within precision-polymers, was used.[268] ROP of *N*-carboxyanhydrides was initiated by 10-undecene-1-amine, followed by the modification on the *N*-

terminus *via* 10-undecenoylchloride to attach vinyl end-groups on both sides, yielding the *C*- and *N*-vinylic amino acid oligomers **O^{Bn}Glu$_3$ (7a)**, **O^{Bn}Glu$_{10}$ (8a)**, **O^{Bn}Asp$_3$ (9a)** and **O^{Bn}Asp$_{10}$ (10a)**, which subsequently were polymerized *via* Grubbs catalyst first generation (Grubbs 1st) catalyzed ADMET polymerization (Figure 19). Amino acid building blocks of the so obtained polymers **AP$_{21}$(^{Bn}Glu$_3$) (7b)**, **AP$_3$(^{Bn}Glu$_{10}$) (8b)**, **AP$_{18}$(^{Bn}Asp$_3$) (9b)** and **AP$_4$(^{Bn}Asp$_{10}$) (10b)** (AP$_{m=\text{polymer-repetitive units}}$(^{Bn}amino acid$_n$)) are thus separated by exactly 19 methylene-units, interrupted by one internal double bond between carbons 9 and 10. The obtained polymers were subsequently purified by preparative GPC to generate samples with low *Đ* and defined molecular weights. The repetitive incorporation of the amino acid blocks into a poly-(alkyl)chain allows to study the assembly behavior between these oligo-amino acid blocks as well as the influence on the secondary structure formation in HFIP-solution and in solid state.

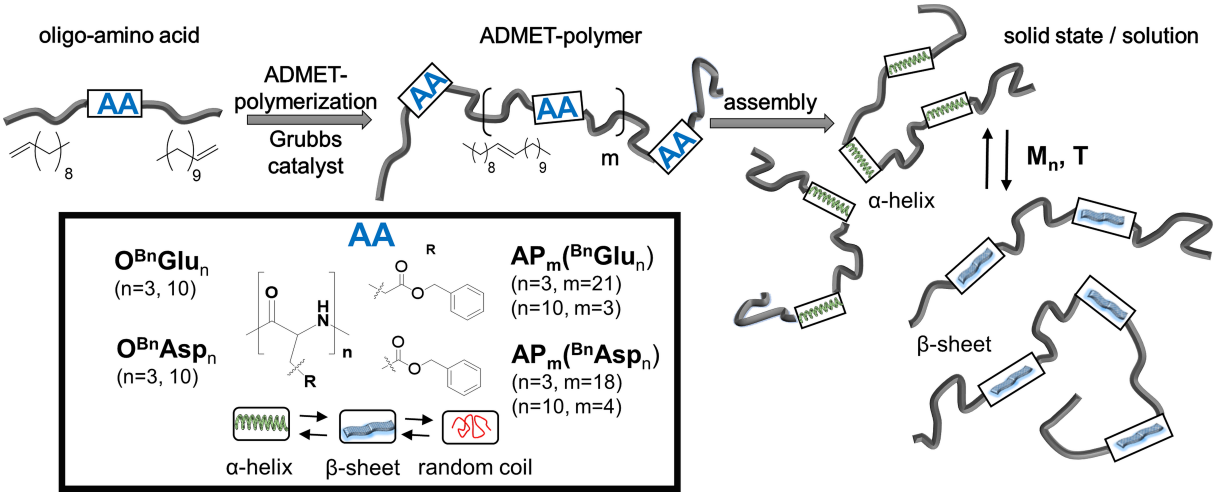

Figure 19. Concept to prepare multisegmented polymers **AP$_m$(^{Bn}Asp$_n$)** or **AP$_m$(^{Bn}Glu$_n$)** containing repetitive amino acid units in their main chain *via* ROP and ADMET-polymerization. Assembly of these polymers is subsequently investigated in HFIP-solution and the solid state by changing the molecular weight, and temperature.

For the investigation of the ROP of NCAs of conformational constrained amino acids 2-aminoisobutyric acid (Aib) and 1-aminocyclohexanecarboxylic acid (ACHC) the used NCAs **11** and **12** were synthesized by Fuchs-Farthing method with triphosgene. For ROP of Aib-NCA (**11**) with common amine initiators chemical environment like solvents (solid state / solution), concentrations and *M*/*I* ratios as well as physical conditions like temperature are varied and the results of the final chain length and end-group analysis are compared by MALDI-TOF-MS and ^{1}H-NMR. The used initiator **A4** was synthesized by conversion of **A3** with $NaCNBH_3$ after amidation of 10-undecenoylchloride with $NH_4^+Cl^-$. Kinetic measurements for the ROP of **Aib-NCA** (**11**) with initiator **A2** in MDF was realized by FTIR-measurements in solution (Figure 20A). The chirality transfer is realized by synthesizing amino acid-methylester hydrochlorides of different L- and D-amino acids **16c** – **16j** and their use as initiators for the ROP of **Aib-NCA** (**11**). Potential helical screw sense preference (P- *vs.* M-helix) for the achiral Aib-domain in **17c** – **17j** introduced by the chiral residues is investigated by CD and FTIR-spectroscopic measurements (Figure 20B). The synthetic concept for the combination of bivalent azo-compounds with conformational constrained amino acids was realized by using the synthesized NH_2- and OH-end-grouped azo-compounds **19**, **20** and **21** as initiators for the ROP **Aib-NCA** (**11**) and **ACHC-NCA** (**12**) (Figure 20C). Synthetic route of Initiator **19** is based on the synthesis of literature[269], initiator **20** was designed by deprotection of NHCOMe-group of **18d** with $NaOH/H_2O$. Initiator **21** was synthesized by two steps *in situ* diazotation of (S)-(-)-1,1'-binaphthyl-2,2'-diamine. The optimized conditions for the

ROP are used from former results of the investigation of ROP. The successful attachment of the initiator for obtained polymers **19a**, **19b**, **20a**, **20b, 21a** and **21b** is realized by ^{1}H-NMR and UV-VIS-spectroscopy, as azo-chromophores are well known for stabilizing *trans*/*cis*-isomers under different conditions. The final conformation of azo-chromophore in polymers **21a** and **21b** is investigated by UV-VIS-spectroscopy after irradiation with light of 254 nm and 366 nm.

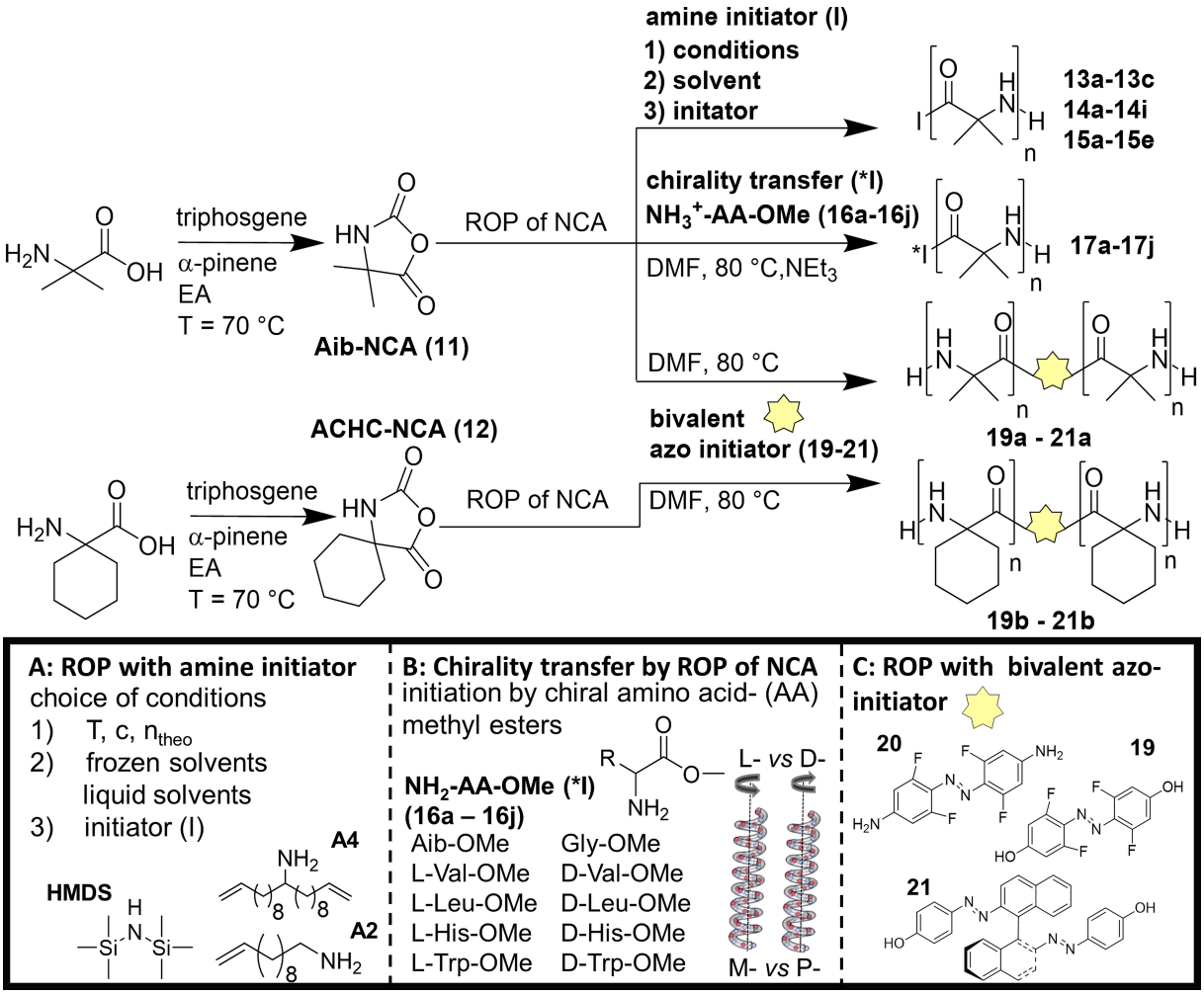

Figure 20. Schematic representation of the investigation of ROP of Aib-NCA with **A**) amine initiators under different conditions, **B**) chiral amino acid-methyl ester as initiators for chirality transfer and **C**) bivalent azo-initiators.

3 Results and discussion

3.1 PE-type-single amino acids hybrid polymers

Parts of the results and discussion as well of the experimental part were already published in

"Precision polymers containing main-chain-amino acids: ADMET polymerization and crystallization" (Freudenberg, J., Poppe, S., Binder, W.H*. *RSC. Adv.* **2017**, *7*, 47507-47519. DOI: 10.1039/C7RA10485E) - Published by The Royal Society of Chemistry and were in parts adapted with permission from The Royal Society of Chemistry (Copyright 2016).

3.1.1 Monomer synthesis

Conceptually, the amino acids were introduced in the polymer structure by fixation of two ω-alkenyl-chains of equal length on either side. Therefore, *N*- and *C*-terminus functionalization was realized by reaction of the amino acid with 10-undecenoyl chloride and afterwards coupling with 10-undecen-1-amine (**A2**) (see Scheme 2).

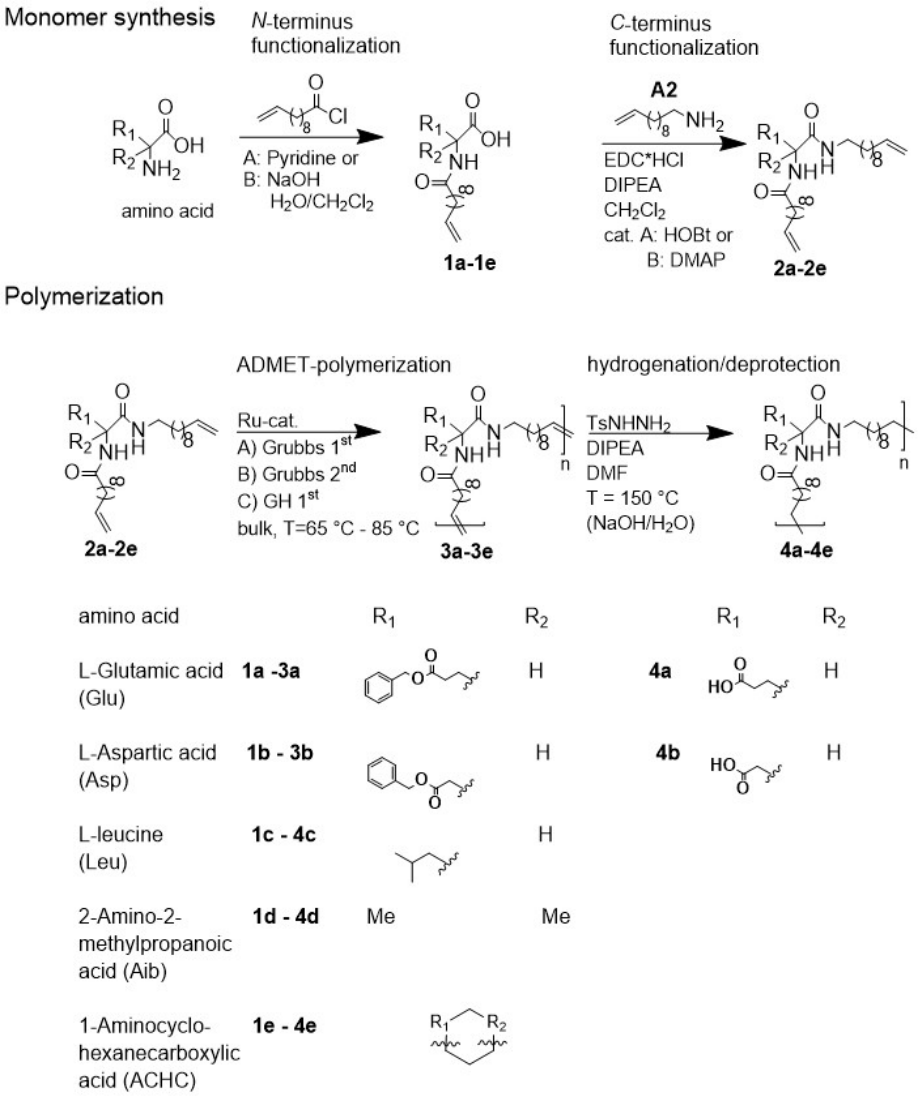

Scheme 2. Synthesis of a) *N*- + *C*-terminus functionalized monomers **2a** – **2e** and b) ADMET-polymers **3a** – **3e** and hydrogenated / deprotected polymers **4a** – **4e**.

For *N*-terminus functionalization pyridine was used as non-ester protected L-glutamic acid and L-aspartic acid **1a** – **1b** or alternatively *via* a two-phase system of aqueous $NaOH/CH_2Cl_2$ mixture (Schotten-Baumann-method) for the synthesis of **1c** – **1e** (for details see Experimental part 4.2.1). Free carboxylic group in products **1a** – **1e** could then be reacted with 10-undecen-1-amine (**A2**), which was synthesized before in a two-step synthesis by reaction of 10-undecenoyl chloride with ammoniumhydroxid to the corresponding amide (**A1**), followed by reduction with $LiAlH_4$ as described in the literature[270] (for details see Experimental part 4.2.2), to yield *N*- and *C*-terminus functionalized monomers **2a** – **2e** (for details see Experimental part 4.2.3). All synthesized monomers **1a** – **1e** and **2a** – **2b** were analysed by ^1H, ^{13}C-NMR and ESI-TOF-MS spectroscopy (see Appendix Figure S1 – S15 and S18 – S30), **A1**-**A2** were analysed by ^1H and ^{13}C-NMR spectroscopy (see Appendix Figure S16 – S17). In Table 6 chosen methods and yields for *N*- and *C*-terminus functionalization of the different amino acids are demonstrated.

Table 6. Chosen methods and yields for *N*- and *C*-terminus functionalization of the different amino acids.

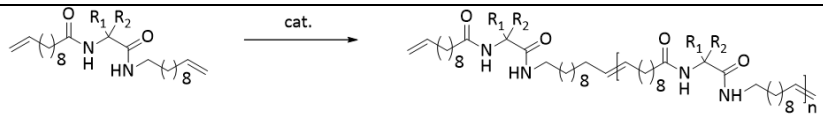

			N-terminus functionalization			*C*-terminus functionalization		
amino acid	R_1	R_2	method	product	yield (%)	cat.:	product	yield (%)
Glu	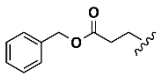	H	A	**1a**	76	A	**2a**	86
Asp	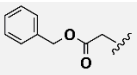	H	A	**1b**	72	A	**2b**	79
Leu		H	B	**1c**	75	A	**2c**	63
Aib	Me	Me	B	**1d**	67	B	**2d**	78
ACHC			B	**1e**	64	B	**2e**	82

3.1.2 ADMET-polymerization and hydrogenation of the polymers

Synthesis of the highly-defined PE-polymers was realized by ADMET-polymerization followed by hydrogenation with *p*-toulenesulfonhydrazide ($TsNHNH_2$) as shown in Scheme 2.

Polymerization of the monomers **2a** – **2e** can be done as a bulk polymerization due to the low melting points. The solid monomers were heated up in an oil bath to 65 °C till they become completely liquid.[265] The appropriate amount of catalyst (100:1 monomer to catalyst ratio) was added to the monomer-melt in which the same amount of catalyst were additionally added to the bulk after several hours. Due to the increasing viscosity during polymerization the reaction temperature was increased stepwise from 85 °C up to 165 °C. Finally, the reaction was quenched by adding THF and precipitating the obtained polymer into cold MeOH (for details see Experimental part 4.3.1).

Due to different activity and isomerization rates[271-274] Grubbs Catalyst first generation (Grubbs 1st), second generation (Grubbs 2nd) and Hoveyda-Grubbs Catalyst first generation (GH 1st) were tested for the chosen reaction conditions. In Table 7 the results of the molecular weights (obtained by NMR and GPC as well as the *Đ*), the yields and the obtained *trans*:*cis* ratio of the internal double bonds for the different catalyst are displayed.
A low isomerization rate[273] and good yields for monomers **3a** – **3c** by using Grubbs 1st catalyst were obtained. GH 1st catalyst under complete oxygen-free conditions also achieved good results with respect to yield and molecular weights of the products, whereas Grubbs 2nd catalyst was found to be the catalyst resulting in the lowest molecular weights. Probing the optimized conditions described by Wagener *et al*.[265] molecular weights as high as 22 kDa were obtained – higher molecular weights were not obtained despite extensive probing. This might be due to the high temperature at which most of the monomers are melting (often above 165 °C), which is limiting the activity of the catalysts. Even though such high reaction temperatures could lead to various side reactions, only a low isomerization rate was observed in MALDI-TOF-MS analysis.

Table 7. Obtained molecular weights calculated by NMR and GPC, *Đ*, yields and *trans:cis* ratio of the internal double bonds for ADMET-polymerization of the monomers **2a** – **2e** to polymers **3a** – **3e** by using different types of catalyst.

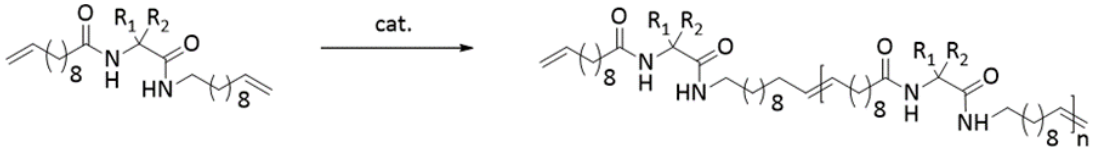

polymer	R_1	R_2	cat.	M_n GPC (Da)	M_n NMR (Da)	DP (n)	*Đ*	*trans*:*cis* ratio	Yield (%)
3a	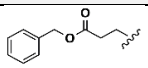	H	Grubbs 1st	7600	9200	17	1.7	68:32	77
			Grubbs 2nd	700	800	2	1.5	89:11	67
			GH 1st	2300	2400	5	2.2	78:22	70
3b	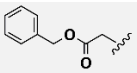	H	Grubbs 1st	10500	22000	41	1.9	68:32	87
			Grubbs 2nd	800	700	2	1.4	82:18	61
			GH 1st	4000	5400	10	1.5	72:28	72
3c	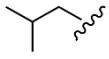	H	Grubbs 1st	3500	4300	10	1.8	75:25	73
			Grubbs 2nd	1000	700	2	1.4	78:22	69
			GH 1st	4100	5500	12	1.6	76:24	71
3d	Me	Me	Grubbs 1st	2500	3000	7	1.4	79:21	73
3e			Grubbs 1st	9400	14600	32	1.9	76:24	70
			GH 1st	11500	18200	40	1.9	79:21	62

Hydrogenation of the terminal and internal double bonds in the backbone to yield the polymer **4a** – **4e** was realized by reaction of the polymers with *p*-toluenesulfonhydrazide ($TsNHNH_2$) and DIPEA in DMF at 150 °C according to literature[275-278] (see Scheme 2, for details see Experimental part 4.3.2). For the hydrogenation the ADMET polymers **3a** – **3e** synthesized with Grubbs 1st generation catalyst were used and molecular weights from 3100 g mol^{-1} to 18500 g mol^{-1} were obtained (Table 8). Reactions were stopped after 6h, complete deprotection of the asparagine and glutamic acid unit in the polymer backbone could be realized by subsequent ester hydrolysis with aqueous NaOH-solution. The resulting mixture was dialysed against MeOH for 3 days to remove the obtained *p*-toluenesulfonic acid and benzyl alcohol in case of **4a** and **4b**. During dialysis, the obtained hydrogenated polymers precipitated due to their complete insolubility in the organic solvents used.

Table 8. Obtained molecular weights calculated by NMR, DP and yields of the unsaturated ADMET polymers 3**a** – **3e** obtained with Grubbs 1st catalyst and saturated polymers **4a** – **4e**.

polymer	M_n NMR (Da)	DP(n)	Yield (%)
3a	9200	17	77
4a	8400	19	72
3b	22000	41	87
4b	18500	43	79
3c	4300	10	73
4c	- [a]	-	62
3d	3000	7	73
4d	3100	7	55
3e	14600	32	70
4e	15500	33	85

[a] Calculation of M_n not possible due to overlapping of the methyl end-groups and methyl groups in the repeating unit.

The monomer and polymer synthesis as well as hydrogenation/deprotection can be followed by ^{1}H-NMR, MALDI-TOF-MS and IR as shown in Figure 21 for the ^{1}H-NMR data of monomer **2c** (top), the ADMET-polymer **3c** (middle) and the hydrogenated polymer **4c** (bottom). Due to completely insoluble of the final product in common organic solvents complete hydrogenation and deprotection can be demonstrated by ^{1}H-NMR in $CDCl_3$ only after adding 15 Vol. % TFA to the mixture. The characteristic signals for the internal double bonds at 5.3 ppm as well as for the terminal double bond at 5.8 ppm and 4.9 ppm are no longer present in the ^{1}H-NMR spectrum of **4c**. Furthermore, protons next to the terminal double bonds at 2.0 ppm are disappearing and signals for the methyl groups at 0.9 ppm become broader due to protons of the resulting methyl end-group. The successful deprotection of the benzyl-group in the case of **4a** and **4b** can be proven by the disappearance of the signals of the CH_2-group next to the aromatic system at 5.1 ppm as well as the characteristic aromatic system signals at 7.3 ppm which is shown in Figure 22 for polymer **4b**. New methyl end-group can be detected at 0.9 ppm and was used for calculation of the molecular weight, indicating successful hydrogenation of the double bonds, whereas all other signals are still present showing slightly changed chemical shifts due to interaction with TFA molecules. Degree of polymerization (DP) calculated for the hydrogenated polymers **4a**, **4b**, **4d** and **4e** are always higher as for unsaturated polymers, which can be due to dialysis after hydrogenation. All other NMR-spectra of the ADMET- and hydrogenated polymers are shown in the Appendix (Figure S31 – S41). The successful hydrogenation can also be proven in IR-spectroscopy by disappearance of the deformation vibration band of the double bonds at 990 cm^{-1} and 915 cm^{-1} in the IR spectrum (Appendix Figure S42 – S51).

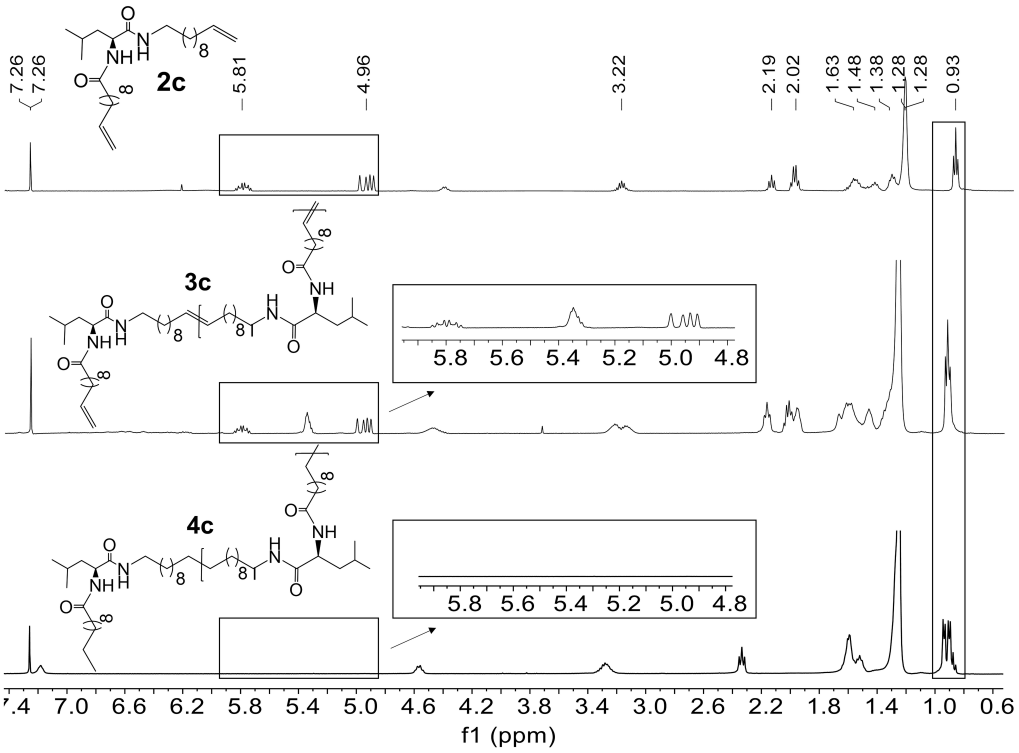

Figure 21. [1]H-NMR spectra of monomer **2c** (top), ADMET-polymer **3c** (middle) and hydrogenated polymer **4c** (bottom) in $CDCl_3$. For **4c** 15 Vol %. TFA was added.

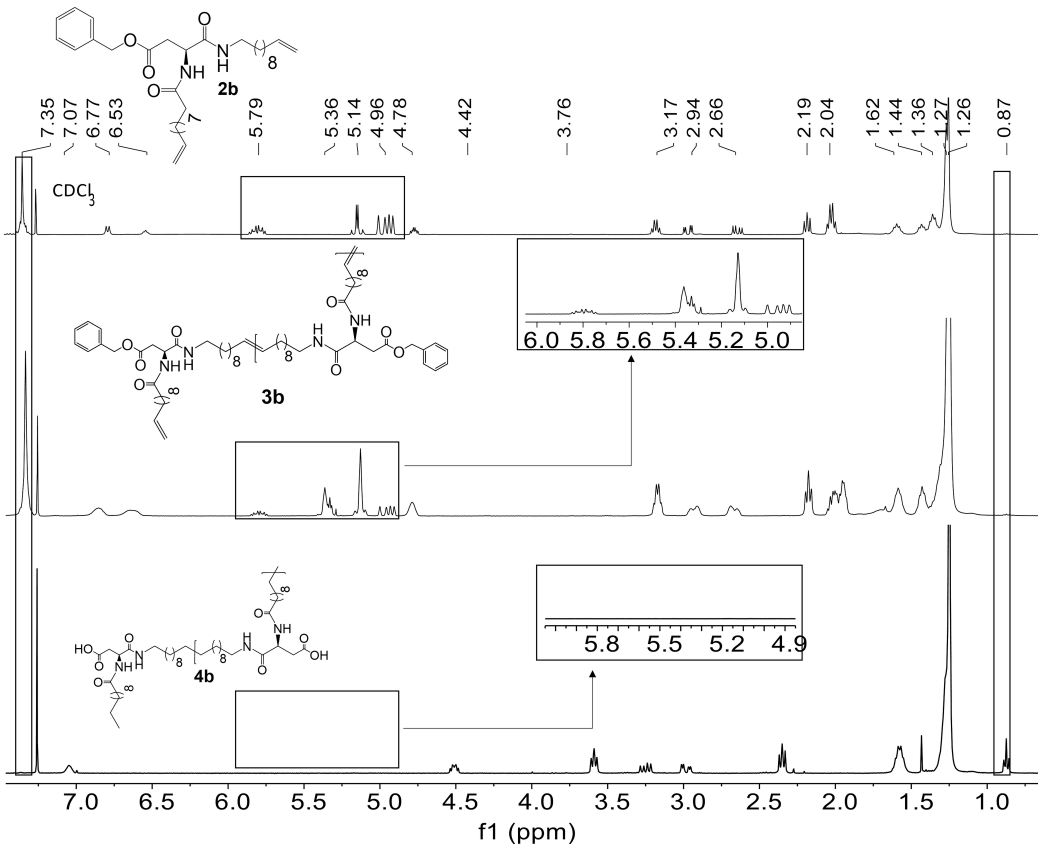

Figure 22. [1]H-NMR spectra of monomer **2b** (top), ADMET-polymer **3b** (middle) and hydrogenated polymer **4b** (bottom) in $CDCl_3$. For **4b** 15 Vol %. TFA was added.

3.1.3 MALDI-TOF-MS-analysis

In Figure 23 and Figure 24 MALDI-TOF-MS spectra of the ADMET-polymer **3b** and the hydrogenated polymer **4e** are shown. All other MALDI-TOF-MS spectra are shown in the Figures S31 – S41 with the exception of **3d**, **4a** and **4d**, which cannot be investigated under the chosen conditions. The MS spectrum of the ADMET-polymer **3b** (Figure 23) shows a mass distribution from 1091 g mol^{-1} to 4165 g mol^{-1} (Figure 23A) with a maximum peak at 1604.041 g mol^{-1}. Two series can be assigned and the distance between signals of the same series amounts to 512 g mol^{-1}. The distance between signals of different series is 14 g mol^{-1}, in which the signal with the lower molecular weight has always a lower intensity (Figure 23B). This signal indicates the loss of a CH_2-Group during ADMET-polymerization due to olefin isomerization, leading to polymers having a slightly different chain length of the alkyl chain[271, 279], with a small amount of isomerization in e.g. **3b**. The low isomerization rate can be proven by the appearance of only one series displaying isomerization products for **3b** and three series for **4e** (Figure 24) whereas high isomerization rates observed at cysteine functionalized precision PE result in 6 series of isomerized side products.[279] The signal at 2117 g mol^{-1} can be assigned to the polymer [E-M_2-EK]$^+$ with potassium as counter ion, which is confirmed by the agreement of the experimental and simulated data (see Figure 23c). Thus, the obtained main series definitely indicates the expected polymer structure by ADMET polymerization including internal and external double bonds and the loss of ethylene in the repeating unit.

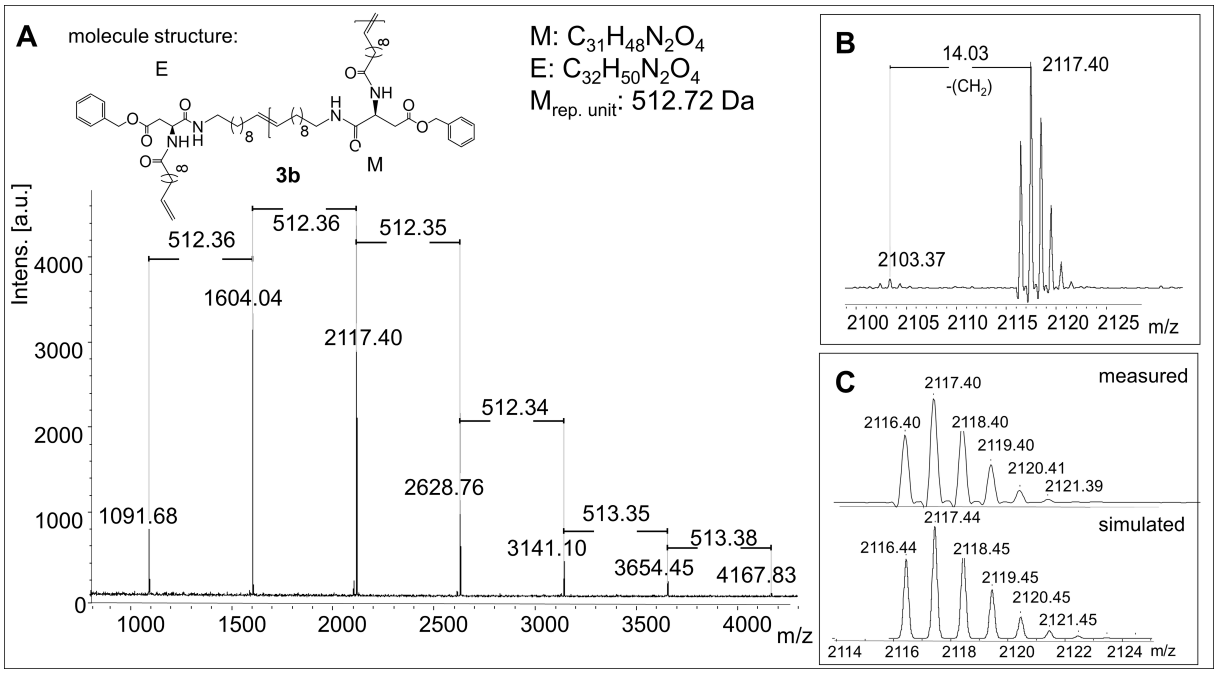

Figure 23. A) MALDI-TOF-MS of ADMET polymer **3b B**) Zoom in to [E-M_2-EK]$^+$ to show isomerization of the olefin **C**) Measured and simulated pattern for [E-M_2-EK]$^+$.

For polymer **4e** (Figure 24) a mass distribution from 937 g mol^{-1} to 2242 g mol^{-1} is obtained, in which the highest absorption peak at 1372 g mol^{-1} indicates the polymer structure [E-M-EK]$^+$. Distance between the main series is 434 g mol^{-1}, which is in agreement with the molecular weight of the repetitive unit. In addition to the obtained main series up to three different series with a distance of 14 g mol^{-1} can be observed, again indicating the isomerization of the olefin. In comparison to **3b**, the isomerization rate is higher and occurs at more than one site. The main series however proofs the complete hydrogenation of the polymer.

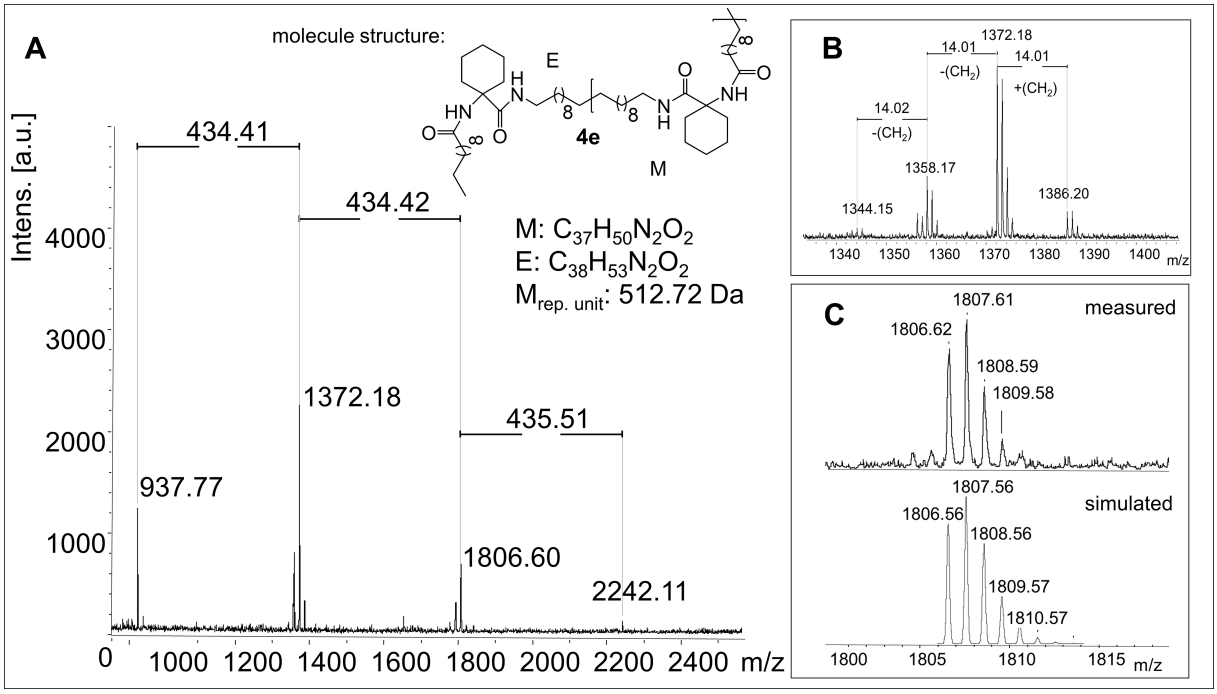

Figure 24. A) MALDI-TOF-MS of ADMET polymer **4e B**) Zoom in to $[E\text{-}M\text{-}EK]^+$ to show isomerization of the olefin **C**) Measured and simulated pattern for $[E\text{-}M\text{-}EK]^+$.

3.1.4 DSC-analysis

The thermal properties of the hydrogenated polymer in comparison to the monomer and the unsaturated polymers were investigated by DSC-measurements. Figure 25 shows the cooling and heating curve for the monomers **2a** and **2b** (dotted lines) and the polymers **4a** and **4b** (straight lines) after ADMET and hydrogenation.

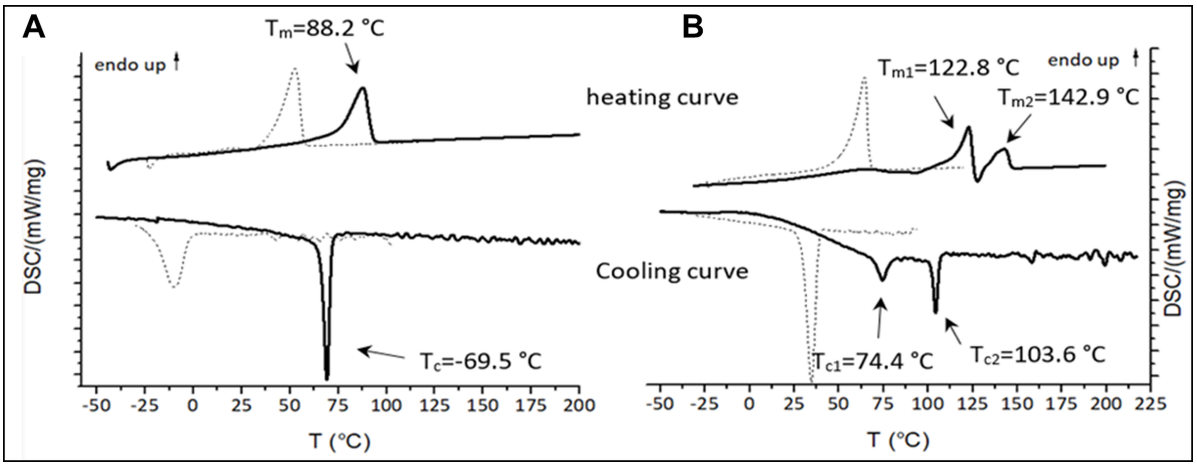

Figure 25. A) DSC thermograms of monomer **2a** (dotted lines) and the hydrogenated polymer **4a** (straight lines) **B**) DSC thermograms of monomer **2b** (dotted lines) and the hydrogenated polymer **4b** (straight lines).

For monomer **2a** melting at 53 °C and crystallization at –10 °C could be observed, whereas monomer **2b** has a significant higher melting and crystallization point (T_m= 64.4 °C; T_c=34.7 °C). After ADMET-polymerization the investigated compounds become completely amorphous, presumably due to sterically hindrance caused by incorporation of the internal double bonds into the polymer.

Crystallization of such polymer strongly depends on the packing of the alkyl chains, which in this case is limited due to the presence of the thus different olefin isomers and the incorporated amino acid in the polymer backbone.
After hydrogenation and deprotection the polymers **4a** and **4b** display a crystalline structure as visible by their melting points. In comparison to the corresponding monomer, melting and crystallization of **4a** and **4b** shifts to significantly higher temperatures, in which **4b** has a higher melting and crystallization temperature than **4a**. However, in comparison to the unsaturated monomers and polymer **4a**, DSC-curves of **4b** are more complex which is due to different melting and crystallization behaviors of these samples. Melting at 122.8 °C and 142.9 °C indicate a melting-recrystallization, which can be due to formation of metastable crystals during the cooling process[280]. Such crystals are melting first and reorganizing again into more stable areas resulting in an exothermal signal in the DSC curve. These areas are melting later, similar to the behavior found for precision polyolefins with different functional groups acting as defects.[281] Furthermore, two crystallization can be observed at 103.6 °C and 74.4 °C, which may be due to microphase separation.

In Table 9 thermal behavior as well as characteristic melting and crystallization data of these samples are summarized. These observations indicate the big influence of the molecular size of the amino acids acting as defects, in which the polymer **4b** bearing aspartic acid after every 19st carbon shows a higher melting and crystallization temperatures than **4a**. Such effects of the defect size on the melting and crystallization were reported early e.g. for alkyl branches[282] and butyl branched polyethylene´s and polyphosphoester´s.[283] For all other monomers **2c** – **2e** and polymers **4c** – **4e** no crystalline behavior could be observed as those amino acids with an aliphatic backbone disturbed crystallinity, whereas amino acids with a functional group able to form define crystal structures. Thus, an additional intermolecular interaction of the carboxylic-acid-defects is proposed for crystallization of the samples, e.g. by dimerization.

Table 9. Thermal behavior of the monomers and polymers with aspartic acid and glutamic acid acting as defects (**2a** – **4a** and **2b** – **4b**).

amino acid		R_1	T_m (°C)	T_c (°C)	ΔH (J g^{-1})	α (%)
Glu	**2a**	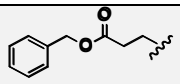	52.8	– 10.1	60.9	25
	3a		---	---	---	---
	4a	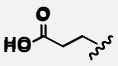	88.2	69.5	26.1	11
Asp	**2b**	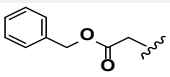	64.4	34.7	51.4	21
	3b		---	---	---	---
	4b	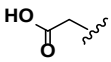	142.8	103.6	60.9	25

3.1.5 XRD-analysis

Crystalline structure of polymers **4a** and **4b** was pre-investigated by WAXS measurements (Figure 26), observing four reflections for both polymers (Table 10). The first reflection in the small angle area at a 2θ of 3.09° for **4a** and 3.60° and **4b** is the (001) reflection, indicative of the distance between two amino acid groups along the chain of 2.86 nm for **4a** and 2.45 nm for **4b**, which is in good agreement with the

length of the precision polymers. At almost exactly the doubled value of 2θ higher order reflection (002) can be detected which was also found for precision sulfone polyethylenes[284], demonstrating that the reflection intensity for **4a** is not as intensive as for **4b**. These (002) reflections are describing the evolution of a lamellar morphology and both (001) and (002) reflections could also be observed for other precision PE-polymers of different methylene sequences lengths bearing DAP-units at 16th, 18th or 20th carbon atom, shifting to higher 2θ values with decreasing length of the alkyl chain.[285] Formation of lamellae in **4a** could be more hindered than in **4b**, caused by the glutamic acid as a major defect, so that the intensity of this reflex for **4a** is significantly smaller than for **4b**. As previously reported for ADMET-PE and high density polyethylene, two characteristic reflections at scattering angles of 21.7 ° and 24.0 ° can be detected, containing information about crystal morphology of the alkyl chains and corresponding to (110) and (200) reflections of a orthorhombic crystal system.[286] For both polymers **4a** and **4b**, broad reflections with maxima at 2θ of 19.58 ° and 21.33 ° and 18.98 ° and 20.68 ° can be observed and thus the crystalline structure is definitely dissimilar to ADMET-PE.[282, 287]

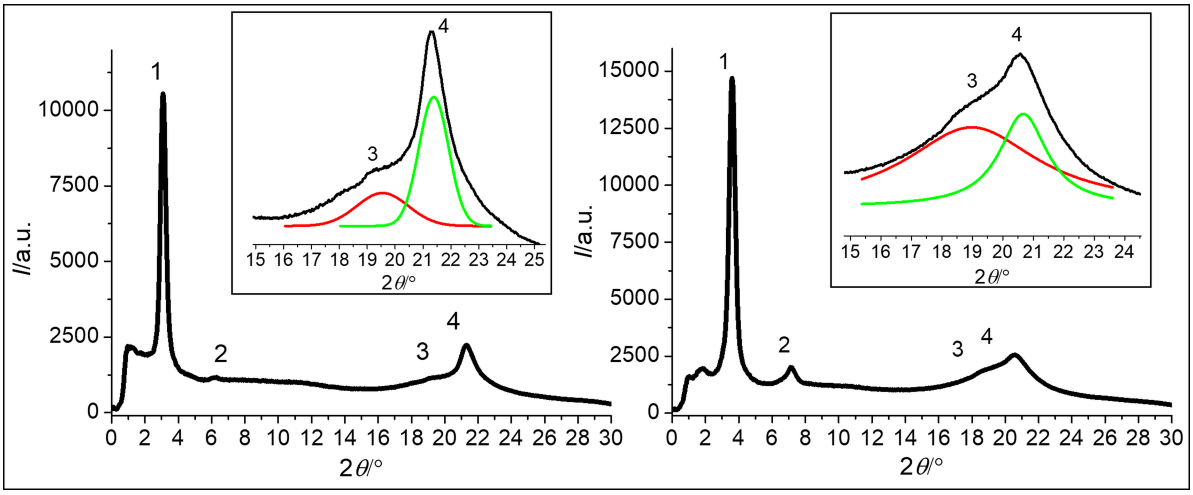

Figure 26. Wide-angle-X-ray diffraction patterns for the defined polymers **4a** (left) and **4b** (right).

The width of the signals can be explained due to the low crystallinity as the defects are large, in accordance with DSC data and literature.[282] Similar to other precision PE-polymers of different methylene spacer length bearing alkyl moieties[282, 287] chlorines[288] and meta-substituted aryl ether branches[281] in the main backbone it is likely that orthorhombic, triclinic and other metastable crystal systems are coexistent as supported by the strong asymmetric distribution of the reflections.[282, 287] Corresponding to the observations for ADMET-poly(ethylene) containing *m*-substituted arylene the amino acid defect presumably can either be excluded from or included into the PE crystals.[281]

Table 10. Obtained WAXS data for hydrogenated polymers **4a** and **4b**.

sample	reflection	2θ / °	q / nm^{-1}	d / nm
4a	1	3.09	2.20	2.86
	2	6.21	4.42	1.42
	3	19.58	13.87	0.45
	4	21.33	15.10	0.42
4b	1	3.60	2.56	2.45
	2	7.14	5.08	1.24
	3	18.98	13.46	0.47
	4	20.68	14.64	0.43

3.2 PE-type oligo-amino acid hybrid polymers

Parts of the results and discussion as well of the experimental part were already published in

"Reprinted (adapted) with permission from (Freudenberg, J.; Binder, W. H.*, Multisegmented Hybrid Polymer Based on Oligo-Amino Acids: Synthesis and Secondary Structure in Solution and in the Solid State. *Macromolecules* **2019,** *52* (12), 4534-4544. DOI: 10.1021/acs.macromol.9b00684). Copyright (2019) American Chemical Society."

3.2.1 Synthesis of multisegmented polymers $AP_m(^{Bn}Glu_n)$ (7b, 8b) and $AP_m(^{Bn}Asp_n)$ (9b, 10b)

The synthetic approach towards the multisegmented polymers is based on a combination of ring-opening polymerization (ROP) of *N*-carboxyanhydrides followed by *N*-terminus functionalization to achieve control over the oligo-amino acids ($O^{Bn}Asp_n$, $O^{Bn}Glu_n$)-segments, followed by ADMET polymerization of appropriately *C*- and *N*-terminal bis-vinyl-functionalized oligo-amino acids to separate them by methylene-segments along a polymer chain (Scheme 3). From a molecular design-point, the interrupting alkyl-units act as flexible spacer unit spatially separating the oligo-amino acids along the polymer chain, but also constraining them within the same chain. In order to check for a potential crystallization of the alkyl-units, chain length (19 CH_2-units) was chosen, able to crystallize into well-known crystal lattices as known from more simple systems with small defects within precision-polymers.[268]

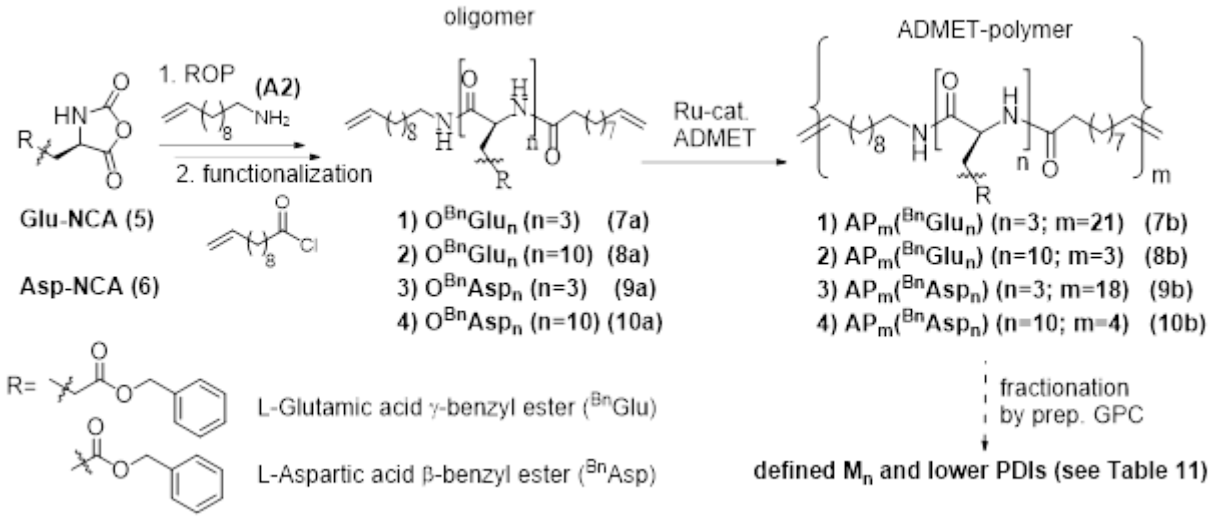

Scheme 3. Synthesis of ADMET-polymers with Grubbs catalyst first generation (Grubbs 1st) after ROP of NCAs and functionalization of the *N*-terminus, followed by fractionation *via* preparative GPC.

ROP of the synthesized *N*-carboxyanhydrides (NCA) **Glu-NCA** (**5**) and **Asp-NCA** (**6**) from corresponding amino acid (for details see Experimental part 4.4.1) with triphosgene was initiated by 10-undecene-1-amine (**A2**), followed by the modification on the *N*-terminus *via* 10-undecenoylchloride to attach vinyl end-groups on both sides, yielding the *C*- and *N*-vinylic amino acid oligomers $\mathbf{O^{Bn}Glu_3}$, $\mathbf{O^{Bn}Glu_{10}}$, $\mathbf{O^{Bn}Asp_3}$ and $\mathbf{O^{Bn}Asp_{10}}$ (O^{Bn}amino $acid_{n=\text{number amino acids units}}$) (for details see Experimental part 4.4.2). Obtained oligomers were subsequently polymerized *via* Grubbs catalyst first generation (Grubbs 1st) catalyzed ADMET polymerization (Scheme 3, for details see Experimental part 4.4.3). Amino acid building blocks of the so obtained polymers $\mathbf{AP_{21}(^{Bn}Glu_3)}$, $\mathbf{AP_3(^{Bn}Glu_{10})}$, $\mathbf{AP_{18}(^{Bn}Asp_3)}$ and $\mathbf{AP_4(^{Bn}Asp_{10})}$ ($AP_{m=\text{polymer-repetitive units}}(^{Bn}\text{amino acid}_n)$) are thus separated by exactly 19 methylene-units, interrupted by one internal double bond between carbons 9 and 10. The obtained polymers were subsequently purified by preparative GPC to generate samples with low *Đ* and defined molecular

weights (for details see Table 11). The repetitive incorporation of the amino acid blocks into a poly-(alkyl)chain allows to study the assembly behaviour between these oligo-amino acid blocks as well as the influence on the secondary structure formation in HFIP-solution and in solid state.

For the synthesis of oligomers **O^{Bn}Glu$_3$ (7a)** , **O^{Bn}Glu$_{10}$ (8a)**, **O^{Bn}Asp$_3$ (9a)** and **O^{Bn}Asp$_{10}$ (10a)** a ROP of **Glu-NCA (5)** and **Asp-NCA (6),** initiated by 10-undecene-1-amine (**A2**) was performed at 0 °C[289], applying vacuum during the reaction to remove the evolving carbon dioxide.[290] Details on the synthesis and characterization (^{1}H-NMR) of the NCAs and the initiator are reported in the Appendix (Figure S16 – S17 and S52 – S53). Previous studies have shown that intramolecular amidation and side reactions with the solvent caused by the high reactivity of the free amine end-group can lead to termination reactions[290] and thus can disturb of the following modification of the *N*-terminus. To exclude the formation of side products, the consumption of the NCAs during the polymerization of **O^{Bn}Glu$_{10}$ (8a)** and **O^{Bn}Asp$_{10}$ (10a)** was followed *via* FTIR spectroscopy, monitoring the characteristic C-O-C anhydride vibration band at 1785 cm^{-1} and 1854 cm^{-1} (Figure 27 A+B) normalized to the benzylic absorption band at 1735 cm^{-1}: starting from the spectra of the virgin **Glu-NCA (5)** or **Asp-NCA (6)** in DMF without the amine initiator as reference value (t=0 min, black curve) a stepwise decrease in intensity of the NCA-vibration band at 1785 cm^{-1} and 1854 cm^{-1} was observed after adding the initiator. After 70 minutes for **Glu-NCA (5)** (Figure 27A pink curve) and 450 minutes for **Asp-NCA (6)** (Figure 27B brown curve) both signals had completely disappeared, indicating the complete conversion of the monomer. Subsequently 10-undecenoylchloride and triethylamine were directly added for the *in-situ* modification of the *N*-terminus.

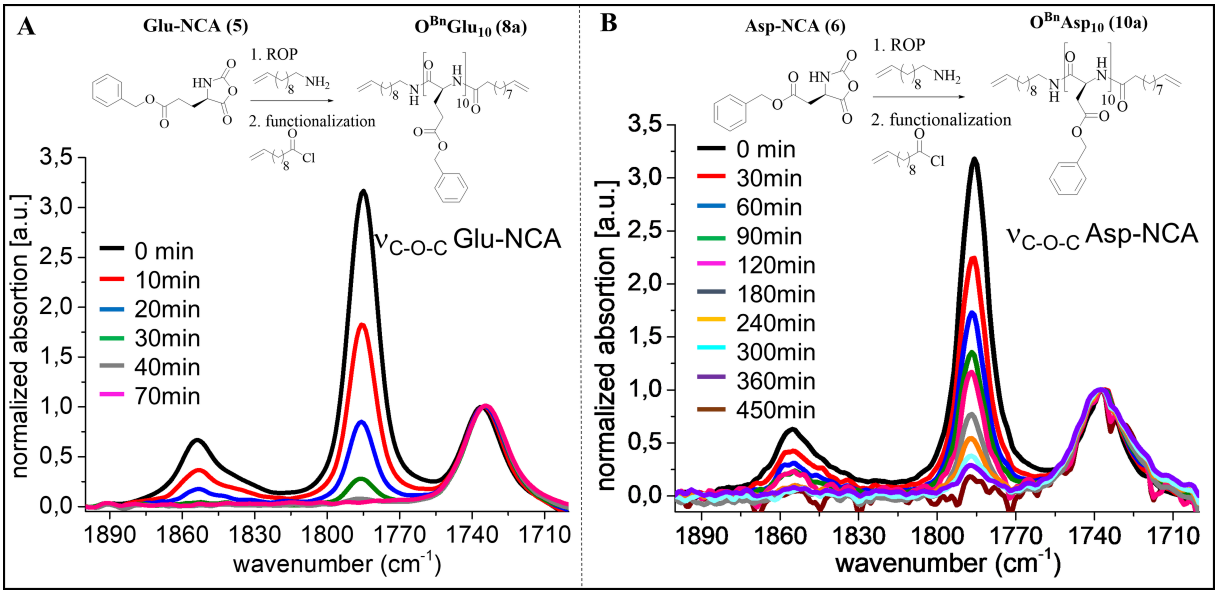

Figure 27. Following of the stepwise NCA-consumption during ROP of **A) Glu-NCA (5)** to **O^{Bn}Glu$_{10}$ (8a)** and **B) Asp-NCA (6)** to **O^{Bn}Asp$_{10}$ (10a)** (right) by FTIR investigation of NCA C-O-C anhydride vibration band at 1785 cm^{-1} and 1854 cm^{-1} (spectra are normalized to the absorption band of the benzyl group at 1735 cm^{-1}).

The final structure of the oligomers could be determined by ^{1}H-NMR and MALDI-TOF-MS measurements. In Figure 28 ^{1}H-NMR of **O^{Bn}Glu$_3$ (7a)** is shown. Protons next to the incurred amide bond on the *C*-terminus at 3.0 ppm clearly identify the attachment of the initiator after ROP of **Glu-NCA (5)**. Furthermore, successful functionalization of the *N*-terminus could be proven by the protons next to the carbonyl group at 2.1ppm. The successful attachment of the alkyl chains was also confirmed by the

characteristic signals for the terminal double bond at 5.8 ppm and 4.9 ppm. The aromatic protons of the repeating unit at 7.3 ppm and the proton next to the chiral centre at 4.2 ppm showing the successful polymerization. Degree of polymerization (DP) was calculated by integration of the terminal double bond protons (H_a + H_b) and the proton of the repeating unit next to the chiral centre (H_1), which could be determined to a chain length of n=3.

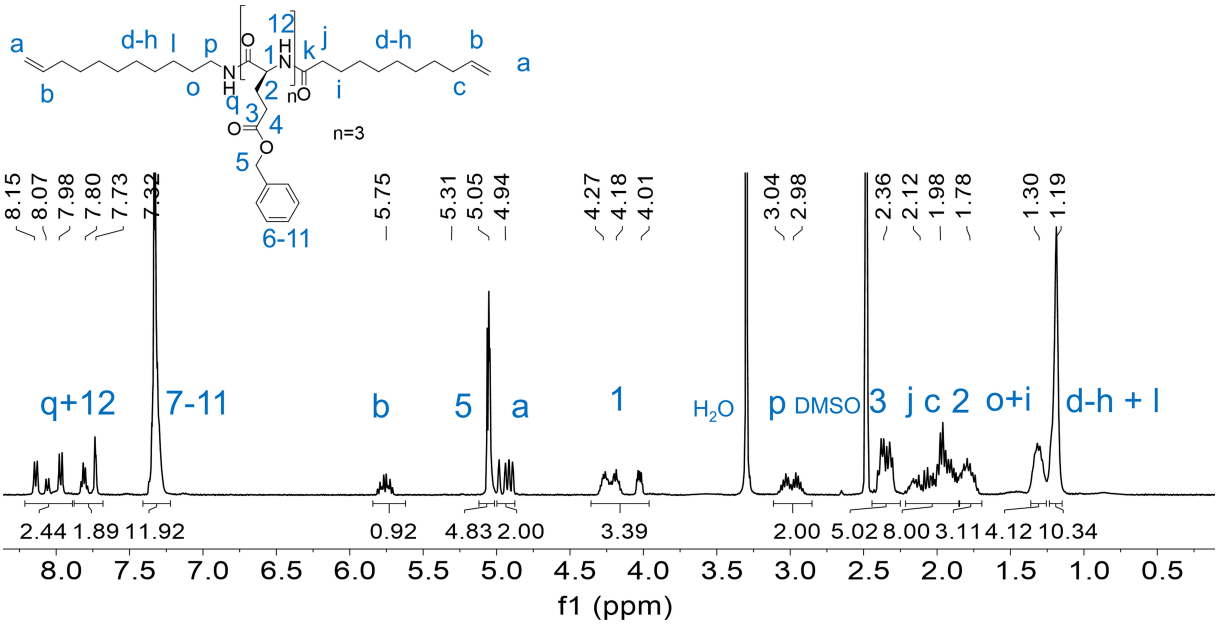

Figure 28. ^{1}H-NMR spectrum of **7a** in DMSO-d_6.

MALDI-TOF-MS measurement of oligomer **O^{Bn}Asp$_{10}$ (10a)** (Figure 29) was performed with dithranol as matrix and KTFA as salt. The MS spectrum of oligomer **10a** shows a mass distribution from 1604 g mol^{-1} to 4271 g mol^{-1} with a maximum peak at 2426 g mol^{-1}. One series can be observed and the distance between the signals amounts to 206 g mol^{-1}. The signal at 2426 g mol^{-1} can be assigned to the oligomer [$C_{132}H_{151}N_{11}O_{31}K^+$] with potassium as counter ion, which is confirmed by the agreement of the experimental and simulated data (see Figure 29 inlet). Thus, the obtained main series definitely indicates the expected oligomer structure and proves the successful polymerization and functionalization of the *N*-terminus.

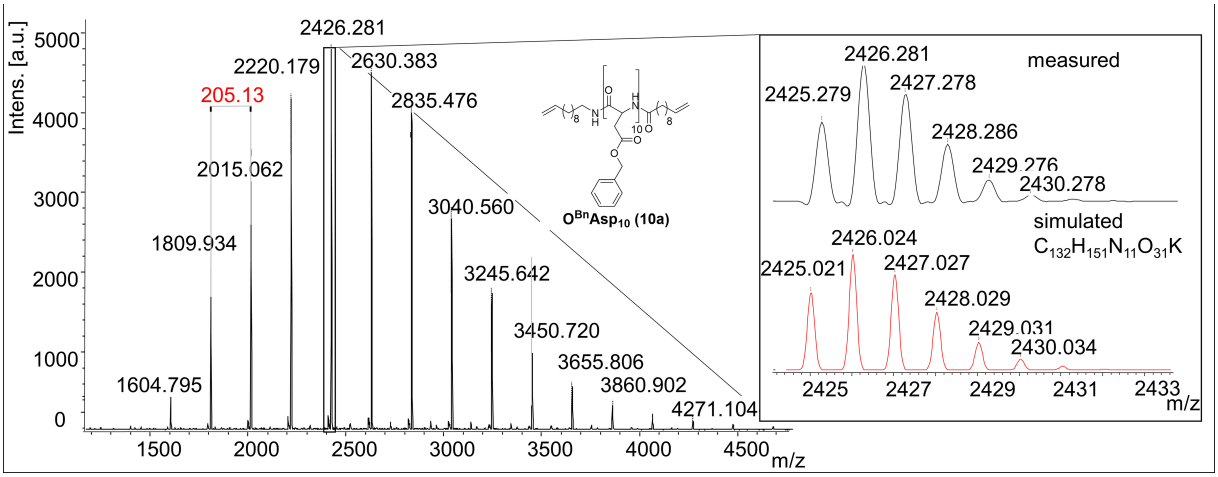

Figure 29. MALDI-TOF-MS of **O^{Bn}Asp$_{10}$ (10a)** using dithranol as matrix and KTFA as salt.

ADMET-polymerization of the so obtained oligomers **O^{Bn}Glu$_3$ (7a)**, **O^{Bn}Glu$_{10}$ (8a)**, **O^{Bn}Asp$_3$ (9a)** and **O^{Bn}Asp$_{10}$ (10a)**, was performed in dichloromethane with Grubbs Catalyst first generation (Grubbs 1st)[291, 292] using the dissolved oligomers, starting with an initial 100:1 monomer to catalyst ratio. The progress of the ADMET-polymerization (**O^{Bn}Asp$_3$ (9a)** to **AP$_{18}$(^{Bn}Asp$_3$) (9b)**) was checked by analytical GPC monitoring the degree of polymerization (Figure 30A). A full conversion with $Đ \approx 2$ was achieved after four days and the reaction was finally quenched by ethyl vinyl ether.
Characterization for all oligo-amino acids and corresponding ADMET-polymers was realized by ^{1}H-NMR-spectroscopy, an additional end-group analysis for all oligo-amino acids was performed *via* MALDI-TOF mass spectrometry, proving in all cases the desired structures (for details see Appendix Figure S54 – S61).

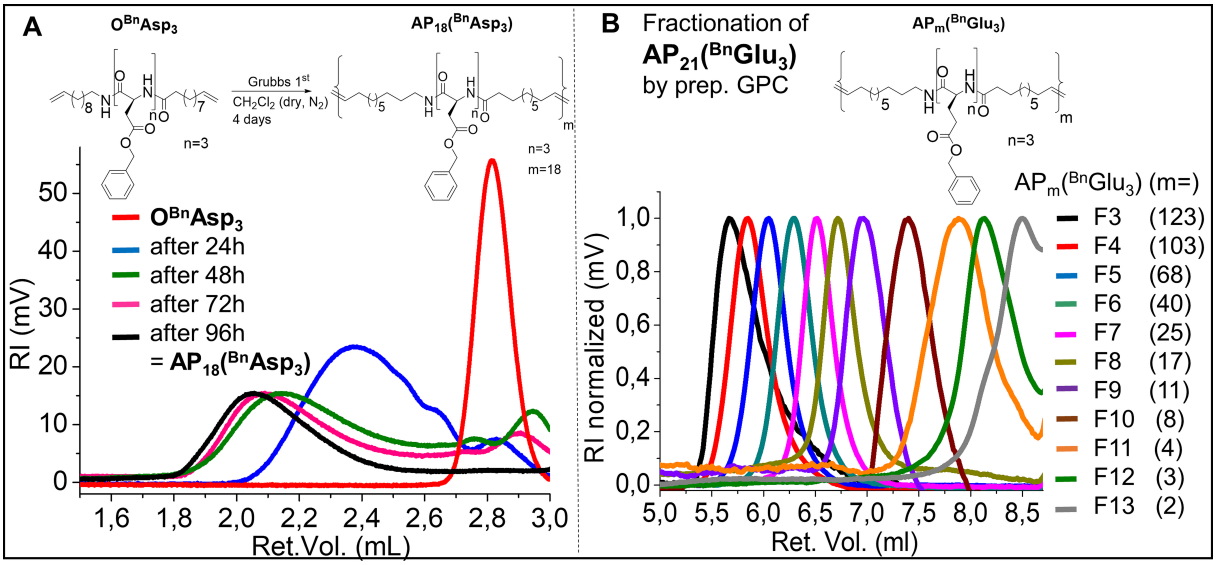

Figure 30. A) Synthesis of the polymer **AP$_{18}$(^{Bn}Asp$_3$) (9b)** by following the time-dependent GPC-curves during ADMET polymerization of **O^{Bn}Asp$_3$ (9a)** and **B)** normalized analytical GPC curves for the obtained fractions of **AP$_{21}$(^{Bn}Glu$_3$) (7b)** after separation by preparative GPC.

As the obtained ADMET polymers displayed relative broad molecular weight distributions, it was aimed to cut a defined molecular weight range to investigate the influence of the chain length towards the secondary structure formation in both, solution and the solid state. Thus, the obtained polymers **AP$_{21}$(^{Bn}Glu$_3$) (7b)**, **AP$_3$(^{Bn}Glu$_{10}$) (8b)**, **AP$_{18}$(^{Bn}Asp$_3$) (9b)** and **AP$_4$(^{Bn}Asp$_{10}$) (10b)** were separated into fractions (**F**) by preparative GPC using DMF as eluent, obtaining defined samples with specific chain length *n* and *m*. In Figure 30B normalized GPC curves for selected fractions **AP$_m$(^{Bn}Glu$_3$) (7b)** (**F3** – **F13**) are shown ranging from (**F3**) (black) with m = 123 to (**F13**) (grey curve) with m = 2, while fractions F1 and F2 contained no polymer. All further chromatograms for preparative GPC of **AP$_{21}$(^{Bn}Glu$_3$) (7b)**, **AP$_3$(^{Bn}Glu$_{10}$) (8b)**, **AP$_4$(^{Bn}Asp$_{10}$) (9b)** and **AP$_{18}$(^{Bn}Asp$_3$) (10b)** along with the analytic GPC curves for the different fractions are shown in detail in the Appendix (Figure S62 – S68).

Analytical GPC data for the obtained oligomers, ADMET-polymers and corresponding fractions after separation by prep. GPC results are shown in Table 11. As expected, the ROP of *N*-carboxyanhydrides showed polydispersities of ~ 1.15 and molecular weights in the range from 0.9 to 1.9 kDa, while the subsequent ADMET polymerization yield molecular weights from 4.5 kDa to 20.0 kDa, with $Đ \approx 2.0$. After fractionation *via* preparative GPC obtaining molecular weights ranging from 1.6 kDa up to 165.5 kDa (**AP$_m$(^{Bn}Glu$_3$) (7b)** (**F13** – **F3**) (m=2–123), **AP$_m$(^{Bn}Glu$_{10}$) (8b)** (**F11** – **F3**) (m=1–27), **AP$_m$(^{Bn}Asp$_3$)**

(**9b**) (**F11 – F3**) (m=5–136) and **AP$_4$(^{Bn}Asp$_{10}$)** (**10b**) (**F13 – F3**) (m=2–70)) and polydispersities down to 1.05.

Table 11. M_n (GPC), $Đ$ and DP (n, m) for the synthesized oligomers **O^{Bn}(AA$_n$)** and ADMET polymers **AP$_m$(^{Bn}AA$_n$)** before and after fractionation.

oligomer O^{Bn}(AA$_n$) **ADMET-polymer AP$_m$(^{Bn}AA$_n$)**

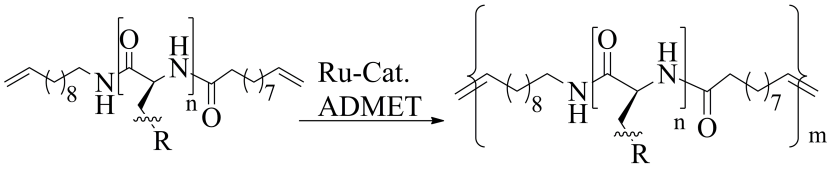

AA	**Glu$_n$**						**Asp$_n$**					
DP (n)	**n=3 (7a + 7b)**			**n=10 (8a + 8b)**			**n=3 (9a + 9b)**			**n=10 (10a + 10b)**		
	M_n (kDa)	$Đ$	m	M_n (kDa)	$Đ$	m	M_n (kDa)	$Đ$	m	M_n (kDa)	$Đ$	m
O^{Bn}(AA$_n$)	0.9	1.17	-	1.9	1.14	-	1.1	1.14	-	1.9	1.10	-
AP$_m$(^{Bn}AA$_n$)	18.7	1.98	21	4.5	1.94	3	20.0	1.89	18	9.0	2.35	4
after fractionation of AP$_m$(^{Bn}AA$_n$) *via* preparative GPC												
F3	122.4	1.40	123	68.7	1.51	27	153.4	1.41	136	165.5	1.55	70
F4	103.3	1.28	103	43.0	1.52	17	142.2	1.35	126	80.0	1.66	34
F5	67.6	1.18	68	28.5	1.41	11	86.0	1.44	76	74.0	1.67	31
F6	40.2	1.15	40	19.4	1.37	8	56.4	1.49	50	67.4	1.32	29
F7	25.0	1.09	25	14.5	1.30	6	36.7	1.47	32	43.3	1.34	18
F8	17.4	1.08	17	9.5	1.29	4	26.5	1.47	23	31.5	1.34	13
F9	11.4	1.09	11	6.3	1.21	3	17.0	1.45	15	22.3	1.24	9
F10	8.0	1.10	8	3.9	1.18	2	9.4	1.28	8	15.0	1.21	6
F11	3.0	1.09	4	2.3	1.17	1	5.2	1.12	5	9.0	1.18	4
F12	2.2	1.08	3							5.4	1.12	3
F13	1.6	1.05	2							3.4	1.13	2

3.2.2 Solid state assembly

Secondary structure formation of the oligomers **O^{Bn}Glu$_3$** (**7a**) and **O^{Bn}Glu$_{10}$** (**8a**) and the fractionated ADMET polymers **AP$_m$(^{Bn}Glu$_3$)** (**7b**) and **AP$_m$(^{Bn}Glu$_{10}$)** (**8b**) was investigated in the solid state *via* FTIR

spectroscopy and DSC measurements. As the distances of the oligo-amino acids within the multisegmented polymers are changed compared to those in the corresponding oligomers, a stacking of helices (see e.g. α-helix bundles[293]) or the formation of stacked β-sheets, induced by refolding of the secondary structure elements was expected. In order to ensure a reproducible-sample preparation, all solid samples were obtained by a evaporation of the solvent (HFIP) at room temperature, as ordering is known to depend on the rate of evaporation[91, 92].

3.2.2.1 Oligomers of $O^{Bn}Glu_n$

First, secondary structure formation of oligomers **$O^{Bn}Glu_3$ (7a)** and **$O^{Bn}Glu_{10}$ (8a)** was investigated *via* solid state FTIR (Figure 31A). **$O^{Bn}Glu_3$ (7a)** (red curve) displayed two characteristic signals at 1625 cm^{-1} and 1690 cm^{-1} in the amide I region completed by the signal at 1521 cm^{-1} in the amide II region clearly identified as a β-sheet structure. In contrast, oligomer **$O^{Bn}Glu_{10}$ (8a)** (black curve) displays two signals at 1652 cm^{-1} and 1625 cm^{-1} in the amide I area and two signals at 1544 cm^{-1} and 1522 cm^{-1} indicative of the coexistence of α-helical conformation and β-sheet. Thus, the α-helical conformation is stabilized with increasing chain length of the amino acid in the polymer backbone. The graphical representation of the (non-)idealized α-helical and β-sheet conformation of $O^{Bn}Glu_n$-esters were presented by Papadopoulos *et al.*[294] Temperature dependent FTIR measurement (Figure 31B) of **$O^{Bn}Glu_{10}$ (8a)** at room temperature (RT, black curve), 60 °C (red curve), 100 °C (blue curve), 140 °C (pink curve) and 200 °C (green curve) does not indicate a significant change in the FTIR curves up to 60 °C. At temperatures from 100 °C (blue curve) to 200 °C (green curve), the signal at 1652 cm^{-1} (α-helix) shifts to 1657 cm^{-1} and decreased in intensity, whereas the signal at 1625 cm^{-1} (β-sheet) became more dominant. In Figure 31C the DSC curves for the first (straight line) and the second heating run (dashed line) for **$O^{Bn}Glu_{10}$ (8a)** are shown, revealing a first order transition at 78 °C in the first heating cycle, which is lost after cooling and reheating the sample. Oligopeptides of ($O^{Bn}Glu_n$) are known to form stable 18/5 helix or a second metasTable 8/2 helix conformation.[294] Due to the observed irreversible first order transition at 78 °C, supported by the shift of the maxima in FTIR from 1652 cm^{-1} to 1657 cm^{-1} (Figure 31B), we propose conformation change of the 7/2 to a 18/5 helix in **$O^{Bn}Glu_{10}$ (8a)**. A higher ordering of the alkyl chains in DSC as well as in WAXS (see Appendix Figure S69) could not be observed, leading to a dominating ordering-effect of the present oligo-amino acids. We therefore concentrated on the analysis by FTIR spectroscopy, to get insight into the potential ordering of the oligo-amino acid sequences in the solid state.

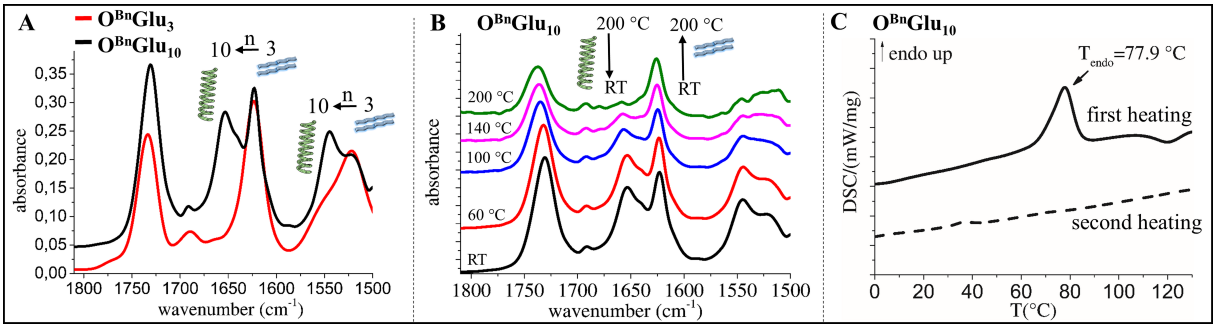

Figure 31. A) FTIR spectra of **$O^{Bn}Glu_3$ (7a)** (red) and **$O^{Bn}Glu_{10}$ (8a)** (black) at room temperature, **B**) temperature dependent FTIR-spectra of **$O^{Bn}Glu_{10}$ (8a)** at room temperature (RT, black curve), 60 °C (red curve), 100 °C (blue curve), 140 °C (pink curve) and 200 °C (green curve) and **C**) DSC-curves for **$O^{Bn}Glu_{10}$ (8a)** of first heating run (straight line) and second heating run (dashed line).

3.2.2.2 Multisegmented polymers of $AP_m(^{Bn}Glu_n)$

Figure 32A displays FTIR spectra of fractions of **$AP_2(^{Bn}Glu_3)$** (**7b**, **F13**, 1.6 kDa, black curve) and **$AP_3(^{Bn}Glu_3)$** (**7b**, **F12**, 2.2 kDa, red curve), revealing signals at 1645 cm^{-1} (amide I) and at 1539 cm^{-1} (amide II region), identifying an absence of a regular secondary structure.[71, 76, 77] With increasing chain length of the polymer **$AP_4(^{Bn}Glu_3)$** (**7b**, **F11**, 3.0 kDa) to **$AP_8(^{Bn}Glu_3)$** (**7b**, **F10**, 8.0 kDa) (Figure 32A green to blue curve) the peak at 1645 cm^{-1} decreased in intensity, neighbored by a newly emerging signal which appeared at 1626 cm^{-1}, indicative of a β-sheet structure confirmed by the shift of the amide II peak from 1539 cm^{-1} to 1529 cm^{-1}.[70, 71, 77] Increasing the chain length further (**$AP_{103}(^{Bn}Glu_3)$** (**7b**, **F4**) (103.3 kDa) (grey)), the signal at 1645 cm^{-1} shifted almost completely to 1626 cm^{-1}, matching with the shift of the signal in the amide II region from 1529 cm^{-1} to 1525 cm^{-1}. Additionally, in the amide I region a new signal at 1690 cm^{-1} appeared, which is also known as a characteristic signal for β-sheet structures.[70, 71, 77] In contrast to the corresponding oligomer **$O^{Bn}Glu_3$** (**7a**) (Figure 32A red curve) formation of β-sheet conformation in the fractions **$AP_2(^{Bn}Glu_3)$** (**7b**, **F13**, 1.6 kDa) - **$AP_8(^{Bn}Glu_3)$** (**7b**, **F11**, 3.0 kDa) is disrupted under the chosen conditions and only fractions with higher molecular weights **$AP_8(^{Bn}Glu_3)$** (**7b**, **F10**, 8.0 kDa) to (**$AP_{103}(^{Bn}Glu_3)$** (**7b**, **F4**, 103.3 kDa, grey curve) show regular formation of the β-sheet structure. As a result β-sheet formation is promoted if more **$O^{Bn}Glu_3$** (**7a**) oligomers are present along the polymer chain – a result in accordance with other oligomeric systems, where β-sheets are proposed to be the more stable conformation.[295] Thus it has been demonstrated that multiple copies of β-sheet oligomeric peptides within one polymer chain are promoting the formation of β-sheet: A process highly reminiscent of amyloid-formation.

In a similar manner **$AP_m(^{Bn}Glu_{10})$** (**8b**) fractions (Figure 32B) demonstrates the formation of an β-sheet conformation with increasing chain length from **$AP_2(^{Bn}Glu_{10})$** (**8b**, **F10**, 3.9 kDa, red curve) to **$AP_3(^{Bn}Glu_{10})$** (**8b**, **F9**, 6.3 kDa, blue curve), **$AP_6(^{Bn}Glu_{10})$** (**8b**, **F7**, 14.5 kDa, green curve) and **$AP_{27}(^{Bn}Glu_{10})$** (**8b**) (**F3**, 68.7 kDa, grey curve) *via* the decrease in intensity of the signal at 1653 cm^{-1}, (amide I) and 1544 cm^{-1} (amide II region) and an increase in intensity at 1626 cm^{-1} and 1521 cm^{-1}.[68, 70, 71, 73, 76, 77] Together with the new signals at 1692 cm^{-1} and 1521 cm^{-1} as well as the increased intensity signal at 1626 cm^{-1}, it indicates an increased amount of β-sheet with increasing molecular weight of the polymer at room temperature. In comparison to the investigated oligomer **$O^{Bn}Glu_3$** (**7a**) (coexistence of α-helical structure and β-sheet (Figure 32A black curve)) the fractions **$AP_1(^{Bn}Glu_{10})$** (**8b**, **F11**, 2.3 kDa) - **$AP_3(^{Bn}Glu_{10})$** (**8b**, **F9**, 6.3 kDa) (Figure 32B) preferred α-helical conformation, whereas fractions with high molecular weights **$AP_6(^{Bn}Glu_{10})$** (**8b**, **F7**, 14.5 kDa) and **$AP_{27}(^{Bn}Glu_{10})$** (**8b**, **F3**, 68.7 kDa) form β-sheet.

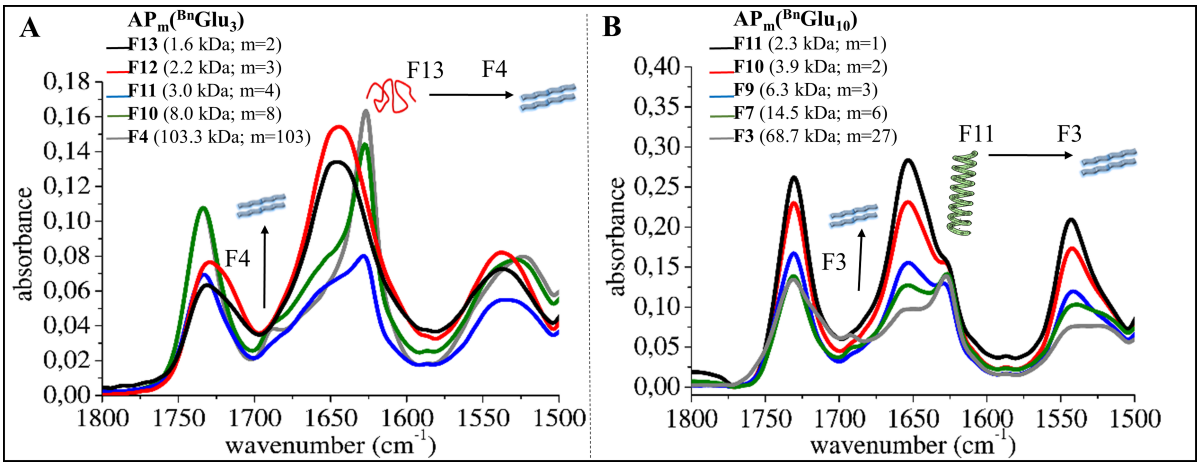

Figure 32. FTIR spectra for selected fractions of **A**) **$AP_m(^{Bn}Glu_3)$** (**7b**) and **B**) **$AP_m(^{Bn}Glu_{10})$** (**8b**) in the amide I and amide II region in the solid state.

As known from previous examples of oligo-amino acids[296, 297], β-sheet conformation is stabilized by intermolecular hydrogen bonds between the NH- and CO-groups of different amino acid units. As the results for fractions of both **AP$_m$(BnGlu$_3$) (7b)** and **AP$_m$(BnGlu$_{10}$) (8b)** indicates a stabilization of the β-sheet structure with increasing chain length of the samples, we hypothesize that intermolecular interactions of amino acid building blocks can be formed better in fractions with higher molecular weight due to the higher amino acid content per chain. The constrained conditions introduced by the long alkyl chains in the ADMET polymer influencing the possibility for intermolecular contacts of the amino acid building blocks, in which amino acid backbones within the same polymer chain can interact and therefore stabilizing the β-sheet structure with increased molecular weight.

3.2.2.3 Thermal behaviour of multisegmented polymers of AP$_m$(BnGlu$_n$)

To investigate the thermal influence on the secondary conformation of the synthesized ADMET polymers in the solid state, temperature dependent FTIR measurements were performed. Figure 33 shows the thermal investigations for **AP$_2$(BnGlu$_{10}$) (8b**, **F10**, 3.9 kDa, Figure 33A), **AP$_6$(BnGlu$_{10}$) (8b, F7**, 14.5 kDa, Figure 33B), **AP$_{27}$(BnGlu$_{10}$) (8b**, **F3**, 68.7 kDa) (Figure 33C) at room temperature (RT, black curve), 60 °C (red curve), 100 °C (blue curve), 140 °C (pink curve) and 200 °C (green curve). As described previously (see Figure 33B), two main signals at 1653 cm^{-1} and 1626 cm^{-1} in the amide I region are characteristic for the coexistence of a β-sheet and helical structure: an increasing amount of β-sheets for the higher molecular weight fractions (from **AP$_2$(BnGlu$_{10}$) (8b**, **F10**, 3.9 kDa, Figure 33A) to **AP$_{27}$(BnGlu$_{10}$) (8b**, **F3**, 68.7 kDa, Figure 33C, black curves) at room temperature is observed. As the temperature was increased stepwise from room temperature RT over 60 °C to 100 °C for **AP$_2$(BnGlu$_{10}$) (8b**, **F10**, Figure 33A, blue curve) the signal at 1653 cm^{-1} decrease in intensity, whereas the shoulder at 1623 cm^{-1} becomes more dominant. At 140 °C (pink curve) the signal for the β-sheet conformation at 1623 cm^{-1} increases further in intensity and at 200 °C the signal at 1653 cm^{-1} only appears as a small shoulder. Furthermore, the signal in the amide II region shifts from 1543 cm^{-1} to 1516 cm^{-1} and a new signal at 1693 cm^{-1} could be observed which is significant for a β-sheet conformation. Thus, a clear transition from α-helical to β-sheet structure with increasing temperature could be observed which remains stable after cooling down to room temperature again and can therefore be regarded as irreversible.

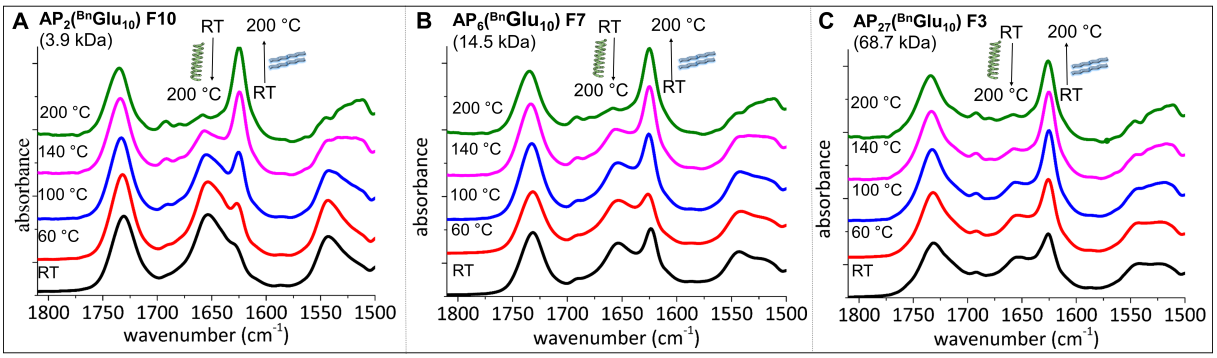

Figure 33. Temperature dependent FTIR measurement of **A**) **AP$_2$(BnGlu$_{10}$) (8b**) (**F10**) (3.9 kDa), **B**) **AP$_6$(BnGlu$_{10}$) (8b**) (**F7**) (14.5 kDa) and **C**) **AP$_{27}$(BnGlu$_{10}$) (8b**) (**F3**) (68.7 kDa) at room temperature (RT, black curve), 60 °C (red curve), 100 °C (blue curve), 140 °C (pink curve) and 200 °C (green curve).

To further analyse these secondary structures changes, quantification of relative amounts for α-helices and β-sheets was realized by using Gaussian functions in the range of 1600 – 1680 cm^{-1} (Table 12) according to literature.[297] Starting from 11 % in **AP$_2$(BnGlu$_{10}$) (8b**) (**F10**) preferring β-sheet conformation, the formation of β-sheet increases slowly from room temperature over 60 °C to 100 °C

to 26 %. The biggest changes for transition from α-helix to β-sheet conformation was found by increasing the temperature further to 140 °C (53 % β-sheet) and 200 °C (85 % β-sheet). This effect was also found for the for **AP$_6$(^{Bn}Glu$_{10}$)** (**8b**) (**F7**) (14.5 kDa) (Figure 33B, black to green curve) and **AP$_{27}$(^{Bn}Glu$_{10}$)** (**8b**) (**F3**) (68.7 kDa) (Figure 33C, black to green curve). As the amount of the β-sheet at room temperature is higher for **AP$_6$(^{Bn}Glu$_{10}$)** (**8b**) (**F7**) (14.5 kDa) (Figure 33B, black curve; 44 % β-sheet) and **AP$_{27}$(^{Bn}Glu$_{10}$)** (**8b**) (**F3**) (68.7 kDa) (Figure 33C, black curve; 64 % β-sheet), the effect for the transition is not significantly pronounced as for the smaller **AP$_2$(^{Bn}Glu$_{10}$)** (**8b**) (**F10**) (3.9 kDa). The molecular weight effect for the formation of the β-sheet structure completely disappears for the samples at 200 °C, as finally all samples display nearly the same relative amount of β-sheet conformation (85 – 90 % β-sheet).

Table 12. Relative amounts for α-helix and β-sheet conformation calculated for temperature dependent FTIR analysis (Figure 33) according to literature.[297]

	AP$_2$(^{Bn}Glu$_{10}$) (8b) F10		**AP$_6$(^{Bn}Glu$_{10}$) (8b) F7**		**AP$_{27}$(^{Bn}Glu$_{10}$) (8b) F3**	
	α-helix	β-sheet	α-helix	β-sheet	α-helix	β-sheet
RT	89	11	56	44	36	64
60 °C	82	18	52	48	35	65
100 °C	74	26	49	51	32	68
140 °C	47	53	44	56	26	74
200 °C	15	85	14	86	10	90

3.2.2.4 Multisegmented polymers of AP$_m$(^{Bn}Asp$_n$)

In a second step the corresponding aspartate polymers (**AP$_m$(^{Bn}Asp$_n$)**) were investigated, revealing an entirely different behaviour: thus for all fractions of **AP$_m$(^{Bn}Asp$_3$)** (**9b**) and **AP$_m$(^{Bn}Asp$_{10}$)** (**10b**) stable α_r-conformation for **AP$_m$(^{Bn}Asp$_3$)** (**9b**) and an α_l-conformation for **AP$_m$(^{Bn}Asp$_{10}$)** (**10b**) (see Appendix Figure S70) were observed, determined by amide I band at 1651 cm^{-1} and 1660 cm^{-1}, respectivly.[93]

Thus, β-sheets could not be found in any of these polymers – a most surprising aspect, as the structural differences between Asp and Glu are comparably minor. It should also be mentioned that for all fractions of **AP$_m$(^{Bn}Asp$_3$)** (**9b**) and **AP$_m$(^{Bn}Asp$_{10}$)** (**10b**) a clear transition from either α_r-helical or α_l-helical conformation to ω-helix without any molecular weight effect could be observed with increasing temperature,[93] with no β-sheet signal in FTIR observed till 200 °C (see Appendix Figure S71 – S72). For oligomers of O^{Bn}Asp$_n$ β-sheet structures were observed only at high temperatures (180 °C), but TGA investigations (not shown) revealed decomposition of **O^{Bn}Asp$_{10}$** (**10a**) and **O^{Bn}Asp$_3$** (**9a**) at 160 °C. We therefore could not investigate the molecular weight depend formation of β-sheet structure in this case, however did not observe a conformational transition to the β-sheets as observed for the respective glutamate oligomers/polymers. In view of the different behaviour of oligo-glutamate and oligo-aspartate in solution[79, 90, 298, 299], this difference is also reflected in the solid state.

3.2.3 Conformational analysis in solution

Finally, CD and FTIR spectroscopic investigations **O^{Bn}Asp$_{10}$** (**10a**) and **O^{Bn}Asp$_3$** (**9a**) and the unfractionated ADMET-polymers **AP$_4$(^{Bn}Asp$_{10}$)** (**10b**) and **AP$_{18}$(^{Bn}Asp$_3$)** (**9b**) in hexafluoroisopropanol

(HFIP), were performed to elucidate their conformation in solution and to understand the chain-length influence, comparing oligomers and respective polymers. HFIP was found to enhance secondary structure formation in synthetic peptides by desiccation and may enhance intramolecular hydrogen bonding contribution in the investigated systems.[300, 301]

3.2.3.1 Oligomers of $O^{Bn}Asp_n$ and multisegmented polymers of $AP_m(^{Bn}Asp_n)$

Different secondary structures for the oligomers in relation to the number of the amino acid repeating unit (**$O^{Bn}Asp_3$ (9a)** *vs.* **$O^{Bn}Asp_{10}$ (10a)**) and the influence of the respective polymers with the same chain length of the oligo-amino acids (**$O^{Bn}Asp_3$ (9a)** *vs.* **$AP_{18}(^{Bn}Asp_3)$ (9b)** and **$O^{Bn}Asp_{10}$ (10a)** *vs.* **$AP_4(^{Bn}Asp_{10})$ (10b)**) could be compared qualitatively. In Figure 34 oligomers **$O^{Bn}Asp_{10}$ (10a)** and **$O^{Bn}Asp_3$ (9a)** and their corresponding ADMET-polymers **$AP_4(^{Bn}Asp_{10})$ (10b)** and **$AP_{18}(^{Bn}Asp_3)$ (9b)** displayed a significant change in secondary structure: **$O^{Bn}Asp_{10}$ (10a)** FTIR spectroscopy revealed an amide I band (Figure 34A, red curve) at 1660 cm^{-1}, which indicates the coexistence of two stable secondary structures, situated exactly between the two characteristic bands of an α_r-helical conformation at 1657 cm^{-1} and an α_l-helical conformation at 1665 cm^{-1}.[93] This signal shifted to 1666 cm^{-1} and decreased in intensity for the ADMET polymer **$AP_4(^{Bn}Asp_{10})$ (10b)** (black curve), indicating the existence of a left handed helical structure and a preferential formation of a β-sheet *via* the appearance of a new signal at 1626 cm^{-1} and a shift from 1549 cm^{-1} to 1528 cm^{-1} in the amide II region.[92, 93]

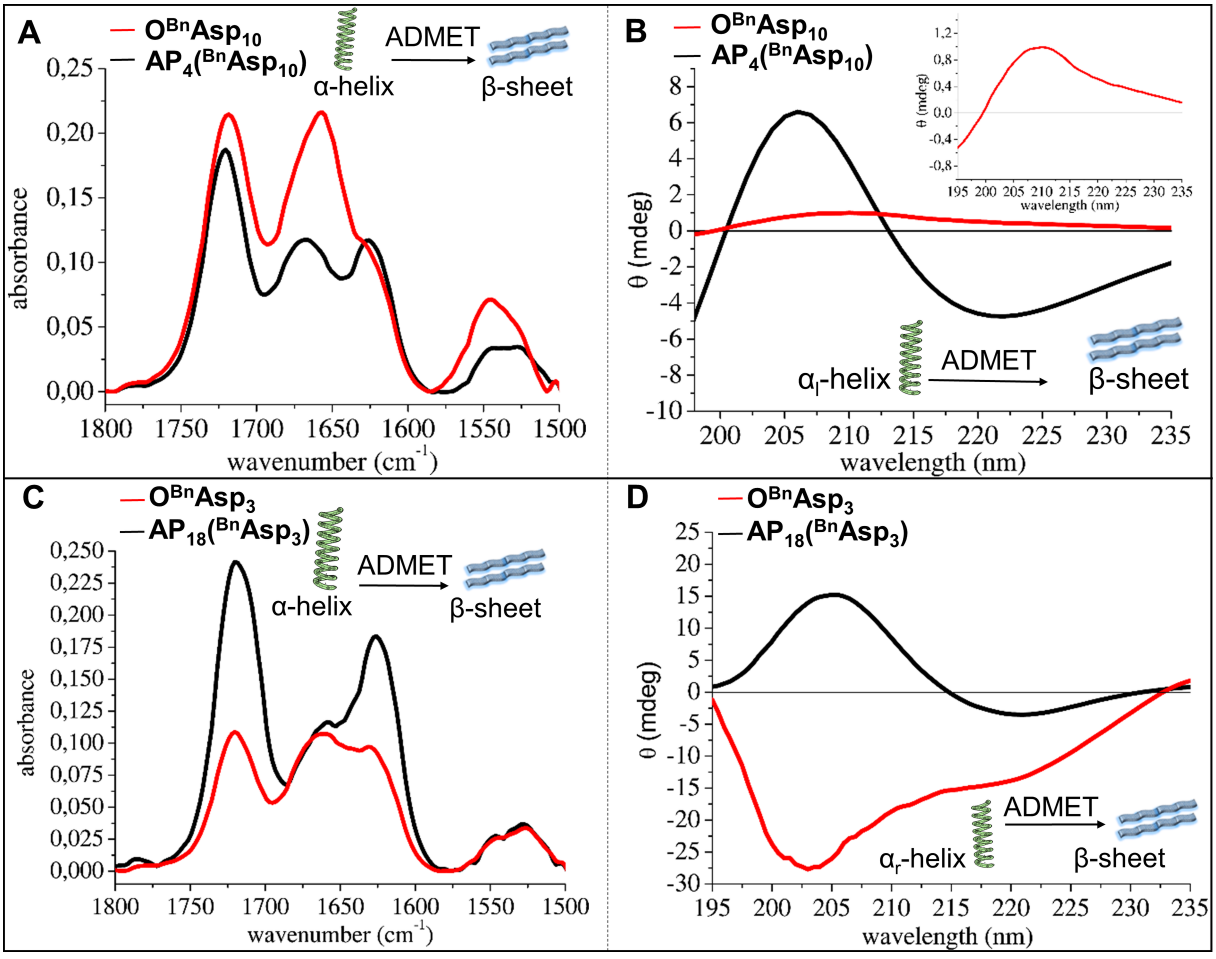

Figure 34. FTIR spectra (**A**, **C**) of the amide I and amide II region at concentrations of 2.0 mg mL^{-1} and CD spectra (**B**, **D**) at 0.2 mg mL^{-1} in HFIP for: **A**+**B**) **$O^{Bn}Asp_{10}$ (10a)** (red) and **$AP_4(^{Bn}Asp_{10})$ (10b)** (black), and **C**+**D**) **$O^{Bn}Asp_3$ (9a)** (red) and **$AP_{18}(^{Bn}Asp_3)$ (9b)** (black).

Additionally, CD spectroscopy (Figure 34B) supported these conformational changes as visible by a transition from the maxima at 224 nm and 210 nm for **O^{Bn}Asp$_{10}$** (**10a**) (red curve) into a local minimum at 221 nm and a maximum at 205 nm for **AP$_4$(^{Bn}Asp$_{10}$)** (**10b**) (black curve).[95] As already known from previous studies, poly-(^{Bn}Asp) esters prefer the formation of a left handed α_l-helical structure with characteristic maxima for the n-π*-transition at 226 nm and π-π*-transition at 212 nm in CD spectroscopy[76]. However, CD spectrum of **O^{Bn}Asp$_{10}$** (**10a**) (red curve) show characteristic signals for a α_l-helical structure even if the magnitudes for the maxima are less pronounced, explainable by a mixture of α_l- and α_r-helical structures due to the *Đ* of the sample (this feature will be discussed further for **O^{Bn}Asp$_3$** (**9a**)). **AP$_4$(^{Bn}Asp$_{10}$)** (**10b**) (black curve) shows the formation of a β-sheet with a characteristic band displaying negative ellipticity and a negative peak occurring at 223 nm proving the result of the FTIR measurement.[93, 95]

Oligomer **O^{Bn}Asp$_3$** (**9a**) (Figure 34C, red curve) displayed a coexistence of the α_r-helical conformation (1658 cm^{-1}) and a β-sheet (1630 cm^{-1}) in the amide I region. Additionally, CD spectroscopy showed two minima at 221 nm and 204 nm, which was found to be characteristic for a α_r-helical conformation (Figure 34D, red). In comparison to previous IR and CD results of **O^{Bn}Asp$_{10}$** (**10a**) (Figure 34A – 34B, red curve), the helical screw sense has been changed from "left-handed" to "right-handed" by decreasing the amino acid repetitive unit in **O^{Bn}Asp$_3$** (**9a**) from 10 to 3. Although the α_l-helical conformation is more stable than the α_r-helical structure in (^{Bn}Asp) esters due to steric hindrance, switches of the helical screw sense may be possible due to the small energy difference between both structures and was already observed for (^{Bn}Asp) esters in films by decreasing the number of the amino acids in the oligomer.[92] Previous studies investigating the effects of solvents on (^{Bn}Asp) ester brushes revealed no correlation between solvent polarity or solubility parameters on α_r- or α_l-helical conformational stabilities.[93]

A significant conformational change towards the β-sheet conformation was observed in the polymer **AP$_{18}$(^{Bn}Asp$_3$)** (**9b**), as indicated by a strong shift in amide I region from 1658 cm^{-1} to 1630 cm^{-1} (Figure 34C, black curve) and a change from two minima at 221 nm and 204 nm into a local minimum at 221 nm and a maximum at 205 nm in CD-spectroscopy (Figure 34D, black curve). Similar, comparing **O^{Bn}Asp$_{10}$** (**10a**) to the ADMET polymer **AP$_4$(^{Bn}Asp$_{10}$)** (**10b**) a transition from an α-helix into β-sheet is observed.

3.2.3.2 Oligomers of O^{Bn}Glu$_n$ and multisegmented polymers of AP$_m$(^{Bn}Glu$_n$)

In contrast the glutamate-oligomers **O^{Bn}Glu$_{10}$** (**8a**) and polymers **AP$_3$(^{Bn}Glu$_{10}$)** (**8b**) (Appendix Figure S73) behave opposite in FTIR spectroscopy displaying already a coexistence of helical and β-sheet conformation as revealed by the amide I signal at 1654 cm^{-1} and 1626 cm^{-1} and a broad signal with a maximum at 1547 cm^{-1} in the amide II region[70, 71, 77], matching thus with previous results for oligo-(^{Bn}Glu) esters with n≤18.[294] The CD spectra (Appendix Figure S73) of both structures **O^{Bn}Glu$_{10}$** (**8a**) (red curve) and **AP$_3$(^{Bn}Glu$_{10}$)** (**8b**) (black curve) shows two local minima at 206 nm and 221 nm, indicative of a α_r-helical conformation.[302] Thus, no significant change in secondary structure formation for the glutamic acid building blocks after embedding into the multisegmented polymer chain could be observed.

Previous studies have shown that α-helical conformations were better stabilized by oligomers and polymers of (^{Bn}Glu) esters than (^{Bn}Asp) esters in solution.[76, 84] Due to these energy differences for stabilizing helical conformations the dynamic switch between different secondary structures like α-helix and β-sheet can be induced in **O^{Bn}Asp$_{10}$** (**10a**) and its corresponding polymer **AP$_4$(^{Bn}Asp$_{10}$)** (**10b**), whereas the amino acid building blocks in **O^{Bn}Glu$_{10}$** (**8a**) and **AP$_3$(^{Bn}Glu$_{10}$)** (**8b**) remains in the same conformation in both, the oligomer and the multisegmented polymer. It has been proposed by several authors previously[91, 92] that the interplay between hydrogen bonds of the NH-amides to either the carbonyl-groups of the Bn-protected side chains or those of the main chain is more pronounced for

O^{Bn}Asp than in O^{Bn}Glu-oligomers. We believe that this effect is responsible for the different behavior of Glu *vs.* Asp oligomeric amino acids.

3.2.3.3 Fractionated multisegmented polymers of AP$_m$(^{Bn}Asp$_n$)

The dynamic switch of α-helical and β-sheet conformation in the synthesized (^{Bn}Asp) esters was further investigated in HFIP-solutions by studying the effect of different chain length (m) (*via* molecular weight, M_n) of the whole ADMET-polymer towards the secondary structure, comparing the oligomer **O^{Bn}Asp$_3$** (**9a**) (red), the corresponding unfractionated polymer **AP$_{18}$(^{Bn}Asp$_3$)** (**9b**) (black) and the fractionated samples **AP$_5$(^{Bn}Asp$_3$)** (**9b**) (**F11**) (blue) and **AP$_{136}$(^{Bn}Asp$_3$)** (**9b**) (**F3**) (green) (see Table 11) by FTIR (Figure 35A) and CD-spectroscopy (Figure 35B). Thus in effect ADMET polymer **AP$_5$(^{Bn}Asp$_3$)** (**9b**) (**F11**) with an average molecular weight of 5.2 kDa (Figure 35A, blue curve, Table 11) indicated a higher relative amount of β-sheet which further increased in case of the non-fractionated **AP$_{18}$(^{Bn}Asp$_3$)** (**9b**) (black curve) with increasing molecular weight to 20.0 kDa indicated by a shift from 1658 cm^{-1} to 1625 cm^{-1}. The polymer with the longest number (m=136) of oligo-amino acid segments **AP$_{136}$(^{Bn}Asp$_3$)** (**9b**) (**F3**) (green curve) (corresponding to a molecular weight of 153.4 kDa) showed a further slight increase in β-sheet secondary structure, clearly demonstrating a molecular weight dependence for the conformational change between helical and β-sheet conformation: a trend supported by CD-spectroscopy (Figure 35B). Interactions of the oligo-amino acids building blocks either within or between the chains stabilize the β-sheet conformation due to the higher amount of amino acids per chain, similar to trends observed in di- and triblock copolymers can be proposed.[296, 297] In general the β-sheet conformation represents the thermodynamically more stable conformation, as proposed by experiments in the solid state.[92] As the secondary structures also depends on the distance for interactions between the amino acids, concentration dependent measurements in HFIP were performed for oligomers **O^{Bn}Asp$_3$** (**9a**) and **O^{Bn}Asp$_{10}$** (**10a**) and the corresponding unfractionated ADMET Polymers **AP$_{18}$(^{Bn}Asp$_3$)** (**9b**) and **AP$_4$(^{Bn}Asp$_{10}$)** (**10b**). For all sample's concentration of 10 mg mL^{-1}, 5 mg mL^{-1}, 2 mg mL^{-1} and 1 mg mL^{-1} in HFIP were adjust and measured *via* FTIR (see Appendix Figure S74-S77). In all cases, the oligomers and polymers stabilized the α-helical conformation at 10 mg mL^{-1}, turning into a coexistence of β-sheet and α-helix with decreasing concentration.

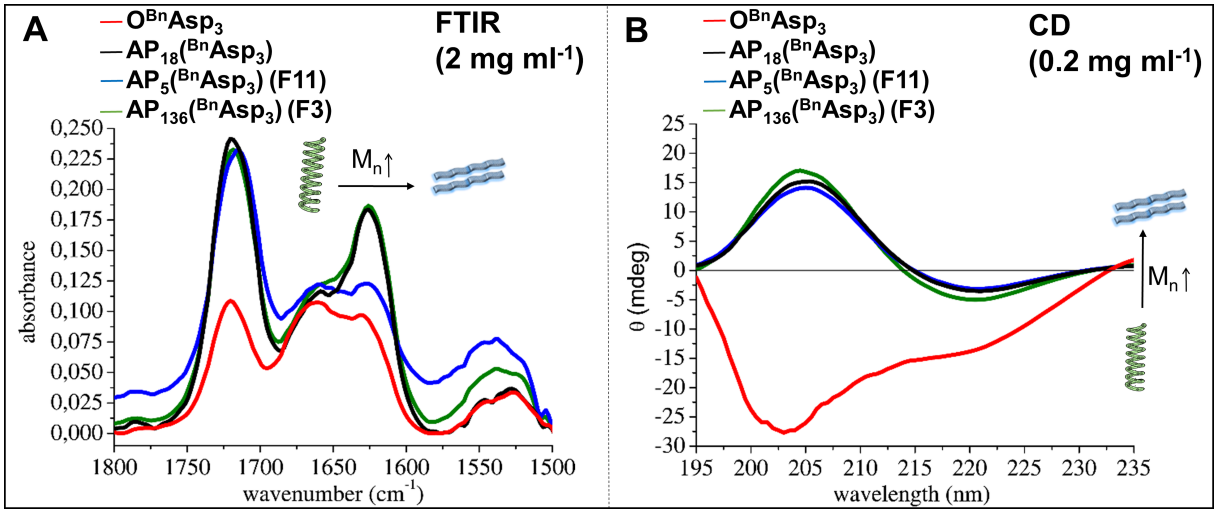

Figure 35. FTIR spectra in amide I and amide II region at 2 mg mL^{-1} (**A**, left) and CD spectra (**B**, right) at 0.2 mg mL^{-1} in HFIP for **O^{Bn}Asp$_3$** (**9a**) (red) (1.1 kDa), non-fractionated **AP$_{18}$(^{Bn}Asp$_3$)** (**9b**) (20.0 kDa) (black), fractionated **AP$_5$(^{Bn}Asp$_3$)** (**9b**) (**F11**) (5.2 kDa) (blue), and **AP$_{136}$(^{Bn}Asp$_3$)** (**9b**) (**F3**) (153.4 kDa) (green).

3.3 Investigation of ROP of Aib-NCA (11) and ACHC-NCA (12)

Parts of the results and discussion as well of the experimental part were already published in

"Reprinted (adapted) with permission from (Freudenberg, J.; Binder, W. H.*, Chirality Control of Screw-Sense in Aib-Polymers: Synthesis and Helicity of Amino Acid Functionalized Polymers. *ACS Macro Let.* **2020**, 9 (5), 686-692. DOI: 10.1021/acsmacrolett.0c00218). Copyright (2020) American Chemical Society."

As it is well known from literature,[303] the polymerization of **11** initiated by a base takes place according to the activated monomer mechanism and can fairly be accelerated by the addition of ring amide compounds, namely 2-oxazolidone and 3-methyl hydantoin. During the polymerization the NCA anion has a pronounced oxoanionic character, which attacks the 2-carbonyl group of the terminal ring unit. In another work, the ROP of (non-)isotope labeled (a-)chiral Aib-NCA with either NEt_3 and DBU as basic initiators or *n*-hexylamine as amine-initiator was compared.[304] In contrast to hexylamine (14 mers), much higher molecular weight polymers could be synthesized while using NEt_3 (30 mers) and DBU (40 mers), since polymerization followed the activated monomer mechanism instead of normal amine mechanism. However, in both cases, a cloud point was observed during the polymerization, indicating the precipitation of the oligomer.

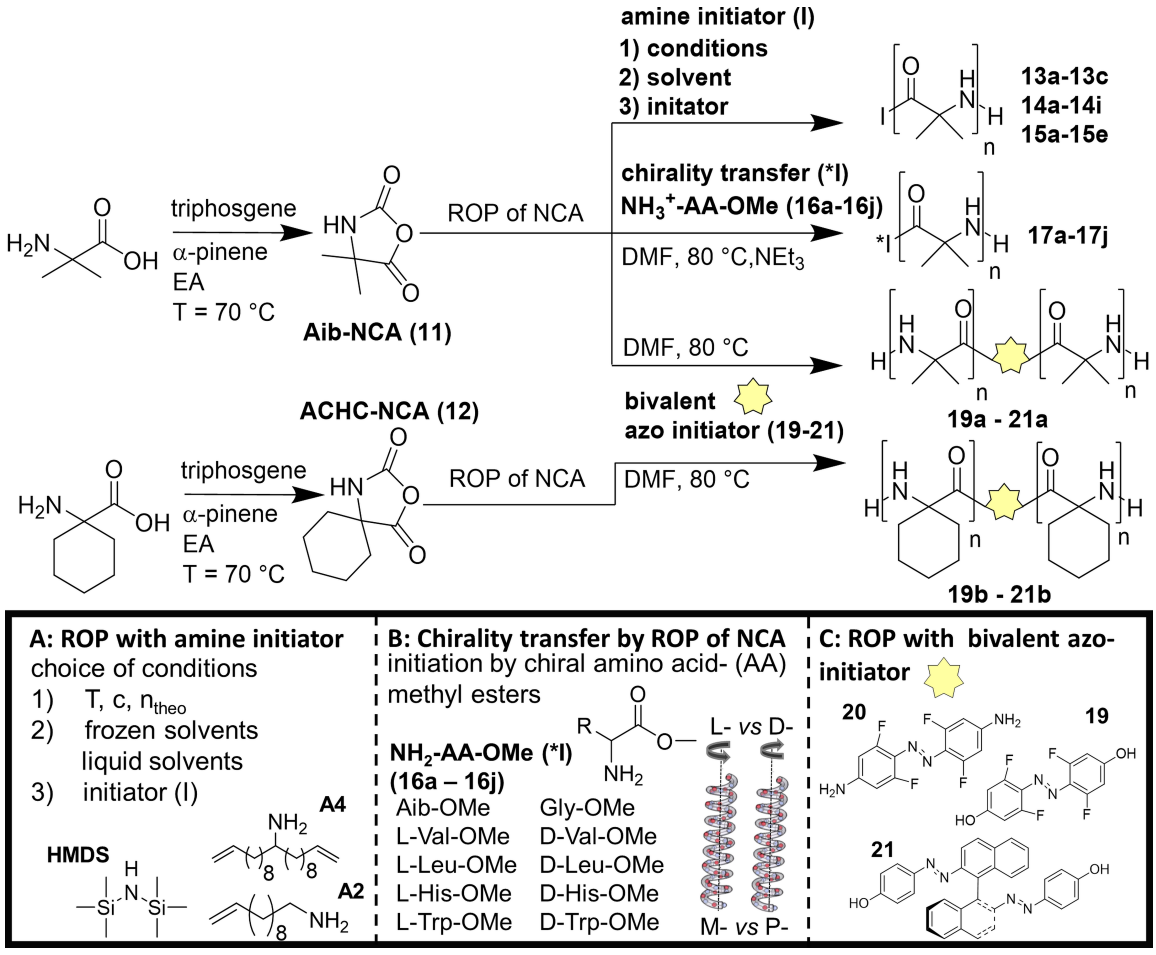

Scheme 4: Synthesis of polymers (PAib) by ROP of **Aib-NCA** (**11**) with amine initiators (**A2**, **A4**, **HMDS**), amino acid-methyl ester hydrochlorides (NH_2-AA-OMe **16a-16j**) and **Aib-NCA** (**11**) and **ACHC-NCA** (**12**) to polymers (PACHC) with the bivalent azo initiator (**19 – 21**).

As the ROP of **Aib-NCA** (**11**) and **ACHC-NCA** (**12**) with other initiators than bases are not well studied, own designed initiators were used for ROP and the final structures of these polymers were investigated by ^{1}H-NMR and MALDI-TOF-MS. For a systematic investigation, the ROP of **Aib-NCA** (**11**) and **ACHC-NCA** (**12**) and following analyses of the final polymers were performed in three parts (Scheme 4). First, the investigation of the ROP of **Aib-NCA** (**11**) with amine initiators under different conditions and in various solvent systems was studied (top), then the ROP with (a-)chiral L-/D-amino acid-methyl esters as initiators was investigated (middle) and third the initiation of **Aib-NCA** (**11**) and **ACHC-NCA** (**12**) by bivalent azo-compounds was explored (bottom).
Synthesis of **Aib-NCA** (**11**) and **ACHC-NCA** (**12**) was realized by the Fuchs-Farthing-method, using triphosgene as reactant and α-pinene as proton catcher (for details see Experimental part 4.5.1, ^{1}H-NMR in Appendix Figure S78). The reaction was accomplished in EA as solvent, as the purity and yields were found to be high for the synthesis of **Glu-NCA** (**5**) and **Asp-NCA** (**6**). Further syntheses of the initiators, chosen methods and analyses of the final polymers will be presented in the following chapters (3.3.1 – 3.3.3).

3.3.1 ROP of Aib-NCA (11) initiated by amine initiator

The ROP of **Aib-NCA** (**11**) with different amine initiators is shown in Scheme 4 (A: ROP with amine initiator). HMDS was obtained commercially and the synthesis of initiator **A2** was described before (chapter 3.1.1 according to literature[270]). Purity of **A2** was proven by ^{1}H-NMR spectroscopy (Appendix Figure S17). For the synthesis of initiator **A4** according to literature[305] 10-undecenoylchloride was converted in 1-dec-9-enyl-undec-10-enylketone (**A3**) in a two-step synthesis using NEt_3 followed by decyclization and decarboxylation with a $NaOH/H_2O$ mixture in the second step. **A3-**amination was realized *via* "Borch reaction" with $NaCNBH_3$ and the final product was purely obtained as proven *via* ^{1}H-NMR and ^{13}C-NMR spectroscopy (For details see Experimental part 4.5.2.1 and Appendix Figure S79-S80). For ROP of **Aib-NCA** (**11**) temperature and chemical parameters like initiator, concentration and *M*/*I* ratio were varied and the molecular weight and the end-group of obtained polymers were characterized *via* MALDI-TOF-MS. Detailed presentation of experimental parameters for chosen reaction systems are shown in Table 13. All other reaction approaches are summarized in Table 15 (see Experimental part 4.5.2.2).

Table 13. Polymerization results and yields for ROP of Aib-NCA (**11**) while varying solvent, monomer to initiator ratio (*M*/*I*), temperature (*T*) and concentrations (*c*). Chain length (n), maximum intensity M_n, min/max M_n and endgroups of the respective polymers are provided by MALDI-TOF measurements.

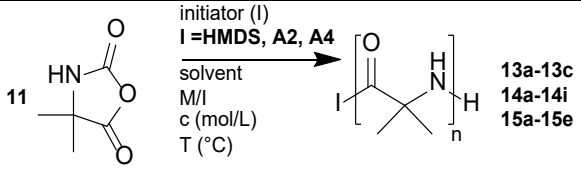

entry	initiator (I) and endgroups on *C*-(E1) and *N*-Terminus (E2)	solvent	M/I	c (mol/L)	T (°C)	yield (%)	M_n MALDI-TOF-MS (Da) (maximum intensity M_n (Min/Max n)
13a	**HMDS** E1: NH_2; E2: H	frozen dioxane	15:1	0.02	11 °C (-24°C)	27	1060.626 (Na^+) (n=12) n=10 – 15
13b			20:1			41	906.485 (K^+) (n=10) n=10 – 15
13c			25:1			32	991.470 (K^+) (n=11) n=11 – 20

entry	initiator (I) and endgroups on *C*- (E1) and *N*-Terminus (E2)	solvent	M/I	c (mol/L)	T (°C)	yield (%)	M_n MALDI-TOF-MS (Da) (maximum intensity M_n (Min/Max n)
14d	**A4** 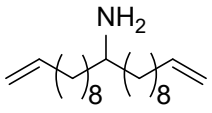 E1: $C_{21}H_{40}N$ E2: H	frozen dioxane	15:1	0.02	11 °C (-24 °C)	55	1451.774 (K^+) (n=13) n=9 – 17
14e			50:1	0.03		53	1536.938 (K^+) (n=14) n=10 – 17
14f			50:1	0.05			1536.986 (K^+) (n=14) n=8 – 24
14g			50:1	0.15			1777.260 (Na^+) (n=17) n=9 – 24
14h			50:1	0.80		60	1006.591 (n=10) + 1793.295 (K^+) (n=17) n=8 – 25
14i		frozen DMA	50:1	0.80	-20 °C (-38 °C)	62	1622.007 (K^+) (n=15) n=10 – 33
15a	**A2** 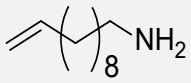 E1: $C_{11}H_{22}N$ E2: H	ET_2O	50:1	2	0 °C	23	1058.595 (K^+) (n=10) n=6 – 19
15b		DCM	50:1	2	0 °C	22	1143.683 (K^+) (n=11) n=6 – 20
15c		Toluene	50:1	2	0 °C	40	1143.602 (K^+) (n=11) n=6 – 19
15d		THF	50:1	2	0 °C	49	1229.037 (K^+) (n=12) n=10 – 22
15e		DMF	12:1	2	80 °C	67	1398.171 (K^+) (n=14) n=11 – 18

*3.3.1.1 ROP of **Aib-NCA (11)** with **HMDS** as initiator*

As it is well known from the ROP of Glu-NCA (**5**) and Asp-NCA (**6**), side reactions like intramolecular amidation and reactions with the solvent caused by the high reactivity of the free amine end-group can lead to termination reactions.[290] In contrast, HMDS was used for controlled polymerization and end-group protection during polymerization within group transfer polymerization (GTP).[191] Consequently, polymererizations were first initiated by HMDS in frozen dioxane. The initiator was tested to ensure that the precipitation of oligomeric Aib species, which was occurring for all other initiating systems, is not caused by side reactions or chain transfer. Furthermore, the polymerization of **Aib-NCA** (**11**) and ring-structured derivates in dioxane systems was found to be not effective in solution at room temperature, but even without initiator the polymerization took place in frozen dioxane with excellent first order kinetics.[306] Additionally, ROP of NCAs in frozen solvents are well known for high control of the final chain length of the polymer.[307] Therefore, first experiments were carried out in frozen dioxane with HMDS as initiator and three different *M*/*I* ratios were adjusted. **Aib-NCA** (**11**) was dissolved in cold dioxane, HMDS was added and the mixture was directly frozen with liquid nitrogen. Then the frozen solution was stored in a freezer for two weeks and thawed (for details see Experimental part 4.5.2.2). After several days, small white particles could be observed in all polymerization systems, which were identified as Aib-oligomers. MALDI-TOF-MS of the finally obtained polymers was performed for molecular weight- and end-group-analysis. In Figure 36 the MALDI-TOF-MS spectrum of the polymer **13a** is shown. The mass spectrum reveals two series and a mass distribution from 890 g mol^{-1} to 1315 g mol^{-1}. The distance between the two series was found to be 16 g mol^{-1}, demonstrating a sodium and a potassium counter ion on the polymer structure. The distance of 85 g mol^{-1} between two

signals of the same series could be identified to the polymer repeating unit of Aib with the maximum at 1060 g mol^{-1} corresponding to a chain length of n=11. End-group analysis revealed a free NH_2-group at the *N*-terminus proving that no side reactions took place during polymerization. The *C*-terminus is connected to a NH_2-group as well, demonstrating the deattachment of silazane during precipitation with MeOH.[191] The measured and simulated pattern of the maximum molecular weight definitely proof the desired structure of the final polymer (Figure 36 inlet).

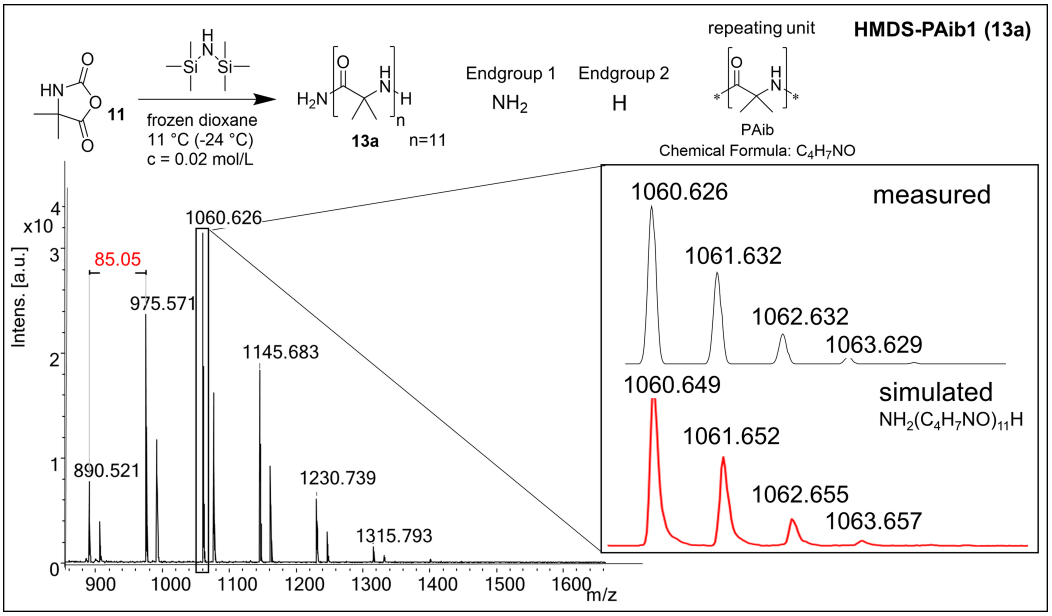

Figure 36. MALDI-TOF-MS spectrum of **13a** and zoom in to measured and simulated pattern for $[E_1\text{-}RU_{n=11}\text{-}E_2Na]^+$ (inlet).

For polymer **13b** and **13c** with a *M*/*I* ratio of 20:1 and 25:1 respectively, no significant changes were observed in MS-spectra (see Appendix Figure S81). In both cases, the polymer repeating unit of Aib, a mass distribution from 890 g mol^{-1} to 1486 g mol^{-1} with its maximum peak at 992 g mol^{-1} and 1060 g mol^{-1} (chain length n=10-12), respectively and the same end-groups (free NH_2-group at *N*-terminus, NH_2-group at *C*-terminus) were found.

*3.3.1.2 ROP of **Aib-NCA (11)** with 1-dec-9-enyl-undec-10-enylamine (**A4**) as initiator*

As no side reactions could be observed for the polymerization with HMDS, initiator **A4** was used in further investigations while keeping the general polymerization procedure (for details see Experimental part 4.5.2.2). The long alkyl chain-initiator has an non-polar character and will possibly increase the solubility of the polymer chain of Aib. Within the syntheses of polymers **14a** – **14d** the *M*/*I* ratios were varied (10:1 – 50:1), whereas no detectable change in the molecular weight distribution and maximum peak (1282 g mol^{-1} *vs.* 1452 g mol^{-1}) was detected in MALDI-TOF-MS analyses (Table 15 Experimental part 4.5.2.2, Appendix Figure S82). As the consumption of the NCA depends on the concentration of the NCA in both, solution and frozen systems[306], the concentration of the monomer in the frozen system was systematically increased. Accordingly, it was checked if the polymerization stops due to the low local concentration of NCA monomers, as in frozen solvents diffusion is prevented. Concentrations of the NCA-monomer were adjusted from 0.03 mol L^{-1} to 0.80 mol L^{-1} (for details see Experimental part 4.5.2.2, Table 15). Obtained polymers **14e** – **14h** were analyzed by MALDI-TOF-MS. The maximum molecular weight peak of polymers **14e** and **14f** shifted to 1536 g mol^{-1}. For polymer **14f** mass distribution increased ranging between 1006 g mol^{-1} to 2217 g mol^{-1}. Further increasing of the NCA-

concentration in frozen dioxane (**14g**: c=0.15 g mol^{-1}, **14h**: c=0.80 g mol^{-1}) led to increased relative intensities for molecular weights over 1537 g mol^{-1}, potentially demonstrating a total higher molecular weight. The highest molecular weight was found to be 2473 g mol^{-1} for polymer **14h**. These results demonstrate the formation of higher molecular weights species during polymerization by using high monomer concentrations in the frozen solvent. However, in all polymerization systems a white precipitation could be observed after several days, so that it can be assumed that the non-polar initiator component did not significantly affect the solubility of the polymer chains.

As solvents with lower melting points are known for a better control in cryo polymerizations,[307] *N*,*N*-dimethylacetamide (DMA) with a melting point of –20 °C was used as solvent for the preparation of **14i** (for details see Experimental part 4.5.2.2, Table 15). As the high monomer concentration within preparation of **14h** (*c*=0.80 g mol^{-1}), led to the highest molecular weights detectable *via* MALD-TOF-MS analysis, the same concentration was adjusted for the ROP of **Aib-NCA** (**11**) in frozen DMA. Procedure for polymerization was done as described for polymers **14a** – **14h**, while the solvent was changed to frozen DMA and the reaction temperature was adjusted to –38 °C. MALDI-TOF-MS analysis of **14i** is shown in Figure 37 demonstrating the formation of the highest molecular weight polymers detectable by MALDI-TOF-MS and revealing a molecular weight distribution from 1091 g mol^{-1} to 3222 g mol^{-1}. The maximum molecular weight peak is located at 1622 g mol^{-1} (Na^+-counter ion) or 1777 g mol^{-1} (K^+-counter ion) and the relative intensities of species with a molecular weight higher than 1622 g mol^{-1} (maximum peak) is high in comparison to the intensities for polymers with a molecular weight less than 1622 g mol^{-1}. Therefore, more polymer species with a molecular weight higher than 1622 g mol^{-1} were detected in MS-spectra, which was additionally proven by ^{1}H-NMR analysis (chain length n=19, see Appendix Figure S83). Results clearly demonstrate the formation of higher molecular weights for polymer **14i** polymerized in frozen DMA instead of dioxane. As precipitation is caused by secondary structure formation in ROP of analogous structured Ala-NCA[187], the assumption made by the results is that the formation of the secondary structure is thus inhibited in DMA (lower melting point and stronger interaction with hydrogen bonds than dioxane) – similar to proteins in frozen water – in turn imparting improved solubility for a then prolonged chain elongation.[308]

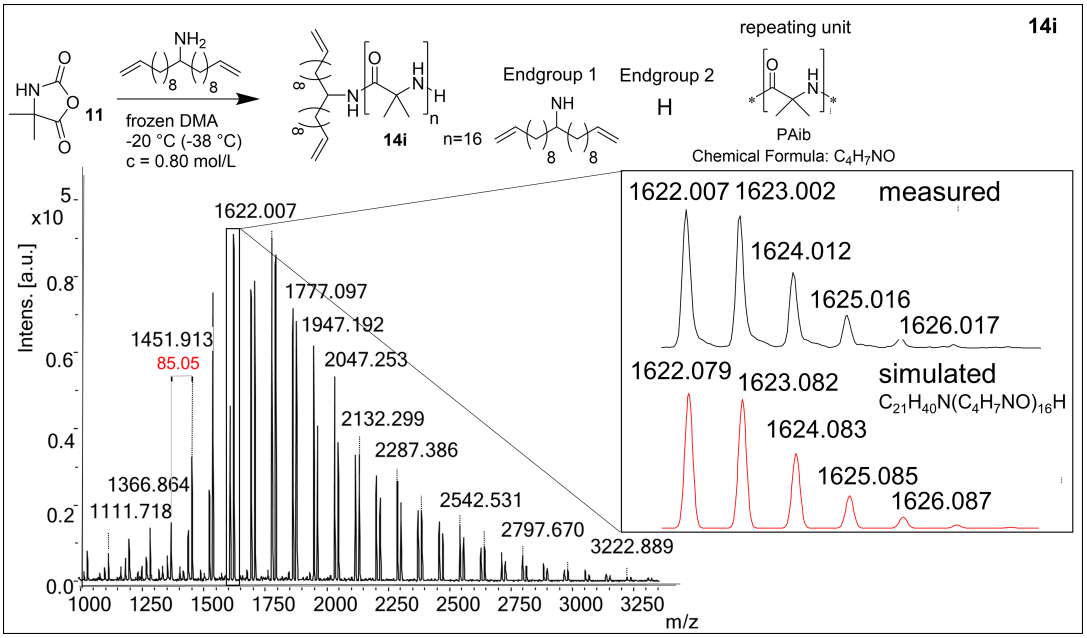

Figure 37. MALDI-TOF-MS spectrum of **14i** and zoom in to measured and simulated pattern for $[E_1\text{-}RU_{n=16}\text{-}E_2K]^+$ (inlet).

*3.3.1.3 ROP of **Aib-NCA (11)** with 10-undecenamine (**A2**) as initiator*

Usually, ROP of NCAs are performed in liquid solvent systems at 0 °C or room temperature.[187] Several solvents like DMF, dioxane or toluene were found to be effective in regard to low polydispersities and high molecular weights. As in all investigated frozen systems the precipitation of the polymer could not be prevented, **Aib-NCA** (**11**) was polymerized in toluene, DCM, Et_2O and THF (for details see Experimental part 4.5.2.2, Table 15), to find a solvent system, in which the final polymer will be soluble and the polymerization can be controlled. The **Aib-NCA** monomer (**11**) was found to be less soluble in DCM and Et_2O, while showing good to superior solubility in toluene and THF. As initiator 10-undecenamine (**A2**) was used, since the investigation of ROP of several NCAs in solution is often realized by the usage of simple amine initiators.[187] The polymerization took place in all investigated solvents with precipitation of the oligomeric species during reaction, but the obtained polymers **15a** – **15d** could only be isolated in low yields. MALDI-TOF-MS analysis of the materials revealed the final polymer structure with the used initiator as end-group on the *C*-terminus (see Appendix Figure S84). Although a *M*/*I* of 50:1 was used, only polymers with a chain length of n=10-20 were detected. Furthermore, the two series (Na^+ and K^+ as counter ion) were assigned to polymers with a free NH_2-group on the *N*-terminus, demonstrating that no side and termination reactions took place and are therefore not responsible for precipitation and low molecular weights.

As NCA-polymerizations of **Glu-NCA** (**5**) and **Asp-NCA** (**6**) (chapter 3.2.1) were found to be effective in DMF as solvent, the polymerization of **Aib-NCA** (**11**) with **A2** as initiator was performed in DMF. Moreover, the temperature was increased to 80 °C as no side or termination reactions were observed in the former polymerizations, while the solubility of peptides usually increases at higher temperatures. In all polymerization systems oligomeric species were precipitating, revealing a chain length of n=10-20, although higher molecular weights were expected for the used *M*/*I*-ratio of 50:1. Therefore, the ratio was changed to *M*/*I* 12:1, to check for a critical chain length at which the oligomer becomes insoluble. To get inside into the kinetics of the polymerization, FTIR-measurements during the ROP of **Aib-NCA** (**11**) with 10-undecenamine (**A2**) as initiator were performed. For evaluation, the FTIR instrument was calibrated by measuring different NCA monomer concentrations (mmol mL^{-1}) in DMF at 80 °C and integrating the areas under the carbonyl signal at 1785 cm^{-1} (see Appendix Figure S85). The regression line was used for determining the real time concentration of the NCA-monomer during the polymerization.

In Figure 38A the 3D-dimensional FTIR-spectroscopic and MALDI-TOF-MS (inlet) for the ROP investigation of **Aib-NCA** (**11**) to **15e** is shown. The investigation of ROP of **Aib-NCA** (**11**) with 10-undecenamine (**A2**) as initiator *via* FTIR was realized by following the stepwise NCA-consumption indicated by the decrease of the NCA-vibration band intensity at 1785 cm^{-1} and 1848 cm^{-1}. After recording virgin **Aib-NCA** (**11**) in solution (0 minutes, grey curve in FTIR), initiator was added and the vibration band intensity (absorbance; z-axis) at 1785 cm^{-1} and 1848 cm^{-1} (x-axis) decreased with time (y-axis, first measuring point at 10 minutes, black curve). After 30 (red curve), 60 (blue curve) and 90 minutes (green curve) the vibration bands are constantly decreasing, demonstrating a uniform NCA-consumption. After 120 minutes (orange curve), oligomers started to precipitate and the NCA-vibration band intensity decreased much slower over a longer time period (cyan curve, 180 min), indicating a slower consumption-rate of the NCA up to its full consumption after 600 minutes (brown curve, disappearance of NCA-vibration band). During polymerization MALDI-TOF-MS spectroscopic investigations were performed after 10 (black), 30 (red), 60 (blue), 90 (green), 120 (orange), 150 (purple), 180 (cyan) and 600 minutes (brown) (Figure 38, inlet). The first recorded MALDI-TOF-MS spectrum after 10 minutes revealed the formation of Aib-oligomers identified by the characteristic distance of 85 g mol^{-1} between the two series (Na^+ or K^+ as counter ion) and the successful initiation by **A2**. At this point a molecular weight distribution between 378 g mol^{-1} (n=2) to 1228 g mol^{-1} (n=12) with

a maximum molecular weight peak at 718 g mol^{-1} related to a repeating unit of n=6 was detected. After 30 minutes, the progressive polymerization could be proven by an increase of molecular weight.

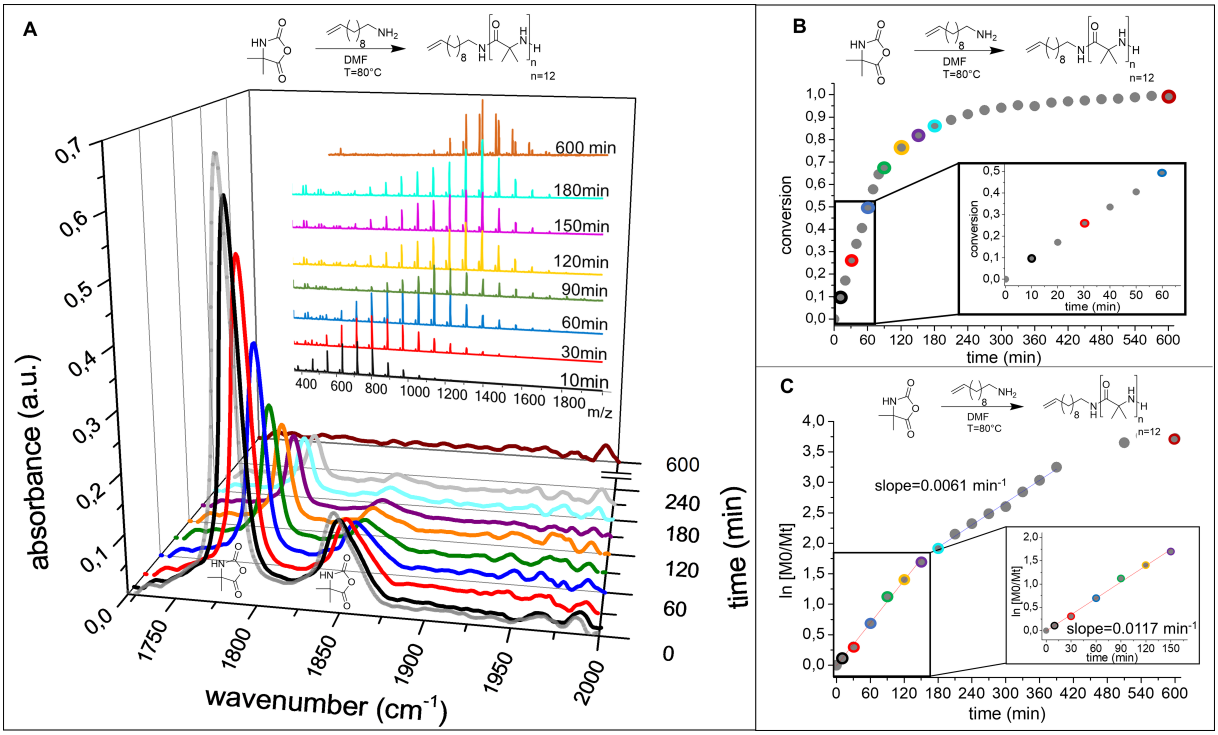

Figure 38. IR-Analysis of the ROP of NCA (**11**), using initiator (**A2**) at T=80 °C and c =2 mol L^{-1}. **A**) Inline monitoring of the NCA-resonance at 1790 cm^{-1} vs. time. Inset: Consecutive MALDI-analysis of the samples drawn at the respective polymerization times. **B**) Plot of conversion vs time (obtained *via* FTIR). **C**) Plot ln[Mo/Mt] vs. time (t) (minutes) inline: slope for the first 150 min with linear behaviour.

Thus, the maximum intense peak shifted to 803 g mol^{-1} (n=7) and the maximum detectable molecular weight was found to be 1483 g mol^{-1} (n=15). Till 120 minutes (yellow curve) the molecular weight maximum intense signal shifted to 1313 g mol^{-1} (n=13) and the molecular weight distribution was detected from 718 g mol^{-1} (n=6) to 1739 g mol^{-1} (n=18). As mentioned, the polymer started to precipitate at this point, showing a clear effect on the molecular weight after 150, 180 and 600 minutes. After 150 minutes, the maximum molecular weight peak did not change in comparison to the MS-spectrum after 120 minutes. After 180 minutes, it shifted to 1398 g mol^{-1}, but no significant changes in the molecular weight distribution were observed. After 600 minutes, NCA-consumption was completed and final MALDI-TOF-MS spectrum revealed a maximum peak at 1398 g mol^{-1}, demonstrating that no change was detected from 180 to 600 minutes. Indeed, the relative intensities for the signals lower than 1398 g mol^{-1} were decreasing and the signals with a lower molecular weight of 1058 g mol^{-1} (n=10) completely disappeared. This indicates the further growth of oligomeric chains with a chain length below n=10 and the difficult chain growth for polymers with a chain length larger n=10. Probably, chain growth was prevented due to insolubility and precipitation of Aib-oligomers. Thus, it is assumed, that only shorter oligomers stayed in solution and continued to polymerize until the NCA was consumed.

In Figure 38B the conversion- *vs.* time-diagram of the ROP of **Aib-NCA** (**11**) to **15e** with 10-undecenamine (**A2**) as initiator is shown. The conversion was calculated by integrating the area under the NCA-vibration band at 1785 cm^{-1} at the corresponding time and comparing it to the original integral value at 0 minutes (eq. 1).

$$\text{Conversion} = 1 - \frac{\boldsymbol{area\,(t)}}{\boldsymbol{area\,(t{=}0min)}} \qquad \textbf{(eq. 1)}$$

The colored dots in the conversion-time-diagram indicate the corresponding conversions for the FTIR-spectra and MALDI-TOF-MS spectra measured after 10 (black), 30 (red), 60 (blue), 90 (green), 120 (orange), 150 (purple), 180 (cyan) and 600 minutes (brown). During the first 60 minutes, a fast polymerization and a constant consumption of NCA-monomer from 9 % (10 min, black dot) over 26 % (30 min, red dot) to exactly 50 % monomer consumption after 60 minutes (blue dot) was observed (inlet Figure 38B). After that point, monomer conversion rate decreased slightly and 67 % (green dot) and 76 % (orange dot) of NCA-monomer were consumed after 90, respectively 120 minutes. Then, the curve showed an asymptotic character typical for living polymerizations shortly before the end of the monomer-consumption. Furthermore, oligomers start to precipitate at this time period, also effecting the monomer consumption rate due to less living chain ends staying in solution. As a result, the conversion progressed slowly, showing 81 % NCA-monomer conversion after 150 minutes (purple dot), 86 % after 180 minutes (cyan dot) and full conversion only after 600 minutes (brown dot).

Living polymerizations are characterized by a constant propagation constant k_p as well as a constant number of active chain ends resulting in first order kinetics and a linear increase in ln [M_0/M_t] *vs.* time plot. The ln [M_0/M_t] *vs*. time plot of the ROP of **Aib-NCA** (**11**) to **15e** with 10-undecenamine (**A2**) as initiator is shown in Figure 38C. For the first 150 minutes, ln [M_0/M_t] increased linearly with time (inlet, black to yellow dot), indicating an ideal living polymerization with the reaction rate of initiation faster than the reaction rate of propagation. Therefore, the observations made by MALDI-TOF-MS investigations like e.g. the absence of termination reactions were confirmed. Besides, the slope of the regression line, which is identified as $k_p \cdot [R^*]$, was calculated (eq. 2, $k_p \cdot [R^*] = 0.0117\ s^{-1}$).

$$\ln \frac{[M_0]}{[M_t]} = k_p \cdot [R^*] \cdot t \qquad \textbf{(eq. 2)}$$

As mentioned, oligomers started to precipitate after 120 minutes, resulting in a decrease of active chain ends in solution. From a kinetic point of view, the precipitation is comparable with termination reactions during polymerization through which the amount of living chain ends is decreasing. Time dependence of ln [M_0/M_t] during termination reactions are characterized by a linear behaviour, but $k_p \cdot [R^*]$ is decreasing as the concentration of active species [R^*] is decreasing as well. In Figure 38C still a linear relationship between ln [M_0/M_t] *vs*. time was observed between 180 to 360 minutes, but the slope decreased ($k_p \cdot [R^*] = 0.0061\ s^{-1}$). Thus, the slower reaction rate could be related to the decreasing concentration of living chain ends in solution, as the propagation constant for the ROP of **Aib-NCA** (**11**) with **A2** as initiator stayed constant. After 420 minutes until the end of the polymerization, the kinetics did not follow a linear behaviour anymore and the further decrease in monomer concentration related to proceeding precipitation of Aib-polymers led to a drastic change of the kinetics. These findings together with the aforementioned results of MALDI-TOF-MS investigations, showing decreasing relative intensities of polymers with a chain length lower than n=10 (Figure 38A), leads to the conclusion, that short, still soluble chains further reacted with remaining NCA-monomer, while constantly oligomers precipitated due to insolubility.

A similar trend for the NCA-monomer consumption was found for the polymerization of Ala-NCA in DMF.[187] At the beginning, a fast polymerization and a linear monomer conversion were observed, but after precipitation of the polymer broader molecular weight distributions were found with increasing polymerization time. Thus, first order kinetic plots of the reactions did not show a linear increase for Ala-NCA polymerization (as well as for other investigated NCAs) as the amount of primary amine end-groups required for propagation continuously decreased due to precipitation. As Aib-polymers are well known for the formation of a sTable 4_{10}-helix and since no initiator- or solvent system was found to

effectively solubilize the oligomeric species, insolubility is probably caused by the formation of secondary structures.[309]

For further characterization of obtained polymer **15e**, ^{1}H-NMR spectroscopy in deuterated HFIP was performed (Figure 39). The successful attachment of the initiator group was confirmed by the characteristic signals for the terminal double bond at 5.8 ppm and 4.9 ppm. The significant signals for the repeating unit of Aib are detectable at 1.3 ppm for the CH_3-protons and 7.2 ppm for the protons of the amide bond. Degree of polymerization (DP) was calculated by integration of the terminal double bond protons (H_a + H_b) and the CH_3-protons of the repeating unit (H_1). Accordingly, a chain length of n=15 was found and the results of the final MALDI-TOF-MS spectrum and the ^{1}H-NMR spectrum of **15e** are in good agreement in regard to the attached end-group and the determined molecular weight.

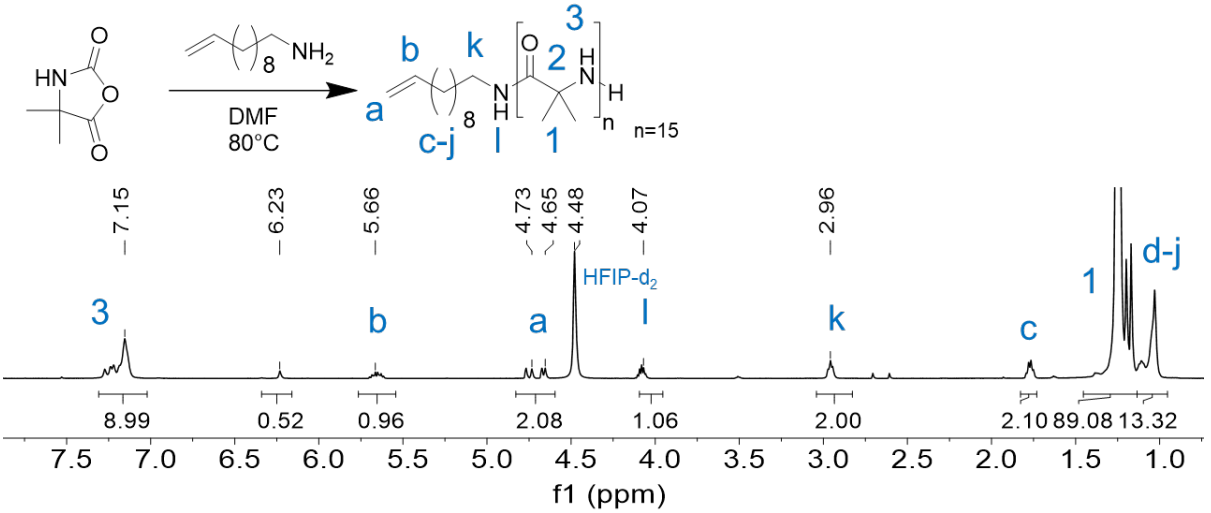

Figure 39. ^{1}H-NMR spectrum of **15e** in HFIP-d_2.

3.3.2 ROP of Aib-NCA (11) initiated by amino acid-methyl esters (16a – 16j)

As ion pairs of primary hydrochloride-initiators are well known for a high controlled ROP of NCAs by producing an equilibrium between active NH_2- and dormant $NH_3^+Cl^-$chain end,[190] the development of new initiator systems in form of amino-acid methyl ester hydrochlorides was realized. Furthermore, the formed achiral Aib-domains are known to form helices with a preference for left- or right-handed screw sense when attached to a chiral residue on *N*- or *C*-terminus, usually synthesized by stepwise synthesis and coupling of individual Aib-residues. For this purpose, ROP of **Aib-NCA** (**11**) with amino acid-methyl esters were performed to better control the polymerization and to investigate the chirality transfer of L- or D-amino acid residues on the achiral Aib-domain (Scheme 4, B: Chirality transfer by ROP of NCA). The respective amino acid-methyl esters (**16a** – **16j**) were synthesized by methyl protection of the corresponding amino-acid with $SOCl_2$ in MeOH (Scheme 5, for details see Experimental part 4.5.3.1), obtaining in total two achiral amino acid methyl-esters (Aib **16a**, Gly **16b**) and eight chiral initiators of L- and corresponding D-amino acids (Val **16c** – **16d**, Leu **16e** – **16f**, His **16g** – **16h** and Trp **16i – 16j**). The obtained amino acid-methyl ester hydrochlorides were analyzed by ^{1}H-NMR (see Appendix Figure S86 – S90) and ^{13}C-NMR spectroscopy proofing the desired structures.

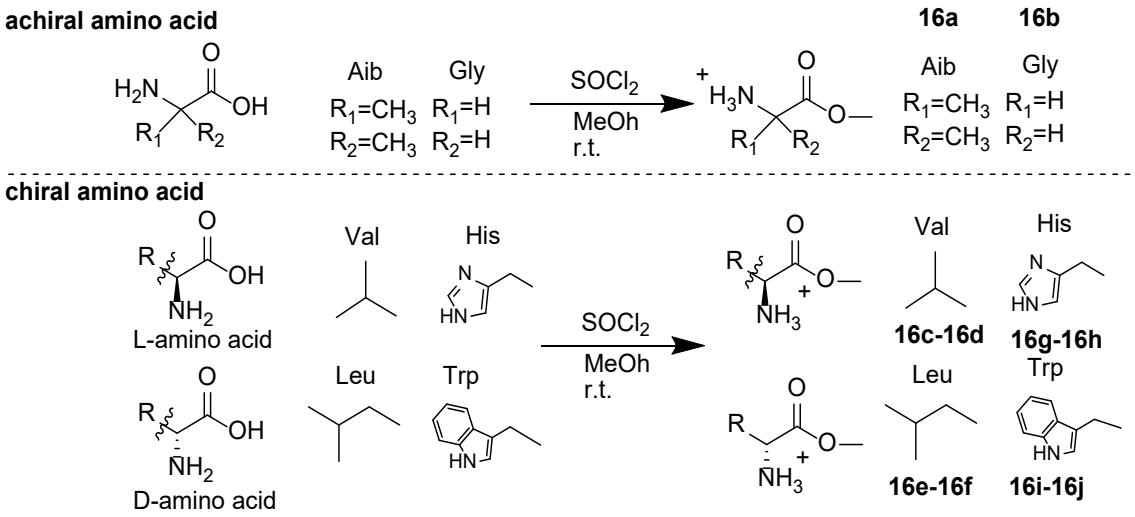

Scheme 5. Synthesis of amino acid-methyl ester hydrochlorides **NH₂-AA-OMe · HCl** (**16a** – **16j**).

To ensure a controlled polymerization, FTIR-measurements for the polymerization of **Aib-NCA** (**11**) with **NH₂-Aib-OMe · HCl** (**16a**) as initiator to **OMe-Aib-PAib** (**17a**) were conducted and the results are shown in Figure 40A.

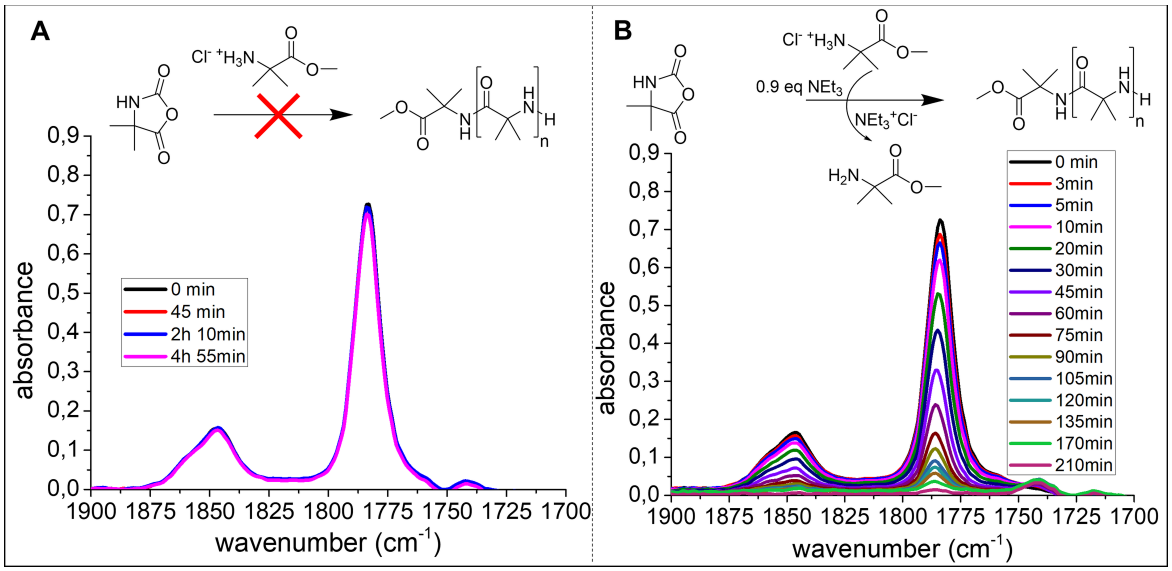

Figure 40: Stepwise NCA-consumption during ROP of **Aib-NCA** (**11**) to **OMe-Aib-PAib** (**17a**) followed by FTIR-investigation of the NCA $_{C\text{-}O\text{-}C}$ anhydride vibration band at 1785 cm^{-1} and 1854 cm^{-1} with **A**) **NH₂-Aib-OMe · HCl** (**16a**) as initiator with no NCA-consumption up to 5 h and **B**) **NH₂-Aib-OMe · HCl** (**16a**) as initiator in combination with 0.9 eq NEt_3 and complete NCA-consumption after 210 min.

First, the NCA-vibration bands of **Aib-NCA** (**11**) at 1785 cm^{-1} and 1854 cm^{-1} were measured without initiator (0 min, black curve). After adding **NH₂-Aib-OMe · HCl** (**16a**) the progress of the polymerization was followed by FTIR investigations and the NCA-vibration bands were measured after 45 minutes (red curve), 2 hours 10 minutes (blue curve) and 4 hours 55 minutes (pink curve). During the investigated time period, no significant change in the intensity and the area under the NCA-vibration band was observed. As a conclusion, no initiation took place by any active NH_2-group of **16a**. In a next

experiment, NEt_3 was added as base to the initiator to deprotonate and activate the NH_3^+-end-group of **NH_2-Aib-OMe · HCl** (**16a**) (Figure 40B). After addition of **Aib-NCA** (**11**) the polymerization was directly initiated by active NH_2-end-groups, proven by decreasing NCA-vibration bands after 3 (red curve) and 5 minutes (blue curve). NCA-vibration bands further decreased with time and disappeared completely after 210 minutes (pink curve), clearly identifying the full conversion of the NCA-monomer.

For all other ROP of NCAs with **16b** – 1**6j** to polymers **17b** – **17j** the activation of the NH_2-group was realized by the addition of NEt_3 (for details see Experimental part 4.5.3.2).

3.3.2.1 ^{1}H-NMR- and MALDI-TOF-MS-analysis

The structure of the obtained polymers and molecular weights determined by NMR spectroscopy (M_n NMR) and MALDI-TOF-MS (maximum intensity signal) are shown in Table 14.

Table 14. Structure, helicity in HFIP-solution, M_n NMR (Da) and M_n MALDI-TOF-MS (Da) for (a-)chiral polymers **17a** – **17j**.

polymer	structure	Helix (P/M) in HFIP-solution	M_n NMR (Da)	M_n MALDI-TOF-MS (Da) (maximum intensity signal) (Min/Max n)
OMe-Aib-PAib (17a)	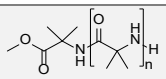	-	1278 (n=14)	1176.380 (K^+) (n=12) n=8 - 16
OMe-Gly-PAib (17b)	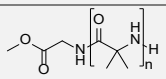	-	1448 (n=16)	1233.395 (K^+) (n=13) n=10 - 17
OMe-L-Val-PAib (17c)	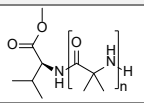	M	1236 (n=13)	1275.252 (K^+) (n=13) n=10 - 19
OMe-D-Val-PAib (17d)	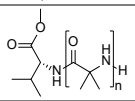	P	1150 (n=12)	1275.213 (K^+) (n=13) n=10 - 17
OMe-L-Leu-PAib (17e)	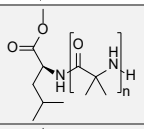	M	1505 (n=16)	1289.156 (K^+) (n=13) n=10 - 19
OMe-D-Leu-PAib (17f)	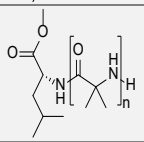	P	1164 (n=12)	1289.178 (K^+) (n=13) n=10 - 19
OMe-L-His-PAib (17g)	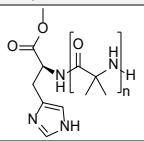	M	1530 (n=16)	1228.356 (K^+) (n=12) n=10 - 20
OMe-D-His-PAib (17h)	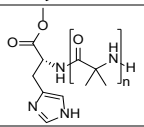	P	1530 (n=16)	1228.339 (K^+) (n=12) n=10 - 18
OMe-L-Trp-PAib (17i)	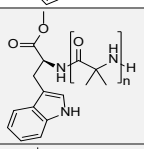	-	--[a]	1362.147 (K^+) (n=13) n=10 - 17
OMe-D-Trp-PAib (17j)	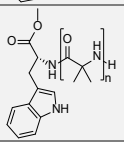	-	--[a]	1277.089 (K^+) (n=12) n=9 - 19

[a] Decomposition in ^{1}H-NMR due to acidic conditions.

For all synthesized polymers (**17a** – **17j**) initiated by amino acid-methyl ester hydrochlorides (**16a** – **16j**) MALDI-TOF-MS and ^{1}H-NMR investigations (in D_2SO_4) were performed. In Figure 41 MALDI-TOF-MS spectrum of **OMe-Aib-PAib** (**17a**) and in Figure 42 ^{1}H-NMR analysis of **NH_2-L-Val-OMe · HCl** (**16c**) in DMSO-d_6 (top) and of **OMe-L-Val-PAib** (**17c**) (bottom) in D_2SO_4 is shown. All other ^{1}H-NMR spectra and MALDI-TOF-MS analyses are shown in the Appendix (Figure S91 – S99).

The MALDI-TOF-MS spectrum (Figure 41) of **OMe-Aib-PAib** (**17a**) revealed a mass distribution from 836 g mol^{-1} to 1516 g mol^{-1} with a maximum peak at 1176 g mol^{-1}. Two series with a distance of 85 g mol^{-1} each were detected, while the lower molecular weight series showed a lower intensity. The distance between signals of different series was determined to be 16 g mol^{-1}, indicating two polymer series with Na^+ and K^+ as counter ion (Figure 41, inlet on top). The signal at 1176 g mol^{-1} was assigned to the polymer $[E_1\text{-}RU_{n=12}\text{-}E_2K]^+$ with potassium as counter ion, which is confirmed by the agreement of the experimental and simulated data (Figure 41, inlet on bottom). As a result of that, the main series definitely indicates the expected polymer structure.

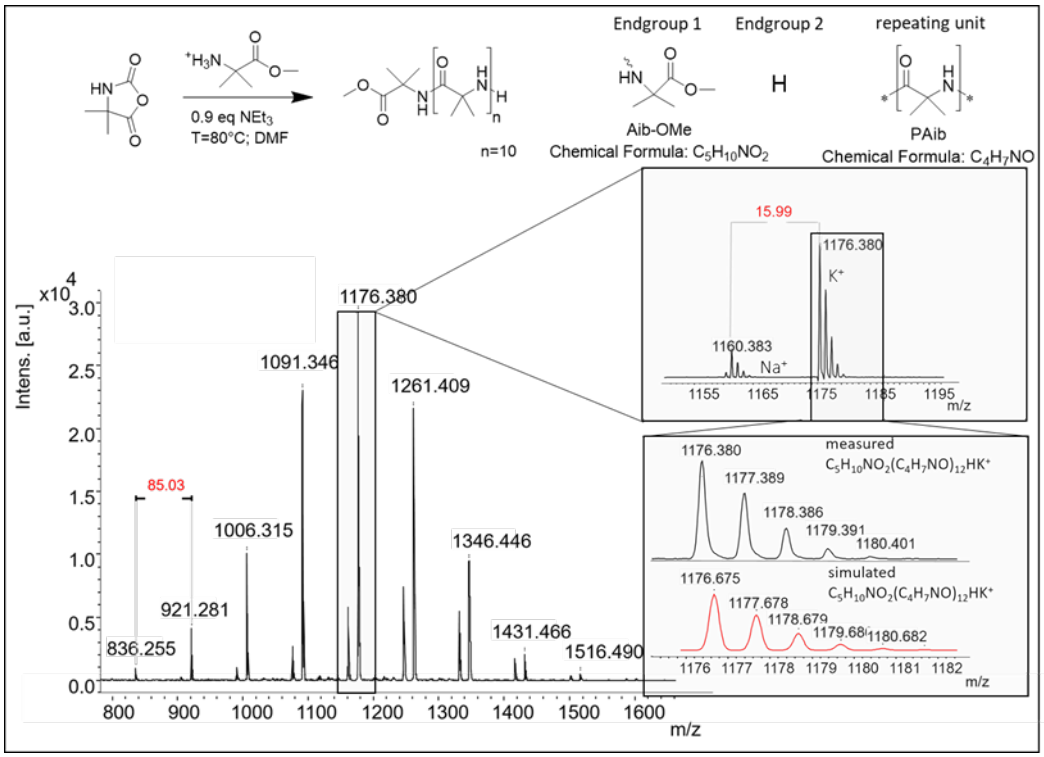

Figure 41. MALDI-TOF-MS spectrum of **OMe-Aib-PAib** (**17a**), zoom in to $[E_1\text{-}RU_{n=12}\text{-}E_2K]^+$ and $[E_1\text{-}RU_{n=12}\text{-}E_2Na]^+$ to show both series with the corresponding end-groups (inlet top) and measured and simulated pattern for $[E_1\text{-}RU_{n=12}\text{-}E_2K]^+$ (inlet bottom).

Successful methyl ester protection of **NH_2-L-Val-OMe · HCl** (**16c**) (top) at the *C*-terminus was proven by ^{1}H-NMR (Figure 42, top) as the characteristic signal of the methyl ester group can be observed at 3.7 ppm. Characteristic signals of the CH-proton of the side chain at 2.2 ppm and of methyl-protons at 1.0 ppm were also assigned, while at 8.7 ppm the NH_3^+-protons were detected. The successful synthesis of **OMe-L-Val-PAib** (**17c**) (Figure 42, bottom) was determined by the presence of the new, broad signal at 1.6 ppm, which can be assigned to methyl-group protons of the repeating Aib-unit. All other signals of the initiating species **NH_2-L-Val-OMe · HCl** (**16c**) like the new signal of the NH-proton at 6.3 ppm of the formed peptide bond during initiation could be assigned proving the presence of the initiator at the *C*-terminus of the polymer. Since D_2SO_4 was used as solvent for **OMe-L-Val-PAib** (**17c**), the signals

of the initiator group partially shifting to higher ppm-values and were detected as broad signals. The resonance of the methyl-ester protons can be used to calculate the molecular weight of the polymer by determining the ratio of the integrals of the CH_3-protons of the repeating unit. The assigned ratio of 14:1 led to a molecular weight of 1320 g mol^{-1} for **OMe-L-Val-PAib** (**17c**) which is in accordance with the maximum peak in MALDI-TOF-MS of 1275 g mol^{-1} (n=13).

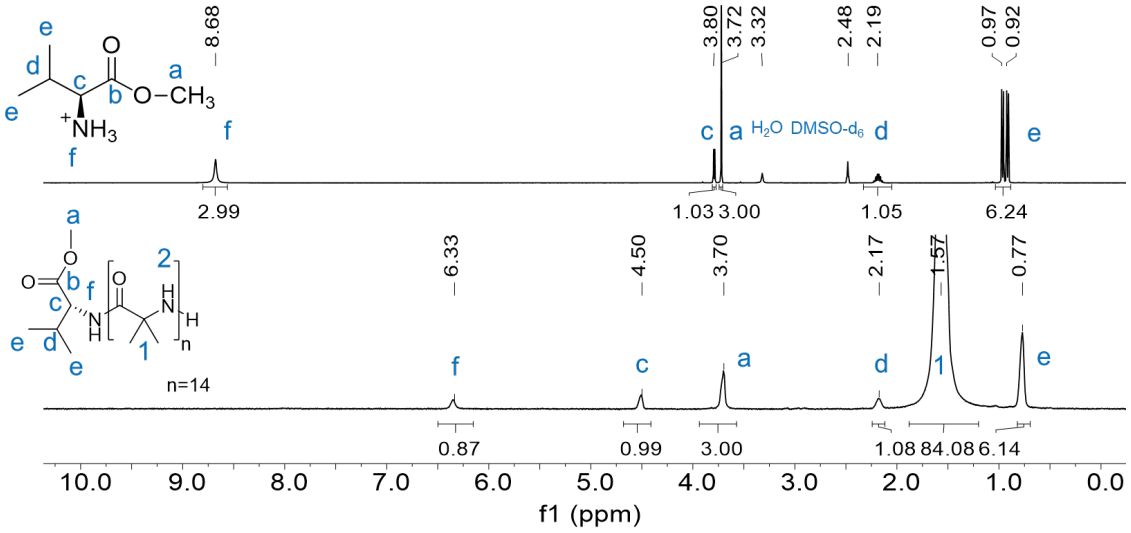

Figure 42. ^{1}H-NMR analysis of **NH_2-L-Val-OMe · HCl** (**16c**) in DMSO-d_6 (top) and of **OMe-L-Val-PAib** (**17c**) (bottom) in D_2SO_4

3.3.2.2 FTIR- and CD-analysis

Since Aib-polymers are well known for their stable conformation of 3_{10}-helices[24, 30, 106-108], polymers **17a** – **17j** were investigated *via* FTIR- and CD-measurements. Temperature-dependent IR-measurements of polymer **17a** at room temperature (RT, black curve), 60 (red curve), 100 (blue curve), 140 (pink curve) and 200 °C (green curve) (see Appendix Figure S100A) revealed an amide I band at 1652 cm^{-1} and an amide II band at 1531 cm^{-1} at all temperatures, demonstrating a stable helical conformation in this temperature range. Furthermore, time-dependent FTIR-measurements of **OMe-Aib-PAib** (**17a)** (see Appendix Figure S100B) at 200 °C after 0 minutes (black curve), 1 (red curve), 1.5 (blue curve), 3 (pink curve), 24 (green curve) and 48 hours (dark blue) and after cooling down to room temperature after 48 hours (violet curve) prove the stability of the helical conformation, as the amide I band at 1652 cm^{-1} and an amide II band at 1531 cm^{-1} sty constant over the whole time period.

As initiators **16c** – **16j** have a chiral center, it will be located on the *C*-terminus of the corresponding polymers **17c** – **17j** after polymerization. To investigate the influence of the introduced chirality on the screw sense direction of formed helices in polymers **17c** – **17j**, solid state FTIR- and CD-measurements in HFIP solution were performed. Solid state FTIR spectra of polymers **17c** – **17j** in the amide I and amide II (see Appendix Figure S101) revealed two main signals at 1650-1651 cm^{-1} in amide I region and at 1535 – 1538 cm^{-1} in amide II region being characteristic for a helical conformation. By comparing the corresponding L- and D-amino acid-methyl esters **17c** *vs.* **17d** (see Appendix Figure S100A black *vs.* red curve), **17e** *vs.* **17f** (see Appendix Figure S101A blue *vs.* pink curve), **17g** *vs.* **17h** (Figure see Appendix Figure S101B green *vs.* violet curve) and **17i** *vs.* **17j** (see Appendix Figure S101B orange *vs.* grey curve) no significant change in the amide I and amide II region was observed.

Next, CD-measurements of polymers **17a** – **17j** in HFIP-solution were performed (Figure 43).

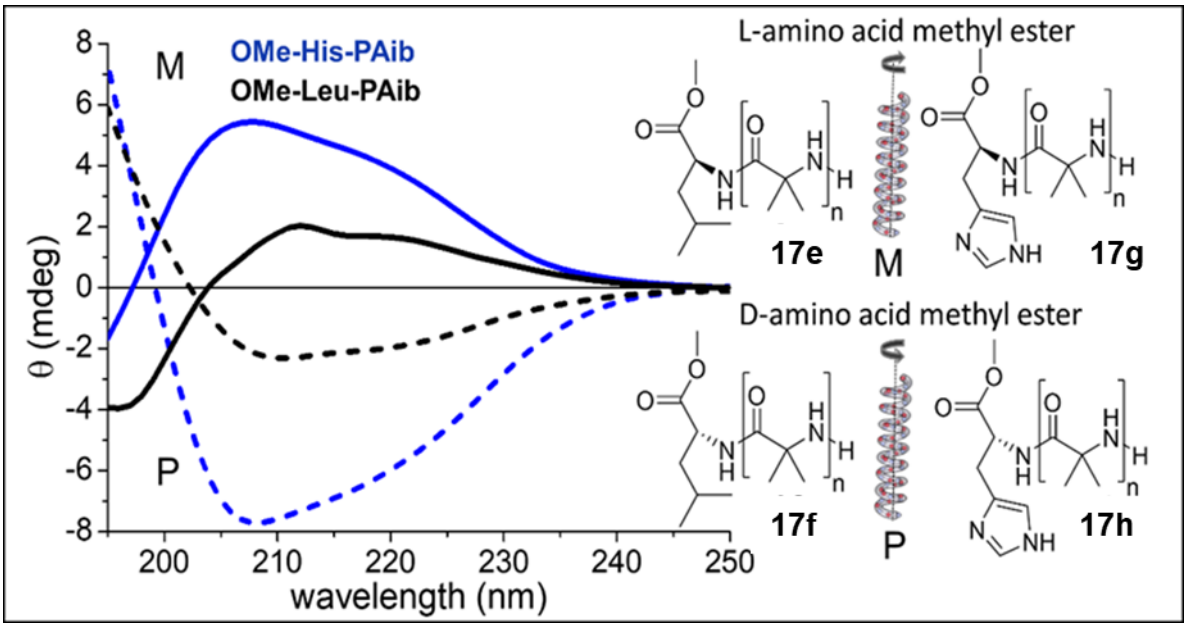

Figure 43: CD spectra in HFIP (0.2 mg mL^{-1}) of **OMe-L-Leu-PAib** (**17e**) (straight curve, black), **OMe-D-Leu-PAib** (**17f**) (dotted curve, black), **OMe-L-His-PAib** (**17g**) (straight curve, blue) and **OMe-D-His-PAib** (**17h**) (dotted curve, blue).

As polymers **OMe-Aib-PAib** (**17a**) and **OMe-Gly-PAib** (**17b**) have no chiral character due to the used achiral initiators, they were therefore used as reference. Both, **OMe-Aib-PAib** (**17a**) and **OMe-Gly-PAib** (**17b**) (see Appendix Figure S102A light and dark grey curve), revealed no signal between 250 nm to 195 nm therefore demonstrating achiral character of the polymers and no specific preference for a certain screw sense direction of the helical conformation determined by FTIR spectroscopy (see Appendix Figure S100). A different result could be obtained for polymers with all chiral amino acids attached: Thus, for **OMe-L-Leu-PAib** (**17e**) (Figure 43 straight curve, black) two local maxima at 221 nm and 211 nm were observed, demonstrating the formation of a helical conformation and the preference for a left-handed (M) screw sense direction. **OMe-D-Leu-PAib** (**17f**) (Figure 43 dotted curve, black) revealed two local minima at 221 nm and 209 nm, also indicating a helical conformation but with a preference for a right-handed (P) screw sense direction. The same behaviour was detected for **OMe-L-His-PAib** (**17g**), revealing local maxima at 220 nm and 208 nm and **OMe-D-His-PAib** (**17h**) with local minima at 221 nm and 208 nm (Figure 43 straight and dotted curve, blue). **OMe-L-Val-PAib** (**17c**) (see Appendix Figure 102B straight curve, red) and **OMe-D-Val-PAib** (**17d**) (see Appendix Figure 102B dotted curve, red) a mirrored behavior of the CD-curves could be observed, revealing a maxima/minima at 214 nm. For **OMe-L-Trp-PAib** (**17i**) and **OMe-D-Trp-PAib** (**17j**) (see Appendix Figure 102C straight and dotted curve, green) a mirrored behavior at wavelengths higher than 220 nm was observed as well, in which both polymers revealed a CD signal at 224 nm (maximum for **OMe-L-Trp-PAib** (**17i**) and minimum for **OMe-D-Trp-PAib** (**17j**)). At lower wavelengths, both CD-spectra show a crossover point at 214 nm and a positive local minimum at 206 nm was found. Furthermore, both CD-spectra proceeded in a positive direction of θ. As described in literature,[310] the high absorption starting from 220 nm is caused by the Trp-side group and corresponding exciton coupling between indole chromophores showing a negative band at 217 nm and a positive band at 207 nm. These signals are overlapping with the CD signal of the secondary structure of the Aib-domain.

Results are similar to previous observations for L-Val-butyl ester[140], in which the heliogenic achiral Aib-domain clearly preferred the formation of a left-handed 3_{10}-helix in MeOH-solution detectable by CD-spectroscopy when attached on the *C*-terminus of an Aib-tetramer. The unfavorable O-O interaction between the main chain carbonyl group and the ester group of the connected residue resulted in the same sign of the torsion angle of the attached residue and a preference for a left-handed helical conformation. [140] A similar behavior was observed for the here investigated systems suggesting that it is therefore independent of an attachment of the amino acid by stepwise synthesis or as initiator in the ROP of **Aib-NCA** (**11**).

3.3.3 ROP of Aib-NCA (11) and ACHC-NCA (12) initiated by bivalent azo-initiators

As the ROP of **Aib-NCA** (**11**) was successful for the initiation with amine-initiator and amino acid-methyl esters at 80 °C in DMF, polymerization was performed with the azo-initiators **19-21**.[311] (Scheme 4, C: ROP with bivalent azo-initiator**)**. The synthesis of the azo-initiators **Azo-OH-DFA** (**19**), **Azo-NH$_2$-DFA** (**20**) and **Azo-Dop-OH** (**21**) is shown in Scheme 6.

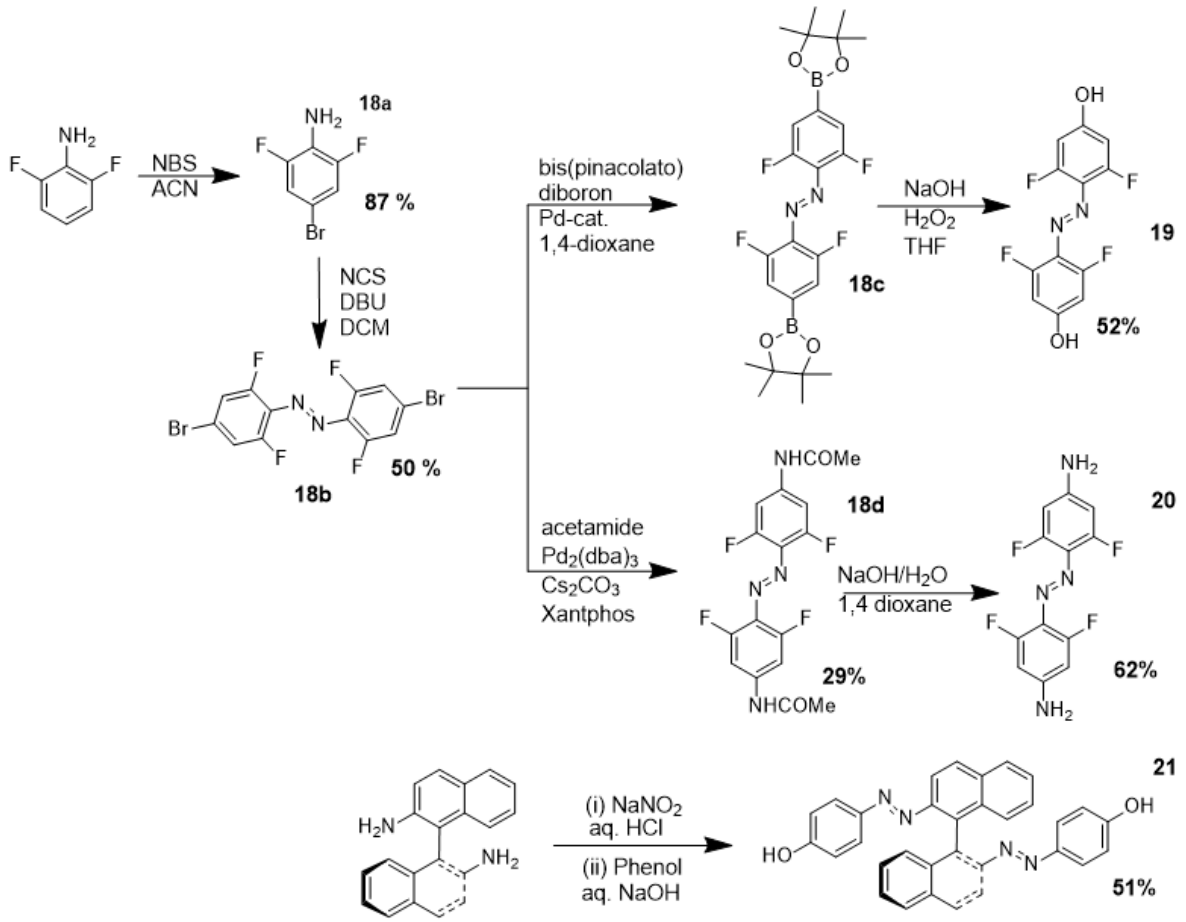

Scheme 6. Synthesis of azo-initiators **Azo-OH-DFA** (**19**), **Azo-NH$_2$-DFA** (**20**) and **Azo-Dop-OH** (**21**).

Azo-OH-DFA (**19**) and **Azo-NH$_2$-DFA** (**20**) were prepared starting with **Azo-Br-DFA** (**18b**), which was synthesized by oxidative coupling of **Br-DFA** (**18a**) with *N*-chlorosuccinimide (NCS) in the presence of an organic base 1,8-diazabicyclo[5.4.0]undec-7-ene (DBU).[312] **Azo-Br-DFA** (**18b**) was then converted with bis(pinacolato)diboron in a Pd-catalyzed reaction to obtain **Azo-Bor-DFA** (**18c**), which was used as starting material in the next step and treated with NaOH and H_2O_2 to obtain **Azo-OH-DFA** (**19**).[313] **Azo-NH$_2$-DFA** (**20**) was obtained by amidation of **Azo-Br-DFA** (**18b**) to **Azo-NHCOME-DFA**

(**18d**),[269] followed by deprotection of the amide group using NaOH / H_2O in dioxane (for details see Experimental part 4.5.4.1). **Azo-Dop-OH** (**21**) was obtained by an azo-coupling reaction of (S)-(-)-1,1'-binaphthyl-2,2'-diamine with $NaNO_2$ and phenol according to literature[311] (for details see Experimental part 4.5.4.2). Compounds **18a** – **18d**, **19**, **20** and **21** were characterised *via* ^{1}H-NMR and ^{19}F-NMR spectroscopy (except **21**), proving in all cases the desired structures of the azo-initiators (see Appendix Figure S103 – S108).

As the ROP of **Aib-NCA** (**11**) was successfully conducted at 80 °C in DMF while using amine-initiators and amino acid-methyl esters, polymerization of **Aib-NCA** (**11**) and **ACHC-NCA** (**12**) initiated by azo-initiators was accomplished by keeping the aforementioned conditions (for details see Experimental part xxx). In all cases, a precipitation during polymerization was observed, giving the first indication for a successful initiation by azo-compounds. The synthesized polymers were analysed by ^{1}H-NMR spectroscopy, as MALDI-TOF-MS did not work out for the synthesised materials.
For polymers **19a**, **19b**, **20a** and **20b** ^{1}H-NMR spectroscopy (see Appendix Figure S109 – S110) revealed the characteristic signals of the repeating unit of Aib or ACHC, respectively. Due to the low solubility even in HFIP-d_2, the characteristic end-group protons attached to the phenyl-ring of the azo-initiator could not be detected. As initiator **19** and **20** are azo-initiators, UV-VIS-measurements were used instead to verify the initiation and the resulting attachment of initiators **19** or **20** on the respective polymers **19a**, **19b**, **20a** and **20b**. Within the UV-VIS-spectrum of **19** two main signals with maxima at 344 nm and 440 nm (Appendix Figure S111A, black curve) were observed. Similar maxima were detected for polymers **19a** (388 nm and 454 nm, Appendix Figure S111A, red curve) and **19b** (376 nm and 484 nm, Appendix Figure S111A, blue curve). The UV-VIS-spectrum of **20** revealed two characteristic signals at 376 nm and 430 nm (Appendix Figure S111B, black curve). With a slight shift of the maxima, these characteristic signals were also found for polymers **20a** (368 nm and 454 nm, Appendix Figure S111B, red curve) and **20b** (360 nm and 458 nm, Appendix Figure S111C, blue curve). Therefore, UV-VIS-measurements clearly indicated the successful initiation and attachment of the azo-initiators.

3.3.3.1 ^{1}H-NMR- and UV-VIS-analysis

^{1}H-NMR analysis of polymers **21a** and **21b** initiated by azo-compound **21** was found to be more informative and useful for end-group analysis. In Figure 44 the ^{1}H-NMR of **21** (top), **21a** (middle) and **21b** (bottom) are shown. The characteristic signals of the azo-initiator **21** are all located in the low field. Typical signals of the phenyl ring at 6.9 and 7.5 ppm, as well as the characteristic signals for the binaphthyl group at 8.2 ppm and 8.4 ppm clearly demonstrate the successful synthesis of **21**. The ^{1}H-NMR spectrum of **21a** (middle) revealed a broad signal at 1.9 ppm, which can be assigned to the repeating unit of the Aib-domain. All other signals can be assigned to the azo-initiator group of **21**, indicating the successful attachment of the initiator during ROP of **Aib-NCA** (**11**). Traces of solvents used during synthesis (DMF) and work-up (acetone) were also observed, but were removed by drying before further investigated. A more complex ^{1}H-NMR spectrum was obtained for **21b**. The repeating unit of the ACHC-side group ring was observed at 1.7 ppm to 2.3 ppm with a characteristic triplet at 2.3 ppm assigned to the protons attached on the end of the six-membered ring (H_4). Comparable to **21**, aromatic signals in a similar ppm-range can be observed, proofing the attachment of the initiator. However, characteristic signals of the azo-initiator are partially overlapping with the other signals in the aromatic area. New signals neighboured to the characteristic signals of **21** give an indication for a second stable conformer (*cis*-conformer) of the azo-initiator, as protons of *trans*- and *cis*-isomers display different chemical shifts.

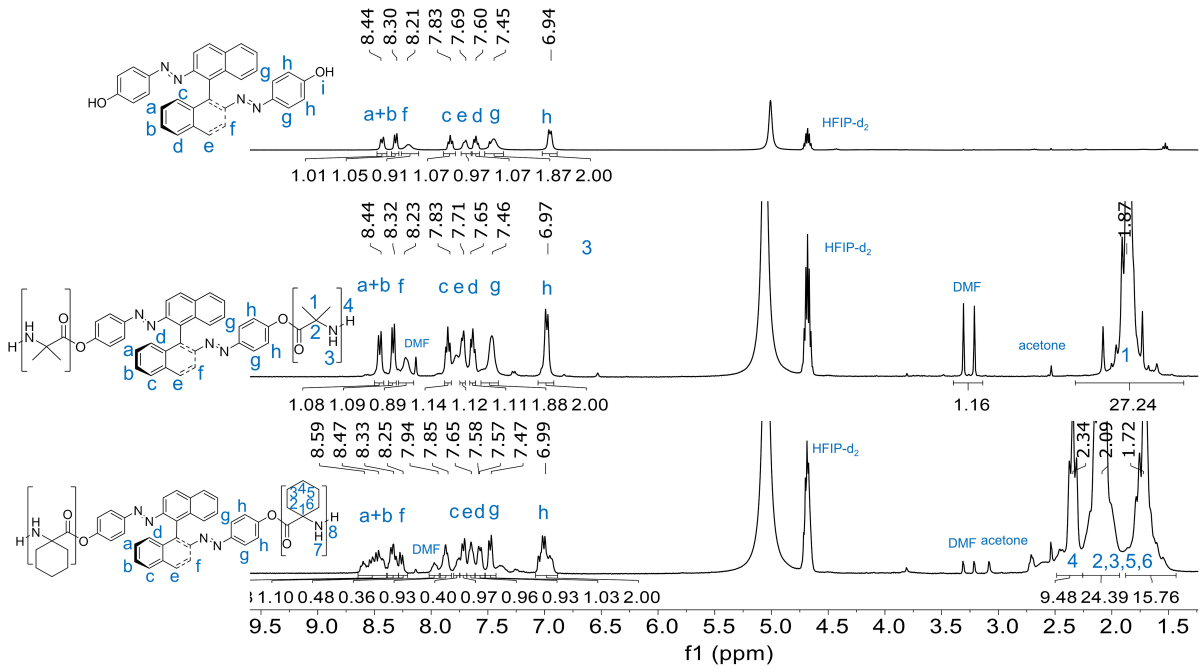

Figure 44. ^{1}H-NMR analysis of **Azo-Dop-OH** (**21**) (top) and **Azo-Dop-PAib** (**21a**) (middle) and **Azo-Dop-ACHC** (**21b**) (bottom) in HFIP-d_2.

The attachment of the initiator and the successfully polymerization was also proven by measuring UV-VIS-spectra of **21**, **21a** and **21b**. It is well known, that azobenzene-type chromophores can form a *trans*- and a *cis*-isomer. The *trans*-isomer is 12 kcal mol^{-1} more stable than the *cis*-isomer and is therefore usually predominant in darkness at room temperature. Nevertheless, a transition of the *trans*- to the *cis*-isomer can be reached by irradiation with light of 320 to 350 nm and contrary, the reverse *cis-trans* isomerization can be introduced thermally or photochemically with irradiation of light of 400 to 450 nm. Therefore, in UV-VIS-spectra usually two main absorption bands for the π–π*–transition of the *trans*-isomer in the UV-region and for the n-π*–transition of the *cis*-isomer at visible wavelengths can be detected. To check the stability of the different isomers present in the azo-initiator and in its corresponding polymers, UV-VIS-spectra of pure azo-initiator **21** and azo-polymers **21a** and **21b** in HFIP were recorded.

The UV-VIS-spectrum of the pure initiator **21** (see Appendix Figure S112A) revealed two main signals at 352 nm for the π–π*–transition of the (*trans*,*trans*)-azobenzene and a signal at 519 nm for the n-π*–transition signal of the (*cis*,*cis*)-azobenzene.[311] As the azo-initiator has two N=N bonds, also a (*trans*,*cis*)-conformation can be adopted. UV-light dependent irradiation with a wavelength of 365 nm and 254 nm led to no change in the absorption spectrum of **21**, demonstrating a thermal stable (*trans*,*trans*)-conformation. As no difference in the UV-Vis-spectra could be recorded after irradiation with both, 254 nm and 365 nm, the photo stationary state of **21** is reached in milliseconds or seconds after irradiation. The stability of the *trans*-conformation within the initiator **21** in the used solvent (HFIP) could be proven by measuring the same UV-Vis absorption spectrum after ten days (Appendix Figure S112B).

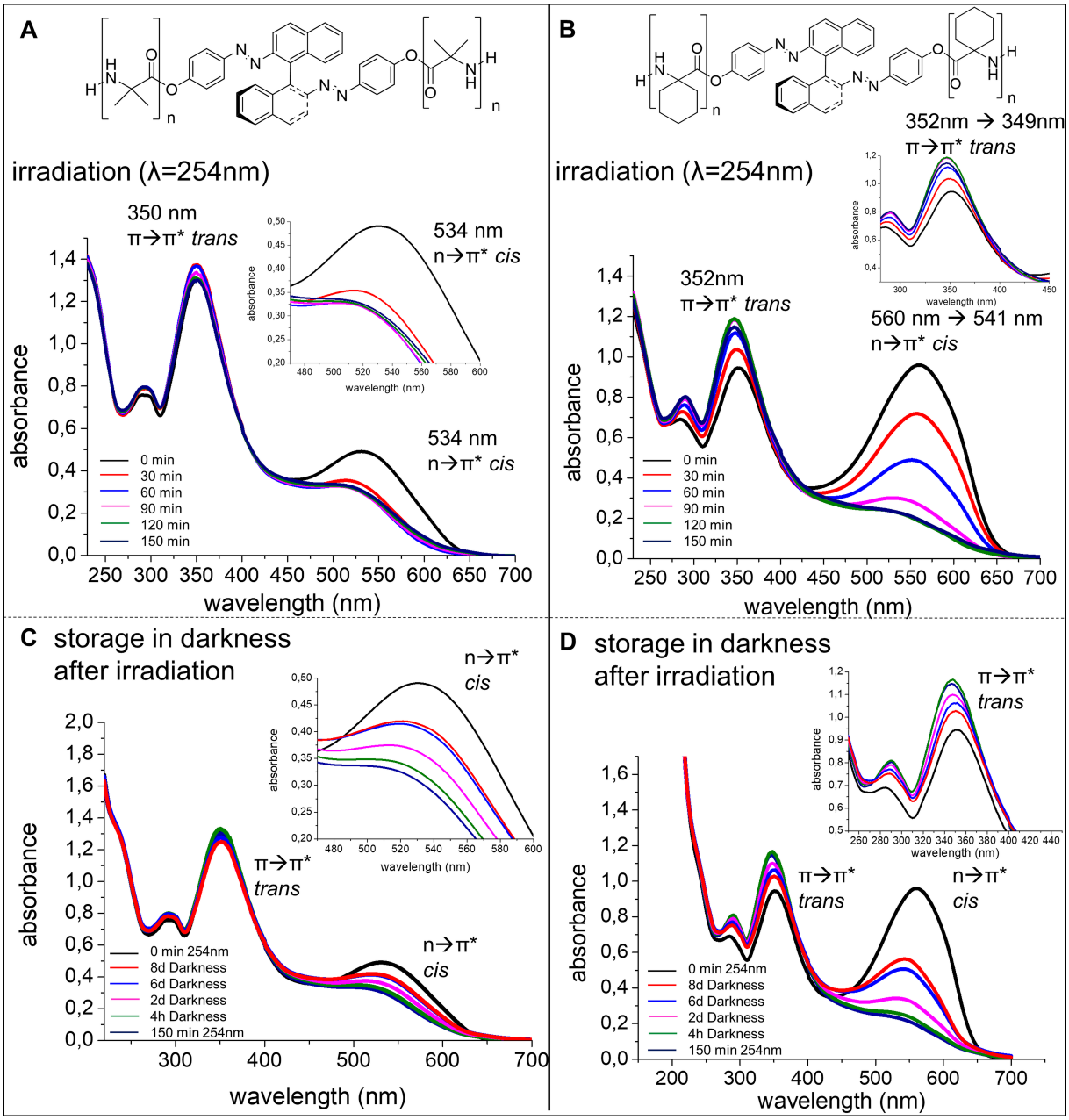

Figure 45. UV-VIS-Spectra without irradiation (black curve) and after irradiation with light (λ=254 nm) after 30 (red curve), 60 (blue curve), 90 (pink curve), 120 (green curve) and 150 min (dark blue curve) of **A**) **Azo-Dop-PAib** (**21a**) and **B**) **Azo-Dop-PACHC** (**21b**) in HFIP and corresponding UV-VIS-spectra of the irradiated samples after storage in darkness (dark blue curve) for 4 h (green curve), 2 d (pink curve), 6 d (blue curve) and 8 d (red curve) with non-irradiated sample spectra (black curve) as reference for **C**) **Azo-Dop-PAib** (**21a**) and **D**) **Azo-Dop-PACHC** (**21b**).

A different behaviour was observed for the polymers **21a** and **21b** prepared by initiating the polymerization of Aib and ACHC with the azo-chromophore **21**. Polymer **21a** (Figure 45A) revealed a π–π*–transition at 350 nm and an n-π*–transition at 534 nm (black curve). After irradiation with light of 366 nm, no change in the UV-VIS-spectrum was observed, whereas an irradiation with light of 254 nm led to a strong decrease of the absorbance intensity at 534 nm and a slight increase of the absorbance intensity at 350 nm within 30 minutes (red curve). After 60 minutes of irradiation (blue curve), the minimum intensity for the n-π*–transition signal at 534 nm and the maximum intensity for the

π-π*–transition signal at 350 nm was reached and no further changes could be observed even after 90 (pink curve), 120 (green curve) and 150 minutes (dark blue curve). A more complex behaviour was observed for polymer **21b** (Figure 45B), revealing a π–π*–transition signal at 352 nm and an n-π*–transition signal at 560 nm for the virgin sample (black curve). After irradiation with light of 254 nm, the n-π*–transition signal at 560 nm strongly decreased in intensity over 30 (red curve), 60 (blue curve) and 90 minutes (pink curve). After 120 (green curve) and 150 minutes (dark blue curve), no further significant changes of the absorption signal were observed. Furthermore, the n-π*–transition absorption signal shifted from 560 nm to 541 nm in the investigated timescale, which led to a colour change from purple to orange. Contrary, the absorbance intensity for the π–π*–transition at 352 nm increased with progressive irradiation, reaching a maximum absorbance value after 120 minutes (green curve).
Due to the usually higher thermodynamic stability of the *trans*-isomer,[314] the absorption signal for the n-π*–transition band is usually much weaker in intensity than the signal for the π–π*–transition of the *cis*-isomer. In the case of **21a**, the absorption spectrum looked similar to typical azo-compounds and the absorption band of the *trans*-isomer was much higher in intensity than for the *cis*-isomer. Contrary, the *cis*- and *trans*-absorption band of **21b** showed equal absorption intensities for the *cis*- and *trans*-isomer, which is a first indication for a more stable *cis*-isomer within **21b**. *Trans*-*cis*-transitions, usually occurring at wavelengths between 340 to 380 nm, could not be introduced by irradiation with light of 365 nm, which indicates either a fast *cis*-*trans*-isomerization after irradiation or an unusual thermal stability of the *cis*-conformation. Azo-compounds usually undergo a *cis*-*trans*-transition by thermal relaxation or irradiation with visible light, but also with UV-light of lower wavelengths like 254 nm.[315]

As the absorption signals of the n-π*–transition of the *trans*-isomer increase and of the π–π*–transition decreased after irradiation with light of 254 nm, it was concluded that the *cis*-isomer is thermally more stable than the *trans*-isomer in **21a** and **21b**. These observations were also made for sterically hindered and ring-closed azo-compounds[316-318] consequently proving the strong effect of the conformational constrained oligo amino acid units on the conformation of the attached azo-initiator **21**.

After irradiation, the samples were stored in darkness to check the thermal stability of both, *trans*- and *cis*-isomer. UV-VIS-Spectra of the irradiated samples **21a** and **21b** after storage in darkness (dark blue curve) for 4 h (green curve), 2 d (pink curve), 6 d (blue curve) and 8 d (red curve) with non-irradiated sample spectra (black curve) as reference are shown in Figure 45C and 47D. The measured spectrum of **21a** revealed a slight increase of the n-π*–transition at 534 nm after 4h. In contrast, the intensity of the π–π*–transition signal for the *trans*-isomer decreased. This process continued after storage of the sample in darkness for two, six and eight days. The signals recovered only partially to their initial values, suggesting that the (*trans*-*trans*)- or (*trans*-*cis*)-conformation is stable for more than eight days. Similar, **21b** showed the same effect but much stronger pronounced, as the initial intensity values for the *cis*- and *trans*-transition signals were nearly equal. After storage in darkness for 4h, a strongly increasing n-π*–transition of the *trans*-isomer and a decreasing π-π*–transition signal of the *cis*-isomer in **21b** could be observed. The observed trend further continued, as after two, six and eight days the π-π*–transition signal further decreased and n-π*–transition signal of the *cis*-isomer strongly increased, indicating a relaxation to the originally state. Furthermore, a slight blue shift was observed and the colour turned back from orange to purple.
Results after irradiation with light of 366 nm and 254 nm and the slow relaxation back to the original state after irradiation with light of 254 nm definitely indicate a thermodynamically more stable *cis*-conformation within **21a** and **21b**, which was found for the first time in such a polymer system.

4 Experimental part

4.1 Materials and methods

All reactions were carried out under inert nitrogen atmosphere unless otherwise noted. Amino acids L-glutamic acid γ-benzyl ester, L-aspartic acid β-benzyl ester, Boc-L-glutamic acid 5-benzyl ester, Boc-L-aspartic acid 4-benzyl ester, D-histidine, D-leucine, D-tryptophan, D-valine and 1,1,1,3,3,3-hexafluoro-2-propanole were purchased from Carbolution-Chemicals. Glycine and L-histidine were purchased from Carl Roth GmbH & Co. KG and acetamide, L-valine and 10-undecenoyl chloride were obtained from Acros Organics. L-tryptophan, 1-aminocyclohexanecarboxylic acid, 2-aminoisobutyric acid, triphosgene, bis(pinacolato)diboron, copper(I) cyanide, diamino-1,1′-binaphthalene and $LiAlH_4$ were purchased from ABCR and L-leucine, tris(dibenzylideneacetone)dipalladium(0), *N*-bromosuccinimide, difluoroaniline, *N*,*N*-dimethylacetamide, Grubbs catalyst 1st Generation, Grubbs catalyst 2nd Generation, Grubbs-Hoveyda catalyst 1st Generation, hexamethyldisilazane, hydroxybenzotriazole hydrate (HOBt Hydrate), oxalyl chloride, sulfuric acid-d_2, trifluoroacetic acid and xantphos were received from Sigma-Aldrich. Potassium acetate was purchased from Fluka and lithium chloride from Alfa Aesar. Methanesulfonic acid was obtained from Merck and dimethyl sulfoxide-d_6 from Chemotrade. All chemicals were used without further preparations or purification steps. The solvents which were used for reactions were dried and freshly distilled before using. THF was dried and distilled over sodium and benzophenone under nitrogen (N_2) atmosphere, for drying of dichloromethane (DCM) and *N*,*N*-dimethylformamide (DMF) CaH_2 was used. For the reactions under protective gas atmosphere N_2 was used, which was purchased from LINDE.

Instruments and measurements

Nuclear magnetic resonance (NMR) spectra were recorded at 27 °C on a NMR spectrometer of VARIAN. ^{1}H-NMR spectroscopy was performed at 400 MHz in $CDCl_3$, DMSO-d_6, D_2SO_4 or HFIP-d_2 as solvents. Chemical shifts (δ) are reported in ppm and referred to the solvent residual signal ($CDCl_3$ 7.26 ppm for ^{1}H, DMSO-d_6 2.50 ppm for ^{1}H, HFIP-d_2 4.52 ppm for ^{1}H). MestReNova (Version 9.0.1) was used for analyzing the data.

Fourier-transformed infrared spectroscopy (FTIR) was measured by a VERTEX 70 IR spectrometer of Bruker by using a single reflex-diamond-ATR-unit for solid state investigations. Solutions experiments in HFIP were performed with a demountable Specac® Omni Cell purchased from Sigma-Aldrich with CaF_2 windows and PTFE spacer between 0.5 mm and 0.2 mm by measuring the pure solvent as background. The absorption bands are reported in cm^{-1} in an area of 1500 – 2500 cm^{-1} to prevent total absorption effects of HFIP. For following the ROP of NCAs a MIR fiber probe was used by measuring the solvent and the initiator as background. The software OPUS 6.5 was used for data interpretation.

Matrix-assisted laser desorption / ionization time-of-flight mass spectrometry (MALDI-TOF-MS) measurements were performed on a Bruker Autoflex III system (Bruker Daltonics) using a nitrogen laser operating at a wave length of λ = 337 nm in reflection or linear mode. The ratio of matrix : analyte : salt was 100 : 10 : 1 and 1 µL of the solution was spotted on the MALDI target. Therefore, the polymer samples were dissolved in THF or DMF with a concentration of 10 mg mL^{-1} and dithranol was used as matrix adjusting a concentration of 10 mg mL^{-1} in THF, while KTFA was used as salt with a concentration of 5 mg mL^{-1} in THF. Data evaluation was carried out on flexAnalysis software (3.4).

ESI-TOF-MS measurements were performed on a Bruker Daltonics microTOF *via* direct injection with a flow rate of 180 µL h^{-1} using positive or negative mode with an acceleration voltage of 4.5 kV. Samples were dissolved in HPLC grade solvents with a concentration of 1 mg mL^{-1} without addition of salt.

For gel permeation chromatography (GPC) measurements of oligomer **$O^{Bn}Asp_3$** a Viscotek GPCmax VE 2002 with a set of a H_{HR} HGuard-17369 and a GMH_{HR}-N-18055 main column was used in THF. Measurements were performed at 22 °C while injecting 100 µL of sample with a concentration of 5 mg mL^{-1} in THF. Detection was realized by refractive index with a VE3580 RI detector of Viscotek at a temperature of 35 °C and a flow rate of 1 mL min^{-1}. External calibration was done with polystyrene standards in a range of 1000 to 115000 g mol^{-1}. The GPC measurements of oligomers (**$O^{Bn}Glu_3$**, **$O^{Bn}Glu_{10}$**, **$O^{Bn}Asp_{10}$**), the obtained ADMET polymers (**$AP_{21}(^{Bn}Glu_3)$**, **$AP_3(^{Bn}Glu_{10})$**, **$AP_{18}(^{Bn}Asp_3)$**, **$AP_4(^{Bn}Asp_{10})$**) and their corresponding fractions, were performed on a Viscotek GPCmax VE 2001 with a set of a H_{HR}-H Guard-17369 and a GMH_{HR}-N-18055 main column in DMF at 60 °C. Detection of the refractive index was realized with a VE 3580 RI detector from Viscotek at 35 °C. The external calibration was done using polystyrene standards in a range of 1000 to 115000 g mol^{-1}. The concentration of all samples was 5 mg mL^{-1}, and the flow rate was 1 mL min^{-1}.

CD-spectroscopic measurements were performed on a JASCO Corp., J-810, Rev. 1.00, at 20 °C using a cuvette with a space length of 1 mm and a sample concentration of 0.1 – 0.2 mg mL^{-1} in HFIP. The spectra were measured with a wavelength ranging from 250 nm to 195 nm with a scan rate of 1 nm s^{-1} performing 50 accumulations. The absorption was reported in mill degree after subtraction of the blank solvent measurement from the sample spectra.

Preparative GPC was performed on a VWR HITACHI Chromaster using a KD-2002.5 column from Shodex in DMF at 55 °C with a flow rate of 0.70 mL min^{-1} and a sample concentration of 15 mg mL^{-1}. The detection was accomplished *via* a refractive index detector from VWR at 50 °C. For analyzing the obtained data EZChrom Elite (version 3.3.2 SP2) was used.

Thin-layer chromatography (TLC) was performed using "Merck silica gel 60" plates. Spots on the TLC plate were visualized using either UV light at a wavelength of 254 or 366 nm, or an oxidizing agent "blue" stain consisting out of $Ce(SO_4)_2 \cdot 4H_2O$ (1 g) and $(NH_4)_6Mo_7O_{24} \cdot 4H_2O$ (1 g) dissolved in a mixture of distilled water (90 mL) and concentrated sulphuric acid (6 mL).

For differential scanning calorimetry (DSC) measurements a NETZSCH DC 204F1 Phoenix, which was calibrated with indium, tin, bismuth, and zinc was used. Nitrogen was used as purge gas and all samples (3 – 8 mg) were placed in standard aluminum pans. For analysis of obtained data Netzsch Proteus – Thermal Analysis (version 5.2.1.) and OriginPro 8G was used. For calculation of the crystallinity α the following equation 3 was used:

$$\alpha = \frac{\Delta H_m}{\Delta H^0{}_m} * 100 \qquad \textbf{(eq. 3)}$$

where $\Delta H^0{}_m$ is the fusion enthalpy of eicosane (ΔH_m=247.3 J g^{-1}).

X-ray diffraction (XRD) measurements of the samples were done as droplet which was heated up on a glass plate to isotropic state followed by cooling the sample with a defined cooling rate of 5 K min^{-1} on a temperature-controlled heating stage. Measuring temperature for **4a** was 60.0 °C and for **4b** 70.0 °C, measuring time for both samples was 30 min. 2D patterns were detected on Vantec 500 detector (Bruker AXS) with a detector to sample distance of 9.00 cm.

UV-VIS absorption spectra were measured on a Jasco V-670 UV/VIS/NIR spectrometer. Optical cells thickness for measurement was 10 mm. The irradiation was performed using UV light (254 nm and 365 nm).

Dialysis tube (molecular weight cut-off (MWCO): 1000 g mol^{-1}) was purchased from Carl Roth GmbH.

4.2 Synthesis of monomers of single-amino acid-PE(-type)-polymers (2a – 2e)

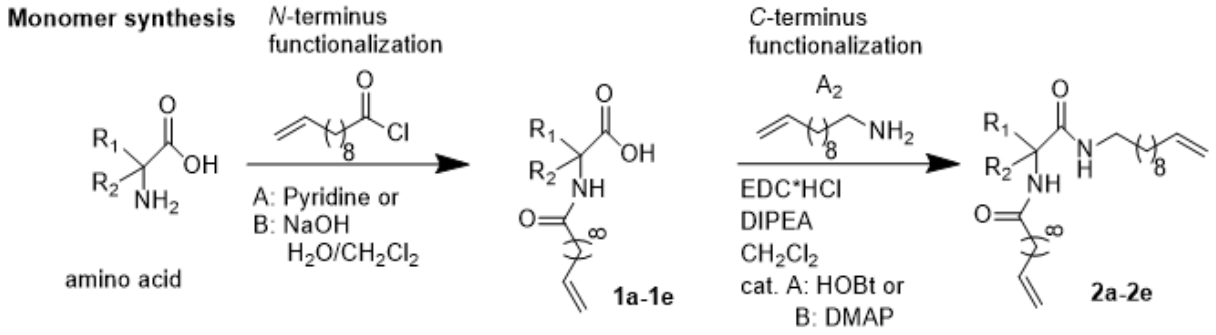

Scheme 7. Synthesis of *N*-terminus functionalized (**1a** – **1e**) and *N*- + *C*-terminus functionalized amino acids (**2a** – **2e**).

4.2.1 N-terminus functionalization

*General procedure for the amino acids bearing a benzyl protection group in the side chain (method A) (**1a** – **1b**)*

N-terminus functionalization was realized by the Einhorn method for the amino acids bearing a benzyl protection group in the side chain. Therefore, the protected amino acid (1 eq) was dissolved in THF (12 mL) and pyridine (10 mL) was added to the solution. The mixture was cooled down to 0 °C and 10-undecenoyl chloride (1.3 eq) was added dropwise to the solution, which was stirred for 24 h at room temperature. Then the reaction mixture was poured into a cold 1M HCl-solution (300 mL) and diethyl ether (200 mL) was added. The organic phase was separated, extracted two times with 1M HCl solution (2x100 mL) and dried over Na_2SO_4. After filtration the mixture was concentrated in vacuum and recrystallized three times in an ethyl acetate : *n*-hexane (1:40) mixture to yield a white solid **1a** – **1b** (72-76 %).

N-Glu (**1a**): ^{1}H-NMR ($CDCl_3$, 27 °C, 400 MHz): δ [ppm] 1.27 (m, 10H, H_d – H_h), 1.60 (m, 2H, H_i), 2.02 – 2.20 (m, 6H, H_4 + H_c + H_j), 2.49 (m, 1H, H_3), 2.57 (m, 1H, H_3), 4.54 (m, 1H, H_2), 4.93 (m, 2H, H_a), 5.12 (s, 2H, H_6), 5.79 (m, 1H, H_b), 6.56 (d, $^3J_{H,H}$ = 7.2 Hz, 1H, H_{13}), 7.31 – 7.45 (m, 5H, H_8 – H_{12}).

^{13}C-NMR ($CDCl_3$, 27 °C, 100 MHz): δ [ppm] 25.4 (C_i), 26.5 (C_3), 28.9 - 29.5 (C_d – C_h), 30.5 (C_4), 33.7 (C_c), 36.3 (C_j), 52.3 (C_2), 66.9 (C_6), 114.1 (C_a), 128.2 - 128.7 (C_8 - C_{12}), 135.5 (C_7), 139.1 (C_b), 171.5 (C_1), 173.6 (C_5), 174.1 (C_k).

N-Glu (**1a**): ESI-TOF-MS (positive mode, without additional salt, *m/z*) $[M]^+$ found 422.226, simulated for $C_{23}H_{33}NO_5Na^+$ 426.225.

N-Asp (**1b**): ^{1}H-NMR ($CDCl_3$, 27 °C, 400 MHz): δ [ppm] 1.27 (m, 10H, H_d – H_h), 1.61 (m, 2H, H_i), 2.02 (m, 2H, H_c), 2.21 (m, 2H, H_j), 2.92 (m, 1H, H_3), 3.09 (m, 1H, H_3), 4.91 (m, 1H, H_2), 4.94 (m, 2H, H_a), 5.14 (s, 2H, H_5), 5.79 (m, 1H, H_b), 6.56 (d, $^3J_{H,H}$ = 7.2 Hz, 1H, H_{12}), 7.31 – 7.45 (m, 5H, H_7 – H_{11}).

N-Asp (**1b**): ^{13}C-NMR ($CDCl_3$, 27 °C, 100 MHz): δ [ppm] 25.4 (C_i), 28.9 - 29.3 (C_d – C_h), 33.8 (C_c), 36.3 (C_j), 36.5 (C_3), 48.5 (C_2), 67.0 (C_5), 114.1 (C_a), 128.2 - 128.6 (C_7 - C_{11}), 135.2 (C_6), 139.1 (C_b), 171.1 (C_1), 173.8 (C_4), 174.1 (C_k).

N-Asp (**1b**): ESI-TOF-MS (positive mode, without additional salt, *m/z*) $[M]^+$ found 412.204, simulated for $C_{22}H_{31}NO_5Na^+$ 412.209.

*General procedure for the amino acids without a protection group in the side chain (method B) (**1c** – **1e**)*

N-terminus functionalization was realized by Schotten-Baumann synthesis for the water-soluble amino acids. The amino acid (1eq) and NaOH (2eq) were dissolved in water (20 mL) and the mixture was cooled in an ice-bath. 10-Undecenoyl chloride (1.1 eq), dissolved in dichloromethane (20 mL), was added dropwise to the solution which was allowed to stir at room temperature for 24 h. The mixture was poured into a cold 1M HCl-solution (200 mL) and the organic phase was separated, dried over Na_2SO_4, filtrated and concentrated in vacuum. The crude product was recrystallized three times in ethyl acetate : *n*-hexane (1:40) mixture to yield a white solid **1c** – **1e** (64-75 %).

N-Leu (**1c**): ^{1}H-NMR ($CDCl_3$, 27 °C, 400 MHz): δ [ppm] 0.95 (m, 6H, H_5 + H_6), 1.28 (m, 10H, H_d – H_h), 1.60 – 1.71 (m, 5H, H_i + H_3 + H_4), 2.02 (m, 2H, H_c), 2.23 (m, 2H, H_j), 4.61 (m, 1H, H_2), 4.94 (m, 2H, H_a), 5.79 (m, 1H, H_b), 5. 96 (m, 1H, H_7).

N-Leu (**1c**): ^{13}C-NMR ($CDCl_3$, 27 °C, 100 MHz): δ [ppm] 21.9 – 22.8 (C_5 + C_6), 24.9 (C_4), 25.5 (C_i), 28.9 – 29.5 (C_d – C_h), 33.7 (C_c), 36.5 (C_j), 41.1 (C_3), 50.8 (C_2), 114.1 (C_a), 139.1 (C_b), 173.9 (C_1), 176.3 (C_k).

N-Leu (**1c**): ESI-TOF-MS (positive mode, without additional salt, *m/z*) $[M]^+$ found 320.215, simulated for $C_{17}H_{31}NO_3Na^+$ 320.220.

N-Aib (**1d**): ^{1}H-NMR ($CDCl_3$, 27 °C, 400 MHz): δ [ppm] 1.27 – 1.36 (m, 10H, H_d – H_h), 1.57-1.62 (m, 8H, H_2 + H_3 + H_i), 2.02 (m, 4H, H_c), 2.20 (m, 2H, H_j), 4.94 (m, 2H, H_a), 5.79 (m, 1H, H_b), 6.02 (m, 1H, H_5).

^{13}C-NMR ($CDCl_3$, 27 °C, 100 MHz): δ [ppm] 24.9 (C_2 + C_3), 25.5 (C_i), 28.9 – 29.5 (C_d – C_h), 33.7 (C_c), 36.8 (C_j), 57.0 (C_1), 114.1 (C_a), 139.1 (C_b), 174.4 (C_k), 177.2 (C_4).

N-Aib (**1d**): ESI-TOF-MS (positive mode, without additional salt, *m/z*) $[M]^+$ found 292.185, simulated for $C_{15}H_{27}NO_3Na^+$ 292.188.

N-ACHC (**1e**): ^{1}H-NMR ($CDCl_3$, 27 °C, 400 MHz): δ [ppm] 1.29 – 1.45 (m, 12H, H_d – H_i), 1.66 (m, 6H, H_3 + H_4 + H_5), 1.89 (m, 2H, H_2 + H_6), 2.04 (m, 4H, H_c + H_2 + H_6), 2.26 (m, 2H, H_j), 4.94 (m, 2H, H_a), 5.69 (m, 1H, H_7), 5.79 (m, 1H, H_b).

N-ACHC (**1e**): ^{13}C-NMR ($CDCl_3$, 27 °C, 100 MHz): δ [ppm] 21.3 (C_3 + C_5), 25.1 – 25.5 (C_i + C_4), 28.9 – 29.5 (C_d – C_h), 32.0 - 33.7 (C_2 + C_6 + C_c), 36.6 (C_j), 59.7 (C_1), 114.1 (C_a), 139.1 (C_b), 175.1 (C_k), 176.0 (C_9).

N-ACHC (**1e**): ESI-TOF-MS (positive mode, without additional salt, *m/z*) $[M]^+$ found 332.217, simulated for $C_{18}H_{31}NO_3Na^+$ 322.220.

4.2.2 Synthesis of the coupling reagent 10-undecene-1-amine (A2)

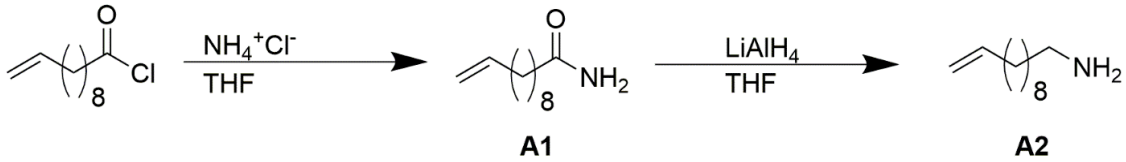

Scheme 8. Synthesis of 10-undecenecarboxamide (**A1**) and 10-undecen-1-amine (**A2**).

Synthesis of 10-undecenecarboxamide (A1)

Synthesis of 10-undecenecarboxamide was done according to literature.[270] In a two-necked round bottom flask, equipped with a magnetic stir bar, a solution of aqueous ammonium hydroxide (250 mL) was added and was cooled down to 0 °C. 10-Undecenoyl chloride (12.69 g; 0.06 mol; 1 eq) was dissolved in THF (50 mL) and was added dropwise to the solution, which was allowed to stir at room temperature for 3 h. The solid product was filtered off, washed with distilled water (3x100 mL) and dried under vacuum to yield 10.85 g (95 %) of 10-undecenecarboxamide (**A1**).

^{1}H-NMR ($CDCl_3$, 27 °C, 400 MHz): δ [ppm] 1.28 – 1.38 (m, 10H, H_d –H_h), 1.63 (m, 2H, H_i), 2.02 (m, 2H, H_c), 2.19 (m, 2H, H_j), 4.93 (m, 2H, H_a), 5.43 (br, 2H, H_l), 5.83 (m, 1H, H_b).

^{13}C-NMR ($CDCl_3$, 27 °C, 100 MHz): δ [ppm] 25.5 (C_h), 28.9 – 29.3 (C_d-C_g), 33.7 (C_c) 35.9 (C_j), 114.1 (C_a), 139.2 (C_b), 175.6 (C_k).

Synthesis of 10-undecene-1-amine (A2)

Synthesis of 10-undecene-1-amine was done according to literature.[270] In an inert atmosphere $LiAlH_4$ (6.50 g; 171.3 mmol; 2.9 eq) was suspended in dry THF (150 mL), was cooled down to 0 °C and 10-undecenecarboxamide (**A1**, 10.85 g; 59.2 mmol; 1.0 eq) dissolved in dry THF (150 mL) was added dropwise to the solution. The mixture was allowed to stir at room temperature for 24 h, was cooled down to 0 °C and was quenched carefully by adding water (20 mL), 1M NaOH-solution (40 mL) and water (20 mL). The mixture was filtered and the filtrate was concentrated in vacuum obtaining the crude product, which was dissolved in diethyl ether (50 mL) and washed with brine (2x100 mL). The organic layer was separated, dried over Na_2SO_4, and purified finally by high vacuum distillation (30 – 38 °C at 0.032 mbar) to yield 5.52 g (55 %) of 10-undecene-1-amine (**A2**).

^{1}H-NMR ($CDCl_3$, 27 °C, 400 MHz): δ [ppm] 1.05 – 1.40 (m, 14H, H_d – H_j), 2.04 (m, 2H, H_c), 2.65 (t, $^{3}J_{H,H}$ = 7.0 Hz, 1H, H_k), 4.95 (m, 1H, H_a), 5,81 (m, 2H, H_b).

^{13}C-NMR ($CDCl_3$, 27 °C, 100 MHz): δ [ppm] 26.7 + 28.8 + 28.9 + 29.0 + 29.1 + 29.3 + 29.4 (C_d-C_h), 33.8 – 33.9 (C_j – C_c), 42.3 (C_k) 114.1 (C_a), 139.2 (C_b).

4.2.3 C-terminus functionalization

*General procedure for chiral AA (**2a** – **2c**)*

All reactions were performed under N_2 atmosphere. The *N*-terminus functionalized amino acid (**1a** – **1c**, 1.0 eq) was dissolved in dry dichloromethane (20 mL) and then **A2** (1.0 eq) was added to the mixture. The solution was cooled down to 0 °C and the coupling reagents DIPEA (3.6 eq), HOBt (13 % H_2O; 1.6 eq) and EDC·HCl (1.6 eq) were added successively. The mixture was allowed to stir at room temperature for 4 hours before it was refluxed overnight. Then the solution was cooled down to room temperature and was extracted with brine (20 mL), 1M HCl (20 mL), brine (20 mL), saturated $NaHCO_3$-solution (20 mL) and brine (20 mL). The organic phase was concentrated under vacuum and the crude product was dissolved in THF (5 mL), precipitated into cold $NaHCO_3$ (150 mL) solution and isolated

by filtration. Afterwards the obtained brown solid was dissolved in Et_2O (20 mL), dried over Na_2SO_4, filtrated and concentrated in vacuum to yield products **2a** – **2c** (63-86 %).

N- + *C*-Glu (**2a**): ^{1}H-NMR ($CDCl_3$, 27 °C, 400 MHz): δ [ppm] 1.26 – 1.34 (m, 20H, H_d – H_h), 1.44 – 1.58 (m, 4H, H_l + H_i), 2.03 – 2.20 (m, 6H, H_4 + H_c + H_j), 2.40 (m, 1H, H_3), 2.54 (m, 1H, H_3), 3.18 (m, 2H, H_m) 4.42 (m, 1H, H_2), 4.93 (m, 4H, H_a), 5.10 (s, 2H, H_6), 5.77 (m, 2H, H_b), 6.43 (d, $^3J_{H,H}$ = 7.2 Hz, 1H, H_{13}), 7.31 – 7.45 (m, 5H, H_8 – H_{12}).

N- + *C*-Glu (**2a**): ^{13}C-NMR ($CDCl_3$, 27 °C, 100 MHz): δ [ppm] 25.5 (C_i), 26.8 (C_i), 27.8 (C_3), 28.9 - 29.5 (C_d – C_h + C_l), 30.6 (C_4), 33.8 (C_c), 36.5 (C_j), 39.6 (C_m), 52.3 (C_2), 66.6 (C_6), 114.1 (C_a), 128.2 - 128.7 (C_8 – C_{12}), 135.8 (C_7), 139.1 (C_b), 170.9 (C_1), 173.4 (C_5), 173.4 (C_k).

N- + *C*-Glu (**2a**): ESI-TOF-MS (positive mode, without additional salt, *m/z*) $[M]^+$ found 577.393, simulated for $C_{34}H_{54}N_2O_4Na^+$ 577.398.

N- + *C*-Asp (**2b**): ^{1}H-NMR ($CDCl_3$, 27 °C, 400 MHz): δ [ppm] 1.27 – 1.40 (m, 22H, H_d – H_h + H_l), 1.59 (m, 2H, H_i), 2.02 – 2.20 (m, 6H, H_4 + H_c + H_j), 2.91 (m, 1H, H_3), 3.08 (m, 1H, H_3), 3.17 (m, 2H, H_m) 4.91 (m, 1H, H_2), 4.94 (m, 4H, H_a), 5.14 (s, 2H, H_5), 5.79 (m, 2H, H_b), 6.56 (d, $^3J_{H,H}$ = 7.2 Hz, 1H, H_{12}), 7.31 – 7.45 (m, 5H, H_7 – H_{11}).

N- + *C*-Asp (**2b**): ^{13}C-NMR ($CDCl_3$, 27 °C, 100 MHz): δ [ppm] 25.5 (C_i), 26.8 (C_i), 28.9 - 29.3 (C_d - C_h + C_l), 33.7 (C_c), 35.7 (C_j), 36.5 (C_3), 39.6 (C_m), 49.1 (C_2), 66.9 (C_5), 114.1 (C_a), 128.2 - 128.6 (C_7 – C_{11}), 135.4 (C_6), 139.2 (C_b), 170.1 (C_1), 172.1 (C_4), 173.3 (C_k).

N- + *C*-Asp (**2b**): ESI-TOF-MS (positive mode, without additional salt, *m/z*) $[M]^+$ found 563.378, simulated for $C_{33}H_{52}N_2O_4Na^+$ 563.382.

N- + *C*-Leu (**2c**): ^{1}H-NMR ($CDCl_3$, 27 °C, 400 MHz): δ [ppm] 0.95 (m, 6H, H_5 + H_6), 1.28 – 1.43 (m, 22H, H_d – H_h + H_l), 1.60 – 1.71 (m, 5H, H_i + H_3 + H_4), 2.02 (m, 2H, H_c), 2.20 (m, 2H, H_j), 3.22 (m, 2H, H_m), 4.61 (m, 1H, H_2), 4.94 (m, 4H, H_a), 5.79 (m, 2H, H_b), 5.96 (m, 1H, H_7).

N- + *C*-Leu (**2c**): ^{13}C-NMR ($CDCl_3$, 27 °C, 100 MHz): δ [ppm] 21.9 – 22.6 (C_5 + C_6), 25.0 (C_4), 25.6 (C_i), 26.8 (C_i), 28.9 – 29.5 (C_d – C_h + C_l), 33.7 (C_c), 36.6 (C_j), 39.5 (C_m), 41.1 (C_3), 51.6 (C_2), 114.1 (C_a), 139.1 (C_b), 172.0 (C_1), 173.1 (C_k).

N- + *C*-Leu (**2c**): ESI-TOF-MS (positive mode, without additional salt, *m/z*) $[M]^+$ found 471.386, simulated for $C_{28}H_{52}N_2O_2Na^+$ 471.392.

*General procedure for achiral AA (**2d** – **2e**)*

All reactions were performed under N_2 atmosphere. To a solution of *N*-terminus functionalized amino acid (**1d** – **1e**, 1.0 eq) and **A2** (1.0 eq) dissolved in 0 °C cold, dry dichloromethane (20 mL) DIPEA (4.5 eq), DMAP (0.02 eq) and EDC·HCl (2.6 eq) were added successively. The solution was heated to reflux for 24 h. After cooling down to room temperature the reaction mixture was extracted with brine (20 mL), 1M HCl (20 mL), brine (20 mL), saturated $NaHCO_3$-solution (20 mL) and brine (20 mL). The organic layer was separated, dried over Na_2SO_4 and concentrated in vacuum to yield **2d** – **2e** (78-82 %).

N- + *C*-Aib (**2d**): ^{1}H-NMR ($CDCl_3$, 27 °C, 400 MHz): δ [ppm] 1.27 – 1.36 (m, 20H, H_d – H_h), 1.47 (m, 2H, H_l), 1.55-1.62 (m, 10H, H_2 + H_3 + H_i), 2.02 (m, 4H, H_c), 2.14 (m, 2H, H_j), 3.22 (m, 2H, H_m), 4.96 (m, 4H, H_a), 5.79 (m, 2H, H_b), 6.09 (m, 1H, H_5), 6.63 (m, 1H, H_5).

N- + *C*-Aib (**2d**): ^{13}C-NMR ($CDCl_3$, 27 °C, 100 MHz): δ [ppm] 24.8 (C_2 + C_3), 25.5 (C_i), 26.8 (C_i), 28.9 – 29.5 (C_d – C_h+ C_l), 33.8 (C_c), 37.4 (C_j), 39.8 (C_m), 57.4 (C_1), 114.1 (C_a), 139.1 (C_b), 173.4 (C_k), 174.5 (C_4).

N- + *C*-Aib (**2d**): ESI-TOF-MS (positive mode, without additional salt, *m/z*) $[M]^+$ found 443.357, simulated for $C_{26}H_{48}N_2O_2Na^+$ 443.361.

N- + *C*-ACHC (**2e**): ^{1}H-NMR ($CDCl_3$, 27 °C, 400 MHz): δ [ppm] 1.29-1.47 (m, 24H, H_d – H_i + H_l), 1.64 (m, 6H, H_3 + H_4 + H_5), 1.88 (m, 2H, H_2 + H_6), 2.04 (m, 6H, H_c + H_2 + H_6), 2.21 (m, 2H, H_j), 3.20 (m, 2H, H_m), 4.97 (m, 4H, H_a), 5.30 (m, 1H, H_7), 5.79 (m, 2H, H_b).

N- + *C*-ACHC (**2e**): ^{13}C-NMR ($CDCl_3$, 27 °C, 100 MHz): δ [ppm] 21.6 (C_3 + C_5), 25.1 – 25.5 (C_i + C_4), 26.9 (C_i), 28.9 – 29.5 (C_d – C_h + C_l), 32.0 – 33.8 (C_2 + C_6 + C_c), 37.5 (C_j), 39.5 (C_m), 59.7 (C_1), 114.1 (C_a), 139.1 (C_b), 175.1 (C_k), 176.0 (C_9).

N- + *C*-ACHC (**2e**): ESI-TOF-MS (positive mode, without additional salt, *m/z*) $[M]^+$ found 483.390, simulated for $C_{29}H_{52}N_2O_2Na^+$ 483.392.

4.3 Synthesis of hydrogenated single-amino acid-PE(-type)-polymers (4a – 4e)

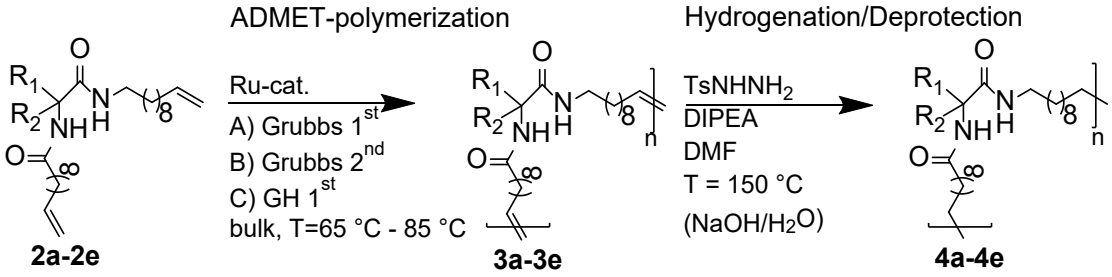

Scheme 9. Synthesis of ADMET-polymers **3a** – **3e** and hydrogenated polymers **4a** – **4e**.

4.3.1 ADMET-polymerization

Polymerization of the monomers **2a** – **2e** was done as bulk polymerization under N_2 atmosphere, following the method proposed by Wagener *et al.*.[265] The solid monomer (**2a** – **2e**) was placed in a dry Schlenk tube, which was subsequently heated in an oil bath to 65 °C. After the monomer became liquid, the appropriate amount of the chosen catalyst (100:1 monomer to catalyst ratio) was added. Vacuum and repeated cycles of flushing with nitrogen were applied during the reaction to remove evolving ethylene. Further small amount of catalyst was additionally added to the bulk-reaction mixture after several hours. Due to increasing viscosity during polymerization the reaction temperature was increased to 85 °C – 165 °C and afterwards the reaction was quenched by adding THF. The reaction mixture was precipitated into cold MeOH to yield **3a** – **3e** (61-87 %).

ADMET-Glu (**3a**): ^{1}H-NMR ($CDCl_3$, 27 °C, 400 MHz): δ [ppm] 1.26 – 1.34 (m, $H_{rep.unit}$, H_d – H_h), 1.44 – 1.59 (m, $H_{rep.unit}$, H_i + H_l), 1.95 – 2.01 (m, $H_{rep.unit}$, H_4 + H_c), 2.16 (m, $H_{rep.unit}$, H_j) 2.41 (m, $H_{rep.unit}$, H_3), 2.55 (m, $H_{rep.unit}$, H_3), 3.20 (m, $H_{rep.unit}$, H_m) 4.41 (m, $H_{rep.unit}$, H_2), 4.96 (m, 4H, H_a), 5.10 (s, $H_{rep.unit}$, H_6), 5.36 (m, $H_{rep.unit}$, H_x + H_y), 5.79 (m, 2H, H_b), 7.34 (m, $H_{rep.unit}$, H_8 – H_{12}).

ADMET-Asp (**3b**): ^{1}H-NMR ($CDCl_3$, 27 °C, 400 MHz): δ [ppm] 1.19 – 1.28 (m, $H_{rep.\ unit}$, H_d – H_h), 1.43 (m, $H_{rep.\ unit}$, H_l), 1.58 (m, $H_{rep.\ unit}$, H_i), 1.95 (m, $H_{rep.\ unit}$, H_c), 2.18 (m, $H_{rep.\ unit}$, H_j), 2.68 (m, $H_{rep.\ unit}$, H_3), 2.90 (m, $H_{rep.\ unit}$, H_3), 3.16 (m, $H_{rep.\ unit}$, H_m), 4.78 (m, $H_{rep.\ unit}$, $H_{2)}$, 4.96 (m, 4H, H_a), 5.13 (m, $H_{rep.\ unit}$, H_5), 5.36 (m, $H_{rep.\ unit}$, H_x + H_y), 5.79 (m, 2H, H_b), 7.33 (m, $H_{rep.\ unit}$, H_7 – H_{11}).

ADMET-Leu (**3c**): ^{1}H-NMR ($CDCl_3$, 27 °C, 400 MHz): δ [ppm] 0.87 (m, $H_{rep.\ unit}$, $H_5 + H_6$), 1.19 – 1.38 (m, 12H, $H_d - H_h + H_l$), 1.46 – 1.66 (m, $H_{rep.\ unit}$, $H_3 + H_4 + H_i$), 2.03 (m, $H_{rep.\ unit}$, H_c), 2.17 (m, $H_{rep.\ unit}$, H_j), 3.19 (m, $H_{rep.\ unit}$, H_l), 4.48 (m, $H_{rep.\ unit}$, H_2), 4.90 (m, 4H, H_a), 5.35 (m, $H_{rep.\ unit}$, $H_x + H_y$), 5.78 (m, 2H, H_b).

ADMET-Aib (**3d**): ^{1}H-NMR ($CDCl_3$, 27 °C, 400 MHz): δ [ppm] 1.27 – 1.36 (m, $H_{rep.unit}$, $H_d – H_h$), 1.48 (m, $H_{rep.unit}$, H_l), 1.55 – 1.59 (m, $H_{rep.unit}$, $H_2 + H_3 + H_i$), 1.94 (m, $H_{rep.unit}$, H_c), 2.16 (m, $H_{rep.unit}$, H_j), 3.23 (m, $H_{rep.unit}$, H_m), 4.96 (m, 2H, H_a), 5.36 (m, $H_{rep.unit}$, $H_x + H_y$), 5.76 (m, 1H, H_b), 6.08 (m, $H_{rep.unit}$, H_5), 6.65 (m, $H_{rep.unit}$, H_6).

ADMET-ACHC (**3e**): ^{1}H-NMR ($CDCl_3$, 27 °C, 400 MHz): δ [ppm] 1.23 – 1.47 (m, $H_{rep.unit}$, $H_d – H_h + H_l + H_i$), 1.62 (m, $H_{rep.unit}$, $H_3 + H_4 + H_5$), 1.86 (m, $H_{rep.unit}$, $H_2 + H_6$), 1.94 – 2.12 (m, $H_{rep.unit}$, $H_c + H_2 + H_6$), 2.21 (m, $H_{rep.unit}$, H_j), 3.20 (m, $H_{rep.unit}$, H_m), 4.91 (m, 4H, H_a), 5. 35 (m, $H_{rep.unit}$, $H_x + H_y$), 5.78 (m, 2H, H_b).

4.3.2 Hydrogenation / deprotection of the oligomers

*General procedure for hydrogenation and deprotection of oligomers bearing a benzyl-protecting group in the side chain (**4a** – **4b**)*

To a solution of the oligomer (**3a** – **3b**, 1.0 eq) in DMF (2 – 4 mL) $TsNHNH_2$ (5.0 eq per double bond) and DIPEA (5.0 eq) were added. The solution was heated to 150 °C for 6 hours. Then the solution was cooled down to 85 °C, NaOH (2.0 eq per protection group) was added and the resulting mixture was stirred overnight. The reaction mixture was cooled down to room temperature and dialyzed against MeOH for 3 days to yield the hydrogenated and deprotected oligomers **4a** – **4b** (72-79 %).

ADMET-Glu H (**4a**): ^{1}H-NMR ($CDCl_3$ + 15 Vol. % TFA, 27 °C, 400 MHz): δ [ppm] 0.87 (m, 6H, H_z), 1.25 – 1.34 (m, $H_{rep.unit}$, $H_b – H_h + H_x + H_y$), 1.54 – 1.60 (m, $H_{rep.unit}$, $H_i + H_l$), 2.00 – 2.16 (m, $H_{rep.unit}$, H_3), 2.39 (m, $H_{rep.unit}$, H_4), 2.54 (m, $H_{rep.unit}$, H_j), 3.29(m, $H_{rep.unit}$, H_m) 4.73 (m, $H_{rep.unit}$, H_2), 7.21 (m, $H_{rep.unit}$, H_{13}), 7.81 (m, $H_{rep.unit}$, H_{14}).

ADMET-Asp H (**4b**):^{1}H-NMR ($CDCl_3$ + 15 Vol. % TFA, 27 °C, 400 MHz): δ [ppm] 0.87 (m, 6H, H_z), 1.19 – 1.28 (m, $H_{rep.unit}$, $H_b – H_h + H_x + H_y$), 1.59 (m, $H_{rep.\ unit}$, $H_i + H_l$), 2.35 (m, $H_{rep.\ unit}$, H_j), 3.01 (m, $H_{rep.\ unit}$, H_3), 3.24 (m, $H_{rep.\ unit}$, H_3), 3.59 (m, $H_{rep.\ unit}$, H_m), 4.50 (m, $H_{rep.\ unit}$, H_2), 7.05 (m, $H_{rep.unit}$, $H_{12} + H_{13}$).

*General procedure for hydrogenation of the oligomers without a protecting group in the side chain (**4c** – **4e**)*

To a solution of the oligomer (**3c** – **3e**, 1.0 eq) in DMF (2 – 4 mL) $TsNHNH_2$ (5.0 eq per double bond) and DIPEA (5.0 eq) were added. The solution was heated up to 150 °C for 6 hours. The resulting mixture was cooled down to room temperature and dialyzed against MeOH for 3 days to yield the hydrogenated oligomers **4c** – **4e** (67-83 %).

ADMET-Leu H (**4c**): ^{1}H-NMR ($CDCl_3$ + 15 Vol. % TFA, 27 °C, 400 MHz): δ [ppm] 0.89 (m, $H_{rep.\ unit}$, $H_5 + H_6 + H_z$), 1.19 – 1.38 (m, 12H, $H_b – H_h + H_x + H_y$), 1.50 – 1.59 (m, $H_{rep.\ unit}$, $H_3 + H_4 + H_i + H_l$), 2.32 (m, $H_{rep.\ unit}$, H_j), 3.25 (m, $H_{rep.\ unit}$, H_m), 4.54 (m, $H_{rep.\ unit}$, H_2), 7.19 (m, $H_{rep.\ unit}$, H_7), 7.39 (m, $H_{rep.\ unit}$, H_8).

ADMET-Aib H (**4d**): ^{1}H-NMR ($CDCl_3$ + 15 Vol. % TFA, 27 °C, 400 MHz): δ [ppm] 0.88 (m, 6H, H_z), 1.25 (m, $H_{rep.unit}$, $H_b – H_h + H_l + H_x + H_y$), 1.55 – 1.59 (m, $H_{rep.unit}$, $H_2 + H_3 + H_i$), 2.28 (m, $H_{rep.unit}$, H_j), 3.29 (m, $H_{rep.unit}$, H_m), 6.70 (m, $H_{rep.unit}$, H_5), 6.99 (m, $H_{rep.unit}$, H_6).

ADMET-ACHC H (**4e**): ^{1}H-NMR ($CDCl_3$ + 15 Vol. % TFA, 27 °C, 400 MHz): δ [ppm] 0.88 (m, 6H, H_z), 1.27 – 1.46 (m, $H_{rep.unit}$, H_b – H_h + H_l + H_x + H_y + H_i), 1.74 (m, $H_{rep.unit}$, H_3 + H_4 + H_5), 1.96 – 2.31 (m, $H_{rep.unit}$,, H_j + H_2 + H_6), 3.37 (m, $H_{rep.unit}$, H_m), 7.12 – 7.26 (m, $H_{rep.unit}$, H_7 + H_8).

4.4 Synthesis of oligo-amino acid-PE(-type)-polymers

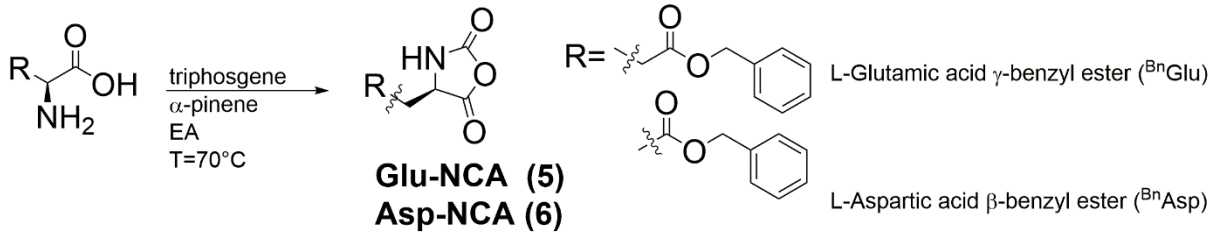

Scheme 10. Synthesis of **Glu-NCA** (**5**) and **Asp-NCA** (**6**).

4.4.1 Synthesis of N-carboxyanhydrides Glu-NCA (5) and Asp-NCA (6)

The synthesis of *N*-carboxyanhydrides Glu-NCA (**5)** and Asp-NCA (**6)** was done according to literature.[319] The amino acid (5-10 g; 1.0 eq) and α-pinene (2.0 eq) were suspended in dry ethyl acetate (10 mL per 1.0 g amino acid) and were heated up to 70 °C. Triphosgene (0.5 eq) was dissolved in dry ethyl acetate (adjusting a concentration of 10 mmol mL^{-1}) and the resulting solution was added dropwise to the reaction mixture over a period of 10 min. After the reaction mixture became clear, it was allowed to react for two more hours to remove excess triphosgene from the reaction mixture. The resulting mixture was cooled down to room temperature and residual HCl and phosgene were purged out with N_2 and trapped in an absorption bottle filled with aqueous NaOH. The solvent was removed in vacuum and the crude product was recrystallized three times in an ethyl acetate : *n*-hexane mixture (1 : 10). After filtration and drying in vacuum, the desired products were yielded as white powders (80-90 %).

Glu-NCA (**5**): ^{1}H-NMR ($CDCl_3$, 27 °C, 400 MHz): δ [ppm] 2.12 (m, 1H, H_4), 2.28 (m, 1H, H_4), 2.59 (t, $^{3}J_{H,H}$ = 6.8 Hz, 2H, H_5), 4.37 (t, $^{3}J_{H,H}$ = 6.0 Hz, 1H, H_3), 5.14 (s, 2H, H_7), 6.48 (s, 1H, H_{14}), 7.31 – 7.45 (m, 5H, H_9 – H_{13}).

^{13}C-NMR ($CDCl_3$, 27 °C, 100 MHz): δ [ppm] 26.9 (C_5), 29.9 (C_4), 57.0 (C_3), 67.1 (C_7), 128.4 – 128.7 (C_9 – C_{13}), 135.2 (C_8), 151.8 (C_1), 169.4 (C_2), 172.4 (C_6).

IR (KBr, cm^{-1}): 3334 (s), 3221 (w), 1881 (w), 1856 (w), 1782 (ss), 1719 (s), 1647 (w), 1610 (w), 1582 (w), 1554 (w), 1535 (w), 1493 (w), 1452 (w), 1417 (w), 1381 (m), 1343 (s), 1308 (m), 1283 (m), 1249 (w), 1187 (s), 1112 (s), 1067 (s), 993 (w), 973 (w), 933 (w), 876 (s), 822 (w), 797 (w), 753 (m), 736 (m), 694 (w), 671 (w), 636 (w), 607 (w), 591 (w).

Asp-NCA (**6**): ^{1}H-NMR ($CDCl_3$, 27 °C, 400 MHz): δ [ppm] 2.88 (dd, $^{3}J_{H,H}$ = 17.8 Hz, $^{2}J_{H,H}$ = 4.3 Hz, 1H, H_4), 3.05 (dd, $^{3}J_{H,H}$ = 17.8 Hz, $^{2}J_{H,H}$ = 4.9 Hz, 1H, H_4), 4.67 (t, $^{3}J_{H,H}$ = 4.5 Hz, 1H, H_3), 5.12 (s, 2H, H_6), 6.15 (s, 1H, H_{13}), 7.31 – 7.45 (m, 5H, H_8 – H_{12}).

^{13}C-NMR (DMSO-d_6, 27 °C, 100 MHz): δ [ppm] 35.1 (C_4), 54,1 (C_3), 66.8 (C_6), 128.6 – 128.9 (C_8 – C_{12}), 136.0 (C_7), 152.6 (C_1), 169.7 (C_2), 171.4 (C_5).

IR (KBr, cm^{-1}): 3605 (w), 3437 (w), 3310 (s), 3181 (w), 3086 (w), 3031 (w), 2971 (w), 2939 (w), 2900 (w), 1983 (w), 1838 (ss), 1788 (ss), 1726 (ss), 1586 (w), 1521 (w), 1496 (s), 1459 (s), 1400 (w), 1354 (s), 1299 (w), 1262 (ss), 1220 (ss), 1177 (ss), 1131 (s), 1110 (s), 1040 (w), 989 (w), 927 (w), 862 (s), 829 (w), 756 (s), 702 (w), 675 (w), 635 (s), 590 (w), 512 (w).

4.4.2 Synthesis of oligomers ($O^{Bn}Glu_{3,\ 10}$ (7a, 8a) and $O^{Bn}Asp_{3,\ 10}$ (9a, 10a)) by ROP of NCAs

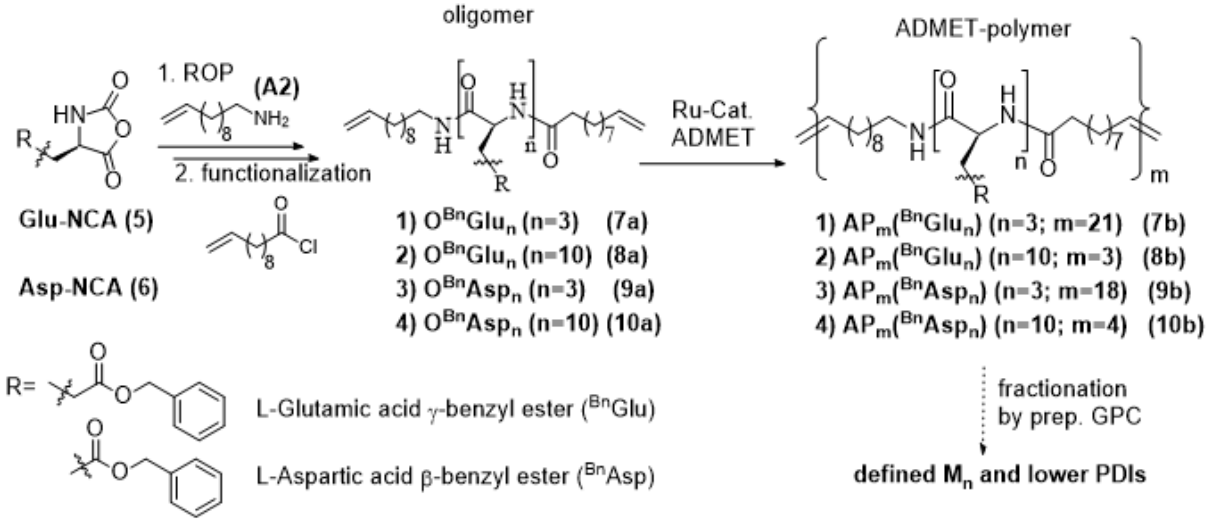

Scheme 11. Synthesis of oligomers **7a** – **10a** by ROP of corresponding **Glu-NCA** (**5**) and **Asp-NCA** (**6**), followed by ADMET-polymerization to obtain ADMET-polymers **7b** – **10b**.

4.4.2.1 Oligo-β-benzyl-L-glutamate, n=3 ($O^{Bn}Glu_3$) (7a)

Glu-NCA (**5**) (3.39 g; 12.88 mmol; 3 eq) was dissolved in dry, oxygen-free THF (20 mL). The solution was cooled down to 0 °C and 10-undecene-1-amine (0.73 g; 4.30 mmol; 1 eq) was added. Vacuum (150 mbar) was applied for 2 hours to remove evolving carbon dioxide, followed by the addition of 10-undecenoyl chloride (1.20 mL; 5.59 mmol; 1.3 eq) and triethylamine (0.90 mL; 6.45mmol; 1.5 eq). The reaction mixture was stirred overnight at room temperature. The resulting precipitate was filtered off and the remaining solution was concentrated in vacuum and precipitated into *n*-pentane (100 mL). After filtration, the obtained crude product was re-dissolved in THF (5 mL) and precipitated into cold 0.25M HCl (100mL). The resulting solid was isolated by centrifugation, dried in a desiccator overnight and further purified by column chromatography on silica (DCM / MeOH : 50 / 3, R_f = 0.15, blue stain) to yield 2.52 g of **$O^{Bn}Glu_3$** (**7a**) (74 %).

^{1}H-NMR (DMSO-d_6, 27 °C, 400 MHz): δ [ppm] 1.19 (m, 22H, H_d – H_h + H_l), 1.31 (m, 4H, H_i + H_o), 1.78 – 2.00 (m, $H_{rep.unit}$, H_2), 1.98 - 2.16 (m, 4H, H_c + H_j) 2.36 (m, $H_{rep.unit}$, H_3), 2.98 – 3.04 (m, 2H, H_p), 4.01 – 4.27 (m, $H_{rep.unit}$, H_1), 4.94 (m, 4H, H_a), 5.05 (s, $H_{rep.unit}$, H_5), 5.75 (m, 2H, H_b), 7.32 (m, $H_{rep.unit}$, H_6 – H_{11}), 7.73 – 8.15 (m, $H_{rep.unit}$, H_{12}), 7.73 – 8.15 (m, 1H, H_q).

MALDI-TOF-MS (positive mode, dithranol, KTFA, *m/z*) $[M]^+$ found 1250.777, simulated for $C_{70}H_{93}N_5O_{13}K^+$ 1250.640.

4.4.2.2 Oligo-β-benzyl-L-glutamate, n=10 ($O^{Bn}Glu_{10}$) (8a)

Glu-NCA (**5**) (3.80 g; 14.43 mmol; 10 eq) was dissolved in dry, oxygen-free DMF (6 mL). After cooling down to 0 °C, 10-undecene-1-amine (0.44 mg; 1.44 mmol; 1 eq) dissolved in dry, oxygen-free DMF (1 mL) was added to the mixture and vacuum (50 mbar) was applied during the whole reaction time. After 60 min, **Glu-NCA** was completely consumed (FTIR control by complete disappearing of $\nu_{C\text{-}O\text{-}C}$ signal at 1785 cm^{-1}). The vacuum was stopped and triethylamine (0.30 mL; 2.16 mmol; 1.5 eq) as well as 10-undecenoyl chloride (0.40 mL; 1.87 mmol; 1.3 eq) were added. The mixture was stirred overnight at room temperature, filtered and concentrated in vacuum. THF (5 mL) was added and the crude product was precipitated into cold 1M HCl (200 mL), isolated by centrifugation, dissolved in $CHCl_3$ and dried over Na_2SO_4. The obtained solution was filtered and the solvent was evaporated in vacuum. The crude

product was dried in a desiccator overnight and further purified by dialysis against MeOH for 3 days to yield **$O^{Bn}Glu_{10}$** (**8a**) (2.43 g, 96 %).

^{1}H-NMR (DMSO-d_6, 27 °C, 400 MHz): δ [ppm] 1.18 – 1.36 (m, 22H, H_d – H_h + H_l), 1.31 (m, 4H, H_i + H_o), 1.78 – 2.00 (m, $H_{rep.unit}$, H_2), 1.98 - 2.16 (m, 6H, H_c + H_j) 2.36 (m, $H_{rep.unit}$, H_3), 2.98 – 3.04 (m, 2H, H_p), 4.01 – 4.27 (m, $H_{rep.unit}$, H_1), 4.94 (m, 4H, H_a), 5.05 (s, $H_{rep.unit}$, H_5), 5.75 (m, 2H, H_b), 7.32 (m, $H_{rep.unit}$, H_6 – H_{11}), 7.73 – 8.15 (m, $H_{rep.unit}$, H_{12}), 7.73 – 8.15 (m, 1H, H_q).

MALDI-TOF-MS (positive mode, dithranol, KTFA, *m/z*) $[M]^+$ found 1194.719, simulated for $C_{66}H_{85}N_5O_{13}K^+$ 1194.578.

*4.4.2.3 Oligo-β-benzyl-L-aspartate, n=3 (**$O^{Bn}Asp_3$**) (**9a**)*

Asp-NCA (**6**) (3.20 g; 12.89 mmol; 3 eq) was dissolved in dry, oxygen-free THF (16 mL). The solution was cooled down to 0 °C and 10-undecene-1-amine (0.73 g; 4.30 mmol; 1 eq) was added to the mixture. The reaction mixture was allowed to stir overnight under applied vacuum (150 mbar), followed by adding 10-undecenoyl chloride (1.20 mL; 5.59 mmol; 1.3 eq) and triethylamine (0.90 mL; 6.45mmol; 1.5 eq) under atmospheric pressure. The reaction mixture was stirred overnight at room temperature, the resulting precipitate was filtered and the solution was concentrated in vacuum. The mixture was precipitated into *n*-pentane (100 mL). After centrifugation, the crude product was re-dissolved in THF (5 mL) and precipitated into cold 0.25M HCl (100mL). The mixture was isolated by centrifugation and the resulting white solid was dried in a desiccator overnight. The polymer was finally purified by flash column chromatography on silica removing the impurities by the addition of chloroform (TLC control, R_f = 0.72). By washing the silica with THF the pure product **$O^{Bn}Asp_3$** (**9a**) was obtained with a yield of 2.52 g (74 %).

^{1}H-NMR ($CDCl_3$, 27 °C, 400 MHz): δ [ppm] 1.27 – 1.37 (m, 22H, H_d – H_h + H_l), 1.47 (m, 2H, H_o), 1.61 (m, 2H, H_i), 2.03 (m, 4H, H_c), 2.18 (m, 2H, H_j), 2.67 – 2.93 (m, $H_{rep.\ unit}$, H_2), 3.18 (m, 2H, H_p), 4.76 (m, $H_{rep.\ unit}$, H_1), 4.97 (m, 4H, H_a), 5.12 (m, $H_{rep.\ unit}$, H_4), 5.82 (m, 2H, H_b), 6.64 (m, $H_{rep.\ unit}$, Hq + H_{11}), 7.33 (m, $H_{rep.\ unit}$, H_5 - H_{10}), 7.51 (m, $H_{rep.\ unit}$, H_q + H11).

MALDI-TOF-MS (positive mode, dithranol, KTFA, *m/z*) $[M]^+$ found 2347.291, simulated for $C_{130}H_{158}N_{10}O_{28}K^+$ 2347.091.

*4.4.2.4 Oligo-β-benzyl-L-aspartate, n=10 (**$O^{Bn}Asp_{10}$**) (**10a**)*

To a solution of **Asp-NCA** (**6**) (3.51 g; 14.14 mmol; 10 eq) in dry, oxygen-free DMF (10 mL), 10-undecene-1-amine (0.24 g; 1.41 mmol; 1 eq) dissolved in DMF (2 mL) was added at 0 °C. Vacuum (50 mbar) was applied and triethylamine (0.29 mL; 2.11 mmol; 1.5 eq) as well as 10-undecenoyl chloride (0.39 mL; 1.83 mmol; 1.3 eq) were added after all **Asp-NCA** was consumed (FTIR control by complete disappearing of $\nu_{C\text{-}O\text{-}C}$ signal at 1785 cm^{-1}). The reaction mixture was stirred overnight at room temperature and the precipitate was filtered off. The solution was concentrated in vacuum, THF (5 mL) was added and the mixture was precipitated into cold 1M HCl (200 mL). After centrifugation, the crude product was dissolved in THF (10 mL) and dried over Na_2SO_4. After filtration, the solution was concentrated in vacuum and the obtained product was dried in a desiccator overnight. The crude product was further purified by dialysis against MeOH to obtain **$O^{Bn}Asp_{10}$ (10a)** (2.01 g, 70 %).

^{1}H-NMR (DMSO-d_6, 27 °C, 400 MHz): δ [ppm] 1.27 – 1.42 (m, 26H, H_d – H_h + H_l + H_i + H_o), 1.96 (m, 4H, H_c), 2.03 (m, 2H, H_j), 2.59 – 2.80 (m, $H_{rep.\ unit}$, H_2), 2.95 (m, 2H, H_p), 4.61 (m, $H_{rep.\ unit}$, H_1), 4.90 (m, 4H, H_a), 5.02 (m, $H_{rep.\ unit}$, H_4), 5.75 (m, 2H, H_b), 7.29 (m, $H_{rep.\ unit,}$ H_6 - H_{10}), 7.51 – 8.26 (m, $H_{rep.\ unit}$, H_q + H_{11}).

MALDI-TOF-MS (positive mode, dithranol, KTFA, *m/z*) $[M]^+$ found 2426.281, simulated for $C_{132}H_{151}N_{11}O_{31}K^+$ 2426.024.

4.4.3 Synthesis of ADMET-polymers $AP_m(^{Bn}Glu_n)$ (7b, 8b) and $AP_m(^{Bn}Asp_n)$ (9b, 10b)

The corresponding oligomer (**$O^{Bn}Glu_3$** (**7a**), **$O^{Bn}Glu_{10}$** (**8a**), **$O^{Bn}Asp_3$** (**9a**), **$O^{Bn}Asp_{10}$** (**10a**)) (2.0 g; 1 eq) was placed in a dry, oxygen-free Schlenk-tube and dry, degassed dichloromethane (6-15 mL) was added followed by Grubbs 1st catalyst (100:1 monomer to catalyst ratio). The mixture was stirred under reflux, while flushing with nitrogen was applied during the whole reaction time (approximately once an hour) to remove evolving ethylene gas. Furthermore, a small amount of catalyst (approximately 1 mg) was additionally added to the reaction mixture after several hours. After 4 days the reaction mixture was cooled down to room temperature, quenched with ethyl vinyl ether (3 mL) and the mixture was allowed to stir overnight. The solvent was removed in vacuum and the crude product was dissolved in toluene : THF 80:20 v/v % mixture followed by a precipitation into cold MeOH. The obtained polymer was isolated by centrifugation, dissolved in THF and further purified by dialysis against MeOH for 3 days to yield the ADMET-polymer **$AP_{21}(^{Bn}Glu_3)$** (**7b**), **$AP_3(^{Bn}Glu_{10})$** (**8b**), **$AP_{21}(^{Bn}Asp_3)$** (**9b**), **$AP_4(^{Bn}Asp_{10})$** (**10b**) (46-71 %).

$AP_{21}(^{Bn}Glu_3)$ (**7b**): yield: 60 %, ^{1}H-NMR (DMSO-d_6, 27 °C, 400 MHz): δ [ppm] 1.19 (m, $H_{rep.\ unit\ alkyl}$, $H_d - H_h$), 1.31 (m, $H_{rep.\ unit\ alkyl}$, $H_i + H_o$), 1.78 – 2.00 (m, $H_{rep.unit\ amino\ acid}$, H_2), 1.98 - 2.16 (m, $H_{rep.\ unit\ alkyl}$, $H_c + H_j$) 2.36 (m, $H_{rep.unit\ amino\ acid}$, H_3), 2.98 – 3.04 (m, $H_{rep.\ unit\ alkyl}$, H_p), 4.01 – 4.27 (m, $H_{rep.unit\ amino\ acid}$, H_1), 5.05 (s, $H_{rep.unit\ amino\ acid}$, H_5), 5.31 (m, $H_{rep.\ unit\ alkyl}$, $H_x + H_y$), 7.32 (m, $H_{rep.unit\ amino\ acid}$, $H_6 - H_{11}$), 7.73 – 8.15 (m, $H_{rep.unit\ amino\ acid}$, H_{12}), 7.73 – 8.15 (m, $H_{rep.\ unit\ alkyl,}$ H_q).

$AP_3(^{Bn}Glu_{10})$ (**8b**): yield: 52 %, ^{1}H-NMR (DMSO-d_6, 27 °C, 400 MHz): δ [ppm] 1.18 – 1.36 (m, $H_{rep.\ unit\ alkyl}$, $H_d - H_h + H_i + H_o$), 1.78 – 2.00 (m, $H_{rep.unit\ amino\ acid}$, H_2), 1.98 - 2.16 (m, $H_{rep.\ unit\ alkyl}$, $H_c + H_j$), 2.36 (m, $H_{rep.unit\ amino\ acid}$, H_3), 2.98 – 3.04 (m, $H_{rep.\ unit\ alkyl}$, H_p), 3.91 – 4.27 (m, $H_{rep.unit\ amino\ acid}$, H_1), 5.05 (s, $H_{rep.unit\ amino\ acid}$, H_5), 5.30 (m, $H_{rep.\ unit\ alkyl}$, $H_x + H_y$), 7.32 (m, $H_{rep.unit\ amino\ acid}$, $H_6 - H_{11}$), 7.73 – 8.15 (m, $H_{rep.unit\ amino\ acid}$, H_{12}), 7.73 – 8.15 (m, $H_{rep.\ unit\ alkyl,}$ H_q).

$AP_{21}(^{Bn}Asp_3)$ (**9b**): yield: 71 %, ^{1}H-NMR (DMSO-d_6, 27 °C, 400 MHz): δ [ppm] 1.27 – 1.47 (m, $H_{rep.\ unit\ alkyl}$, $H_d - H_h + H_l + H_o + H_i$), 2.03 (m, $H_{rep.\ unit\ alkyl}$, H_c), 2.18 (m, $H_{rep.\ unit\ alkyl}$, H_j), 2.67 – 2.93 (m, $H_{rep.\ unit\ amino\ acid}$, H_2), 3.52 (m, $H_{rep.\ unit\ alkyl}$, H_p), 4.57 (m, $H_{rep.\ unit\ amino\ acid}$, $H1$), 5.10 (m, $H_{rep.\ unit\ amino\ acid}$, H_4), 5.33 (m, $H_{rep.\ unit\ alkyl}$, $H_x + H_y$), 7.33 (m, $H_{rep.\ unit\ amino\ acid}$, H_5 - H_{10}), 7.51 (m, $H_{rep.\ unit}$, $H_q + H_{11}$).

$AP_4(^{Bn}Asp_{10})$ (**10b**): yield: 46 %, ^{1}H-NMR (DMSO-d_6, 27 °C, 400 MHz): δ [ppm] 1.17 – 1.47 (m, $H_{rep.\ unit\ alkyl}$, $H_d - H_h + H_l + H_o + H_i$), 1.96 (m, $H_{rep.\ unit\ alkyl}$, H_c), 2.04 (m, $H_{rep.\ unit\ alkyl}$, H_j), 2.60 – 2.80 (m, $H_{rep.\ unit\ amino\ acid}$, H_2), 2.95 (m, $H_{rep.\ unit\ alkyl}$, H_p), 4.61 (m, $H_{rep.\ unit\ amino\ acid}$, H_1), 5.02 (m, $H_{rep.\ unit\ amino\ acid}$, H_4), 5.32 (m, $H_{rep.\ unit\ alkyl}$, $H_x + H_y$), 7.30 (m, $H_{rep.\ unit\ amino\ acid}$, H_6 - H_{10}), 7.51 – 8.14 (m, $H_{rep.\ unit}$, $H_q + H_{11}$).

4.5 Synthesis of artificial oligo-amino acids

4.5.1 Synthesis of N-carboxyanhydrides (NCAs) of achiral amino acids (11, 12)

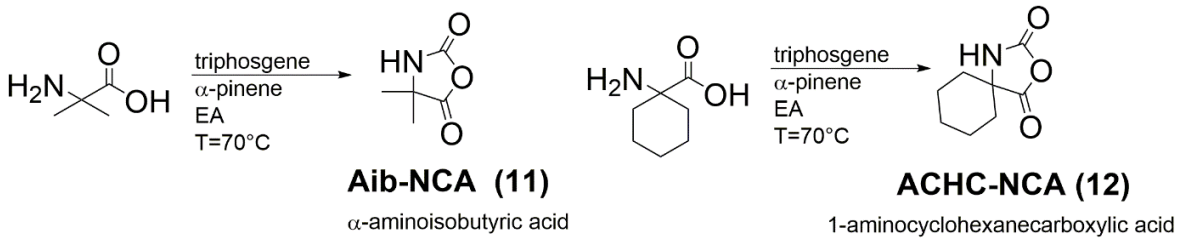

Scheme 12. Synthesis of **Aib-NCA** (**11**) and **ACHC-NCA** (**12**).

*4.5.1.1 Synthesis of **Aib-NCA (11)***

Aib (15.4 g; 0.175 mol; 1.0 eq) and α-pinene (47.68g; 0.350 mol; 2.0 eq) were suspended in dry ethyl acetate (170 mL). Triphosgene (35.5 g; 0,120 mol; 0.68 eq) was added and the reaction mixture was heated up to 70 °C. After the reaction mixture became clear (1 day), it was allowed to react for five more hours to remove excess triphosgene from the reaction mixture. The mixture was cooled down to room temperature and residual HCl and phosgene were purged out with N_2 and trapped in an absorption bottle filled with aqueous NaOH. The solvent was removed in vacuum and the crude product was recrystallized three times in an ethyl acetate : *n*-hexane mixture (1 : 10), filtrated and dried in vacuum to yield **Aib-NCA** (**11**) as white crystalline powder (12.9 g; 57 %).

^{1}H-NMR (DMSO-d_6, 27 °C, 400 MHz): δ [ppm] 1.40 (s, 6H, $H_4 + H_5$), 9.08 (br, 1H, H_6).

^{13}C-NMR (DMSO-d_6, 27 °C, 100 MHz): δ [ppm] 25.1 ($C_4 + C_5$), 59.7 (C_3), 150.8 (C_1), 175 (C_2).

IR (KBr, cm^{-1}): 3605 (w), 3437 (w), 3309 (s), 3181 (w), 3086 (w), 3030 (w), 2970 (w), 2938 (w), 2900 (w), 1983 (w), 1837 (ss), 1787 (ss), 1725 (ss), 1586 (w), 1558 (w), 1521 (m), 1496 (m), 1399 (s), 1354 (s), 1299 (m), 1262 (s), 1220 (w), 1177 (s), 1131 (s), 1110 (s), 1040 (w), 988 (w), 926 (s), 862 (w), 829 (w), 756 (s), 702 (m), 675 (m), 635 (s), 590 (w), 512 (w).

*4.5.1.2 Synthesis of **ACHC-NCA (12)***

ACHC (18.0 g; 0.126 mol; 1.0 eq) and α-pinene (34.33 g; 0.252 mol; 2.0 eq) were suspended in dry ethyl acetate (170 mL). Triphosgene (24.3 g; 0,082 mol; 0.65 eq) was added and the reaction mixture was heated up to 70 °C. After the reaction mixture became clear (4 days), it was allowed to react for five more hours to remove excess triphosgene from the reaction mixture. The mixture was cooled down to room temperature and residual HCl and phosgene were purged out with N_2 and trapped in an absorption bottle filled with aqueous NaOH. The solvent was removed in vacuum and the crude product was recrystallized three times in an ethyl acetate : *n*-hexane mixture (1 : 10), filtrated and dried in vacuum to yield **ACHC-NCA** (**12**) as white crystalline powder (14,3 g; 67 %).

^{1}H-NMR (DMSO-d_6, 27 °C, 400 MHz): δ [ppm] 1.33 (m, 1H, H_8), 1.40 – 1.55 (m, 3H, $H_4 + H_8$), 1.56 – 1.67 (m, 2H, H_6), 1.68 – 1.73 (m, 4H, $H_5 + H_7$), 9.44 (br, H_9).

^{13}C-NMR (DMSO-d_6, 27 °C, 100 MHz): δ [ppm] 21.1 ($C_5 + C_7$), 24.5 (C_6), 33.7 ($C_4 + C_8$), 62.7 (C_3), 151.3 (C_1), 174.1 (C_2).

IR (KBr, cm^{-1}): 3606 (w), 3541 (w), 3353 (ss), 2937 (s), 2865 (w), 2821 (m), 1861 (ss), 1794 (ss), 1645 (w), 1541 (w), 1507 (m), 1451 (w), 1423 (w), 1355 (w), 1323 (s), 1271 (s), 1199 (s), 1151 (w), 1043 (s), 1004 (m), 938 (w), 914 (ss), 847 (w), 771 (w), 675 (w), 631 (m), 601 (w), 558 (m), 508 (w).

4.5.2 Synthesis of artificial oligo-amino acids initiated by amine initiators

*4.5.2.1 Synthesis of 1-dec-9-enyl-undec-10-enylamine (initiator **A4**)*

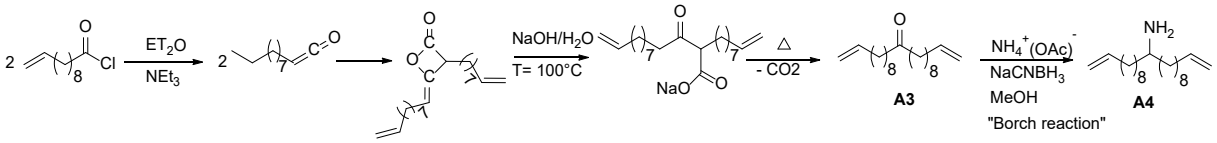

Scheme 13. Synthesis of **A3** and **A4**.

Synthesis of 1-dec-9-enyl-undec-10-enylketone (A3)

Synthesis of **1-dec-9-enyl-undec-10-enylketone** (**A3**) was done according to literature.[305] 10-undecenoyl chloride (20.49 g; 101.08 mmol; 1 eq) was dissolved in Et_2O (120 mL) and cooled down to 0 °C. NEt_3 (26.0 mL; 187.58 mmol; 1.86 eq) was added slowly, instantly forming white triethylammonium chloride salt. The reaction mixture was allowed to stir at room temperature for 3 days and the solid was filtered off. The filtrate was concentrated and dried under vacuum. Distilled H_2O (100 mL) and NaOH (8.80 g; 0.21 mol) was added and the two-phase system was refluxed for 6 hours. The resulting homogeneous, orange solution was cooled down to room temperature and 2M HCl (130 mL) was added. The solution was extracted with Et_2O (3x 50 mL) and the organic layers were combined. The organic phase was washed with 1M HCl (2x20 mL), saturated $NaHCO_3$-solution (2x20 mL) and distilled water (2x20 mL). The organic phase was dried over Na_2SO_4, filtered and recrystallized three times in MeOH to yield 8.76 g (28 %) of **1 dec-9-enyl-undec-10-enylketone** (**A3**).

^{1}H-NMR ($CDCl_3$, 27 °C, 400 MHz): δ [ppm] 1.28 – 1.37 (m, 21H, H_d –H_h), 1.55 (m, 4H, H_i), 2.04 (m, 4H, H_c), 2.37 (t, $^3J_{H,H}$ = 7.5 Hz, 4H, H_j), 4.94 (m, 4H, H_a), 5.79 (m, 2H, H_b).

^{13}C-NMR ($CDCl_3$, 27 °C, 100 MHz): δ [ppm] 25.5 (C_i), 28.9 – 29.3 ($C_{d\text{-}h}$), 33.7 (C_c), 36.0 (C_j), 114.1 (C_a), 139.1 (C_b), 175.6 (C_k).

Synthesis of 1-dec-9-enyl-undec-10-enylamine (A4)

Synthesis of **1-dec-9-enyl-undec-10-enylamine** (**A4**) was done according to literature.[305] In an inert atmosphere **1-dec-9-enyl-undec-10-enylketone** (**A3**) (2.00 g; 5.98 mmol; 1 eq), ammonium acetate (4.61 g; 59.8 mmol; 10 eq), $NaCNBH_3$ (2.02 g; 30.50 mmol; 5.1 eq) and molsieve (3Å) were suspended in dry MeOH (40 mL) and the reaction mixture was stirred overnight at 55 °C, followed by refluxing for 6 hours. After cooling down to room temperature, the mixture was filtrated. Distilled H_2O (200 mL) was added and the aqueous phase was extracted with Et_2O (3x50 mL). The organic phases were combined and washed with 1M NaOH (2x30 mL) and brine (2x30 mL). The organic phase was dried over Na_2SO_4, filtrated and dried in vacuum. The crude product was purified by column chromatography removing all impurities with EA / *n*-hexane : 1/3 followed by using THF as eluent to obtain **1-dec-9-enyl-undec-10-enylamine** (**A4**) as a colourless liquid with a yield of 1.25 g (68 %).

^{1}H-NMR ($CDCl_3$, 27 °C, 400 MHz): δ [ppm] 1.28 (m, 21H, H_d –H_h), 1.37 (m, 4H, H_i), 1.52 (m, 4H, H_j), 2.02 (m, 4H, H_c), 2.95 (m, 1H, H_k), 4.58 (m, 2H, H_l), 4.93 (m, 4H, H_a), 5.80 (m, 2H, H_b).

^{13}C-NMR ($CDCl_3$, 27 °C, 100 MHz): δ [ppm] 25.5 (C_i), 28.9 – 29.3 ($C_{d\text{-}h}$), 33.8 (C_c), 35.2 (C_j), 51.9 (C_k), 114.1 (C_a), 139.1 (C_b).

4.5.2.2 Synthesis of polymers initiated by amine initiator

A) Frozen solvents: In a typical reaction **Aib-NCA** (**11**) (100-500 mg; *c* mol/L; *M*/*I* eq) was dissolved in oxygen-free, dry solvent. The solution was precooled to 0 °C. **Initiator** (***I***) (*M*/*I* eq) was added and the reaction mixture was directly frozen with liquid nitrogen and stored in a freezer. After several days, the product precipitated as white solid. After two weeks, the reaction mixture was thawed and dialyzed against acetone to get **13a** – **14i.**

B) Liquid solvents: In a typical reaction **initiator** (***I***) (*M*/*I* eq) was dissolved in oxygen-free, dry solvent. The solution was heated up or cooled down to the reaction temperature. **Aib-NCA** (**11**) (100-500 mg; *c* mol/L; *M*/*I* eq) was added and the reaction mixture was allowed to react overnight (for **15e**: 600 min as identified by FTIR-measurements). In all cases, the product precipitated as white solid during

polymerization. The solution was cooled down or warmed up to room temperature and dialyzed against acetone to get **15a** – **15e**.

Table 15. Initiator (*I*), solvent, M/I-ratios, *c* (mol/L) and T (°C) for the ROP of **Aib-NCA** (**11**).

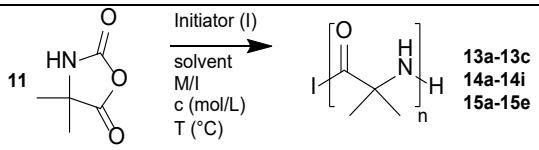

entry	initiator (*I*) and endgroups on *C*-(E1) and *N*-terminus (E2)	solvent	M/I	c (mol L^{-1})	T (°C)	yield (%)	M_n MALDI-TOF-MS (Da) (maximum intensity M_n (Min/Max n)
13a	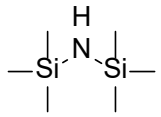 **"HMDS"** E1: NH_2 E2: H	frozen Dioxane	15:1	0.02	11 °C (-24 °C)	27	1060.626 (Na^+) (n=12) n=10-15
13b			20:1			41	906.485 (K^+) (n=10) n=10-15
13c			25:1			32	991.470 (K^+) (n=11) n=11-20
14a	**A4** 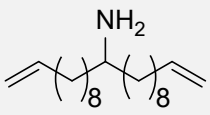 E1: $C_{21}H_{40}N$ E2: H	frozen Dioxane	10:1	0.02	11 °C (-24 °C)	55	1451.845 (K^+) (n=13) n=7-17
14b			15:1			53	1282.509 (K^+) (n=11) n = 9-16
14c			25:1			48	1451.870 (K^+) (n=13) n=9-18
14d			50:1			53	1451.774 (K^+) (n=13) n=9-17
14e			50:1	0.03		61	1536.938 (K^+) (n=14) n=10-17
14f			50:1	0.05		63	1536.986 (K^+) (n=14) n=10-24
14g			50:1	0.15		57	1777.260 (K^+) (n=16) n=9-24
14h			50:1	0.80		62	1006.591 (n=10) + 1793.295 (K^+) (n=17) n=8-25
14i		frozen DMA	50:1	0.80	-20 °C (-38 °C)	60	1622.007 (K^+) (n=15) n=10-33
15a	**A2** 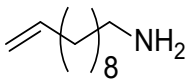 E1: $C_{11}H_{22}N$ E2: H	ET_2O	50:1	2.0	0 °C	23	1058.595 (K^+) (n=10) n=6-19
15b		DCM	50:1	2.0	0 °C	22	1143.683 (K^+) (n=11) n=6-20
15c		Toluene	50:1	2.0	0 °C	40	1143.602 (K^+) (n=11) n=6-19
15d		THF	50:1	2.0	0 °C	49	1229.037 (K^+) (n=12) n=10-22
15e		DMF	12:1	2.0	80 °C	67	1399.171 (K^+) (n=14) n=11-18

HMDS-PAib1 (**13a**). White solid; 27 % yield; MALDI-TOF-MS (positive mode, dithranol, KTFA, *m/z*) $[M]^+$ found 1060.626, simulated for $NH_2(C_4H_7NO)_{12}HNa^+$ 1060.649.

HMDS-PAib2 (**13b**). White solid; 41 % yield; MALDI-TOF-MS (positive mode, dithranol, KTFA, *m/z*) $[M]^+$ found 906.485, simulated for $NH_2(C_4H_7NO)_{10}HK^+$ 906.517.

HMDS-PAib3 (**13c**). White solid; 32 % yield; MALDI-TOF-MS (positive mode, dithranol, KTFA, *m/z*) $[M]^+$ found 991.470, simulated for $NH_2(C_4H_7NO)_{11}HK^+$ 991.570.

21Amin-PAib1 (**14a**). White solid; 55 % yield; MALDI-TOF-MS (positive mode, dithranol, KTFA, *m/z*) $[M]^+$ found 1451.845, simulated for $C_{21}H_{40}N(C_4H_7NO)_{13}HK^+$ 1451.973.

21Amin-PAib2 (**14b**). White solid; 53 % yield; MALDI-TOF-MS (positive mode, dithranol, KTFA, *m/z*) $[M]^+$ found 1282.509, simulated for $C_{21}H_{40}N(C_4H_7NO)_{11}HK^+$ 1281.867.

21Amin-PAib3 (**14c**). White solid; 48 % yield; MALDI-TOF-MS (positive mode, dithranol, KTFA, *m/z*) $[M]^+$ found 1451.870, simulated for $C_{21}H_{40}N(C_4H_7NO)_{13}HK^+$ 1451.973.

21Amin-PAib4 (**14d**). White solid; 53 % yield; MALDI-TOF-MS (positive mode, dithranol, KTFA, *m/z*) $[M]^+$ found 1451.774, simulated for $C_{21}H_{40}N(C_4H_7NO)_{13}HK^+$ 1451.973.

21Amin-PAib5 (**14e**). White solid; 61 % yield; MALDI-TOF-MS (positive mode, dithranol, KTFA, *m/z*) $[M]^+$ found 1536.938, simulated for $C_{21}H_{40}N(C_4H_7NO)_{14}HK^+$ 1537.026.

21Amin-PAib6 (**14f**). White solid; 63 % yield; MALDI-TOF-MS (positive mode, dithranol, KTFA, *m/z*) $[M]^+$ found 1536.986, simulated for $C_{21}H_{40}N(C_4H_7NO)_{14}HK^+$ 1537.026.

21Amin-PAib7 (**14g**). White solid; 57 % yield; MALDI-TOF-MS (positive mode, dithranol, KTFA, *m/z*) $[M]^+$ found 1777.260, simulated for $C_{21}H_{40}N(C_4H_7NO)_{17}HNa^+$ 1777.213.

21Amin-PAib8 (**14h**). White solid; 62 % yield; MALDI-TOF-MS (positive mode, dithranol, KTFA, *m/z*) $[M]^+$ found 1793.295, simulated for $C_{21}H_{40}N(C_4H_7NO)_{17}HNa^+$ 1793.187.

21Amin-PAib9 (**14i**). White solid; 60 % yield; ^{1}H-NMR (HFIP-d_2, 27 °C, 400 MHz): δ [ppm] 1.45 – 1.69 (m, $H_{rep.\ unit}$, H_d –H_h + H_1), 1.85 (m, 4H, H_i), 2.19 (m, 4H, H_c), 3.92 (br, 1H, H_k), 5.10 (m, 4H, H_a), 6.60 (m, 2H, H_b), 6.67 – 7.00 (m, 1H, H_l), 7.60 (m, $H_{rep.\ unit}$, H_3).

MALDI-TOF-MS (positive mode, dithranol, KTFA, *m/z*) $[M]^+$ found 1622.007, simulated for $C_{21}H_{40}N(C_4H_7NO)_{15}HK^+$ 1622.079.

11Amin-PAib1 (**15a**). White solid; 17 % yield; MALDI-TOF-MS (positive mode, dithranol, KTFA, *m/z*) $[M]^+$ found 1058.595, simulated for $C_{11}H_{22}N(C_4H_7NO)_{10}HK^+$ 1058.674.

11Amin-PAib2 (**15b**). White solid; 23 % yield; MALDI-TOF-MS (positive mode, dithranol, KTFA, *m/z*) $[M]^+$ found 1143.683, simulated for $C_{11}H_{22}N$ $(C_4H_7NO)_{11}HK^+$ 1143.727.

11Amin-PAib3 (**15c**). White solid; 22 % yield; MALDI-TOF-MS (positive mode, dithranol, KTFA, *m/z*) $[M]^+$ found 1143.602, simulated for $C_{11}H_{22}N$ $(C_4H_7NO)_{11}HK^+$ 1143.727.

11Amin-PAib4 (**15d**). White solid; 67 % yield; MALDI-TOF-MS (positive mode, dithranol, KTFA, *m/z*) $[M]^+$ found 1229.037, simulated for $C_{11}H_{22}N$ $(C_4H_7NO)_{13}HK^+$ 1398.885.

11Amin-PAib4 (**15e**). White solid; 67 % yield; ^{1}H-NMR (HFIP-d_2, 27 °C, 400 MHz): δ [ppm] 1.05 – 1.40 (m, $H_{rep.\ unit}$, H_d –H_j +H_1), 1.80 (m, 2H, H_c), 2.96 (m, 2H, H_k), 4.07 (m, 1H, H_l) 4.73 (m, 2H, H_a), 5.66 (m, 1H, H_b), 7.15 (m, $H_{rep.\ unit}$, H_3).

MALDI-TOF-MS (positive mode, dithranol, KTFA, *m/z*) $[M]^+$ found 1399.171, simulated for $C_{11}H_{22}N(C_4H_7NO)_{13}HK^+$ 1228.779.

4.5.3 Synthesis of artificial oligo-amino acids initiated by amino acid-methyl ester (17a – 17j)

*4.5.3.1 Synthesis of amino acid-methyl ester hydrochlorides (**16a** – **16j**)*

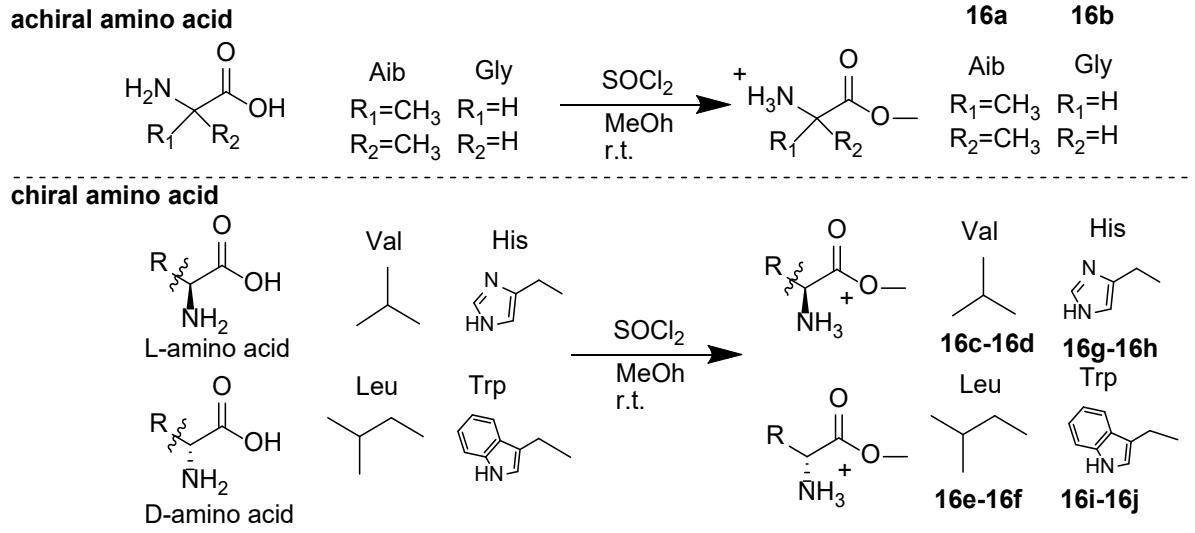

Scheme 14. Synthesis of amino acid-methyl esters **NH_2-AA-OMe · HCl** (**16a** – **16j**).

General procedure: (L-/D-)AA (1 eq) were suspended in dry MeOH (10 mL per 1g) and cooled to 0 °C. Thyonilchloride (1.2 eq) was added dropwise to the suspension and the reaction mixture was stirred at room temperature overnight. The solution was concentrated in vacuum and the obtained crude product was recrystallized three times in MeOH:Et_2O mixture, separated and dried in vacuum to give **NH_2-AA-OMe • HCl** (**16a-16j**) (65 % – 89 %).

2-aminoisobutyric acid methyl ester hydrochloride (NH_2-Aib-OMe • HCl) (16a). White solid; 85 % yield; ^{1}H-NMR (DMSO-d_6, 27 °C, 400 MHz): δ [ppm] 1.47 (s, 6H, H_d), 3.70 (s, 3H, H_a), 8.86 (br, 3H, H_e).

^{13}C-NMR (DMSO-d_6, 27 °C, 100 MHz): δ [ppm] 23.8 (C_d), 53.5 (C_c), 56.3 (C_a) 172.4 (C_b).

Glycine methyl ester hydrochloride (NH_2-Gly-OMe • HCl) (16b). White solid; 89 % yield; ^{1}H-NMR (DMSO-d_6, 27 °C, 400 MHz): δ [ppm] 3.70 (s, 6H, H_a), 3.74 (s, 3H, H_c), 8.57 (br, 3H, H_d).

^{13}C-NMR (DMSO-d_6, 27 °C, 100 MHz): δ [ppm] 39.8 (C_c), 52.9 (C_a), 168.4 (C_b).

L-Valine methyl ester hydrochloride (NH_2-L-Val-OMe • HCl) (16c). White solid; 88 % yield; ^{1}H-NMR (DMSO-d_6, 27 °C, 400 MHz): δ [ppm] 0.94 (dd, $^{3}J_{H,H}$=6.9 Hz, $^{4}J_{H,H}$=19.7 Hz, 6H, H_e), 2.19 (m, 1H, H_d), 3.72 (s, 3H, H_a), 3.80 (d, $^{3}J_{H,H}$=4.8 Hz, 1H, H_c), 8.68 (br, 3H, H_f).

^{13}C-NMR (DMSO-d_6, 27 °C, 100 MHz): δ [ppm] 19.0 (C_e), 29.7 (C_d), 52.9 (C_a), 57.7 (C_c), 169.5 (C_b).

D-Valine methyl ester hydrochloride (NH_2-D-Val-OMe • HCl) (16d). White solid; 80 % yield; ^{1}H-NMR (DMSO-d_6, 27 °C, 400 MHz): δ [ppm] 0.94 (dd, $^3J_{H,H}$=10.9 Hz, $^4J_{H,H}$=20.5 Hz, 6H, H_e), 2.19 (m, 1H, H_d), 3.72 (s, 3H, H_a), 3.80 (d, $^3J_{H,H}$=4.6 Hz, 1H, H_c), 8.68 (br, 3H, H_f).

^{13}C-NMR (DMSO-d_6, 27 °C, 100 MHz): δ [ppm] 18.9 (C_e), 29.7 (C_d), 53.0 (C_a), 57.7 (C_c), 169.6 (C_b).

L-Leucine methyl ester hydrochloride (NH_2-L-Leu-OMe • HCl) (16e). White solid; 82 % yield; ^{1}H-NMR (DMSO-d_6, 27 °C, 400 MHz): δ [ppm] 0.87 (d, $^3J_{H,H}$=6.5 Hz, 6H, H_f), 1.63 (t, $^3J_{H,H}$=7.4 Hz, 2H, H_d), 1.74 (m, 1H, H_e), 3.72 (s, 3H, H_a), 3.92 (t, $^3J_{H,H}$=6.9 Hz, 1H, H_c), 8.59 (br, 3H, H_g).

^{13}C-NMR (DMSO-d_6, 27 °C, 100 MHz): δ [ppm] 22.4 (C_f), 24.2 (C_e), 40.0 (C_d), 50.9 (C_a), 53.1 (C_c), 170.7 (C_b).

D-Leucine methyl ester hydrochloride (NH_2-D-Leu-OMe • HCl) (16f). White solid; 77 % yield; ^{1}H-NMR (DMSO-d_6, 27 °C, 400 MHz): δ [ppm] 0.87 (d, $^3J_{H,H}$=6.5 Hz, 6H, H_f), 1.63 (t, $^3J_{H,H}$=7.4 Hz, 2H, H_d), 1.74 (m, 1H, H_e), 3.72 (s, 3H, H_a), 3.92 (t, $^3J_{H,H}$=8.3 Hz, 1H, H_c), 8.66 (br, 3H, H_g).

^{13}C-NMR (DMSO-d_6, 27 °C, 100 MHz): δ [ppm] 22.4 (C_f), 24.2 (C_e), 40.0 (C_d), 50.9 (C_a), 53.1 (C_c), 170.7 (C_b).

L-Histidine methyl ester dihydrochloride (NH_2-L-His-OMe • 2HCl) (16g). White solid; 65 % yield; ^{1}H-NMR (DMSO-d_6, 27 °C, 400 MHz): δ [ppm] 3.30 (m, 2H, H_d), 3.70 (s, 3H, H_a), 4.45 (t, $^3J_{H,H}$=7.1 Hz, 1H, H_c), 7.50 (s, 1H, H_f), 9.05 (s, 1H, H_h).

^{13}C-NMR (DMSO-d_6, 27 °C, 100 MHz): δ [ppm] 24.6 (C_d), 53.6 (C_c), 56.2 (C_a), 119.6 (C_f), 125.8 (C_e), 135.0 (C_h), 169.7 (C_b).

D-Histidine methyl ester dihydrochloride (NH_2-D-His-OMe • 2HCl) (16i). White solid; 78 % yield; ^{1}H-NMR (DMSO-d_6, 27 °C, 400 MHz): δ [ppm] 3.32 (m, 2H, H_d), 3.70 (s, 3H, H_a), 4.45 (t, $^3J_{H,H}$=7.1 Hz, 1H, H_c), 7.50 (s, 1H, H_f), 9.05 (s, 1H, H_h).

^{13}C-NMR (DMSO-d_6, 27 °C, 100 MHz): δ [ppm] 25.5 (C_d), 51.5 (C_c), 53.5 (C_a), 118.5 (C_f), 127.1 (C_e), 134.4 (C_h), 168.9 (C_b).

L-Tryptophan methyl ester hydrochloride (NH_2-L-Trp-OMe • HCl) (16h). White pale solid; 69 % yield; ^{1}H-NMR (DMSO-d_6, 27 °C, 400 MHz): δ [ppm] 3.31 (m, 2H, H_d), 3.60 (s, 3H, H_a), 4.16 (t, $^3J_{H,H}$ = 6.0 Hz, 1H, H_c), 6.98 (t, $^3J_{H,H}$ = 7.4 Hz, 1H, H_h), 7.07 (t, $^3J_{H,H}$ = 8.0 Hz, 1H, H_i), 7.25 (s, 1H, H_l), 7.36 (dd, $^3J_{H,H}$ = 8.0 Hz, $^2J_{H,H}$ = 4.2 Hz, 1H, H_j), 7.50 (d, $^3J_{H,H}$ = 4.6 Hz, 1H, H_g), 8.79 (br, 3H, H_n), 11.21 (s, 1H, H_m).

^{13}C-NMR (DMSO-d_6, 27 °C, 100 MHz): δ [ppm] 26.5 (C_d), 53.0 (C_c), 53.2 (C_a), 106.8 (C_e), 112.0 (C_j), 118.5 – 119.0 (C_h + C_g), 121.5 (C_i), 125.4 (C_l), 127.4 (C_f), 136.7 (C_k), 170.1 (C_b).

D-Tryptophan methyl ester hydrochloride (NH_2-D-Trp-OMe • HCl) (16j). White pale solid; 69 % yield; ^{1}H-NMR (DMSO-d_6, 27 °C, 400 MHz): δ [ppm] 3.31 (m, 2H, H_d), 3.60 (s, 3H, H_a), 4.16 (t, $^3J_{H,H}$ = 6.0 Hz, 1H, H_c), 6.98 (t, $^3J_{H,H}$ = 7.4 Hz, 1H, H_h), 7.07 (t, $^3J_{H,H}$ = 7.5 Hz, 1H, H_i), 7.25 (s, 1H, H_l), 7.36 (d, $^3J_{H,H}$ = 12.1 Hz, 1H, H_j), 7.50 (d, $^3J_{H,H}$ = 4.6 Hz, 1H, H_g), 8.79 (br, 3H, H_n), 11.21 (s, 1H, H_m).

^{13}C-NMR (DMSO-d_6, 27 °C, 100 MHz): δ [ppm] 26.5 (C_d), 53.0 (C_c), 53.2 (C_a), 106.8 (C_e), 112.0 (C_j), 118.5 – 119.0 (C_h + C_g), 121.5 (C_i), 125.4 (C_l), 127.4 (C_f), 136.7 (C_k), 170.1 (C_b).

*4.5.3.2 Synthesis of polymers (**17a – 17j**) initiated by amino acid-methyl esters*

The corresponding **initiator** (**NH_2-AA-OMe · HCl**) (0.1 eq) was dissolved in oxygen-free, dry DMF (2 mol/L). Oxygen-free, dry NEt_3 (0.09 eq) was added and the solution was heated up to 80 °C. **Aib-NCA** (3 - 4 mmol; 1 eq) was added and the reaction mixture was stirred at 80 °C overnight. The solution was cooled down to room temperature and dialyzed against acetone. The final polymers were dried in high vacuum to get **OMe-AA-PAib** (**17a** – **17j**) (42 – 71 %).

Table 16. Synthesis and yields for polymers **17a** – **17j** by ROP of **Aib-NCA** (**11**) initiated by corresponding amino acid-methyl esters (**NH_2-AA-OMe · HCl**) **16a** – **16j.**

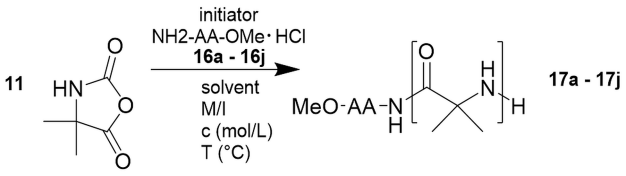

polymer	polymer structure	yield (%)	M_n NMR (Da)	M_n MALDI-TOF-MS (Da) (maximum intensity signal (Min/Max n)
OMe-Aib-PAib (**17a**)	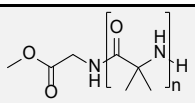 **17a**	63	1278 (n=14)	1176.380 (K^+) (n=12) n=9 - 17
OMe-Gly-PAib (**17b**)	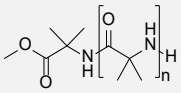 **17b**	62	1448 (n=16)	1233.395 (K^+) (n=13) n=10 - 18
OMe-L-Val-PAib (**17c**)	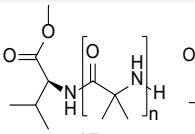 **17c**	54	1236 (n=13)	1275.252 (K^+) (n=13) n=10- 19
OMe-D-Val-PAib (**17d**)	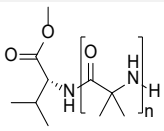 **17d**	60	1150 (n=12)	1275.213 (K^+) (n=13) n=10 - 17
OMe-L-Leu-PAib (**17e**)	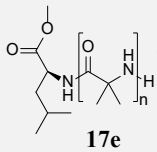 **17e**	71	1505 (n=16)	1289.156 (K^+) (n=13) n=10 - 19
OMe-D-Leu-PAib (**17f**)	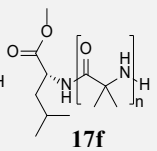 **17f**	62	1164 (n=12)	1289.178 (K^+) (n=13) n=10 - 19
OMe-L-His-PAib (**17g**)	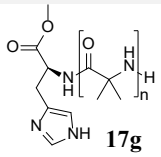 **17g**	36	1530 (n=16)	1228.356 (K^+) (n=12) n=10 - 20
OMe-D-His-PAib (**17h**)	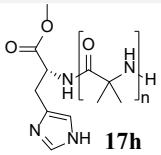 **17h**	44	1530 (n=16)	1228.339 (K^+) (n=12) n=10 - 18
OMe-L-Trp-PAib (**17i**)	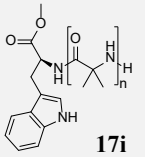 **17i**	42	--	1362.147 (K^+) (n=13) n=10 - 17
OMe-D-Trp-PAib (**17j**)	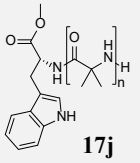 **17j**	51	--	1277.089 (K^+) (n=12) n=9 - 18

OMe-Aib-PAib (17a). White solid; 63% yield; ^{1}H-NMR (D_2SO_4 (96-98 wt. % in D_2O), 27 °C, 400 MHz): δ [ppm] 1.96 (m, $H_{rep.\ unit}$, H_l + H_d), 4.09 (s, 3H, H_a), 6.73 (br, 1H, H_e).

MALDI-TOF-MS (positive mode, dithranol, KTFA, *m/z*) $[M]^+$ found 1176.380, simulated for $C_5H_{10}NO_2(C_4H_7NO)_{12}HK^+$ 1176.675.

OMe-Gly-PAib (17b). White solid; 62 % yield; ^{1}H-NMR (D_2SO_4 (96-98 wt. % in D_2O), 27 °C, 400 MHz): δ [ppm] 1.96 (m, $H_{rep.\ unit}$, H_l), 4.11 (m, 3H, H_a), 4.68 (s, 3H, H_c), 6.73 (br, 1H, H_d).

MALDI-TOF-MS (positive mode, dithranol, KTFA, *m/z*) $[M]^+$ found 1233.395, simulated for $C_3H_6NO_2(C_4H_7NO)_{13}HK^+$ 1233.697.

OMe-L-Val-PAib (17c). White solid; 54 % yield; ^{1}H-NMR (D_2SO_4 (96-98 wt. % in D_2O), 27 °C, 400 MHz): δ [ppm] 0.77 (d, $^3J_{H,H}$ = 6.4 Hz, 6H, H_e), 1.57 (m, $H_{rep.\ unit}$, H_1), 2.17 (m, 1H, H_d), 3.70 (br, 3H, H_a), 4.50 (br, 1H, H_c), 6.33 (br, 1H, H_f).

MALDI-TOF-MS (positive mode, dithranol, KTFA, *m/z*) $[M]^+$ found 1275.250, simulated for $C_6H_{12}NO_2(C_4H_7NO)_{13}HK^+$ 1275.744.

OMe-D-Val-PAib (17d). White solid; 60 % yield; ^{1}H-NMR (D_2SO_4 (96-98 wt. % in D_2O), 27 °C, 400 MHz): δ [ppm] 0.76 (br, 6H, H_e), 1.57 (m, $H_{rep.\ unit}$, H_1), 2.16 (m, 1H, H_d), 3.70 (s, 3H, H_a), 4.50 (br, 1H, H_c), 6.36 (br, 1H, H_f).

MALDI-TOF-MS (positive mode, dithranol, KTFA, *m/z*) $[M]^+$ found 1275.213, simulated for $C_6H_{12}NO_2(C_4H_7NO)_{13}HK^+$ 1275.744.

OMe-L-Leu-PAib (17e). White solid; 71% yield; ^{1}H-NMR (D_2SO_4 (96-98 wt. % in D_2O), 27 °C, 400 MHz): δ [ppm] 1.04 - 1.11 (dd, $^3J_{H,H}$ = 21.7, 5.8 Hz, 6H, H_f), 1.96 (m, $H_{rep.\ unit}$, $H_1 + H_d + H_e$), 4.06 (s, 3H, H_a), 5.10 (br, 1H, H_c), 6.72 (br, 1H, H_g).

MALDI-TOF-MS (positive mode, dithranol, KTFA, *m/z*) $[M]^+$ found 1289.111, simulated for $C_7H_{14}NO_2(C_4H_7NO)_{13}HK^+$ 1289.759.

OMe-D-Leu-PAib (17f). White solid; 62% yield; ^{1}H-NMR (D_2SO_4 (96-98 wt. % in D_2O), 27 °C, 400 MHz): δ [ppm] 1.04 - 1.11 (dd, $^3J_{H,H}$ = 21.3, 6.5 Hz, 6H, H_f), 1.96 (m, $H_{rep.\ unit}$, $H_1 + H_d + H_e$), 4.07 (s, 3H, H_a), 5.09 (br, 1H, H_c), 6.73 (br, 1H, H_g).

MALDI-TOF-MS (positive mode, dithranol, KTFA, *m/z*) $[M]^+$ found 1228.356, simulated for $C_7H_{10}N_3O_2(C_4H_7NO)_{12}HK^+$ 1228.681.

OMe-L-His-PAib (17g). White solid; 36 % yield; ^{1}H-NMR (D_2SO_4 (96-98 wt. % in D_2O), 27 °C, 400 MHz): δ [ppm] 1.58 (m, $H_{rep.\ unit}$, H_1), 3.16 - 3.35 (br, 2H, H_d), 3.70 (br, 3H, H_a), 4.91 (br, 1H, H_c), 6.35 (br, 1H, H_i), 7.12 (br, 1H, H_f), 8.22 (br, 1H, H_g).

MALDI-TOF-MS (positive mode, dithranol, KTFA, *m/z*) $[M]^+$ found 1228.356, simulated for $C_7H_{10}N_3O_2(C_4H_7NO)_{12}HK^+$ 1228.681.

OMe-D-His-PAib (17h). White solid; 44 % yield; ^{1}H-NMR (D_2SO_4 (96-98 wt. % in D_2O), 27 °C, 400 MHz): δ [ppm] 1.57 (m, $H_{rep.\ unit}$, H_1), 3.17 – 3.36 (br, 2H, H_d), 3.69 (s, 3H, H_a), 4.90 (s, 1H, H_c), 6.34 (s, 1H, H_i), 7.11 (s, 1H, H_f), 8.22 (s, 1H, H_g).

MALDI-TOF-MS (positive mode, dithranol, KTFA, *m/z*) $[M]^+$ found 1228.355, simulated for $C_7H_{10}N_3O_2(C_4H_7NO)_{12}HK^+$ 1228.681.

OMe-L-Trp-PAib (17i). White pale solid; 42 % yield; ^{1}H-NMR (D_2SO_4 (96-98 wt. % in D_2O), 27 °C, 400 MHz): decomposition due to acidic conditions

MALDI-TOF-MS (positive mode, dithranol, KTFA, *m/z*) $[M]^+$ found 1362.147, simulated for $C_{12}H_{13}N_2O_2(C_4H_7NO)_{13}HK^+$ 1362.755.

OMe-D-Trp-PAib (17j). White pale solid; 51 % yield; ^{1}H-NMR (D_2SO_4 (96-98 wt. % in D_2O), 27 °C, 400 MHz): decomposition due to acidic conditions

MALDI-TOF-MS (positive mode, dithranol, KTFA, *m/z*) $[M]^+$ found 1277.060, simulated for $C_{12}H_{13}N_2O_2(C_4H_7NO)_{12}HK^+$ 1277.702.

4.5.4 Synthesis of artificial oligo-amino acids initiated by azo-initiators

*4.5.4.1 Synthesis of azo-initiator **Azo-OH-DFA (19)** and **Azo-NH$_2$-DFA (20)***

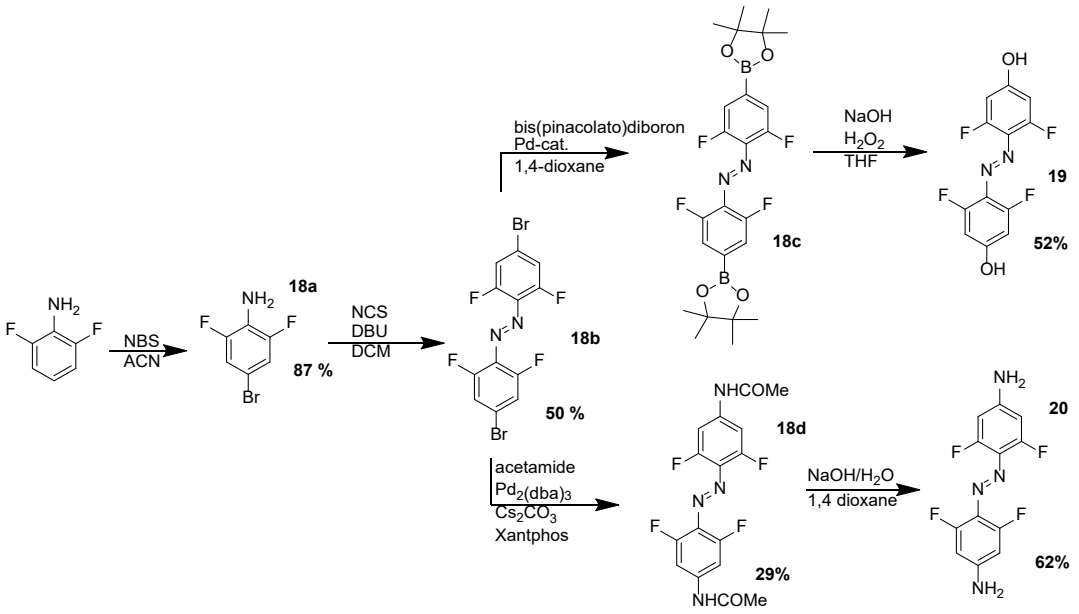

Scheme 15. Synthesis of azo-initiators **19** and **20**.

*Synthesis of **Br-DFA (18a)***

Synthesis was done according to literature.[269] 2,6-Difluoroaniline (25.01 g; 0.19 mol; 1 eq) was dissolved in acetonitrile (400 mL) and stirred for 10 minutes at room temperature. NBS (35.15 g; 0.20 mol; 1.02 eq) was added to the solution and the reaction mixture was allowed to stir overnight at room temperature. The obtained red solution was concentrated in vacuum and *n*-hexane (350 mL) was added. The mixture was extracted with distilled water (2 x 250 mL) and dried over Na_2SO_4. After filtration *n*-hexane was removed in vacuum and the crude product was purified by column chromatography (DCM / *n*-hexane: 1 / 4, R_f = 0.) to give **Br-DFA** (**18a**) as a pale white solid with a yield of 35.11 g (87 %).

^{1}H-NMR ($CDCl_3$, 27 °C, 400 MHz): δ [ppm] 3.73 (s, 2H, H_b), 6.99 (dd, $^3J_{H,H}$=6.3 Hz, $^4J_{H,H}$=1.5 Hz, 2H, H_a).

^{19}F-NMR ($CDCl_3$, 27 °C, 376 MHz): δ [ppm] -130.7 (s, 2F, F_{Ar}).

*Synthesis of **Azo-Br-DFA (18b)***

Synthesis was done according to literature.[269] **Br-DFA** (**18a**, 2.34 g; 11.23 mmol; 1 eq) and DBU (3.42 g; 22.47 mmol; 2 eq) were dissolved in dry, oxygen-free DCM (40 mL) and cooled down to -78 °C. NCS (3.00 g; 22.47 mmol; 2 eq) was added to the mixture and the obtained red solution was stirred for 30 minutes at -78 °C. The reaction was quenched with aqueous saturated Na_2CO_3-solution (20 mL) and the organic phase was washed with distilled water (100 mL) and 1M HCl (100 mL). The solution was dried over Na_2SO_4, filtered and concentrated in vacuum. The obtained crude product was treated with TFA (20 mL) and stirred 30 minutes at room temperature to obtain a maximum amount of *trans*-configuration. TFA was removed in vacuum and the crude product was purified by column chromatography (DCM / *n*-hexane : 1 / 10, R_f = 0.) to give **Azo-Br-DFA** (**18b**) as red crystals (1.17 g; 50 %).

^{1}H-NMR (DMSO-d_6, 27 °C, 400 MHz): δ [ppm] 7.67 (d, $^{4}J_{H,H}$=7.5 Hz, 4H, $H_{a,\ cis}$), 7.76 (d, $^{4}J_{H,H}$=9.2 Hz, 4H, $H_{a,\ trans}$).

^{19}F-NMR ($CDCl_3$, 27 °C, 376 MHz): δ [ppm] -119.4 (d, J=9.3 Hz, $F_{Ar,\ trans}$), -119.1 (d, J=7.0 Hz, $F_{Ar,\ cis}$).

*Synthesis of **Azo-Bor-DFA (18c)***

Synthesis was done according to literature.[313] A Schlenck tube was securated and transferred into glovebox. **Azo-Br-DFA** (**18b**, 519.9 mg; 1.26 mmol; 1 eq), KOAc (737.2 mg; 7.51 mmol; 6 eq), bis(pinacolato)diboron (961.4 mg; 3.79 mmol; 3 eq) and $Pd(dppf)Cl_2 \cdot CH_2Cl_2$ (103.8 mg; 0.126 mmol; 0.1 eq) were weighed in and dry, oxygen-free dioxane (15 mL) was added. The solution was heated up to 75 °C and stirred overnight. The reaction mixture was concentrated in vacuum and DCM (20 mL) and water (20 mL) were added. The two phases were separated and the organic phase was washed with water (3x20 mL). The organic phase was dried over Na_2SO_4, filtered and the solvent was removed in vacuum. The crude product was purified by flash column chromatography (EA, R_f = 0.95) and was directly used in the next step.

*Synthesis of **Azo-OH-DFA (19)***

Synthesis was done according to literature.[313] **Azo-Bor-DFA** (**18c**, 5.20 g; 10.27 mmol; 1 eq) was dissolved in THF (150 mL) and 2M NaOH (24 mL) and aqueous H_2O_2-solution (50-60 %; 2.3 mL) was added to the solution. The reaction mixture was stirred for 1.5 h at room temperature. The reaction mixture was concentrated in vacuum and was neutralized by 1M HCl and EtOAc (200 mL) was added. The phases were separated and the organic layer was washed with distilled water (3x 100 mL). The organic phase was dried over Na_2SO_4, filtered and the solvent was removed in vacuum. The crude material was purified by column chromatography (EtOAc / *n*-hexane : 1 / 1, R_f = 0.57) to yield **Azo-OH-DFA** (**19**) as red powder (2.07 g; 52 % over two steps).

^{1}H-NMR (DMSO-d_6, 27 °C, 400 MHz): δ [ppm] 6.63 (d, $^{3}J_{H,H}$ = 11.4 Hz, 4H, H_a), 11.11 (br, 2H, H_b).

^{19}F-NMR ($CDCl_3$, 27 °C, 376 MHz): δ [ppm] -119.4 (s, 2F, F_{Ar}).

ESI-TOF-MS (negative mode, without additional salt, *m/z*) $[M]^-$ found 285.028, simulated for $C_{12}H_7N_2O_2F_4^-$ 285.028.

*Synthesis of **Azo-NHCOME-DFA (18d)***

Synthesis was done according to literature.[269] **Azo-Br-DFA** (**18a**, 1.29 g; 3.13 mmol; 1 eq), acetamide (1.17 g; 19.81 mmol; 6.3 eq), Cs_2CO_3 (3.69 g; 11.33 mmol; 3.8 eq), Pd_2dba_3 (0.17 g; 0.19 mmol; 0.06 eq) and Xantphos (0.39 g; 0.67 mmol; 0.22 eq), were weighed in a Schlenck tube and oxygen free, dry dioxane (10mL) was added. The reaction mixture was heated up to 90 °C and stirred for 5 hours. The solution was cooled down to room temperature and concentrated in vacuum. EtOAc (30 mL) was added and the organic phase was extracted with distilled water (30 mL). The phases were separated and the aqueous phase was extracted with EtOAC (3x30 mL). The organic phases were combined, filtrated and the solvent was removed in vacuum. The crude material was purified by coloum chromatographie (EtOAc / *n*-hexane : 3 / 1, R_f = 0.38) to yield **Azo-NHCOME-DFA** (**18d**) as red powder (0.36 g; 29 %).

^{1}H-NMR (DMSO-d_6, 27 °C, 400 MHz): δ [ppm] 2.03 (s, 6H, $H_{b,\ cis}$), 2.10 (s, 6H, $H_{b,\ trans}$), 7.32 (d, $^{3}J_{H,H}$ = 10.8 Hz, 4H, $H_{a,\ cis}$), 7.48 (d, $^{3}J_{H,H}$ = 11.9 Hz, 4H, $H_{a,\ trans}$), 10.43 (s, 2H, $H_{c,\ cis}$), 10.59 (s, 2H, $H_{c,\ trans}$).

^{19}F-NMR (DMSO-d_6, 27 °C, 376 MHz): δ [ppm] -119.3 (s, 2F, F_{Ar}).

*Synthesis of **Azo-NH$_2$-DFA (20)***

Azo-NHCOME-DFA (**18d**, 0.36 g; 0.91 mmol; 1 eq) was dissolved in dioxane (50 mL) and 30 wt. % aqueous NaOH (20 mL) was added to the solution. The reaction mixture was refluxed for 1h followed by stirring overnight at 80 °C. The solution was neutralized with conc. HCl and the precipitate was filtered off. The filtrate was extracted with EtOAc (3x 50 mL) and the organic phases were combined. The precipitate was dissolved in EtOAc (100 mL) and the organic layers were combined. The organic phase was dried over Na_2SO_4, filtered and the solvent was removed in vacuum. The crude material was purified by coloum chromatographie (EtOAc / *n*-hexane : 2 / 1, R_f = 0.67) to yield **Azo-NH$_2$-DFA** (**20**) as orange powder (0.20 g; 77 %).

^{1}H-NMR (DMSO-d$_6$, 27 °C, 400 MHz): δ [ppm] 6.27 (d, $^3J_{H,H}$ = 12.3 Hz, 4H, H$_a$), 6.39 (br, 2H, H$_b$).

^{19}F-NMR (DMSO-d$_6$, 27 °C, 376 MHz): δ [ppm] -120.3 (s, 2F, F_{Ar}).

ESI-TOF-MS (negative mode, without additional salt, *m/z*) $[M]^-$ found 283.252, simulated for $C_{12}H_7N_4F_4^-$ 283.060.

*4.5.4.2 Synthesis of azo-initiator **Azo-Dop-OH (21)***

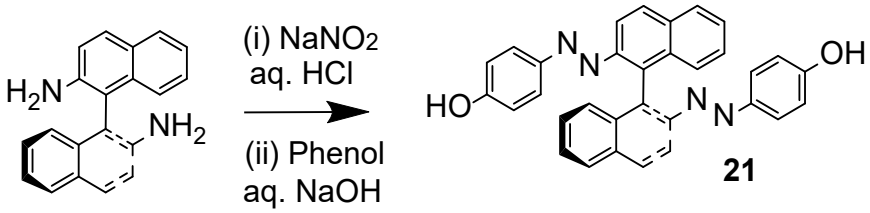

Scheme 16. Synthesis of azo-initiator **21**.

Synthesis was done according to literature.[311] (S)-(-)-1,1'-Binaphthyl-2,2'-diamine (1.02 g; 3.59 mmol; 1 eq) was dissolved in a solution of water (17mL) and concentrated HCl (2.5 mL) and the reaction mixture was cooled down to -5 °C. Sodium nitrite (0.58 g; 8.45 mmol; 2.35 eq) dissolved in water (10 mL) was cooled down to -5 °C and was added dropwise to the reaction mixture. The resulting mixture was added dropwise to a solution of phenol (0.77 g; 8.21 mmol; 2.29 eq) and NaOH (0.93g; 23.25 mmol) in water (15 mL) at -5 °C. After the solution turned from yellow over red and orange to brown 1M HCl (18 mL) was added and the suspension was extracted with DCM (100 mL). The organic layer was separated and washed with 1M HCl (50 mL) and water (50 mL), dried over Na_2SO_4 and filtered. The solvent was removed in vacuum and the crude product was purified by column chromatography ($CHCl_3$ / MeOH : 10 / 1, R_f = 0.53) to yield **Azo-Dop-OH** (**21**) as orange crystals (0.89 g; 51 %).

^{1}H-NMR ($CDCl_3$, 27 °C, 400 MHz): δ [ppm] 5.26 (br, 2H, H$_i$), 6.58 (m, 4H, H$_h$), 7.21 (m, 4H, H$_g$), 7.28 (m, 2H, H$_d$), 7.44 (d, $^3J_{H,H}$ = 8.2 Hz, 2H, H$_e$), 7.48 (ddd, $^3J_{H,H}$ = 8.1 Hz, $^3J_{H,H}$ = 6.8 Hz, $^2J_{H,H}$ = 1.2 Hz, 2H, H$_c$), 7.97 (d, $^3J_{H,H}$ = 8.1 Hz, 2H, H$_f$), 8.04 (d, $^3J_{H,H}$ = 8.9 Hz, 2H, H$_a$ + H$_b$), 8.11 (d, $^3J_{H,H}$ = 8.9 Hz, 2H, H$_a$ + H$_b$).

ESI-TOF-MS (negative mode, without additional salt, *m/z*) $[M]^-$ found 493.177, simulated for $C_{32}H_{21}N_4O_2^-$ 493.166.

*4.5.4.3 Synthesis of polymers (**19a, 19b, 20a, 20b, 21a, 21b**) initiated by azo-initiators*

*Synthesis of **Azo-OHPAib-DFA (19a)** and **Azo-OHPACHC-DFA (19b)***

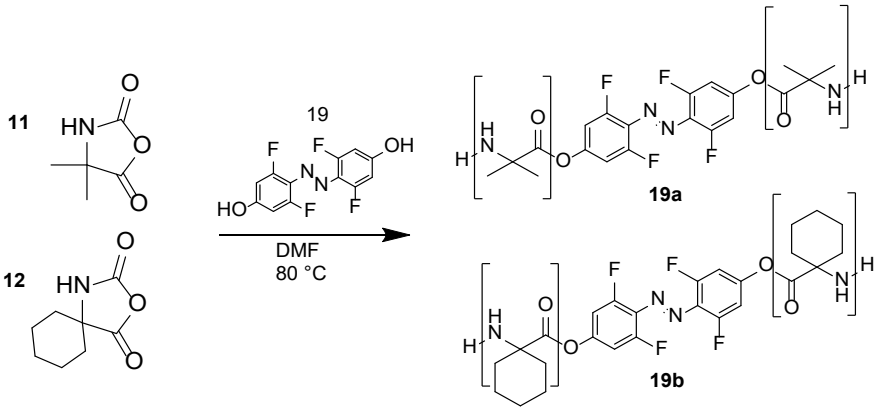

Scheme 17. Synthesis of polymers **19a** and **19b** by ROP of **11** or **12** initiated by azo-initiator **19**.

Azo-OH-DFA (**19**, 10.0 mg; 0.04 mmol; 0.05 eq) was dissolved in oxygen-free, dry DMF (2 mol/L). The solution was heated up to 80 °C and **Aib-NCA** (**11**, 93.6 mg; 0.72 mmol; 1 eq) or **ACHC-NCA** (**12**, 123.5 mg; 0.73 mmol; 1 eq) was added and the reaction mixture was stirred at 80 °C overnight. The solution was cooled down to room temperature and dialyzed against acetone to get **Azo-OHPAib-DFA** (**19a**) or **Azo-OHPACHC-DFA** (**19b**) (41-49 %).

Azo-OHPAib-DFA (**19a**) ^{1}H-NMR (HFIP-d_2, 27 °C, 400 MHz): δ [ppm] 1.70 (m, $H_{rep.\ unit}$, H_1), 7.61 (br, $H_{rep.\ unit}$, H_3).

Azo-OHPACHC-DFA (**19b**) ^{1}H-NMR (HFIP-d_2, 27 °C, 400 MHz): δ [ppm] 1.55 – 1.75 (m, $H_{rep.\ unit}$, $H_3 + H_5$), 1.90 – 1.96 (m, $H_{rep.\ unit}$, H_4), 2.16 – 2.47 (m, $H_{rep.\ unit}$, $H_2 + H_6$), 7.54 (br, $H_{rep.\ unit}$, H_3).

*Synthesis of **Azo-NH$_2$PAib-DFA (20a)** and **Azo-NH$_2$PACHC-DFA (20b)***

Azo-NH$_2$-DFA (**20**, 10.6 mg; 0.04 mmol; 0.05 eq) was dissolved in oxygen-free, dry DMF (2 mol/L). The solution was heated up to 80 °C and **Aib-NCA** (**11**, 90.3 mg; 0.70 mmol; 1 eq) or **ACHC-NCA** (**12**, 126.3 mg; 0.75 mmol; 1 eq) was added and the reaction mixture was stirred at 80 °C overnight. The solution was cooled down to room temperature and dialyzed against acetone to get **Azo-NH$_2$PAib-DFA** (**20a**) or **Azo-NH$_2$PACHC-DFA** (**20b**) (45-48 %).

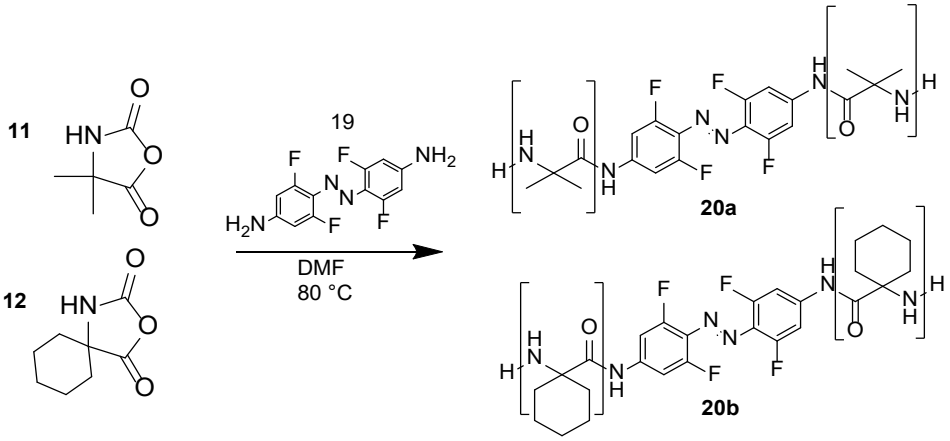

Scheme 18. Synthesis of polymers **20a** and **20b** by ROP of **11** or **12** initiated by azo-initiator **20**.

Azo-NH$_2$PAib-DFA (**20a**) ^{1}H-NMR (HFIP-d$_2$, 27 °C, 400 MHz): δ [ppm] 1.73 (m, H$_{rep.\ unit}$, H$_1$), 7.64 (br, H$_{rep.\ unit}$, H$_3$).

Azo-NH$_2$PACHC-DFA (**20b**) ^{1}H-NMR (HFIP-d$_2$, 27 °C, 400 MHz): δ [ppm] 1.51 – 1.73 (m, H$_{rep.\ unit}$, H$_3$ + H$_4$ + H$_5$), 1.87 (m, H$_{rep.\ unit}$, H$_4$), 2.06– 2.47 (m, H$_{rep.\ unit}$, H$_2$ + H$_6$), 7.54 (br, H$_{rep.\ unit}$, H$_3$).

*Synthesis of **Azo-DOP-PAib (21a)** and **Azo-Dop-PACHC (21b)***

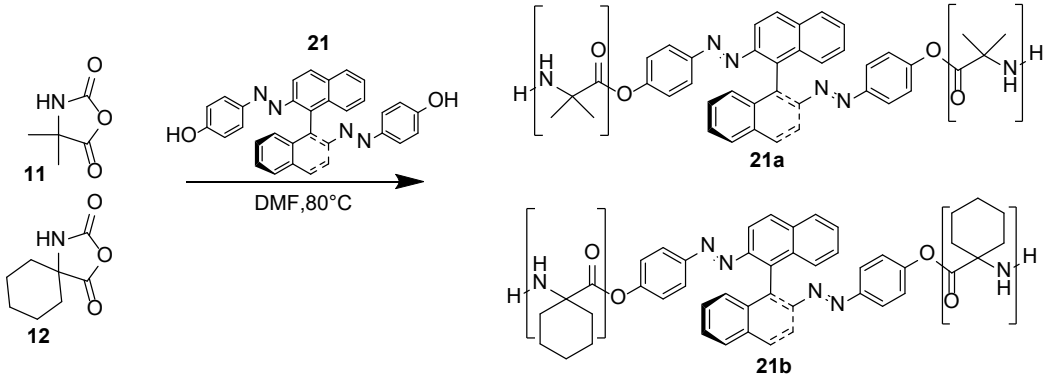

Scheme 19. Synthesis of polymers **21a** and **21b** by ROP of **11** or **12** initiated by azo-initiator **21**.

Synthesis of Azo-Dop-PAib (21a)

Azo-Dop-OH (**21**, 44.82 mg; 0.09 mmol; 0.5 eq) was dissolved in oxygen-free, dry DMF (0.73 mL; 2 mol/L). The orange solution was heated up to 80 °C and **Aib-NCA** (**11**) (187.25 mg; 1.45 mol; 8 eq) was added. The reaction mixture was stirred at 80 °C overnight, cooled down to room temperature and dialyzed against acetone to get **Azo-Dop-PAib** (**21a**) (44 %).

^{1}H-NMR (HFIP-d$_2$, 27 °C, 400 MHz): δ [ppm] 1.73 – 2.02 (m, H$_{rep.\ unit}$, H$_1$), 6.63 (br, 4H, H$_h$), 7.06 (br, 4H, H$_g$), 7.51 (br, 2H, H$_d$), 7.60 (br, 2H, H$_e$), 7.97 (br, 2H, H), 8.28 (br, 2H, H$_f$), 8.52 (br, 4H, H$_a$+H$_b$).

Synthesis of Azo-Dop-PACHC (21b)

Azo-Dop-OH (**21**, 37.50 mg; 0.08 mmol; 0.5 eq) was dissolved in oxygen-free, dry DMF (0.61 mL; 2 mol/L). The orange solution was heated up to 80 °C and **ACHC-NCA** (**12**, 206.1 mg; 1.22 mmol; 8 eq) was added. The reaction mixture was stirred at 80 °C overnight, cooled down to room temperature and dialyzed against acetone to get **Azo-Dop-PACHC** (**21b**) (37 %).

^{1}H-NMR (HFIP-d$_2$, 27 °C, 400 MHz): δ [ppm] 1.61 – 2.37 (m, H$_{rep.\ unit}$, H$_2$ + H$_3$ + H$_4$ + H$_5$ + H$_6$), 6.63 (br, 4H, H$_h$), 7.06 (br, 4H, H$_g$), 7.51 (br, 2H, H$_d$), 7.60 (br, 2H, H$_e$), 7.97 (br, 2H, H), 8.28 (br, 2H, H$_f$), 8.52 (br, 4H, H$_a$+H$_b$).

5 Summary

In this work a strategy for synthesizing and characterization of newly developed hybrid polyalkyl-polymers with single/oligo-amino acids at every 19th CH_2 carbon atom was reported. The polymers were investigated in solid state and solution in their crystallization behavior of the PE-type alkyl chain middle segments as well as the secondary structure formation of the oligo-amino acid building blocks.

To ensure and investigate the crystallization of the middle-segmented PE-type chains, model complexes consisting of single-amino acids (chiral/achiral, polar/non-polar) embedded into PE-type alkyl chains were designed. The single-amino acids were embedded as "defects" into a highly defined PE-type alkyl chain and the crystallization behavior of these hybrid polymers were investigated in dependence of the "defect"-nature.

Therefore, chiral/achiral as well as polar/nonpolar single-amino acids were functionalized on the *N*- and *C*-terminus with alkyl branches, bearing terminal double bonds at each end. The synthesis of the highly defined polymers with molecular weights up to 22 kDa was realized by ADMET polymerization under melt-polymerization conditions, followed by complete hydrogenation of the internal double bonds with *p*-toulenesulfonhydrazide ($TsNHNH_2$) (Scheme 20, top). For ADMET polymerization Grubbs 1st, Grubbs 2nd and Grubbs Hoveyda 1st catalyst were tested, the former was found to be the best catalyst in handling and in synthesizing low isomerized, high molecular weight polymers in good yields, proving the structures of the obtained products by GPC, MALDI-TOF-MS, ^{1}H-NMR- and IR-spectroscopy.

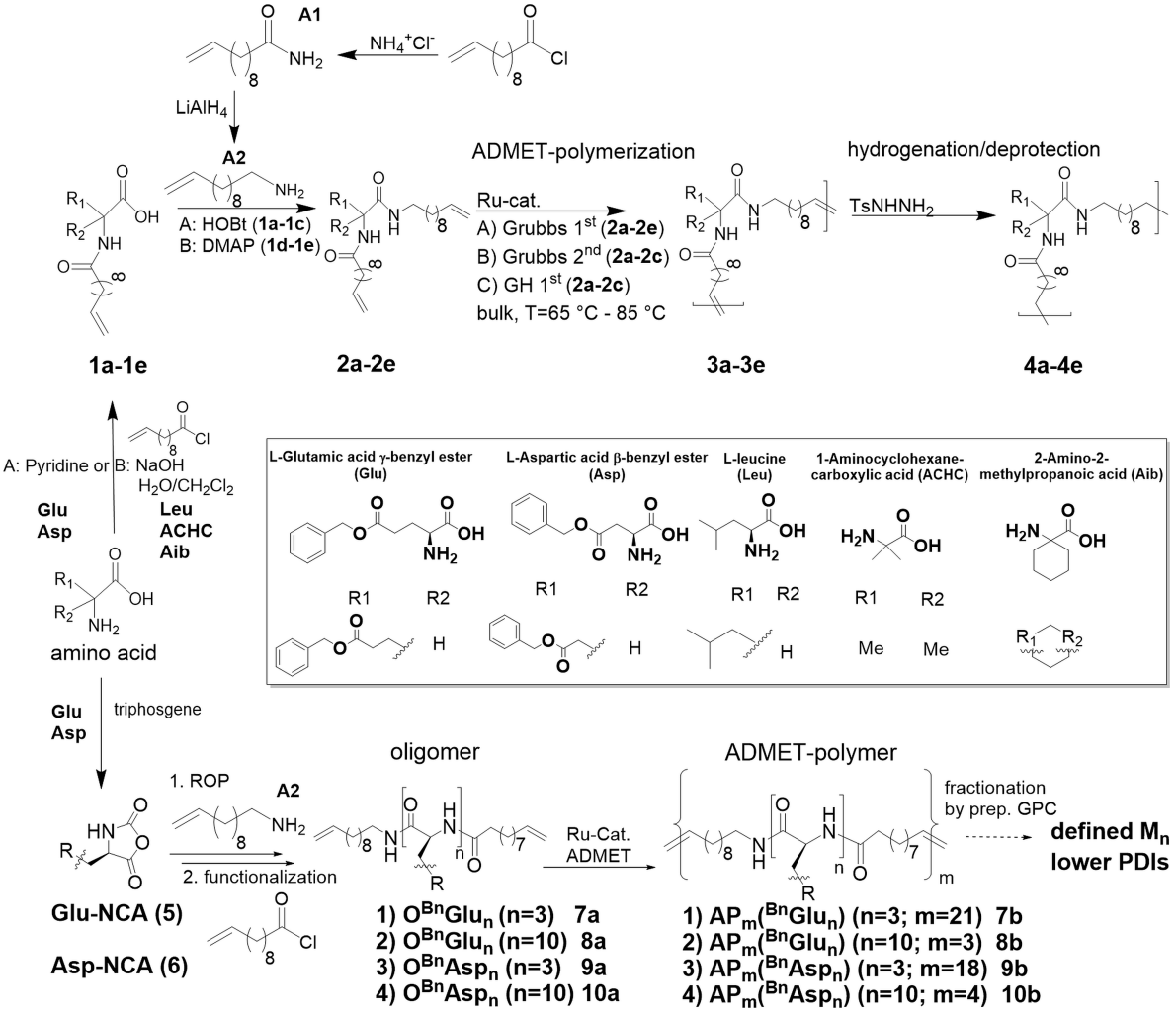

Scheme 20. Synthetic route for the synthesis of hybrid polymers **4a** – **4e** (top) and **7b** – **10b** (bottom).

Thermal investigation of the monomers and polymers demonstrated that all compounds having a non-polar amino acid (L-leucine, 2-aminoisobutyric acid, 1-aminocyclohexanecarboxylic acid) in the chain are amorphous, whereas the monomers and the hydrogenated polymers of polar amino acids (glutamic and aspartic acid) show crystalline morphologies (Figure 46, left). Melting points for glutamic acid modified monomers and polymers are lower in comparison to aspartic acid, demonstrating that the bigger the size of the defect the lower the ability to pack into the crystal. The hydrogenated polymer bearing aspartic acid moieties (**4b**) shows a complex thermal behavior, which is represented by melting-recrystallization and two crystallization points. WAXD-measurements show four reflections for both **4a** and **4b**, indicating a distance between the two amino acid groups of 2.86 nm for **4a** and 2.45 nm for **4b** along the PE-chain, together with the formation of a lamellar structure. An orthorhombic crystal in which amino acids can either be excluded from or included into the PE crystals is assumed.

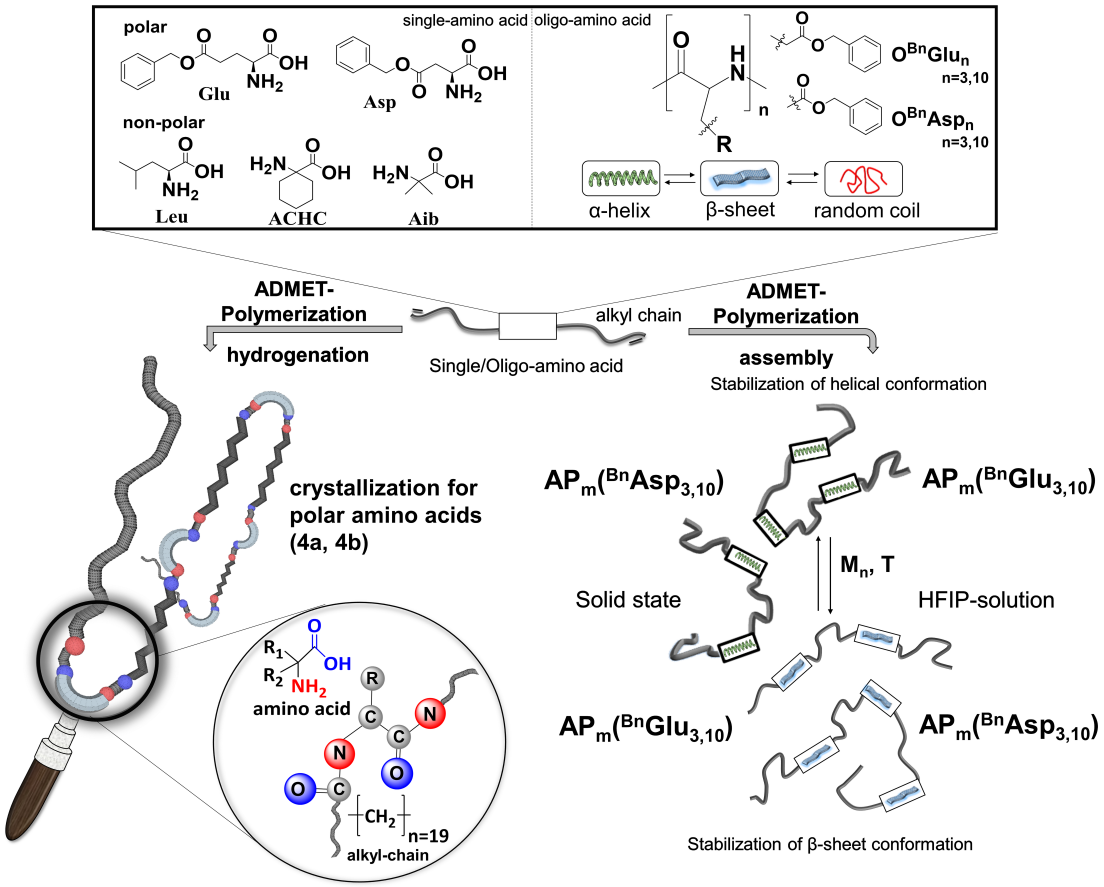

Figure 46. Summarized results for the investigation of PE-single-amino acid-hybrids (left) with observed crystallization for embedded single Glu- (**4a**) and Asp- (**4b**) segments and PE-oligo-amino acid-hybrids with stabilization of helical conformation for $AP_m(^{Bn}Asp_{3,10})$ in solid state and $AP_m(^{Bn}Glu_{3,10})$ in HFIP-solution as well as stabilization of β-sheet conformation for $AP_m(^{Bn}Asp_{3,10})$ in HFIP-solution and $AP_m(^{Bn}Glu_{3,10})$ in solid state (right).

Furthermore, oligo-amino acids embedded into PE-type polymers were designed to investigate the secondary structure formation of the amino acid building blocks. The oligo-amino acids act as dynamic folding elements, introducing conformational changes within these multisegmented polymers in dependence of their nature, chain length, and temperature in either HFIP-solution or the solid state.

For this purpose, conformational changes of secondary structures of oligomers (**$O^{Bn}Asp_{3,\ 10}$** and **$O^{Bn}Glu_{3,\ 10}$**), embedded into multisegmented copolymers **$AP_m(^{Bn}Glu_{3,\ 10})$** and **$AP_m(^{Bn}Asp_{3,10})$,** with the

oligomers present in multiple (m=2-136) copies along the polymer chain were studied. Thus, oligo-amino acids (**O^{Bn}Asp$_{3,\ 10}$** and **O^{Bn}Glu$_{3,\ 10}$**) were prepared by ring-opening polymerization of the corresponding *N*-carboxyanhydrides, followed by ADMET-polymerization to yield the multi-segmented polymers **AP$_{21}$(^{Bn}Glu$_3$)**, **AP$_3$(^{Bn}Glu$_{10}$)**, **AP$_{18}$(^{Bn}Asp$_3$)** and **AP$_4$(^{Bn}Asp$_{10}$)** (Scheme 20, bottom).

Fractionation by preparative GPC yielded narrow molecular weight fractions (polydispersities down to 1.05) that could be analyzed by CD and IR-spectroscopy to get insight into their secondary structure in both, HFIP-solution and the solid state. Significant conformational changes were observed comparing oligomers and the respective ADMET-polymers: in the solid state **AP$_m$(^{Bn}Glu$_3$)** and **AP$_m$(^{Bn}Glu$_{10}$)** FTIR-measurements indicated a stabilization of the β–sheet conformation with increasing chain length (m) of the polymer, presumably due to enhanced intermolecular interactions between amino acid building blocks of the same polymer chain, which are preferred in glutamic acid in contrast to the respective aspartic acid samples. With increasing temperature, the β-sheet structure is preferred, assuming to be the thermodynamically favored conformation (Figure 46, right).

Solution experiments reveal a different behavior: for **O^{Bn}Asp$_{10}$** a conformational change from a α_l-helix to a β–sheet took place in HFIP-solution after ADMET polymerization to **AP$_4$(^{Bn}Asp$_{10}$)**, whereas for **O^{Bn}Glu$_{10}$** and the corresponding ADMET-polymer **AP$_3$(^{Bn}Glu$_{10}$)** a stabilization of the helical conformation in HFIP-solution was observed as detected by CD spectroscopy. After preparative GPC, FTIR and CD spectroscopic measurements revealed a clear stabilization of the β-sheet structure in HFIP-solution with increasing chain length for the **AP$_{5–136}$(^{Bn}Asp$_3$)** (**F11** – **F3**) (5.2 – 153.4 kDa) fractions (Figure 46, right). The investigations clearly showed that different chemical and environmental aspects influence the secondary structures of the synthesized polymers, most of all the number of oligo amino-acid sequences within a multisegmented polymer in solution, whereas differences are blurred out in the solid state, especially at higher temperatures, finally preferring the formation of β-sheets in the solid state. The here reported observations for the first time systematically investigate conformational changes of multisegmented polymers containing dynamically foldable oligo-amino acids, leading to a deeper understanding of such conformational changes in solution and the solid state.

As conformational constrained-amino acids offer a variety of individual properties in the class of biomaterials, oligo-Aib and oligo-ACHC oligomers were designed and systematically investigated in their final conformation. The main focus was the investigation of the ROP of the corresponding NCAs with different initiator systems and the characterization of their final chain length and end-groups.

The ROP of **Aib-NCA** (**11**) were investigated by the usage of different initiation systems. First, ROP of **Aib-NCA** (**11**) initiated by amine initiator HMDS, **A2** and **A4** was investigated under different conditions by varying the temperature, solvent, concentration and *M*/*I* ratio (Scheme 21, top).
Polymerization could be achieved in both, solution and frozen solvents. Best results in regard to molecular weights were obtained in frozen DMA, as the molecular weight could be determined to 1622 g mol^{-1} (n=16) with a maximum peak at n=33. The kinetic for the polymerization in DMF at 80 °C by initiation of **A2** was investigated by FTIR-measurements, revealing a constant decrease in intensity of the NCA-vibration band in FTIR and an increasing molecular weight in MALDI-TOF-MS for the first 120 minutes. Comparison of ln M_0/M_t *vs.* time for the measured time periods revealed a living character of the polymerization for the first 120 minutes. After precipitation of oligomeric Aib-units after 120 minutes, the reaction still revealing a linear slope of ln M_0/M_t *vs.* time but a slower reaction rate together with a slower decreasing rate of the NCA-vibration band intensity in FTIR and a stagnating increasing molecular weight in MALDI-TOF-MS. After 600 minutes, the polymerization was finished as the NCA-vibration band disappeared, demonstrating complete consumption of the NCA-monomer.

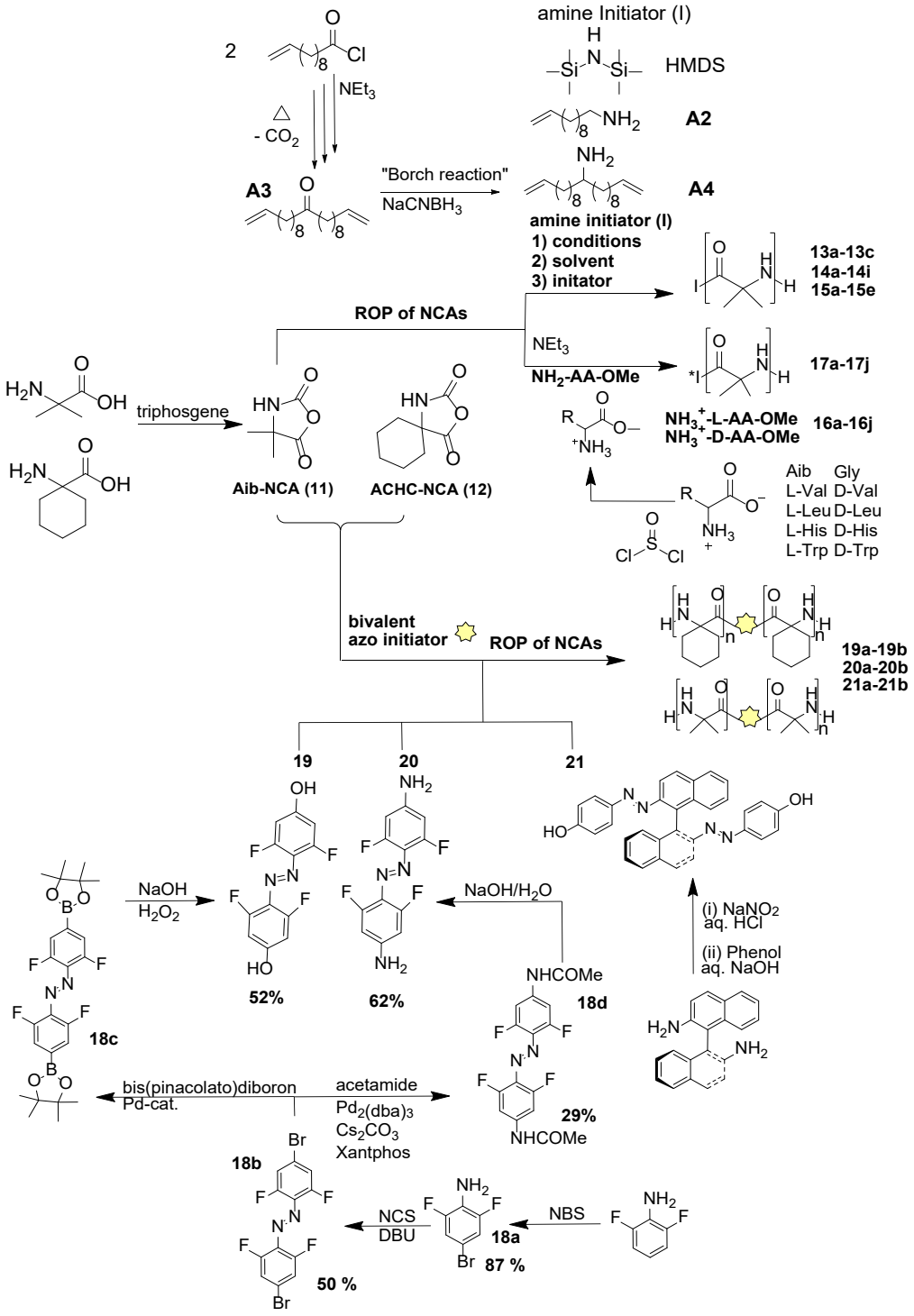

Scheme 21. Synthetic route for the investigation of the ROP of **Aib-NCAs** (**11**) and **ACHC-NCA** (**12**).

As oligomers of conformational constrained amino acid Aib stabilizing a racemic mixture of left- and right-handed 3_{10}-helical conformation, the attachment of chiral residues on the achiral Aib-domain can result in a preference for a left- or right-handed screw sense direction, which mainly depends on the nature, the position and the protecting group of the attached residue.

Therefore, the (a-)chiral amino acid-methyl esters **16a – 16j** were used for polymerization of **Aib-NCA** (**11**) **17a – 17j** (Scheme 21, middle). In all cases, the desired structures could be proven by ^{1}H-NMR and MALDI-TOF-MS measurements. Solid state FTIR- and CD-measurements in HFIP-solution were conducted, revealing no detectable preference for right- or left helical screw sense in solid state. In

contrast, CD-measurements in HFIP-solution revealed a left-handed screw sense preference in helical Aib-domain for L-amino acid-methyl ester-initiators (**17c**, **17e**, **17g**, **17i**) and a right-handed helical screw sense preference for D-amino acid-methyl ester (**17d**, **17f**, **17h**, **17j**) (Figure 47, left).

Based on literature considerations, very high strains, incooperated in an azo-compound itself, can lead to a thermal stable *cis*-isomer due to steric hindrance, becoming even more stable than the distorted *trans*-conformation.
Therefore, bivalent azo-initiators **19**, **20** and **21** were synthesized and used for the ROP of **Aib-NCA** (**11**) and **ACHC-NCA** (**12**) (Scheme 21, bottom). For polymers **19a, 19b** and **20a, 20b** polymerization occurred detectable *via* ^{1}H-NMR, the attachment of the initiator **19** and **20** on the polymer repeating unit was proven by UV-VIS-measurements. Ring opening polymerization of **Aib-NCA** (**11**) and **ACHC-NCA** (**12**) could successfully initiated with azo-initiator **21** and the desired structure for polymers **21a** and **21b** was proven *via* ^{1}H-NMR and UV-VIS-measurements.
Finally, polymer **21a** and **21b** were further investigated by UV-VIS-spectroscopy, revealing a decrease in intensity for the n-π*–transition signal and an increasing absorbance signal for the π–π*–transition after irradiation with light at 254 nm. After irradiation the samples were stored in darkness and both signals relaxing back partially in their original states before irradiation. The c*is*-isomer of the attached azo-initiator is therefore thermally stabilized in **21a** and **21b** (Figure 47, right).

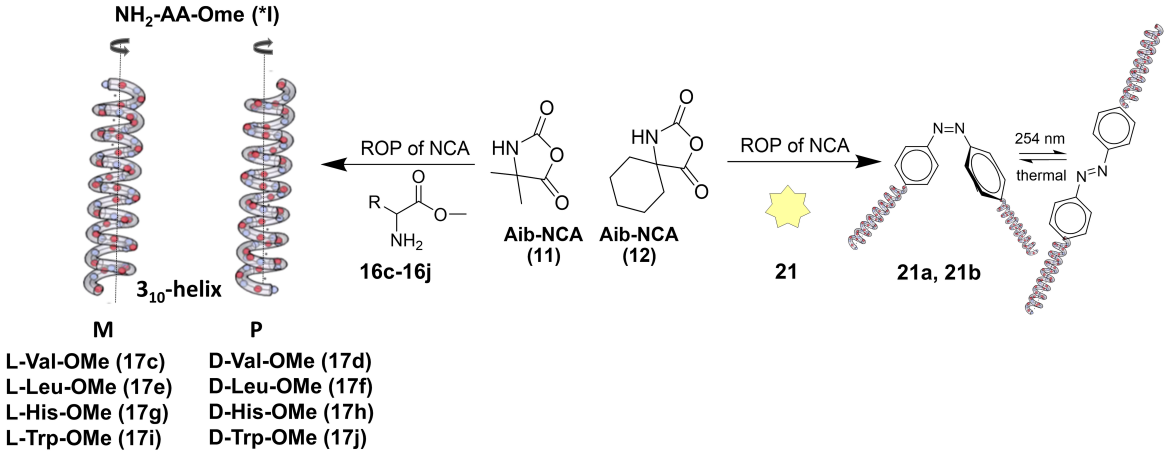

Figure 47. Results for the introduction of a left-handed helix preference for L-amino acid-methyl ester and right-handed helical screw sense preference for D-amino acid esters in Aib-domains after initiation of ROP of **Aib-NCA** (**11**) (left) and thermal stabilization of *cis*-isomer in azo- chromophores attached on Aib- and ACHC-domains after ROP of **Aib-NCA** (**11**) and **ACHC-NCA** (**12**) with azo-initiator **21**.

The present work extends the insights into the secondary structure formation of $O^{Bn}Glu_n$ and $O^{Bn}Asp_n$ as the reported observations for the first time systematically investigate conformational changes of multisegmented polymers containing dynamically foldable oligo-amino acids, leading to a deeper understanding of such conformational changes in solution and in the solid state. The incooperation into different types of non-polypeptide middle segments and the resulting changes in secondary structure formation of these two oligomers may have new insights into their dynamic folding behavior.

Furthermore, the here developed synthetic approach not only widens the scope of Aib-polymer science, but also allows for a larger scale preparation of a large library of Aib-polymers in the future for investigations of this interesting novel poly(amino)-acid. The attachement of chiral amine initiators as well as dynamic chirality switcher and the investigation of the resulting preference for a certain screw sense direction would be of great interest and a great topic for the future.

6 References

1. Gomes, C. M.; Faísca, P. F., *Protein folding: An introduction*. Springer: **2019**; p 1-63.
2. Whitford, P. C.; Onuchic, J. N., What protein folding teaches us about biological function and molecular machines. *Curr. Opin. Struct. Biol.* **2015,** *30*, 57-62.
3. Dill, K. A.; MacCallum, J. L., The Protein-Folding Problem, 50 Years On. *Science* **2012,** *338* (6110), 1042-1046.
4. Whitford, D., *Proteins: structure and function*. John Wiley & Sons: **2013**.
5. Jakubke, H. D.; Sewald, N., *Peptides from A to Z: A Concise Encyclopedia*. Wiley: Weinheim, **2008**; p 1-402.
6. Wagner, I.; Musso, H., New Naturally Occurring Amino Acids. *Angew. Chem. Int. Ed.* **1983,** *22* (11), 816-828.
7. Barret, R., 2 - Importance and Evaluation of the pKa. In *Therapeutical Chemistry*, Barret, R., Ed. Elsevier: **2018**; pp 21-51.
8. Rudinger, J., Characteristics of the amino acids as components of a peptide hormone sequence. In *Peptide Hormones*, Parsons, J. A., Ed. Macmillan Education UK: London, **1976**; pp 1-7.
9. Nomenclature and Symbolism for Amino Acids and Peptides. *Eur. J. Biochem.* **1984,** *138* (1), 9-37.
10. Fischer, G., Chemical aspects of peptide bond isomerisation. *Chem. Soc. Rev.* **2000,** *29* (2), 119-127.
11. Sigel, A.; Sigel, H., Probing of Proteins by Metal Ions and Their Low-Molecular-Weight Complexes. In *Met. Ions Biol. Syst.*, Martin, B., Ed. CRC Press: **2001**; Vol. 38, p 2.
12. Huang, F. F.; Rha, C., Protein structures and protein fibers—a review. *Polym. Eng. Sci.* **1974,** *14* (2), 81-91.
13. Bonduelle, C., Secondary structures of synthetic polypeptide polymers. *Polym. Chem.* **2018,** *9* (13), 1517-1529.
14. Nelson, D. L.; Cox, M. M., *Lehninger principles of biochemistry (4th ed.)*. W.H. Freeman and Company: New York, **2004**.
15. Cieplak, A. S., Protein folding, misfolding and aggregation: The importance of two-electron stabilizing interactions. *PLoS One* **2017,** *12* (9), e0180905-e0180905.
16. Song, Z.; Fu, H.; Wang, R.; Pacheco, L. A.; Wang, X.; Lin, Y.; Cheng, J., Secondary structures in synthetic polypeptides from N-carboxyanhydrides: design, modulation, association, and material applications. *Chem. Soc. Rev.* **2018,** *47* (19), 7401-7425.
17. Ramachandran, G. N.; Ramakrishnan, C.; Sasisekharan, V., Stereochemistry of polypeptide chain configurations. *J. Mol. Biol.* **1963,** *7* (1), 95-99.
18. Hollingsworth, S. A.; Karplus, P. A., A fresh look at the Ramachandran plot and the occurrence of standard structures in proteins. *BioMol Concepts* **2010,** *1* (3-4), 271.
19. Lovell, S. C.; Davis, I. W.; Arendall III, W. B.; de Bakker, P. I. W.; Word, J. M.; Prisant, M. G.; Richardson, J. S.; Richardson, D. C., Structure validation by Cα geometry: ϕ,ψ and Cβ deviation. *Proteins: Struct., Funct., Bioinf.* **2003,** *50* (3), 437-450.
20. Pauling, L.; Corey, R. B.; Branson, H. R., The structure of proteins: Two hydrogen-bonded helical configurations of the polypeptide chain. *Proc. Natl. Acad. Sci.* **1951,** *37* (4), 205-211.
21. Woolfson, D. N.; Ryadnov, M. G., Peptide-based fibrous biomaterials: some things old, new and borrowed. *Curr. Opin. Chem. Biol.* **2006,** *10* (6), 559-567.
22. Pavone, V.; Benedetti, E.; Di Biasio, B.; Pedone, C.; Santini, A.; Bavoso, A.; Toniolo, C.; Crisma, M.; Sartore, L., Critical Main-Chain Length for Conformational Conversion From 310-Helix to α-Helix in Polypeptides. *J. Biomol. Struct. Dyn.* **1990,** *7* (6), 1321-1331.
23. Nesloney, C. L.; Kelly, J. W., Progress towards understanding β-sheet structure. *Bioorg. Med. Chem.* **1996,** *4* (6), 739-766.
24. Toniolo, C., Intramolecularly hydrogen-bonded peptide conformations. *CRC Crit. Rev. Biochem.* **1980,** *9* (1), 1-44.
25. James Milner-White, E.; Poet, R., Loops, bulges, turns and hairpins in proteins. *Trends Biochem. Sci.* **1987,** *12*, 189-192.
26. Chou, P. Y.; Fasman, G. D., Prediction of beta-turns. *Biophys. J.* **1979,** *26* (3), 367-383.

27. Lewis, P. N.; Momany, F. A.; Scheraga, H. A., Chain reversals in proteins. *Biochim. Biophys. Acta, Protein Struct.* **1973,** *303* (2), 211-229.
28. Wilmot, C. M.; Thornton, J. M., Analysis and prediction of the different types of β-turn in proteins. *J. Mol. Biol.* **1988,** *203* (1), 221-232.
29. Kabsch, W.; Sander, C., Dictionary of protein secondary structure: Pattern recognition of hydrogen-bonded and geometrical features. *Biopolymers* **1983,** *22* (12), 2577-2637.
30. Rose, G. D.; Glerasch, L. M.; Smith, J. A., Turns in Peptides and Proteins. In *Adv. Protein Chem.*, Anfinsen, C. B.; Edsall, J. T.; Richards, F. M., Eds. Academic Press: **1985**; Vol. 37, pp 1-109.
31. Hutchinson, E. G.; Thornton, J. M., A revised set of potentials for β-turn formation in proteins. *Protein Sci.* **1994,** *3* (12), 2207-2216.
32. Baker, E. N.; Hubbard, R. E., Hydrogen bonding in globular proteins. *Prog. Biophys. Mol. Biol.* **1984,** *44* (2), 97-179.
33. Tonlolo, C.; Benedetti, E., The polypeptide 310-helix. *Trends Biochem. Sci.* **1991,** *16*, 350-353.
34. Vieira-Pires, R. S.; Morais-Cabral, J. H., 310 helices in channels and other membrane proteins. *J. Gen. Physiol.* **2010,** *136* (6), 585-592.
35. Karpen, M. E.; De Haseth, P. L.; Neet, K. E., Differences in the amino acid distributions of 310-helices and α-helices. *Protein Sci.* **1992,** *1* (10), 1333-1342.
36. Robbins, A. H.; Stout, C. D., The structure of aconitase. *Proteins: Struct., Funct., Bioinf.* **1989,** *5* (4), 289-312.
37. Venkataram Prasad, B. V.; Balaram, P.; Benedetti, E., The Stereochemistry of Peptides Containing α-Aminoisobutyric Acid. *Crit. Rev. Biochem. Mol. Biol* **1984,** *16* (4), 307-348.
38. Toniolo, C.; Benedetti, E., Structures of polypeptides from α-amino acids disubstituted at the α-carbon. *Macromolecules* **1991,** *24* (14), 4004-4009.
39. Costantini, S.; Colonna, G.; Facchiano, A. M., Amino acid propensities for secondary structures are influenced by the protein structural class. *Biochem. Biophys. Res. Commun.* **2006,** *342* (2), 441-451.
40. Cohen, C.; Szent-Gyorgyi, A. G., Optical rotation and helical polypeptide chain configuration in α-proteins. *J. Am. Chem. Soc.* **1957,** *79* (1), 248-248.
41. Urnes, P.; Doty, P., Optical Rotation And The Conformation Of Polypeptides And Proteins. In *Adv. Protein Chem.*, Anfinsen, C. B.; Anson, M. L.; Bailey, K.; Edsall, J. T., Eds. Academic Press: **1962**; Vol. 16, pp 401-544.
42. Robinson, C.; Bott, M. J., Optical Rotation and Chain Folding in Synthetic Polypeptides and Gelatin. *Nature* **1951,** *168* (4269), 325-326.
43. Berman, H.; Henrick, K.; Nakamura, H.; Markley, J. L., The worldwide Protein Data Bank (wwPDB): ensuring a single, uniform archive of PDB data. *Nucleic Acids Res.* **2006,** *35* (suppl_1), D301-D303.
44. Sussman, J. L.; Lin, D.; Jiang, J.; Manning, N. O.; Prilusky, J.; Ritter, O.; Abola, E. E., Protein Data Bank (PDB): Database of Three-Dimensional Structural Information of Biological Macromolecules. *Acta Crystallogr. D* **1998,** *54* (6 Part 1), 1078-1084.
45. Bandekar, J., Amide modes and protein conformation. *Biochim. Biophys. Acta, Protein Struct. Mol. Enzymol.* **1992,** *1120* (2), 123-143.
46. Thomas Jr., G. J., New structural insights from Raman spectroscopy of proteins and their assemblies. *Biopolymers* **2002,** *67* (4-5), 214-225.
47. Rygula, A.; Majzner, K.; Marzec, K. M.; Kaczor, A.; Pilarczyk, M.; Baranska, M., Raman spectroscopy of proteins: a review. *J. Raman Spectrosc.* **2013,** *44* (8), 1061-1076.
48. Hinds, M. G.; Norton, R. S., NMR spectroscopy of peptides and proteins. *Mol. Biotechnol.* **1997,** *7* (3), 315-331.
49. Clore, G. M.; Gronenborn, A. M., *NMR of Proteins*. Macmillan International Higher Education: **1993**.
50. Oppenheimer, N. J.; James, T. L., *Nuclear Magnetic Resonance. Part A. Spectral Techniques and Dynamics*. Elsevier: **1989**.
51. Oppenheimer, N. J.; James, T. L., Nuclear magnetic resonance. B: structure and mechanism. *Methods Enzymol.* **1989,** *177*.

52. James, T. L.; Dotsch, V.; Schmitz, U., *Nuclear magnetic resonance of biological macromolecules*. Elsevier: **2001**.
53. Adochitei, A.; Drochioiu, G., Rapid Characterization of peptide secondary structure by FT-IR spectroscopy. *Rev. Roum. Chim.* **2011,** *56*, 783-791.
54. Kong, J.; Yu, S., Fourier Transform Infrared Spectroscopic Analysis of Protein Secondary Structures. *Acta Biochim. Biophys. Sin.* **2007,** *39* (8), 549-559.
55. Susi, H.; Byler, D. M., Resolution-enhanced fourier transform infrared spectroscopy of enzymes. In *Methods Enzymol.*, Academic Press: **1986**; Vol. 130, pp 290-311.
56. Surewicz, W. K.; Mantsch, H. H.; Chapman, D., Determination of protein secondary structure by Fourier transform infrared spectroscopy: A critical assessment. *Biochemistry* **1993,** *32* (2), 389-394.
57. Glassford, S. E.; Byrne, B.; Kazarian, S. G., Recent applications of ATR FTIR spectroscopy and imaging to proteins. *Biochim. Biophys. Acta, Proteins Proteomics* **2013,** *1834* (12), 2849-2858.
58. Haris, P. I., Infrared Spectroscopy of Protein Structure. In *Encyclopedia of Biophysics*, Roberts, G. C. K., Ed. Springer Berlin Heidelberg: Berlin, Heidelberg, **2013**; pp 1095-1106.
59. Kelly, S. M.; Jess, T. J.; Price, N. C., How to study proteins by circular dichroism. *Biochim. Biophys. Acta* **2005,** *1751* (2), 119-39.
60. Pelton, J. T.; McLean, L. R., Spectroscopic Methods for Analysis of Protein Secondary Structure. *Anal. Biochem.* **2000,** *277* (2), 167-176.
61. Greenfield, N. J., Applications of circular dichroism in protein and peptide analysis. *Trends Anal. Chem.* **1999,** *18* (4), 236-244.
62. Francesco Simone, R.; Johnny, H.; Andrea, C.; Giovanni, D., AFM-Based Single Molecule Techniques: Unraveling the Amyloid Pathogenic Species. *Curr. Pharm. Des.* **2016,** *22* (26), 3950-3970.
63. Miller, L. M.; Bourassa, M. W.; Smith, R. J., FTIR spectroscopic imaging of protein aggregation in living cells. *Biochim. Biophys. Acta, Biomembr.* **2013,** *1828* (10), 2339-2346.
64. Barth, A., Infrared spectroscopy of proteins. *Biochim. Biophys. Acta, Bioenerg.* **2007,** *1767* (9), 1073-1101.
65. Hui, Y. H., Infrared and Raman Spectroscopy in Food Science. In *Handbook of food science, technology, and engineering*, Ismail, A.; Cocciardi, R.; Alvarez, C.; Sedman, J., Eds. CRC press: Boca Raton, **2005**; pp 44-10.
66. Doty, P.; Bradbury, J. H.; Holtzer, A. M., Polypeptides. IV. The Molecular Weight, Configuration and Association of Poly-γ-benzyl-L-glutamate in Various Solvents. *J. Am. Chem. Soc.* **1956,** *78* (5), 947-954.
67. Blout, E. R.; Karlson, R. H., Polypeptides. III. The Synthesis of High Molecular Weight Poly-γ-benzyl-L-glutamates[1]. *J. Am. Chem. Soc.* **1956,** *78* (5), 941-946.
68. Doty, P.; Holtzer, A. M.; Bradbury, J. H.; Blout, E. R., Polypeptides II. The Configuration of Polymers of γ-Benzyl-L-Glutamate in solution. *J. Am. Chem. Soc.* **1954,** *76* (17), 4493-4494.
69. Blout, E. R.; Karlson, R. H.; Doty, P.; Hargitay, B., Polypeptides. I. The synthesis and the molecular weight of high molecular weight polyglutamic acids and esters[1]. *J. Am. Chem. Soc.* **1954,** *76* (17), 4492-4493.
70. Masuda, Y.; Miyazawa, T., Infrared spectra and molecular conformations of poly-γ-benzyl-L-glutamate. *Macromol. Chem.* **1967,** *103* (1), 261-267.
71. Ishida, M.; Takai, M.; Okabayashi, H.; Masuda, H.; Nishio, E.; O'Connor, C. J., FTIR evidence for antiparallel β-sheet structures of long oligomeric N-acetyl-l-glutamic acid benzyl esters. *Vib. Spectrosc* **2001,** *27* (2), 135-138.
72. Goodman, M.; Felix, A. M.; Deber, C. M.; Brause, A. R.; Schwartz, G., Conformational aspects of polypeptides. XI. The nitroaromatic effect. *Biopolymers* **1963,** *1* (4), 371-400.
73. Doty, P.; Yang, J. T., Polypeptides. VII. Poly-γ-Benzyl-L-Glutamate: The Helix-Coil transition in solution. *J. Am. Chem. Soc.* **1956,** *78* (2), 498-500.
74. Bovey, F. A.; Tiers, G. V. D.; Filipovich, G., Polymer NSR spectroscopy. I. The motion and configuration of polymer chains in solution. *J. Polym. Sci.* **1959,** *38* (133), 73-90.

75. Bradbury, E. M.; Crane-Robinson, C.; Paolillo, L.; Temussi, P., N.m.r. studies of the helix-coil transition of polypeptides in non-protonating solvent mixtures. *Polymer* **1973,** *14* (7), 303-308.
76. Novotná, P.; Urbanová, M., Vibrational circular dichroism study of solvent- and temperature-induced conformational changes in poly-γ-benzyl-l-glutamate and poly-β-benzyl-l-aspartate. *Vib. Spectrosc* **2013,** *66*, 1-7.
77. Okabayashi, H.; Ishida, M.; Tamaoki, H.; Masuda, H.; O'Connor, C. J., Fourier transform IR study of aggregational behavior of N-acetyl-L- and N-butyloxycarbonyl-L-glutamic acid oligomeric benzyl esters in dioxane and benzene: beta-turn --> antiparallel beta-sheet transition. *Biopolymers* **2002,** *65* (2), 129-41.
78. Fraser, R. D. B.; Harrap, B. S.; Ledger, R.; Macrae, T. P.; Stewart, F. H. C.; Suzuki, E., Stability of the α-helix in poly(γ-benzyl L-glutamate) and related polymers. *Biopolymers* **1967,** *5* (9), 797-808.
79. Blout; Blout, E. R.; Karlson, R. H., Poly-ß-benzyl aspartates: Optical rotation and the sense of the helix. *J. Am. Chem. Soc.* **1958,** *80* (5), 1259-1260.
80. Bradbury, E. M.; Brown, L.; Downie, A. R.; Elliott, A.; Hanby, W. E.; McDonald, T. R. R., α-Helices and a New Polypeptide Fold in Poly-β-Benzyl-L-Aspartate. *Nature* **1959,** *183* (4677), 1736-1737.
81. Bradbury, E. M.; Downie, A. R.; Elliott, A.; Hanby, W. E.; Wilson, A. H., The stability and screw sense of the α-helix in poly-β-benzyl-L-aspartate. *Proc. R. Soc. London, Ser. A* **1960,** *259* (1296), 110-128.
82. Bradbury, E. M.; Downie, A. R.; Elliott, A.; Hanby, W. E., Screw Sense of the α-Helix in Poly-β-benzyl-L-aspartate. *Nature* **1960,** *187* (4734), 321-321.
83. Karlson, R. H.; Norland, K. S.; Fasman, G. D.; Blout, E. R., The Helical Sense of Poly-β-benzyl-L-aspartate. Synthesis and Rotatory Dispersion of Copolymers of β-Benzyl-L and D-Aspartate with γ-Benzyl-L-glutamate1. *J. Am. Chem. Soc.* **1960,** *82* (9), 2268-2275.
84. E. M. Bradbury; A. R. Downie; A. Elliott; Hanby, W. E., The stability and screw sense of the ω-helix in poly-ß-benzyl-L-aspartate. *Proc. R. Soc. Lond. A* **1961,** *259* (1296), 110-128.
85. Goodman, M.; Deber, C. M.; Felix, A. M., Conformational Aspects of Polypeptides. VII. Reversal of The Helical Sense of Poly-L-Aspartate Esters. *J. Am. Chem. Soc.* **1962,** *84* (19), 3773-3774.
86. Ooi, T.; Scott, R. A.; Vanderkooi, G.; Scheraga, H. A., Conformational Analysis of Macromolecules. IV. Helical Structures of Poly-L-Alanine, Poly-L-Valine, Poly-β-Methyl-L-Aspartate, Poly-γ-Methyl-L-Glutamate, and Poly-L-Tyrosine. *J. Chem. Phys.* **1967,** *46* (11), 4410-4426.
87. Hashimoto, M., Studies of Poly-β-benzyl-L-aspartate Helix. II. The Circular Dichroism and Optical Rotatory Dispersion of Copolymers of β-p-Methyl, Chloro, or Cyanobenzyl-L-aspartate with β-Benzyl-L-aspartate. *Bull. Chem. Soc. Jpn.* **1966,** *39*, 2713-2720.
88. Hashimoto, M.; Aritomi, J., Studies of poly-beta-benzyl-l-aspartate helix. I. The synthesis and rotatory dispersion of copolymers of beta-p-methyl, chloro, cyano, or nitrobenzyl-l-aspartate with beta-benzyl-l-aspartate. *Bull. Chem. Soc. Jpn.* **1966,** *39* (12), 2707-2713.
89. Masahisa, H.; Satoshi, A., Studies of Poly-β-benzyl-L-aspartate Helix. III. Infrared Spectra of Copolymers of β-Benzyl-L-aspartate with β-p-Methyl, Chloro, Cyano, or Nitrobenzyl-L-aspartate in a Chloroform Solution. *Bull. Chem. Soc. Jpn.* **1967,** *40* (7), 1698-1701.
90. Bradbury, E. M.; Carpenter, B. G.; Goldman, H., Conformational studies of polymers and copolymers of L-aspartate esters. I. Preparation and solution studies. *Biopolymers* **1968,** *6* (6), 837-850.
91. Obata, H.; Kanetsuna, H., Crystallinity and conformational changes in poly(β-benzyl L-aspartate). *Journal of Polymer Science Part A-2: Polymer Physics* **1971,** *9* (11), 1977-1989.
92. Hiroko, K.; Hisaaki, K., Effect of molecular weight on conformation of poly(β-benzyl L-aspartate) in films. *J. Polym. Sci., Part B: Polym. Phys.* **1972,** *10* (10), 1931-1939.
93. Yang, C.-T.; Wang, Y.; Chang, Y.-C., Effect of Solvents and Temperature on the Conformation of Poly(β-benzyl-l-aspartate) Brushes. *Biomacromolecules* **2010,** *11* (5), 1308-1313.

94. Bradbury, E. M.; Brown, L.; Downie, A. R.; Elliott, A.; Fraser, R. D. B.; Hanby, W. E., The structure of the ω-form of poly-β-benzyl-L-aspartate. *J. Mol. Biol.* **1962,** *5* (2), 230-247.
95. Kondo, Y.; Iizuka, E.; Oka, A.; Hayakawa, T., Circular dichroism of poly(β-benzyl-l-aspartate) films in the α, β and ω conformations. *Polymer* **1977,** *18* (2), 111-113.
96. Tsujita, Y.; Takahashi, T.; Takizawa, A., Coacervation effect of cast solution on the structure and properties of Poly(ß-benzyl L-aspartate). *Sen'i Gakkaishi* **1981,** *37* (11), 467-471.
97. Le Bailly, B. A. F.; Clayden, J., Dynamic foldamer chemistry. *Chem. Commun.* **2016,** *52* (27), 4852-4863.
98. Ute, K.; Fukunishi, Y.; Jha, S. K.; Cheon, K.-S.; Muñoz, B.; Hatada, K.; Green, M. M., Dynamic NMR Determination of the Barrier for Interconversion of the Left- and Right-Handed Helical Conformations in a Polyisocyanate. *Macromolecules* **1999,** *32* (4), 1304-1307.
99. Solà, J.; Morris, G. A.; Clayden, J., Measuring Screw-Sense Preference in a Helical Oligomer by Comparison of 13C NMR Signal Separation at Slow and Fast Exchange. *J. Am. Chem. Soc.* **2011,** *133* (11), 3712-3715.
100. Crisma, M.; Toniolo, C., Helical screw-sense preferences of peptides based on chiral, Cα-tetrasubstituted α-amino acids. *Pept. Sci* **2015,** *104* (1), 46-64.
101. De Zotti, M.; Formaggio, F.; Crisma, M.; Peggion, C.; Moretto, A.; Toniolo, C., Handedness preference and switching of peptide helices. Part II: Helices based on noncoded α -amino acids. *J. Pept. Sci.* **2014,** *20*.
102. Toniolo, C.; Crisma, M.; Formaggio, F.; Peggion, C., Control of peptide conformation by the Thorpe-Ingold effect (Cα-tetrasubstitution). *Pept. Sci* **2001,** *60* (6), 396-419.
103. Inai, Y.; Tagawa, K.; Takasu, A.; Hirabayashi, T.; Oshikawa, T.; Yamashita, M., Induction of One-Handed Helical Screw Sense in Achiral Peptide through the Domino Effect Based on Interacting Its N-Terminal Amino Group with Chiral Carboxylic Acid. *J. Am. Chem. Soc.* **2000,** *122* (47), 11731-11732.
104. Appavu, R.; Mohan, D.; Kakumanu, R.; Munisamy, G., Fundamental of Secondary Structures in Peptide Based Synthetic Nanovaccine Development. *Transcriptomics* **2016,** *4*, 131.
105. Venanzi, M.; Gatto, E.; Formaggio, F.; Toniolo, C., The importance of being Aib. Aggregation and self-assembly studies on conformationally constrained oligopeptides. *J. Pept. Sci.* **2017,** *23* (2), 104-116.
106. Venkatachalam, C. M., Stereochemical criteria for polypeptides and proteins. V. Conformation of a system of three linked peptide units. *Biopolymers* **1968,** *6* (10), 1425-1436.
107. Bonora, G. M.; Mapelli, C.; Toniolo, C.; Wilkening, R. R.; Stevens, E. S., Conformational analysis of linear peptides: 5. Spectroscopic characterization of β-turns in Aib-containing oligopeptides in chloroform. *Int. J. Biol. Macromol.* **1984,** *6* (4), 179-188.
108. Dwivedi, A. M.; Krimm, S.; Malcolm, B. R., Vibrational analysis of peptides, polypeptides, and proteins. XXIV. Conformation of poly(α-aminoisobutyric acid). *Biopolymers* **1984,** *23* (10), 2025-2065.
109. Toniolo, C.; Benedetti, E., In Molecular Conformation and Biological Interactions; Balaram, P.; Ramaseshan, S., Eds. *Indian Academy of Science: Bangalore, India* **1991**, 511-521.
110. Benedetti, E.; Di Blasio, B.; Pavone, V.; Pedone, C.; Toniolo, C.; Crisma, M., Characterization at atomic resolution of peptide helical structures. *Biopolymers* **1992,** *32* (4), 453-456.
111. Gilead, S.; Gazit, E., Inhibition of Amyloid Fibril Formation by Peptide Analogues Modified with α-Aminoisobutyric Acid. *Angew. Chem. Int. Ed.* **2004,** *43* (31), 4041-4044.
112. Valle, G.; Toniolo, C.; Bonora, G. M., Structures of N-acetyl-α-aminoisobutyric acid, $C_6H_{11}NO_3$, and N-trifluoroacetyl-α-aminoisobutyric acid, $C_6H_8F_3NO_3$. *Acta Crystallogr. C* **1985,** *41* (2), 235-238.
113. Mayr, W.; Jung, G.; Strähle, J., Die Kristallstruktur von α-(tert-Butyloxycarbonylamino)isobuttersäure. *Liebigs Ann. Chem.* **1980,** *1980* (5), 715-724.
114. Van Roey, P.; Smith, G. D.; Balasubramanian, T. M.; Marshall, G. R., tert-Butyloxycarbonyl-α-aminoisobutyryl-α-aminoisobutyrate benzyl ester, $C_{20}H_{30}N_2O_5$. *Acta Crystallogr. C* **1983,** *39* (7), 894-896.
115. Benedetti, E.; Bavoso, A.; Di Blasio, B.; Pavone, V.; Pedone, C.; Crisma, M.; Bonora, G. M.; Toniolo, C., Linear oligopeptides. 81. Solid-state and solution conformation of

homooligo(α-aminoisobutyric acids) from tripeptide to pentapeptide: evidence for a 3_{10} helix. *J. Am. Chem. Soc.* **1982,** *104* (9), 2437-2444.
116. Di Blasio, B.; Santini, A.; Pavone, V.; Pedone, C.; Benedetti, E.; Moretto, V.; Crisma, M.; Toniolo, C., Crystal-state conformation of homo-oligomers of α-aminoisobutyric acid: Molecular and crystal structure of pBrBz-$(Aib)_6$-OMe. *Struct. Chem.* **1991,** *2* (5), 523-527.
117. Bavoso, A.; Benedetti, E.; Di Blasio, B.; Pavone, V.; Pedone, C.; Toniolo, C.; Bonora, G. M., Long polypeptide 3_{10}-helices at atomic resolution. *Proc. Natl. Acad. Sci.* **1986,** *83* (7), 1988-1992.
118. Pavone, V.; di Blasio, B.; Santini, A.; Benedetti, E.; Pedone, C.; Toniolo, C.; Crisma, M., The longest, regular polypeptide 3_{10} helix at atomic resolution. *J. Mol. Biol.* **1990,** *214* (3), 633-635.
119. Toniolo, C.; Crisma, M.; Bonora, G. M.; Benedetti, E.; Dl Blasio, B.; Pavone, V.; Pedone, C.; Santini, A., Preferred conformation of the terminally blocked $(Aib)_{10}$ homo-oligopeptide: A long, regular 3_{10}-helix. *Biopolymers* **1991,** *31* (1), 129-138.
120. Gessmann, R.; Brückner, H.; Petratos, K., Three complete turns of a 3_{10}-helix at atomic resolution: the crystal structure of Z-$(Aib)_{11}$-OtBu. *J. Pept. Sci.* **2003,** *9* (11-12), 753-762.
121. Soto, C., Protein misfolding and disease; protein refolding and therapy. *FEBS Lett.* **2001,** *498* (2-3), 204-207.
122. Soto, C., Unfolding the role of protein misfolding in neurodegenerative diseases. *Nat. Rev. Neurosci.* **2003,** *4* (1), 49-60.
123. Formaggio, F.; Bettio, A.; Moretto, V.; Crisma, M.; Toniolo, C.; Broxterman, Q. B., Disruption of the β-sheet structure of a protected pentapeptide, related to the β-amyloid sequence 17–21, induced by a single, helicogenic Cα-tetrasubstituted α-amino acid. *J. Pept. Sci.* **2003,** *9* (7), 461-466.
124. Soto, C.; Sigurdsson, E. M.; Morelli, L.; Kumar, R. A.; Castaño, E. M.; Frangione, B., β-sheet breaker peptides inhibit fibrillogenesis in a rat brain model of amyloidosis: implications for Alzheimer's therapy. *Nat. Med. (N. Y., NY, U. S.)* **1998,** *4* (7), 822-826.
125. Chugh, J. K.; Wallace, B. A., Peptaibols: models for ion channels. *Biochem. Soc. Trans.* **2001,** *29* (4), 565-570.
126. Daniel, J. F. d. S.; Rodrigues Filho, E., Peptaibols of Trichoderma. *Nat. Prod. Rep.* **2007,** *24* (5), 1128-1141.
127. Whitmore, L.; Wallace, B. A., The Peptaibol Database: a database for sequences and structures of naturally occurring peptaibols. *Nucleic Acids Res.* **2004,** *32*, D593-D594.
128. David, W.; Jukka, E., Synthetic Antibiotic Peptides Database. *Protein Pept. Lett.* **2002,** *9* (1), 53-57.
129. Fox, R. O.; Richards, F. M., A voltage-gated ion channel model inferred from the crystal structure of alamethicin at 1.5-Å resolution. *Nature* **1982,** *300* (5890), 325-330.
130. Karle, I. L.; Flippen-Anderson, J. L.; Agarwalla, S.; Balaram, P., Crystal structure of [Leu1]zervamicin, a membrane ion-channel peptide: implications for gating mechanisms. *Proc. Natl. Acad. Sci.* **1991,** *88* (12), 5307-5311.
131. Snook, C. F.; Woolley, G. A.; Oliva, G.; Pattabhi, V.; Wood, S. P.; Blundell, T. L.; Wallace, B. A., The structure and function of antiamoebin I, a proline-rich membrane-active polypeptide. *Structure* **1998,** *6* (6), 783-792.
132. Hummel, R.-P.; Toniolo, C.; Jung, G., Konformationsübergänge zwischen enantiomeren 3_{10}-Helices. *Angew. Chem.* **1987,** *99* (11), 1180-1182.
133. Kubasik, M.; Kotz, J.; Szabo, C.; Furlong, T.; Stace, J., Helix–helix interconversion rates of short ^{13}C-labeled helical peptides as measured by dynamic NMR spectroscopy. *Biopolymers* **2005,** *78* (2), 87-95.
134. Zotti, M. D.; Formaggio, F.; Crisma, M.; Peggion, C.; Moretto, A.; Toniolo, C., Handedness preference and switching of peptide helices. Part I: Helices based on protein amino acids. *J. Pept. Sci.* **2014,** *20* (5), 307-322.
135. Toniolo, C.; Bonora, G. M.; Benedetti, E.; Bavoso, A.; Di Blasio, B.; Pavone, V.; Pedone, C., Peptaibol antibiotics: Conformational preferences of synthetic emerimicin fragments. *Biopolymers* **1983,** *22* (5), 1335-1356.

136. Bardi, R.; Piazzesi, A. M.; Toniolo, C.; Raj, P. A.; Raghothama, S.; Balaram, P., Conformations of the amino aterminal tetrapeptide of emerimicins and antiamoebins in solution and in the solid state. *Int. J. Biol. Macromol.* **1986,** *8* (4), 201-206.
137. Crisma, M.; Valle, G.; Formaggio, F.; Bianco, A.; Toniolo, C., Helical screw sense of peptide molecules. X-Ray diffraction structures of two oligopeptides with a single chiral centre. *J. Chem. Soc., Perkin Trans. 2,* **1993,** (5), 987-991.
138. Crisma, M.; Valle, G.; Pantano, M.; Formaggio, F.; Bonora, G. M.; Toniolo, C.; Kamphuis, J., Peptides from chiral Cαα-disubstituted glycines. On the helical screw sense of isovaline peptides. *J. Recl TravChim Pays-Bas* **1995,** *114* (7), 325-331.
139. Crisma, M.; Valle, G.; Formaggio, F.; Toniolo, C., Helical screw sense of peptide molecules. Diastereomeric -Pro-Ala-$(Aib)_4$-sequences. *Zeitschrift für Kristallographie - Crystalline Materials* **1998,** *213* (11), 599.
140. Pengo, B.; Formaggio, F.; Crisma, M.; Toniolo, C.; Maria Bonora, G.; B. Broxterman, Q.; Kamphuis, J.; Saviano, M.; Iacovino, R.; Rossi, F.; Benedetti, E., Linear oligopeptides. Part 406.1 Helical screw sense of peptide molecules: the pentapeptide system (Aib)4/L-Val[L-(αMe)Val] in solution. *J. Chem. Soc., Perkin Trans. 2,* **1998,** (7), 1651-1658.
141. Benedetti, S.; Saviano, M.; Iacovino, R.; Crisma, M.; Formaggio, F.; Toniolo, C., Helical screw sense of peptide molecules. Crystal structures of three Aib-based pentapeptides[1]. *Z. Kristallogr.* **1999,** *214*, 160.
142. Karle, I. L.; Ranganathan, D.; Lakshmi, C., Demonstration of a cystine unit as a promising turn scaffold for the design of a parallel U-shaped two-helix bundle motif: Crystal structure of the homodimer $Cys(Aib_n)_2$ (n = 3, 4). *Biopolymers* **2001,** *59* (5), 301-304.
143. Tanaka, M.; Oba, M.; Imawaka, N.; Tanaka, Y.; Kurihara, M.; Suemune, H., Conformational Study of Heteropentapeptides Containing an α-Ethylated α,α-Disubstituted Amino Acid: (S)-Butylethylglycine (=2-Amino-2-ethylhexanoic Acid) within a Sequence of Dimethylglycine (=2-Aminoisobutyric Acid) Residues. *Helv. Chim. Acta* **2001,** *84* (1), 32-46.
144. Oba, M.; Tanaka, M.; Kurihara, M.; Suemune, H., Conformation of Peptides Containing a Chiral α-Ethylated α,α-Disubstituted α-Amino Acid: (S)-α-Ethylleucine (=(2S)-2-Amino-2-ethyl-4-methylpentanoic Acid) within Sequences of Dimethylglycine and Diethylglycine Residues. *Helv. Chim. Acta* **2002,** *85* (10), 3197-3218.
145. Crisma, M.; Andreetto, E.; De Zotti, M.; Moretto, A.; Peggion, C.; Formaggio, F.; Toniolo, C., Crystal-state 3D-structural characterization of novel, Aib-based, turn and helical peptides. *J. Pept. Sci.* **2007,** *13* (3), 190-205.
146. Clayden, J.; Castellanos, A.; Solà, J.; Morris, G. A., Quantifying End-to-End Conformational Communication of Chirality through an Achiral Peptide Chain. *Angew. Chem. Int. Ed.* **2009,** *48* (32), 5962-5965.
147. Demizu, Y.; Tanaka, M.; Doi, M.; Kurihara, M.; Okuda, H.; Suemune, H., Conformations of peptides containing a chiral cyclic α, α-disubstituted α-amino acid within the sequence of Aib residues. *J. Pept. Sci.* **2010,** *16* (11), 621-626.
148. Solà, J.; Fletcher, S. P.; Castellanos, A.; Clayden, J., Nanometer-Range Communication of Stereochemical Information by Reversible Switching of Molecular Helicity. *Angew. Chem. Int. Ed.* **2010,** *49* (38), 6836-6839.
149. Solà, J.; Helliwell, M.; Clayden, J., N- versus C-Terminal Control over the Screw-Sense Preference of the Configurationally Achiral, Conformationally Helical Peptide Motif $Aib_8GlyAib_8$. *J. Am. Chem. Soc.* **2010,** *132* (13), 4548-4549.
150. Boddaert, T.; Solà, J.; Helliwell, M.; Clayden, J., Chemical communication: conductors and insulators of screw-sense preference between helical oligo(aminoisobutyric acid) domains. *Chem. Commun.* **2012,** *48* (28), 3397-3399.
151. Brown, R. A.; Marcelli, T.; De Poli, M.; Solà, J.; Clayden, J., Induction of Unexpected Left-Handed Helicity by an N-Terminal L-Amino Acid in an Otherwise Achiral Peptide Chain. *Angew. Chem. Int. Ed.* **2012,** *51* (6), 1395-1399.
152. De Poli, M.; De Zotti, M.; Raftery, J.; Aguilar, J. A.; Morris, G. A.; Clayden, J., Left-Handed Helical Preference in an Achiral Peptide Chain Is Induced by an l-Amino Acid in an N-Terminal Type II β-Turn. *J. Org. Chem.* **2013,** *78* (6), 2248-2255.

153. Byrne, L.; Solà, J.; Boddaert, T.; Marcelli, T.; Adams, R. W.; Morris, G. A.; Clayden, J., Foldamer-mediated remote stereocontrol: >1,60 asymmetric induction. *Angew. Chem. Int. Ed.* **2014,** *53* (1), 151-155.
154. De Poli, M.; Byrne, L.; Brown, R. A.; Solà, J.; Castellanos, A.; Boddaert, T.; Wechsel, R.; Beadle, J. D.; Clayden, J., Engineering the Structure of an N-Terminal β-Turn To Maximize Screw-Sense Preference in Achiral Helical Peptide Chains. *J. Org. Chem.* **2014,** *79* (10), 4659-4675.
155. De Poli, M.; Clayden, J., Thionoglycine as a multifunctional spectroscopic reporter of screw-sense preference in helical foldamers. *Org. Biomol. Chem.* **2014,** *12* (5), 836-843.
156. Pike, S. J.; Diemer, V.; Raftery, J.; Webb , S. J.; Clayden, J., Designing Foldamer–Foldamer Interactions in Solution: The Roles of Helix Length and Terminus Functionality in Promoting the Self-Association of Aminoisobutyric Acid Oligomers. *Chem. Eur. J* **2014,** *20* (48), 15981-15990.
157. Pike, S. J.; Boddaert, T.; Raftery, J.; Webb, S. J.; Clayden, J., Participation of non-aminoisobutyric acid (Aib) residues in the 3_{10} helical conformation of Aib-rich foldamers: a solid state study. *New J. Chem.* **2015,** *39* (5), 3288-3294.
158. Demizu, Y.; Yabuki, Y.-u.; Doi, M.; Sato, Y.; Tanaka, M.; Kurihara, M., Conformations of helical Aib peptides containing a pair of l-amino acid and d-amino acid. *J. Pept. Sci.* **2012,** *18* (7), 466-475.
159. Benedetti, E.; Saviano, M.; Iacovino, R.; Pedone, C.; Santini, A.; Crisma, M.; Formaggio, F.; Toniolo, C.; Broxterman, Q. B.; Kamphuis, J., Helical screw sense of peptide molecules: The pentapeptide system $(Aib)_4$/L-Val[L-(αMe)Val] in the crystal state. *Biopolymers* **1998,** *46* (7), 433-443.
160. Benedetti, E.; Bavoso, A.; Di Blasio, B.; Pavone, V.; Pedone, C.; Toniolo, C.; Bonora, G. M., Peptaibol antibiotics: a study on the helical structure of the 2-9 sequence of emerimicins III and IV. *Proc. Natl. Acad. Sci. U. S. A.* **1982,** *79* (24), 7951-7954.
161. Demizu, Y.; Yamagata, N.; Sato, Y.; Doi, M.; Tanaka, M.; Okuda, H.; Kurihara, M., Controlling the helical screw sense of peptides with C-terminal L-valine. *J. Pept. Sci.* **2010,** *16* (3), 153-158.
162. Gessmann, R.; Brückner, H.; Petratos, K., The peptide Z-Aib-Aib-Aib-L-Ala-OtBu. *Acta Crystallogr. C* **2014,** *70* (Pt 4), 405-407.
163. Le Bailly, B. A. F.; Clayden, J., Controlling the sign and magnitude of screw-sense preference from the C-terminus of an achiral helical foldamer. *Chem. Commun.* **2014,** *50* (59), 7949-7952.
164. De Poli, M.; Zawodny, W.; Quinonero, O.; Lorch, M.; Webb, S. J.; Clayden, J., Conformational photoswitching of a synthetic peptide foldamer bound within a phospholipid bilayer. *Science* **2016,** *352* (6285), 575-580.
165. Valle, G.; Crisma, M.; Toniolo, C.; Beisswenger, R.; Rieker, A.; Jung, G., First observation of a helical peptide containing a chiral residue without a preferred screw sense. *J. Am. Chem. Soc.* **1989,** *111* (17), 6828-6833.
166. Demizu, Y.; Doi, M.; Sato, Y.; Tanaka, M.; Okuda, H.; Kurihara, M., Screw-Sense Control of Helical Oligopeptides Containing Equal Amounts of L- and D-Amino Acids. *Chem. Eur. J* **2011,** *17* (40), 11107-11109.
167. Merrifield, R. B., Solid Phase Peptide Synthesis. I. The Synthesis of a Tetrapeptide. *J. Am. Chem. Soc.* **1963,** *85* (14), 2149-2154.
168. van Hest, J. C. M.; Tirrell, D. A., Protein-based materials, toward a new level of structural control. *Chem. Commun.* **2001,** (19), 1897-1904.
169. Kricheldorf, H. R., Polypeptide und 100 Jahre Chemie der α-Aminosäure-N-carboxyanhydride. *Angew. Chem.* **2006,** *118* (35), 5884-5917.
170. Nikos, H.; Iatrou, H.; Pitsikalis, M.; Sakellariou, G., Synthesis of Well-Defined Polypeptide-Based Materials via the Ring-Opening Polymerization of α-Amino Acid N -Carboxyanhydrides. *Chem. Rev.* **2009,** *109*, 5528-78.
171. Deng, C.; Wu, J.; Cheng, R.; Meng, F.; Klok, H.-A.; Zhong, Z., Functional polypeptide and hybrid materials: Precision synthesis via α-amino acid N-carboxyanhydride polymerization and emerging biomedical applications. *Prog. Polym. Sci.* **2014,** *39* (2), 330-364.

172. Lu, H.; Wang, J.; Song, Z.; Yin, L.; Zhang, Y.; Tang, H.; Tu, C.; Lin, Y.; Cheng, J., Recent advances in amino acid N-carboxyanhydrides and synthetic polypeptides: chemistry, self-assembly and biological applications. *Chem. Commun.* **2014,** *50* (2), 139-155.
173. González-Henríquez, C. M.; Sarabia-Vallejos, M. A.; Rodríguez-Hernández, J., Strategies to Fabricate Polypeptide-Based Structures via Ring-Opening Polymerization of N-Carboxyanhydrides. *Polymers* **2017,** *9* (11), 551.
174. Song, Z.; Tan, Z.; Cheng, J., Recent Advances and Future Perspectives of Synthetic Polypeptides from N-Carboxyanhydrides. *Macromolecules* **2019,** *52* (22), 8521-8539.
175. Leuchs, H., Ueber die Glycin-carbonsäure. *Ber. Dtsch. Chem. Ges.* **1906,** *39* (1), 857-861.
176. Leuchs, H.; Manasse, W., Über die Isomerie der Carbäthoxyl-glycyl glycinester. *Ber. Dtsch. Chem. Ges.* **1907,** *40* (3), 3235-3249.
177. Leuchs, H.; Geiger, W., Über die Anhydride von α-Amino-N-carbonsäuren und die von α-Aminosäuren. *Ber. Dtsch. Chem. Ges.* **1908,** *41* (2), 1721-1726.
178. Wessely, F.; Pawloy, H.; Rizzi, W., Untersuchungen über α-Amino-N-carbonsäureanhydride. VII. Über die Umsetzung mit Grignardschen Verbindungen. *Monatsh. Chem. Verw. Teile Anderer Wiss.* **1955,** *86* (1), 75-87.
179. Ben-Ishai, D.; Katchalski, E., Synthesis of N-Carboxy-α-amino Acid Anhydrides from N-Carbalkoxy-α-amino Acids by the Use of Phosphorus Tribromide. *J. Am. Chem. Soc.* **1952,** *74* (14), 3688-3689.
180. Fuchs, F., Über N-Carbonsäure-anhydride. *Ber. Dtsch. Chem. Ges.* **1922,** *55* (9), 2943-2943.
181. Fuller, W. D.; Verlander, M. S.; Goodman, M., A procedure for the facile syntheis of amino-acid N-carboxyanhydrides. *Biopolymers* **1976,** *15* (9), 1869-1871.
182. Smeets, N. M. B.; van der Weide, P. L. J.; Meuldijk, J.; Vekemans, J. A. J. M.; Hulshof, L. A., A Scalable Synthesis of l-Leucine-N-carboxyanhydride. *Org. Process Res. Dev.* **2005,** *9* (6), 757-763.
183. Kramer, J. R.; Deming, T. J., General Method for Purification of α-Amino acid-N-carboxyanhydrides Using Flash Chromatography. *Biomacromolecules* **2010,** *11* (12), 3668-3672.
184. Otake, Y.; Nakamura, H.; Fuse, S., Rapid and Mild Synthesis of Amino Acid N-Carboxy Anhydrides: Basic-to-Acidic Flash Switching in a Microflow Reactor. *Angew. Chem. Int. Ed.* **2018,** *57* (35), 11389-11393.
185. Vacogne, C. D.; Schlaad, H., Controlled ring-opening polymerization of α-amino acid N -carboxyanhydrides in the presence of tertiary amines. *Polymer* **2017,** *124*, 203-209.
186. Deming, T. J., Polypeptide and Polypeptide Hybrid Copolymer Synthesis via NCA Polymerization. In *Peptide Hybrid Polymers*, Klok, H.-A.; Schlaad, H., Eds. Springer Berlin Heidelberg: Berlin, Heidelberg, **2006**; pp 1-18.
187. Habraken, G. J. M.; Wilsens, K. H. R. M.; Koning, C. E.; Heise, A., Optimization of N-carboxyanhydride (NCA) polymerization by variation of reaction temperature and pressure. *Polym. Chem.* **2011,** *2* (6), 1322-1330.
188. Habraken, G. J. M.; Peeters, M.; Dietz, C. H. J. T.; Koning, C. E.; Heise, A., How controlled and versatile is N-carboxy anhydride (NCA) polymerization at 0 °C? Effect of temperature on homo-, block- and graft (co)polymerization. *Polym. Chem.* **2010,** *1* (4), 514-524.
189. Deming, T. J.; Curtin, S. A., Chain Initiation Efficiency in Cobalt- and Nickel-Mediated Polypeptide Synthesis. *J. Am. Chem. Soc.* **2000,** *122* (24), 5710-5717.
190. Dimitrov, I.; Schlaad, H., Synthesis of nearly monodisperse polystyrene–polypeptide block copolymers via polymerisation of N-carboxyanhydrides. *Chem. Commun.* **2003,** (23), 2944-2945.
191. Lu, H.; Cheng, J., Hexamethyldisilazane-Mediated Controlled Polymerization of α-Amino Acid N-Carboxyanhydrides. *J. Am. Chem. Soc.* **2007,** *129* (46), 14114-14115.
192. Zhao, W.; Gnanou, Y.; Hadjichristidis, N., Organocatalysis by hydrogen-bonding: a new approach to controlled/living polymerization of α-amino acid N-carboxyanhydrides. *Polym. Chem.* **2015,** *6* (34), 6193-6201.
193. Deming, T. J., Facile synthesis of block copolypeptides of defined architecture. *Nature* **1997,** *390* (6658), 386-389.

194. Deming, T. J., Cobalt and iron initiators for the controlled polymerization of α-amino acid-N-carboxyanhydrides. *Macromolecules* **1999,** *32* (13), 4500-4502.
195. Goodwin, A. A.; Bu, X.; Deming, T. J., Reactions of α-amino acid-N-carboxyanhydrides (NCAs) with organometallic palladium(0) and platinum(0) compounds: structure of a metallated NCA product and its role in polypeptide synthesis. *J. Organomet. Chem.* **1999,** *589* (1), 111-114.
196. Seidel, S. W.; Deming, T. J., Use of Chiral Ruthenium and Iridium Amido−Sulfonamidate Complexes for Controlled, Enantioselective Polypeptide Synthesis. *Macromolecules* **2003,** *36* (4), 969-972.
197. Gradišar, Š.; Žagar, E.; Pahovnik, D., Ring-Opening Polymerization of N-Carboxyanhydrides Initiated by a Hydroxyl Group. *ACS Macro Let.* **2017,** *6* (6), 637-640.
198. Yuan, J.; Sun, Y.; Wang, J.; Lu, H., Phenyl Trimethylsilyl Sulfide-Mediated Controlled Ring-Opening Polymerization of α-Amino Acid N-Carboxyanhydrides. *Biomacromolecules* **2016,** *17* (3), 891-896.
199. Zhao, W.; Lv, Y.; Li, J.; Feng, Z.; Ni, Y.; Hadjichristidis, N., Fast and selective organocatalytic ring-opening polymerization by fluorinated alcohol without a cocatalyst. *Nat. Commun.* **2019,** *10* (1), 3590.
200. Aliferis, T.; Iatrou, H.; Hadjichristidis, N., Living Polypeptides. *Biomacromolecules* **2004,** *5* (5), 1653-1656.
201. Vayaboury, W.; Giani, O.; Cottet, H.; Deratani, A.; Schué, F., Living Polymerization of α-Amino Acid N-Carboxyanhydrides (NCA) upon Decreasing the Reaction Temperature. *Macromol. Rapid Commun.* **2004,** *25* (13), 1221-1224.
202. Wang, X.; Song, Z.; Tan, Z.; Zhu, L.; Xue, T.; Lv, S.; Fu, Z.; Zheng, X.; Ren, J.; Cheng, J., Facile Synthesis of Helical Multiblock Copolypeptides: Minimal Side Reactions with Accelerated Polymerization of N-Carboxyanhydrides. *ACS Macro Let.* **2019,** *8* (11), 1517-1521.
203. Grazon, C.; Salas-Ambrosio, P.; Ibarboure, E.; Buol, A.; Garanger, E.; Grinstaff, M. W.; Lecommandoux, S.; Bonduelle, C., Aqueous Ring-Opening Polymerization-Induced Self-Assembly (ROPISA) of N-Carboxyanhydrides. *Angew. Chem. Int. Ed.* **2020,** *59* (2), 622-626.
204. Yang, Z.; Bai, T.; Ling, J.; Shen, Y., Hydroxyl-tolerated polymerization of N-phenoxycarbonyl α-amino acids: A simple way to polypeptides bearing hydroxyl groups. *J. Polym. Sci., Part A: Polym. Chem.* **2019,** *57* (8), 907-916.
205. Sun, J.; Schlaad, H., Thiol−Ene Clickable Polypeptides. *Macromolecules* **2010,** *43* (10), 4445-4448.
206. Lu, H.; Bai, Y.; Wang, J.; Gabrielson, N. P.; Wang, F.; Lin, Y.; Cheng, J., Ring-Opening Polymerization of γ-(4-Vinylbenzyl)-(L)-Glutamate N-Carboxyanhydride for the Synthesis of Functional Polypeptides. *Macromolecules* **2011,** *44* (16), 6237-6240.
207. Tang, H.; Zhang, D., Multi-functionalization of helical block copoly(α-peptide)s by orthogonal chemistry. *Polym. Chem.* **2011,** *2* (7), 1542-1551.
208. Zhang, Y.; Lu, H.; Lin, Y.; Cheng, J., Water-Soluble Polypeptides with Elongated, Charged Side Chains Adopt Ultra-Stable Helical Conformations. *Macromolecules* **2011,** *44* (17), 6641-6644.
209. Yan, L.; Yang, L.; He, H.; Hu, X.; Xie, Z.; Huang, Y.; Jing, X., Photo-cross-linked mPEG-poly(γ-cinnamyl-l-glutamate) micelles as stable drug carriers. *Polym. Chem.* **2012,** *3* (5), 1300-1307.
210. Zhou, J.; Chen, P.; Deng, C.; Meng, F.; Cheng, R.; Zhong, Z., A Simple and Versatile Synthetic Strategy to Functional Polypeptides via Vinyl Sulfone-Substituted l-Cysteine N-Carboxyanhydride. *Macromolecules* **2013,** *46* (17), 6723-6730.
211. Xu, Q.; He, C.; Xiao, C.; Yu, S.; Chen, X., ε-Methacryloyl-l-lysine based polypeptides and their thiol–ene click functionalization. *Polym. Chem.* **2015,** *6* (10), 1758-1767.
212. Perlin, P.; Gharakhanian, E. G.; Deming, T. J., Homoallylglycine residues are superior precursors to orthogonally modified thioether containing polypeptides. *Chem. Commun.* **2018,** *54* (48), 6196-6199.
213. Yuan, J.; Zhang, Y.; Sun, Y.; Cai, Z.; Yang, L.; Lu, H., Salt- and pH-Triggered Helix–Coil Transition of Ionic Polypeptides under Physiology Conditions. *Biomacromolecules* **2018,** *19* (6), 2089-2097.

214. Engler, A. C.; Lee, H.-i.; Hammond, P. T., Highly Efficient "Grafting onto" a Polypeptide Backbone Using Click Chemistry. *Angew. Chem. Int. Ed.* **2009,** *48* (49), 9334-9338.
215. Huang, Y.; Zeng, Y.; Yang, J.; Zeng, Z.; Zhu, F.; Chen, X., Facile functionalization of polypeptides by thiol-yne photochemistry for biomimetic materials synthesis. *Chem. Commun.* **2011,** *47* (26), 7509-7511.
216. Krannig, K.-S.; Huang, J.; Heise, A.; Schlaad, H., Photochemical thiol–yne functionalization of polypeptide scaffolds. *Polym. Chem.* **2013,** *4* (14), 3981-3986.
217. Zhang, R.; Zheng, N.; Song, Z.; Yin, L.; Cheng, J., The effect of side-chain functionality and hydrophobicity on the gene delivery capabilities of cationic helical polypeptides. *Biomaterials* **2014,** *35* (10), 3443-3454.
218. Liu, W.; Zhu, M.; Xiao, J.; Ling, Y.; Tang, H., Synthesis and UCST-type phase behavior of polypeptide with alkyl side-chains in alcohol or ethanol/water solvent mixtures. *J. Polym. Sci., Part A: Polym. Chem.* **2016,** *54* (21), 3425-3435.
219. Rhodes, A. J.; Deming, T. J., Soluble, Clickable Polypeptides from Azide-Containing N-Carboxyanhydride Monomers. *ACS Macro Let.* **2013,** *2* (5), 351-354.
220. Habraken, G. J. M.; Koning, C. E.; Heuts, J. P. A.; Heise, A., Thiol chemistry on well-defined synthetic polypeptides. *Chem. Commun.* **2009,** (24), 3612-3614.
221. Kramer, J. R.; Deming, T. J., Preparation of Multifunctional and Multireactive Polypeptides via Methionine Alkylation. *Biomacromolecules* **2012,** *13* (6), 1719-1723.
222. Gharakhanian, E. G.; Deming, T. J., Versatile Synthesis of Stable, Functional Polypeptides via Reaction with Epoxides. *Biomacromolecules* **2015,** *16* (6), 1802-1806.
223. Gharakhanian, E. G.; Bahrun, E.; Deming, T. J., Influence of Sulfoxide Group Placement on Polypeptide Conformational Stability. *J. Am. Chem. Soc.* **2019,** *141* (37), 14530-14533.
224. Wu, G.; Ge, C.; Liu, X.; Wang, S.; Wang, L.; Yin, L.; Lu, H., Synthesis of water soluble and multi-responsive selenopolypeptides via ring-opening polymerization of N-carboxyanhydrides. *Chem. Commun.* **2019,** *55* (54), 7860-7863.
225. Ishikawa, K.; Endo, T., Synthesis and polymerization of .gamma.-trichloroethyl-L-glutamate N-carboxyanhydride: a polypeptide that can be functionalized with a nucleophilic agent. *J. Am. Chem. Soc.* **1988,** *110* (6), 2016-2017.
226. Tang, H.; Zhang, D., General Route toward Side-Chain-Functionalized α-Helical Polypeptides. *Biomacromolecules* **2010,** *11* (6), 1585-1592.
227. Ding, J.; Xiao, C.; Tang, Z.; Zhuang, X.; Chen, X., Highly Efficient "Grafting From" an α-Helical Polypeptide Backbone by Atom Transfer Radical Polymerization. *Macromol. Biosci.* **2011,** *11* (2), 192-198.
228. Liu, Y.; Chen, P.; Li, Z., Molecular Bottlebrushes with Polypeptide Backbone Prepared via Ring-Opening Polymerization of NCA and ATRP. *Macromol. Rapid Commun.* **2012,** *33* (4), 287-295.
229. Song, Z.; Zheng, N.; Ba, X.; Yin, L.; Zhang, R.; Ma, L.; Cheng, J., Polypeptides with Quaternary Phosphonium Side Chains: Synthesis, Characterization, and Cell-Penetrating Properties. *Biomacromolecules* **2014,** *15* (4), 1491-1497.
230. Deng, Y.; Xu, Y.; Wang, X.; Yuan, Q.; Ling, Y.; Tang, H., Water-Soluble Thermoresponsive α-Helical Polypeptide with an Upper Critical Solution Temperature: Synthesis, Characterization, and Thermoresponsive Phase Transition Behaviors. *Macromol. Rapid Commun.* **2015,** *36* (5), 453-458.
231. Ding, J.; Xiao, C.; He, C.; Li, M.; Li, D.; Zhuang, X.; Chen, X., Facile preparation of a cationic poly(amino acid) vesicle for potential drug and gene co-delivery. *Nanotechnology* **2011,** *22* (49), 494012.
232. Chen, C.; Wang, Z.; Li, Z., Thermoresponsive Polypeptides from Pegylated Poly-l-glutamates. *Biomacromolecules* **2011,** *12* (8), 2859-2863.
233. Liao, Y.; Dong, C.-M., Synthesis, conformation transition, liquid crystal phase, and self-assembled morphology of thermosensitive homopolypeptide. *J. Polym. Sci., Part A: Polym. Chem.* **2012,** *50* (9), 1834-1843.
234. Cheng, Y.; He, C.; Xiao, C.; Ding, J.; Zhuang, X.; Chen, X., Versatile synthesis of temperature-sensitive polypeptides by click grafting of oligo(ethylene glycol). *Polym. Chem.* **2011,** *2* (11), 2627-2634.

235. Tang, H.; Li, Y.; Lahasky, S. H.; Sheiko, S. S.; Zhang, D., Core−Shell Molecular Bottlebrushes with Helical Polypeptide Backbone: Synthesis, Characterization, and Solution Conformations. *Macromolecules* **2011,** *44* (6), 1491-1499.
236. Cho, C. S.; Nah, J. W.; Jeong, Y. I.; Cheon, J. B.; Asayama, S.; Ise, H.; Akaike, T., Conformational transition of nanoparticles composed of poly(γ-benzyl l-glutamate) as the core and poly(ethylene oxide) as the shell. *Polymer* **1999,** *40* (24), 6769-6775.
237. Lutz, J.-F.; Schütt, D.; Kubowicz, S., Preparation of Well-Defined Diblock Copolymers with Short Polypeptide Segments by Polymerization of N-Carboxy Anhydrides. *Macromol. Rapid Commun.* **2005,** *26* (1), 23-28.
238. Cho, C.-S.; Kim, S.-W.; Komoto, T., Synthesis and structural study of an ABA block copolymer consisting of poly(γ-benzyl L-glutamate) as the a block and poly(ethylene oxide) as the B block. *Makromol. Chem.* **1990,** *191* (4), 981-991.
239. Tsutsumiuchi, K.; Aoi, K.; Okada, M., Synthesis of Polyoxazoline−(Glyco)peptide Block Copolymers by Ring-Opening Polymerization of (Sugar-Substituted) α-Amino Acid N-Carboxyanhydrides with Polyoxazoline Macroinitiators. *Macromolecules* **1997,** *30* (14), 4013-4017.
240. Lee, H.-F.; Sheu, H.-S.; Jeng, U. S.; Huang, C.-F.; Chang, F.-C., Preparation and Supramolecular Self-Assembly of a Polypeptide-block-polypseudorotaxane. *Macromolecules* **2005,** *38* (15), 6551-6558.
241. Caillol, S.; Lecommandoux, S.; Mingotaud, A.-F.; Schappacher, M.; Soum, A.; Bryson, N.; Meyrueix, R., Synthesis and Self-Assembly Properties of Peptide−Polylactide Block Copolymers. *Macromolecules* **2003,** *36* (4), 1118-1124.
242. Degée, P.; Dubois, P.; Jérôme, R.; Teyssié, P., Synthesis and characterization of biocompatible and biodegradable poly(ϵ-caprolactone-b-γ-benzylglutamate) diblock copolymers. *J. Polym. Sci., Part A: Polym. Chem.* **1993,** *31* (1), 275-278.
243. Rong, G.; Deng, M.; Deng, C.; Tang, Z.; Piao, L.; Chen, X.; Jing, X., Synthesis of Poly(ε-caprolactone)-b-Poly(γ-benzyl-l-glutamic acid) Block Copolymer Using Amino Organic Calcium Catalyst. *Biomacromolecules* **2003,** *4* (6), 1800-1804.
244. Kricheldorf, H. R.; Hauser, K., Polylactones. 55. A−B−A Triblock Copolymers of Various Polypeptides. Syntheses Involving 4-Aminobenzoyl-Terminated Poly(ε-caprolactone) as B Block. *Biomacromolecules* **2001,** *2* (4), 1110-1115.
245. Cheon, J.-B.; Jeong, Y.-I.; Cho, C.-S., Effects of temperature on diblock copolymer micelle composed of poly(γ-benzyl L-glutamate) and poly(N-isopropylacrylamide). *Polymer* **1999,** *40* (8), 2041-2050.
246. Klok, H.-A.; Langenwalter, J. F.; Lecommandoux, S., Self-Assembly of Peptide-Based Diblock Oligomers. *Macromolecules* **2000,** *33* (21), 7819-7826.
247. Williams, A. J.; Gupta, V. K., Self-Assembly of a Rodlike Polypeptide on Solid Surfaces: Role of Solvent, Molecular Weight, and Time of Assembly. *J. Phys. Chem. B* **2001,** *105* (22), 5223-5230.
248. Williams, A.; Gupta, V., Structure and formation of self-assembled monolayers of helical poly (γ-benzyl L-glutamate) by surface plasmon resonance and infrared spectroscopy. *Thin Solid Films* **2003,** *423*, 228-234.
249. Klok, H.-A.; Hernández, J. R.; Becker, S.; Müllen, K., Star-shaped fluorescent polypeptides. *J. Polym. Sci., Part A: Polym. Chem.* **2001,** *39* (10), 1572-1583.
250. Steig, S.; Cornelius, F.; Witte, P.; Staal, B. B. P.; Koning, C. E.; Heise, A.; Menzel, H., Synthesis of polypeptide based rod–coil block copolymers. *Chem. Commun.* **2005,** (43), 5420-5422.
251. Habraken, G. J. M.; Koning, C. E.; Heise, A., Peptide block copolymers by N-carboxyanhydride ring-opening polymerization and atom transfer radical polymerization: The effect of amide macroinitiators. *J. Polym. Sci., Part A: Polym. Chem.* **2009,** *47* (24), 6883-6893.
252. Zhang, X.; Li, J.; Li, W.; Zhang, A., Synthesis and Characterization of Thermo- and pH-Responsive Double-Hydrophilic Diblock Copolypeptides. *Biomacromolecules* **2007,** *8* (11), 3557-3567.
253. Audouin, F.; Knoop, R. J. I.; Huang, J.; Heise, A., Star polymers by cross-linking of linear poly(benzyl-L-glutamate) macromonomers via free-radical and RAFT polymerization. A

simple route toward peptide-stabilized nanoparticles. *J. Polym. Sci., Part A: Polym. Chem.* **2010,** *48* (20), 4602-4610.
254. Knoop, R. J. I.; Habraken, G. J. M.; Gogibus, N.; Steig, S.; Menzel, H.; Koning, C. E.; Heise, A., Synthesis of poly(benzyl glutamate-b-styrene) rod-coil block copolymers by dual initiation in one pot. *J. Polym. Sci., Part A: Polym. Chem.* **2008,** *46* (9), 3068-3077.
255. Agut, W.; Taton, D.; Lecommandoux, S., A Versatile Synthetic Approach to Polypeptide Based Rod−Coil Block Copolymers by Click Chemistry. *Macromolecules* **2007,** *40* (16), 5653-5661.
256. Agut, W.; Brûlet, A.; Schatz, C.; Taton, D.; Lecommandoux, S., pH and Temperature Responsive Polymeric Micelles and Polymersomes by Self-Assembly of Poly[2-(dimethylamino)ethyl methacrylate]-b-Poly(glutamic acid) Double Hydrophilic Block Copolymers. *Langmuir* **2010,** *26* (13), 10546-10554.
257. Lu, H.; Cheng, J., N-Trimethylsilyl Amines for Controlled Ring-Opening Polymerization of Amino Acid N-Carboxyanhydrides and Facile End Group Functionalization of Polypeptides. *J. Am. Chem. Soc.* **2008,** *130* (38), 12562-12563.
258. Brzezinska, K. R.; Curtin, S. A.; Deming, T. J., Polypeptide End-Capping Using Functionalized Isocyanates: Preparation of Pentablock Copolymers. *Macromolecules* **2002,** *35* (8), 2970-2976.
259. Kros, A.; Jesse, W.; Metselaar, G. A.; Cornelissen, J. J. L. M., Synthesis and Self-Assembly of Rod–Rod Hybrid Poly(γ-benzyl L-glutamate)-block-Polyisocyanide Copolymers. *Angew. Chem. Int. Ed.* **2005,** *44* (28), 4349-4352.
260. Deng, C.; Rong, G.; Tian, H.; Tang, Z.; Chen, X.; Jing, X., Synthesis and characterization of poly(ethylene glycol)-b-poly (l-lactide)-b-poly(l-glutamic acid) triblock copolymer. *Polymer* **2005,** *46* (3), 653-659.
261. Arimura, H.; Ohya, Y.; Ouchi, T., The Formation of Biodegradable Polymeric Micelles from Newly Synthesized Poly(aspartic acid)-block-Polylactide AB-Type Diblock Copolymers. *Macromol. Rapid Commun.* **2004,** *25* (6), 743-747.
262. Kong, X.; Jenekhe, S. A., Block Copolymers Containing Conjugated Polymer and Polypeptide Sequences: Synthesis and Self-Assembly of Electroactive and Photoactive Nanostructures. *Macromolecules* **2004,** *37* (22), 8180-8183.
263. Karatzas, A.; Iatrou, H.; Hadjichristidis, N.; Inoue, K.; Sugiyama, K.; Hirao, A., Complex Macromolecular Chimeras. *Biomacromolecules* **2008,** *9* (7), 2072-2080.
264. Kim, K. T.; Vandermeulen, G. W. M.; Winnik, M. A.; Manners, I., Organometallic−Polypeptide Block Copolymers: Synthesis and Properties of Poly(ferrocenyldimethylsilane)-b-poly- (γ-benzyl-l-glutamate). *Macromolecules* **2005,** *38* (12), 4958-4961.
265. Li, H.; Caire da Silva, L.; Schulz, M. D.; Rojas, G.; Wagener, K. B., A review of how to do an acyclic diene metathesis reaction. *Polym. Int.* **2017,** *66* (1), 7-12.
266. Atallah, P.; Wagener, K. B.; Schulz, M. D., ADMET: The Future Revealed. *Macromolecules* **2013,** *46* (12), 4735-4741.
267. Mutlu, H.; de Espinosa, L. M.; Meier, M. A. R., Acyclic diene metathesis: a versatile tool for the construction of defined polymer architectures. *Chem. Soc. Rev.* **2011,** *40* (3), 1404-1445.
268. Leonard, J. K.; Hopkins, T. E.; Chaffin, K.; Wagener, K. B., Semicrystalline Lysine Functionalized Precision Polyolefins. *Macromol. Chem. Phys.* **2008,** *209* (14), 1485-1494.
269. Bléger, D.; Schwarz, J.; Brouwer, A. M.; Hecht, S., o-Fluoroazobenzenes as Readily Synthesized Photoswitches Offering Nearly Quantitative Two-Way Isomerization with Visible Light. *J. Am. Chem. Soc.* **2012,** *134* (51), 20597-20600.
270. Lambert, K. M.; Bobbitt, J. M.; Eldirany, S. A.; Kissane, L. E.; Sheridan, R. K.; Stempel, Z. D.; Sternberg, F. H.; Bailey, W. F., Metal-Free Oxidation of Primary Amines to Nitriles through Coupled Catalytic Cycles. *Chem. Eur. J* **2016,** *22* (15), 5156-5159.
271. Petkovska, V. I.; Hopkins, T. E.; Powell, D. H.; Wagener, K. B., Functionality Dependent Olefin Activity in Acyclic Diene Metathesis Polymerization: Mass Spectrometry Characterization of Amino Acid Functionalized Olefins. *Anal. Chem.* **2006,** *78* (11), 3624-3631.

272. Courchay, F. C.; Sworen, J. C.; Ghiviriga, I.; Abboud, K. A.; Wagener, K. B., Understanding Structural Isomerization during Ruthenium-Catalyzed Olefin Metathesis: A Deuterium Labeling Study. *Organometallics* **2006,** *25* (26), 6074-6086.
273. Lehman, S. E.; Wagener, K. B., Comparison of the Kinetics of Acyclic Diene Metathesis Promoted by Grubbs Ruthenium Olefin Metathesis Catalysts. *Macromolecules* **2002,** *35* (1), 48-53.
274. Schrodi, Y., Evolution and applications of second-generation ruthenium olefin metathesis catalysts. *Aldrichim. Acta* **2007,** *40* (2), 45.
275. Kobayashi, S.; Pitet, L. M.; Hillmyer, M. A., Regio- and Stereoselective Ring-Opening Metathesis Polymerization of 3-Substituted Cyclooctenes. *J. Am. Chem. Soc.* **2011,** *133* (15), 5794-5797.
276. Li, Z.-L.; Li, L.; Deng, X.-X.; Zhang, L.-J.; Dong, B.-T.; Du, F.-S.; Li, Z.-C., Periodic Vinyl Copolymers Containing γ-Butyrolactone via ADMET Polymerization of Designed Diene Monomers with Built-in Sequence. *Macromolecules* **2012,** *45* (11), 4590-4598.
277. Berda, E. B.; Wagener, K. B., Inducing Pendant Group Interactions in Precision Polyolefins: Synthesis and Thermal Behavior. *Macromolecules* **2008,** *41* (14), 5116-5122.
278. Reimann, S.; Baumeister, U.; Binder, W. H., Macromol. Chem. Phys. 20/2014. *Macromol. Chem. Phys.* **2014,** *215* (20), 1929-1929.
279. Petkovska, V. I.; Hopkins, T. E.; Powell, D. H.; Wagener, K. B., MALDI-TOF Detection of Olefin Structural Isomerization in Metathesis Chemistry. *Macromolecules* **2005,** *38* (14), 5878-5885.
280. Song, S.; Miao, W.; Wang, Z.; Gong, D.; Chen, Z.-R., Synthesis and characterization of precisely-defined ethylene-co-aryl ether polymers via ADMET polymerization. *Polymer* **2015,** *64*, 76-83.
281. Song, S.-F.; Guo, Y.-T.; Wang, R.-Y.; Fu, Z.-S.; Xu, J.-T.; Fan, Z.-Q., Synthesis and Crystallization Behavior of Equisequential ADMET Polyethylene Containing Arylene Ether Defects: Remarkable Effects of Substitution Position and Arylene Size. *Macromolecules* **2016,** *49* (16), 6001-6011.
282. Rojas, G.; Inci, B.; Wei, Y.; Wagener, K. B., Precision Polyethylene: Changes in Morphology as a Function of Alkyl Branch Size. *J. Am. Chem. Soc.* **2009,** *131* (47), 17376-17386.
283. Zheng, Y.-R.; Tee, H. T.; Wei, Y.; Wu, X.-L.; Mezger, M.; Yan, S.; Landfester, K.; Wagener, K.; Wurm, F. R.; Lieberwirth, I., Morphology and Thermal Properties of Precision Polymers: The Crystallization of Butyl Branched Polyethylene and Polyphosphoesters. *Macromolecules* **2016,** *49* (4), 1321-1330.
284. Gaines, T. W.; Trigg, E. B.; Winey, K. I.; Wagener, K. B., High Melting Precision Sulfone Polyethylenes Synthesized by ADMET Chemistry. *Macromol. Chem. Phys.* **2016,** *217* (21), 2351-2359.
285. Reimann, S.; Danke, V.; Beiner, M.; Binder, W. H., Synthesis of supramolecular precision polymers: Crystallization under conformational constraints. *J. Polym. Sci., Part A: Polym. Chem.* **2017,** *55* (22), 3736-3748.
286. Butler, M. F.; Donald, A. M.; Bras, W.; Mant, G. R.; Derbyshire, G. E.; Ryan, A. J., A Real-Time Simultaneous Small- and Wide-Angle X-ray Scattering Study of In-Situ Deformation of Isotropic Polyethylene. *Macromolecules* **1995,** *28* (19), 6383-6393.
287. Inci, B.; Lieberwirth, I.; Steffen, W.; Mezger, M.; Graf, R.; Landfester, K.; Wagener, K. B., Decreasing the Alkyl Branch Frequency in Precision Polyethylene: Effect of Alkyl Branch Size on Nanoscale Morphology. *Macromolecules* **2012,** *45* (8), 3367-3376.
288. Alamo, R. G.; Jeon, K.; Smith, R. L.; Boz, E.; Wagener, K. B.; Bockstaller, M. R., Crystallization of Polyethylenes Containing Chlorines: Precise vs Random Placement. *Macromolecules* **2008,** *41* (19), 7141-7151.
289. Vacogne, C. D.; Schlaad, H., Controlled ring-opening polymerization of α-amino acid N-carboxyanhydrides in the presence of tertiary amines. *Polymer* **2017,** *124*, 203-209.
290. Habraken, G. J. M.; Wilsens, K. H. R. M.; Koning, C. E.; Heise, A., Optimization of N-carboxyanhydride (NCA) polymerization by variation of reaction temperature and pressure. *Polym. Chem.* **2011,** *2* (6), 1322.

291. Baughman, T. W.; Wagener, K. B., Recent Advances in ADMET Polymerization. *Adv. Polym. Sci* **2005,** *176*, 1-42.
292. Schulz, M. D.; Wagener, K. B., Solvent Effects in Alternating ADMET Polymerization. *ACS Macro Lett.* **2012,** *1* (4), 449-451.
293. Kirkham, S.; Castelletto, V.; Hamley, I. W.; Reza, M.; Ruokolainen, J.; Hermida-Merino, D.; Bilalis, P.; Iatrou, H., Self-Assembly of Telechelic Tyrosine End-Capped PEO and Poly(alanine) Polymers in Aqueous Solution. *Biomacromolecules* **2016,** *17* (3), 1186-1197.
294. Papadopoulos, P.; Floudas, G.; Klok, H. A.; Schnell, I.; Pakula, T., Self-Assembly and Dynamics of Poly(γ-benzyl-l-glutamate) Peptides. *Biomacromolecules* **2004,** *5* (1), 81-91.
295. Kung, V. M.; Cornilescu, G.; Gellman, S. H., Impact of Strand Number on Parallel β-Sheet Stability. *Angew. Chem. Int. Ed.* **2015,** *54* (48), 14336-14339.
296. Matolyak, L. E.; Keum, J. K.; Van de Voorde, K. M.; Korley, L. T. J., Synthetic approach to tailored physical associations in peptide-polyurea/polyurethane hybrids. *Org. Biomol. Chem.* **2017,** *15* (36), 7607-7617.
297. Johnson, J. C.; Wanasekara, N. D.; Korley, L. T. J., Influence of secondary structure and hydrogen-bonding arrangement on the mechanical properties of peptidic-polyurea hybrids. *J. Mater. Chem. B* **2014,** *2* (17), 2554.
298. Bradbury, E. M.; Brown, L.; Downie, A. R.; Elliott, A.; Fraser, R. D. B.; Hanby, W. E., The structure of the ω-form of poly-β-benzyl-L-aspartate. *J. Mol. Biol.* **1962,** *5* (2), 230-IN3.
299. Sasaki, S.; Yasumoto, Y.; Uematsu, I., .pi.-Helical conformation of poly(.beta.-phenethyl L-aspartate). *Macromolecules* **1981,** *14* (6), 1797-1801.
300. Venkatraman, J.; Shankaramma, S. C.; Balaram, P., Design of Folded Peptides. *Chem. Rev.* **2001,** *101* (10), 3131-3152.
301. Buck, M., Trifluoroethanol and colleagues: cosolvents come of age. Recent studies with peptides and proteins. *Q Rev Biophys* **1998,** *31* (3), 297-355.
302. Pu, M.; Hara, M., Effects of ionic group incorporation into model polypeptide, poly(γ-benzyl-L-glutamate) (PBLG). *Polymer* **2014,** *55* (19), 4890-4898.
303. Sekiguchi, H.; Froyerd, G., Anionic polymerization mechanism of n-carboxy-α-amino acid anhydrides. *J. Polym. Sci.* **1975,** *52* (1), 157-171.
304. Ueda, A.; Oba, M.; Izumi, Y.; Sueyoshi, Y.; Doi, M.; Demizu, Y.; Kurihara, M.; Tanaka, M., Helical structures of homo-chiral isotope-labeled α-aminoisobutyric acid peptides. *Tetrahedron* **2016,** *72* (39), 5864-5871.
305. Hopkins, T. E.; Wagener, K. B., Amino Acid and Dipeptide Functionalized Polyolefins. *Macromolecules* **2003,** *36* (7), 2206-2214.
306. Grant, N. H.; Clark, D. E.; Alburn, H. E., Accelerated Polymerization of N-Carboxyamino Acid Anhydrides in Frozen Dioxane1. *J. Am. Chem. Soc.* **1966,** *88* (17), 4071-4074.
307. Li, X.-C.; Hu, C.-S.; Li, H.-J.; Li, P.-Y.; Haleem, A.; He, W.-D., Ring-opening cryo-polymerization of N-carboxy-α-amino acid anhydride of γ-benzyl l-Glutamate. *Polymer* **2018,** *151*, 1-5.
308. Strambini, G. B.; Gabellieri, E., Proteins in frozen solutions: evidence of ice-induced partial unfolding. *Biophys. J.* **1996,** *70* (2), 971-976.
309. Kricheldorf, H. R.; von Lossow, C.; Schwarz, G., Primary Amine-Initiated Polymerizations of Alanine-NCA and Sarcosine-NCA. *Macromol. Chem. Phys.* **2004,** *205* (7), 918-924.
310. Muto, K.; Yoshida, R.; Yashida, R.; Ishii, T.; Handa, T., Circular dichroism of the backbone and side chains separated from natural circular dichroism of poly-L-tryptophan by the fluorescence detected circular dichroism method. *J. Am. Chem. Soc.* **1986,** *108* (20), 6416-6417.
311. Li, Q.; Green, L.; Venkataraman, N.; Shiyanovskaya, I.; Khan, A.; Urbas, A.; Doane, J. W., Reversible Photoswitchable Axially Chiral Dopants with High Helical Twisting Power. *J. Am. Chem. Soc.* **2007,** *129* (43), 12908-12909.
312. Antoine John, A.; Lin, Q., Synthesis of Azobenzenes Using N-Chlorosuccinimide and 1,8-Diazabicyclo[5.4.0]undec-7-ene (DBU). *J. Org. Chem.* **2017,** *82* (18), 9873-9876.
313. Iamsaard, S.; Anger, E.; Aßhoff, S. J.; Depauw, A.; Fletcher, S. P.; Katsonis, N., Fluorinated Azobenzenes for Shape-Persistent Liquid Crystal Polymer Networks. *Angew. Chem. Int. Ed.* **2016,** *55* (34), 9908-9912.

314. Ding, L.; Zhang, L.; Han, H.; Huang, W.; Song, C.; Xie, M.; Zhang, Y., Hyperbranched Azo-Polymers Synthesized by Acyclic Diene Metathesis Polymerization of an AB2 Monomer. *Macromolecules* **2009,** *42* (14), 5036-5042.
315. Ding, L.; Zhang, P.; Fu, C.; Yin, J.; Mao, Y.; Liu, N.; Li, S.; Yang, C.; Zhao, R.; Deng, K., Synthesis of Temperature and Light Sensitive Copolymers with Controlled Aggregation during Phase Transitions. *Macromol. Chem. Phys.* **2019,** *220* (22), 1900349.
316. Norikane, Y.; Katoh, R.; Tamaoki, N., Unconventional thermodynamically stable cis isomer and trans to cis thermal isomerization in reversibly photoresponsive [0.0](3,3′)-azobenzenophane. *Chem. Commun.* **2008,** (16), 1898-1900.
317. Patton, D.; Park, M.-K.; Wang, S.; Advincula, R. C., Evanescent Waveguide and Photochemical Characterization of Azobenzene-Functionalized Dendrimer Ultrathin Films. *Langmuir* **2002,** *18* (5), 1688-1694.
318. Kusukawa, T.; Fujita, M., "Ship-in-a-Bottle" Formation of Stable Hydrophobic Dimers of cis-Azobenzene and -Stilbene Derivatives in a Self-Assembled Coordination Nanocage. *J. Am. Chem. Soc.* **1999,** *121* (6), 1397-1398.
319. Ulkoski, D.; Meister, A.; Busse, K.; Kressler, J.; Scholz, C., Synthesis and structure formation of block copolymers of poly(ethylene glycol) with homopolymers and copolymers of l-glutamic acid γ-benzyl ester and l-leucine in water. *Colloid Polym. Sci.* **2015,** *293* (8), 2147-2155.

7 Appendix

S1. – S15. Characterization of N-terminus functionalized monomers 1a – 1e

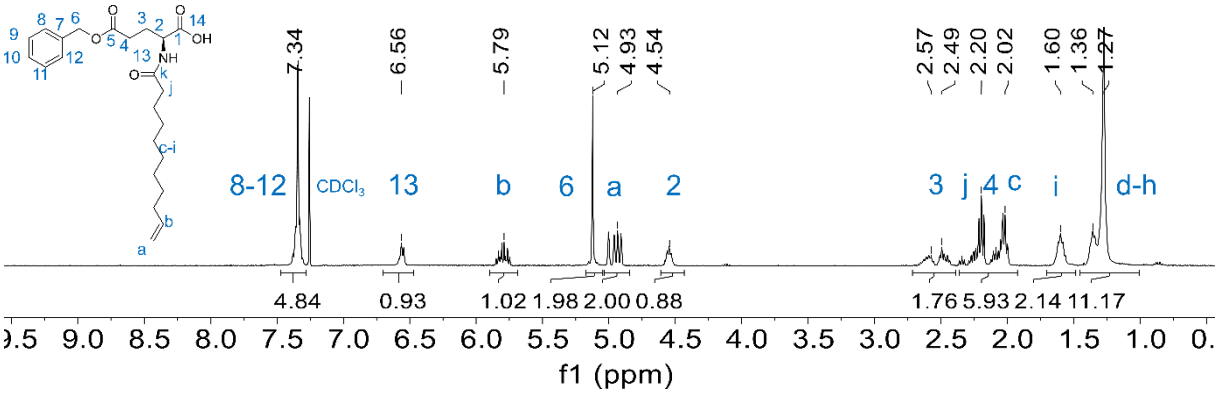

Figure S1. [1]H-NMR spectrum of **1a**.

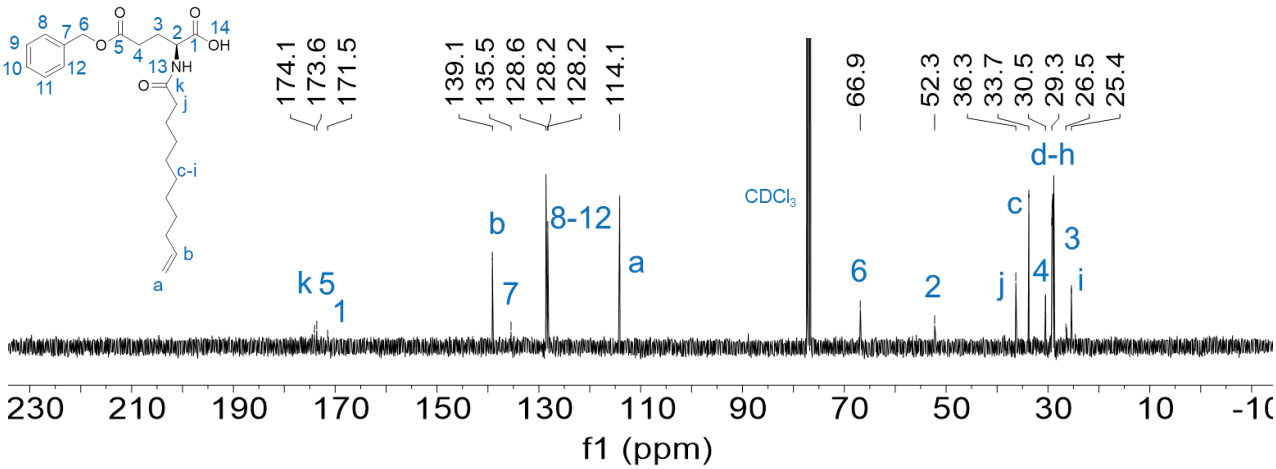

Figure S2. [13]C-NMR spectrum of **1a.**

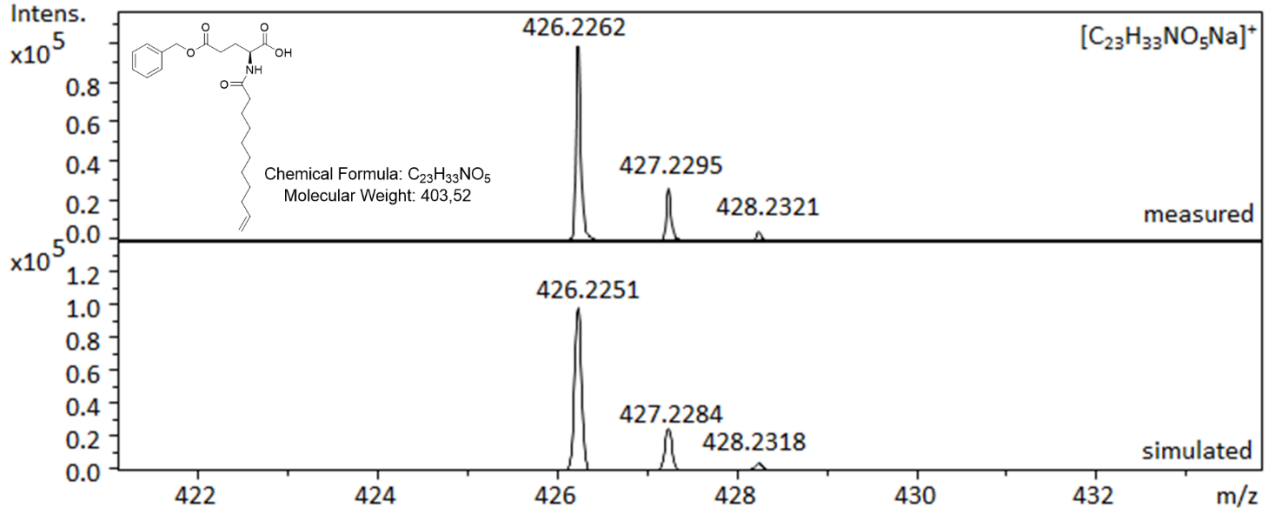

Figure S3. ESI-TOF-MS spectrum of **1a**.

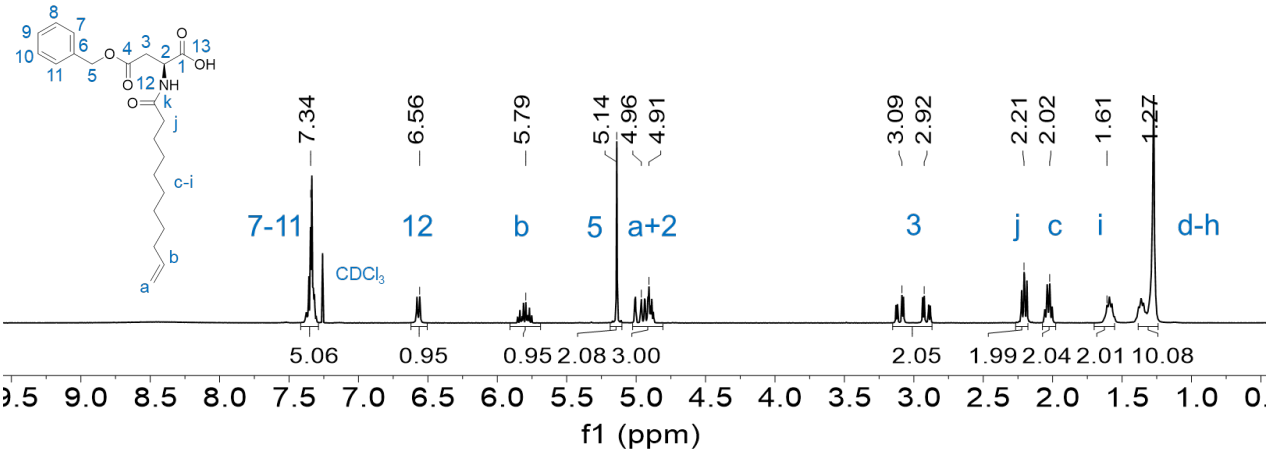

Figure S4. [1]H-NMR spectrum of **1b**.

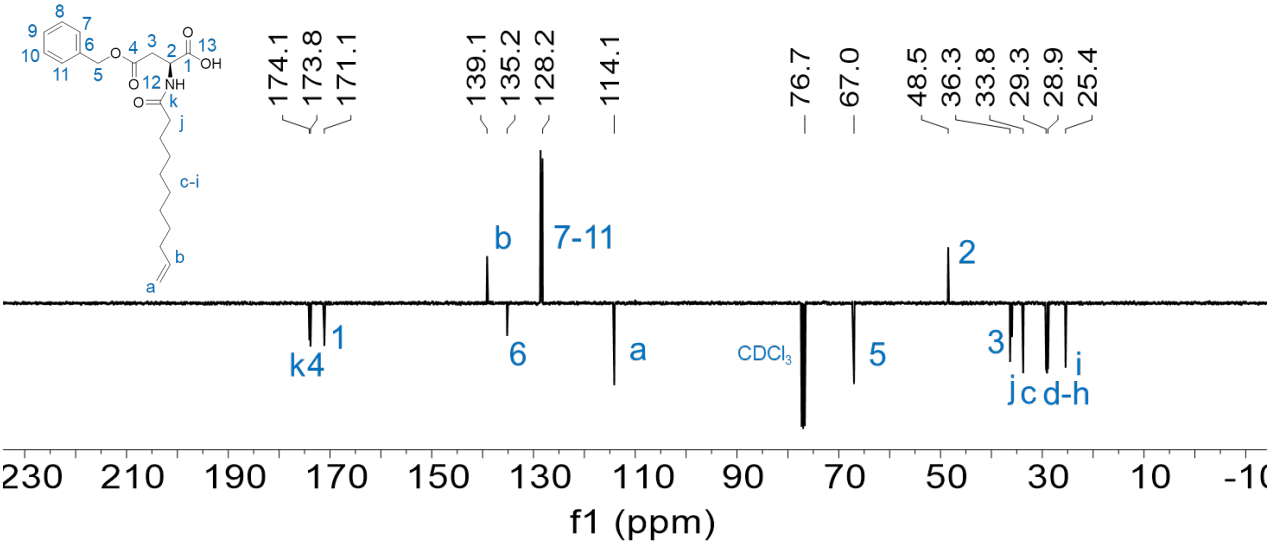

Figure S5. [13]C-APT spectrum of **1b**.

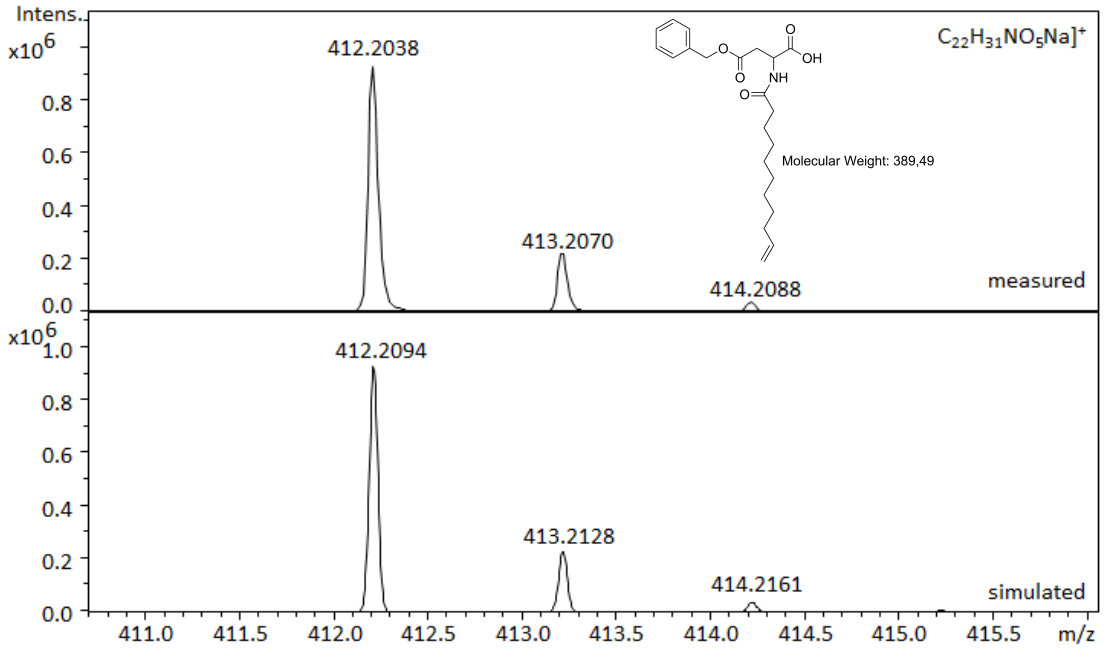

Figure S6. ESI-TOF-MS spectrum of **1b**.

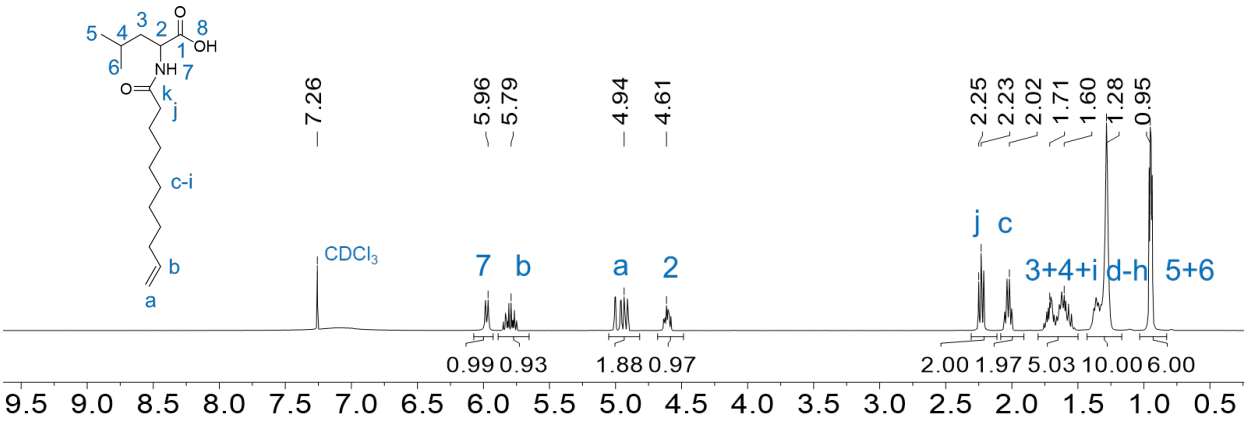

Figure S7. [1]H-NMR spectrum of **1c**.

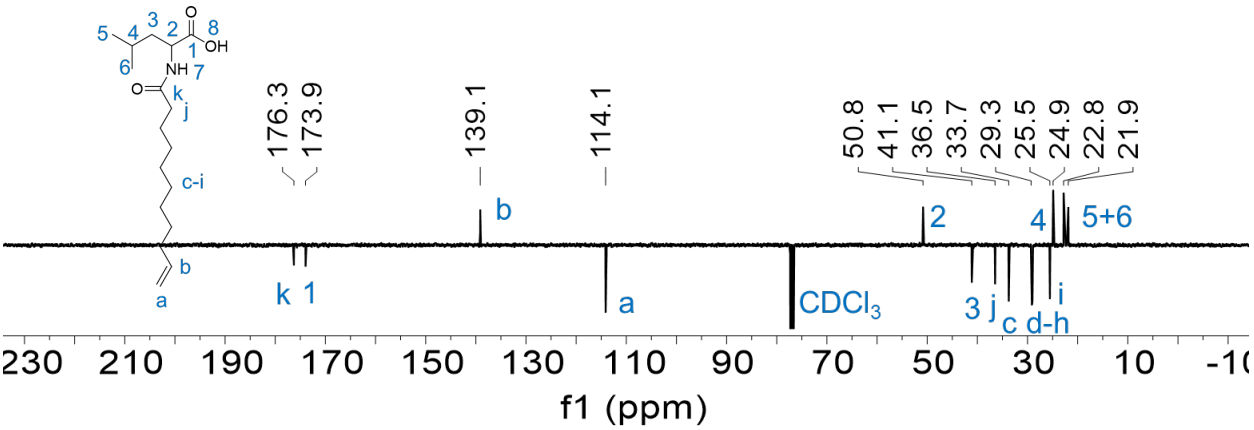

Figure S8. [13]C-APT spectrum of **1c**.

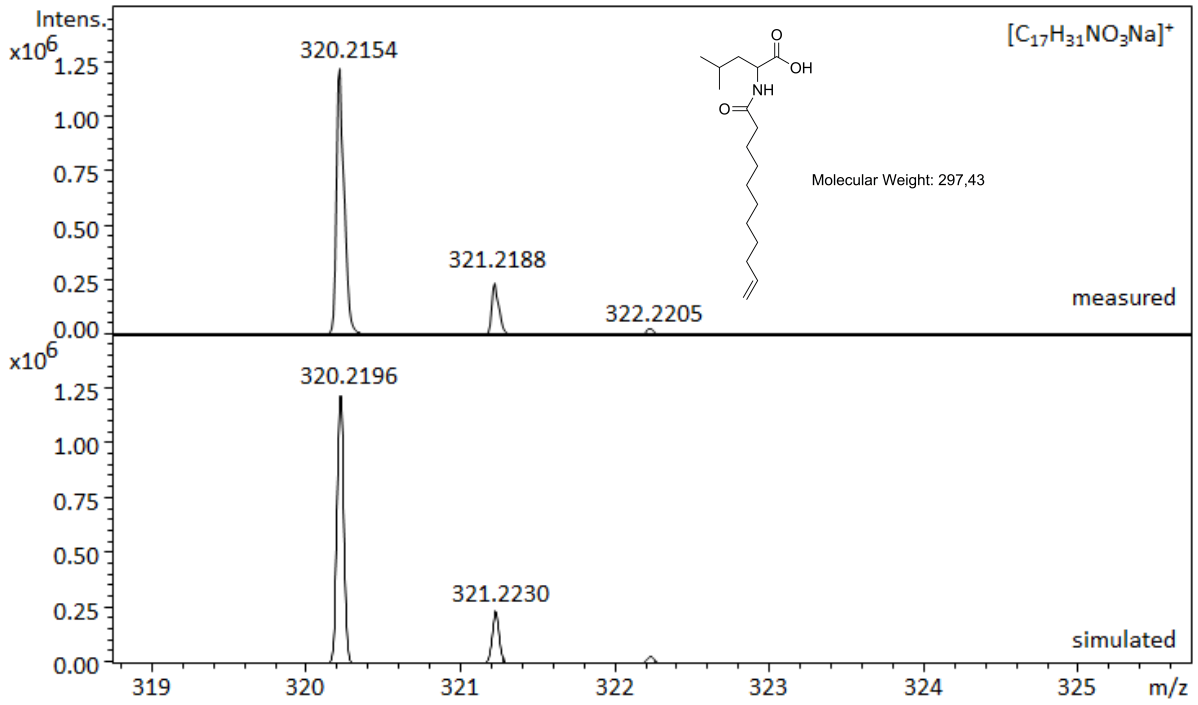

Figure S9. ESI-TOF-MS spectrum of **1c**.

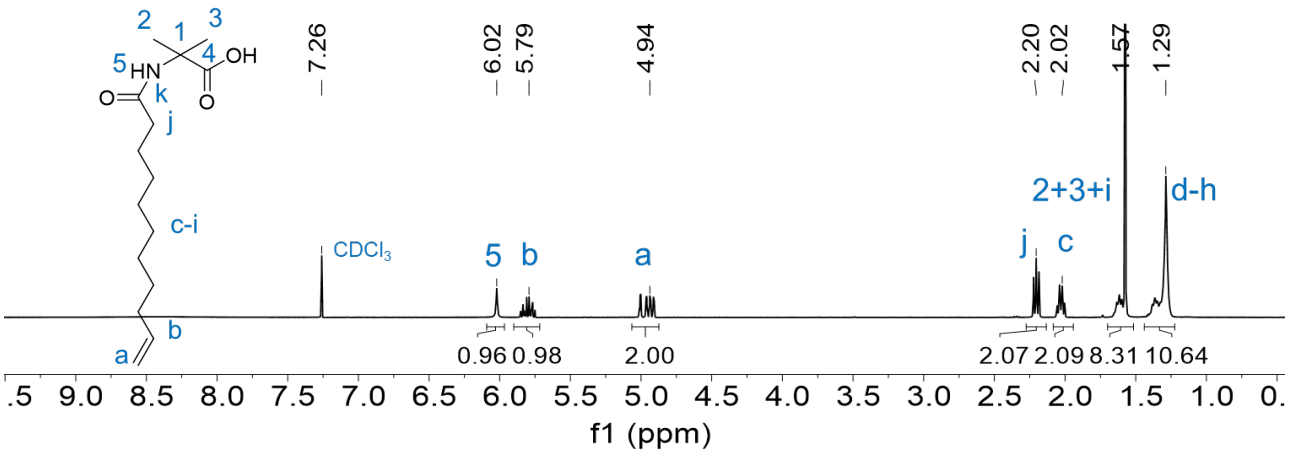

Figure S10. [1]H-NMR spectrum of **1d**.

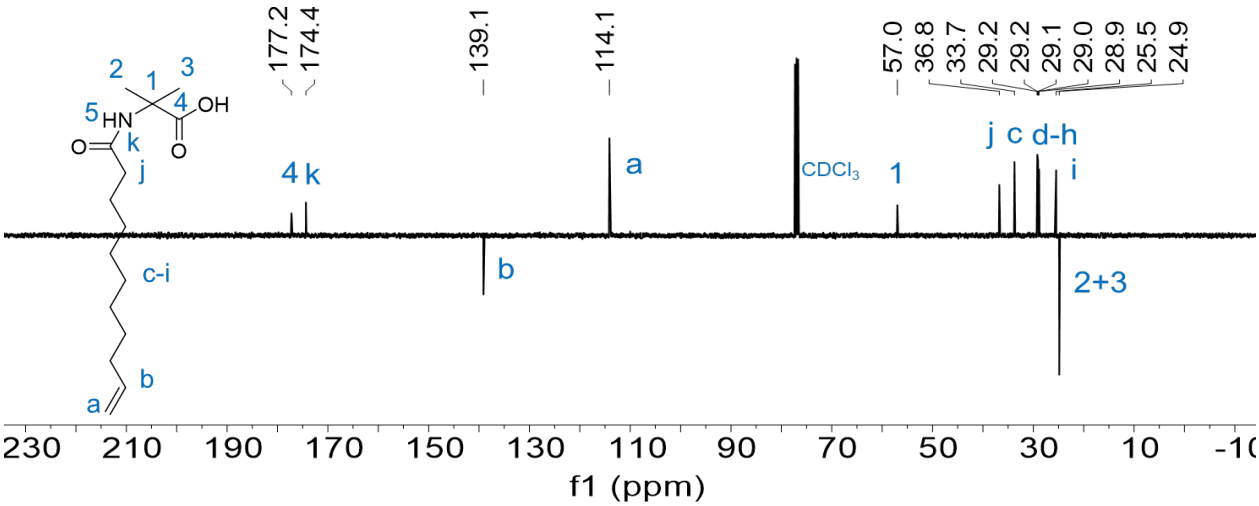

Figure S11. [13]C-APT spectrum of **1d**.

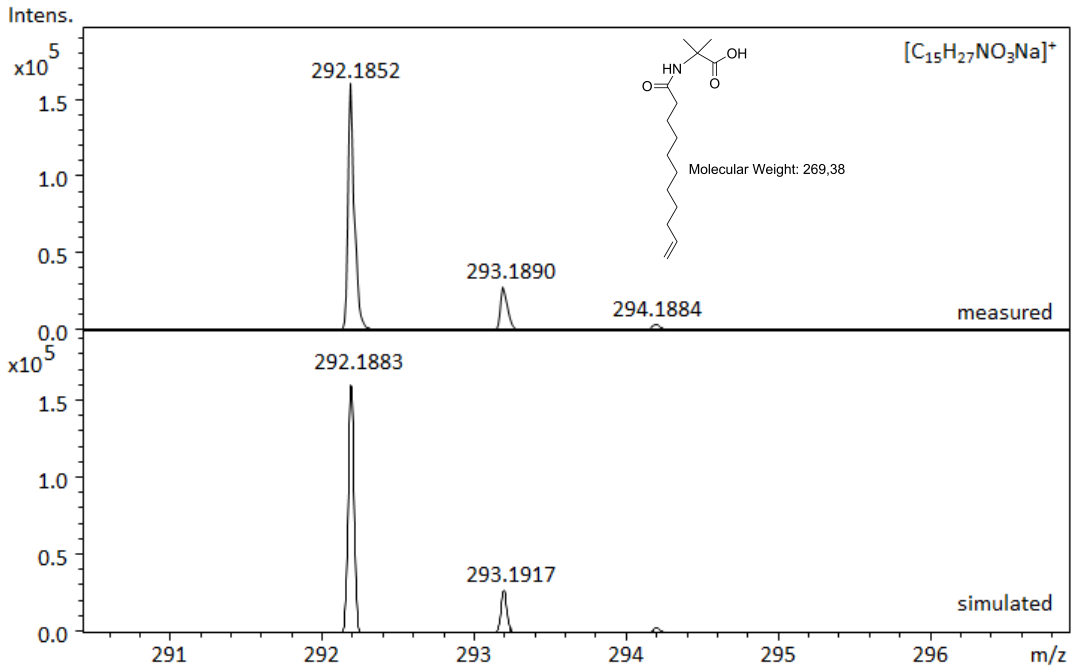

Figure S12. ESI-TOF-MS spectrum of **1d**.

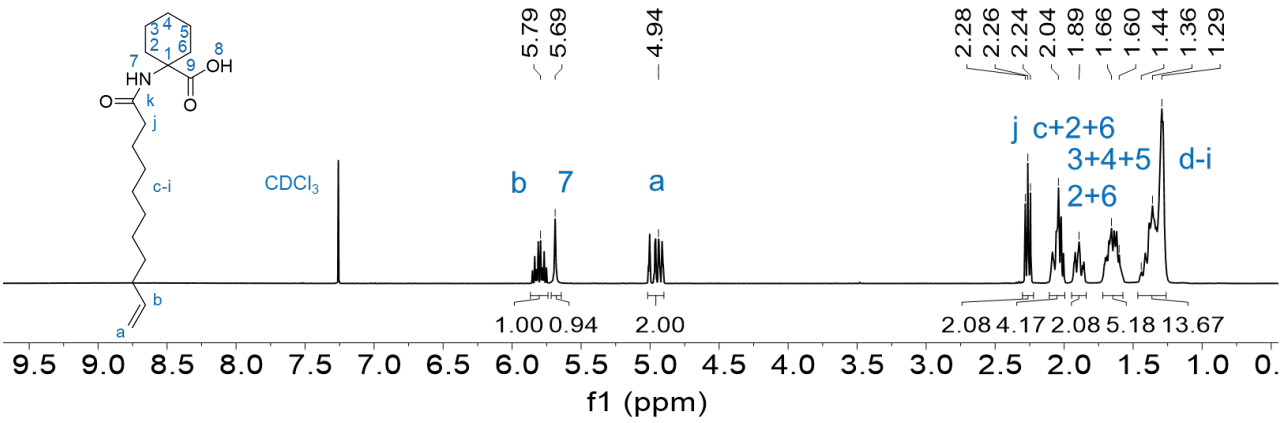

Figure S13. [1]H-NMR spectrum of **1e**.

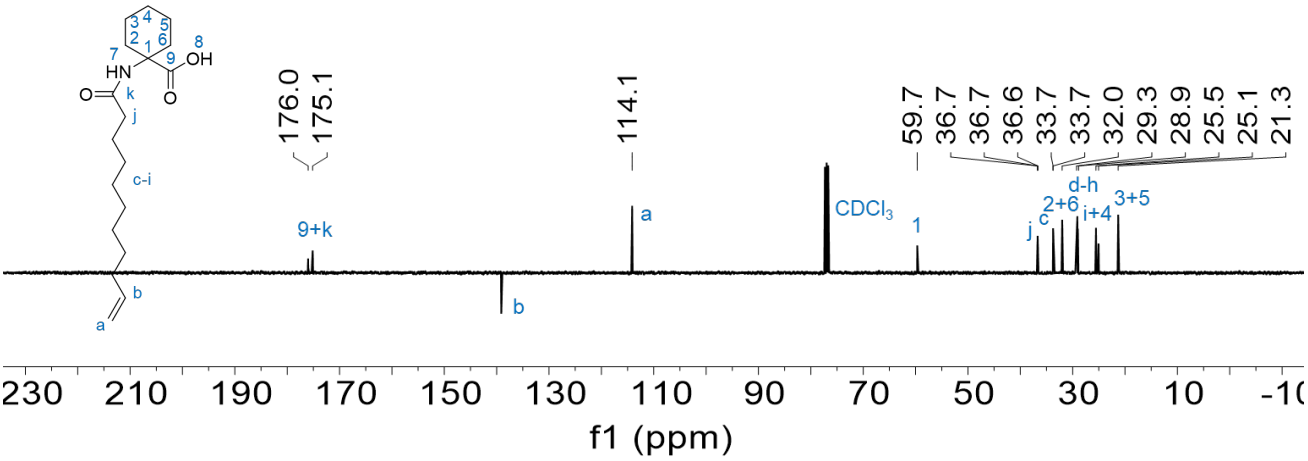

Figure S14. [13]C-APT spectrum of **1e**.

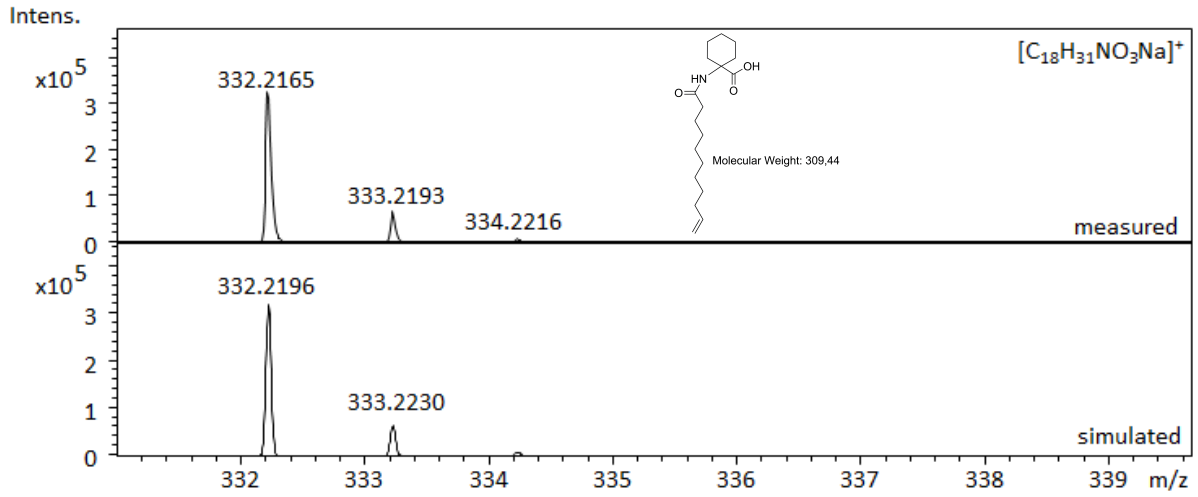

Figure S15. ESI-TOF-MS spectrum of **1e**.

S16. – S17. Characterization of coupling reagent A2.

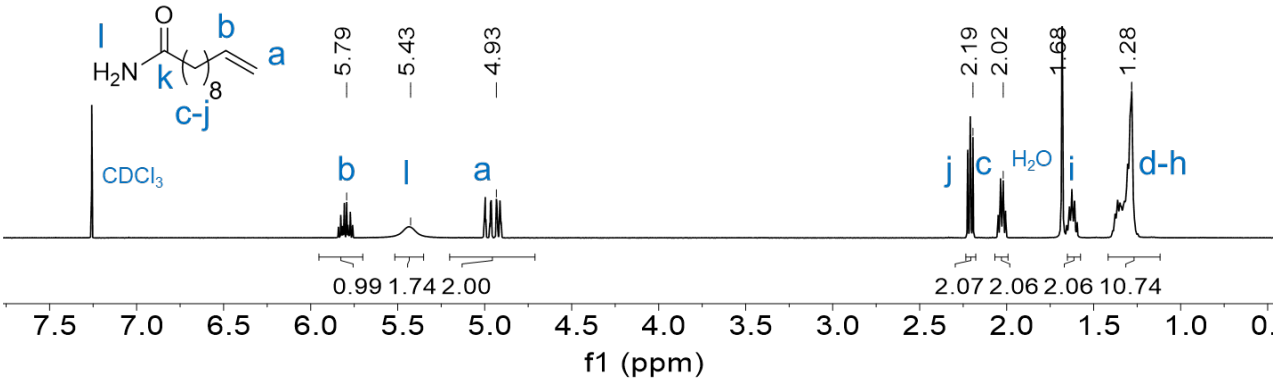

Figure S16. [1]H-NMR spectrum of **A1**.

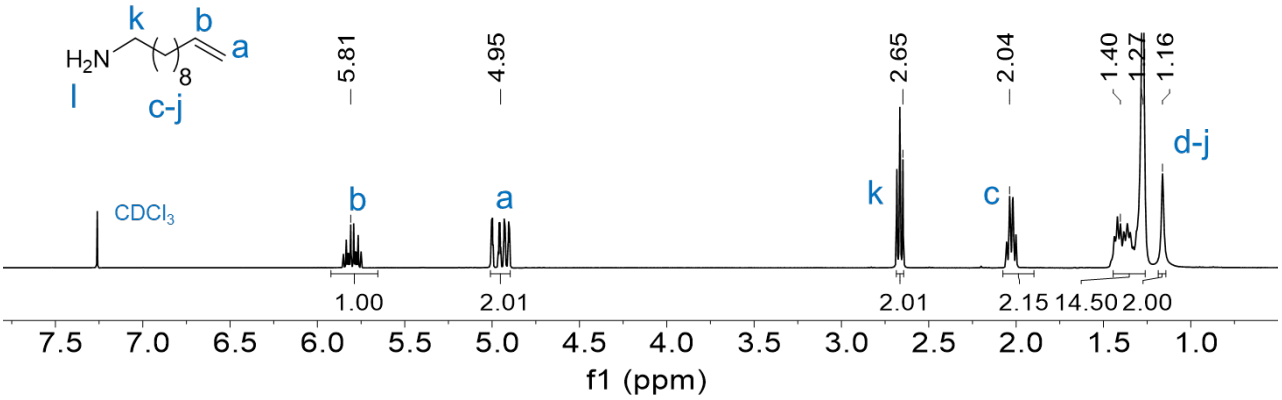

Figure S17. [1]H-NMR spectrum of **A2**.

S18. – S30. Characterization of N- + C-terminus functionalized monomers 2a – 2e

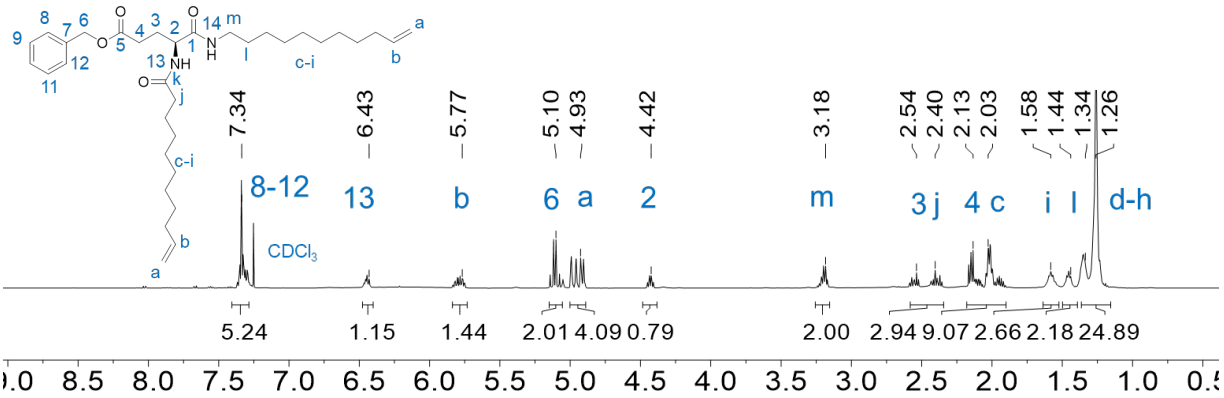

Figure S18. [1]H-NMR spectrum of **2a**.

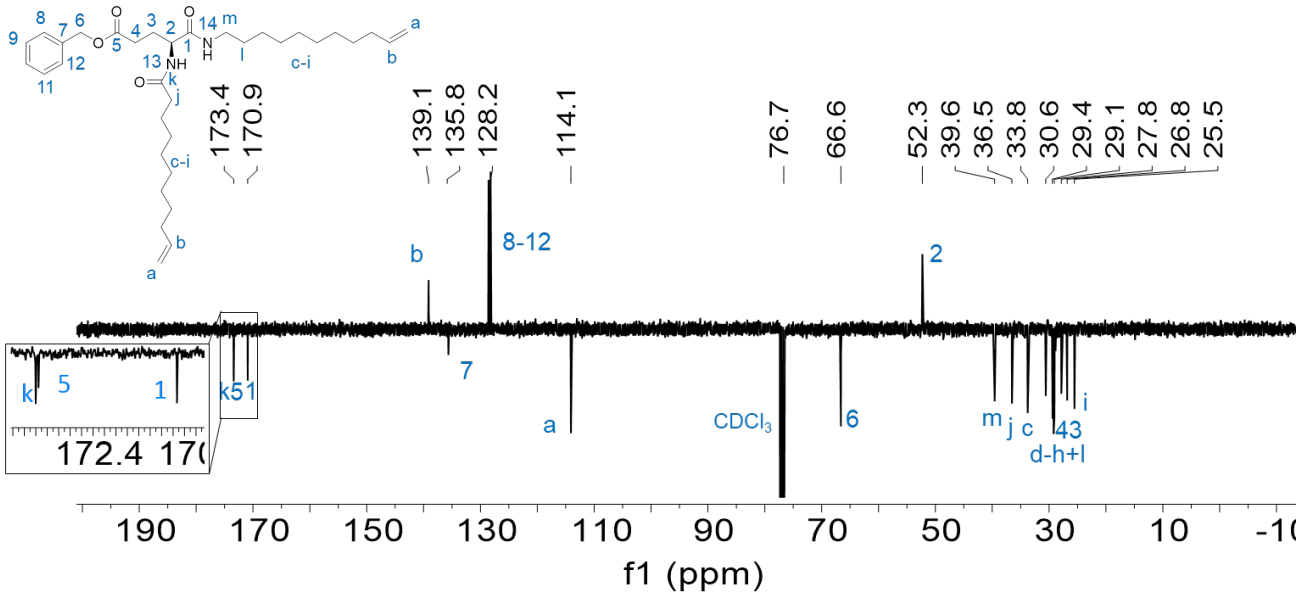

Figure S19. ^{13}C-APT spectrum of **2a**.

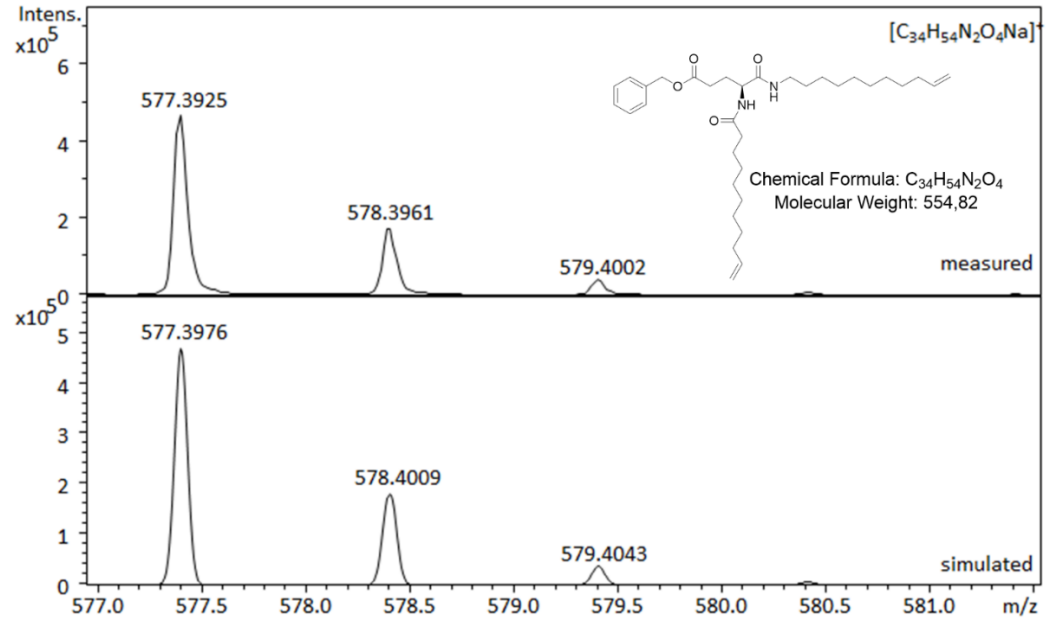

Figure S20. ESI-TOF-MS spectrum of **2a**.

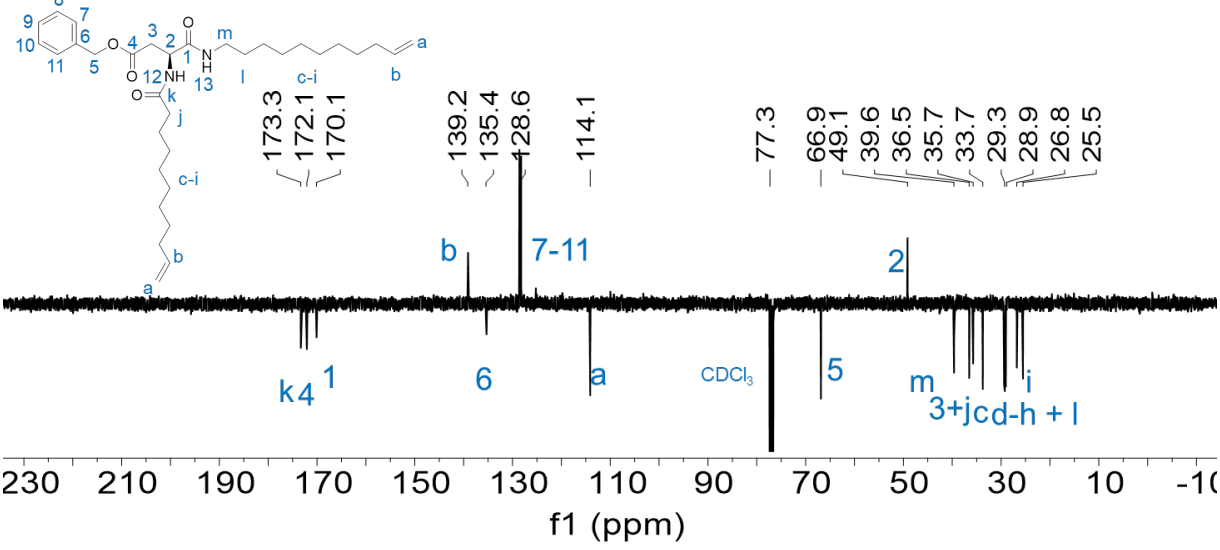

Figure S21. ^{13}C-APT spectrum of **2b**.

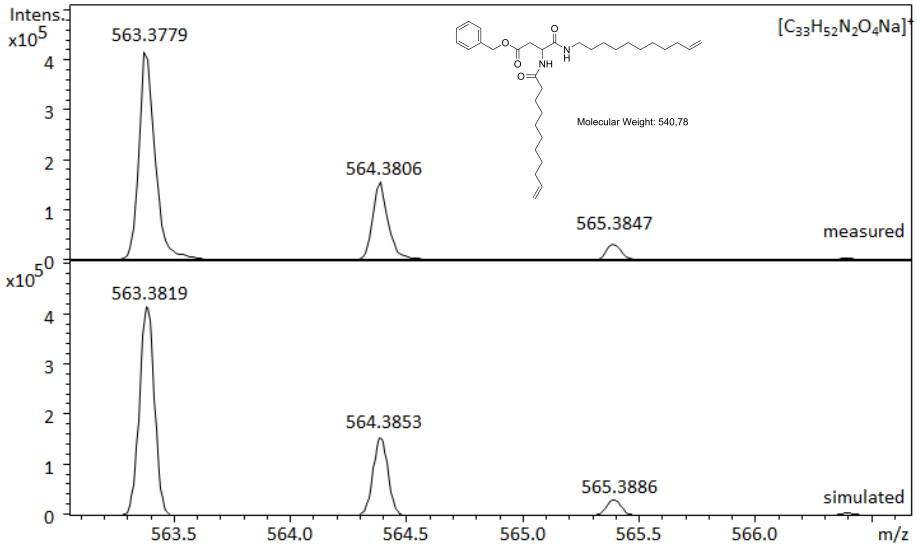

Figure S22. ESI-TOF-MS spectrum of **2b**.

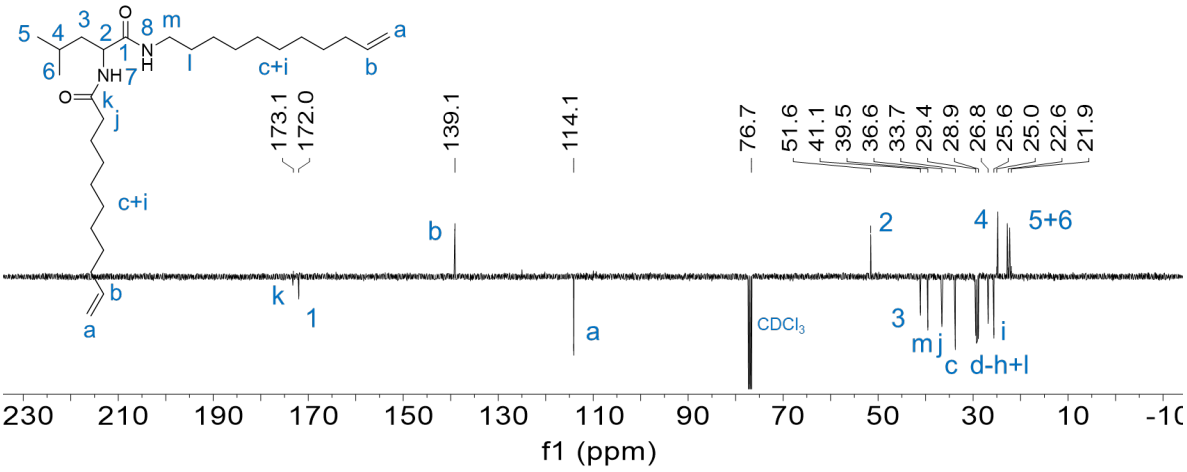

Figure S23. ^{13}C-APT spectrum of **2c**.

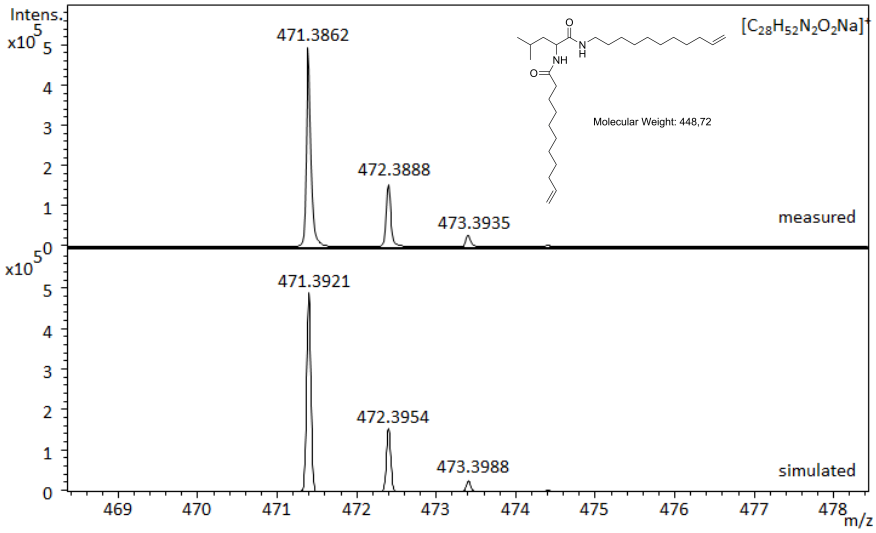

Figure S24. ESI-TOF-MS spectrum of **2c**.

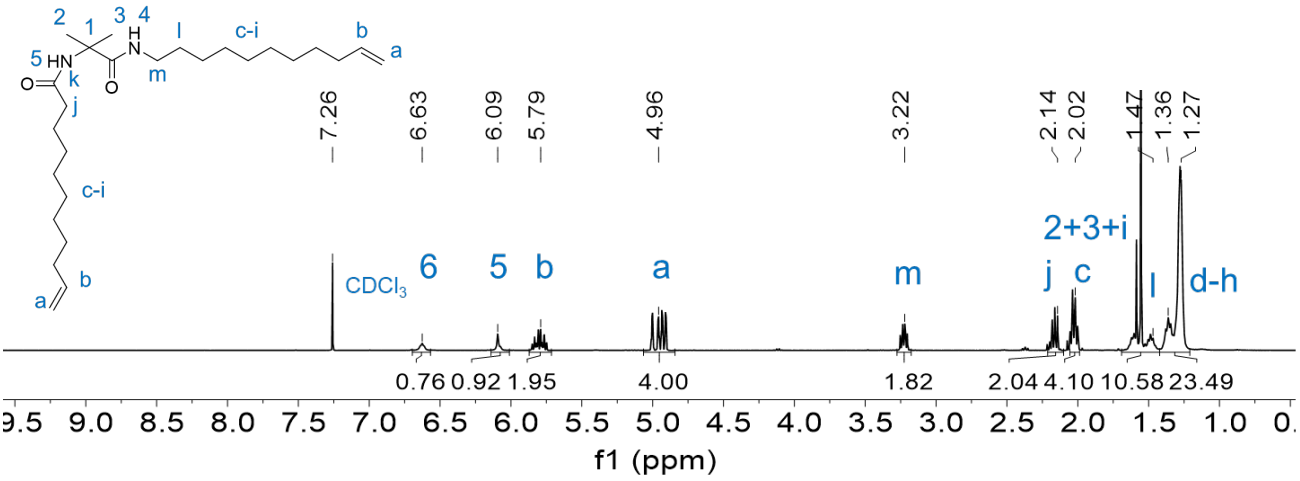

Figure S25. [1]H-NMR spectrum of **2d**.

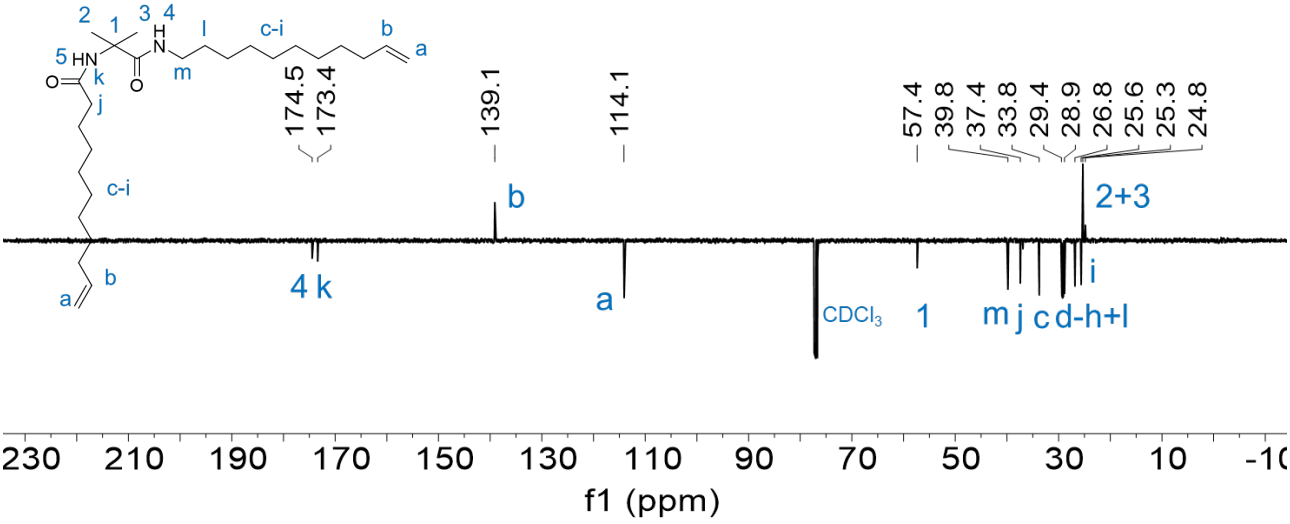

Figure S26. [13]C-APT spectrum of **2d**.

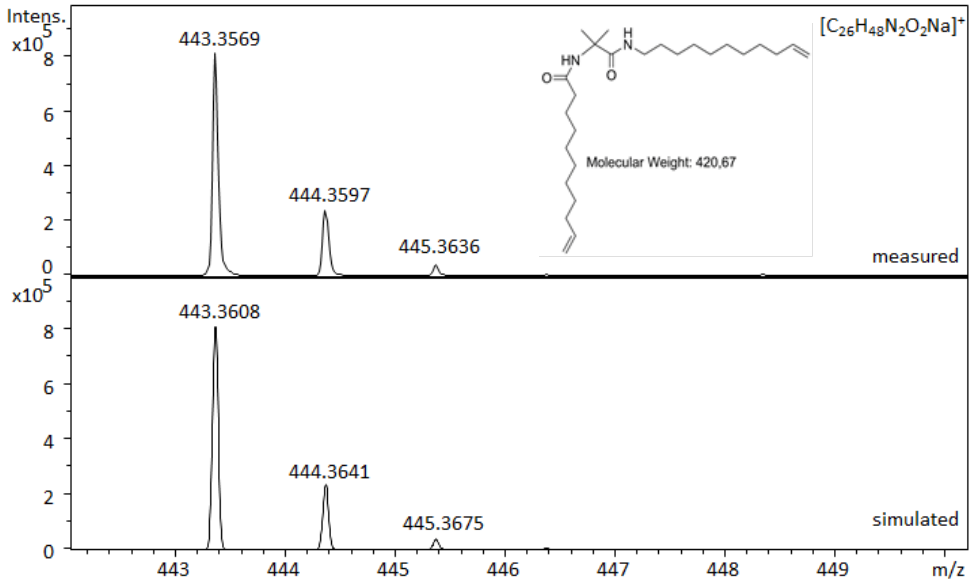

Figure S27. ESI-TOF-MS spectrum of **2d**.

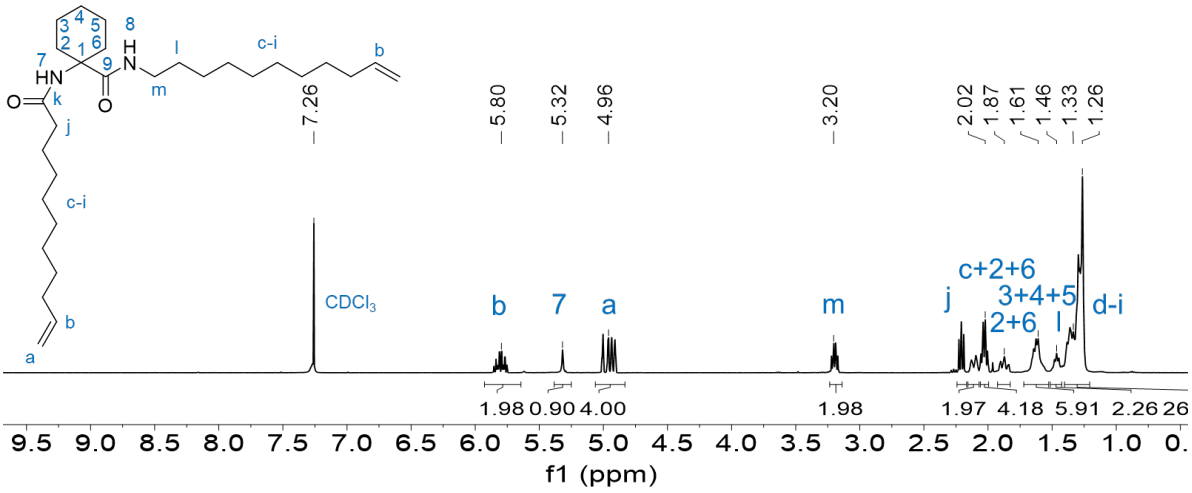

Figure S28. [1]H-NMR spectrum of **2e**.

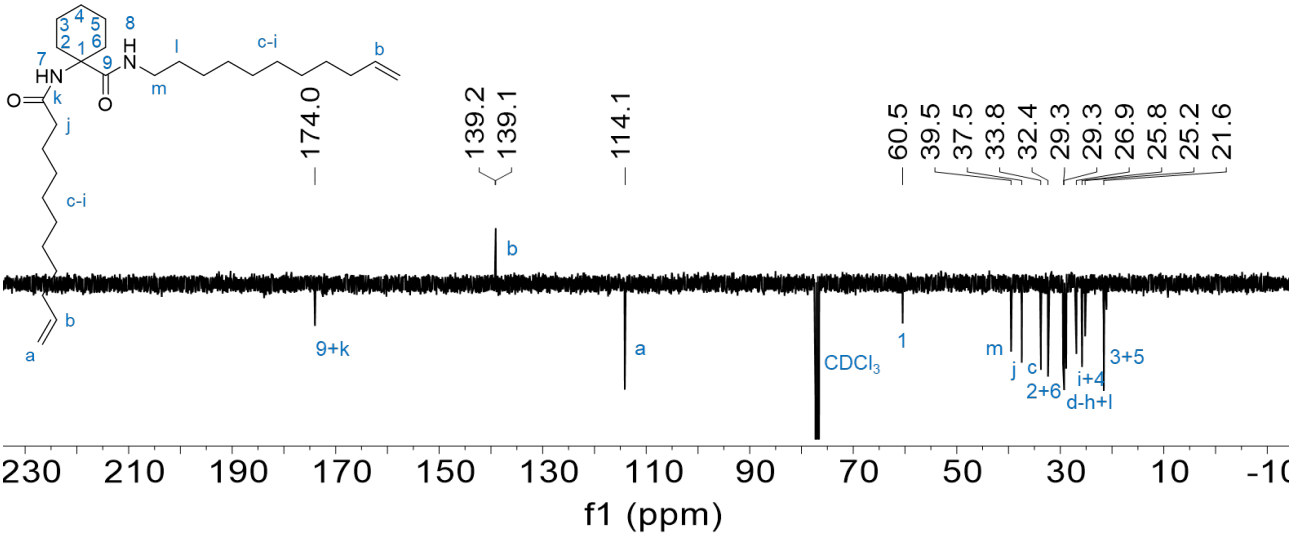

Figure S29. [13]C-APT spectrum of **2e**.

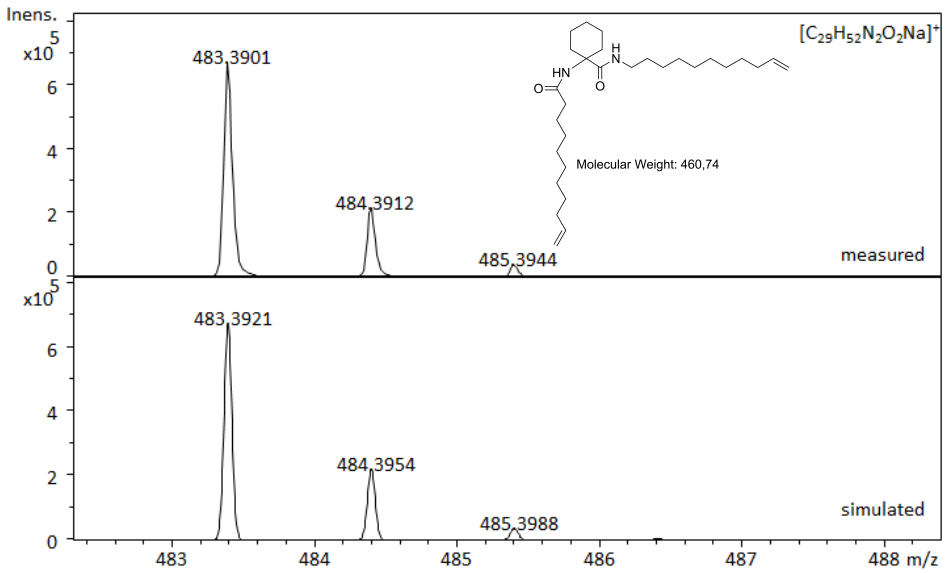

Figure S30. ESI-TOF-MS spectrum of **2e**.

S31. – S36. Characterization of ADMET-polymers 3a – 3e

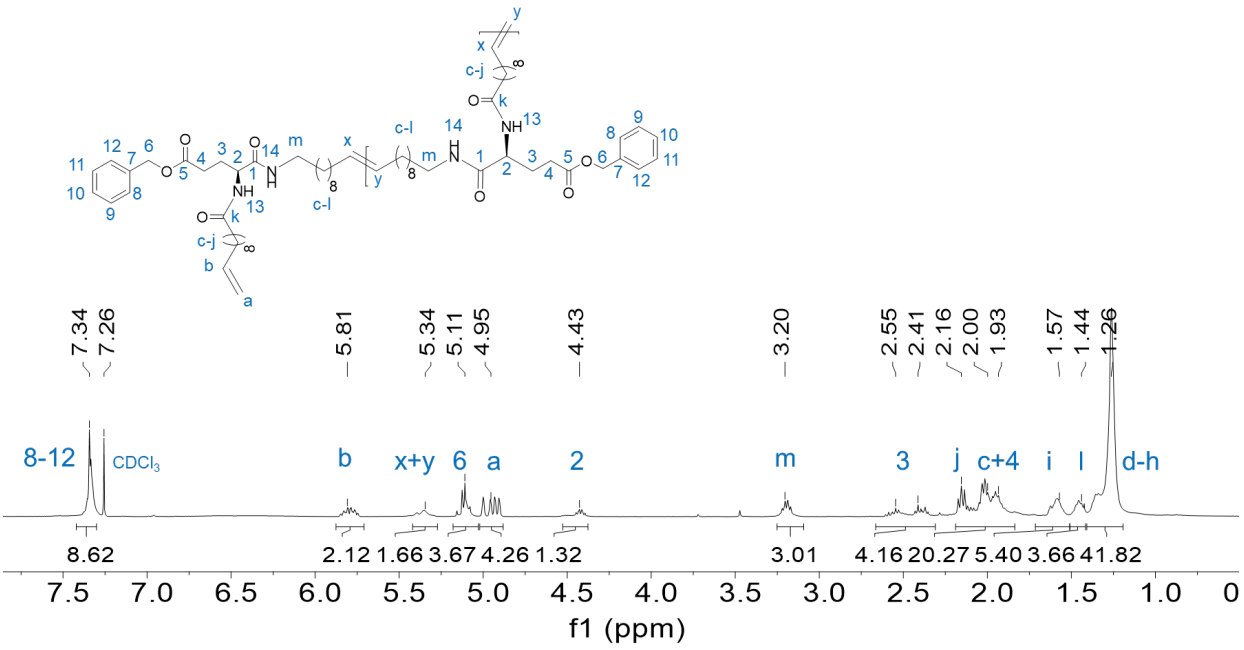

Figure S31. ^{1}H-NMR spectrum of **3a**.

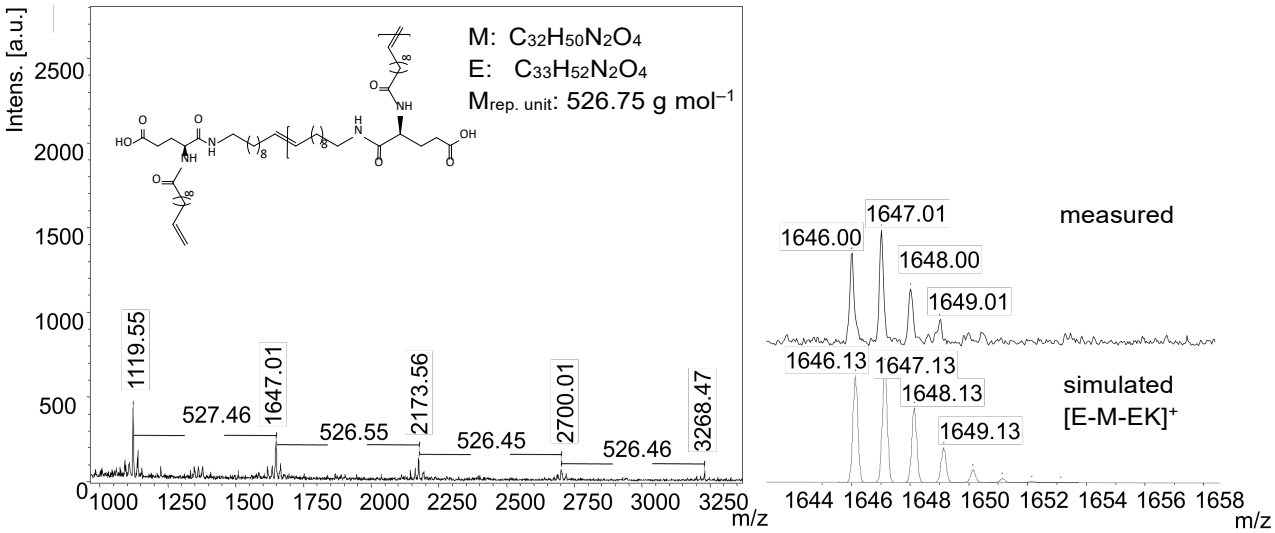

Figure S32. MALDI-TOF-MS spectrum of ADMET polymer **3a**.

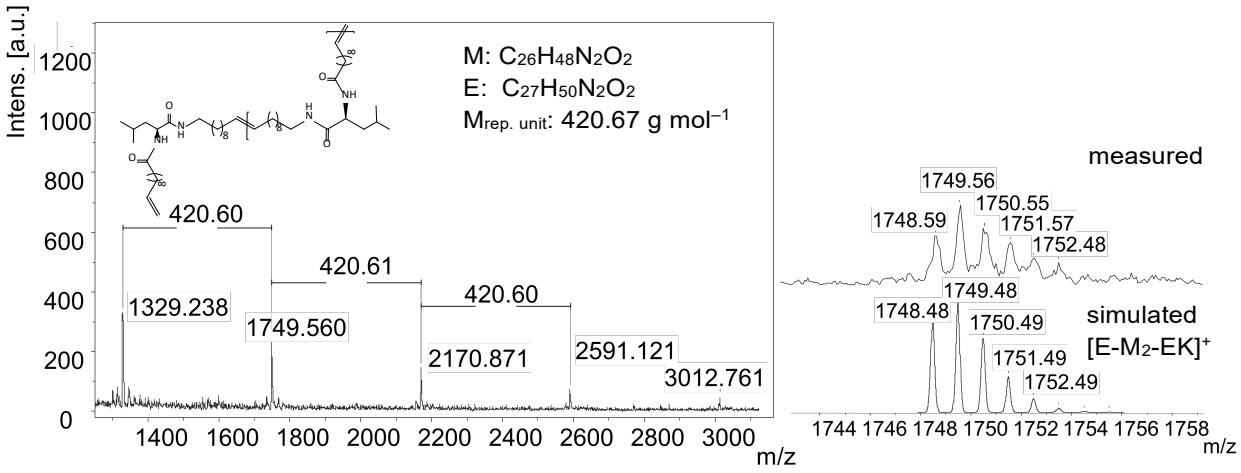

Figure S33. MALDI-TOF-MS spectrum of ADMET polymer **3c**.

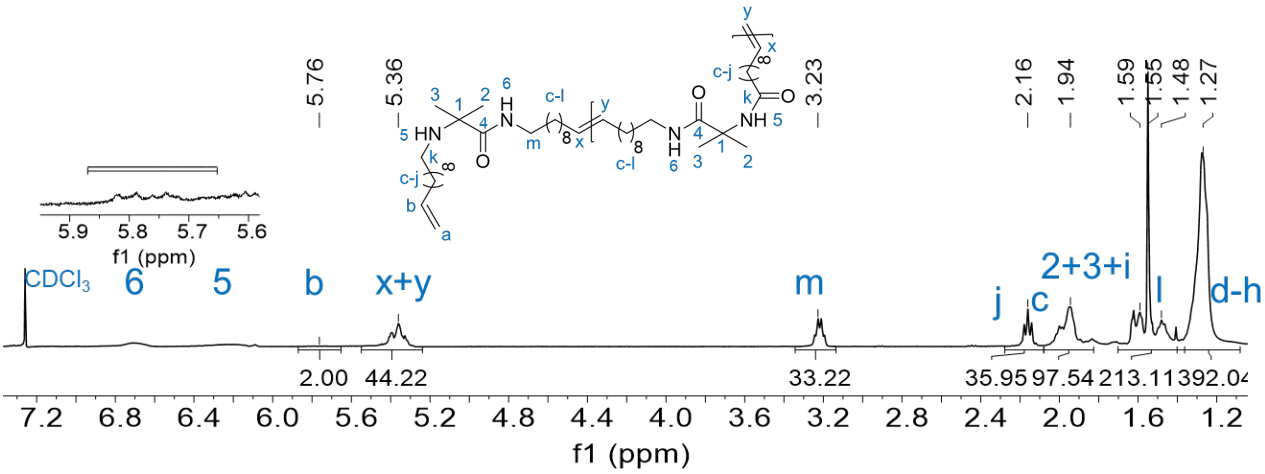

Figure S34. ^{1}H-NMR spectrum of **3d**.

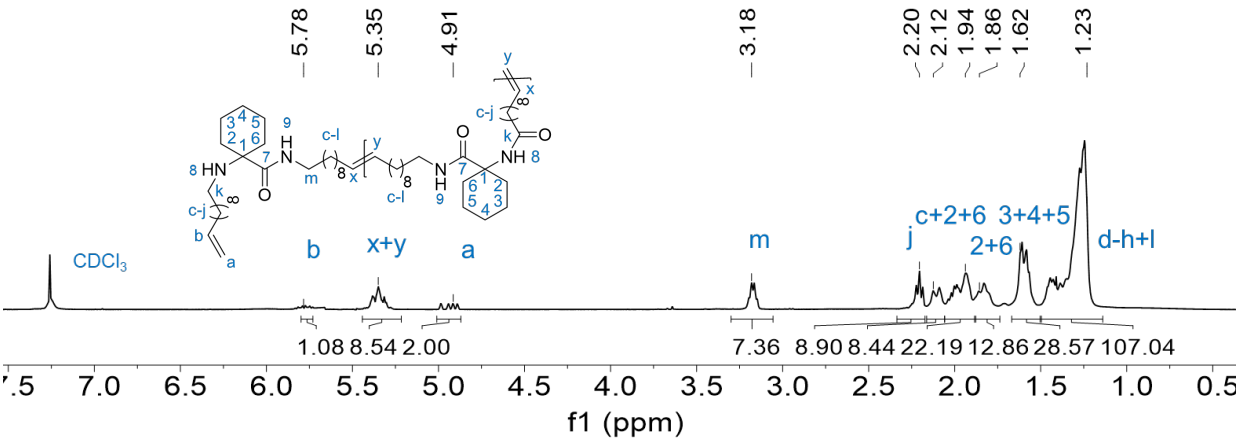

Figure S35. ^{1}H-NMR spectrum of **3e**.

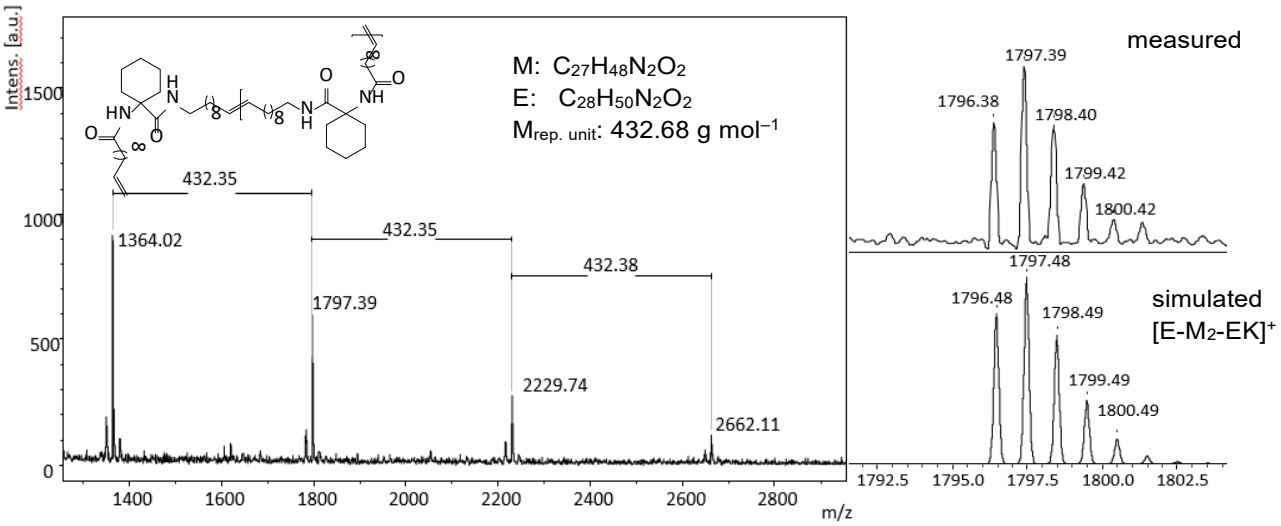

Figure S36. MALDI-TOF-MS spectrum of **3e**.

S37. – S41. Characterization of hydrogenated ADMET-polymers 4a – 4e

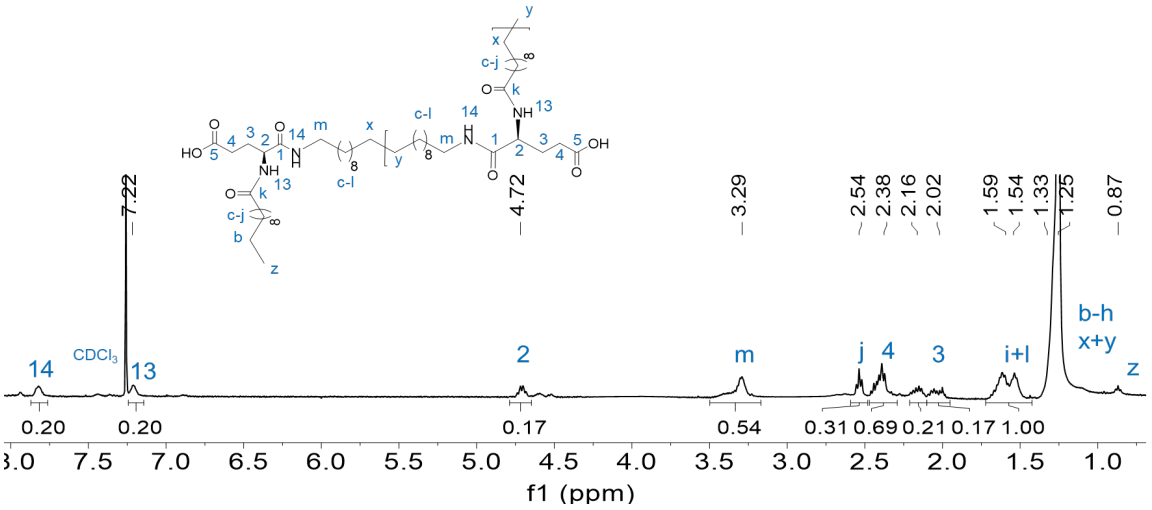

Figure S37. ^{1}H-NMR spectrum of **4a**.

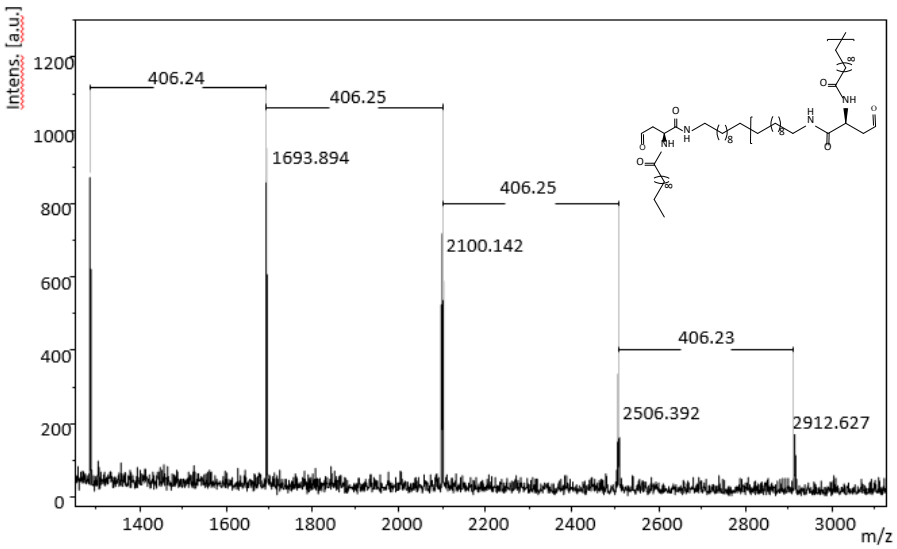

Figure S38. MALDI-TOF-MS spectrum of **4b**. High laser energy leads to loss of H_2O in the molecule during measurements.

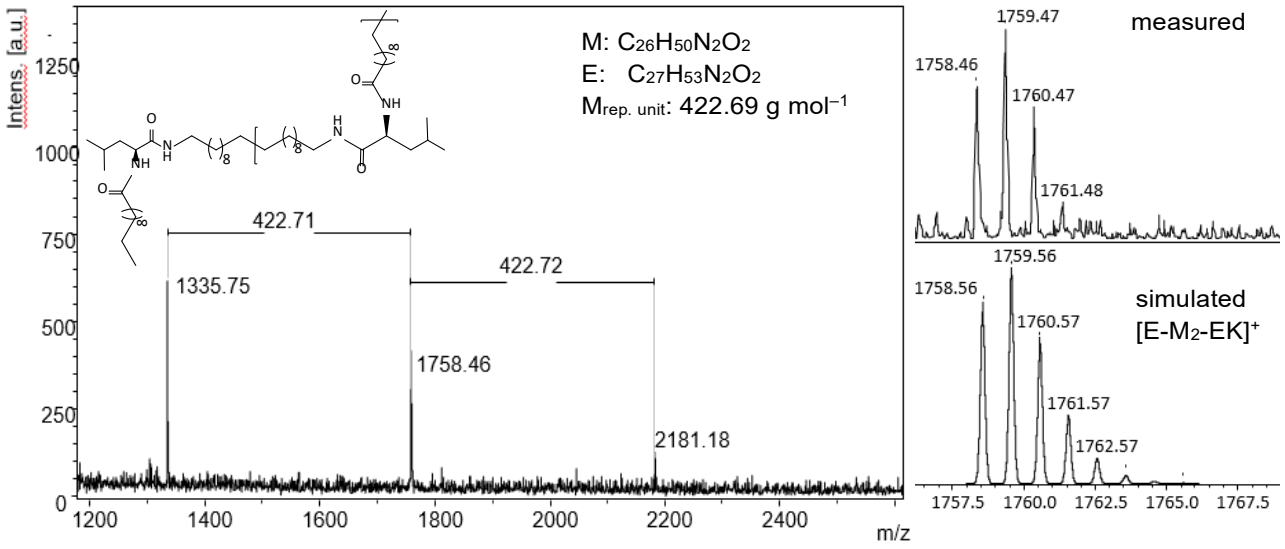

Figure S39. MALDI-TOF-MS spectrum of **4c**.

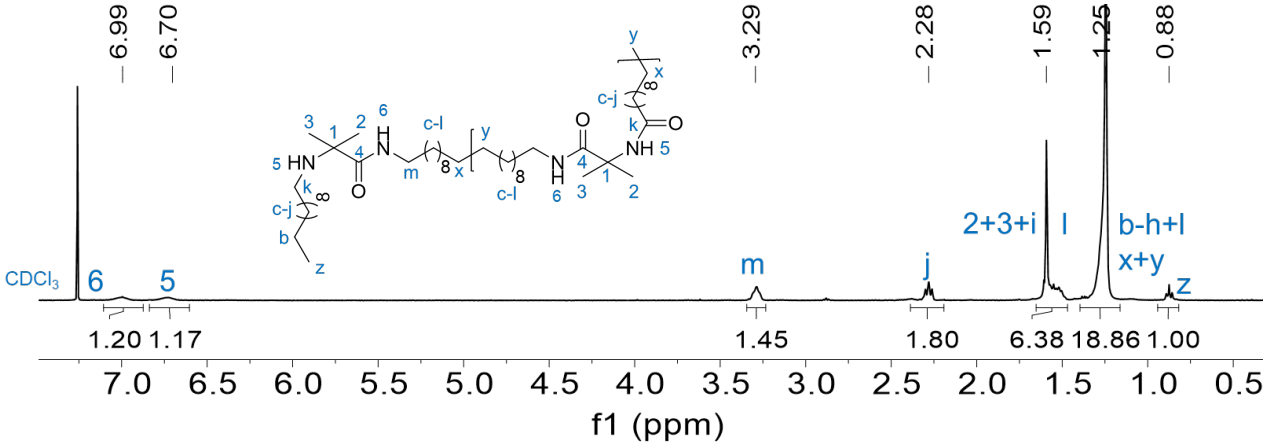

Figure S40. [1]H-NMR spectrum of **4d**.

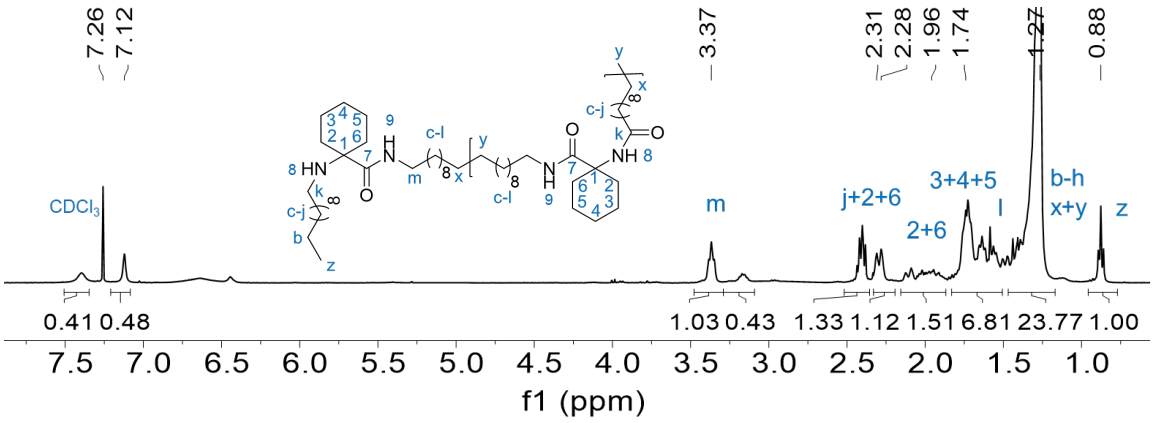

Figure S41. [1]H-NMR spectrum of **4e.**

S42. – S51. IR Spectra of polymers 3a – 3e and hydrogenated polymers 4a – 4e

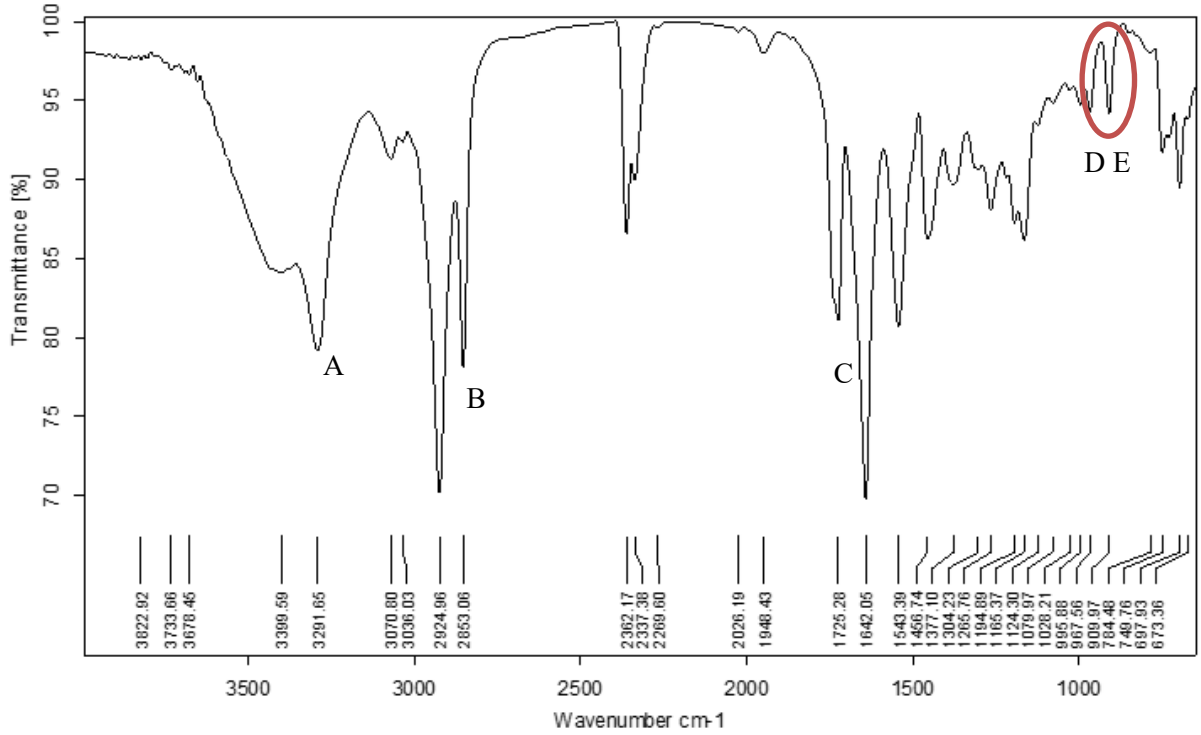

Figure S42. IR spectrum of **3a**: A. 3291 cm^{-1} $\nu_{asymm.}$ CONH; B. 2924 – 2853 cm^{-1} ν CH_2; C. 1642 cm^{-1} δ CONH; D. 967 cm^{-1} δ RCH=CHR; E. 909 cm^{-1} δ RCH=CH_2.

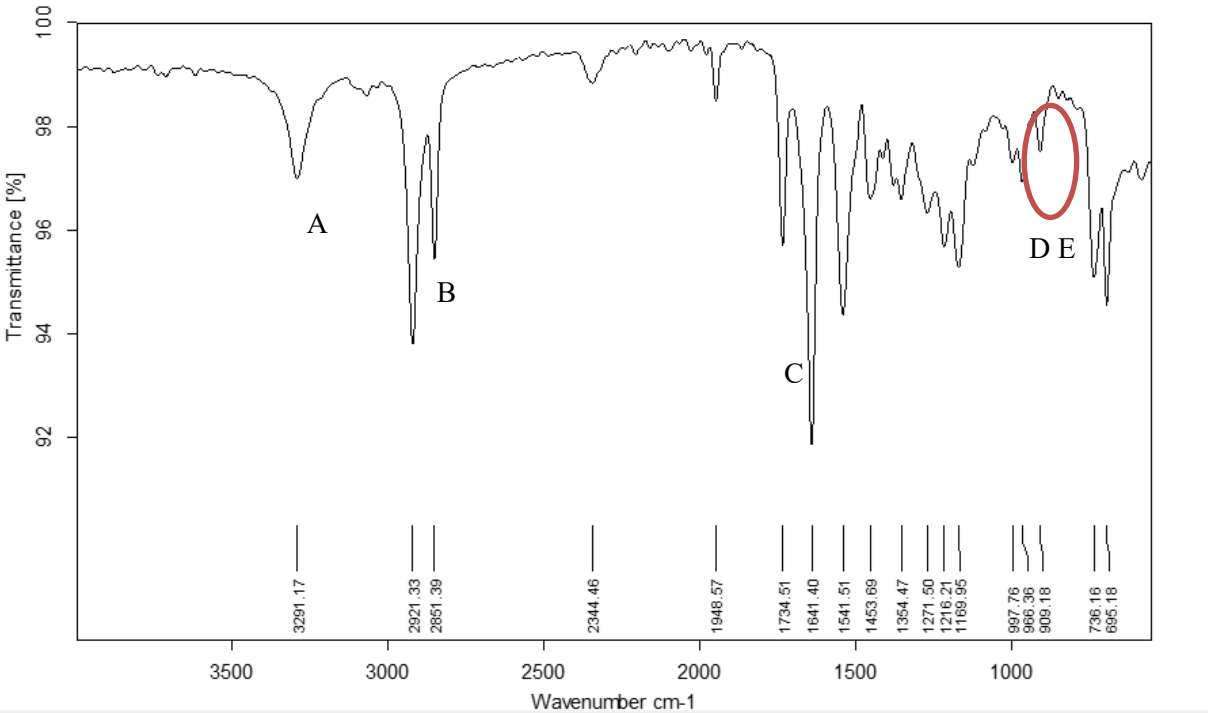

Figure S43. IR spectrum of **3b**: A. 3291 cm^{-1} $\nu_{asymm.}$ CONH; B. 2921 – 2851 cm^{-1} ν CH_2; C. 1641 cm^{-1} δ CONH; D. 966 cm^{-1} δ RCH=CHR; E. 909 cm^{-1} δ RCH=CH_2.

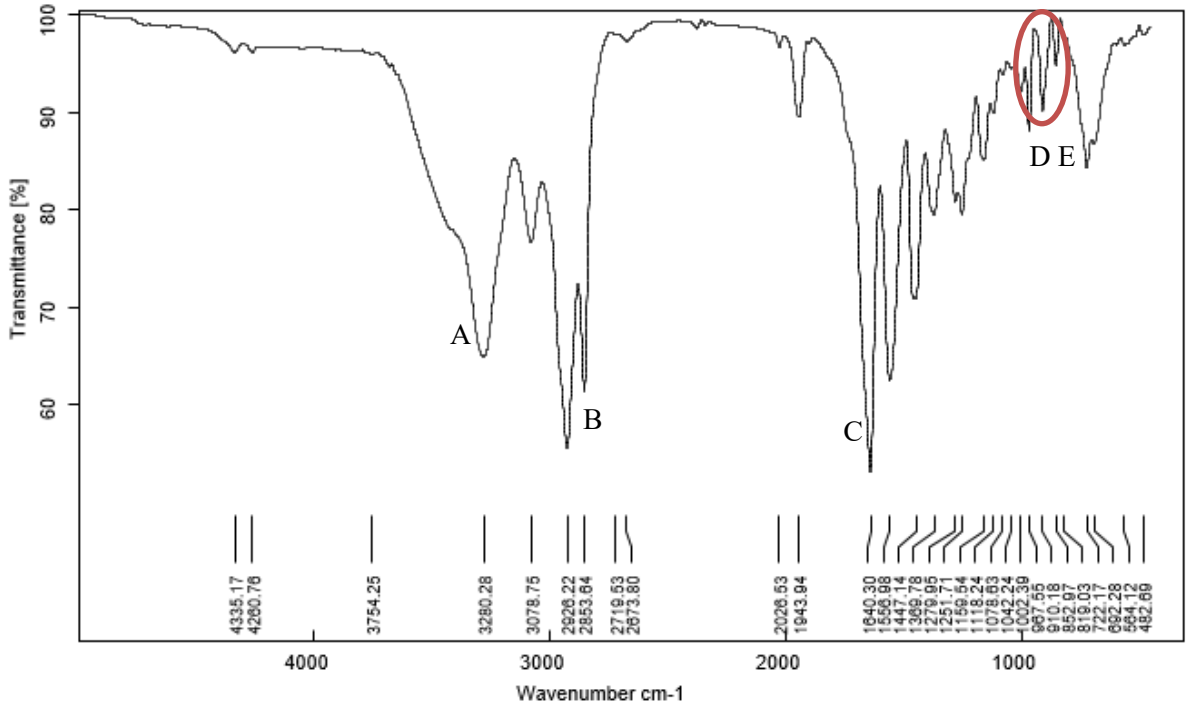

Figure S44. IR spectrum of **3c**: A. 3280 cm^{-1} $\nu_{asymm.}$ CONH; B. 2926 – 2853 cm^{-1} ν CH_2; C. 1640 cm^{-1} δ CONH; D. 967 cm^{-1} δ RCH=CHR; E. 910 cm^{-1} δ RCH=CH_2.

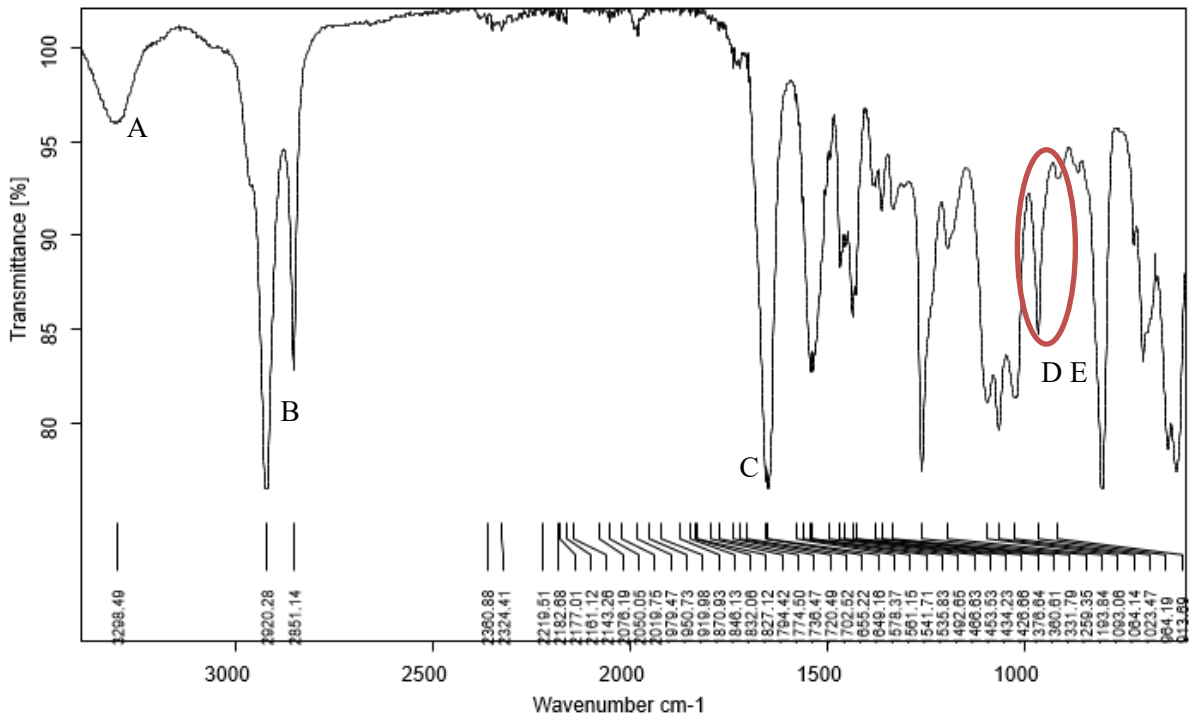

Figure S45. IR spectrum of **3d**: A. 3298 cm^{-1} $\nu_{asymm.}$ CONH; B. 2920 – 2851 cm^{-1} ν CH_2; C. 1658 cm^{-1} δ CONH; D. 964 cm^{-1} δ RCH=CHR; E. 913 cm^{-1} δ RCH=CH_2.

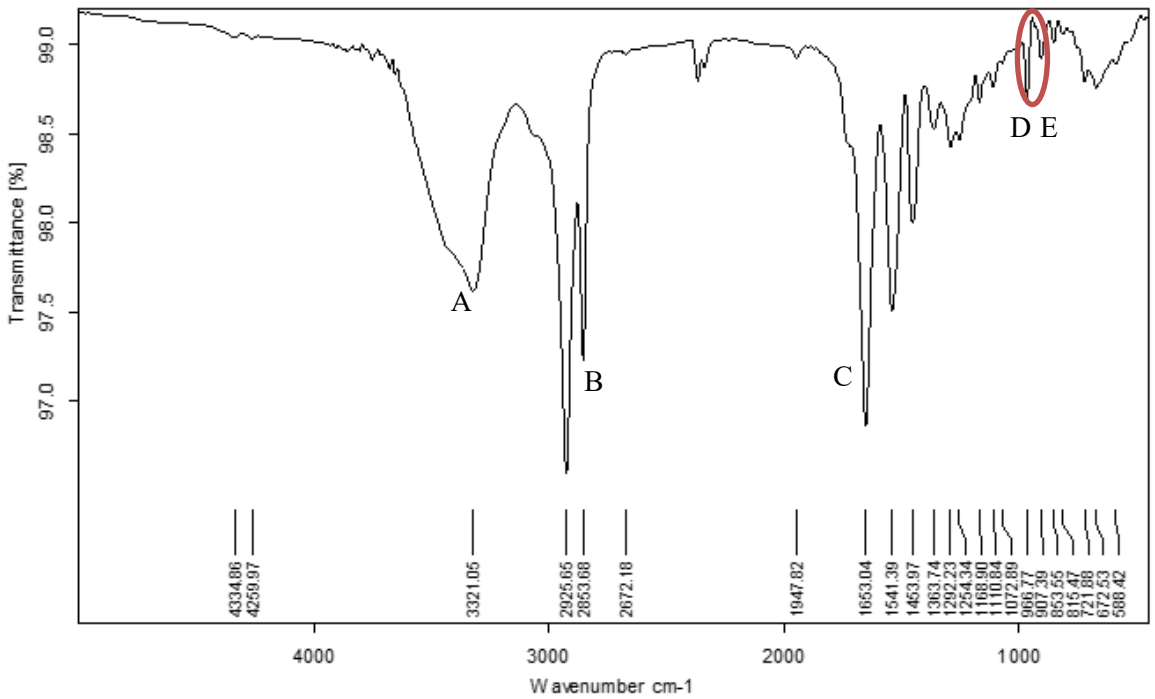

Figure S46. IR spectrum of **3e**: A. 3221 cm^{-1} $\nu_{asymm.}$ CONH; B. 2925 – 2853 cm^{-1} ν CH_2; C. 1653 cm^{-1} δ CONH; D. 966 cm^{-1} δ RCH=CHR; E. 907 cm^{-1} δ RCH=CH_2.

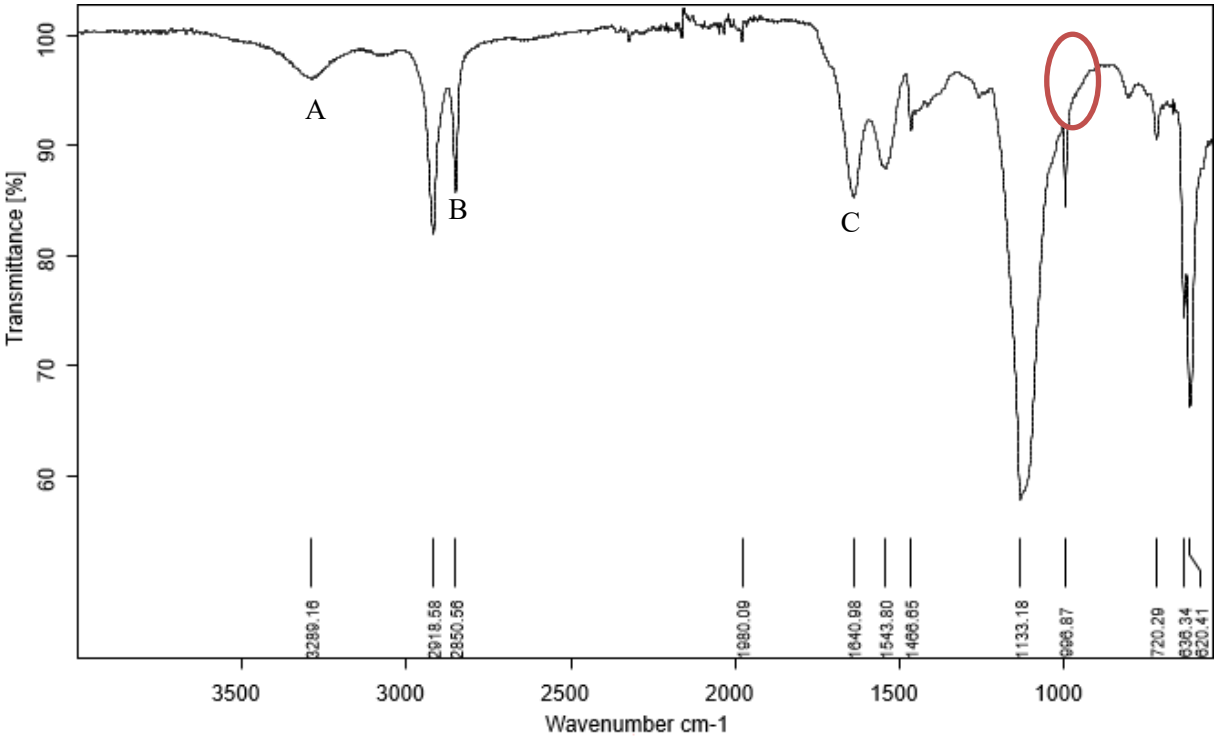

Figure S47. IR spectrum of **4a**: A. 3289 cm^{-1} $\nu_{asymm.}$ CONH; B. 2918 – 2850 cm^{-1} ν CH_2; C. 1640 cm^{-1} δ CONH.

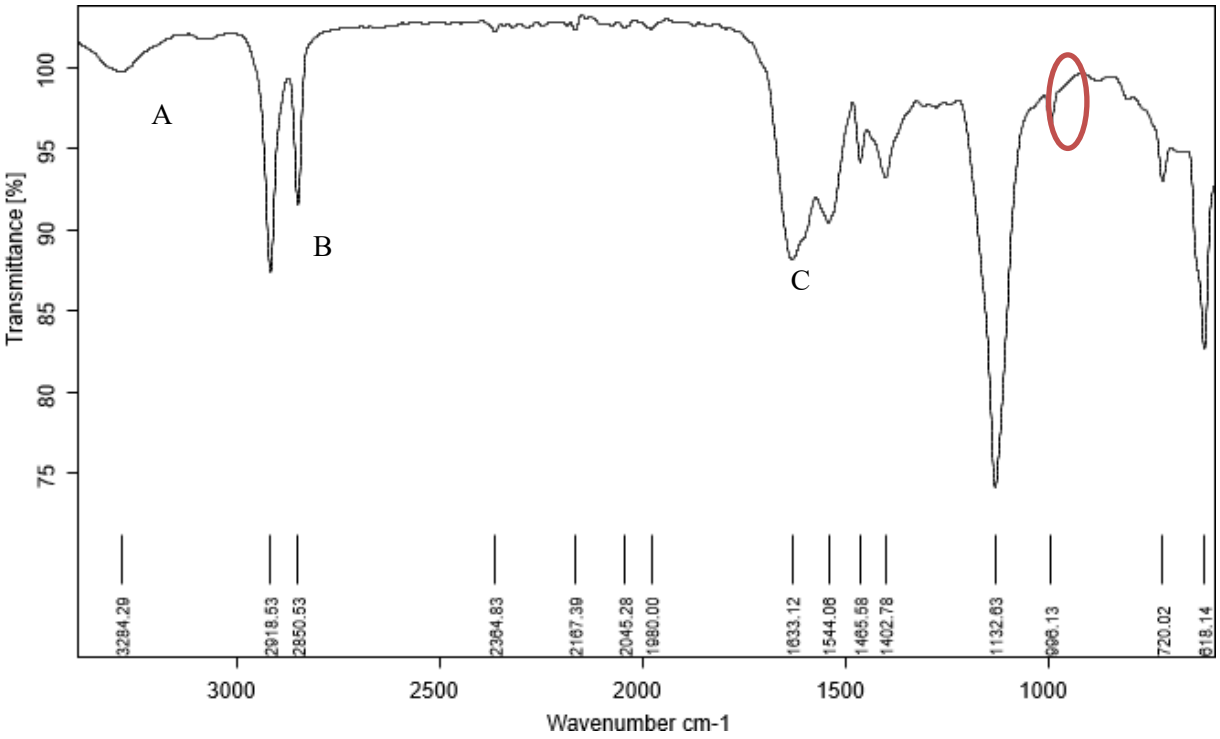

Figure S48. IR spectrum of **4b**: A. 3284 cm^{-1} $\nu_{asymm.}$ CONH; B. 2918 – 2850 cm^{-1} ν CH_2; C. 1633 cm^{-1} δ CONH.

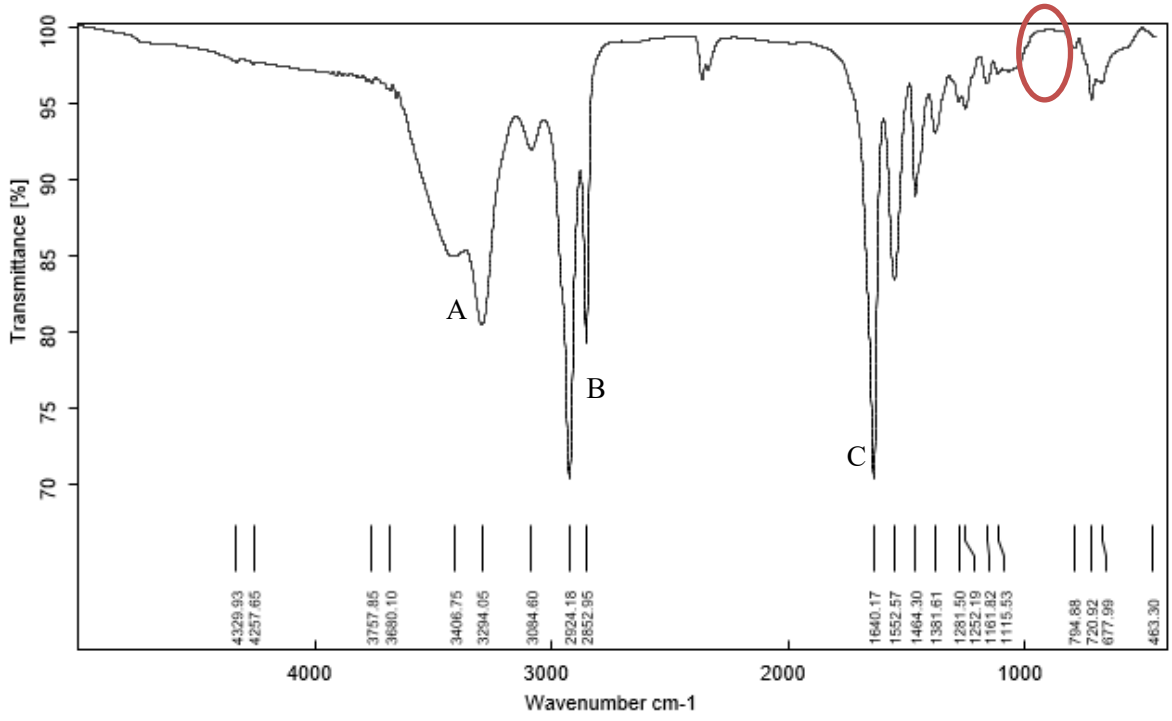

Figure S49. IR spectrum of **4c**: A. 3406 – 3294 cm^{-1} $\nu_{asymm.}$ CONH; B. 2924 – 2852 cm^{-1} ν CH_2; C. 1640 cm^{-1} δ CONH.

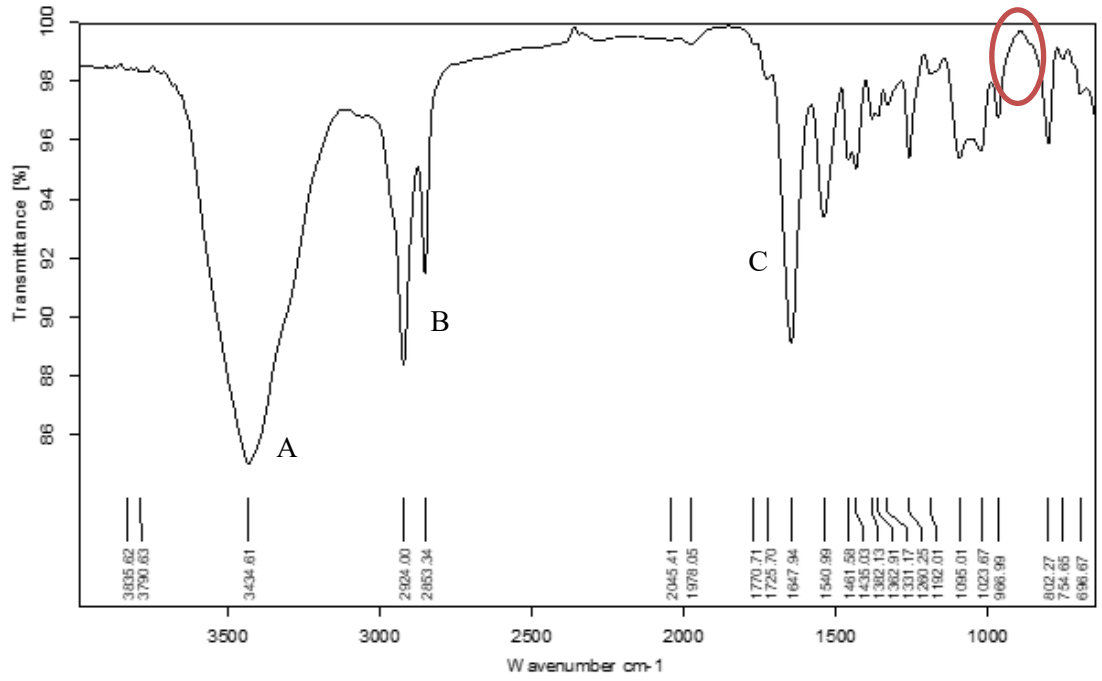

Figure S50. IR spectrum of **4d**: A. 3434 cm^{-1} $\nu_{asymm.}$ CONH; B. 2924 – 2853 cm^{-1} ν CH_2; C. 1647 cm^{-1} δ CONH.

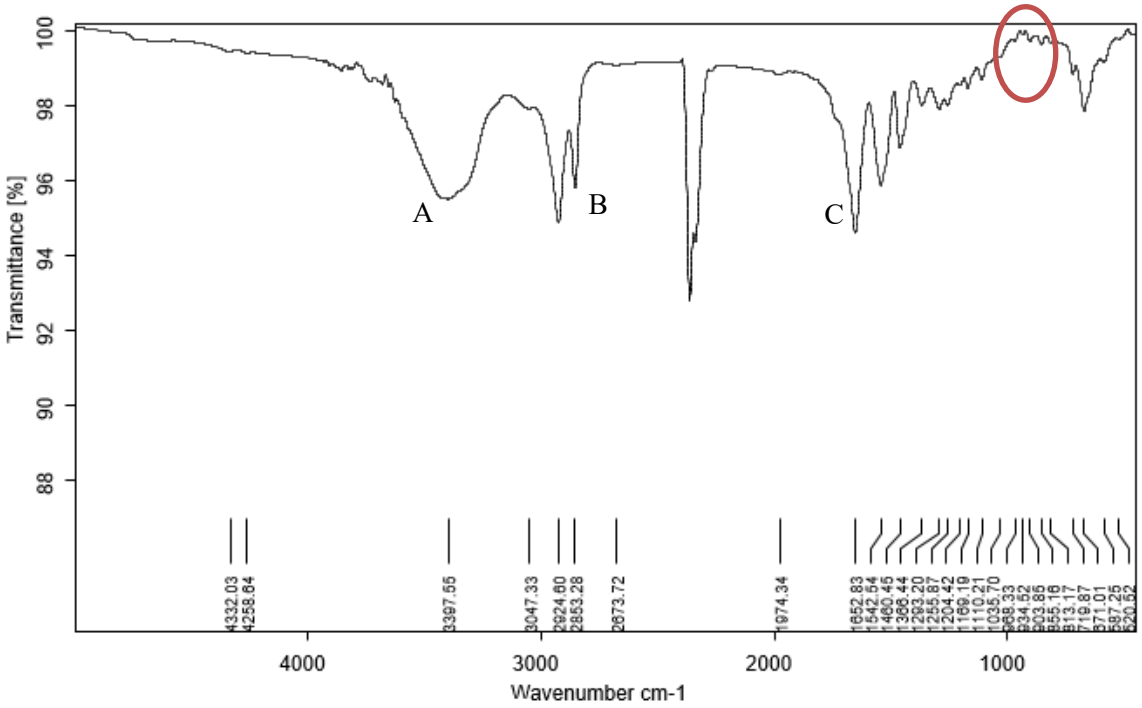

Figure S51. IR spectrum of **4e**: A. 3397 cm^{-1} $\nu_{asymm.}$ CONH; B. 2924 – 2853 cm^{-1} ν CH_2; C. 1652 cm^{-1} δ CONH.

S52. – S53. Characterization of Glu-NCA (5) and Asp-NCA (6)

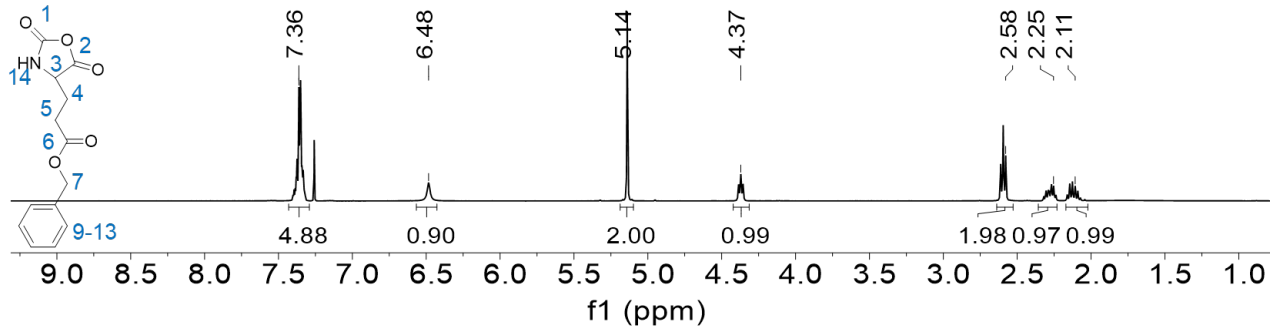

Figure S52. ^{1}H-NMR spectrum of **5**.

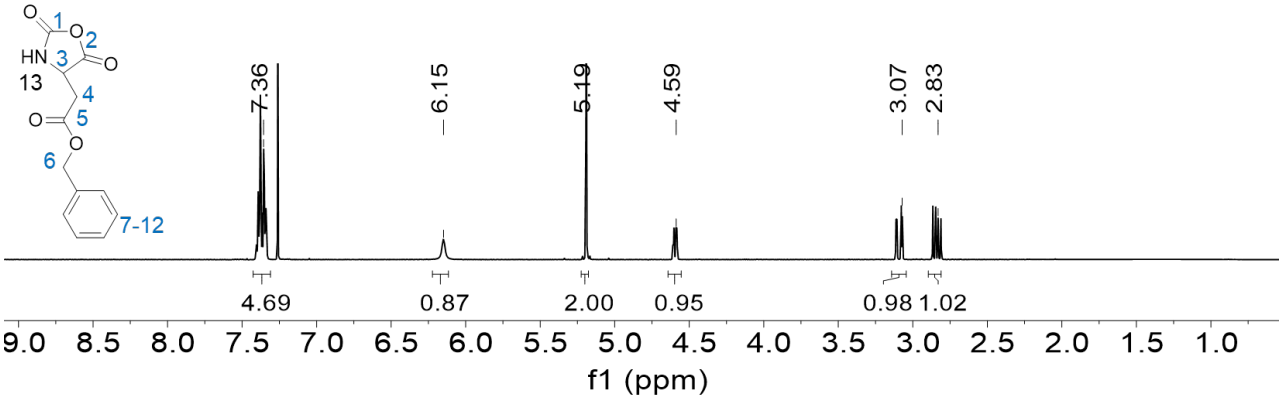

Figure S53. ^{1}H-NMR spectrum of **6**.

S54. – S61. Characterization of oligomers 7a – 10a

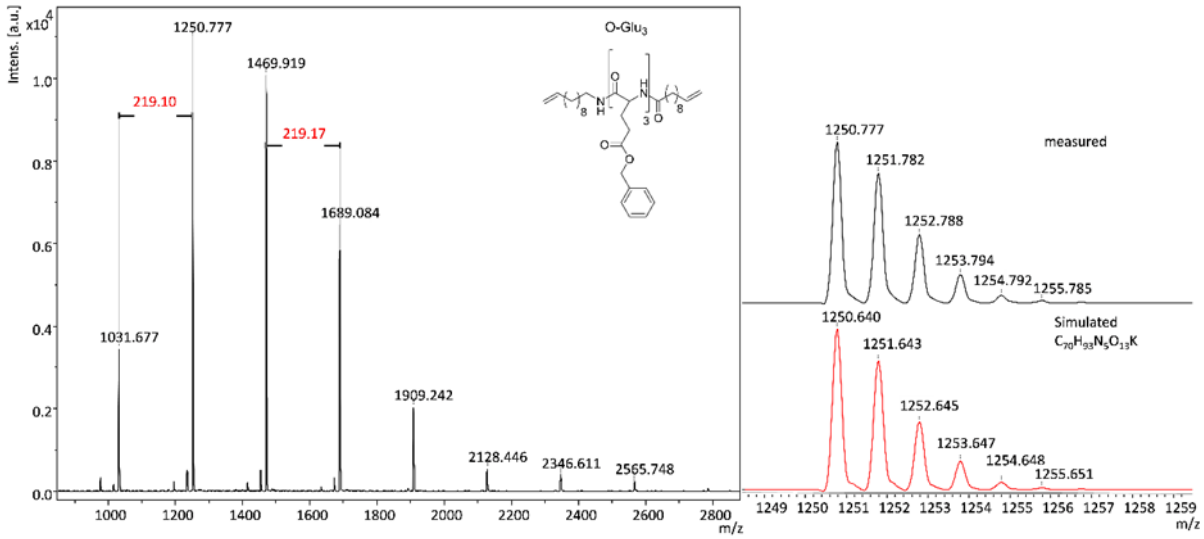

Figure S54. MALDI-TOF-MS spectrum of **O^{Bn}Glu$_3$** (**7a**) using dithranol as matrix and KTFA as salt.

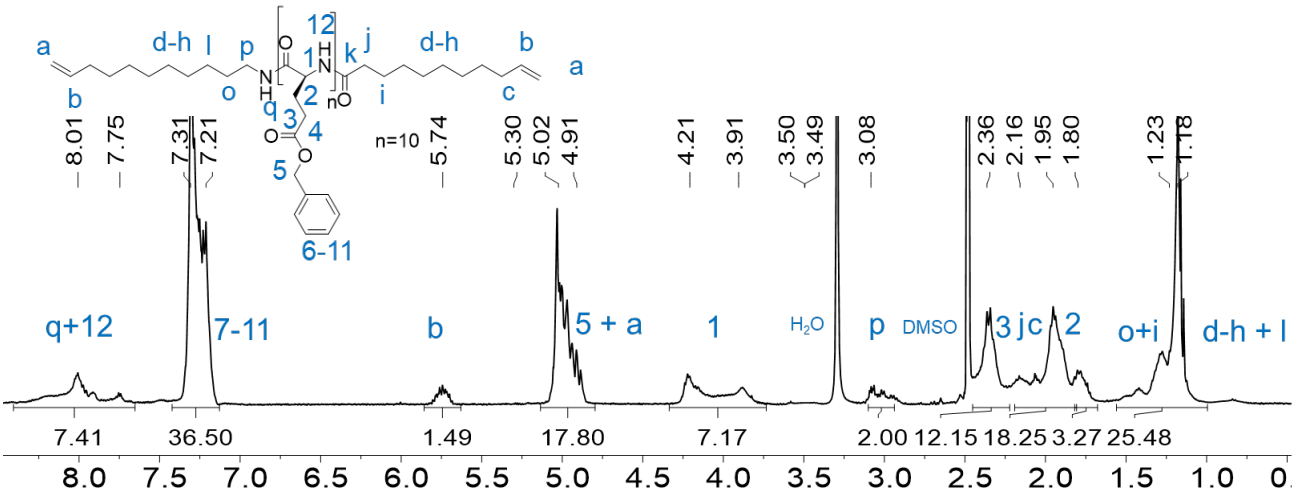

Figure S55. ^{1}H-NMR spectrum of **8a**.

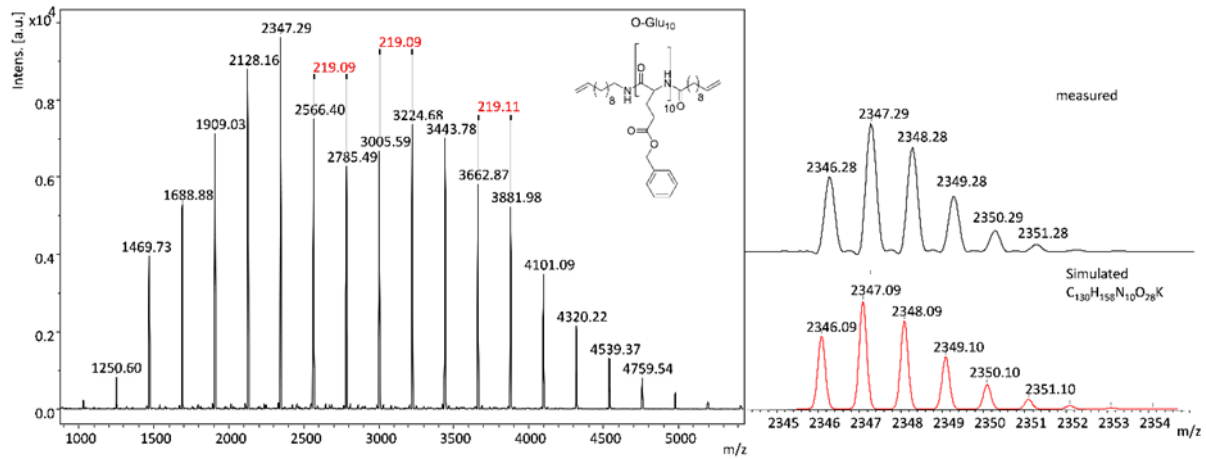

Figure S56. MALDI-TOF-MS spectrum of **O^{Bn}Glu$_{10}$ (8a)** using dithranol as matrix and KTFA as salt.

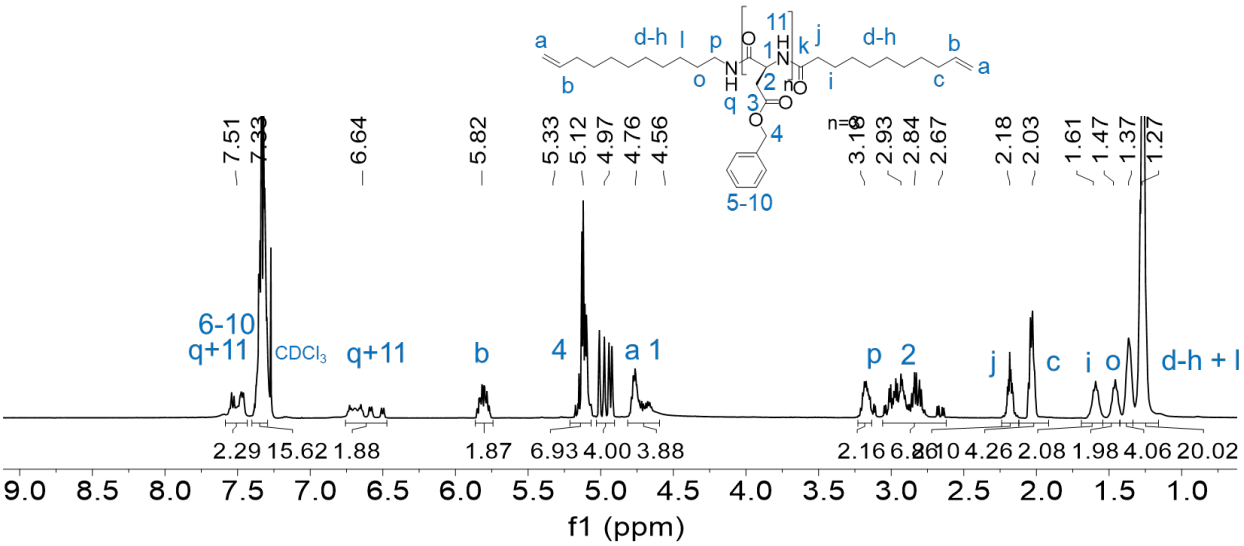

Figure S57. ^{1}H-NMR spectrum of **9a**.

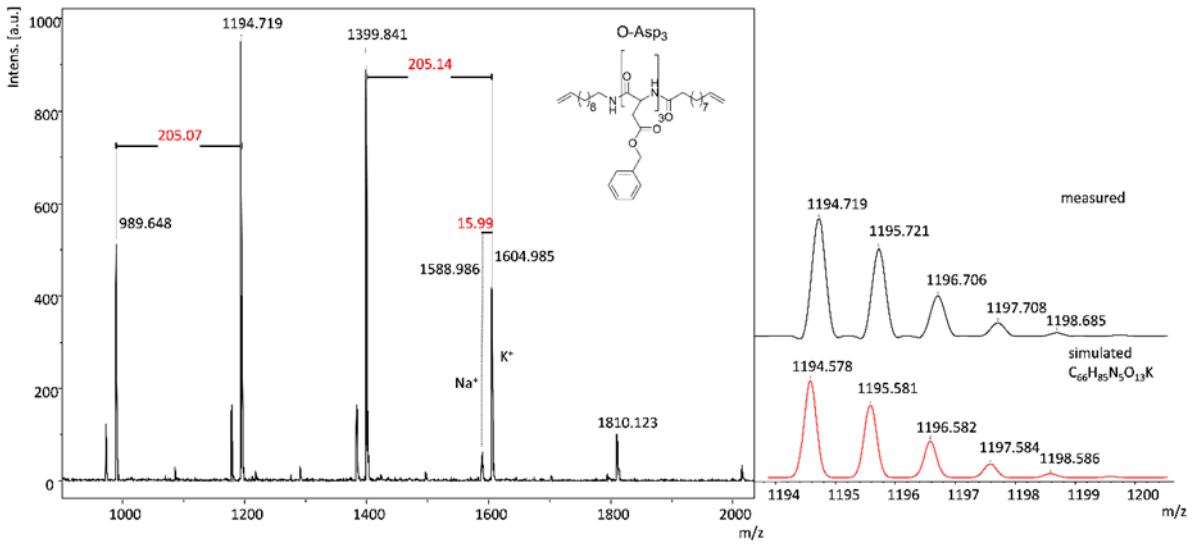

Figure S58. MALDI-TOF-MS spectrum of **O^{Bn}Asp$_3$** (**9a**) using dithranol as matrix and KTFA as salt.

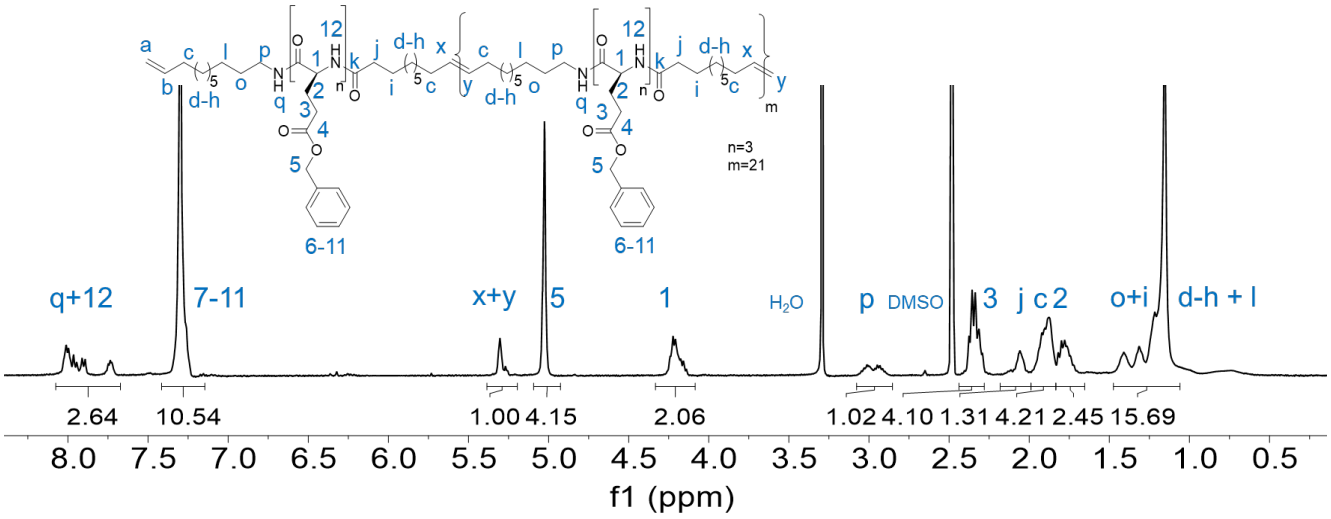

Figure S59. ^{1}H-NMR spectrum of **7b**.

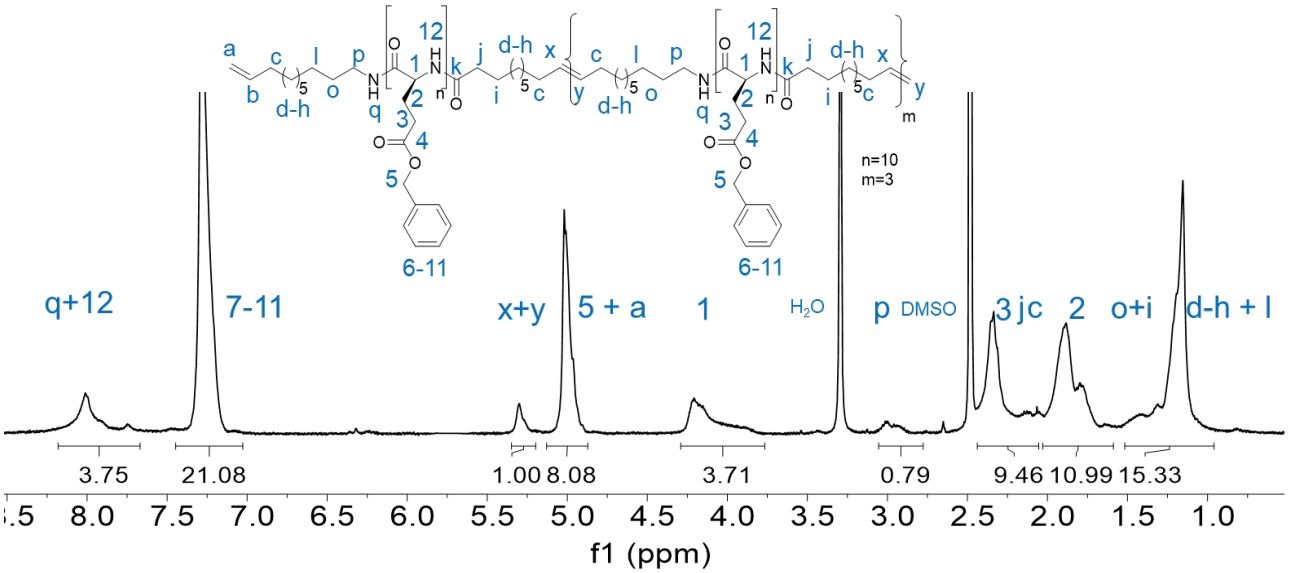

Figure S60. ^{1}H-NMR spectrum of **8b**.

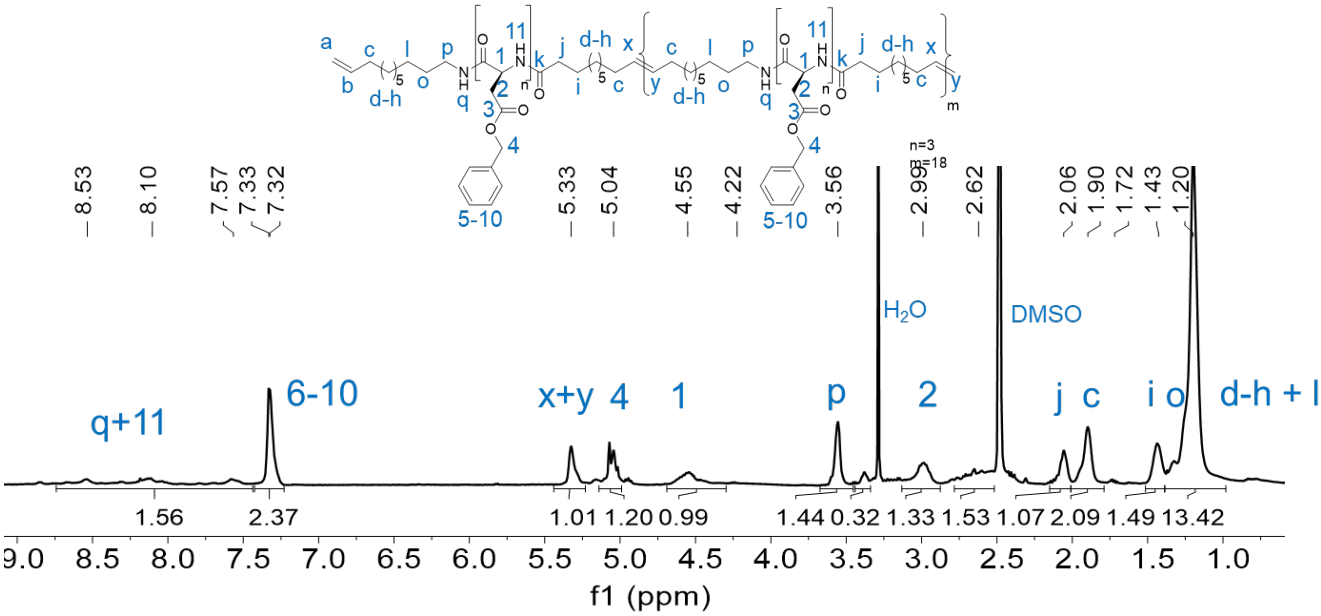

Figure S61. ^{1}H-NMR spectrum of **9b**.

S62. – S65. Preparative GPC curves for the fractionated ADMET-polymers

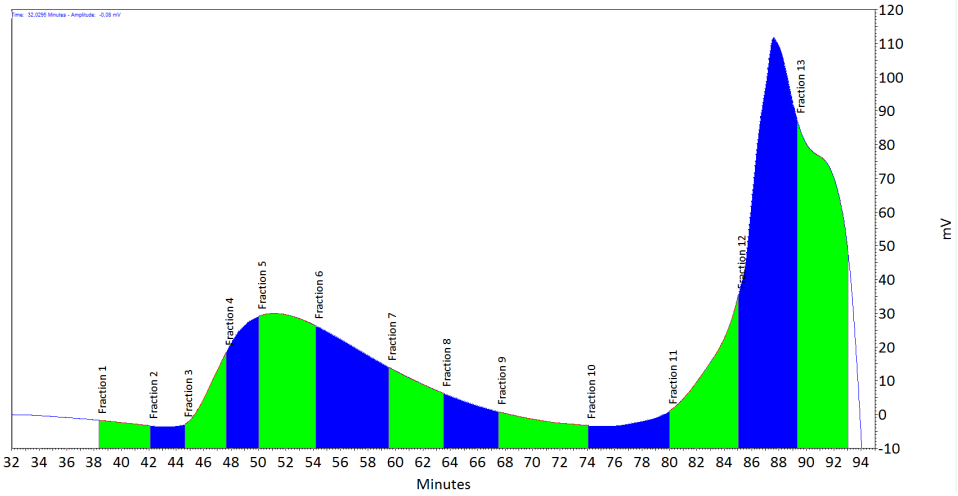

Figure S62. Preparative GPC curve for fractionation of **$AP_{21}(^{Bn}Glu_3)$ (7b)** in DMF (for fraction 1+2 no polymer could be obtained, for detailed information see Table 11).

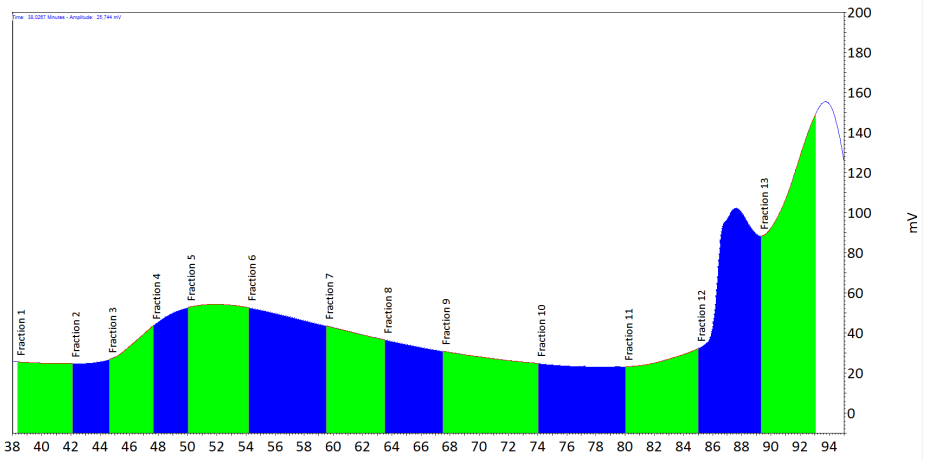

Figure S63. Preparative GPC curve for fractionation of **$AP_3(^{Bn}Glu_{10})$ (8b)** in DMF (for fraction 1+2 no polymer could be obtained, for detailed information see Table 11).

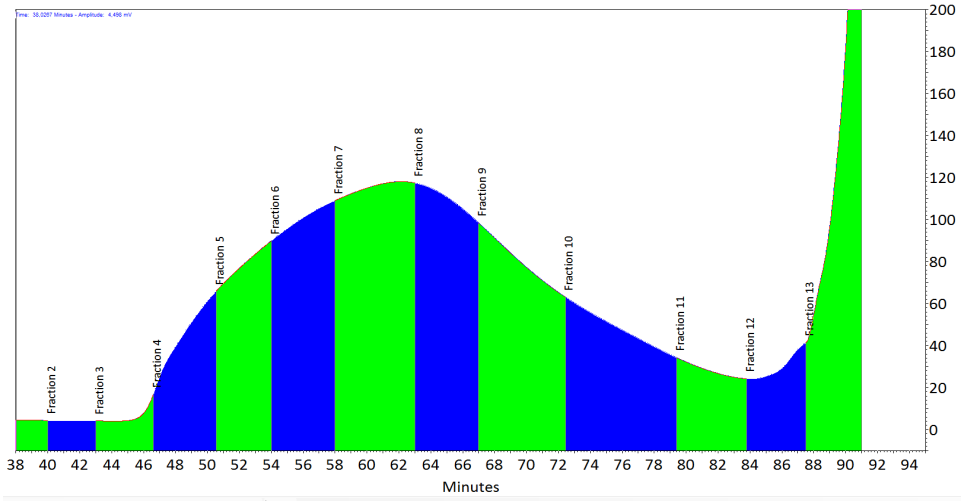

Figure S64. Preparative GPC curve for fractionation of **AP$_{18}$(^{Bn}Asp$_3$) (9b)** in DMF (for fraction 1+2 no polymer could be obtained, for detailed information see Table 11).

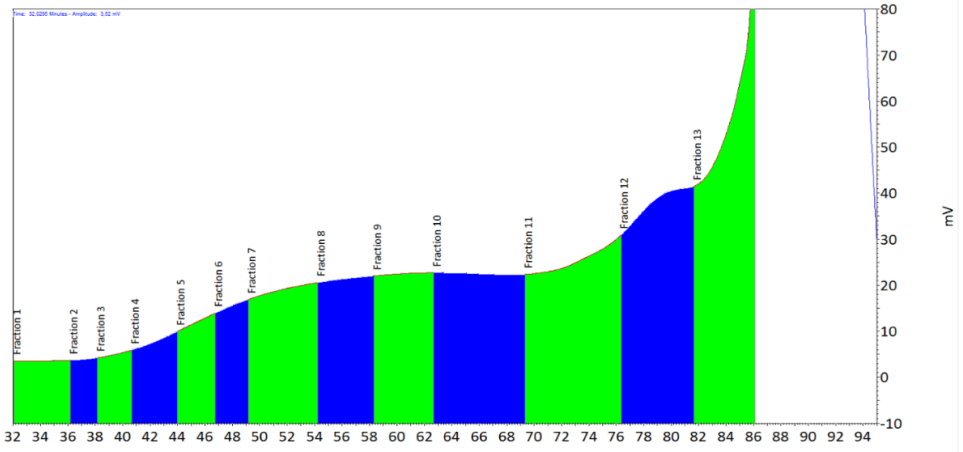

Figure S65. Preparative GPC curve for fractionation of **AP$_4$(^{Bn}Asp$_{10}$) (10b)** in DMF (for fraction 1+2 no polymer could be obtained, for detailed information see Table 11).

S66 – 68. Analytical GPC curves for the fractionated ADMET-polymers

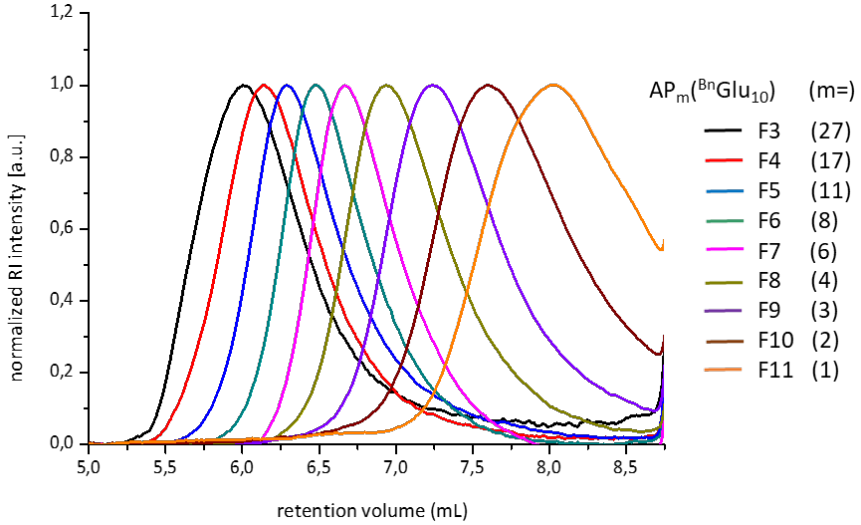

Figure S66. Normalized analytical GPC curves for obtained fractions of **AP$_3$(^{Bn}Glu$_{10}$) (8b)** after separation by preparative GPC.

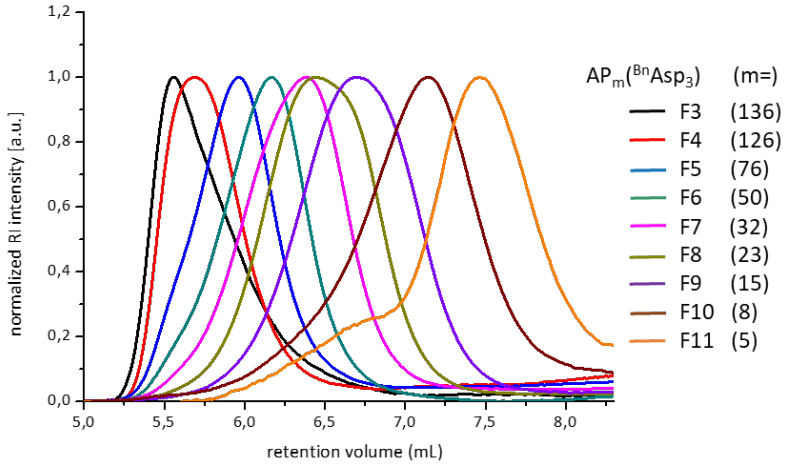

Figure S67. Normalized analytical GPC curves for obtained fractions of **AP$_{18}$(^{Bn}Asp$_3$)** (**9b**) after separation by preparative GPC.

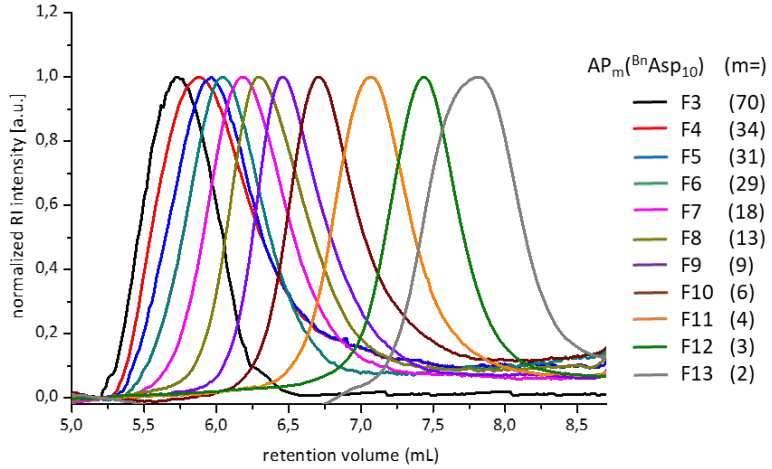

Figure S68. Normalized analytical GPC curves for obtained fractions of **AP$_4$(^{Bn}Asp$_{10}$)** (**10b**) after separation by preparative GPC .

S69. WAXS-investigation of O^{Bn}Glu$_{10}$ (8a) and AP$_3$(^{Bn}Glu$_{10}$) (8b)

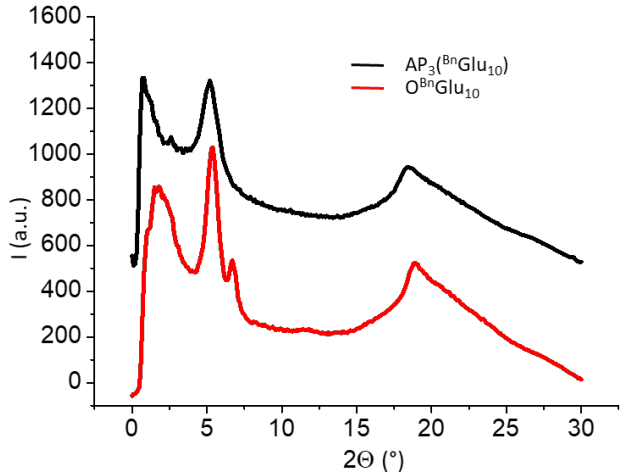

Figure S69. Wide-angle-X-ray diffraction patterns for **O^{Bn}Glu$_{10}$** (**8a**) (red) and **AP$_3$(^{Bn}Glu$_{10}$)** (**8b**) (black).

S70. FTIR in solid state for chosen fractions of $AP_m(^{Bn}Asp_3)$ and $AP_m(^{Bn}Asp_{10})$

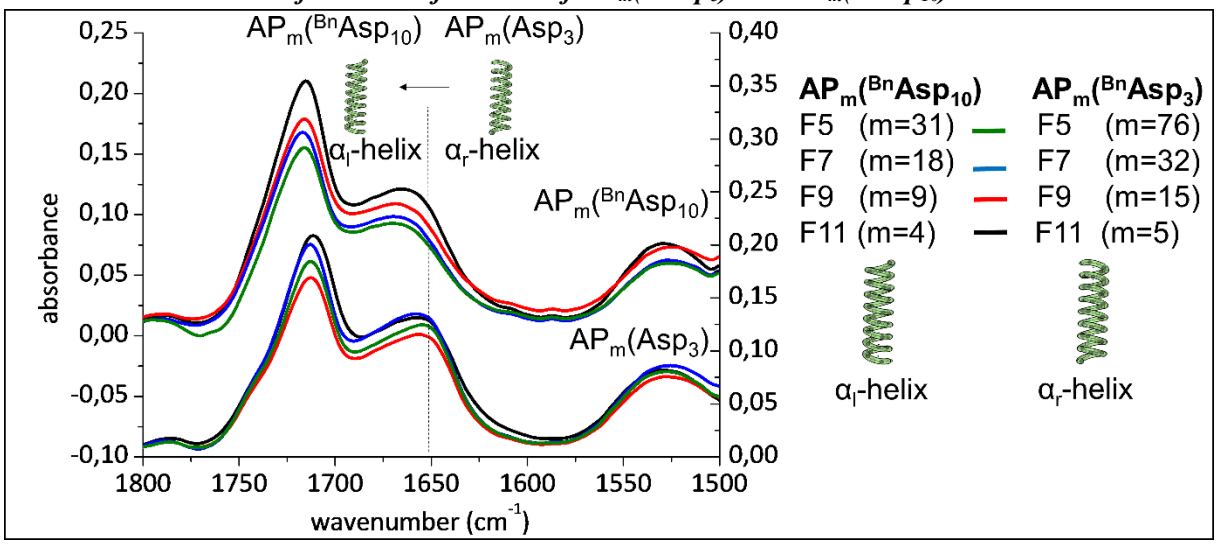

Figure S70. Solid state FTIR spectra for chosen fractions of **$AP_m(^{Bn}Asp_{10})$ (10b)** (top) and **$AP_m(^{Bn}Asp_3)$ (9b)** (bottom). No significant changes for different molecular weights (fractions) of the same ADMET-polymer could be observed, but a transition from right-handed to left-handed helical screw sense for increasing number of amino acids per building block.

S71. – S72. T-dependent FTIR in solid state for chosen fractions of $AP_m(^{Bn}Asp_3)$ and $AP_m(^{Bn}Asp_{10})$

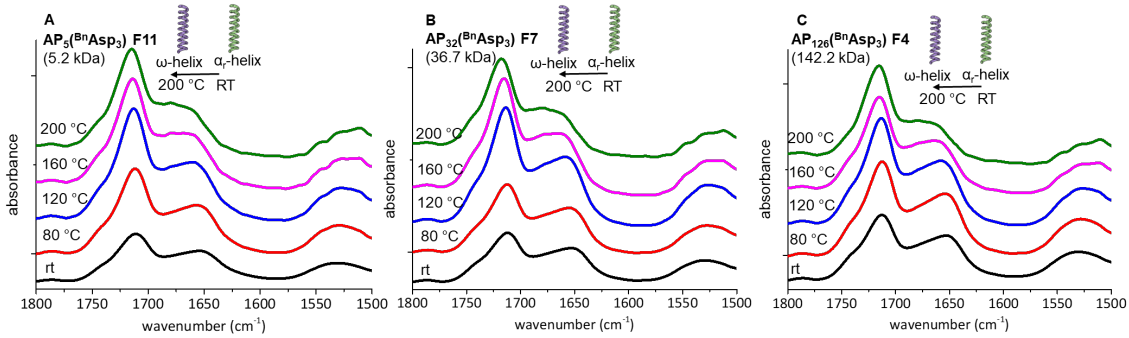

Figure S71. Temperature dependent FTIR measurement of A) **$AP_5(^{Bn}Asp_3)$ (F11)** (5.2 kDa), B) **$AP_{32}(^{Bn}Asp_3)$ (F7)** (36.7 kDa) and C) **$AP_{126}(^{Bn}Asp_3)$ (F4)** (142.2 kDa) at room temperature (RT, black curve), 80 °C (red curve), 120 °C (blue curve), 160 °C (pink curve) and 200 °C (green curve).

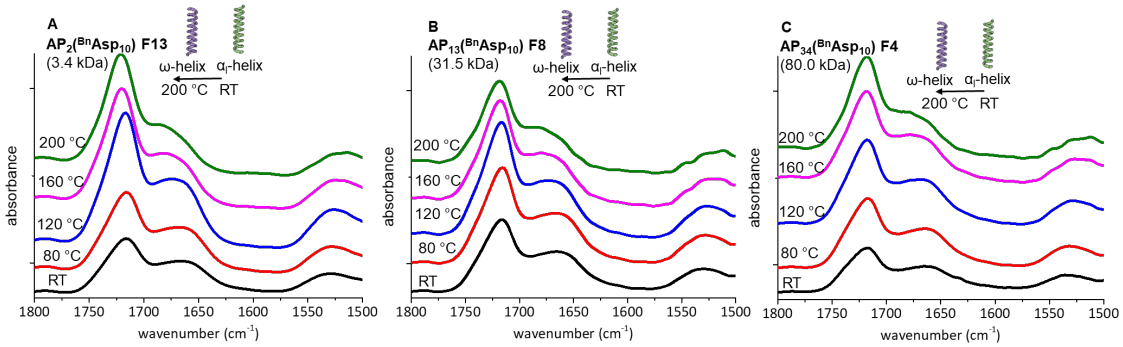

Figure S72. Temperature dependent FTIR measurement of A) **$AP_2(^{Bn}Asp_{10})$ (F13)** (3.4 kDa), B) **$AP_{13}(^{Bn}Asp_{10})$ (F8)** (31.5 kDa) and C) **$AP_{34}(^{Bn}Asp_{10})$ (F4)** (80.0 kDa) at room temperature (RT, black curve), 80 °C (red curve), 120 °C (blue curve), 160 °C (pink curve) and 200 °C (green curve).

S73. FTIR and CD-measurement of oligomer $O^{Bn}Glu_{10}$ (8a) and polymer $AP_3(^{Bn}Glu_{10})$ (8b) (unfractionated) in HFIP-solution.

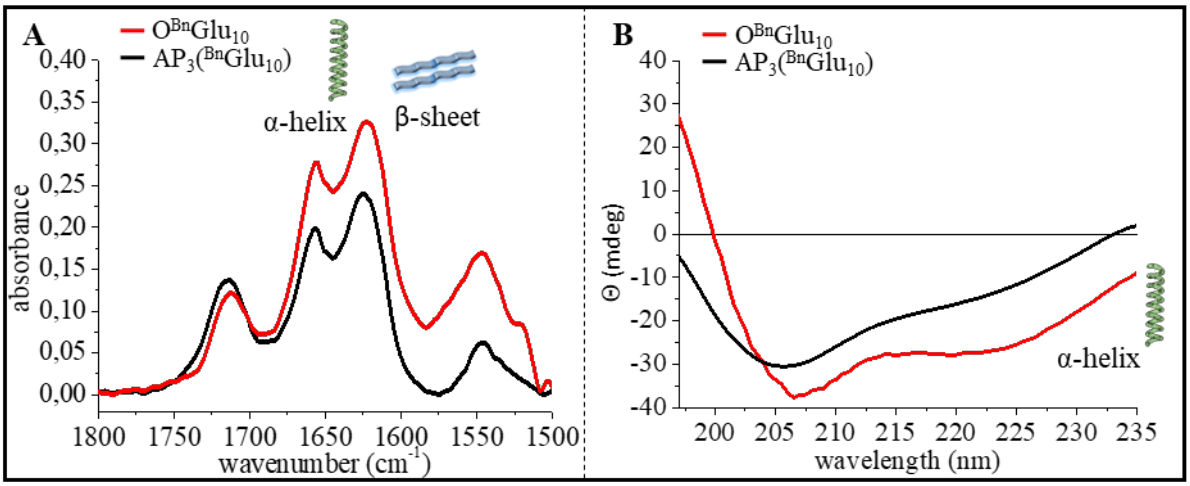

Figure S73. FTIR spectra (A) of the amide I and amide II region at concentrations of 2.0 mg mL^{-1} and CD spectra (B) at concentrations of 0.2 mg mL^{-1} in HFIP for **$O^{Bn}Glu_{10}$ (8a)** (red) and **$AP_3(^{Bn}Glu_{10})$ (8b)** (black).

S74. - S77. Concentration dependent FTIR measurements of oligomers and corresponding ADMET-polymers (unfractionated) in HFIP-solution.

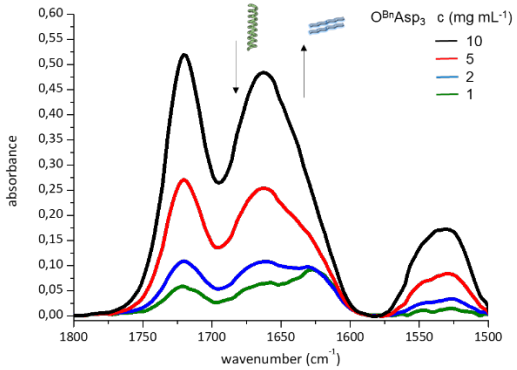

Figure S74. Concentration dependent measurement for **$O^{Bn}Asp_3$ (9a)** at 10 mg mL^{-1} (black), 5 mg mL^{-1} (red), 2 mg mL^{-1} (blue) and 1 mg mL^{-1} (green) with 0.5 mm PTFE spacer. With decreasing concentration, an increasing amount of β-sheet structure was observed.

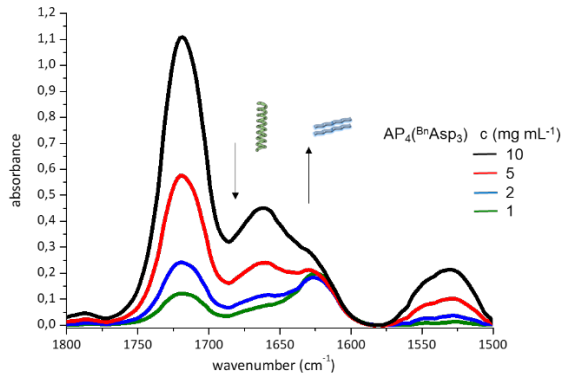

Figure S75. Concentration dependent measurement for **AP$_4$(^{Bn}Asp$_3$)** (**9b**) at 10 mg mL^{-1} (black), 5 mg mL^{-1} (red), 2 mg mL^{-1} (blue) and 1 mg mL^{-1} (green) with 0.5 mm PTFE spacer. With decreasing concentration, an increasing amount of β-sheet structure was observed.

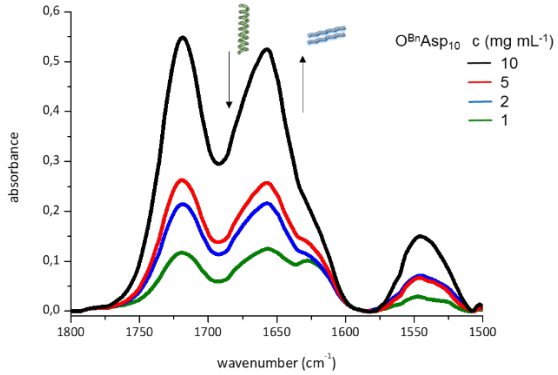

Figure S76. Concentration dependent measurement for **O^{Bn}Asp$_{10}$** (**10a**) at 10 mg mL^{-1} (black), 5 mg mL^{-1} (red), 2 mg mL^{-1} (blue) and 1 mg mL^{-1} (green) with 0.5 mm PTFE spacer. With decreasing concentration, an increasing amount of β-sheet structure was observed.

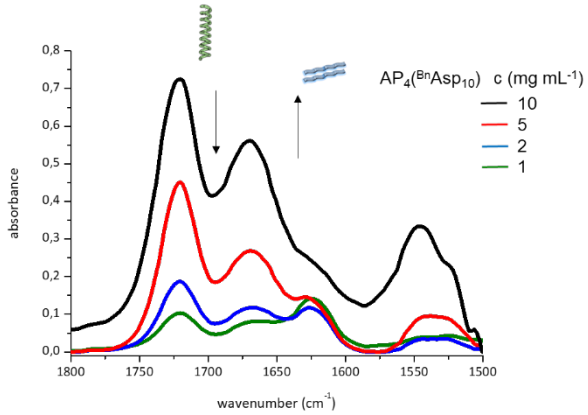

Figure S77. Concentration dependent measurement for **AP$_4$(^{Bn}Asp$_{10}$)** (**10b**) at 10 mg mL^{-1} (black), 5 mg mL^{-1} (red), 2 mg mL^{-1} (blue) and 1 mg mL^{-1} (green) with 0.5 mm PTFE spacer. With decreasing concentration, an increasing amount of β-sheet structure was observed.

S78. Characterization of Aib-NCA (11) and ACHC-NCA (12)

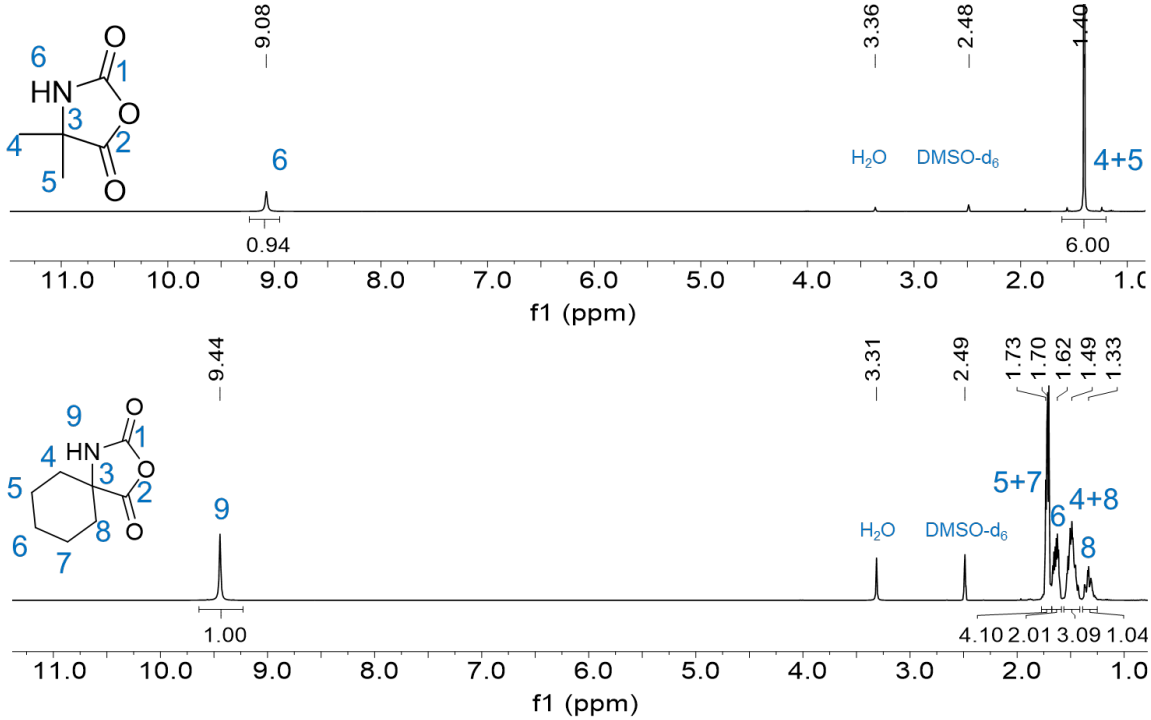

Figure S78. ^{1}H-NMR spectra of **11** (top) and **12** (bottom).

S79. – S80. Characterization of initiator A4

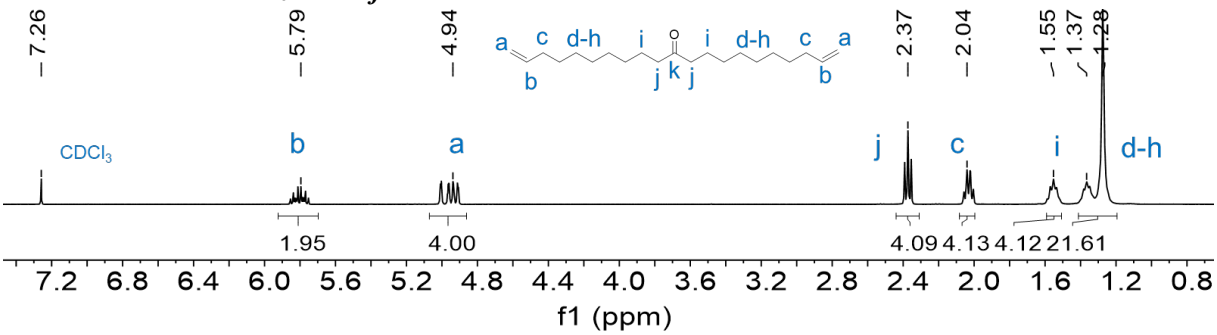

Figure S79. ^{1}H-NMR spectrum of **A3**.

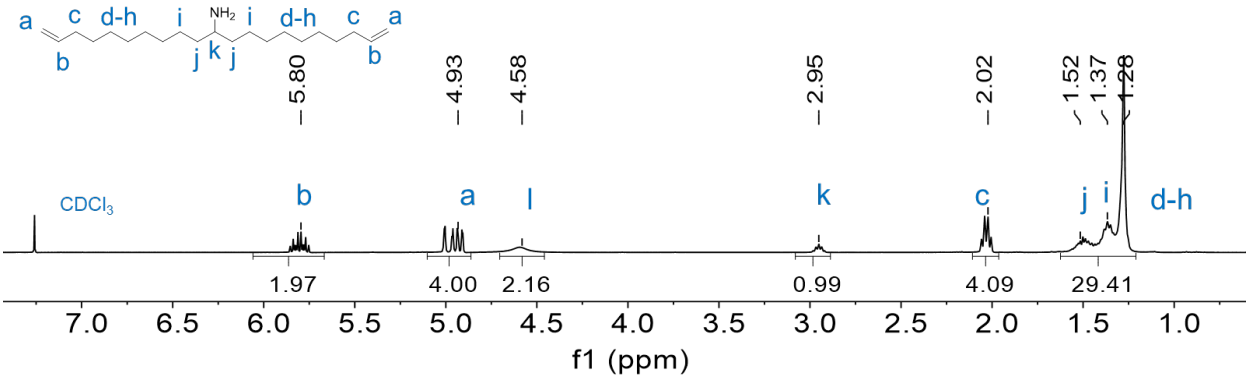

Figure S80. ^{1}H-NMR spectrum of **A4**.

S81. Characterization of polymers initiated by HMDS

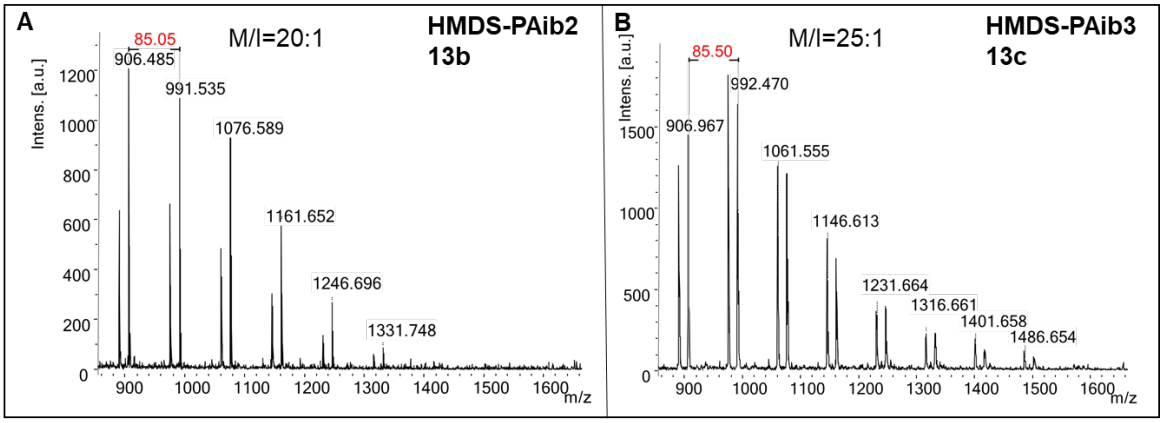

Figure S81. MALDI-TOF-MS spectra of **A**) **13b** and **B**) **13c** using dithranol as matrix and KTFA as salt.

S82. – S83. Characterization of polymers initiated by A4

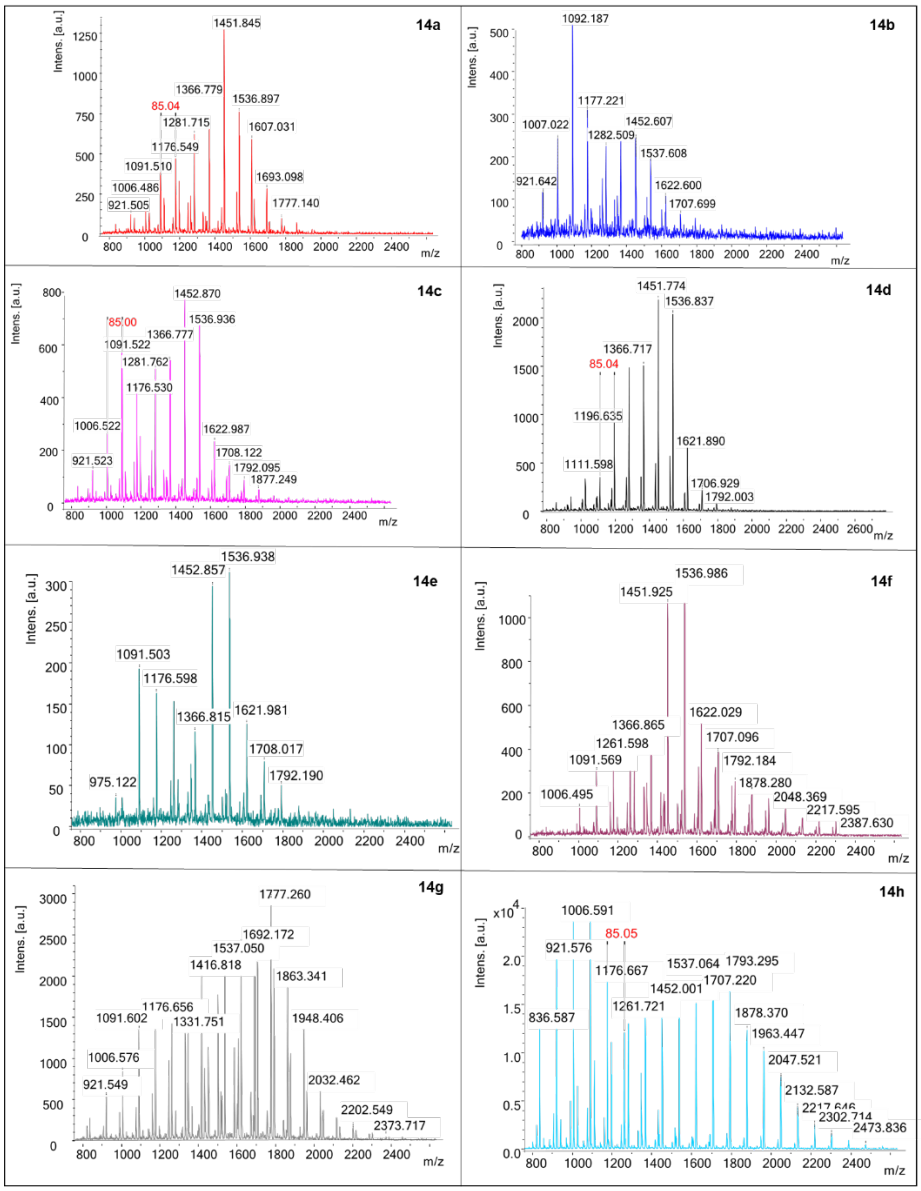

Figure S82. MALDI-TOF-MS spectra of **14a – 14h** using dithranol as matrix and KTFA as salt.

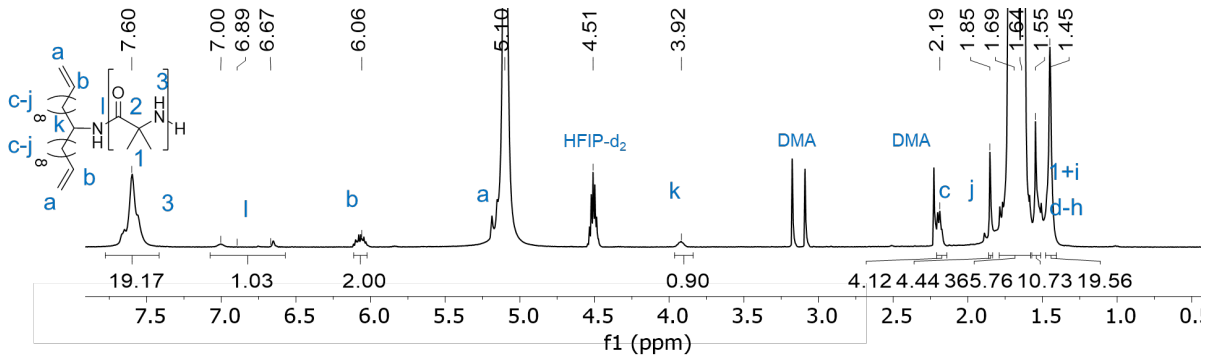

Figure S83. ^{1}H-NMR spectrum of **14i** in HFIP-d_2.

S84. Characterization of polymers initiated by A2

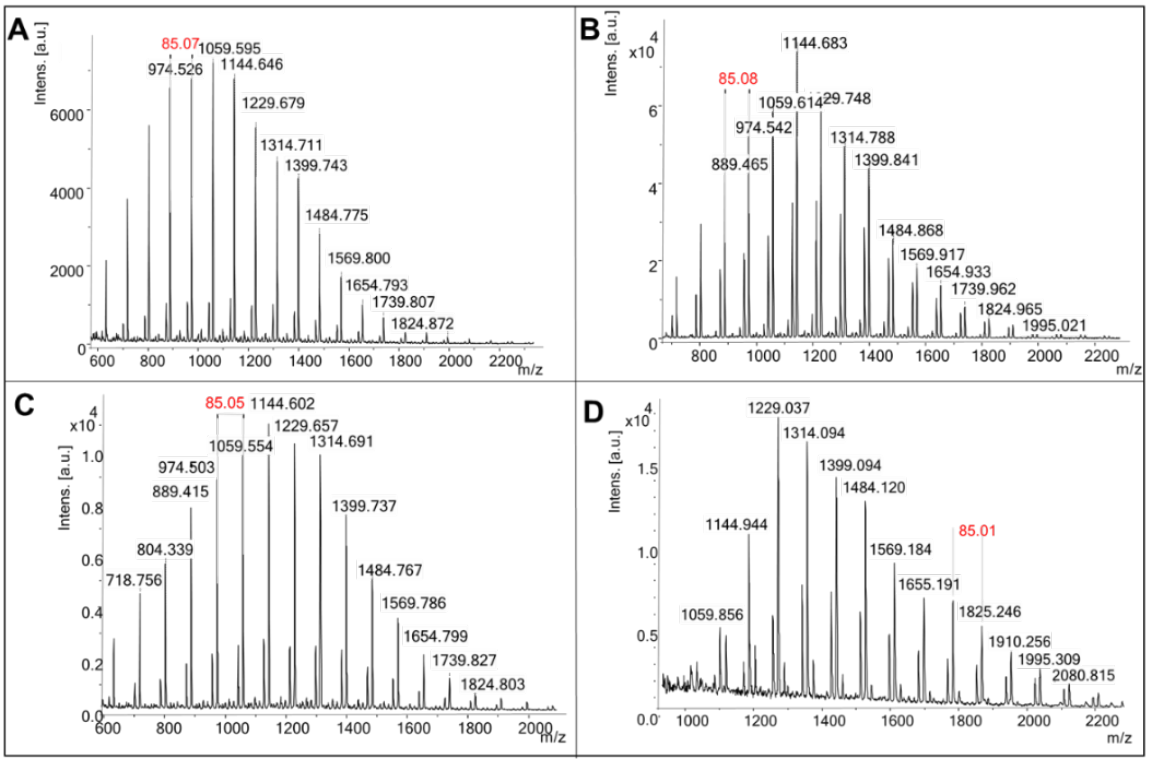

Figure S84. MALDI-TOF-MS spectra of **A**) **15a**, **B**) **15b**, **C**) **15c** and **D**) **15d** using dithranol as matrix and KTFA as salt.

S85. Calibration of FTIR with Aib-NCA (11)

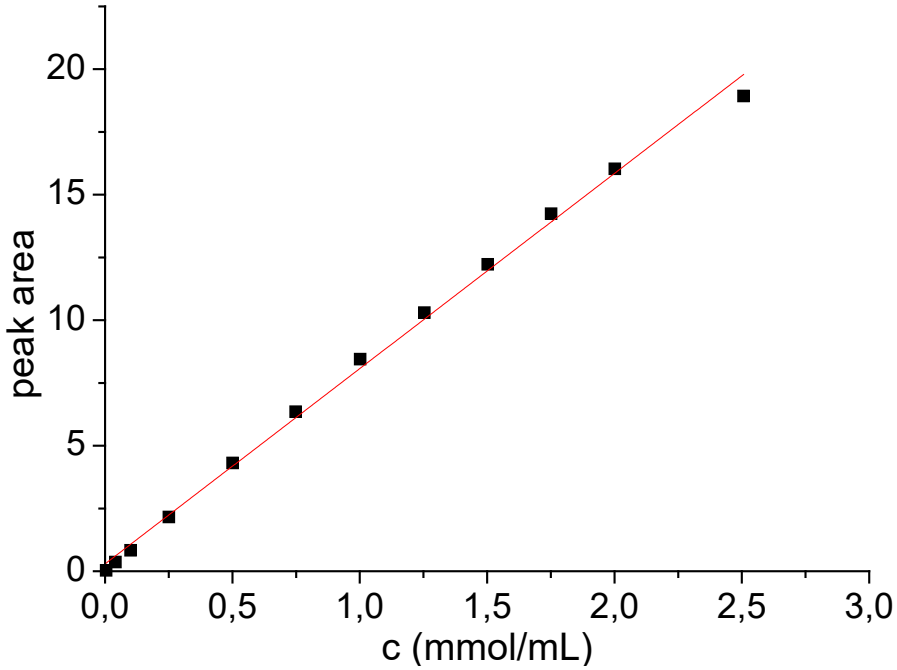

Figure S85. FTIR-calibration plot of the peak areas of the carbonyl peak at 1785 cm^{-1} *vs.* the **Aib-NCA** (**11**) monomer concentration (mmol mL^{-1}) in DMF at 80 °C.

S86. – S90. Characterization of amino acid-methyl ester hydrochlorides (16a – 16j)

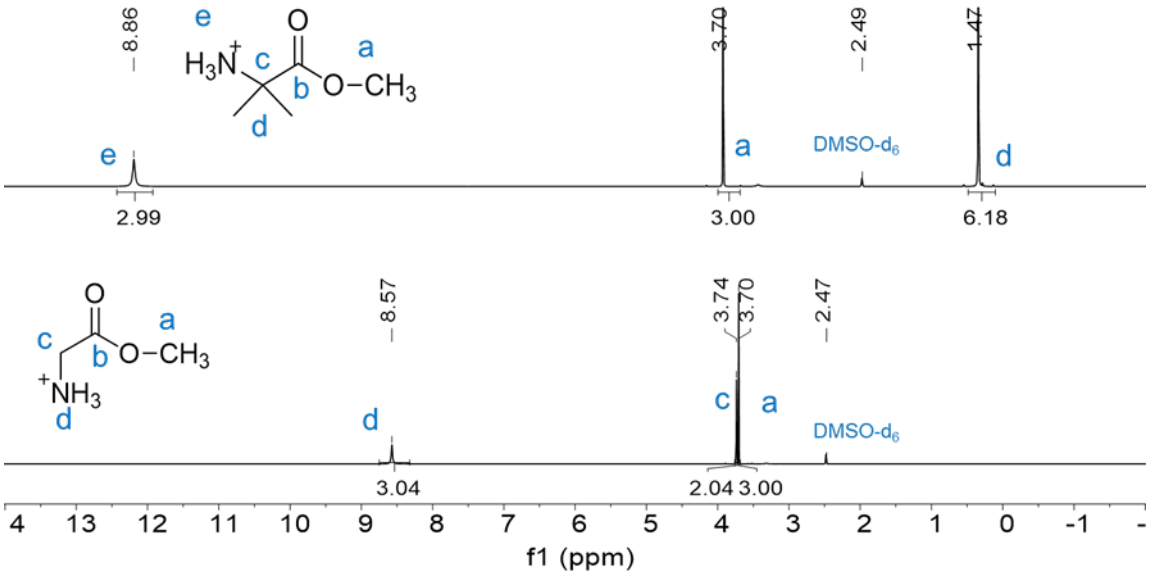

Figure S86. ^{1}H-NMR spectra of **NH_2-Aib-OMe · HCl** (**16a**) (top) and **NH_2-Gly-OMe · HCl** (**16b**) (bottom).

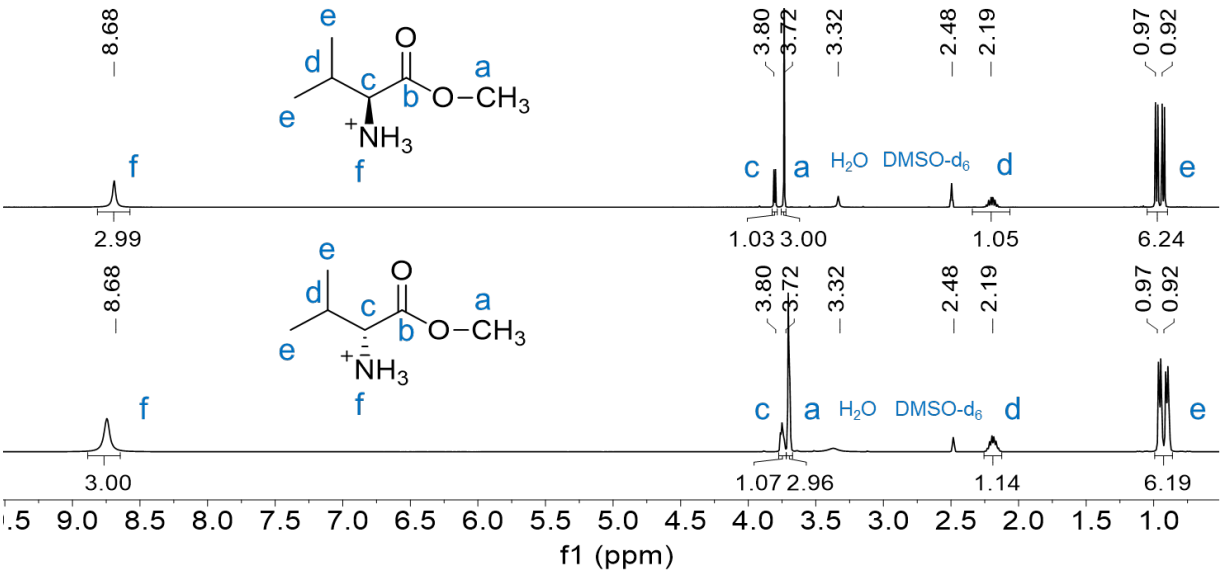

Figure S87. ^{1}H-NMR spectra of **NH_2-L-Val-OMe · HCl (16c)** (top) and **NH_2-D-Val-OMe · HCl (16d)** (bottom).

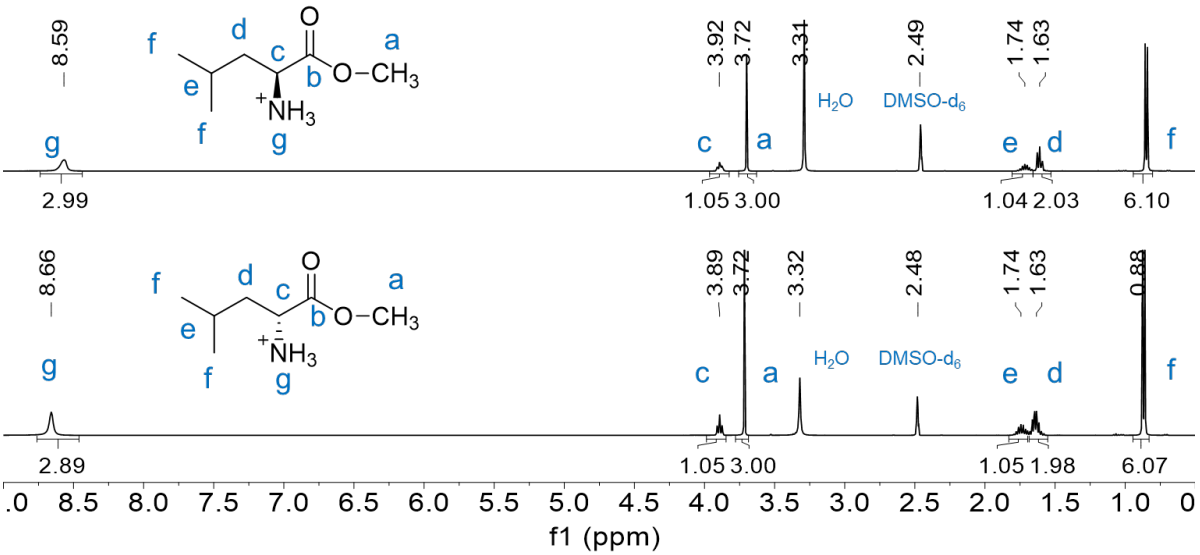

Figure S88. ^{1}H-NMR spectra of **NH_2-L-Leu-OMe · HCl (16e)** (top) and **NH_2-D-Leu-OMe · HCl (16f)** (bottom).

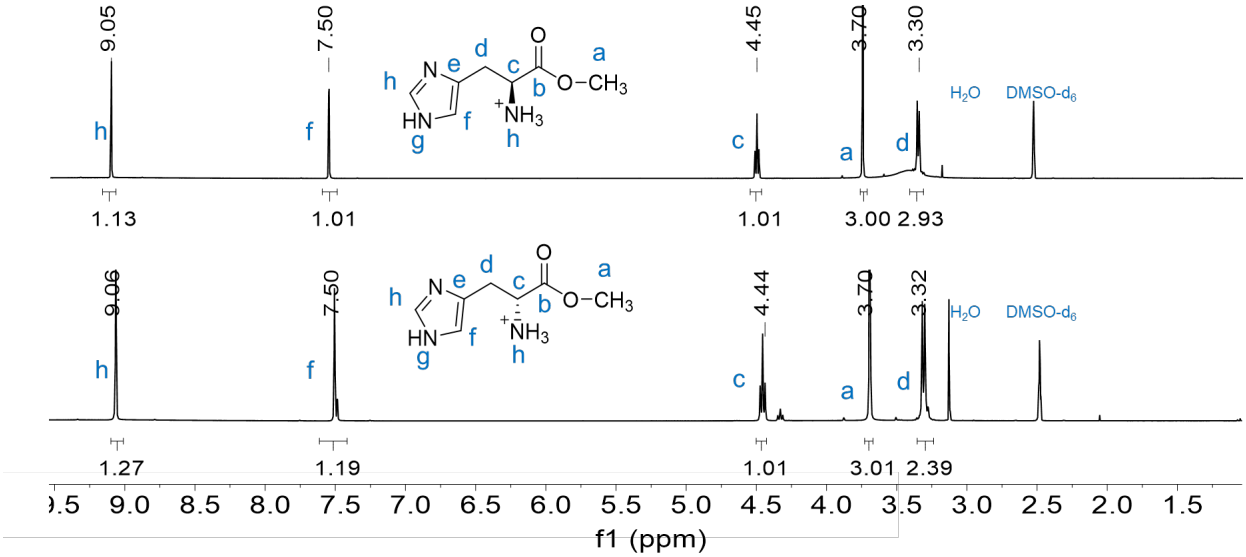

Figure S89. ^{1}H-NMR spectra of **NH_2-L-His-OMe · HCl (16g)** (top) and **NH_2-D-His-OMe · HCl (16h)** (bottom).

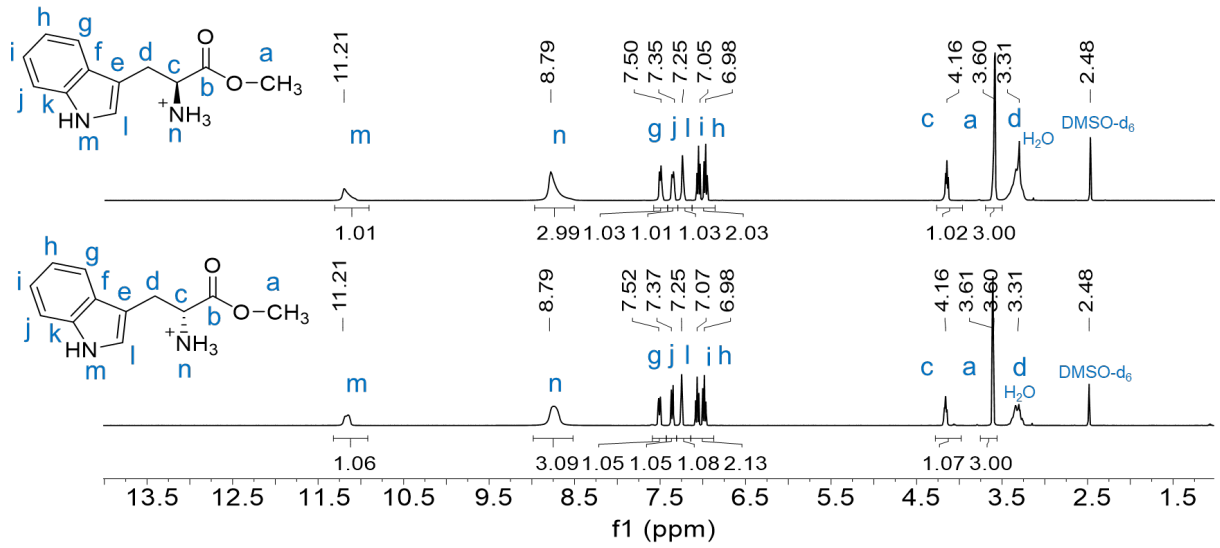

Figure S90. ^{1}H-NMR spectra of **NH_2-L-Trp-OMe · HCl (16i)** (top) and **NH_2-D-Trp-OMe · HCl (16j)** (bottom).

S91. – S99. Characterization of polymers 17a – 17j

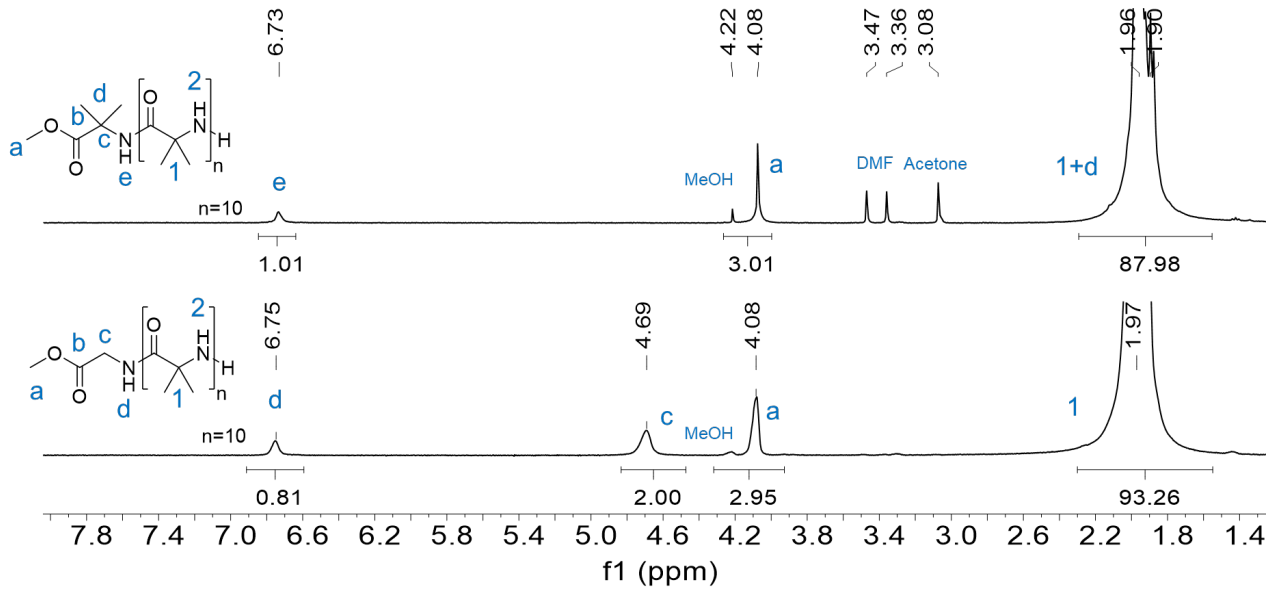

Figure S91. ^{1}H-NMR spectra of **OMe-Aib-PAib** (**17a**) (top) and **OMe-Gly-PAib** (**17b**) (bottom).

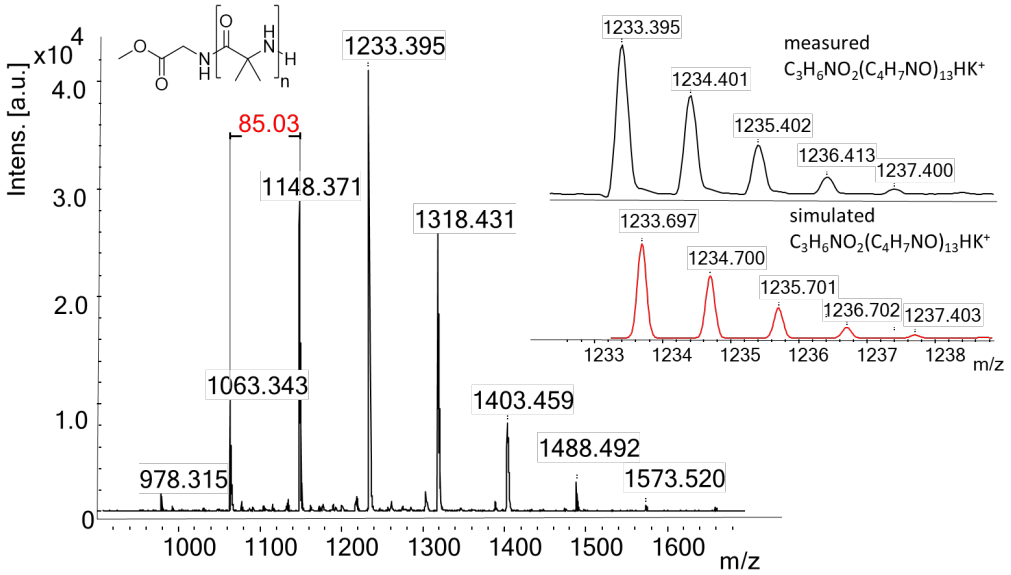

Figure S92. MALDI-TOF-MS spectrum of **OMe-Gly-PAib** (**17b**) using dithranol as matrix and KTFA as salt.

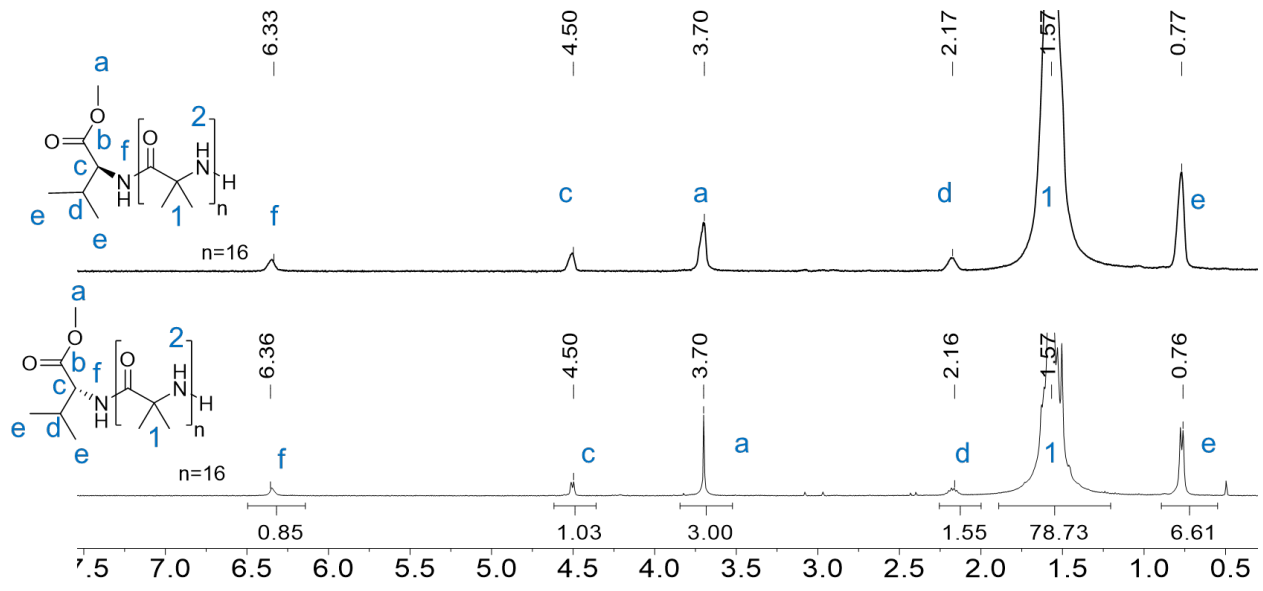

Figure S93. [1]H-NMR spectra of **OMe-L-Val-PAib** (**17c**) (top) and **OMe-D-Val-PAib** (**17d**) (bottom).

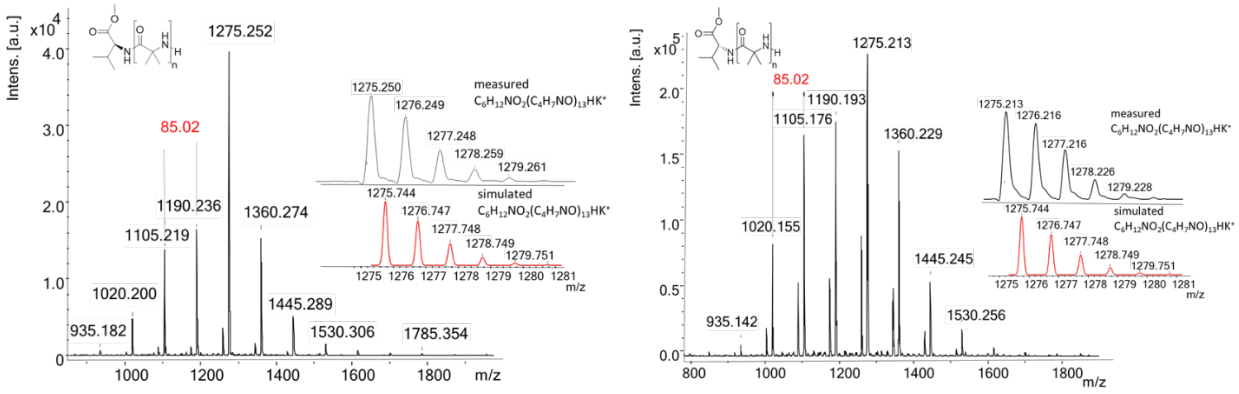

Figure S94. MALDI-TOF-MS spectra of **OMe-L-Val-PAib** (**17c**) and **OMe-D-Val-PAib** (**17d**) using dithranol as matrix and KTFA as salt.

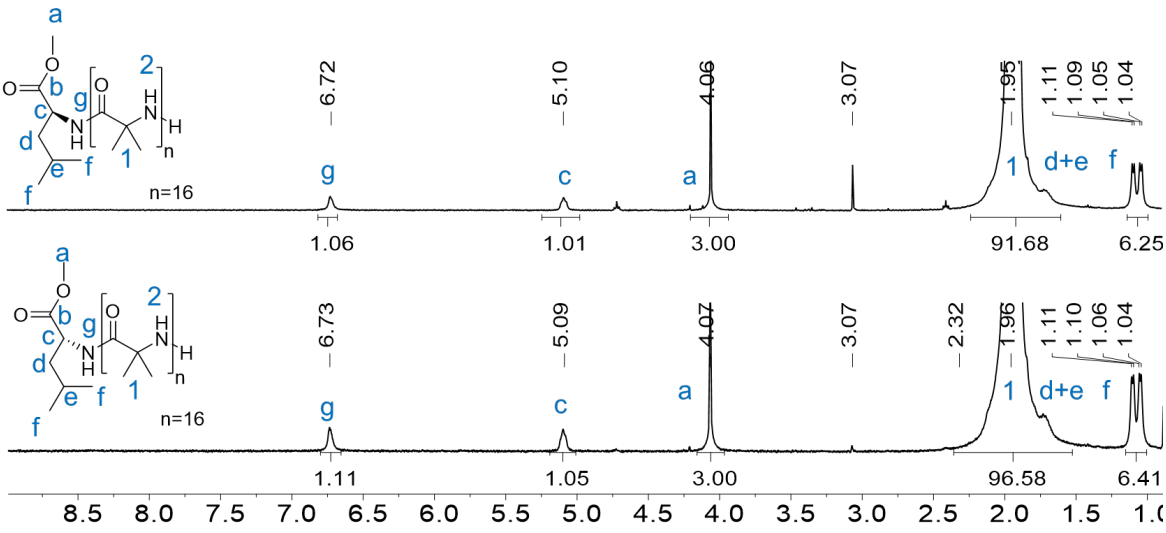

Figure S95. [1]H-NMR spectra of **OMe-L-Leu-PAib** (**17e**) (top) and **OMe-D-Leu-PAib** (**17f**) (bottom).

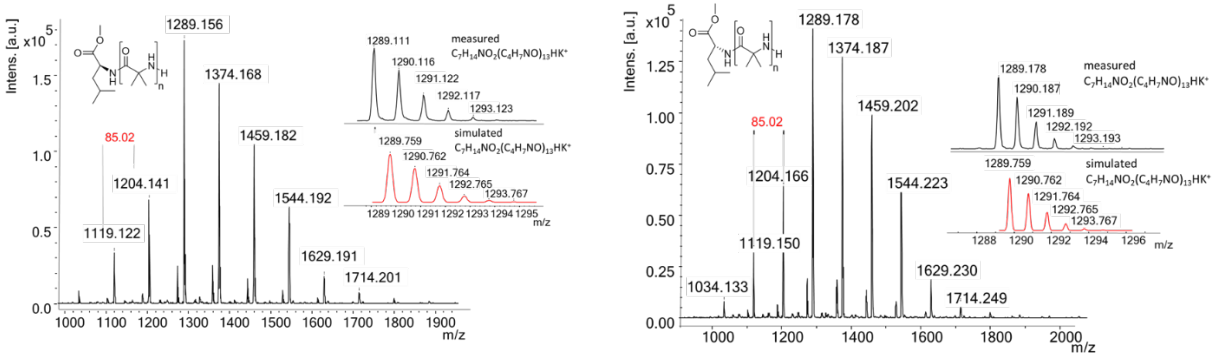

Figure S96. MALDI-TOF-MS spectra of **OMe-L-Leu-PAib** (**17e**) and **OMe-D-Leu-PAib** (**17f**) using dithranol as matrix and KTFA as salt.

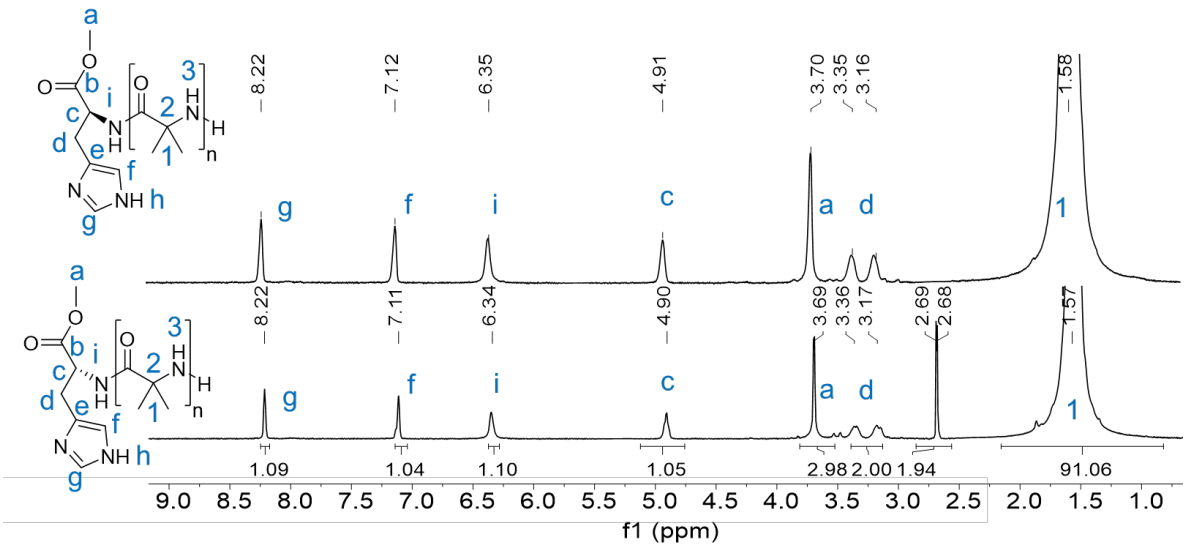

Figure S97. ^{1}H-NMR spectra of **OMe-L-His-PAib** (**17g**) (top) and **OMe-D-His-PAib** (**17h**) (bottom).

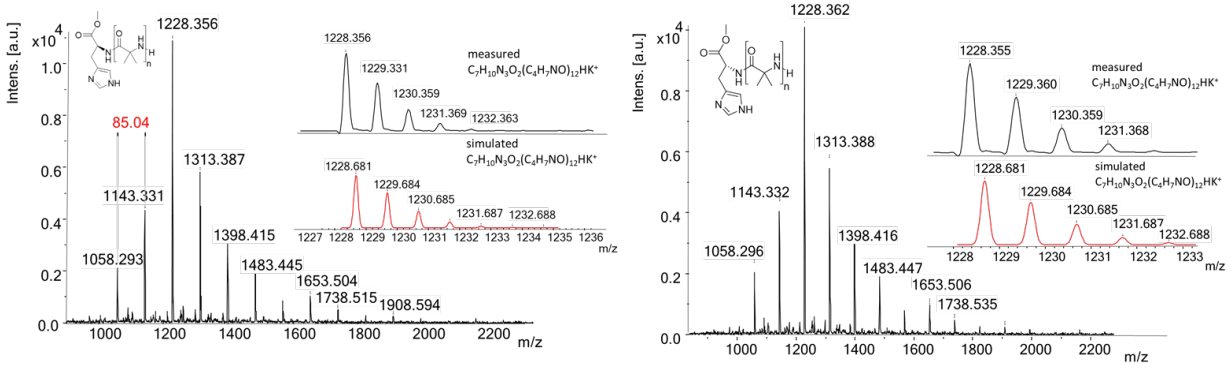

Figure S98. MALDI-TOF-MS spectra of **OMe-L-His-PAib** (**17g**) and **OMe-D-His-PAib** (**17h**) using dithranol as matrix and KTFA as salt.

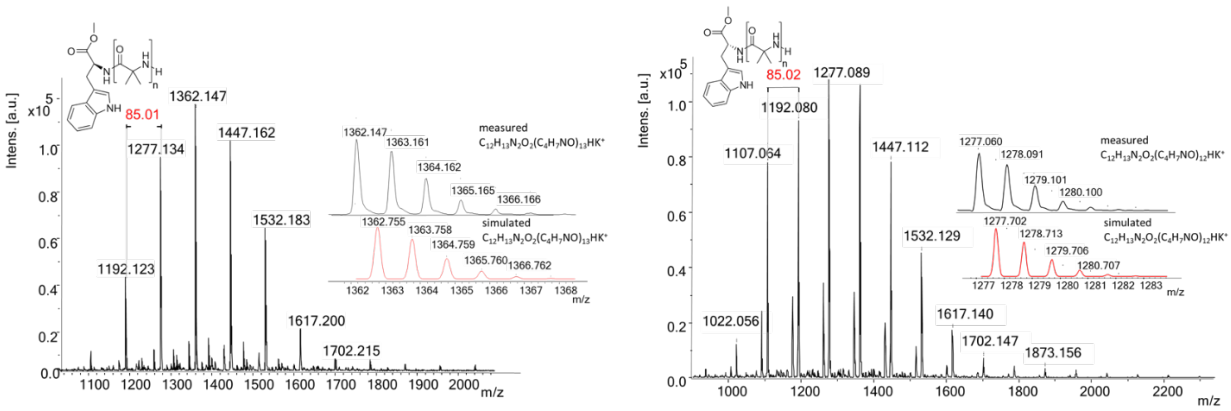

Figure S99. MALDI-TOF-MS spectra of **OMe-L-Trp-PAib** (**17i**) and **OMe-D-Trp-PAib** (**17j**) using dithranol as matrix and KTFA as salt.

S100. – S101. IR-investigation for polymers 17a – 17j

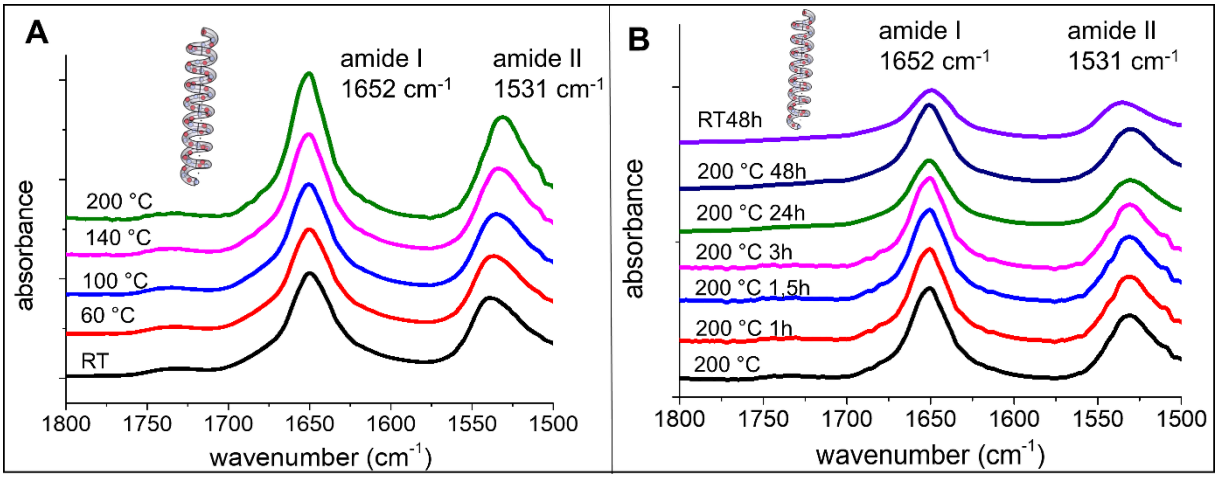

Figure S100. A) Temperature and **B**) time dependent FTIR-spectra of **OMe-Aib-PAib** (**17a**) in the amide I and amide II region in the solid state.

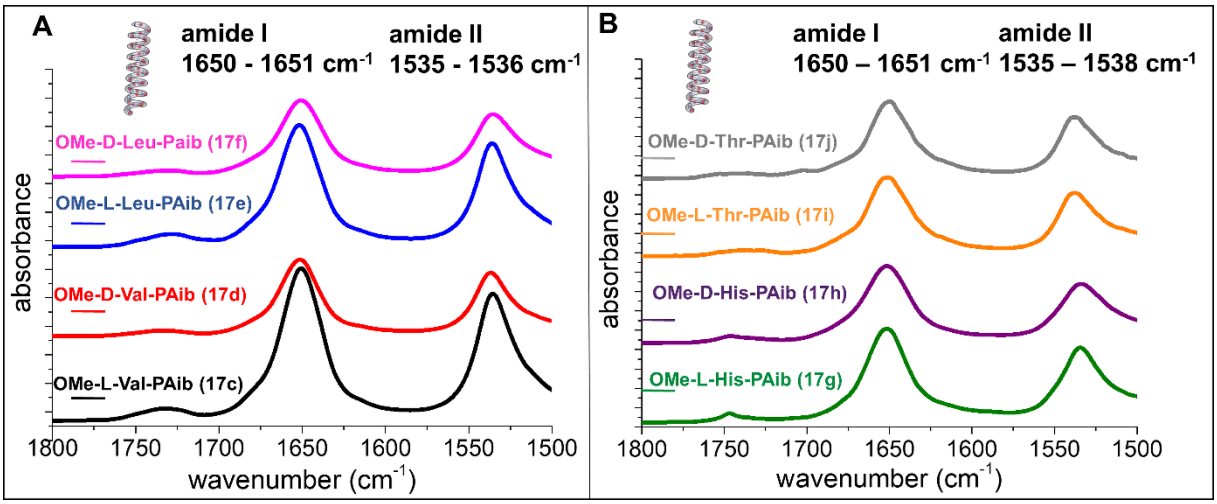

Figure S101. FTIR-spectra of **A**) **OMe-L-Val-PAib** (**17c**), **OMe-D-Val-PAib** (**17d**), **OMe-L-Leu-PAib** (**17e**) and **OMe-D-Leu-PAib** (**17f**) and **B**) **OMe-L-His-PAib** (**17g**), **OMe-D-His-PAib** (**17h**), **OMe-L-Trp-PAib** (**17i**), **OMe-D-Trp-PAib** (**17j**) in the amide I and amide II region at room temperature in the solid state.

S102. CD-analysis of 17a-17d and 17i-17j in HFIP

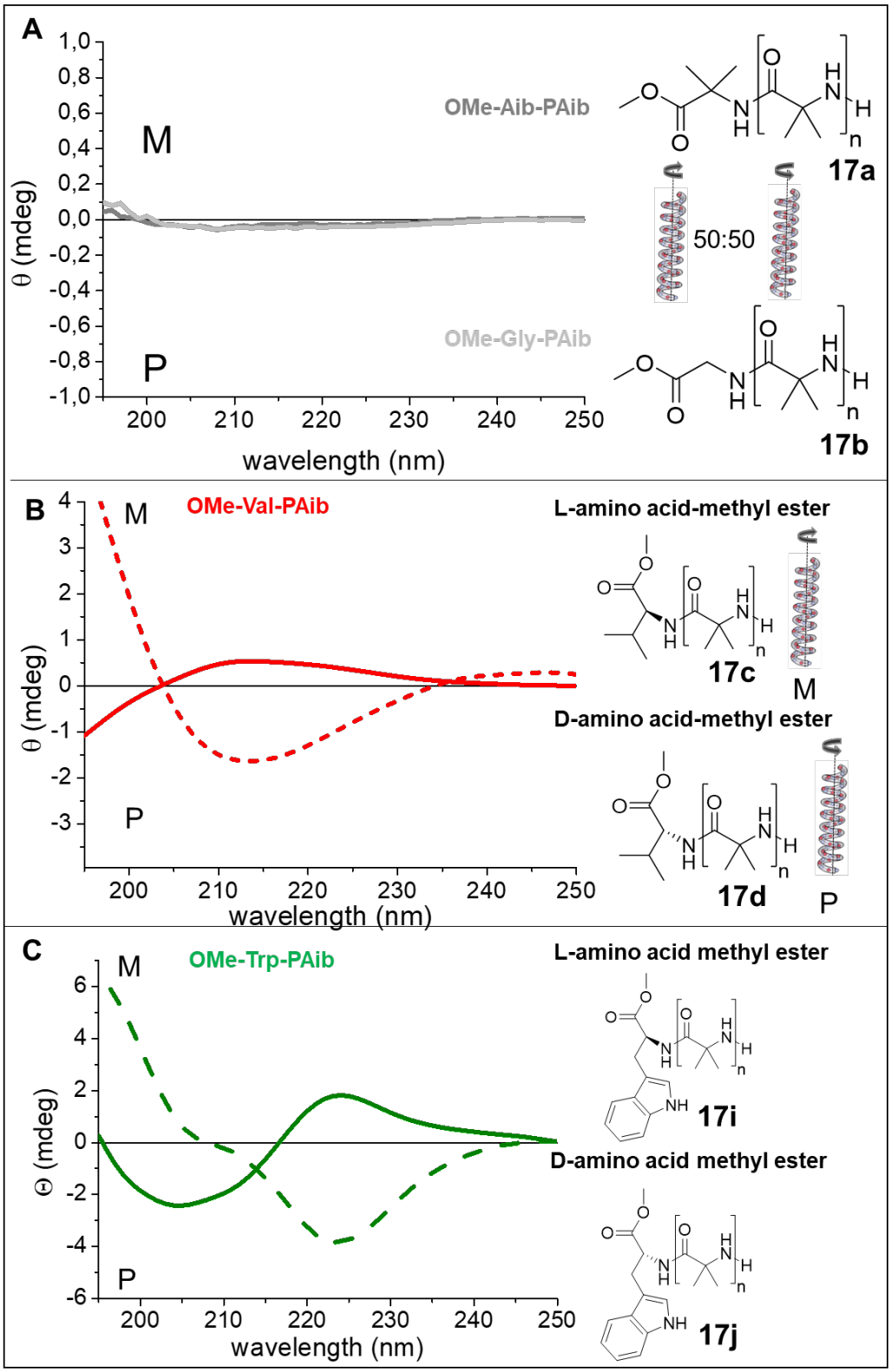

Figure S102. CD spectra at 0.2 mg mL^{-1} in HFIP for **A**) **OMe-Aib-PAib (17a)** (straight curve, dark grey) and **OMe-Gly-PAib (17b)** (straight curve, light grey) **B**) **OMe-L-Val-PAib (17c)** (straight curve, red) and **OMe-D-Val-PAib (17d)** (dotted curve, red) and **C**) **OMe-L-Trp-PAib (17i)** (straight curve, green) and **OMe-D-Trp-PAib (17j)** (dotted curve, green).

S103. – S108. Characterization of azo-initiators 18-21

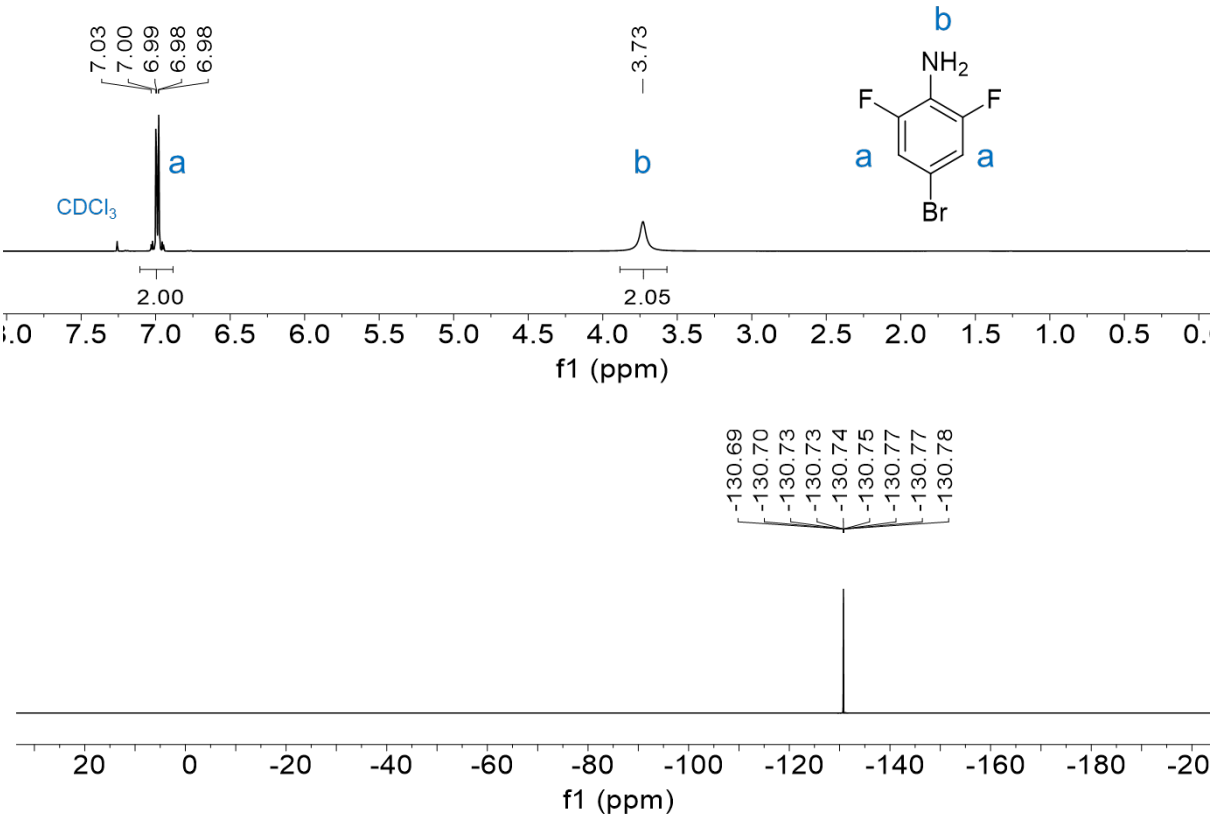

Figure S103. [1]H-NMR (top) and [19]F-NMR spectra (bottom) of **18a**.

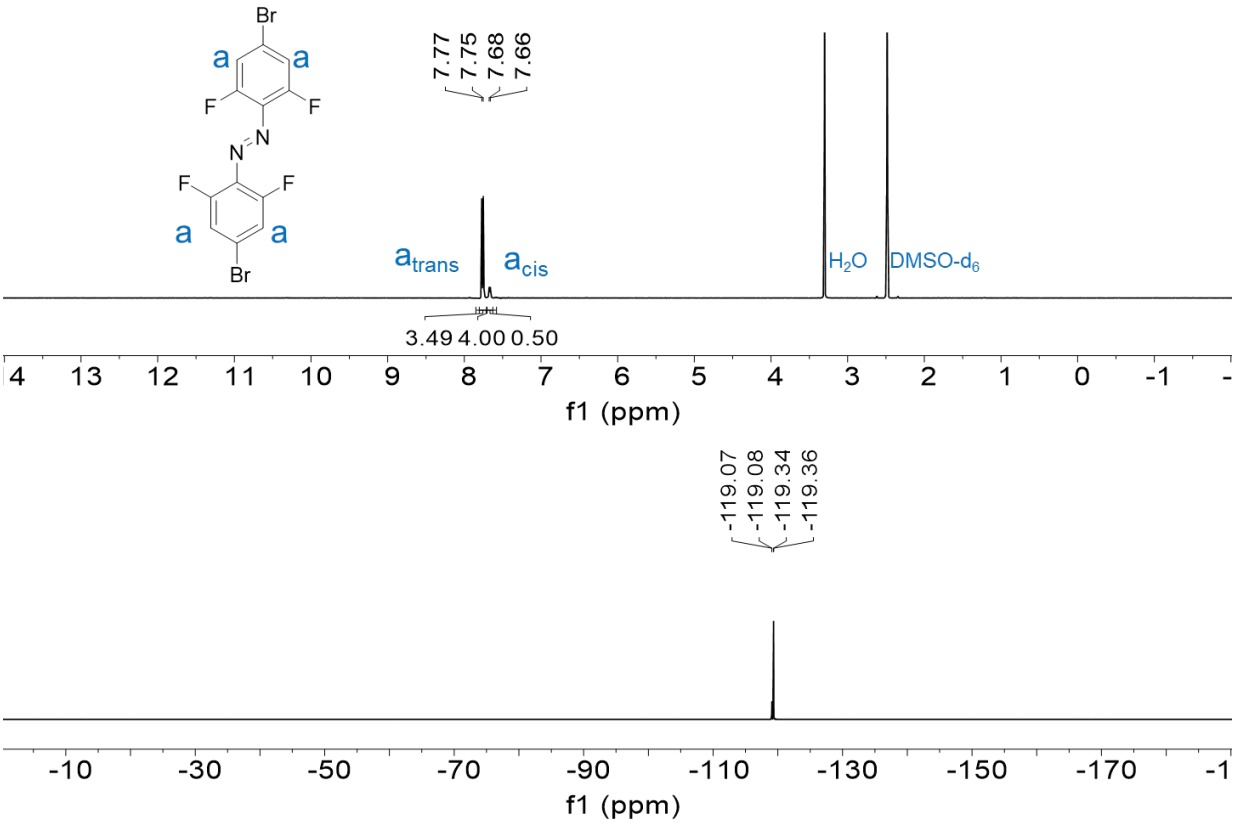

Figure S104. [1]H-NMR (top) and [19]F-NMR spectra (bottom) of **18b**.

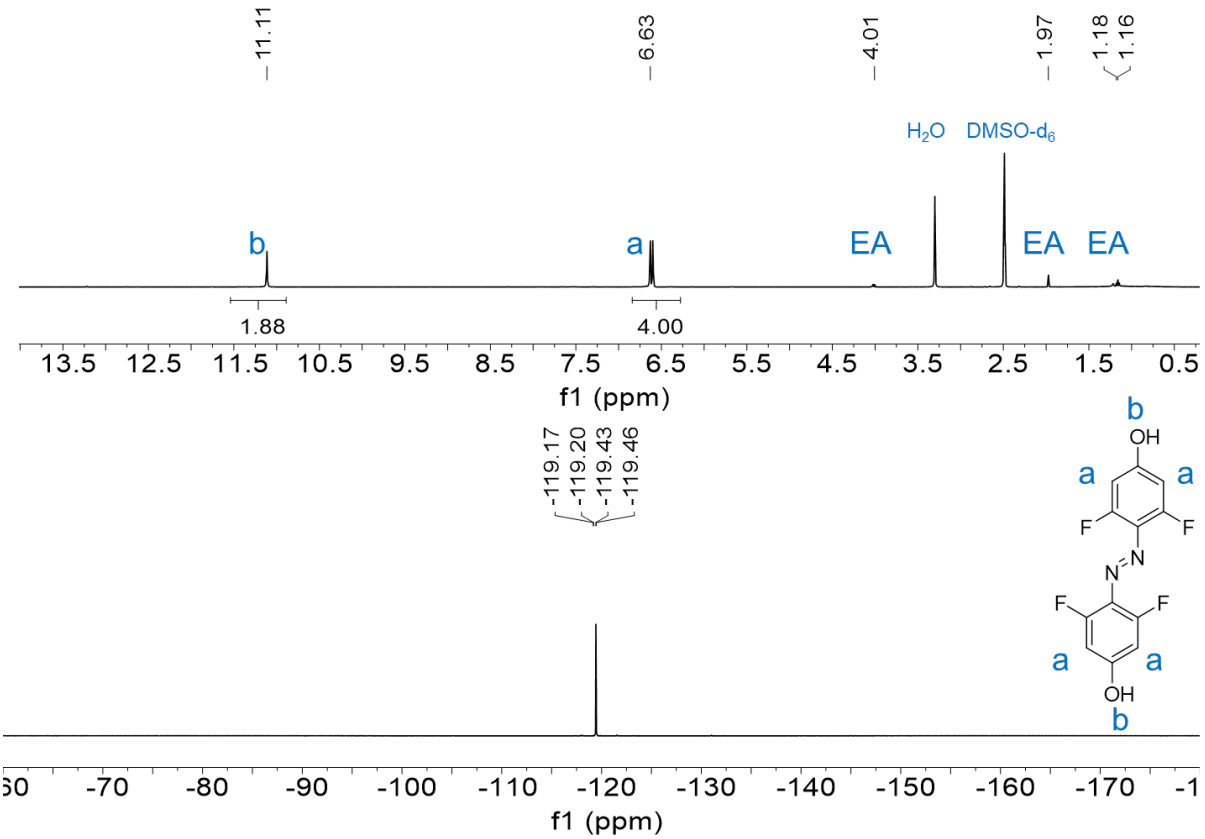

Figure S105. [1]H-NMR (top) and [19]F-NMR spectra (bottom) of **19**.

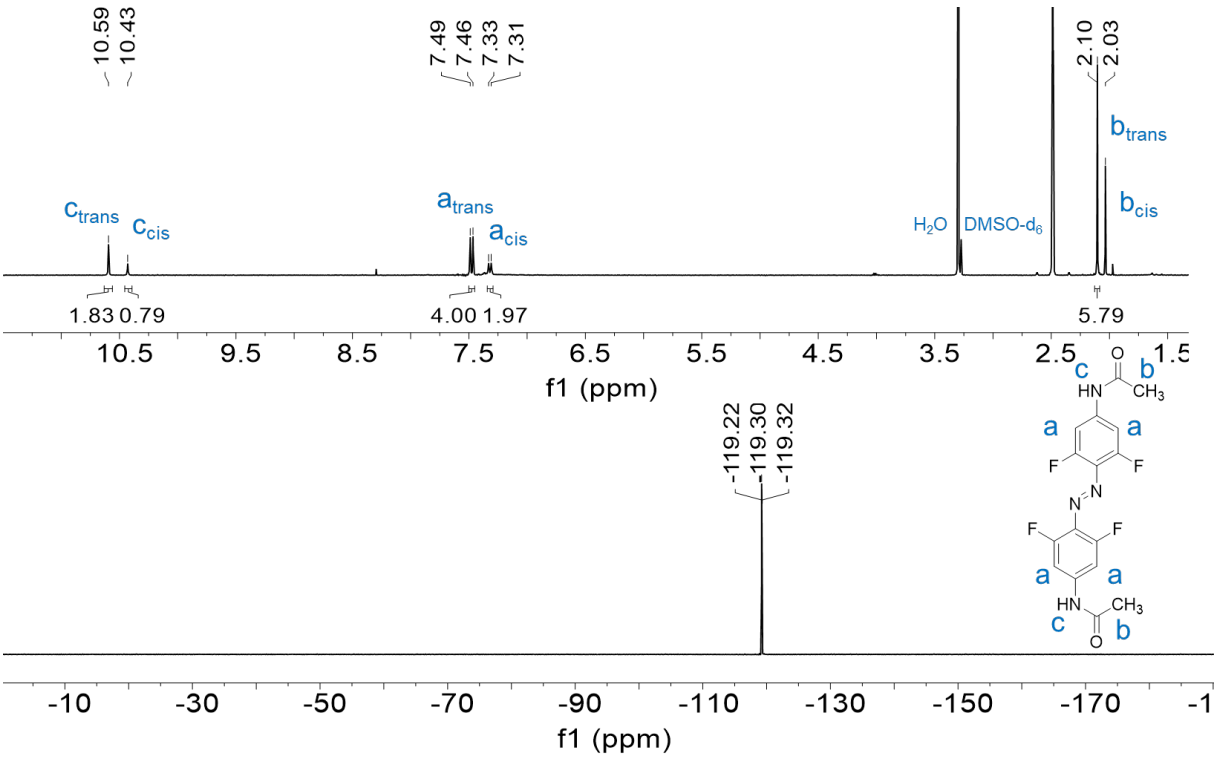

Figure S106. [1]H-NMR (top) and [19]F-NMR spectra (bottom) of **18d**.

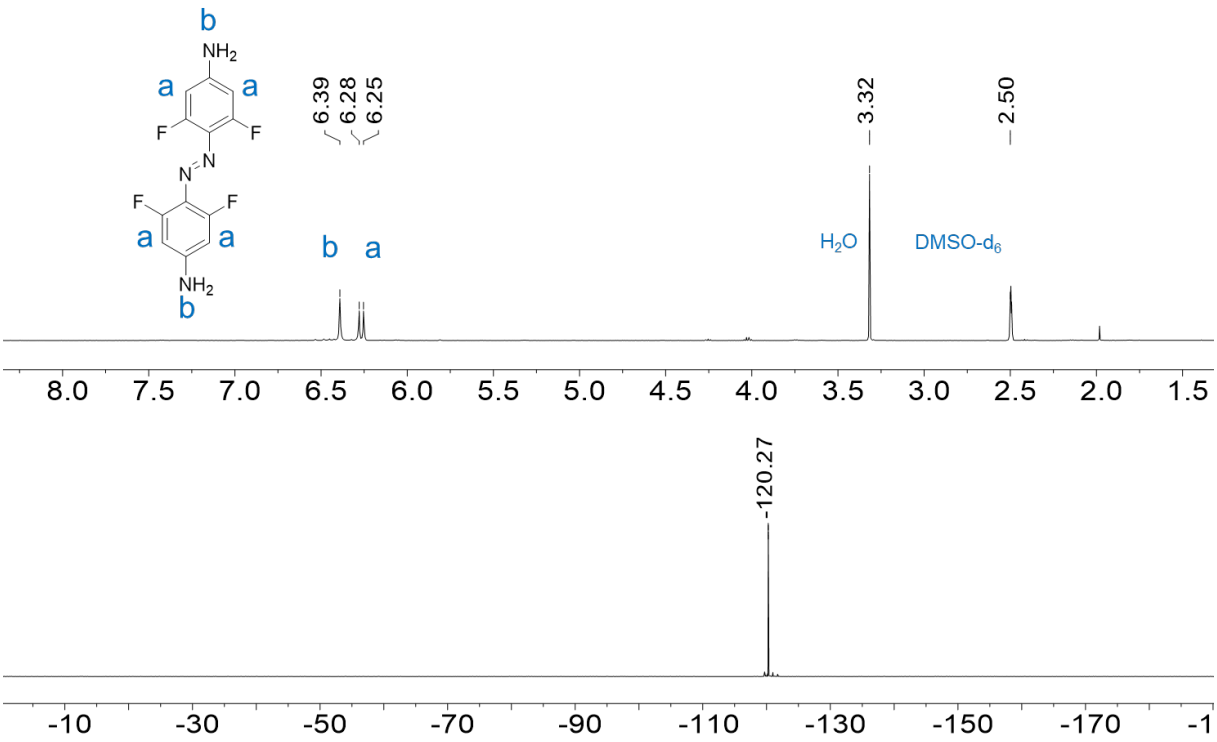

Figure S107. [1]H-NMR (top) and [19]F-NMR spectra (bottom) of **20**.

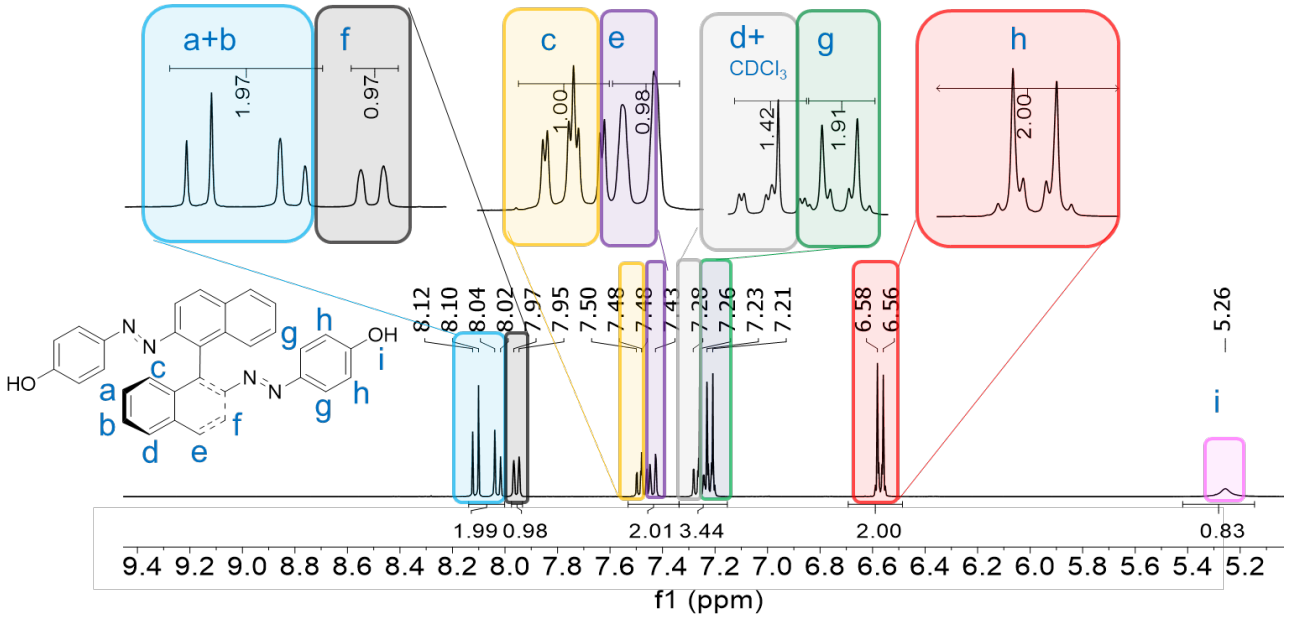

Figure S108. [1]H-NMR spectrum of **21** in $CDCl_3$.

S109. – 112. Characterization of polymers 19a, 19b, 20a, 20b

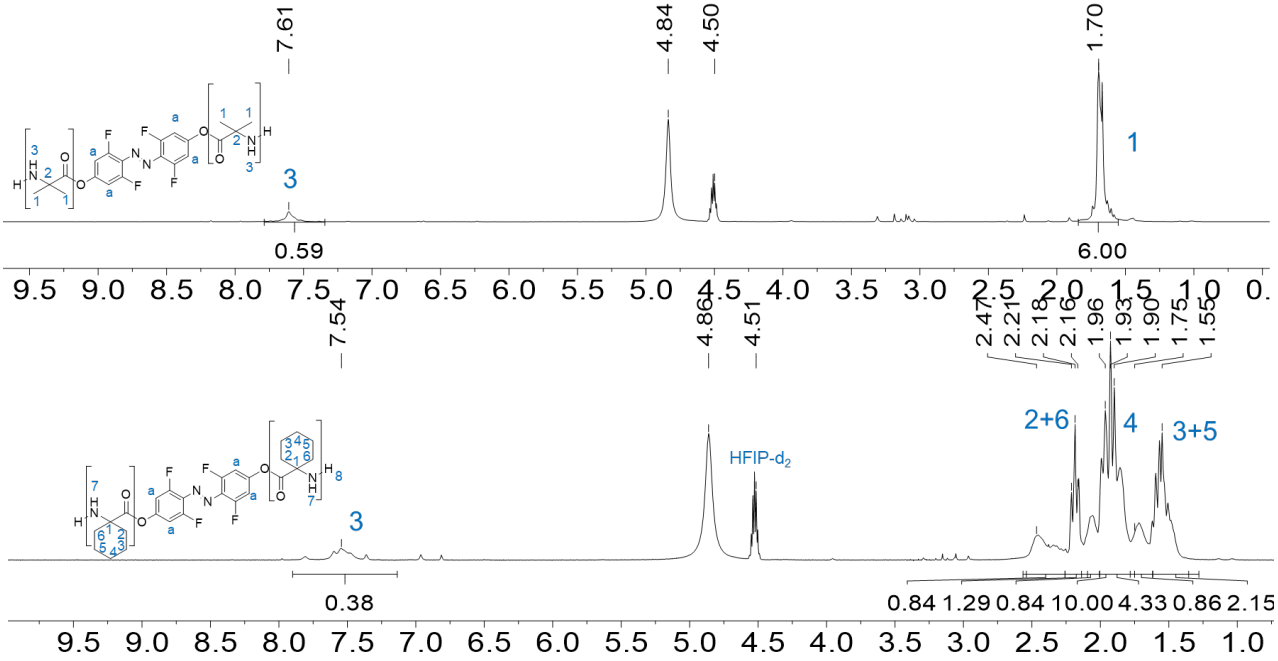

Figure S109. ^{1}H-NMR spectra of **19a** (top) and **19b** (bottom) in HFIP-d_2.

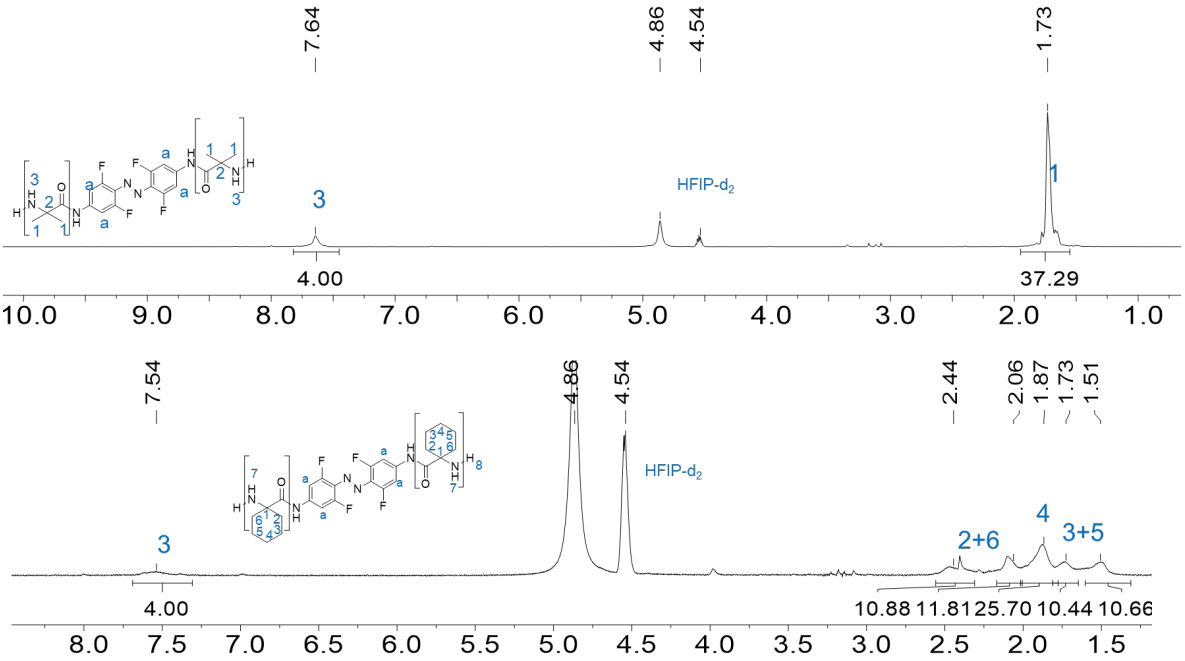

Figure S110. ^{1}H-NMR spectra of **20a** (top) and **20b** (bottom) in HFIP-d_2.

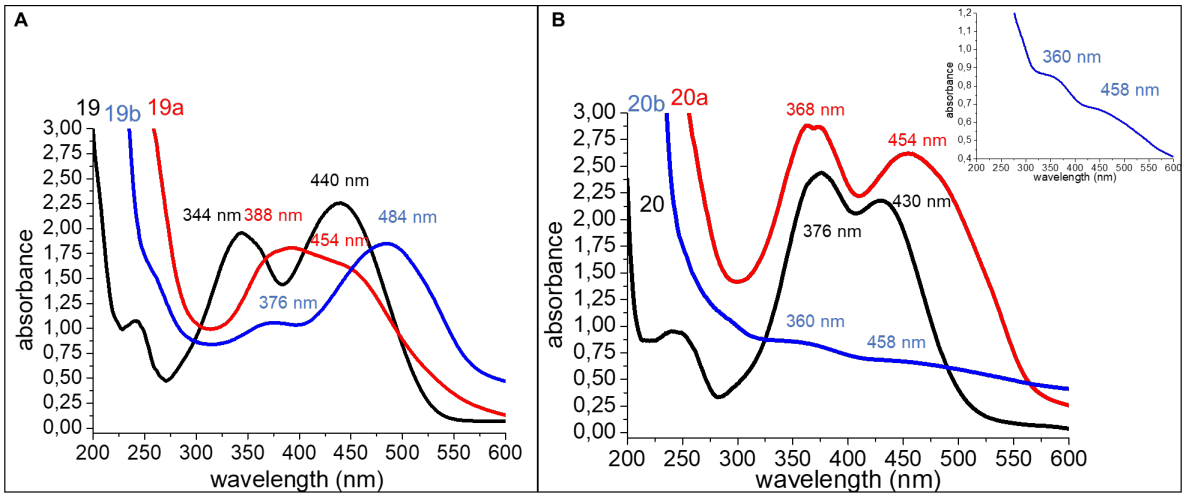

Figure S111. UV-VIS-spectra of **A**) **19** (black), **19a** (red) and **19b** (blue) and **B**) **20** (black), **20a** (red) and **20b** (blue), inlet: zoom into UV-VIS-spectrum of **20b**, in which absorbance signal intensity is low due to low concentration of sample.

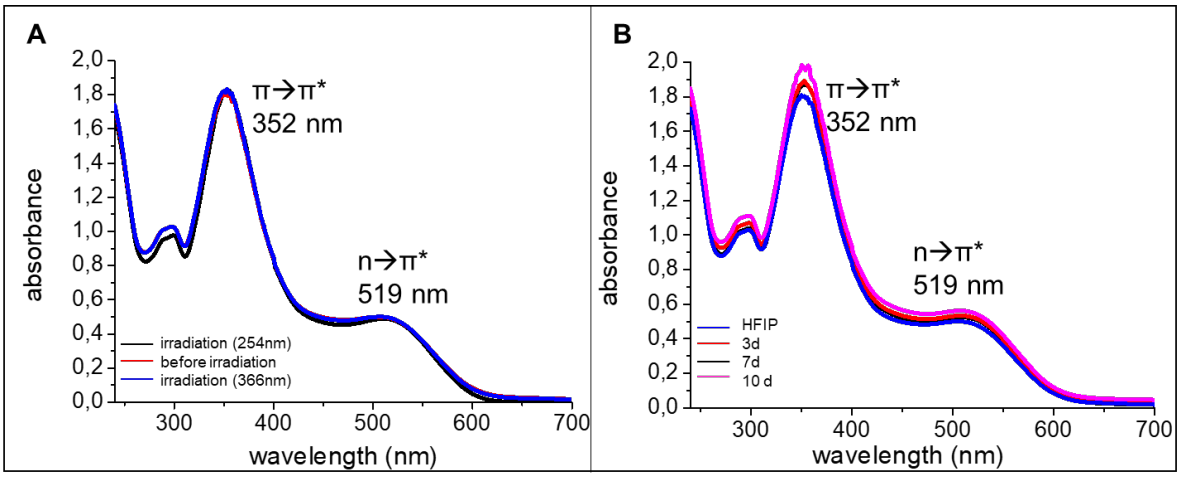

Figure S112. UV-VIS- spectra of **21** in HFIP-solution **A**) before irradiation (red curve) and after irradiation with light (λ=254 nm) (black curve) and (λ=366 nm) (blue curve) and **B**) after 3 days (red curve) 7 days (black curve) and 10 days (pink curve) revealing stability without decomposition in the used solvent (higher absorbance after several days due to evaporation of the solvent).

ACS Macro Letters

May 2020 • Volume 9, Issue 5

pubs.acs.org/acsmacrolett

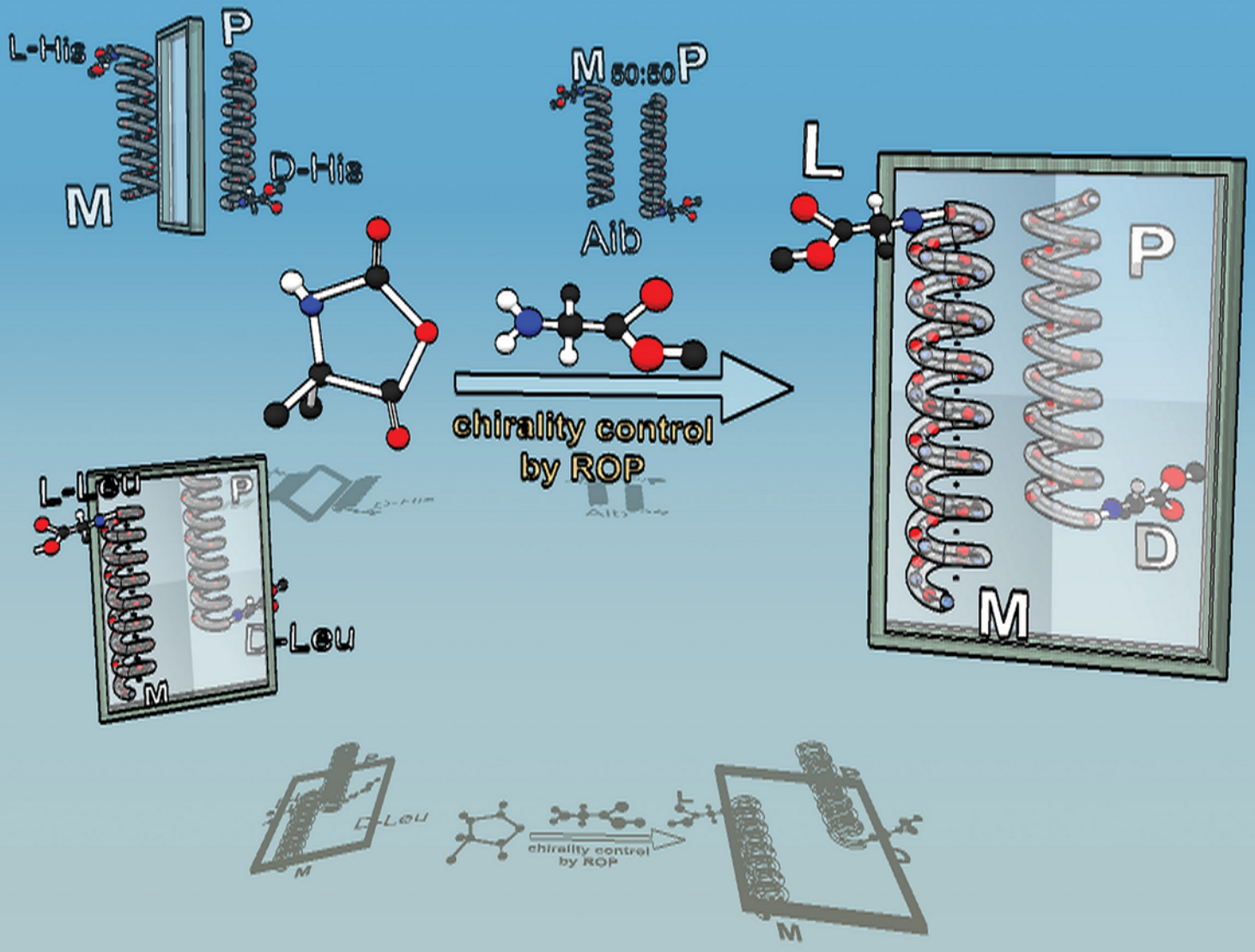

ACS Publications
Most Trusted. Most Cited. Most Read.

www.acs.org

8 Curriculum vitate

• Jan Freudenberg •

Lebenslauf

Persönliche Daten

Geburtsdatum:	10.11.1992
Geburtsort:	Weißenfels
Staatsangehörigkeit:	deutsch

Schulische Ausbildung

ab 10/2016 **Martin-Luther-Universität Halle-Wittenberg (Promotionsstudent)**

- Ausarbeitung und Anfertigung einer Promotionsarbeit

10/2014 – 09/2016 **Martin-Luther-Universität Halle-Wittenberg (Masterstudium Chemie)**

- Abschluss Master Chemie in der Regelstudienzeit von vier Semestern

10/2011 – 10/2014 **Martin-Luther-Universität Halle-Wittenberg (Bachelorstudium Chemie)**

- Abschluss Bachelor Chemie in der Regelstudienzeit von sechs Semestern

08/2003 – 07/2011 **Goethegymnasium Weißenfels (Abitur)**

Fähigkeiten/Kenntnisse

Synthetische Kenntnisse

Eigenständige Durchführung (Labormaßstab) von:

- Polymerisationen (lebend, Kondensation, Addition)
- Organischen Synthesen

Analytische Kenntnisse

Erfahrungen in der Durchführung eigener Messungen mit:

- MALDI-TOF-MS-Spektrometer, ESI-TOF-MS-Spektrometer
- IR-, UV-VIS-Spektrometer
- Präparative GPC/HPLC im Labormaßstab

Computer

- Sehr gute Kenntnisse in Microsoft Word, Excel und Power Point
- Sehr gute Kenntnisse in Software zur Bearbeitung chemischer Aufgabestellungen und Auswertung von Messdaten wie z.B. Origin, MestReNova, ChemDraw

Fremdsprachen

- Sehr gute Kenntnisse in Englisch

Halle (Saale), den

_____

Jan Freudenberg

Publikationsliste

J. Freudenberg, W.H. Binder*, Chirality Control of Screw-Sense in Aib-Polymers: Synthesis and Helicity of Amino Acid Functionalized Polymers. *ACS Macro Let.* **2020**, 9, 686-692. DOI: 10.1021/acsmacrolett.0c00218

J. Freudenberg, W.H. Binder*, Multisegmented Hybrid Polymer Based on Oligo-Amino Acids: Synthesis and Secondary Structure in Solution and in the Solid State. *Macromolecules*, **2019**, 52, 12, 4534-4544. DOI: 10.1021/acs.macromol.9b00684

J. Freudenberg, S. Poppe, W.H. Binder*, Precision polymers containing main-chain-amino acids: ADMET polymerization and crystallization. *RSC Adv.*, **2017**, 7, 47507-47519. DOI: 10.1039/C7RA10485E

P. Liebing, **J. Freudenberg**, C. Heiser, K. Merzweiler*, Novel Copper(I) Clusters with 2-(Diphenylphosphanyl)anilide Ligands. Synthesis and Crystal Structures of $[Cu_6X_2(NHR)_4]$ (X = Cl, Br, I; R = C_6H_4-2-PPh_2). *Z. Anorg. Allg. Chem.*, **2017**, 643, 203-208. DOI: 10.1002/zaac.201600364

Konferenzbeiträge

Freudenberg, J.; Binder, W. H., Crystallization and aggregation behavior of polymer-peptide conjugates, APME (Advanced Polymers via Macromolecular Engineering), 21. – 25. Mai 2017, Ghent, Belgien, Poster.

Halle (Saale), den

Jan Freudenberg

9 Eigenständigkeitserklärung

Erklärung

Hiermit versichere ich, dass ich die vorliegende Arbeit selbstständig und ausschließlich unter Verwendung der angegebenen Quellen und Hilfsmittel verfasst habe. Die Arbeit ist in gleicher oder ähnlicher Fassung noch in keinem anderen Studiengang und an keiner anderen Universität als Prüfungsleistung vorgelegt worden.

Halle (Saale), den

_____

Jan Freudenberg